

**Understanding the roles of
fumarate in *Plasmodium* metabolism and
succinimide in MjGATase stabilization**

A Thesis Submitted for the Award of the Degree of

Doctor of Philosophy

by

Aparna Vilas Dongre



Thesis Supervisor: Prof. Hemalatha Balaram

**Molecular Biology and Genetics Unit,
Jawaharlal Nehru Centre for Advanced Scientific Research,
(Deemed to be University)
Bangalore-560064, India**

December 2020

(This page is intentionally left blank)

Declaration

I hereby declare that this thesis entitled, “**Understanding the roles of fumarate in *Plasmodium* metabolism and succinimide in MjGATase stabilization**” is an authentic record of research work, which has been carried out by me under the supervision of **Prof. Hemalatha Balam** at the Molecular Biology and Genetics Unit, Jawaharlal Nehru Centre for Advanced Scientific Research, Bangalore, India and this work has not been submitted elsewhere for the award of any other degree.

In keeping with the general practice of reporting scientific observations, due acknowledgements have been made wherever the work described has been based on the findings of other investigators. Any omission, which might have occurred by oversight or misjudgement, is regretted.



Aparna Vilas Dongre

JNCASR, Bengaluru

Date:

(This page is intentionally left blank)



Molecular Biology and Genetics Unit,
Jawaharlal Nehru Centre for Advanced Scientific Research,
Jakkur, Bangalore – 560 064, India.

Hemalatha Balaram, Ph.D.

Professor

Certificate

This is to certify that the work described in this thesis entitled “**Understanding the roles of fumarate in *Plasmodium* metabolism and succinimide in MjGATase stabilization**” is the result of investigations carried out by **Ms Aparna Vilas Dongre** in the Molecular Biology and Genetics Unit, Jawaharlal Nehru Centre for Advanced Scientific Research, Bengaluru, India under my supervision, and that the results presented in this thesis have not been previously formed the basis for the award of any other diploma, degree or fellowship.

Hemalatha Balaram

Prof. Hemalatha Balaram,

JNCASR, Bengaluru

Date:

◇ Telephone: 91-80-22082812 ◇ Telefax: 91-80-22082766 ◇ Email: hb@jncasr.ac.in

List of Publications

- 1) Kumar S., Prakash S., Gupta K., **Dongre A.**, Balaram P., Balaram H. Unexpected functional implication of a stable succinimide in the structural stability of *Methanocaldococcus jannaschii* glutaminase. **Nature Communications**. 2016 Sep 28;7(1):1-4.
- 2) ***Dongre A.**, *Das S., Bellur A., Kumar S., Chandrashekarmath A., Balaram P., §Balasubramanian S., §Balaram H. Structural basis for the hyperthermostability of an archaeal glutaminase induced by post-translational succinimide formation (*Manuscript to be communicated*)

* Equal Contribution

§ Joint corresponding authors

- 3) Jayaraman V., **Dongre A.**, Chandrashekarmath A., Balaram H. Significance of fumarate generated during AMP synthesis examined by metabolic rewiring in *Plasmodium spp.* parasites (*manuscript under preparation*)

Acknowledgements

My Ph.D. has been quite a long and fruitful journey. It was made possible by encouragement, support and constructive criticism I received along the way from a large number of people. I hereby take the opportunity to express my gratitude for them.

To begin with, I thank *Prof. Hemalatha Balaram*, my supervisor who accorded me the opportunity to work under her guidance. She has been with me all along the way mentoring, inspiring, supporting and at times criticizing me and shaping my scientific temper. Her zest for science is contagious. She has also been a source of many thoughtful “tea time” discussions regarding science, history, politics and has helped me develop a taste for some good books as well.

I would like to thank all MBGU faculty members, Prof. Anuranjan Anand, Prof. Ranga Uday Kumar, Prof. MRS Rao, Prof. Tapas Kundu, Prof. Maneesha Inamdar, Prof. Kaustuv Sanyal, Prof. Namita Surolia, Dr. Ravi Manjithaya, and faculties from other departments, Dr. Meher Prakash, Dr. Sarit Agasti, Dr. James Chelliah, Dr. Sheeba Vasu and Dr. Kushagra Bansa for their words of appreciation and constructive criticism during departmental presentation which helped me get a better perspective of my work. The interdisciplinary scientific environment offered by JNCASR nurtures the scientific minds well.

A part of my thesis work involved collaborative project with Prof. Balasubramanian Sundaram’s group at CPMU, JNCASR. He has taught me whatever I know about MD simulations today. His student Dr. Sudip Das has been extremely patient with me, explaining me smallest of the results in great detail. We have had some immensely helpful scientific discussions.

All the crystallography work was carried out at X-ray facility at Molecular Biophysics Unit, Indian Institute of Science, Bangalore. Prof. B. Gopal has been generous with us to provide us time on the X-ray machines whenever requires and it has been instrumental to our research. His inputs during solving the crystal structure have been valuable. I would also like to thank Prof. M.R.N. Murthy at Molecular Biophysics Unit, Indian Institute of Science, Bangalore who guided us to solve the crystal structure the right way and taught us the correct way of interpreting X-ray data. Our efforts to solve the structure of MjGATase wild type enzyme could not have met with success without immensely valuable inputs from Dr. Udipi A. Ramagopal, Associate Professor & Dean Academics, Poornaprajna Institute of Scientific Research, Bangalore, India.

I would like to thank *Dr. Ravi Phadke* (HOD, Department of Microbiology, Ramnarain Ruia college) and *Dr. S Shanmugasundaram* (HOD, Microbial Gene Technology, Madurai Kamaraj University) who inspired me to do science and nurtured my interest in science.

I am honoured to have had an opportunity to interact with *Prof. Padmanabhan Balaram* during the course of my Ph.D. He taught me to keenly analyse and appreciate protein structure. His scientific wisdom has always been and will always be a source of inspiration.

The role of a healthy work environment cannot be emphasised enough. I am grateful to past and present members of my laboratory who maintained an extremely zealous lab culture. I have learnt a lot from each of them. When I entered lab as a novice Ph.D. student, I was helped at each and every step by Dr. Sanjeev Kumar, Dr. Vijay Jayaraman, Dr. Saurav Roy, Dr. Arpit Shukla, Dr. Santosh S, Dr. Prasoon Thota, Dr. Lakshmeesha KN and Jyothi, Umesh, Manu and Sonia. I carried forward works of Dr. Sanjeev and Dr. Vijay who taught me every experimental skill I needed to acquire to start my journey. Along with them, the current lab members and a few who left recently, Arpitha, Ashutosh, Resmi, Nivedita, Anusha, Rahul Madan, Neelakshi, Pavithra, Dr. Ruchika and Dr. C. N Rahul have been extremely helpful, encouraging and entertaining and I sincerely thank them for making the lab a great place to work. The enthusiasm displayed by rotation students, Veena, Rashi, Pragya, Srijana, Sarika and Satya was infectious and each of them contributed immensely.

I would like to thank other MBGU seniors, batchmates and juniors for their suggestions during MBGU annual work presentations. Those work presentation sessions were very helpful and a good platform for all students to come together on weekly basis. I specially thank Dr. Amrutha, Dr. Nikhil, Dr. Arnab, Dr. Rohan, Dr. Deboshree, Dr. Palak and Dr. Vijay (CBL). I shared some good memories with my batchmates Rima, Praveen, Aditya, Suchismita, Krishnendu, Pallavi, Siddharth, Veena and Bhavana during our early times in JNCASR and I thank them for their support all throughout.

This long journey in JNC would have been difficult without some wonderful friends I made along the way. My friends Rishav, Veena, Surbhi, Yamini, Ruchika and Resmi who have been my clan, keeping me sane during tough times and were my family away from family.

I would like to thank the staff of X-ray facility at Molecular Biophysics Unit of Indian Institute of Science, Bangalore for extending their support every time we used the facility.

I would like to thank various facilities in JNCASR: Academics, library, canteen, hostel, dhanvantari, security and others. I would also like to thank Dr. Prakasha (Animal facility) and Suma ma'am (Microscopy) for their help. I hereby also acknowledge JNCASR for financial support. I earnestly thank JNCASR community for providing a conducive scientific environment.

Last but not the least is my family who I wholeheartedly want to thank. My father has been supportive and trusting of all my life choices. Through his actions, he teaches me to be humble, honest and passionate about work. My mother's unconditional love and boundless compassion propels me through any storm I encounter in my personal or professional life. It is my baby sister from whom I learn to take life lightly and live in the moment. I am forever indebted to them for being my rocks!

A new addition to my life is my in-laws to whom I thank earnestly. They not only understood the importance of my work but also constantly supported and encouraged me.

I cannot imagine last few years of my life without this one person, Margesh! He has been my pillar from day one of my Ph.D. His unconditional love, support and encouragement is the reason I could sail through this journey!

Thank you all!

(This page is intentionally left blank)

Synopsis of Thesis

Understanding the roles of fumarate in *Plasmodium* metabolism and succinimide in MjGATase stabilization

Submitted by

Aparna Vilas Dongre

Molecular Biology & Genetics Unit (MBGU),

Jawaharlal Nehru Centre for Advanced Scientific Research (JNCASR), Bangalore.

Thesis supervisor: Prof. Hemalatha Balaram

Overview of the work

Apicomplexan parasites of genus *Plasmodium* synthesize purine nucleotides via the salvage pathway rather than *de novo* pathway. Our laboratory has been studying various biochemical aspects of the *Plasmodium* purine salvage pathway. The two purine mononucleotides adenosine 5' monophosphate (AMP) and guanosine 5' monophosphate (GMP) are synthesized from inosine 5' monophosphate (IMP) via independent branches of the purine synthesis pathway. My thesis consists of two distinct lines of work that were started simultaneously and the results obtained for both sections are discussed in detail. One line of work pertains to understanding the metabolic significance of fumarate generated from AMP synthesis branch from *Plasmodium* whereas the other line of work involves studying the structural features of succinimide-induced thermostability in an archaeal glutamine amidotransferase.

Plasmodium parasites primarily salvage the nucleobase hypoxanthine from host erythrocytes along with small amounts of adenosine and other nucleosides (Bissati et al. 2008; El Bissati et al. 2006; Rager et al. 2001). Hypoxanthine is converted to inosine 5' monophosphate (IMP) in a reaction catalysed by hypoxanthine guanine (xanthine) phosphoribosyltransferase (HG(X)PRT). IMP is a nodal nucleotide that can be branched either into AMP or GMP synthesis. The first step of AMP synthesis from IMP catalysed by adenylosuccinate synthetase (ADSS) adds a molecule of aspartate on IMP, generating succinyl AMP (sAMP, adenylosuccinate). Second reaction catalysed by adenylosuccinate lyase releases fumarate from sAMP, converting it to AMP. Earlier NMR studies from our laboratory, conducted with exogenously added ¹³C labelled fumarate, had demonstrated that fumarate is not a metabolic waste; rather it is metabolised into malate, aspartate, pyruvate and lactate. In the current study, we sought to determine the consequences of depleting the endogenous fumarate generated during AMP synthesis, within the parasites.

The GMP synthesis arm involves conversion of IMP to XMP, catalysed by IMP dehydrogenase followed by conversion of XMP to GMP catalysed by GMP synthetase. These two enzymes have also been studied extensively in our laboratory from *Plasmodium* as well as from a hyperthermophilic archaeon, *Methanocaldococcus jannaschii*. GMP synthetase consists of two subunits/domains: ATP pyrophosphatase (ATPPase) and glutamine amidotransferase (GATase). Extensive study of

Methanocaldococcus jannaschii GATase (MjGATase) led to a serendipitous discovery of a stable succinimidyl residue at position 109 – formed post-translationally during deamidation of asparagine - which was probed thoroughly, mass-spectrometrically (Kumar et al. 2016). In the study presented in this thesis, we elucidated the structural basis for thermostability of (MjGATase) induced by the post-translational succinimide formation. Deamidation of asparaginyl (or glutaminyl) residues in proteins is a spontaneously occurring, non-enzymatic post-translational modification, occurring under physiological conditions, that results in formation of aspartate or β -aspartate/iso-aspartate products via a succinimide intermediate and leads to destabilization of protein structure with concomitant loss of function. Deamidation *in vivo*, occurs predominantly in aged proteins (under physiological conditions) and *in vitro* in proteins/enzymes/antibodies stored for prolonged periods. In the current study, we solved the structure of MjGATase by X-ray crystallography to gain insights into the structural features that accord succinimide-induced hyperthermostability.

Understanding the significance of fumarate generated during AMP synthesis to the asexual stages of *Plasmodium spp.* parasites

Malaria, caused by parasites of *Plasmodium spp.* is responsible for millions of deaths worldwide, each year. It has been a global concern for centuries, imposing a significant economic burden on countries affected by it. Population of young children (under the age of 5) and pregnant women are predominantly affected by this disease, with majority of cases found in underdeveloped and developing countries (World Health Organization, 2019). The emergence of drug resistance to front line antimalarials among parasite populations has posed a need to discover new drug targets. Understanding of the parasite metabolism is crucial to exploit the differences between host and parasite metabolism, which can open up new avenues of drug targets unique to the parasite. Metabolism in *Plasmodium spp.* parasites has been the focus of many research studies and valuable insights have been obtained through them (Cobbold and McConville 2014; Van Dooren, Stimmler, and McFadden 2006; Ke et al. 2015; MacRae et al. 2013).

Purine and pyrimidine nucleotides are the building blocks of DNA and RNA in addition to being part of the structure of some of the coenzymes like NAD, FAD and Coenzyme A. Steady supply of purine nucleotides is crucial for survival and growth of highly proliferating asexual stage *Plasmodium* parasites; hence, the purine salvage pathway of parasites is an attractive drug target. Purine salvage in apicomplexan parasites is mediated predominantly via adenosine kinase (AK) or hypoxanthine guanine phosphoribosyltransferase (HGPRT) (Chaudhary et al. 2004; Ghérardi and Sarciron 2007). *Plasmodium* parasites predominantly salvage nucleobases and nucleosides such as hypoxanthine, adenosine and inosine from host erythrocytes along with minor import of guanine, guanosine and xanthosine (Bissati et al. 2008). Hypoxanthine, either directly imported from host or generated from adenosine via sequential actions of adenosine deaminase and purine nucleoside phosphorylase, is converted to inosine 5' monophosphate (IMP) in a reaction catalysed by hypoxanthine guanine (xanthine) phosphoribosyltransferase (HG(X)PRT). Parasite genome lacks genes encoding AK or

adenine phosphoribosyl transferase (APRT). IMP is a nodal metabolite as it serves as a precursor for both adenosine 5' monophosphate (AMP) and guanosine 5' monophosphate (GMP) biosynthesis. IMP to GMP conversion is catalysed by the sequential actions of IMP dehydrogenase (IMPDH) and GMP synthetase (GMPS). In a first step towards AMP synthesis, adenylosuccinate synthetase (ADSS) catalyses addition of aspartate onto IMP, converting it to succinyl AMP (sAMP) with concomitant conversion of GTP to GDP. Adenylosuccinate lyase (ASL) converts sAMP to AMP, removing aspartate carbon skeleton as fumarate. AMP is deaminated back to IMP via the action of AMP deaminase (AMPD) in a cyclic inter-conversion process termed the purine nucleotide cycle (PNC) (Bogusky, Lowenstein, and Lowenstein 1976). Regenerated IMP can re-enter purine synthesis (Fig. 1).

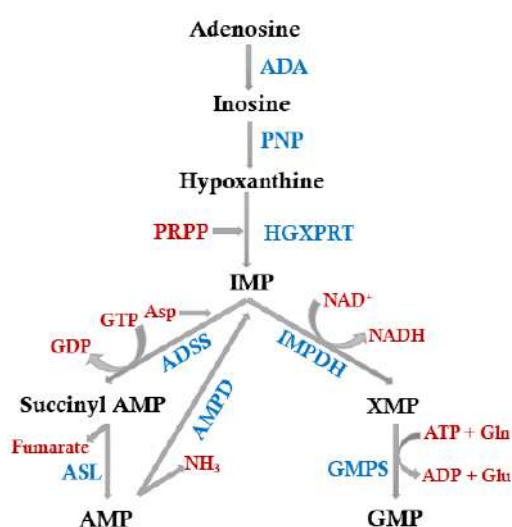


Figure 1. Schematic representation of purine salvage pathway of *Plasmodium spp.* parasites. Parasites salvage hypoxanthine and adenosine from the host erythrocytes and convert them to adenylate and guanylate nucleotides through two independent branches.

During the synthesis of AMP from IMP, with each molecule of AMP, a molecule of fumarate is generated. Given that the amount of AMP generated in asexual stage parasites would be high, the amount of fumarate generated will also be sizable which can be further amplified by a functional purine nucleotide cycle. Fumarate is an intermediate of tricarboxylic acid (TCA) cycle, a pathway that is functional yet dispensable to *Plasmodium* parasites in the asexual stages and the flux through TCA cycle during asexual stage life cycle is minimal. During the asexual stage life cycle, the energy requirement of parasites is fulfilled via aerobic glycolysis, in a metabolic scenario that is similar to cancer cells (Abdel-Haleem et al. 2017; Salcedo-Sora et al. 2014).

As mentioned earlier, parasite genome lacks genes encoding adenosine kinase and adenine phosphoribosyltransferase. The retention of HG(X)PRT and absence of AK in Plasmodia is intriguing as AMP generation from AK is rather energy efficient with only one molecule of ATP utilized to convert a molecule of adenosine into AMP in a one-step reaction



HG(X)PRT reaction utilizes phosphoribosyl pyrophosphate (PRPP) that is formed from ribose-5-phosphate and ATP (the generation of substrate itself involves utilization of a molecule of ATP). The subsequent ADSS/ASL reactions, utilize GTP and aspartate; generation of GTP also requires ATP, rendering the whole pathway (HGXPRT/ADSS/ASL) even more energy-consuming. Given these metabolic scenarios where flux through TCA is minimal and AMP is synthesized via HG(X)PRT/ADSS/ASL pathway, the question arises - what could be the metabolic significance of fumarate generated through this pathway to the asexual stages of *Plasmodium* parasites. The study described in this thesis is a collation of experiments carried out in an attempt to find answers to these questions. In order to examine the importance of fumarate to overall parasite metabolism, its production through ADSS/ASL pathway needs to be abrogated and the cellular processes and pathways affected by depletion of fumarate need to be studied. However, conversion of IMP through ADSS and ASL reactions to AMP is the only pathway by which parasite can synthesize AMP; hence, ablation of fumarate production by inhibition/gene deletion of either ADSS or ASL would abolish AMP generation which would be lethal to the parasites. This scenario demands de-coupling of AMP synthesis and fumarate production within the cell which can be achieved by introducing an alternate pathway for AMP synthesis (independent of fumarate generation) followed by deletion/inhibition of ADSS and/or ASL enzyme function and examination of the effects of that perturbation on the overall cellular metabolism through *in vitro* assays and metabolomic studies.

Chapter one provides a general introduction about *Plasmodium* species distribution, parasite life cycle and metabolism which will familiarize the reader with the important life cycle stages and different metabolic pathways of the parasite.

Chapter two details the materials and methods used during the study. It includes protocols followed for routine *Plasmodium* culturing, synchronization, parasite enrichment and transfections in addition to routine molecular biology protocols. Methodologies of the various strategies used to express an alternate purine salvage pathway in *Plasmodium* parasites, strategies attempted to knock out endogenous ADSS/ASL genes and the method for chemical inhibition of adss are described in detail in this chapter. Genetic manipulations were also attempted in murine malaria parasite *P. berghei* simultaneously, the protocols for the same are also reported.

Chapter three provides comprehensive account of results obtained for the objectives laid out in the study. All three objectives of the study have been provided with an introduction (a literature review) followed by results and discussion. First objective of the study was to generate transgenic *Plasmodium* lines expressing an alternate pathway for AMP synthesis to facilitate decoupling of AMP synthesis from fumarate production. Since adenosine kinase mediated purine salvage dominates in other apicomplexan parasites, we chose this enzyme to bypass HG(X)PRT mediated AMP synthesis in *Plasmodium falciparum* and *Plasmodium berghei*. Transgenic parasite lines of *P. falciparum* and *P. berghei*

expressing yeast adenosine kinase were generated, validated and used for further studies. Attempts were made to knock-out and knock-down enzymes of endogenous AMP synthesis pathway using available gene disruption techniques such as double-crossover homologous recombination (Maier et al. 2006), CRISPR-Cas9 (Ghorbal et al. 2014) and conditional protein knock-down via DHFR degradation domain-trimethoprim combination (Muralidharan et al. 2011). In *P. berghei* transgenic parasites expressing yeast adenosine kinase, ASL knock-out was attempted using pJAZZ construct procured from Plasmogem (Schwach et al. 2015). Despite considerable efforts and use of different strategies, desired gene knock-outs could not be obtained in either *P. falciparum* or *P. berghei* parasites, metabolically rewired to express an alternate AMP synthesis enzyme, suggesting that ADSS/ASL mediated AMP synthesis and perhaps fumarate production are indispensable to the parasite during asexual life-cycle. We also used a chemical genetics approach and inhibited AMP synthesis via adenylosuccinate synthetase using hadacidin (Shigeura and Gordon 1962a, 1962b). Growth phenotypes of transgenic parasites in presence and absence of hadacidin were analysed. Discussion includes succinct account of key results, future experiments, and analysis of failure to obtain desired gene knock-outs. At the end of this chapter, our attempts to standardize metabolomics with *P. falciparum* culture have been recounted. These three chapters complete the parasitology section of the thesis.

Study of the structural basis for the hyperthermostability of an archaeal glutaminase induced by post-translational succinimide formation

Next two chapters discuss structural features responsible for hyperthermostability of *Methanocaldococcus jannaschii* glutamine amidotransferase (MjGATase) subunit induced by a post-translationally formed succinimidyl residue.

Organisms surviving at high temperatures (thermophiles) are able to do so because of their thermally stable proteins/enzymes. The structural and functional features of thermophilic proteins that facilitate their optimal activity at high temperatures makes them desirable candidates for those interested in studying molecular mechanisms of protein thermostability. Amino acid sequences of thermostable proteins are similar to their mesophilic counterparts but subtle differences in tertiary structure, primary sequence and other modifications (e.g. PTMs) grant thermal stability to thermophilic proteins. A vast number of 'mechanisms of thermostability' have been studied till date and the search and examination of new mechanisms is still ongoing. Previous studies from our laboratory on MjGATase led to the serendipitous discovery of a stable succinimidyl residue (SNN109), formed as a result of a post-translational modification - deamidation of asparagine 109. Asn109 was present as a succinimidyl moiety in bulk of the protein overexpressed and purified from *E. coli*. The succinimide harbouring protein was thermally and chemically stable resisting hydrolysis at 100 °C and 8 M guanidium hydrochloride (Kumar et al. 2016).

Asparagine deamidation and aspartate isomerization are spontaneous, non-enzymatic processes occurring in aged proteins *in vivo* or proteins stored for prolonged periods *in vitro* and during both the processes, five membered succinimide ring is formed as an intermediate (Fig. 2 a) (Robinson 2002; Robinson and Robinson 2001). The succinimide intermediate is highly unstable and undergoes dehydration to form either L-Asp or L-iso-Asp; it can also undergo racemization to form D-succinimide that can be hydrolysed to D-Asp or D-isoAsp (Fig. 2 b) (Clarke 1987; Geiger and Clarke 1987)

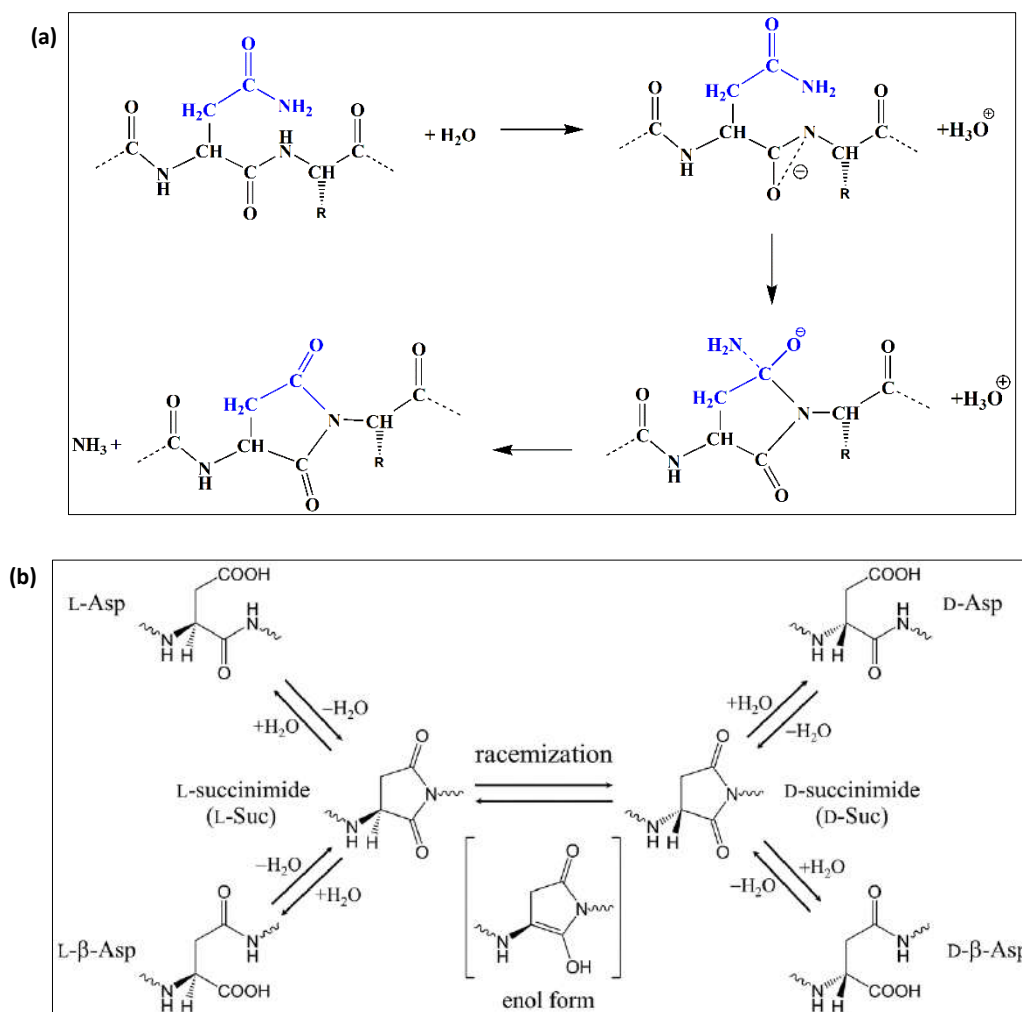


Figure 2: Formation and hydrolysis of succinimide intermediate. (a) Schematic representation of the process of deamidation of asparaginyl residue in a peptide leading to succinimide intermediate formation. (b) Schematic representation of succinimide racemization leading to D/L-Asp or D/L-iso-Asp formation. Image (b) adopted from Takahashi, O., Kirikoshi, R., & Manabe, N. (2016). Racemization of the Succinimide Intermediate Formed in Proteins and Peptides: A Computational Study of the Mechanism Catalyzed by Dihydrogen Phosphate Ion. *International journal of molecular sciences*, 17(10), 1698. under Creative Common CC BY license.

Deamidation and isomerization reactions are almost always detrimental causing destabilization of protein structure and concomitant loss of function. Spontaneous deamidation of stored therapeutic antibodies leading to their reduced efficacy is a major concern in the pharmaceutical industry. However, in MjGATase, intermediate of Asn109 deamidation is stable and it, in turn, stabilises the entire protein as demonstrated through extensive mass spectrometric analysis and site-directed

mutagenesis (Kumar et al. 2016). To our knowledge, it was the first report of succinimide-induced thermostability mechanism in proteins.

In this study, we sought to solve the structure of MjGATase protein to capture the stable succinimide to understand the structural features that stabilize the succinimidyl residue and in turn the entire protein. Molecular dynamic simulations are a useful tool to investigate and visualize atomistic details of protein dynamics (movement). For the present study, we collaborated with Prof. Balasubramanian Sundaram's group at Chemistry and Physics of Materials Unit, JNCASR who performed MD simulations on wild type and mutant (lacking succinimidyl residue) structures of MjGATase to understand, at atomistic level, the contributions of succinimidyl residue towards maintaining the overall protein stability.

Chapter four provides literature review on known mechanisms of thermostability, enzymatic and non-enzymatic deamidation processes, a brief account of other non-enzymatic post-translational modifications, functional implications of iso-aspartate formation in proteins, an account of few examples of stable succinimidyl residues found in other proteins (examples taken from RCSB-PDB) and the influence of stable succinimides (in peptides) on structure of peptide backbones. The section also contains brief introduction to the molecular dynamic simulation tools used, replica exchange with solute scaling (REST2) (Wang, Friesner, and Berne 2011) and Well-tempered metadynamics (WT-MTD) (Barducci, Bussi, and Parrinello 2008). A major problem encountered during simulations of biological macro-molecules is the insufficient sampling of conformational space. As MjGATase is an inherently stable protein, tools that could sample enough conformational space to reflect small changes were required; REST2 and WT-MTD mitigate this problem by sampling large conformational space.

In chapter five, Materials and Methods, Results, Discussion and Future directions of this section of the thesis have been combined. Methods used to purify, crystallize and solve structure of MjGATase (wild type and mutants) have been reported in detail.

Structure of MjGATase solved by X-ray crystallography has been thoroughly analysed with specific focus on the succinimidyl residue: its interactions with neighbouring residues, long-range contacts and tertiary contacts connecting the stable succinimidyl residue with the active site residues. Structure of WT MjGATase covalently bound to the non-hydrolysable glutamine analogue, acivicin (5CS) was also solved. In addition, structure of D110G mutant, in which succinimide forms but readily undergoes hydrolysis, was also solved and analysed. As discussed in Introduction, presence of succinimidyl residue in a peptide has structural implications, which were also noticed in MjGATase protein structure. These have been assessed and the observations are summarized. Electron density of tripeptide region 108-110 (ENG) in MjGATase_D110G was fragmented although electron density for rest of the residues was well-mapped. This suggests that absence of the succeeding negatively charged residue renders the tripeptide region highly flexible and the resultant increased dynamics makes it difficult to capture electron density in that region.

Further, the stabilizing interactions of succinimidyl residue have been discussed. We postulate that post-translational succinimide formation might be more widespread among hyperthermophilic organisms than we currently presume. This conjecture is based on the observed conservation of E(N/D)(D/E) tripeptide sequence in ~100 other archaeal glutamine amidotransferase (subunits of GMP synthetase) sequences. At the end, I have briefly reported the results obtained by advanced simulation tools used in the study (*All simulations were performed by Dr. Sudip Das, Ph.D. from Prof. Balasubramanian Sundaram's laboratory, Chemistry and Physics of Materials Unit, JNCASR*). Simulation data illustrate that succinimide lacking protein is more flexible compared to succinimide containing protein and it corroborates our experimental observations – succinimide containing protein is more thermostable than the protein lacking it – providing a plausible molecular level explanation for it.

At the end of this chapter, the future prospects for this section of the thesis have been discussed. One of the mechanisms granting thermostability to proteins is the increased occurrence of prolyl residues (Avil, Molecular, and Aut 2004; Herning et al. 1992; Watanabe et al. 1991, 1994). Although both succinimidyl and prolyl residues are cyclic and impose a local conformational constrain, the effect varies as seen from the mutant of MjGATase in which Asn109 was replaced with Pro109. The mutant was found to have lost thermal stability conspicuously compared to the wild type protein. We solved and analysed the structure of MjGATase_N109P to understand reasons behind drastic decrease in thermostability of this mutant. Preliminary observations have been summarized and future experiments in this regard have been proposed. The mechanism behind 'succinimide-formation' needs to be probed further and few factors which could plausibly be involved have been discussed. Stable succinimides in proteins are majorly identified by solving structure, however, it may not always be possible to do so. More efficient techniques for the same can be mass spectrometry and few of the studies which describe the use of MS for succinimide-detection in peptide digests have been noted. Extrapolating and incorporating the known mechanisms of thermostability in desired (industrially important) proteins is the principal motive behind studying these mechanisms. We postulate future experiments/ analyses to be performed to attempt incorporation of "stable-succinimide" in industrially important proteins to endow thermostability upon them.

References

1. Abdel-Haleem, Alyaa M. et al. 2017. "The Emerging Facets of Non-Cancerous Warburg Effect." *Frontiers in Endocrinology* 8(OCT): 1–7.
2. Avil, Francesc X, Biologia Molecular, and Universitat Aut. 2004. "Applications on Loop Modeling and Protein Function."
3. Barducci, Alessandro, Giovanni Bussi, and Michele Parrinello. 2008. "Well-Tempered Metadynamics: A Smoothly Converging and Tunable Free-Energy Method." *Physical Review Letters* 100(2): 1–4.
4. El Bissati, Kamal et al. 2006. "The Plasma Membrane Permease PfNT1 Is Essential for Purine Salvage in the Human Malaria Parasite Plasmodium Falciparum." *Proceedings of the National Academy of Sciences of the United States of America* 103(24): 9286–91.
5. Bissati, Kamal El et al. 2008. "Genetic Evidence for the Essential Role of PfNT1 in the Transport and Utilization of Xanthine, Guanine, Guanosine and Adenine by Plasmodium Falciparum." *Molecular and Biochemical Parasitology* 161(2): 130–39.
6. Bogusky, R. T., L. M. Lowenstein, and J. M. Lowenstein. 1976. "The Purine Nucleotide Cycle. A Pathway for Ammonia Production in the Rat Kidney." *Journal of Clinical Investigation* 58(2): 326–35.
7. Chaudhary, Kshitiz et al. 2004. "Purine Salvage Pathways in the Apicomplexan Parasite Toxoplasma Gondii." *Journal of Biological Chemistry* 279(30): 31221–27.
8. Clarke, Steven. 1987. "Propensity for Spontaneous Succinimide Formation from Aspartyl and Asparaginylic Residues in Cellular Proteins." *International Journal of Peptide and Protein Research* 30(6): 808–21.
9. Cobbold, Simon A, and Malcolm J McConville. 2014. "The Plasmodium Tricarboxylic Acid Cycle and Mitochondrial Metabolism." In *Encyclopedia of Malaria*, eds. Marcel Hommel and Peter G Kremsner. New York, NY: Springer New York, 1–18. https://doi.org/10.1007/978-1-4614-8757-9_13-1.
10. Van Dooren, Giel G., Luciana M. Stimmler, and Geoffrey I. McFadden. 2006. "Metabolic Maps and Functions of the Plasmodium Mitochondrion." *FEMS Microbiology Reviews* 30(4): 596–630.
11. Geiger, T., and S. Clarke. 1987. "Deamidation, Isomerization, and Racemization at Asparaginylic and Aspartyl Residues in Peptides. Succinimide-Linked Reactions That Contribute to Protein Degradation." *Journal of Biological Chemistry* 262(2): 785–94.
12. Geneva: World Health Organization. 2019. *World Malaria Report 2019*.
13. Ghérardi, Arnaud, and Marie Elisabeth Sarciron. 2007. "Molecules Targeting the Purine Salvage Pathway in Apicomplexan Parasites." *Trends in Parasitology* 23(8): 384–89.
14. Ghorbal, Mehdi et al. 2014. "Genome Editing in the Human Malaria Parasite Plasmodium Falciparum Using the CRISPR-Cas9 System." *Nature Biotechnology* 32(8): 819–21.
15. Herning, Thierry et al. 1992. "Role of Proline Residues in Human Lysozyme Stability: A Scanning Calorimetric Study Combined with X-Ray Structure Analysis of Proline Mutants." *Biochemistry* 31(31): 7077–85.
16. Ke, Hangjun et al. 2015. "Genetic Investigation of Tricarboxylic Acid Metabolism during the

- Plasmodium Falciparum Life Cycle.” *Cell Reports* 11(1): 164–74.
17. Kumar, Sanjeev et al. 2016. “Unexpected Functional Implication of a Stable Succinimide in the Structural Stability of Methanocaldococcus Jannaschii Glutaminase.” *Nature Communications* 7: 12798. <http://www.nature.com/doi/10.1038/ncomms12798>.
 18. MacRae, James I et al. 2013. “Mitochondrial Metabolism of Sexual and Asexual Blood Stages of the Malaria Parasite Plasmodium Falciparum.” *BMC biology* 11(1): 67.
 19. Maier, Alexander G., Joanna A M Braks, Andrew P. Waters, and Alan F. Cowman. 2006. “Negative Selection Using Yeast Cytosine Deaminase/Uracil Phosphoribosyl Transferase in Plasmodium Falciparum for Targeted Gene Deletion by Double Crossover Recombination.” *Molecular and Biochemical Parasitology* 150(1): 118–21.
 20. Muralidharan, Vasant et al. 2011. “Asparagine Repeat Function in a Plasmodium Falciparum Protein Assessed via a Regulatable Fluorescent Affinity Tag.” *Proceedings of the National Academy of Sciences of the United States of America* 108(11): 4411–16.
 21. Rager, Nicolle et al. 2001. “Localization of the Plasmodium Falciparum PfNT1 Nucleoside Transporter to the Parasite Plasma Membrane.” *Journal of Biological Chemistry* 276(44): 41095–99.
 22. Robinson, N. E. 2002. “Protein Deamidation.” *Proceedings of the National Academy of Sciences* 99(8): 5283–88.
 23. Robinson, N E, and A B Robinson. 2001. “Molecular Clocks.” *Proceedings of the National Academy of Sciences of the United States of America* 98(3): 944–49.
 24. Salcedo-Sora, J. Enrique, Eva Caamano-Gutierrez, Stephen A. Ward, and Giancarlo A. Biagini. 2014. “The Proliferating Cell Hypothesis: A Metabolic Framework for Plasmodium Growth and Development.” *Trends in Parasitology* 30(4): 170–75.
 25. Schwach, Frank et al. 2015. “PlasmoGEM, a Database Supporting a Community Resource for Large-Scale Experimental Genetics in Malaria Parasites.” *Nucleic Acids Research* 43(D1): D1176–82.
 26. Shigeura, Harold T, and Charles N Gordon. 1962a. 237 *Hadacidin, a New Inhibitor of Purine Biosynthesis*.
 27. 1962b. 237 *The journal of biological chemistry* The Mechanism of Action of Hadacidine.
 28. Wang, Lingle, Richard A. Friesner, and B. J. Berne. 2011. “Replica Exchange with Solute Scaling: A More Efficient Version of Replica Exchange with Solute Tempering (REST2).” *Journal of Physical Chemistry B* 115(30): 9431–38.
 29. Watanabe, Kunihiko et al. 1994. “Multiple Proline Substitutions Cumulatively Thermostabilize Bacillus Cereus ATCC7064 Oligo-1,6-Glucosidase.” *European Journal of Biochemistry* 283: 277–83.
 30. Watanabe, Kunihiko, Kyoko Chishiro, Kazuhisa Kitamura, and Yuzuru Suzuki. 1991. “Proline Residues Responsible for Thermostability Occur with High Frequency in the Loop Regions of an Extremely Thermostable Oligo-1,6-Glucosidase from Bacillus Thermoglucosidasius KP1006.” *Journal of Biological Chemistry* 266(36): 24287–94.

Abbreviations

5CS	2-amino-3-(cystein-s-yl)-isoxazolidin-5-yl-acetic acid
AAT	Aspartate aminotransferase
ADP	Adenosine 5' diphosphate
ADSS	Adenylosuccinate synthetase
AGEs	Advanced glycation end-products
AK	Adenosine kinase
AMP	Adenosine 5' monophosphate
APRT	Adenine phosphoribosyl transferase
AQUA	Advanced quick assembly
ASL	Adenylosuccinate lyase
Asn	Asparagine
Asp	Aspartate
ATP	Adenosine 5' triphosphate
BSD	Blasticidin
cAMP	Cyclic AMP
CAS	CRISPR associated
CD	Cytosine deaminase
CRISPR	Clustered regulatory interspersed short palindromic repeats
DDD	DHFR degradation domain
D-iso-Asp	D-iso-aspartate
DNA	Deoxyribonucleic acid
dNTP's	Deoxy nucleoside triphosphates
DTT	Dithiothreitol
ECM	Extracellular matrix
EDTA	Ethylene diamino tetraacetic acid
EGTA	ethylene glycol-bis (β -aminoethyl ether)-N,N,N',N'-tetraacetic acid
FAD	Flavin adenine dinucleotide
FH	Fumarate hydratase
GATase	Glutamine amidotransferase
Gln	Glutamine
Glu	Glutamate
Gly	Glycine
GMP	Guanosine 5' monophosphate
GMPS	GMP synthetase
GSH	Glutathione
GSSH	Oxidised glutathione
HA	Haemagglutinin
hDHFR	Human dihydrofolate reductase
HGPRT	Hypoxanthine guanine phosphoribosyl transferase
HGXPRT	Hypoxanthine guanine xanthine phosphoribosyl transferase
HLRCC	Hereditary leiomyomatosis and renal cell cancer
Hyp	Hypoxanthine
IMP	Inosine 5' monophosphate
IMPDH	IMP dehydrogenase
IPTG	Isopropyl β - d-1-thiogalactopyranoside
kbp	Kilobase pair

kDa	Kilo Dalton
LB	Luria Bertani
MDH	Malate dehydrogenase
MDS	Molecular dynamic simulations
Mj	<i>Methanocaldococcus jannaschii</i>
MQO	Malate quinone oxidoreductase
NAD	Nicotinamide adenine dinucleotide
Ni-NTA	Nickle-nitrilotriacetic acid
NMN	Nicotinamide mononucleotide
O.D.	Optical density
ORF	Open reading frame
PCR	Polymerase chain reaction
PIMT	Protein L-isoaspartyl methyltransferase
PM1KO	Plasmepsin 1 knock-out
PMSF	Phenylmethyl sulfonyl fluoride
PNC	Purine nucleotide cycle
PNP	Purine nucleoside phosphorylase
PRPP	Phosphoribosyl pyrophosphate
PTM	Post-translational modification
RBC	Red blood cell
REST2	Replica exchange with solute scaling
RFA	Regulatable fluorescent affinity
RNA	Ribonucleic acid
ROS	Reactive oxygen species
rpm	Revolutions per minute
RPMI	Roswell Park Memorial Institute
sAMP	Succinyl AMP/adenylosuccinate
SDS	Sodium lauryl sulfate
SDS-PAGE	Sodium lauryl sulfate-polyacrylamide gel electrophoresis
SNN	Succinimide
TB	Terrific broth
UTR	Untranslated region
WT	Wild type
WT-MTD	Well-tempered-metadynamics
XMP	Xanthosine 5' monophosphate
yFCU	yeast cytosine deaminase/uridine phosphoribosyltransferase

Table of Contents

Investigating the significance of fumarate generated during purine nucleotide cycle (PNC) to the asexual stages of <i>Plasmodium spp.</i> parasites	4
Chapter 1	5
1. Introduction.....	6
1.1. Brief history of malaria.....	6
1.2. The global health burden of malaria.....	6
1.3. Species distribution of <i>Plasmodium</i>	7
1.4. Life cycle of <i>Plasmodium falciparum</i>	8
1.5. Metabolism in <i>Plasmodium spp.</i>	12
1.5.1. Glycolysis	14
1.5.2. TCA cycle.....	16
1.5.3. Electron transport chain.....	20
1.5.4. Nucleotide metabolism	21
1.6. Fumarate: Metabolic and Non-metabolic roles	25
1.6.1. Fate of fumarate generated through PNC in rat skeletal muscles	27
Chapter 2.....	32
2. Materials and Methods.....	33
2.1. Materials.....	33
2.2. Methods.....	34
2.2.1. Generation of plasmid constructs for <i>Plasmodium</i> transfections.....	34
2.2.2. Protein purification.....	38
2.2.3. Thin layer chromatography for detection of enzyme activity	39
2.2.4. Processing of whole blood.....	39
2.2.5. Revival of parasite stocks	39
2.2.6. Parasite Culture.....	39
2.2.7. Cryopreservation of parasites	40
2.2.8. Synchronization of parasites	40
2.2.9. Enrichment of late stages by density gradient centrifugation on Percoll®	40
2.2.10. Magnetic separation of late stage parasites	41
2.2.11. Saponin lysis of RBCs to obtain free parasites	42
2.2.12. Genomic DNA isolation from <i>P. falciparum</i> parasites.....	42
2.2.13. Parasite transfections	43
2.2.14. Western blot.....	45
<i>Plasmodium berghei</i> protocols	46
2.2.16. Maintenance of <i>Plasmodium berghei</i>	46
2.2.17. Transfection of <i>Plasmodium berghei</i> parasites	47

2.2.18. Genomic DNA isolation.....	48
Chapter 3.....	51
3. Results, Discussion and Future Directions.....	52
3.1. Results.....	52
3.1.1. Generation and Validation of <i>P. falciparum</i> line expressing alternative purine salvage enzyme	52
3.1.2. Attempts of gene(s) disruption in <i>P. falciparum</i> and <i>P. berghei</i>	63
3.1.3. Hadacidin inhibition studies with transgenic parasites, <i>P. falciparum</i> 3D7 ^{yAK}	88
3.2. Discussion.....	97
3.2.1. Persistent essentiality of <i>adss</i> and <i>asl</i> in metabolically rewired parasites.....	97
3.2.2. Future uses of transgenic parasite lines generated.....	101
3.3. Future Directions.....	103
Understanding the structural basis for the hyperthermostability of an archaeal glutaminase induced by post-translational succinimide formation.....	111
Chapter 4.....	112
4. Introduction.....	113
4.1. Mechanisms of protein thermostability.....	113
4.1.1. Primary sequence of proteins and associated intrinsic properties.....	113
4.1.2. Shortening or deletion of loops.....	113
4.1.3. Hydrophobic and aromatic interactions.....	113
4.1.4. Increased occurrence of proline residues.....	114
4.1.5. Increased number of hydrogen bonds, ion pairs and salt bridges.....	114
4.1.6. Post-translational modifications (PTMs).....	114
4.1.7. Counter selection of thermolabile amino acids.....	115
4.1.8. Oligomerization.....	115
4.1.9. Release of conformational strain.....	116
4.2. Deamidation.....	116
4.2.1. Reaction mechanisms of non-enzymatic deamidation.....	118
4.2.2. Factors affecting deamidation in peptides and proteins.....	120
4.3. An account of other non-enzymatic post-translational modifications.....	121
4.3.1. Oxidation.....	122
4.3.2. Lysine Acylation.....	123
4.3.3. Polyphosphorylation.....	124
4.3.4. Succination.....	124
4.3.5. S-cyanylation.....	124
4.3.6. Glycation.....	124
4.4. Functional implications of iso-aspartate formation.....	125
4.5. Stable succinimides in proteins and their functions.....	126
4.6. The influence of a stable succinimide on peptide backbone.....	129

4.7.	Glutamine amidotransferase (GATase).....	129
4.7.1.	Structural features of Glutamine amidotransferases	130
4.8.	Molecular Dynamic Simulation.....	132
Chapter 5.....		137
5.1.	Materials and Methods	138
5.1.1.	Protein purification.....	138
5.1.2.	Crystallization and data collection.....	138
5.1.3.	Structure solution and refinement.....	140
5.2.	Results and Discussion.....	144
5.2.1.	Crystal structure of MjGATase	144
5.2.2.	Structural Implication of a stable succinimidyl residue in MjGATase	151
5.2.3.	Structure of MjGATase_D110G mutant	152
5.2.4.	Interactions stabilizing succinimidyl residue in MjGATase	155
5.2.5.	Stable succinimide formation as an adaptive mechanism of protein thermostability in hyperthermophiles	159
5.2.6.	Molecular Dynamic Simulation	162
5.3.	Future Directions.....	165
5.3.1.	Evolutionary selection of a succinimidyl residue.....	166
5.3.2.	Detection of stable succinimidyl residue in proteins	175
5.3.3.	Can this PTM be engineered to enhance stability and reduce floppiness?	176
5.3.4.	Factors governing succinimide formation in MjGATase	178
Annexure I.....		182
Annexure II		184
Rights and Permissions.....		211
References		223

Investigating the significance of fumarate generated during purine nucleotide cycle (PNC) to the asexual stages of *Plasmodium spp.* parasites

Chapter 1

Introduction

This chapter provides a general introduction about *Plasmodium* species distribution, parasite life cycle and metabolism which will familiarize the reader with the important life cycle stages and different metabolic pathways of the parasite.

1. Introduction

1.1. Brief history of malaria

The word malaria is an amalgamation of medieval Italian words, *mal'aria*; *mal* meaning bad and *aria* meaning air. The disease was thought to be caused by foul air associated with mushy lands and low-lying swamps, hence the name. In 1880, a French army surgeon Charles Louis Alphonse Laveran noticed a parasite in blood of individuals suffering from malaria. Laveran was awarded the Nobel prize in 1907 for his discovery. Camillo Golgi described two forms of the disease; one showing tertian periodicity (fever every other day) and the other with quartan periodicity (fever every third day). The discovery that malaria parasites are transmitted by mosquitoes was made by Ronald Ross, a British officer in the Indian medical services and received the Nobel prize in 1902 his discovery. The names *Plasmodium malariae* and *Plasmodium vivax* were given by Italian physician and zoologist Giovanni Battista Grassi and Raimondo Filetti in 1890, respectively. Giovanni Batista Grassi was also the first one to establish the complete life cycle of *Plasmodium falciparum* and to discover that malaria transmission occurs via female anopheline mosquitoes. An American physician William H. Welch named the more malignant malarial parasite *Plasmodium falciparum*. *Plasmodium ovale* was named by John William Watson Stephens who observed this parasite species in blood of an East African patient whose erythrocytes were oval and had fimbriated edges. He named the species ovale in recognition of oval shape of the infected RBCs. *Plasmodium knowlesi*, the species that causes malaria in long-tailed and pig-tailed macaques has been recently found to cause malaria in humans through zoonotic transfer (Arrow et. al., 2004; Cox 2010).

1.2. The global health burden of malaria

Malaria has been a global health concern for centuries. According to World Malaria Report 2019, published by World Health Organization, an estimated 228 million cases of malaria occurred worldwide in 2018 vis-à-vis 251 million cases that were reported in 2010 (Geneva: World Health Organization 2019). Although malaria mortality rate has declined in 2018 compared to that in 2010, the sheer numbers of deaths caused due to the disease remain alarming. The disease inflicts significant economic burden on the nations and individuals affected by it. The population that is primarily affected by malaria is of young children (under the age of 5) and pregnant women. Majority of these cases occur in sub-Saharan Africa with south-east Asia, Eastern Mediterranean, Western Pacific, and the Americas also being at risk. In 2017, India alone harboured 4% of all the malaria cases worldwide (Geneva: World Health Organization 2019).

1.3. Species distribution of *Plasmodium*

Five species of *Plasmodium* are known to infect human host: *P. falciparum*, *P. vivax*, *P. ovale*, *P. malariae* and occasionally, *P. knowlesi*, a species that usually infects primates. Of these, *P. falciparum* is deadliest of all and is responsible for majority of the deaths worldwide with most prevalence in sub-Saharan Africa. *P. vivax* is the second most significant species and is more prevalent in Southeast Asia and Latin America. The commonly reported malaria cases from India are caused by *P. vivax* and *P. falciparum* with occasional reports of *P. malariae* infections from eastern India (Das et al., 2012). Species distribution of *Plasmodium spp.* with their respective vertebrate host systems and their geographical distributions is shown in Table 1.1.

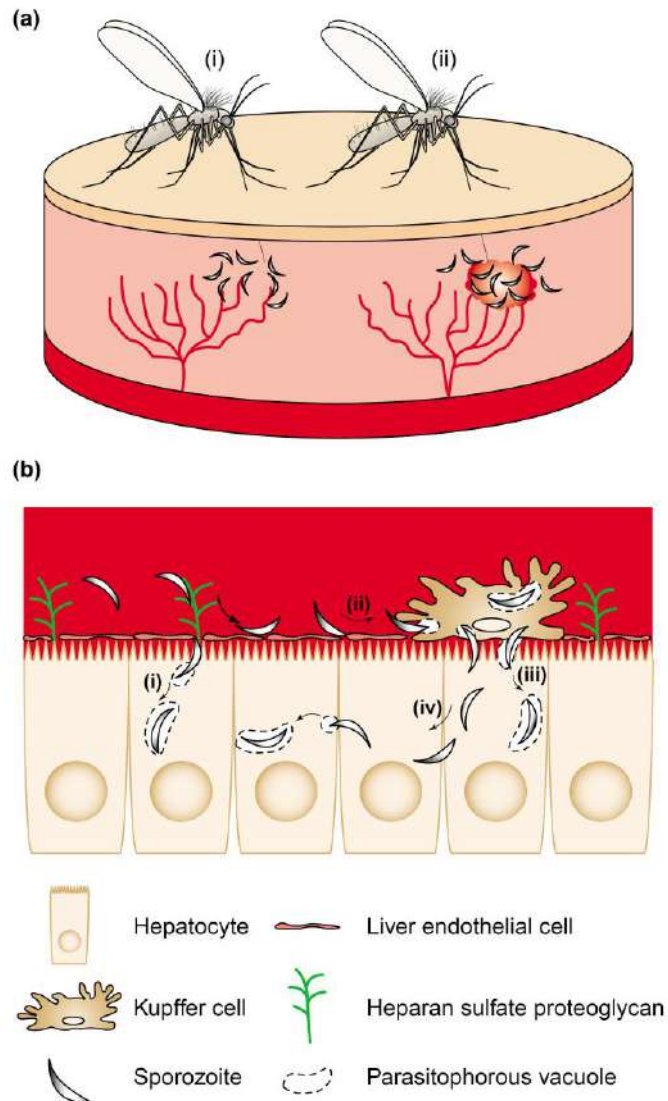
Table 1.1: Species distribution of *Plasmodium* parasites with their respective vertebrate hosts and geographical distribution

Parasite	Host	Geographic Distribution
<i>Plasmodium reichenowi</i>	Chimpanzee	Africa
<i>Plasmodium falciparum</i>	Human	Africa, Asia, South/Central America
<i>Plasmodium fieldi</i>	Macaque	Southeast Asia
<i>Plasmodium simiovale</i>	Macaque	Southeast Asia
<i>Plasmodium hylobati</i>	Macaque	Southeast Asia
<i>Plasmodium inui</i>	Macaque	Southeast Asia
<i>Plasmodium knowlesi</i>	Macaque	Southeast Asia
<i>Plasmodium coatneyi</i>	Macaque	Southeast Asia
<i>Plasmodium simium</i>	Spider Monkey	South America
<i>Plasmodium vivax</i>	Human	Africa, Asia, South/Central America
<i>Plasmodium cynomolgi</i>	Macaque	Southeast Asia
<i>Plasmodium gonderi</i>	Madril	Africa
<i>Plasmodium malariae</i>	Human	Africa, Asia, South/Central America
<i>Plasmodium brasilianum</i>	Spider/Howler/Night Monkey	South America
<i>Plasmodium ovale</i>	Human	Africa
<i>Hepatocystis sp.</i>	Bat/Primate	Africa, Asia
<i>Plasmodium atheruri</i>	Rodent	Africa
<i>Plasmodium vinkei</i>	Rodent	Africa
<i>Plasmodium chabaudi</i>	Rodent	Africa
<i>Plasmodium berghei</i>	Rodent	Africa
<i>Plasmodium yoelii</i>	Rodent	Africa
<i>Plasmodium mexicanum</i>	Lizard	North America
<i>Plasmodium chiricahuae</i>	Lizard	North America
<i>Plasmodium elongatum</i>	Bird	Worldwide
<i>Plasmodium gallinaceum</i>	Bird	Southeast Asia
<i>Plasmodium relictum</i>	Bird	Worldwide
<i>Plasmodium floridense</i>	Lizard	Caribbean/Central America
<i>Plasmodium azurophilum</i>	Lizard	Caribbean/Central America
<i>Plasmodium faichildi</i>	Lizard	Central America
<i>Plasmodium agamae</i>	Lizard	Africa
<i>Plasmodium gigantum</i>	Lizard	Africa
<i>Plasmodium mackerassae</i>	Lizard	Australia

*Table reproduced from TREE OF LIFE web project (<http://tolweb.org/tree/phylogeny.html>) with permission from authors.

1.4. Life cycle of *Plasmodium falciparum*

The complete life cycle of malaria parasites involves two hosts and consists of a sporogonic cycle, an exo-erythrocytic cycle and an (intra) erythrocytic cycle. The asexual stages of the life cycle (exo-erythrocytic and intra-erythrocytic cycles) take place in vertebrate hosts such as humans, rodents, monkeys, birds etc. while the sexual stages (sporogonic cycle) take place in non-vertebrate host, *Anopheles* mosquitos. A malaria-infected, female *Anopheles* mosquito, during a blood meal, inoculates 20-200 sporozoites into vertebrate (humans in case of *P. falciparum*) host skin where they stay for a short time, possibly permeating the epidermis to enter the bloodstream (Fig. 1.1 a) (Kappe et. al., 2003). Sporozoites are highly motile and must *traverse* and *invade* cells (Vaughan and Kappe, 2017). Once sporozoites enter the bloodstream, they are sequestered through the hepatic artery or the portal vein towards the hepatic sinusoids, which are composed of highly perforated endothelial cells and specialized macrophages, the Kupffer cells (Garcia et. al., 2006) (Fig. 1.1 b). Circumsporozoite protein (CSP) or thrombospondin-related anonymous protein (TRAP), which are the most abundant sporozoite surface proteins, might be responsible for mediating retention of sporozoites in the hepatic sinusoid (Ménard et al. 1997). Multiple hypotheses propose how sporozoites could enter the hepatocytes. One hypothesis suggests that sporozoites enter hepatocytes through Kupffer cells. Transmigration through Kupffer cells always occurs through formation of parasitophorous vacuole (PV) around sporozoites. Sporozoites then exit the PV, leaving the Kupffer cell behind, and invade hepatocytes (Kappe et al. 2003) (Fig. 1.1 b) Alternatively, CSP on the sporozoite surface recognizes and binds to highly sulfated heparin sulfate proteoglycans (HSPGs) that protrude through the open fenestration of the endothelium, penetrate through the endothelial cells and invade the hepatocytes to commence the exoerythrocytic cycle (Vaughan and Kappe 2017).



TRENDS in Parasitology

Figure 1.1: Invasion of hepatocytes by sporozoites. (a) Upon entering the bloodstream, sporozoites are sequestered through the hepatic artery or the portal vein towards the hepatic sinusoids. (b) The entry of sporozoites into hepatocytes is hypothesized to occur via two routes. (i) One hypothesis is that sporozoites bind to and enter via heparan sulfate proteoglycans and the other suggests that (ii) they enter through Kupffer cells and the migration is mediated by a parasitophorous vacuole formed around the sporozoite. Image is reproduced from Kappe, Stefan H. I., Karine Kaiser, and Kai Matuschewski. 2003. "The Plasmodium Sporozoite Journey: A Rite of Passage." *Trends in Parasitology* 19(3):135–43 with permission.

The liver stage parasites undergo schizogony, i.e. nuclear division without cell division, during maturation and only in the final phase of this process do invasive exoerythrocytic merozoites form (Vaughan and Kappe, 2017). Mature liver stage schizont contains between 4,200–29,000 merozoites (Baer et al., 2007). These merozoites - which are capable of infecting erythrocytes - recognize, attach and enter the erythrocytes in under 60 sec (Cowman and Crabb, 2006). This short time frame could be because the antigens on the surface of the extracellular form of the parasite are particularly vulnerable to immune attack by the host system. In case of *P. vivax* and *P. ovale*, a dormant form termed

hypnozoites, can also persist in the liver and cause relapses by invading the bloodstream weeks, or even years later (Mikolajczak et al., 2015).

Merozoites utilize apicomplexan invasion organelles such as the apical complex, pellicle and surface coat, to recognize and enter the host erythrocyte. Primary interaction between the polar merozoite and the host erythrocyte is at any point on the surface of merozoite (Fig. 1.2) and the interaction is low-affinity and reversible. Subsequently, the merozoite re-orientates itself to juxtapose with the erythrocyte membrane. A wide variety of proteins (> 50) have been hypothesized to be involved in mediating the interaction between erythrocytes and merozoites (Cowman and Crabb, 2006) (Fig. 1.2). The three well studied, distinct functional classes are: merozoite surface proteins (MSPs), which form a structurally complex coat around the merozoites; *P. falciparum* reticulocyte binding protein (RBP) homologues (PfRHs) and *P. falciparum* erythrocyte binding antigens (PfEBAs) (related to *P. vivax* duffy antigen binding protein). Apical membrane antigen (AMA1) is an essential parasite encoded receptor, the exact function of which is unknown but it is proposed to play a role in merozoite reorientation (Mitchell et al., 2004), rhoptry secretion, erythrocyte binding (Fraser et al., 2001; Kato et al., 2005), and formation of moving junction (Alexander et al., 2005; Lamarque et al., 2011; Wright and Rayner, 2014).

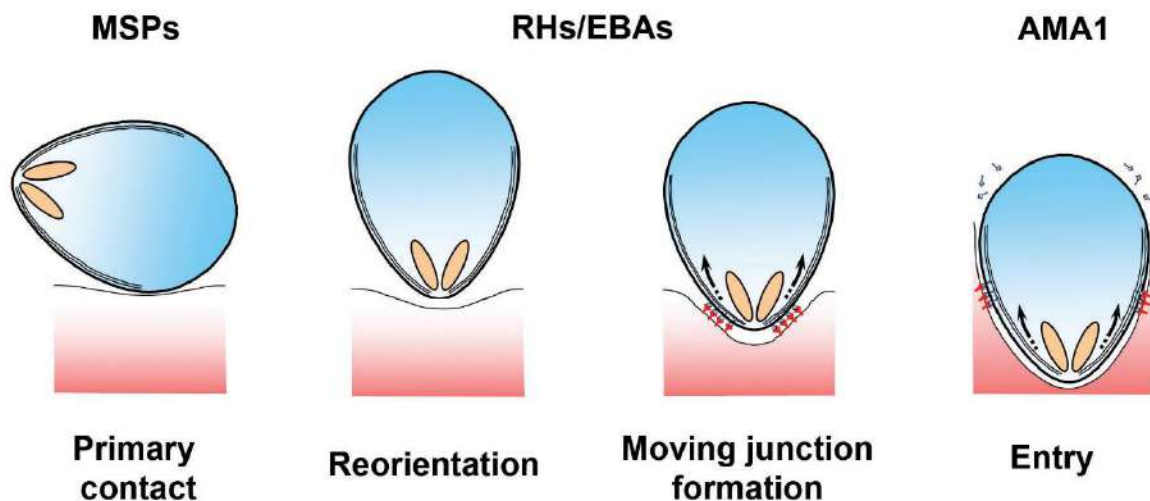


Figure 1.2: Erythrocyte invasion by merozoites. It is a complex, multi-step process. Merozoite randomly attached to RBC surface reorients itself to align the apical complex with RBC membrane. Formation of a moving junction is a crucial process for host cell invasion to occur and AMA1 is an important protein among other proteins found at the MJ. AMA1 and the associated proteins found at the MJ are conserved across Apicomplexan parasites. The figure was reproduced from Wright GJ, Rayner JC (2014) *Plasmodium falciparum* Erythrocyte Invasion: Combining Function with Immune Evasion. PLoS Pathog 10(3): e1003943 under Creative Commons Attribution License (Wright and Rayner, 2014). Abbreviations: MSP, Merozoite surface protein; RH, reticulocyte binding protein homologues; EBAs (erythrocyte binding antigens); AMA1, apical membrane antigen 1.

Within the erythrocytes, the parasites undergo asexual multiplication (intra-erythrocytic schizogony) and develop through ring, trophozoites and schizont stages. The schizonts eventually rupture and merozoites re-infect fresh erythrocytes as the intra-erythrocytic cycle continues. Some merozoites (1-2%) are committed to sexual development, through a process called gametocytogenesis that generates male and female gametocytes, which are ingested by mosquitoes during a blood meal (Fig. 1.3).

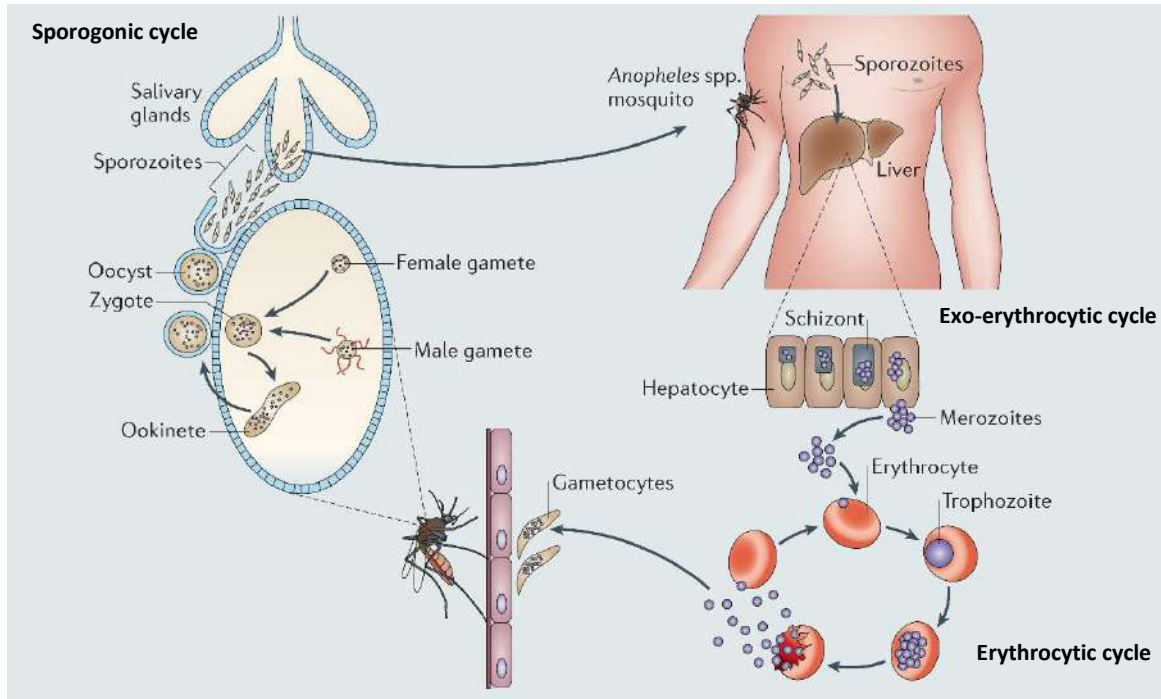


Figure 1.3: Complete life cycle of *Plasmodium falciparum*. The sexual reproduction occurs in the mosquito and is termed as sporogonic cycle. The asexual stages of the life cycle take place in vertebrate host (human) and is divided into exo-erythrocytic and intra-erythrocytic cycle. A small percentage of intra-erythrocytic merozoites differentiate into male and female gametocytes. Erythrocytic cycle is responsible for the clinical manifestation of the disease. Image reproduced from de Koning-Ward, T., Gilson, P. & Crabb, B. Advances in molecular genetic systems in malaria. *Nat Rev Microbiol* 13, 373–387 (2015) with permission.

The ~ 48-hour intra-erythrocytic cycle of *P. falciparum* is responsible for clinical manifestation of malaria in humans.

During these different stages of its complex life cycle, the *Plasmodium* parasite encounters substantially different metabolic environments in mosquito and human hosts. Changes in the surrounding metabolic environments is reflected as changes in metabolic needs and capabilities of the parasite. Whereas temperature inside of human host is 37 °C, the temperature of mosquito midgut is 20 °C (Billker et al., 1997). The metabolic environments encountered by the parasite in the two host systems are also different (Murphy 1998b).

Metabolism of intra-erythrocytic cycle of *P. falciparum* has been extensively studied over the past few decades since these stages are relatively easier to culture in the laboratory and are responsible for the pathology associated with the disease. Understanding of the basic metabolism of the parasite is crucial since development of selective, rational and effective antiparasitic drugs depends on exploiting the metabolic differences of the parasite and its host (Boitz et al., 2013). In the next sections, some major metabolic pathways of the parasite have been discussed.

1.5. Metabolism in *Plasmodium* spp.

Understanding of the parasites' metabolism has grown over last few decades owing to the advancement in genetic and analytical techniques. *Plasmodium* parasites are highly proliferative cells that undergo mitosis to produce 16-24 merozoites (Cobbold and Mcconville, 2014). Therefore, the metabolism of intra-erythrocytic stages of *Plasmodium* seems to have evolved not just to fulfil the energy demand but also to support growth requirements (such as biosynthesis of nucleotides, lipids, and proteins along with the generation of reducing equivalents and energy) of rapidly proliferating cells. Streamlined metabolic networks and capability of supporting anabolic reactions via aerobic fermentative glycolysis and glutaminolysis seem to be the preconditions of being proliferating cells rather than consequences of it (Salcedo-Sora et al. 2014) as seen in cancer cells which are highly proliferative cells. These hallmarks of rapidly proliferating cells are also observed in asexual stage *Plasmodium* parasites and parallels can be drawn between metabolism of cancer cells and *Plasmodium* parasites. Figure 1.4 summarizes the carbon and mitochondrial metabolism of parasites. Some important metabolic pathways are discussed in detail in the following sections.

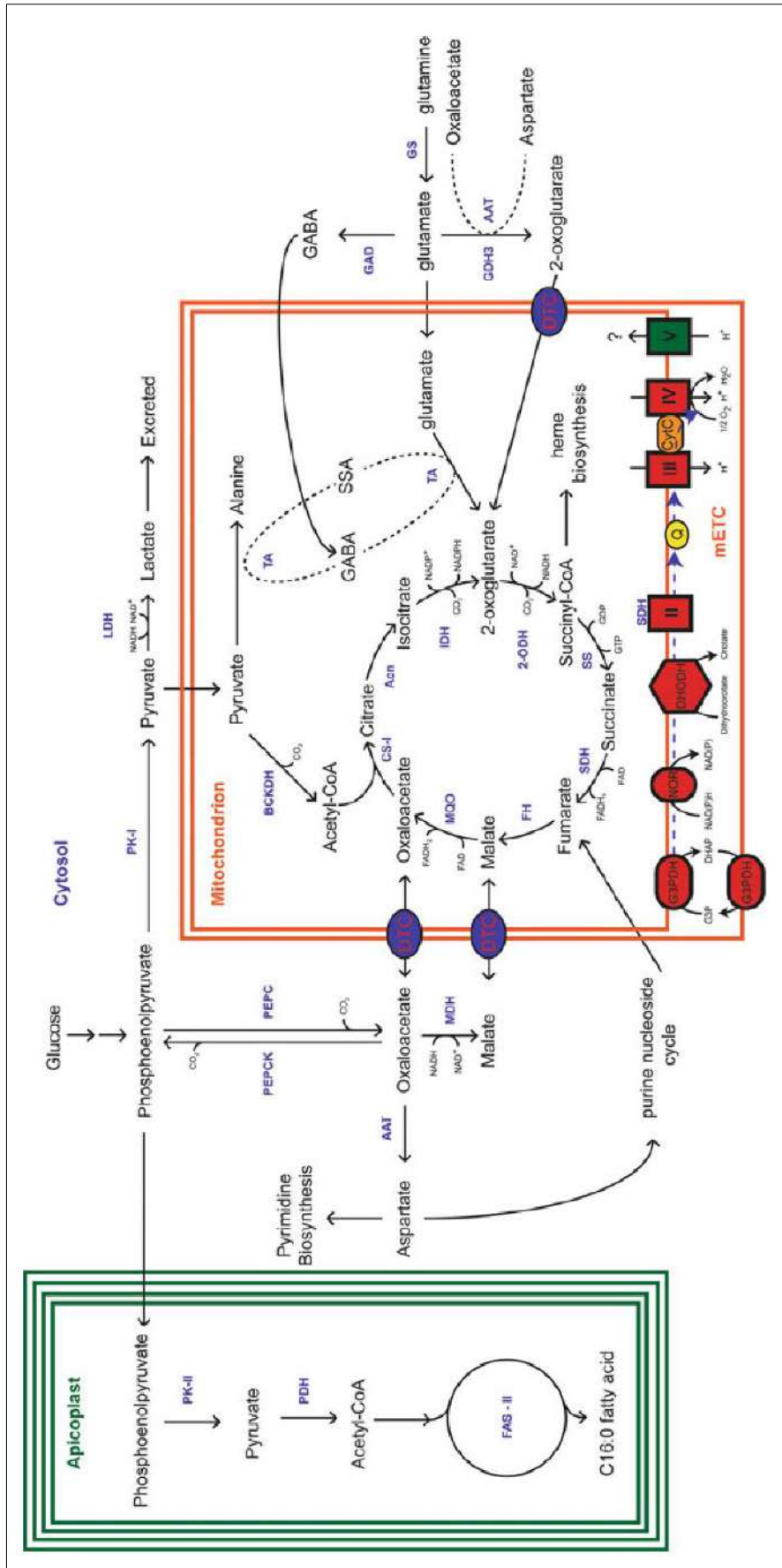


Figure 1.4: Carbon and mitochondrial metabolism of Plasmodium spp. parasites. Major biochemical pathways are schematically represented. Like many other cells, metabolism in Plasmodium parasites is compartmentalized and a variety of transporters are required for transport of metabolites across these different compartments. Image reproduced from Cobbold S.A., McConville M.J. (2014) The Plasmodium Tricarboxylic Acid Cycle and Mitochondrial Metabolism. In: Hommel M., Kremsner P. (eds) Encyclopedia of Malaria. Springer, New York, NY. with permission. Four walled apicoplast is represented in green while double membraned mitochondrion is represented in red.

1.5.1. Glycolysis

Biochemical studies established the dependence of intra-erythrocytic parasites on aerobic fermentative glycolysis for ATP generation, early on (Ali and Fletcher, 1985; Sherman, 1979). The uptake of glucose by infected RBCs is found to be ~75-100 fold higher as compared to uninfected RBCs (Roth, 1990; Sherman, 1979) and more than 80% of the glucose is converted to lactate (MacRae et al., 2013). This process of aerobic fermentative glycolysis generating lactate as the major end product was shown to be the attribute of cancer cells and is termed as Warburg effect (WE) (Warburg, 1956). However, several other non-cancerous cells such as those involved in immunity (effector T cells, activated macrophage/dendritic cells) (Newsholme et al., 1986; Palmer et al., 2015; van der Windt and Pearce, 2012), angiogenesis (endothelial cells) (De Bock et al., 2013) and pluripotency (induced pluripotent stem cells/embryonic stem cells)(Folmes et al., 2011; Kondoh et al., 2007), were also shown to display WE (Fig. 1.5). It is counterintuitive that rapidly proliferating cells prefer energetically inefficient glucose fermentation to lactate (that generates 2 ATP molecules) for ATP generation, rather than energetically much more efficient oxidative phosphorylation (generates 38 ATP molecules). Whether WE is a cause or a consequence of rapid cell proliferation is debatable.

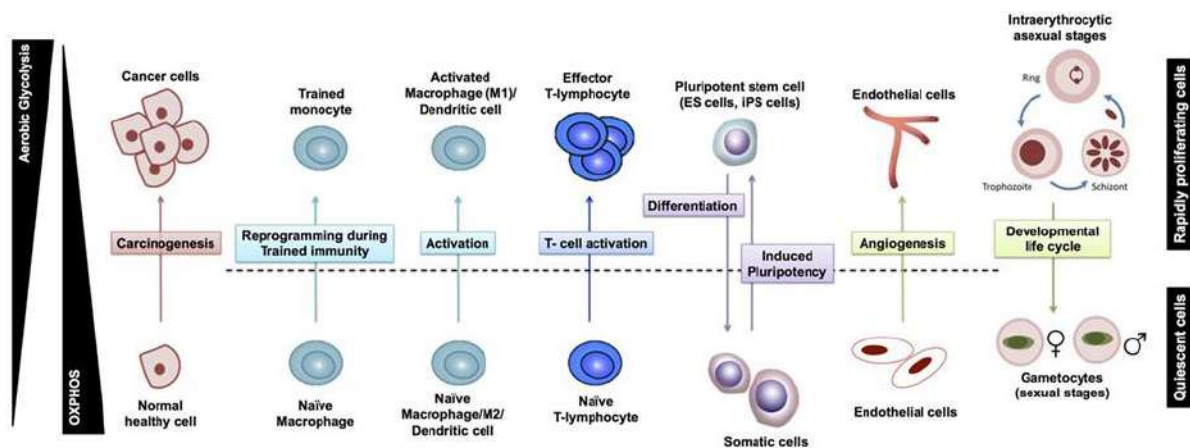


Figure 1.5: Warburg effect seen cancerous and non-cancerous cells. Besides cancer cells, some other rapidly proliferating cells also utilize high amount of glucose and rely on aerobic glycolysis for supply of energy. In the non-proliferating modes of the respective cells, glucose is utilized via oxidative phosphorylation pathway. Therefore, aerobic glycolysis seems to be the hallmark of rapidly dividing cells. Whether it is the switch that induces rapid proliferation or rapid proliferation results in the metabolic switch is yet to be discovered. Image reproduced from Abdel-Haleem AM, Lewis NE, Jamshidi N, Mineta K, Gao X and Gojobori T (2017) The Emerging Facets of Non-Cancerous Warburg Effect. *Front. Endocrinol.* 8:279. doi: 10.3389/fendo.2017.00279 under Creative Commons Attribution License.

For fulfilling increased energy demands during intra-erythrocytic stages, parasites do not depend on the host glycolytic pathway; rather glucose is transported inside the parasite via a high-affinity facilitative hexose transporter, PfHT1 (Krishna et al., 2000; Woodrow et al., 2000). However, mature mammalian erythrocytes lack nucleus and other cellular organelles as well as the pathways for synthesis of nutrients required to support the growth of rapidly dividing intracellular parasites. It was shown that in *P. yoelii* and *P. berghei* infected mouse erythrocytes, glucose is transported into the erythrocytes via a non-saturable diffusion system that appears in the membrane of these erythrocytes post infection

(Tanabe, 1990). In *P. falciparum* infected erythrocytes, the host membrane was shown to become permeable to low molecular mass carbohydrates and amino acids such as glucose and alanine respectively. Membrane permeation was mediated by new permeability pathways and these transporters are non-saturable and are not inhibited by cytochalasin B, a potent inhibitor of carrier protein mediated transport (Tanabe, 1990). From the erythrocytes, glucose is taken up by the parasite via PfHT1 and metabolized via aerobic glycolysis.

Upon entry into the parasite, glucose is acted upon by hexokinase (PfHK) that catalyses phosphorylation of glucose to glucose-6-phosphate. PfHK shares only 26 % sequence identity with human hexokinase 1, making it a promising drug target (Olafsson et. al., 1992). There is a possible hydrophobic membrane anchor sequence present at the C terminus of PfHK, suggesting that the enzyme is present on parasite plasma membrane, which could improve the efficiency of glucose phosphorylation at the site of uptake. The enzyme is expressed maximally during the trophozoite stage (Olafsson and Certa, 1994).

Another important regulatory glycolytic enzyme is 6-phospho-1-fructokinase (PFK) which catalyses fructose-6-phosphate to fructose-1,6-bisphosphate conversion. *P. falciparum* genome contains two genes encoding PFK, one on chromosome 9 (*PfPFK9*) and the other on chromosome 11 (*PfPFK11*). Out of these two, only PfPFK9 possesses all the features essential for PFK activity. The *PfPFK9* gene encodes an ATP dependent phosphofructokinase which consists of two domains, α and β with the latter being catalytically active and uses ATP as a substrate. α domain also exhibits a very small but distinct amount of catalytic activity (Mony et al., 2009). The enzyme displays allosteric properties similar to mammalian enzymes; inhibited by ATP while being activated by fructose-6-phosphate. However, the enzyme exhibits different allosteric regulation. Phosphoenolpyruvate, the penultimate intermediate of glycolytic pathway, which also acts as an inhibitor of mammalian PFKs, is found to be an activator of plasmodial enzyme. On the other hand, ADP was found to inhibit PfPFK (Buckwitz et. al., 1990). Activation rather than inhibition by PEP of plasmodial PFK could be an adaptation to support enhanced glycolytic activity.

Third reaction that is considered rate limiting in glycolysis is the conversion of phosphoenolpyruvate to pyruvate catalysed by pyruvate kinase. *P. falciparum* genome codes two non-identical isoforms of pyruvate kinase, PfPK type I and type II, of which PfPKI is localized to cytosol while PfPKII is an apicoplast-targeted enzyme. Both the isoforms are expressed during intra-erythrocytic stage (Chan et. al., 2007; Oelshlegel et. al., 1975). While cytosolic PfPKI is involved in glycolysis, apicoplast localized PfPKII might be involved in lipid metabolism. PfPKI is unaffected by fructose-1,6-bisphosphate, a general activator of pyruvate kinases. However, the enzyme is inhibited by ATP and citrate (Chan and Sim, 2004). Analysis of apicomplexan genomes reveals that PKII is confined to all Apicomplexans and carries an apicoplast targeting signal sequence (Chan et. al., 2007).

Higher quantities of ATP, NAD⁺ and inorganic phosphates are required to sustain higher glycolytic flux. The need for regeneration of NAD⁺ could be fulfilled during the reduction of pyruvate to lactate via lactate dehydrogenase (PfLDH) that concomitantly also catalyses oxidation of NADH to NAD⁺ and is therefore undoubtedly essential for parasite survival. PfLDH has an enlarged active site as compared to its mammalian counterpart indicating differences between the host and the parasite enzymes which can be exploited for selective drug design (Dunn et al., 1996). The enzyme is prone to substrate inhibition at high concentration of pyruvate; however, the magnitude of inhibition is small (Shoemark et al., 2007), suggesting an adaptation of the enzyme to support high glycolytic flux. Regeneration of NAD⁺ by LDH reaction thus circumvents the reliance on mitochondrial NADH utilizing reactions. Not many studies have been performed on the utilization of inorganic phosphate by *Plasmodium* parasites. In one of the few studies performed by K Nagarajan, he demonstrated that free *P. berghei* parasites incorporate P³² labelled inorganic phosphate (in high energy phosphate bonds of ATP) upto 18 μM, after which the percentage incorporation does not increase. Under similar experimental conditions, uninfected reticulocytes did not incorporate P³² (Natarajan, 1968). Although this study does suggest higher requirement of inorganic phosphates by *Plasmodium* parasites, lack of any further studies makes it difficult to comment on involvement of inorganic phosphate in regulation of glycolytic flux. A small proportion of pyruvate generated from glycolysis is funnelled into tricarboxylic acid (TCA) cycle through its conversion to acetyl-CoA, catalysed by mitochondrial branched chain ketoacid dehydrogenase (BCKDH) (Oppenheim et al., 2014), rather than pyruvate dehydrogenase (PDH) complex. The TCA cycle metabolism in *Plasmodium* parasites and its regulation are discussed in the next section.

1.5.2. TCA cycle

Complete oxidation of glucose involves its ultimate conversion to CO₂; beginning with glycolysis in cytosol followed by Kerbs' cycle/tricarboxylic acid cycle in mitochondria. TCA metabolism, that occurs in the mitochondrial matrix is fundamental to all eukaryotic cells as it is the major source of generation of energy-containing compounds such as NADH, FADH₂, GTP and is also a connecting link between carbohydrate, lipid and protein metabolism - through acetyl-CoA. Given the aerobic fermentative glycolysis exhibited by *Plasmodium* parasites, it was previously believed that the singular mitochondrion of parasites might be redundant for asexual stages of the parasite life cycle and that the parasite lacks a functional TCA cycle. However, susceptibility of parasites to mitochondrial cytochrome bc₁ (complex III) inhibitor, atovaquone, established essentiality of this organelle (Fry and Pudney, 1992; Srivastava et al., 1997). Experiments with exogenously added labelled fumarate (2,3-¹³C) by Bulusu and co-workers (Bulusu et al., 2011) revealed labelled TCA cycle intermediates, confirming the operation of a functional TCA cycle in *Plasmodium spp.* parasites, which was later confirmed by mass spectrometry-based metabolomics experiments using ¹³C-glucose by MacRae and co-workers (MacRae et al. 2013). In the absence of a mitochondrial PDH complex in Apicomplexans, glycolysis derived pyruvate is converted to acetyl-CoA through BCKDH enzyme complex in these organisms (Cobbold et al., 2013; Oppenheim et al., 2014). Although deletion of BCKDH in *P. berghei*

was non-lethal; it led to striking reduction in growth rate of asexual stages - in normocytes but not in reticulocytes - and severely impaired virulence of sexual stages in mice (Oppenheim et al., 2014). The differential growth of *P. berghei* BCKDH mutants in erythrocytes and reticulocytes can be attributed to the differences in metabolism between the two. The metabolome of reticulocytes is much more complex as compared to that of erythrocytes, which supports the growth of metabolically compromised parasites (Srivastava et al. 2015).

A comprehensive reverse genetic analysis of TCA cycle enzymes by Ke and co-workers revealed that six out of the eight TCA cycle enzymes could be knocked out in intra-erythrocytic stages of *P. falciparum* parasites with gene deletion mutants exhibiting similar growth phenotypes as that of the wild type parasites. Fumarate hydratase (FH) which catalyses conversion of fumarate to malate and malate:quinone oxidoreductase (MQO) that subsequently converts malate to oxaloacetate were the only two genes that could not be deleted despite use of different approaches (Ke et al., 2015) depicting the essentiality of these two enzymes. The study also ascertained that the TCA cycle displays metabolic plasticity in that it is majorly fuelled by glutamine rather than glucose during the intra-erythrocytic stages (Fig. 1.6 a) but can switch to glucose derived carbon flux, which could be an adaptation to the complex life cycle of *Plasmodium* parasite, during which it encounters strikingly different host metabolic environments. This was demonstrated by increased flux of glucose derived carbon in parasites lacking α -ketoglutarate dehydrogenase ($\Delta kd h$) that cannot funnel glutamine into the cycle (Fig. 1.6 b). In $\Delta kd h$ mutants, the flux of glucose through TCA cycle was found to be higher indicating metabolic rewiring. The essentiality of FH is attributed to its role in purine salvage pathway for regeneration of aspartate required to ensure continued functionality of purine nucleotide cycle (Jayaraman et al. 2018) whereas MQO is interpreted to have a non-enzymatic structural function in mitochondrial biogenesis; although, this hypothesis lacks experimental evidence. (Ke et al., 2015). The study also concluded that function of TCA cycle is dispensable during certain stages of sexual cycle as well but is absolutely essential for parasite transmission.

However, a different study by Niikura and co-workers demonstrated that genetic disruption of both FH and MQO is possible in *P. berghei* parasites. *P. berghei* $\Delta m q o$ parasites were more fitness compromised compared to *P. berghei* $\Delta f h$ parasites and were unable to establish experimental cerebral malaria in mice but could not cause any obvious changes in mitochondrial membrane potential as assessed by MitoTracker® (Niikura et al. 2017).

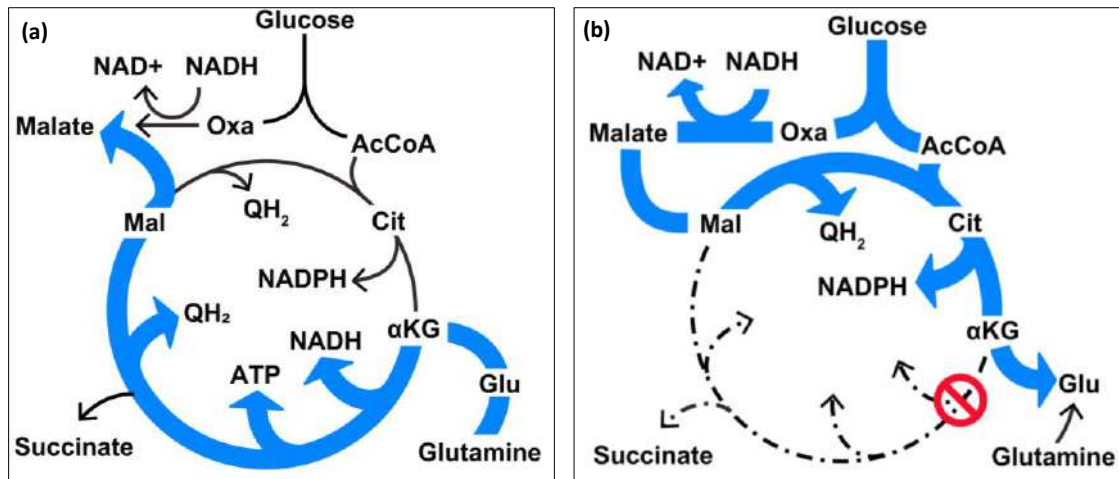


Figure 1.6: Regulation of TCA cycle in *P. falciparum*. Schematic representation of TCA cycle of *P. falciparum* reproduced from Ke H, Lewis IA, Morrisey JM, et al. Genetic investigation of tricarboxylic acid metabolism during the *Plasmodium falciparum* life cycle. *Cell Rep.* 2015;11(1):164–174. doi: 10.1016/j.celrep.2015.03.011 under Creative Commons Attribution-NonCommercial-No Derivatives License. (a) Glutamine is the preferred carbon source that drives TCA cycle in wild type *P. falciparum* parasites. (b) However, if glutamine utilization is hampered due to disruption of α -ketoglutarate dehydrogenase (Δ kdh), glucose derived carbon flux through TCA is increased. Abbreviations: QH₂, Ubiquinol; AcCoA, acetyl Coenzyme A; Mal, malate; Oxa, oxaloacetate; Cit, citrate; α KG, α ketoglutarate; Glu, glutamate.

A variety of catabolic pathways converge on citric acid cycle, channelling intermediates into the cycle thereby contributing anaplerotically. Glutamine, oxaloacetate and fumarate are major anaplerotic contributors to the TCA cycle.

Glutamine drives the TCA cycle in *Plasmodium* parasites during asexual stage, as noted earlier (Fig. 1.6 a). Glutamate synthetase (GS) converts glutamine to glutamate, that is subsequently converted to α -ketoglutarate in a reaction catalysed by glutamate dehydrogenase (GDH). α -ketoglutarate enters mitochondria presumably via α -ketoglutarate/malate transporter (Ke, H et al. 2015) and is metabolized further through TCA cycle.

Glycolytically generated PEP was shown to be converted to oxaloacetate (OAA) via the CO₂ fixing enzyme, phosphoenolpyruvate carboxylase (PEPC) (Storm et al., 2014). Deletion of *pepc* gene was found to be lethal and viable knock out parasites could only be obtained in media supplemented with malate or fumarate suggesting that PEPC mediates important metabolic function by operating the mitochondrial malate shuttle. OAA generated by PEPC reaction in the parasite cytosol is converted to malate via cytosolic malate dehydrogenase (MDH), which concomitantly oxidises NADH to NAD⁺. Malate can then enter mitochondria via the α -ketoglutarate/malate transporter. Inside the mitochondrial matrix, malate can either be acted upon by MQO, producing OAA or by FH (in a reverse reaction) and be converted to fumarate (Fig. 1.7). MQO reaction regenerates ubiquinol that functions in mitochondrial electron transport chain (mETC) and is therefore important for parasite survival (Hartuti et al., 2018). In the context of mitochondrial malate shuttle, PEPC mediated anaplerosis of malate into the TCA cycle appears to be essential (Storm et al., 2014).

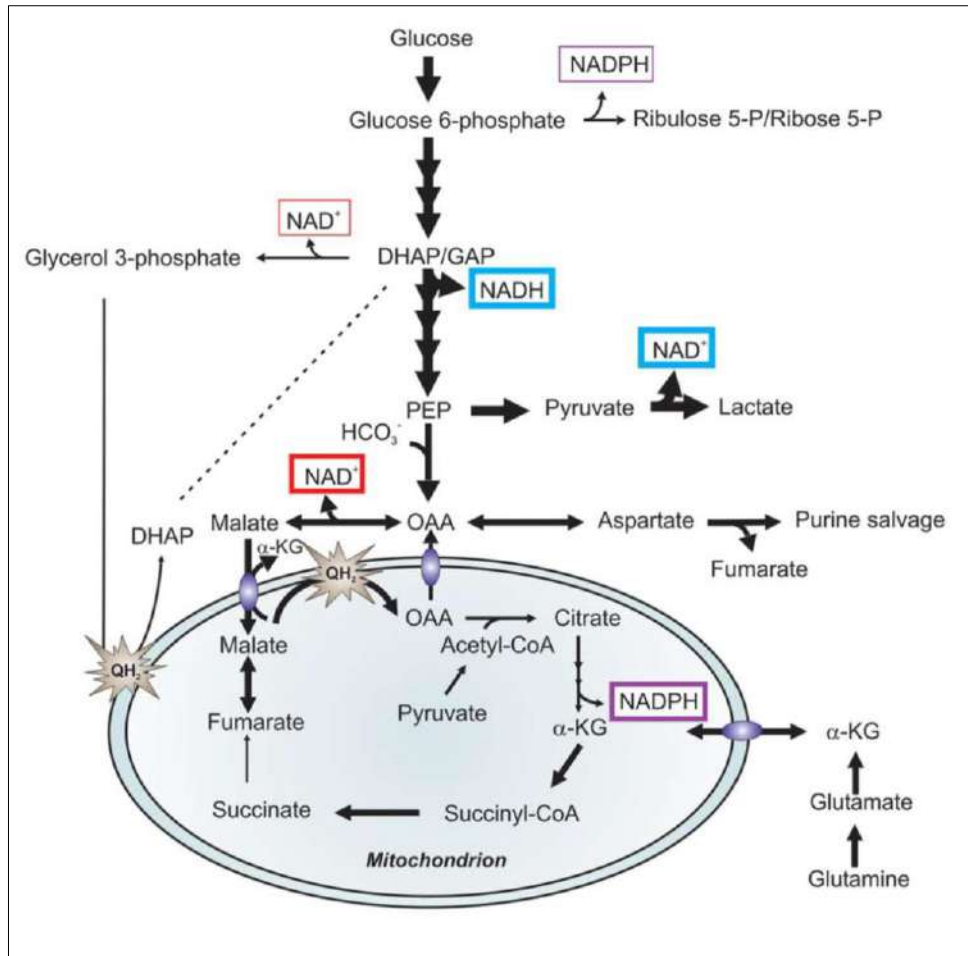


Figure 1.7: PEPC mediated anaplerosis in TCA cycle. Phosphoenolpyruvate carboxylase catalyses conversion of phosphoenolpyruvate to oxaloacetate in cytosol. Oxaloacetate cannot be transported across the mitochondrial matrix, rather it is converted to malate via cytosolic malate dehydrogenase. The malate thus generated can be transported across mitochondrial membrane into the matrix of mitochondria where it is converted back to OAA or in a reverse reaction of fumarate hydratase, converted to fumarate. The schematic representation depicts contribution of PEPC to the overall metabolism of Plasmodium parasites. Image reproduced from Storm, Janet, Sonal Sethia, Gavin J. Blackburn, Achuthanunni Chokkathukalam, David G. Watson, Rainer Breitling, Graham H. Coombs, Sylke Müller, 2014. "Phosphoenolpyruvate Carboxylase Identified as a Key Enzyme in Erythrocytic Plasmodium Falciparum Carbon Metabolism." *PLoS Pathogens* 10(1) under the Creative Commons Attribution License. Abbreviations: DHAP, dihydroxyacetone phosphate; GAP, glyceraldehyde 3-phosphate; OAA, Oxaloacetate.

Another metabolite that is a TCA cycle intermediate and is generated in cytosol through a different pathway is fumarate. Fumarate is generated as a by-product of adenylosuccinate lyase (ASL) reaction of purine salvage pathway (Bulusu et al., 2009). The sole fumarate utilizing enzyme in *Plasmodium* parasites is fumarate hydratase and is localized to the mitochondria (Jayaraman et al., 2018). The transporter that transports fumarate from cytosol to mitochondria is yet uncharacterised; however, experiments using ^{14}C labelled fumarate showed labelling of malate, aspartate, pyruvate and lactate attesting that fumarate is indeed transported to mitochondria (Bulusu et al., 2011) and is metabolized through FH and MQO reactions of the TCA cycle, in turn connecting nucleotide metabolism to energy metabolism in parasites.

1.5.3. Electron transport chain

Mitochondrial ETC (mETC) in parasites of genus *Plasmodium* mainly consists of three enzyme complexes which maintain the mitochondrial potential: complex II (Succinate: ubiquinone oxidoreductase), III (cytochrome *bc₁* complex) and IV (cytochrome c oxidase). Additionally, *Plasmodium spp.* parasites express several dehydrogenases such as a non-essential, type II NAD(P)H oxidoreductase that acts as an alternate complex I (Ke et al., 2019), an essential dihydroorotate dehydrogenase (DHODH), two isoforms of glycerol-3-phosphate dehydrogenase (G3PDH) of which one is cytosolic/NAD⁺ linked and essential (PF3D7_1216200) while the other is localised to mitochondria/FAD⁺ linked and is dispensable (PF3D7_0306400) (Van Dooren, Stimmler, and McFadden 2006). Finally, a prokaryotic-like malate: quinone oxidoreductase, that is essential in *P. falciparum* but could be deleted in *P. berghei* parasites. All of the five dehydrogenases reduce ubiquinone (Q) to ubiquinol (QH₂). Ubiquinol, in turn, donates electrons to complex III thereby driving the electron transport chain (Painter et al., 2007). The predominant function of mETC during asexual stages is not ATP generation; rather mETC furnishes electrons which drive the membrane bound proton pumps thereby maintaining mitochondrial membrane potential. Moreover, mETC also appears to be critical for regeneration of ubiquinol essential for the functioning of DHODH, an enzyme involved in *de novo* pyrimidine biosynthesis. Expression of a fumarate-utilizing, ubiquinol-independent DHODH - *Saccharomyces cerevisiae* DHODH - in *P. falciparum* renders the parasites resistant to mETC inhibitor, atovaquone, suggesting the key function of mitochondria in regeneration of ubiquinol for pyrimidine biosynthesis (Painter et al., 2007).

Recent findings by Sullivan and co-workers delineated the role of mitochondrial respiration in proliferative metabolism i.e. metabolism in rapidly dividing cells, which revealed that mETC is essential for aspartate biosynthesis in rapidly proliferating cells (Sullivan et al., 2015). Aspartate is derived from glutamine that is converted to α -ketoglutarate via glutamate synthase (GS) and glutamate dehydrogenase reactions (GDH) (Glutamine \rightarrow glutamate \rightarrow α -ketoglutarate \rightarrow oxaloacetate \rightarrow aspartate). α -KG is subsequently converted to OAA via oxidative TCA cycle metabolism. OAA gets converted to aspartate via a transamination reaction involving glutamate and catalysed by aspartate aminotransferase (AAT). GDH is a NAD(P)⁺ dependent enzyme and the NAD(P)⁺ required for the reaction is thought to be regenerated via mETC. The study demonstrated that aspartate addition rescued the growth of proliferating cells treated with respiration inhibitors rotenone, antimycin, and oligomycin (which also inhibits re-oxidation of NAD(P)H due to insufficiency of electron acceptor) (Sullivan et al. 2015). Aspartate is required for synthesis of DNA/RNA/proteins – biomolecules required in greater amounts by proliferating cells, suggesting an anabolic role for respiration in these cells. Although asexual stage *Plasmodium* parasites can obtain aspartate from haemoglobin degradation, it could still be insufficient to fulfil parasites' metabolic requirements and aspartate generated through mitochondrial respiration could be needed in the parasites. However, this hypothesis needs experimental evidence in *Plasmodium*.

1.5.4. Nucleotide metabolism

Purine and pyrimidine nucleotides are the building blocks of DNA and RNA in addition to being part of the structure of some of the coenzymes like NAD, Coenzyme A and are indispensable for survival and proliferation of all cell types. Asexual stages of *Plasmodium* parasites, being rapidly proliferating cells, require high amounts of these building blocks. Nucleotides can either be synthesized *de novo* or can be salvaged from preformed nucleobases/ nucleosides. *Plasmodium* parasites salvage preformed purine nucleobases from the erythrocytes whereas pyrimidines are synthesized via *de novo* pathway (Gutteridge and Trigg, 1970; Walsh and Sherman, 1968). As mentioned earlier, parasite metabolism appears to have adapted to differing metabolic requirements in different hosts. Mature human erythrocytes contain abundant amounts of purines but the concentration of pyrimidines is limited (Cassera et al., 2011), therefore through the course of evolution, parasite might have retained the *de novo* pathway of pyrimidine synthesis in order to complement the host metabolism.

1.5.4.1. *de novo* pyrimidine biosynthesis in *Plasmodium*

Long before genome analysis of *P. falciparum* revealed presence of all 6 genes coding for enzymes of the *de novo* pyrimidine synthesis pathway (Gardner et al., 2002), the activities of most of these enzymes were studied and reported in different parasite species (Gero et. al., 1984; Krungkrai et. al., 1990; O' Sullivan et. al., 1980; Rathod and Rieckmann, 1982). The *de novo* pyrimidine biosynthetic pathway begins with carbamoyl phosphate and aspartic acid and follows essentially the same steps in all organisms from prokaryotes to eukaryotes including humans. Carbamoylaspartate dehydrates to form the pyrimidine ring structure which is eventually converted to uridine 5' monophosphate (UMP), the nodal intermediate for cytosine 5' monophosphate (CMP) and thymidine 5' monophosphate (TMP) generation (Fig. 1.8)

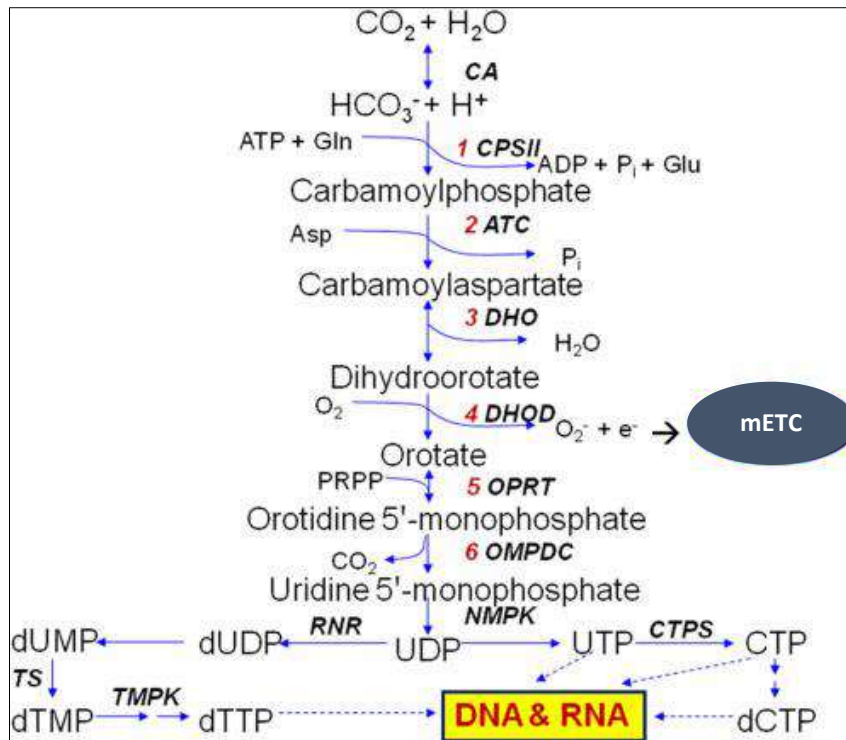


Figure 1.8: De novo pyrimidine synthesis pathway in *Plasmodium* parasites. Image is reproduced from Insights into the pyrimidine biosynthetic pathway of human malaria parasite *Plasmodium falciparum* as chemotherapeutic target, Sudaratana R. Krungkrai, Jerapan Krungkrai, Asian Pacific Journal of Tropical Medicine, June 2016 under a creative commons license. Abbreviations: CA, carbonic anhydrase; CPSII, carbamoyl phosphate synthase II; ATC, aspartic transcarbamoylase; DHO, dihydroorotase; DHOD/DHODH, dihydroorotate dehydrogenase; OPRT, orotate phosphoribosyltransferase; OMPDC, OMP decarboxylase; NMPK, nucleoside monophosphate kinase; RNR, ribonucleotide reductase; CTPS, CTP synthase; TMPK, TMP kinase; TS, thymidylate synthetase.

DHODH that catalyses conversion of dihydroorotate to orotate requires coenzyme Q that is regenerated in the mitochondria via the mETC and as noted in the earlier section, the function of mETC in *Plasmodium* is to sustain continued pyrimidine synthesis during the intra-erythrocytic stages. Inhibitors of mETC are therefore thought to act by inhibiting pyrimidine synthesis in *Plasmodium* parasites. mETC inhibitors inhibit growth of asexual stages and early sexual stages (gametocytes) but not late-stage gametocytes, suggesting that *de novo* pyrimidine biosynthesis is not essential for late-stage gametocytes and that (Murphy, 1998a) the pool of preformed pyrimidine nucleotides are sufficient for further maturation process of gametocytes (Fleck et al., 1996; Talman et al., 2004).

1.5.4.2. Purine salvage pathway in *Plasmodium*

Compared to pyrimidines, purines concentrations in plasma are higher (Slowiaczek and Tattersall, 1982) from where, they are imported in the erythrocytes and in turn are taken up by parasites. Due to these high concentrations of purines present in host cells, *Plasmodium* parasites could have retained the more energy efficient salvage pathway for purines rather than energetically expensive *de novo* pathway. Purine salvage pathway from *Plasmodium* parasites has been more extensively studied as the enzymes of the pathway differ considerably from the host enzymes making this pathway an attractive drug target,

which is confirmed by inhibition of parasite growth in *in vitro* cultures upon addition of mycophenolic acid, an inhibitor of enzyme IMPDH ($IC_{50} = 5.4 \mu\text{M}$) (Hedstrom 2009; Veletzky et al. 2014). Hypoxanthine and adenosine are predominantly salvaged from RBCs by the parasite via PfNT1 transporter. Adenosine cannot be directly converted to AMP as *Plasmodium* parasites lack adenosine kinase enzyme; rather it is sequentially converted to inosine and hypoxanthine by adenosine deaminase (ADA) and purine nucleotide phosphorylase (PNP) respectively. Hypoxanthine is phosphorylated to inosine 5' monophosphate (IMP), that is a nodal intermediate from which both adenosine 5' monophosphate (AMP) and guanosine 5' monophosphate (GMP) are synthesized (Fig. 1.9). AMP can be deaminated and converted to IMP by AMP deaminase enzyme, which constitutes a purine nucleotide cycle. A detailed account of purine-import and salvage in *Plasmodium* parasites is represented in Figure 3.2 discussed in chapter 3.

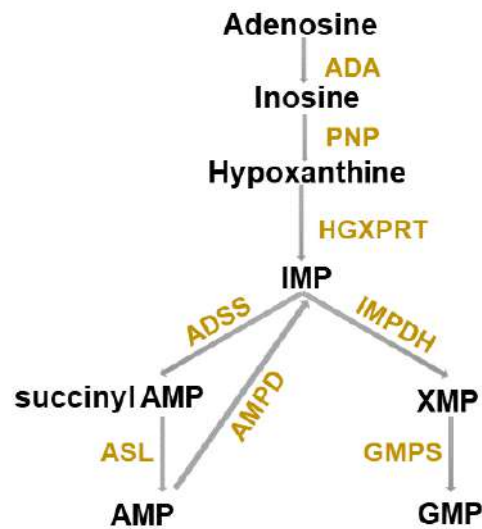


Figure 1.9: Reactions of purine salvage and biosynthesis pathways in *Plasmodium*. Adenosine and hypoxanthine are salvaged from host cells. Adenosine is converted to hypoxanthine and which then enters the purine synthesis pathway. The steps of purine synthesis pathway have been shown. Enzymes are coloured in brown and intermediates in black. Abbreviations: HGXPRT, hypoxanthine guanine xanthine phosphoribosyl transferase; AMPD, AMP deaminase; ADA, adenosine deaminase; PNP, purine nucleoside phosphorylase; ADSS, adenylosuccinate synthetase; ASL, adenylosuccinate lyase; IMPDH, IMP dehydrogenase; GMPS, GMP synthase.

1.5.4.3. Purine nucleotide cycle (PNC)

As mentioned earlier, conversion of IMP to AMP and deamination of AMP back to IMP is known as purine nucleotide cycle (Fig. 1.9, 1.10). The net reaction of the cycle is



It was shown by Argon and Lowenstein that in exercising skeletal muscles, PNC is responsible for fuelling TCA cycle through generation of fumarate. Increased TCA flux could be utilized to generate more ATP for the exercising muscles (Aragón and Lowenstein, 1980). Moreover, PNC generated ammonia was speculated to be utilized for the synthesis of glutamine in exercising muscles. Glutamine

is transported from muscles to the kidneys where it is used to neutralize acidity of urine via deamination of glutamine (Arinze, 2005). Disruption of PNC in muscle cells leads to alterations of ATP content of the muscles, thereby causing muscle dysfunction (Sabina et al., 1980). Other than exercising skeletal muscles, PNC is also known to occur in liver and kidneys (Bogusky et al., 1976; Moss and McGivan, 1975; Tornheim et al., 1986), however, the function of PNC in these organs is uncharacterized.

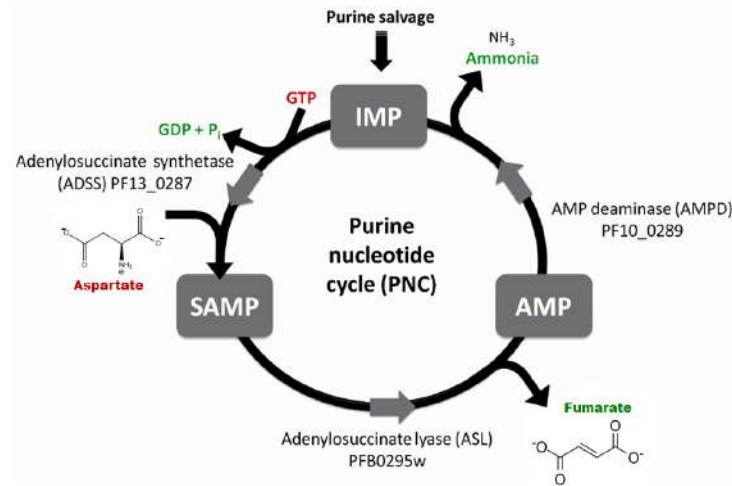
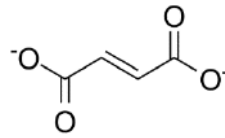


Figure 1.10: Purine nucleotide cycle. The cyclic pathway begins with formation of succinylAMP from IMP by addition of aspartate via adenylosuccinate synthetase (ADSS) reaction which also dephosphorylates a molecule of GTP. The aspartate nitrogen is transferred to IMP while the carbon backbone leaves as fumarate during the next reaction catalysed by adenylosuccinate lyase (ASL). AMP is acted upon by AMPD which deaminates AMP and converts it back to IMP. The substrates of the reaction are shown in red while the products are shown in green. Figure reproduced from (with slight modifications) Jayaraman, V., Bulusu, V., & Balaram, H. (2012). Crosstalk between purine nucleotide metabolism and mitochondrial pathways in *Plasmodium falciparum*. *Current Science*, 102(5), 757 with permission.

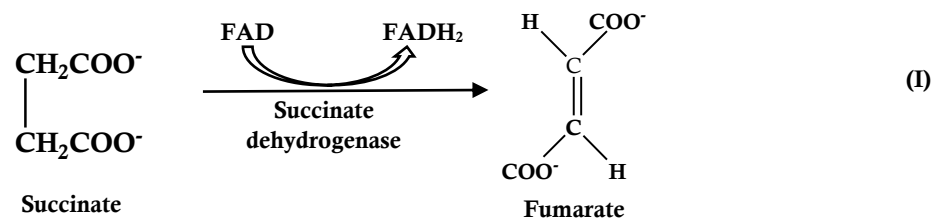
In *Plasmodium* parasites, although the presence of AMPD suggests operation of a functional PNC, recent study from our laboratory demonstrated that AMPD is dispensable during all stages of parasite's life cycle (Nagappa et al., 2019). Overexpression of AMPD was lethal suggesting that drain of AMP through AMPD reaction is not tolerated in *Plasmodium*.

The fate of fumarate generated from PNC in *Plasmodium* parasites is as yet not fully apprehended. The plausible roles of fumarate generated through PNC in *Plasmodium* are discussed in the following section.

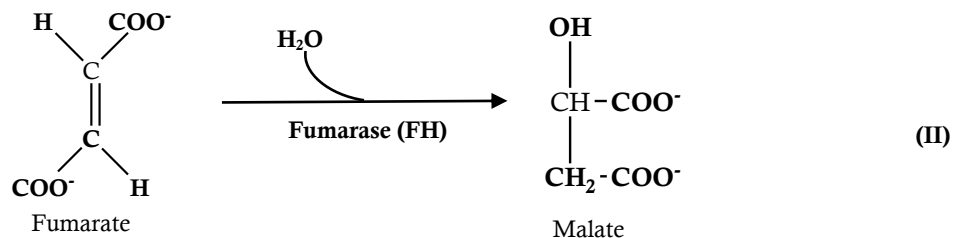
1.6. Fumarate: Metabolic and Non-metabolic roles



Fumarate is a moderately reactive α , β -unsaturated electrophilic metabolite that is an intermediate of the TCA cycle, generated by oxidation of succinate in a reaction catalysed by succinate dehydrogenase (I). Fumarate is also generated as a by-product during urea cycle, purine nucleotide cycle as well as a by-product of degradation of glucogenic amino acids (Frezza 2017).



Fumarate is metabolised through TCA cycle via the reaction catalysed by fumarate hydratase (FH) (II). FH adds a molecule of water converting the C-C double bond of fumarate into a C-C single bond of malate.



Mammalian cells possess two isoforms of FH: a mitochondrial isoform and a cytosolic one (Yogev et al., 2011). Whereas the mitochondrial FH is involved in TCA metabolism, the function of cytosolic FH appears to be conversion of fumarate generated in cytosol to malate as the latter can be transported to mitochondria. Thus far, transporters that can transport fumarate from cytosol to mitochondria have not been characterized. *Plasmodium* parasites contain only one isoform of FH which is localized to parasite mitochondria (Jayaraman et al. 2018); hence, transport of fumarate to mitochondria is a prerequisite.

Fumarate can react with the thiol group of cysteine residues in proteins via Michael addition reaction and covalently modify the cysteine to S-(2-succinyl) cysteine (2SC) (Fig. 1.11). This post-translational modification (PTM) is termed *succination* and it is non-enzymatic and irreversible (Alderson et al. 2006). *Succination* is different from *succinylation*, the latter is an enzymatic PTM that leads to the formation of amide, ester, or thioester bonds. Succination preferentially occurs at cysteine residues with low pKa

values (~3-4), such as cysteines located in active site pockets. Succination occurs exclusively at cysteines and the cysteine-fumarate adduct (2SC) is the first known PTM of protein caused by an intermediate of TCA cycle (Alderson et al. 2006). The functional consequence of this PTM includes loss of function of the succinated protein. This suggests a plausible role for fumarate in the regulation of cell metabolism and homeostasis. Succination is not a PTM confined to proteins of specific biological processes and hence accumulation of fumarate can impact a wide range of cellular processes such as redox homeostasis (Zheng et al. 2015), metabolic disorder such as diabetes (Blatnik, Thorpe, and Baynes 2008; Harmel and Fiedler 2018), cytoskeleton organization (Piroli et al. 2014), signalling pathways and tumorigenesis (Kulkarni et al. 2019; Menko et al. 2014; Y. Yang et al. 2012).

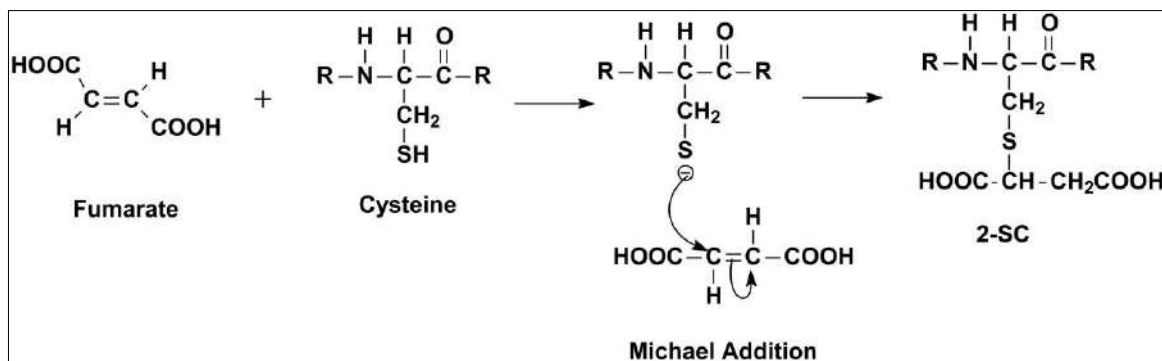


Figure 1.11: Reaction mechanism of cysteine succination. The α , β unsaturated electrophile reacts with the free thiol group of a cysteine residue in a Michael addition reaction, modifying cysteine to S-(2-Succinyl)-Cysteine (2SC). Figure reproduced from Inactivation of Glyceraldehyde-3-Phosphate Dehydrogenase by Fumarate in Diabetes; Matthew Blatnik, Norma Frizzell, Suzanne R. Thorpe, John W. Baynes; Diabetes Jan 2008, 57 (1) 41-49; DOI: 10.2337/db07-0838 with permission.

Research has long ago unravelled link between cellular metabolism and cancer/oncogenesis since the observation of Warburg effect (Warburg, 1956) in cancer/tumour cells - a metabolic dysfunction considered as a hallmark of cancer cells. Similarly, metabolic dysregulation resulting in accumulation of fumarate has been shown to be an attribute of renal cell cancer (Kulkarni et al., 2019; Menko et al., 2014; M. Yang et al., 2012; Y. Yang et al., 2012). Mutation in fumarate hydratase gene is associated with hereditary leiomyomatosis and renal cell cancer (HLRCC) which is characterized by high levels of intracellular fumarate. HLRCC is an autosomal dominant condition in which susceptible individuals are at a risk of development of cutaneous leiomyomas, early onset multiple uterine leiomyomas and an aggressive form of type II papillary renal cancer (Kulkarni et al., 2019; Menko et al., 2014; Y. Yang et al., 2012). In FH deficient cells, Keap1, a E3 ubiquitin ligase is succinated by excess fumarate and consequently inactivated. Keap1 is an inhibitor of nuclear erythroid related factor 2 (NRF2); inactivation of Keap1 results in induction of NRF2 and an ensuing potent antioxidant response since the downstream targets of NRF2 have an important role in redox homeostasis (Kulkarni et al., 2019). At molecular level, fumarate-cysteine adduct formation was shown to be mediated by protonated form of fumarate (HOOC-CH=CH-COOH) that exists at lower pH. FH deficient HLRCC cells exhibit lower cellular pH which would therefore be conducive to succination.

Moreover, excess fumarate is shown to succinate glutathione (GSH), converting it to succinicGSH, a covalent adduct between fumarate and glutathione. SuccinicGSH is shown to introduce oxidative stress (due to depletion of GSH) that is necessary and sufficient to induce cellular senescence (Zheng et al., 2015). These observations suggest a role for fumarate hydratase as a tumour suppressor gene, as it clears out an oncometabolite fumarate from the system.

Fumarate is also involved in conferring antibiotic persistence in *E. coli*, phenomenon in which a small fraction of cells that survive lethal concentrations of antibiotics. Fumarate imparts antibiotic persistence by acting as a terminal electron acceptor thereby avoiding generation of hydroxyl radicals ($\bullet\text{OH}$) that are responsible for antibiotic mediated bacterial killing (Kim et al., 2016).

1.6.1. Fate of fumarate generated through PNC in rat skeletal muscles

The reactions of purine nucleotide cycle involve utilization of NH_3 from aspartate whereas rest of the aspartate carbon skeleton leaves PNC as fumarate. Mitochondrial transporters transporting fumarate from cytosol to mitochondria are as yet unknown but mammalian cells possess a cytosolic isoform of FH that can convert cytosolic fumarate to malate, which can then enter mitochondria (Fig. 1.12). Inside the mitochondria, malate is oxidized to OAA via mitochondrial malate dehydrogenase (MDH). OAA can then get transaminated to aspartate through aspartate aminotransferase (AAT), localized either in cytosol or mitochondria. In rat skeletal muscles, mitochondrial AAT acts upon OAA converting it to aspartate that is shuttled out of mitochondria and aspartate re-enters the purine nucleotide cycle (Arinze, 2005) (Fig. 1.12)

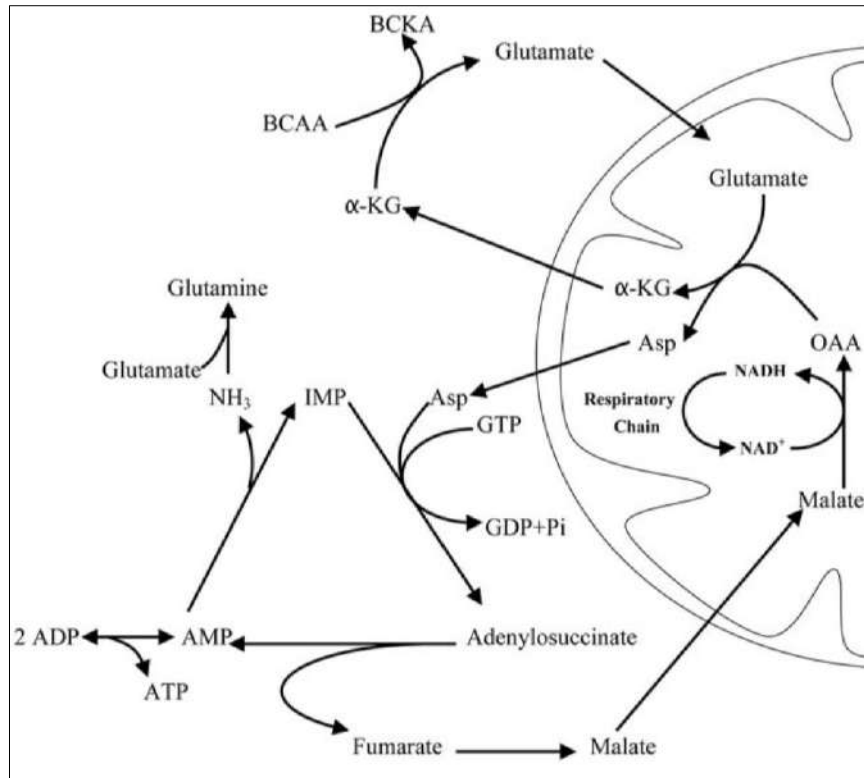


Figure 1.12: Fate of fumarate generated through PNC in rat skeletal muscle. In rat skeletal muscles, fumarate is converted to malate in the cytosol that is then transported to mitochondria. Mitochondrial oxidation of malate to oxaloacetate could be necessary to maintain redox balance in the cytosol and to generate ATP through NADH oxidation mediated by mitochondrial ETC. OAA is transaminated to aspartate via AAT reaction and aspartate re-enters PNC. Figure reproduced from Ifeanyi J. Arinze, Facilitating Understanding of the Purine Nucleotide Cycle and the One-carbon Pool, *The International Union of Biochemistry and Molecular Biology*, Vol. 33, No. 3, pp. 165–168, 2005 under creative common licences. Abbreviations: BCAA, branched chain amino acids; BCKA, branched chain α-keto acids; Asp, aspartate; α-KG, α-ketoglutarate.

Objectives of the study

As mentioned earlier, *Plasmodium* parasites also generate fumarate as a by-product during the biosynthesis of AMP via ADSS/ASL reactions (Fig. 1.9, 1.10). ADSS/ASL is the singular route of AMP production in parasites; therefore, for every molecule of AMP synthesized, a molecule of fumarate is also generated. Given that the amount of AMP required by a highly proliferating cell would be substantial, the quantity of fumarate generated would also be sizable. In this context, following question arises: what could be the metabolic significance of fumarate generated via this pathway in the parasite cytosol?

The present study is a collation of experiments carried out in an attempt to find answers to these questions. Earlier studies from our laboratory traced the metabolic fingerprints of exogenously added labelled fumarate within *P. falciparum* parasites using ¹³C NMR. The study undoubtedly established that fumarate is not a metabolic waste, rather it is efficiently metabolised by the asexual stage parasites. Addition of labelled fumarate resulted in labelling of aspartate, malate, pyruvate, lactate, nucleic acids and proteins (Bulusu et al. 2011).

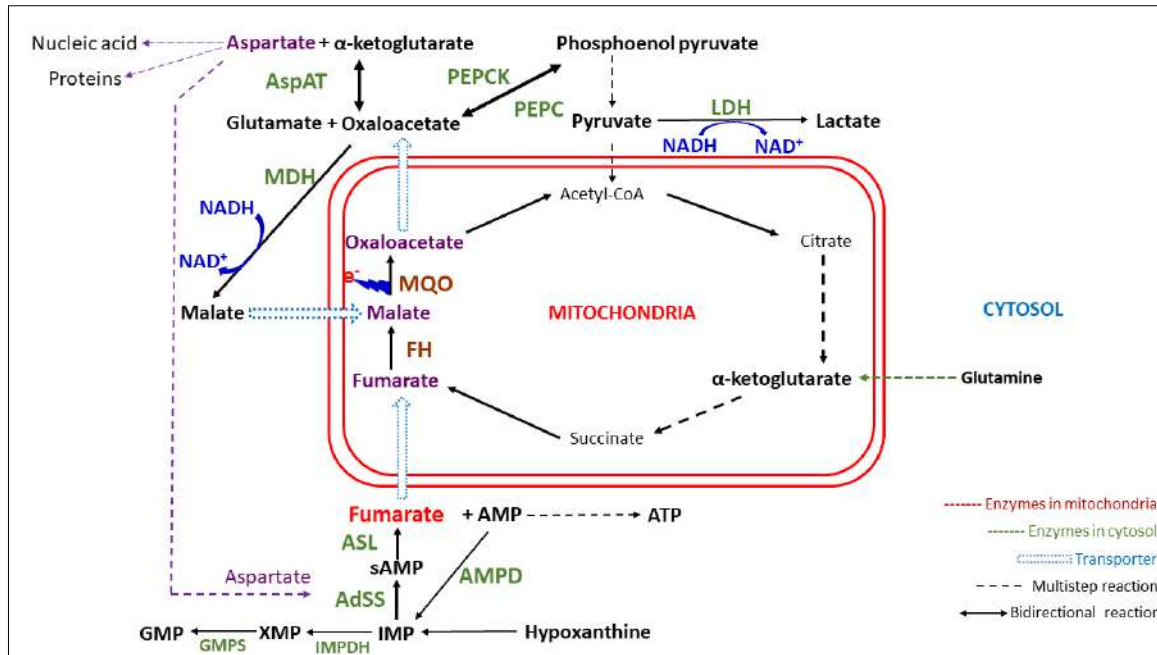


Figure 1.13: Schematic of the possible metabolic fate of fumarate in *P. falciparum*. Based on the results of study performed previously in our laboratory, we speculated the metabolic fate of fumarate in *P. falciparum* asexual stage parasites. Fumarate is highlighted in red colour. As *P. falciparum* FH is shown to be localized to the mitochondrion, fumarate needs to be transported inside the mitochondria via as yet unknown transporter. Once inside the mitochondrion, fumarate acts as a substrate for the FH reaction and gets converted to malate. Mitochondrial enzymes are represented in brown colour. Malate is further converted to oxaloacetate via MQO, a reaction that also contributes to maintenance of mitochondrial membrane potential. Malate can simultaneously be imported from cytosol into the mitochondria via a malate: oxoglutarate transporter. OAA can enter TCA cycle or can be transported out of the mitochondrion and into the cytosol where it can participate in a transamination reaction catalysed by aspartate aminotransferase (AspAT) and get converted to aspartate. Aspartate can then get incorporated in the nucleic acids via pyrimidines, into proteins and can also funnel back to PNC. All cytosolic enzymes are represented in green colour. Abbreviations: AspAT, aspartate aminotransferase; AdSS, adenylosuccinate synthetase; ASL, adenylosuccinate lyase; AMPD, AMP deaminase; GMPS, GMP synthetase; IMPDH, IMP dehydrogenase; FH, fumarate hydratase; MQO, malate quinone oxidoreductase; MDH, malate dehydrogenase; PEPCK, phosphoenolpyruvate carboxylase; PEPC, phosphoenolpyruvate carboxylase; LDH, lactate dehydrogenase.

Figure 1.13 summarises our understanding of the metabolic path traced by fumarate in the parasite. As indicated in the figure, aspartate enters AMP synthesis through ADSS and ASL and leaves as fumarate. Since *P. falciparum* lacks a cytosolic counterpart of FH, fumarate needs to be transported to mitochondria. Transporters that mediate the transport of fumarate from cytosol to mitochondria in *Plasmodium spp.* are unannotated, however, we speculate that a malate: oxoglutarate translocator might non-specifically mediate fumarate transport. Inside the mitochondrion, sequential actions of FH and MQO convert fumarate to malate and OAA. FH and MQO are the only two essential TCA cycle enzymes that could not be deleted (Ke et al., 2015). Their essentiality can be attributed to the requirement of these enzymes for the utilization of fumarate and associated maintenance of mitochondrial membrane potential necessary for transport of proteins, ions and solutes across mitochondria. OAA can be transported out of mitochondria through dicarboxylate: tricarboxylate carrier (DTC) into the cytosol where it can participate in a transamination reaction with glutamate to form aspartate and α-ketoglutarate - a reaction mediated by aspartate aminotransferase. OAA can also

be acted upon by PEP carboxykinase that converts it to PEP. PEP via the pyruvate kinase reaction can be converted to pyruvate that can partition between LDH or BCKDH reactions. Aspartate generated through the AAT reaction can get incorporated into nucleic acids via pyrimidines (Bulusu et al. 2011) and into proteins or can re-enter the ADSS/ASL reaction. Apart from the direct involvement of carbon skeleton of fumarate in different pathways, we also hypothesize that fumarate enhances glycolysis by increasing NAD^+ concentration in the cell. This could be facilitated by:

- i) increased flux through LDH reaction (over and above the pre-existing Warburg effect) and
- ii) increased flux through cytosolic MDH reaction as illustrated in figure 1.13.

Cytosolic malate dehydrogenase in *Plasmodium* catalyses reduction of oxaloacetate to malate with concomitant oxidation of NADH to NAD^+ . Malate is shown to be excreted from the parasites (Bulusu et al. 2011) while increased NAD^+ is a prerequisite to support enhanced glycolytic flux during asexual stages. This led us to speculate that fumarate might also be involved in supporting rapid proliferation of asexual stage parasites. However, these speculations are based on the observations of the NMR experiments carried out using exogenously added fumarate and the objective of the current study is to investigate the metabolism of fumarate generated within the parasite as a consequence of the ADSS/ASL reaction. To study the cellular pathways and processes to which fumarate contributes, its production through ADSS/ASL pathway needs to be abrogated and the cellular processes and pathways then affected due to fumarate-depletion need to be examined. As conversion of IMP through ADSS and ASL reactions to AMP is the only pathway by which parasite can synthesize AMP; ablation of fumarate production by inhibition/gene deletion of either ADSS or ASL would abolish AMP generation which would be lethal to the parasites. This scenario demands de-coupling AMP synthesis from fumarate production within the cell, which can be achieved by introducing an alternate pathway for AMP synthesis (one independent of fumarate generation) followed by deletion/inhibition of ADSS and/or ASL enzyme function and the consequent effects on cellular metabolism can be examined by performing *in vitro* assays and metabolomic studies. With this aim, we laid out the following objectives for the study:

- 1) Generation and validation of *P. falciparum*/*P. berghei* parasite lines expressing alternative purine salvage enzyme, *Saccharomyces cerevisiae* adenosine kinase
- 2) Genetic approach: disruption of *adss/asl* gene(s) in transgenic parasites possessing alternate AMP synthesis pathway
- 3) Chemical biology approach: examination of effect of ADSS inhibition by hadacidin on transgenic parasites expressing an alternate AMP synthesis pathway
- 4) Metabolomics studies on transgenic parasites to investigate the metabolic fate of fumarate in *Plasmodium* parasites.

Chapter 3 describes the experiments performed to fulfil these objectives and results obtained are analysed.

Chapter 2

Materials and Methods

This chapter details the materials and methods used during the study. It includes protocols followed for routine *Plasmodium* culturing, synchronization, parasite enrichment and transfections in addition to routine molecular biology protocols. Various strategies used to express an alternate purine salvage pathway in *Plasmodium* parasites, strategies attempted to knock out endogenous ADSS/ASL and chemical inhibition approach are reported. Genetic manipulations were also attempted in murine malaria parasite *P. berghei* simultaneously, the protocols for the same are also reported.

2. Materials and Methods

2.1. Materials

All reagents used were of highest quality and procured from Sigma Aldrich, Thermo Fischer Scientific, SRL or In-Vitrogen unless specified otherwise. *Plasmodium falciparum* and *Plasmodium berghei* strains were procured from the Malaria Research and Reference Reagent Resource Center (MR4). Primers were custom synthesized from Sigma-Aldrich, Bangalore. All restriction enzymes and Taq DNA polymerase were procured from New England Biolabs. Phusion polymerase was procured from Thermo Fischer. Bacterial media components were purchased from HiMedia, Mumbai while *Plasmodium* media components were procured from Sigma-Aldrich. Albumax II and Fetal Bovine Serum (FBS) were sourced from Gibco (In Vitrogen). Plasmid isolation kits, PCR purification kits and Gel extraction kits were from Qiagen. Endo-free plasmid isolation mini and maxi kits were purchased from Qiagen and Macherey-Nagel (MN). P3, P5 and SE solution kits for nucleofection were purchased from Lonza, Germany. In-Fusion HD cloning kit was purchased from Clontech (TaKaRa Bio), USA.

Centromeric plasmids used for protein expression in *P. falciparum* (pFCENv1 and pFCENv2) and *P. berghei* (pBCEN5) were a kind gift from Prof. Shiroh Iwanaga, Mie University, School of Medicine, Tsu, Japan. CRISPR-Cas9 plasmids pL6-eGFP, pUF1-Cas9, pL7-kahrp and pL6-Bsgv6, used for gene knockout, were a kind gift from Dr. Jose-Juan Lopez-Rubio, Biology of Host-Parasite Interactions Unit, Institut Pasteur, Paris, France. Plasmid pGDB and *P. falciparum* PM1KO parasite line used for conditional knockdown were a kind gift from Prof. Daniel E. Goldberg, Department of Medicine, Division of Infectious Diseases, Washington University School of Medicine, USA. Plasmids used for knockout, pCC1 and pCC4 were a kind gift from Prof. Alan F. Cowman, Infectious Diseases and Immune Defence, Walter and Eliza Hall Institute of Medical Research, Australia. pARL plasmid for single crossover recombination mediated knockout was a kind gift from Dr. Suman Dhar, Special Centre for Molecular Medicine, Jawaharlal Nehru University. pJAZZ-*Dasl* construct, TSA and pir strains of *E. coli* were procured from Plasmogem. Positive selection drug WR99210 was a kind gift from Jacobus Pharmaceuticals, Princeton, NJ, USA. Blasticidin was purchased from Invitrogen, USA. DSM1 was procured from MR4. Hadacidin was procured from Developmental Therapeutics Program, National Cancer Institute, USA. Fitting of data was performed using GraphPad Prism v5.

BALB/c mice aged between 6-8 weeks (male or female) were from Animal Facility, JNCASR. O+, A+ or B+ blood used for culturing *P. falciparum* was drawn from healthy donors with informed consent. Permission for *in-vitro* parasite culture and animal work was obtained from the Institutional Bio-safety Committee and Institutional Animal Ethics Committee of the Jawaharlal Nehru Centre for Advanced Scientific Research (JNCASR). Mass spectra were recorded at Central Instrumentation facility (CIF), Molecular Biology and Genetics Unit, JNCASR using Q Exactive HF (Thermo Scientific, USA) coupled to a Dionex UltiMate 3000 UHPLC (Thermo Scientific, USA).

2.2. Methods

2.2.1. Generation of plasmid constructs for *Plasmodium* transfections

Two sets of plasmid constructs were generated for this study. One set involves plasmid constructs for over expression of a gene(s) to bypass the endogenous AMP generation pathway. Other set involved constructs generated to obtain a knock-out or conditional knock-down of adenylosuccinate synthase and adenylosuccinate lyase genes in *P. falciparum* and *P. berghei*. All the constructs were generated in *E. coli* DH5 α strain and confirmed by DNA sequencing. Table 2.1 lists protein expression constructs generated for this study, the primer pairs and restriction enzymes used. Table 2.2 lists constructs generated for the purpose of knockout or conditional knockdown along with the primer pairs and restriction enzymes used for the same. Table 2.3, presented at the end of this section, provides sequences of all the oligonucleotide primers used in this study.

Table 2.1: Constructs generated for episomal expression of genes

Sr. No	Name of construct	Parent plasmid	Primer pair	Restriction enzymes
1	pET21b-yAK	pET21b	PI & PII	NdeI/XhoI
2	pFCENv2-yAK	pFCENv2	P1 & P2	AflIII/AvrII
3	pFCENv2-ASL	pFCENv2	P21 & P22	AflIII/AvrII
4	pBCEN5-yAK	pBCEN5	P27 & P28	BamHI / XbaI

2.2.1.1. Cloning and expression of yeast adenosine kinase in *E coli*

The coding sequence of adenosine kinase was amplified by PCR from yeast (*Saccharomyces cerevisiae*) genomic DNA using primers PI/PII. The PCR fragment was cloned in pET21b in-frame with a 6X His-tag at the C-terminus using NdeI/XhoI restriction enzymes. Positive clone (pET21b-yAK) was confirmed by colony PCR, insert release and DNA sequencing.

2.2.1.2. Cloning of yAK in pFCENv2 plasmid for heterologous expression in *P. falciparum*

For cloning into pFCENv2 plasmid, yAK gene was PCR amplified from yeast genomic DNA using primers P1/P2, digested with AvrII and AflIII enzymes and cloned into AvrII/AflIII digested pFCENv2 plasmid, in frame with 3X HA tag. Clones were confirmed by insert release and DNA sequencing. A confirmed clone of pFCENv2-yAK was used for transfection in *P. falciparum* parasites following the protocols described below.

2.2.1.3. Cloning of yAK in pbCEN5 plasmid for heterologous expression in *P. berghei*

yAK gene along with a HA tag was subcloned from pFCENv2-yAK vector to pbCEN5 plasmid between BamHI/XhoI sites using primers P27/P28. Clones were confirmed by colony PCR, insert release and DNA sequencing. A confirmed clone of pbCEN5-yAK was used for transfection in *P. berghei* ANKA parasites following the protocol described below.

Table 2.2: Knock out and Knock- down constructs used in the study

Sr. No	Name of construct	Parent plasmid	Primer pair	Restriction enzymes
1	pCC1- Δ asl	pCC1	5'asl: P3 & P4	SacII/AflIII
			3'asl: P5 & P6	NcoI/AvrII
2	pL7- Δ adss	pL6-eGFP	5'adss: P7 & P8	SpeI/AflIII
			3'adss: P9 & P10	EcoRI/NcoI
			sgRNA- P25/P31 & P26/P32	In-fusion kit
3	pL7- Δ asl	pL6-eGFP	5'asl: P11 & P12	SpeI/AflIII
			3'asl: P13 & P14	EcoRI/NcoI
			sgRNA- P23/P31 & P24/P32	In-fusion kit
4	pARL- Δ adss	pARL	P15 & P16	KpnI/AvrII
5	pGDB- Δ adss	pGDB	P17 & P18	XhoI/AvrII
6	pGDB- Δ asl	pGDB	P19 & P20	XhoI/AvrII

2.2.1.4. Generation of plasmid construct for gene deletion

pCC plasmid vectors were a kind gift from Prof. Alan F. Cowman, Infectious Diseases and Immune Defence, Walter and Eliza Hall Institute of Medical Research, Australia. 5' homology arm sequence of *asl* (1360 bp) was amplified from *P. falciparum* 3D7 genomic DNA using primers P3 and P4 and cloned between SacII/AflIII. Positive clones were screened by colony PCR and insert release. One such clone, pCC1-5'asl was used for subsequent manipulation. The 3' *asl* homology arm (970 bp) was amplified from *P. falciparum* 3D7 genomic DNA using primers P5 and P6 and cloned in pCC1-5'asl vector between NcoI/AvrII sites. A few positive colonies were obtained which were further confirmed by insert release and DNA sequencing. The confirmed clone, pCC1- Δ asl was used in further experiments.

2.2.1.5. Generation of plasmid constructs for gene disruption using CRISPR-Cas9 genome editing technique

Plasmid vectors required for CRISPR Cas9 mediated gene knock out in *P. falciparum* were a kind gift from Dr. Jose-Juan Lopez-Rubio, Biology of Host-Parasite Interactions Unit, Institut Pasteur, Paris, France. Homology arms for adenylosuccinate synthetase gene were cloned in pL6-eGFP plasmid vector by replacing eGFP homology arm segments. 5' adss homology arm sequence (625 bp) was amplified from *P. falciparum* 3D7 genomic DNA using oligonucleotide primers P7 and P8 and cloned in pL6 between SpeI/AflIII sites. Similarly, 3'adss homology arm sequence (738 bp) was amplified from same genomic DNA using oligonucleotide primers P9 and P10 and cloned between EcoRI/NcoI sites. Positive clones were confirmed by colony PCR and DNA sequencing. The confirmed clone, pL6- Δ adss was used in further experiments.

2.2.1.6. Cloning of sgRNA in pL6- Δ adss vector

CRISPR Cas9 technique consisting of two vector systems developed for use in *Plasmodium falciparum* by Mehdi Ghrobal and co-workers (Ghorbal et al. 2014) was used in this study. pL6 vector is used for cloning the homology arms required for the homology directed repair (HDR) pathway and the short guide RNA (sgRNA) required for recognition of target. The sgRNAs were designed using EuPaGDT: a web tool tailored to design CRISPR guide RNAs for eukaryotic pathogens (Tarleton and Peng 2015). Multiple approaches were employed to clone a 20 nt sgRNA segment in pL6 vector as the initial attempts were unsuccessful. All these approaches are summarized below.

a) sgRNA cloning between BtgZI restriction sites in pL6-eGFP vector

BtgZI is a Type IIS restriction enzyme that recognizes asymmetric DNA sequences and cleaves outside of its recognition sequence. HPLC purified, 24-bases long synthetic oligonucleotides (sgRNA oligos for adss, P29/P30, Table 2.3) with BtgZI compatible overhangs for pL6 were obtained from Sigma-Aldrich. The oligonucleotides were annealed *in vitro* and ligated with BtgZI linearized pL6- Δ adss (pL6 vector in which 5' and 3' homology arms for *adss* gene have been already cloned) using T4 DNA ligase.

b) Cloning using In-Fusion (Clontech) cloning kit

In-fusion HD cloning kit was purchased from Clontech (Takara) (Catalogue No. 639648). In-Fusion enzymes fuse DNA fragments that possess 15 bp overlap with each other. Oligonucleotides (P23 & P24 for *asl* and P25 & P26 for *adss*, Table 2.3) for the purpose of In-Fusion cloning consisted of desired sgRNA sequence flanked on either side by 15 bases that were complementary with the pL6 vector sequence. These HPLC purified synthetic oligonucleotides were custom made from Sigma-Aldrich. These oligonucleotides were annealed *in vitro* and pL6 vector was digested with BtgZI. The annealed oligonucleotides were mixed with digested pL6- Δ adss in excess. The reaction mix (10 μ L) consisted of vector DNA (~ 50 ng), insert DNA (annealed oligonucleotides, ~ 150 ng), 2 μ L In-Fusion enzyme mix and DNase free water. The reaction mix was prepared on ice and transferred to 50 °C water bath for 15 minutes. At the end of 15 minutes, the reaction mix was immediately placed on ice and 100 μ L of freshly prepared *E. coli* DH5 α competent cells were transformed with 2.5 μ L of reaction mix.

c) Overlap PCR followed by cloning using In-Fusion cloning kit

This strategy involved generation of two PCR products that had an overlapping sequence corresponding to desired sgRNA to be cloned on one end and sequences overlapping with pL6 vector (Fig. 2.1 a) on the other (outer) ends (Fig. 2.1 b). For cloning of sgRNA_{adss}, PCR 1 was performed using primer pair P25/P31 while PCR 2 was performed using P26/P32 primers (Table 2.3). Schematic representation of the strategy is shown below.

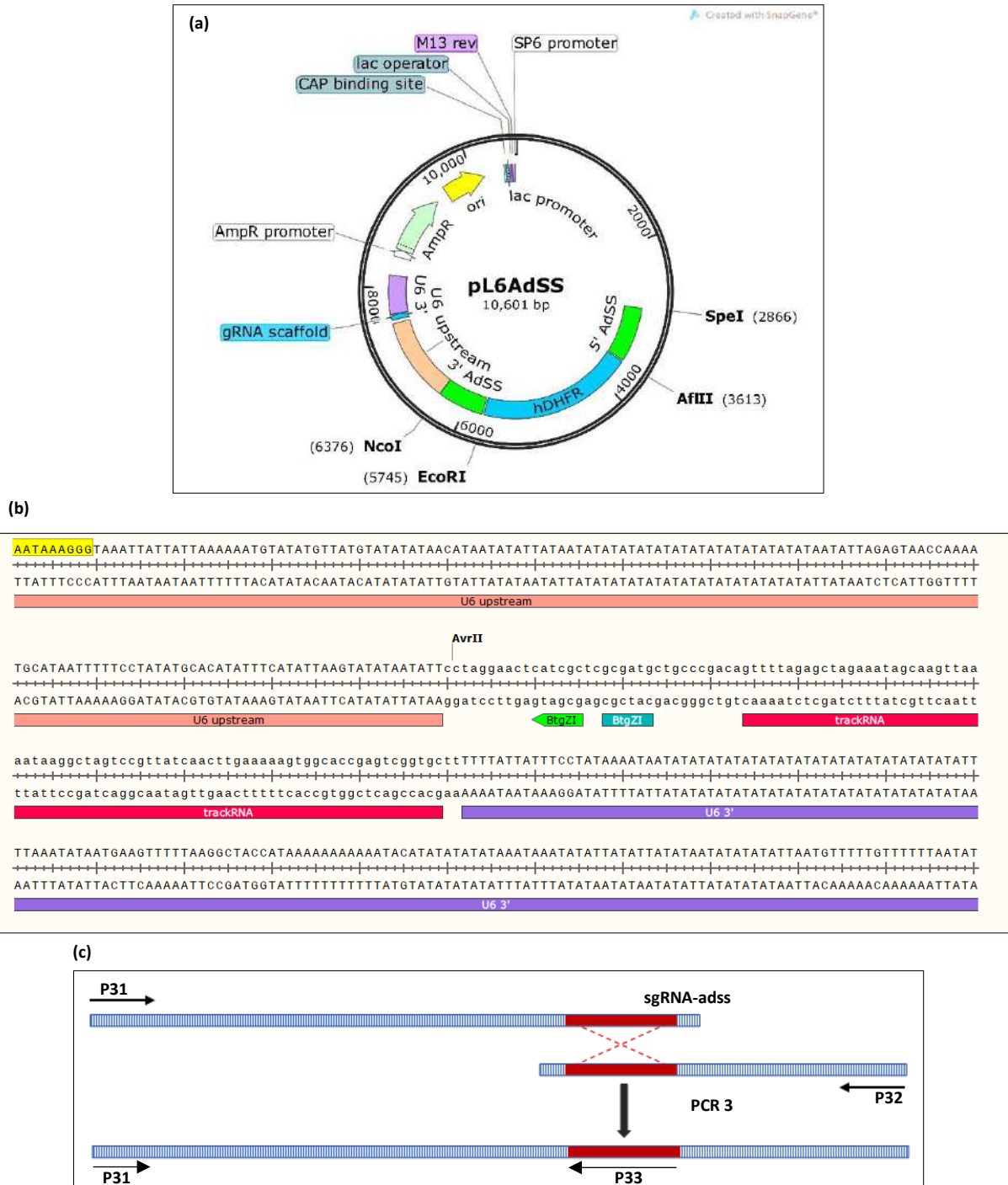


Figure 2.1: Schematic representation of strategy used for cloning sgRNA in pL6-adss. (a) Plasmid map of pL6-adss that was used for cloning of sgRNA_adss, generated using SnapGene viewer. 5' adss and 3' adss homology arms are shown in green. (b) gRNA scaffold region of pL6 vector. sgRNA of adss is cloned between two BtgZI restriction enzyme sites. Sequences of oligonucleotides P31 and P32 are from U6 upstream and U6 3' (UTR) regions, respectively (c) Overlap PCR strategy that led to successful cloning of sgRNA in pL6-adss.

Two segments from pL6 plasmids from the gRNA scaffold region with U6 promoter and terminator, were amplified in two separate PCR reactions. PCR 1 was performed with primers P25/P31 which generated an amplicon of 434 bp while PCR 2 was performed P26/P32 that generated an amplicon of 235 bp. Primers P25; 5'-

AACTTGCTATTTCTAGCTCTAAAAC**GAGAAAACCCACCAACTGTAATATT**
 ATATACTTAATATGAAATA- 3' and P26; 5'-
 TATTTTCATATTAAGTATATAATATT**ACAGTTGGTGGGGTTTTCTCGTTTTA**
 GAGCTAGAAATAGCAAGTT- 3' contained sgRNA sequence for *adss* (highlighted in bold in the primer sequence above). The two fragments had an overlap of 70 bp. They were then used as a template for a third PCR with primers P31/P32 to generate an amplicon of 669 bp that contained the desired sgRNA sequence for *adss* (Fig. 2.1 c). pL6- Δ adss plasmid (Fig. 3.1 a) was first digested with BtgZI at 60 °C for 2 hours followed by AvrII at 37 °C for 2 hours. Digested vector was cleaned using Qiagen Gel Extraction kit (Cat No./ID: 28115) and used for In-Fusion reaction. The amplicon obtained from PCR 3 had sequence homology to pL6 U6 promoter on one side and tracrRNA on the other side (Fig. 2.1 b). This amplicon was then cloned in pL6- Δ adss plasmid using In-Fusion cloning kit following manufacturer's instructions (Clontech (TaKaRa Bio), USA). *E. coli* DH5 α competent cells were transformed with the In-Fusion reaction mix (2.5 μ L) and the resultant colonies were screened for positive clones using primers P33/P25.

Generation of knock-out construct for *asl* was initiated by cloning of sgRNA into pL6-eGFP plasmid vector by following overlap PCR method described above using primers P23/P31 & P24/P32. Clones of pL6-sgRNA(*asl*) were confirmed by colony PCR and DNA sequencing. 5' *asl* homology arm sequence (512 bp) was amplified from *P. falciparum* 3D7 genomic DNA using oligonucleotide primers P11 and P12 and cloned in pL6-sgRNA(*asl*) between SpeI/AflIII sites. Similarly, 3' *asl* homology arm sequence (460 bp) was amplified from same genomic DNA using oligonucleotide primers P13 and P14 and cloned between EcoRI/NcoI sites. Positive clones were confirmed by colony PCR and DNA sequencing. *P. falciparum* 3D7^{yAK} parasites were transfected with the confirmed clone, pL7- Δ asl.

2.2.1.7. Generation of plasmid constructs for conditional knockdown in *P. falciparum*

~ 1 kbp DNA fragment from 3' end of the gene is amplified by PCR from *P. falciparum* 3D7 genomic DNA and cloned in pGDB vector between AvrII/XhoI sites. The clones pGBD- Δ adss and pGDB- Δ asl were generated by cloning 1035 bp and 1043 bp from 3' end of *adss* and *asl* respectively, amplified using primers P17/ P18 (*adss*) and P19/ P20 (*asl*). The inserts were cloned in pGDB using AQUA (advanced quick assembly) cloning technique, a homology sequence-based cloning (Beyer et al. 2015). The colonies were screened by colony PCR and correct clone was confirmed by DNA sequencing.

2.2.2. Protein purification

For purification of recombinant yAK, *E. coli* Rosetta cells were transformed with the confirmed clone (pET21b-yAK). The culture was grown to 0.6 O.D. and induced using 0.3 mM IPTG and incubated further for 4 hours at 37 °C. Cells were pelleted down and resuspended in buffer A (50 mM Tris HCl, pH 7.5, 150 mM NaCl, 1 mM DTT, 1 mM PMSF and 10 % glycerol) and sonicated. Cellular debris was removed by centrifugation at 24,000 x g for 30 minutes at 4 °C. Cleared supernatant was incubated with nickel nitrilotriacetic acid (Ni-NTA) agarose beads NI-NTA (His-Bind® Resin, Qiagen, USA) for

3 hours at 4 °C. The solution was then loaded onto a glass column pre-equilibrated with buffer A and beads were then washed with 50 column-volumes of buffer A containing 20 mM imidazole to wash off any contaminants. Protein was eluted in 250 mM, 500 mM and 1000 mM imidazole. 250 mM imidazole fractions were pooled, dialysed in buffer A to remove imidazole and used for further analysis.

2.2.3. Thin layer chromatography for detection of enzyme activity

Phosphorylation reactions (10 µl) contained [γ -³²P]-ATP (100 nCi µL⁻¹), 50 mM Tris HCl, pH 7.5, 2 mM MgCl₂, 4 mM ATP (cold, not radiolabelled) and 500 µM adenosine. Reactions were started by addition of 50 ng of the purified protein (yAK) to the reaction mix. After incubation for 12 hours at room temperature, 1 µL reaction mixture was spotted on PEI-cellulose TLC plate. The mobile phase used was 1-butanol, glacial acetic acid and water (50: 25: 25). Reaction products were visualised by exposing the TLC plates on Phospho-imager by Fujifilm.

2.2.4. Processing of whole blood

O+, B+ or A+ blood was collected from healthy donors using vacutainers containing acid citrate dextrose buffer. The blood was processed within 24 hours from the time of collection. Whole blood was transferred from vacutainers to sterile Falcon tubes and centrifuged at 800 x g for 5 minutes. The upper buffy coat layer was discarded and packed erythrocyte pellet was resuspended in equal volume of incomplete medium (RPMI 1640 with 25 mM HEPES) and centrifuged at 800 x g for 5 minutes. Three washes were performed using incomplete medium and finally the pellet was resuspended in equal volume (to achieve 50 % RBC suspension) of incomplete medium and stored at 4 °C (for not more than 2 weeks).

2.2.5. Revival of parasite stocks

Parasite stock was removed from liquid nitrogen container, transferred to laminar air flow and the surface of cryovial was wiped with 70 % ethanol. The contents of the vial were thawed by gently rubbing between palms. Once thawed, the contents of vial were transferred to a sterile 50 ml Falcon tube with a pipette and the cell volume measured. 0.1 volume of 12 % NaCl was added to the Falcon tube dropwise with intermittent swirling of the tube. The tube was then placed on a stand for 5 minutes without disturbance followed by addition of 10 volumes of 1.6 % NaCl dropwise, swirling the tube gently. The tube was centrifuged at 400 x g for 5 minutes. Supernatant was discarded and pellet was resuspended in 10 volumes of warm complete media (incomplete medium with 0.5 % AlbuMaxII, 0.45 % glucose, 0.2 % sodium bicarbonate and 100 µM hypoxanthine) and centrifuged. Supernatant was discarded and pellet was then resuspended in 5 ml complete medium with 100 µL (50 % suspension) fresh erythrocytes and transferred to a T25 flask with filtered cap. The flask was placed in an incubator.

2.2.6. Parasite Culture

P. falciparum 3D7 parasites were cultured in human erythrocytes (O+, B+ or A+ based on availability) collected from a healthy donor following the protocol established by Trager and Jensen (Trager and Jensen 1977). RPMI 1640 medium was prepared as incomplete medium containing RPMI, 25 mM

HEPES and gentamycin. Complete medium was prepared as per requirement by supplementing incomplete medium with 0.5 % AlbuMaxII, 0.2 % NaHCO₃, 0.45 % glucose and 100 µM hypoxanthine. All cultures were maintained at 2 % haematocrit. The culture was grown at 37 °C in CO₂ incubator (5% CO₂) and medium changed every 24 hr. Parasitemia was estimated when required by microscopic examination of Giemsa-stained smears.

2.2.7. Cryopreservation of parasites

P. falciparum parasites are usually frozen using Stockholm Sorbitol Method. This method gives lower initial parasitemia but more synchronized culture during first two life cycles after revival of stocks, as late stages are killed during thawing. Stocks of *P. falciparum* are made when cultures are predominantly in ring stages with at least 6-8 % parasitemia in a 2 % haematocrit culture. 5 ml culture was harvested by centrifugation at 400 x g for 5 minutes. Supernatant was discarded and pellet was resuspended in 300 µL of fetal bovine serum with gentle mixing followed by addition of 500 µL freezing medium (28 % sorbitol, 3 % glycerol and 0.65 % NaCl) with constant swirling of the tube. The resulting cell suspension was transferred to a sterile cryovial, flash frozen in liquid nitrogen and subsequently transferred to a liquid nitrogen tank.

2.2.8. Synchronization of parasites

Parasite cultures were synchronized in ring stage (not later than 10 to 12 h post-invasion) to eliminate the mature forms using sorbitol which lyses only erythrocytes with late stage parasites due to their increased permeability owing to presence of new permeability pathway channels on the surface of these erythrocytes (Lambros and Vanderberg 1979), thereby synchronizing the culture in ring stages. 5 % sorbitol was prepared in sterile water and filter sterilized through 0.2 µm filter. For synchronization, parasite culture was centrifuged at 500 x g for 5 minutes. Supernatant was discarded and pellet resuspended in 10 volumes of 5 % sorbitol. The suspension was incubated at room temperature for 10 min with intermittent mixing. At the end of 10 minutes, cell suspension was centrifuged at 500 x g for 5 min. Pellet was washed with 10 volumes of warm (37 °C) complete medium. Washing process was repeated twice and the resulting pellet was then resuspended in complete medium to obtain 2 % haematocrit and put back in culture at 37 °C. To attain tightly synchronized parasites, sorbitol synchronization was performed for 2 consecutive life cycles.

2.2.9. Enrichment of late stages by density gradient centrifugation on Percoll®

Percoll® is a medium for density gradient centrifugation of cells. It consists of colloidal suspension (23% w/w in water) of silica particles of 15-30 nm diameter that are coated with polyvinylpyrrolidone (PVP). Late stage parasites (trophozoites and schizonts) being lower in density as compared to uninfected RBCs and ring stage parasite-infected RBCs form a layer on top of the 70% Percoll® solution thus leading to their enrichment (Rivadeneira, Wasserman, and Espinal 1983). Iso-osmotic solution of Percoll® was prepared by diluting 9 parts of Percoll® with 1 part of 10x PBS (pH 7.4) to form a 90 % Percoll® solution. This solution was further diluted by mixing 8 ml of it with 2 ml of 1x PBS, making a 70 % Percoll® solution. The solution was filtered through 0.45 µm filter. Parasite culture with

predominantly late-stage parasites was harvested by centrifuging at 500 x g for 5 minutes. The supernatant was discarded and pellet was resuspended in 1x PBS to obtain 10 % haematocrit suspension. This suspension was layered over equal-volume of 70 % Percoll® solution by slowly trickling it along the wall of the Falcon tube. The tube was then centrifuged in a swing bucket rotor at 700 g for 10 minutes at room temperature without brake (deceleration = 0). The resulting parasite layer formed at the interface of Percoll® and 1x PBS was collected carefully and washed twice with incomplete medium and used for analysis. An enrichment of up to 80 % can be achieved by varying the Percoll® gradient.

2.2.10. Magnetic separation of late-stage parasites

In spite of the PVP coated silica particles, Percoll® enrichment can be a stressful procedure for parasite health; magnetic beads-based separation of trophozoites and schizonts is a useful alternative (Spadafora *et. al.*, 2011). Trophozoite and schizont stage parasites contain large amounts of hemozoin, a molecule that has paramagnetic properties. Magnetic Assisted Cell Sorting (MACS) technique exploits this paramagnetic nature of hemozoin in trophozoite and schizont stage parasites via positive selection. MACS columns are composed of ferromagnetic particles coated with cell-safe material. When placed in magnetic field, the particles amplify the magnetic field 10000 folds inducing a high magnetic field within the column. Parasite culture with predominantly late stage parasites was harvested by centrifugation at 500 x g for 5 minutes. The supernatant was discarded and pellet was resuspended in incomplete medium to obtain 10 % haematocrit. The LS column(s) (Miltenyi Biotec, USA) was placed on the MACS separator (Miltenyi Biotec, USA) that was mounted on a stand. The column was equilibrated with 5 ml warm (37 °C) incomplete medium. 10 % haematocrit suspension was then loaded onto the column and the flow-through was collected in a sterile Falcon tube. Once all of the suspension was passed through, the flow-through was again loaded onto the column. This step was repeated thrice. This step helps in enhancing the binding of trophozoites and schizonts to the column. After the binding step, column was washed with ~20 ml incomplete medium. The columns were then unmounted from the magnetic separator and parasites were eluted using 3-4 ml incomplete media while holding the column away from the magnetic field. Due to the removal of magnetic field, trophozoites and schizonts are dislodged from the column and are eluted out. This method yields up to 80-90 % enrichment of trophozoites and schizonts (Fig. 2.2).

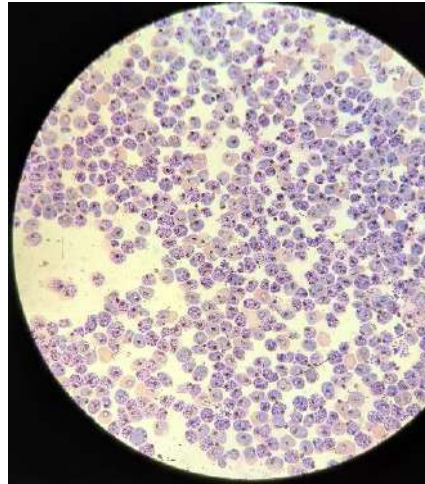


Figure 2.2: *P. falciparum* parasites separated using MACS. A microscopic field showing *P. falciparum* parasites separated using MACS columns and stained using Giemsa.

2.2.11. Saponin lysis of RBCs to obtain free parasites

Trophozoite and schizont stage parasites are released from erythrocytes by saponin lysis. Saponin renders the erythrocyte and parasitophorous vacuolar membranes permeable to macromolecules but leaves the parasite plasma membrane intact thereby preventing their lysis. Saponin solution (0.15 % w/v) was prepared in 1x PBS or incomplete medium and chilled to 4 °C. Parasite culture was harvested and pellet washed twice with cold 1x PBS. The pellet was then resuspended in 2 volumes of saponin solution, incubated for exactly 5 minutes. The reaction was quenched at the end of 5 minutes by adding 10 volumes of ice-cold 1x PBS. The cell suspension was then centrifuged at 4000 x g for 15 minutes at 4 °C. The parasite pellet was washed twice with ice-cold 1x PBS by centrifugation at 4000 x g for 5 minutes each at 4 °C. The pellet was then flash frozen and stored at -80 °C until further use.

2.2.12. Genomic DNA isolation from *P. falciparum* parasites

Genomic DNA was isolated from saponin released free parasites. Parasite pellet was resuspended in TE buffer, 1/100th volume of original culture volume i.e. pellet obtained from 40 mL culture is resuspended in 400 µL TE buffer. Pellet was resuspended using a cut tip to avoid shearing of cells. To the cell suspension, proteinase K was added to a final concentration of 20 µg ml⁻¹ followed by SDS (stock concentration 20 %) to a final concentration of 0.5 %. The resulting solution was mixed by gently inverting the tube few times. The mixture was incubated overnight at 55-60 °C. At the end of incubation, 1 volume of Tris-saturated phenol and 1 volume of chloroform was added to the same. The tubes were tumbled gently for 10 minutes until complete mixing of organic and aqueous phases occurred and then centrifuged at 10,000 x g for 5 minutes at 4 °C. The aqueous phase was transferred to a fresh tube and phenol: chloroform extraction was performed again following which the mixture was extracted using 1 volume of chloroform alone and the aqueous phases were pooled. To the aqueous phase, 1/10th volume of 3 M sodium acetate (pH 5.2) was added followed by addition of absolute ethanol (of >99 % purity). The tube was inverted several times to mix the solution and transferred to -20 °C for 1 hour to enhance DNA precipitation. Tube was then centrifuged at 10,000 x g for 10

minutes at 4 °C. Supernatant was discarded and pellet was washed with 70 % ethanol solution and centrifuged. The supernatant was discarded and pellet was air dried. The dried pellet was dissolved in 50-100 µL sterile TE. Small amount (~ 2 µL) of genomic DNA solution was run on an agarose gel to examine the quality of isolated parasite genomic DNA.

2.2.13. Parasite transfections

P. falciparum parasites were transfected with the plasmid of interest using one of the 4 protocols described below. When large quantities (100 µg) of plasmid were required for transfection, DNA was isolated using the endotoxin-free maxi-prep kit from Qiagen. For small scale plasmid DNA isolation (up to 35 µg), endotoxin-free mini prep kit from MN (MACHEREY-NAGEL, Germany) was used. To transfect parasites using Bio-rad electroporator (Gene Pulser X cell) and cytomix, previously published protocols were followed. To transfect parasites using Amaxa (Lonza) 4D nucleofector, P3 or SE solution kits were used with appropriate pulse codes mentioned in literature.

2.2.13.1. Pre-loading of erythrocytes using Bio-Rad electroporator

O+ blood was freshly collected from a -healthy donor and a 50 % erythrocyte suspension was prepared. 400 µL of 50 % erythrocyte suspension was used for pre-loading. Erythrocytes were washed with 5 mL ice-cold incomplete cytomix (120 mM KCl, 0.15 mM CaCl₂, 2 mM EGTA, 5 mM MgCl₂, 10 mM K₂HPO₄/KH₂PO₄ (pH 7.6), 25 mM HEPES (pH 7.6)). To the washed erythrocyte pellet, 50-100 µg plasmid DNA dissolved in incomplete cytomix was added. The volume was made up to 400 µL using ice-cold incomplete cytomix. Cell suspension was transferred to a pre-chilled 2 mm cuvette and electroporated using Bio-Rad Gene Pulser X-cell. For an exponential wave protocol, the voltage applied was 310 V, capacitance was 950 µF and resistance was fixed at ∞ (without the PC module)(Hasenkamp, Russell, and Horrocks 2012; Maier et al. 2006). Time constant was noted (A time constant between 12 to 20 milliseconds is desirable). After pulsing, the cell suspension was transferred immediately onto ice for 30 sec after which 1 ml warm complete medium was added. The contents of the cuvette were then transferred to a T25 flask and 500 µL of schizont stage culture with 4-5 % parasitemia was added. The volume of culture was made up to 5 ml using complete medium and flask was transferred to 37 °C. Medium was changed after a few hours to remove traces of cytomix from the culture. 24 hours post transfection, a Giemsa-stained smear was prepared to estimate parasitemia. Appropriate drug pressure was commenced once healthy parasites were observed. Fresh erythrocytes were added to the culture to achieve haematocrit of 2 % to avoid loss of culture due to excess parasitemia. Post-transfection, culture was maintained in a meticulous fashion by media changes every 24 hours for initial 10 days. Thereafter, media was changed twice a week and small amounts of old erythrocytes were discarded and replenished with 50 µL fresh erythrocytes. Smears were prepared to monitor appearance of transfectants.

2.2.13.2. Transfection of ring stage parasites using Bio-Rad electroporator

Parasite culture was synchronized twice in consecutive generations using 5% sorbitol to obtain tightly synchronized parasites. 5 ml ring stage parasite culture with 6-8 % parasitemia was centrifuged and

pellet was gently washed with ice-cold incomplete cytomix. Supernatant was discarded, to the pellet 50-100 μg plasmid DNA, resuspended in incomplete cytomix, was added. The volume was made up to 400 μL with ice-cold incomplete cytomix. Cell suspension was then transferred to a pre-chilled 2 mm Bio-Rad cuvette. Electroporation was performed by using Bio-Rad Gene Pulser X-cell by applying voltage of 310 V, capacitance 950 μF and resistance ∞ (Hasenkamp et al. 2012). The time constant was noted (A time constant between 12 to 20 ms is desirable). After pulsing, cuvette was immediately transferred onto ice for 30 sec following which 1 mL pre warmed complete medium was added to the cuvette aseptically. Electroporated cell suspension was transferred to a 5 ml Falcon tube and volume was made up to 5 ml. The tube was centrifuged at 300 x g for 5 minutes. The supernatant was discarded and pellet was carefully resuspended in 5 ml complete medium and transferred to a T25 flask. Media change was given 24 hours post transfection and a Giemsa-stained smear was made to estimate parasitemia. Appropriate drug pressure was initiated once healthy parasites were seen. Post transfection, cultures were maintained as described above.

2.2.13.3. Transfection of schizont stage parasites using Amaxa (Lonza) 4D nucleofector

Tightly synchronized schizont stage parasites were obtained by two sorbitol synchronizations in consecutive life cycles followed by Percoll® or MACS enrichment in the second cycle, after which enriched late stage parasites were put back in culture to invade fresh erythrocytes. Synchronization window of 4-6 hours is desirable. Synchronized schizonts were then purified by MACS and incubated at 37 °C for 1 hour to recover. 100 μL transfection solution was made by mixing 82 μL of P3 (Lonza) solution and 18 μL of supplement 1 (Lonza). To the P3 transfection solution, 10 μg of plasmid DNA (dissolved in TE) was added. The schizonts were pelleted after the recovery period, supernatant discarded and pellet resuspended in 100 μL P3 transfection solution containing plasmid DNA. The final volume was made up to maximum 110 μL . The cell suspension was transferred to cuvette provided with the P3 kit. Transfection was performed at room temperature in Amaxa (Lonza) 4D nucleofector using pulse code FP-158 (Moon et al. 2013). Immediately after transfection, cuvette was transferred to the laminar air flow chamber and 1 ml pre-warmed complete medium was added. The entire solution was then transferred to a T25 flask along with 2 ml complete medium (at 37 °C) and fresh erythrocytes were added to make up the haematocrit to 20%. The flask was kept on shaking at 100 rpm for 2 hours at 37 °C (in the incubator) to allow the schizonts to burst and reinvade efficiently. The culture was then transferred to a T75 flask and 10 ml fresh warm complete medium was added to the culture and transferred back to the incubator. Media was changed 24 hours post transfection and smear was made to detect parasites. Drug pressure was initiated only after visualization of parasites by Giemsa smear. Cultures were maintained in the same manner as described above for pre-loading protocol.

2.2.13.4. Pre-loading of erythrocytes using Amaxa (Lonza) nucleofector

O+ blood was freshly collected from a healthy donor (preferably on the day of transfection) and a 50% erythrocyte suspension was prepared. The parasite culture was tightly synchronized by repeated sorbitol synchronization of rings in two consecutive life cycles. Parasite culture at schizont stage with

4-5 % parasitemia is desirable to infect transfected erythrocytes. 40 μ L RBC suspension was centrifuged and supernatant discarded. 100 μ L SE (Lonza) transfection solution was prepared by mixing 82 μ L SE solution and 18 μ L supplement 1 (Lonza) solution. To this mix, 10 μ g plasmid DNA was added (dissolved in TE at a concentration of 1 μ g/ μ L). The RBC pellet was resuspended in this transfection solution + DNA mixture and mixed gently using a pasture pipette. The resulting cell suspension was then transferred to a cuvette provided with SE kit. Nucleofection of erythrocytes was performed using pulse code CM-162 (Caro, Miller, and DeRisi 2012). The cuvette was transferred immediately to a laminar air flow chamber and 1 ml of pre-warmed complete medium was added to it. The cell suspension was then transferred to a T25 flask and volume made up to 5 ml with pre-warmed complete medium. 500 μ L of schizont-stage parasite culture was added to complete transfection and flask put back in the incubator. Media change was given 4-5 hours later to remove traces of SE solution. 24 hours post transfection, another media change was given and smear made to estimate parasite health and parasitemia. Drug pressure was initiated after observing healthy parasites in the culture. Culture was maintained in the manner as described above.

2.2.14. Western blot

a) *Preparation of parasite cell lysate.*

Free parasites were isolated by saponin lysis and pellets stored in -80 °C until use. A pellet from 25 ml culture with 8-10 % parasitemia was removed from -80 °C and to it 2 μ L of protease inhibitor cocktail was added immediately. The pellet was thawed at on ice in the presence of protease inhibitor cocktail. Once the pellet was thawed, equal volumes 2x SDS loading dye mixed with β -mercaptoethanol was added to it. The solution was mixed gently and kept in boiling water bath for 7-8 minutes with intermittent mixing to ensure complete lysis of parasites. After boiling, the cell lysate was centrifuged at 24, 000 x g for 15 minutes. The supernatant was carefully transferred to another tube and supernatant volume equivalent to 10 ml of culture was loaded on to a 12 % SDS-PAGE gel. The gel was run at 150 V till the dye front reached the end of the gel. Transfer was performed using semi-dry method.

b) *Transfer*

Transfer buffer (24 mM Tris HCl, 192 mM glycine and 20% methanol) was prepared and chilled. The blotting papers were thoroughly soaked in chilled transfer buffer. The PVDF membrane was activated in 100 % methanol. Once the gel run was complete the membrane, gel and blotting papers were arranged in the following order:

Bottom--- Blotting papers---PVDF membrane---gel---Blotting papers---**Top**

Care was taken to remove any air bubbles trapped between the sheets. The semi dry transfer was performed at 25 V for 30 min in a Bio-Rad instrument.

c) *Development of blot*

After the transfer was complete, the blot was removed from the transfer apparatus and washed with distilled water. It was then soaked in Ponceau solution (2% Ponceau (w/v) in 3% acetic acid). Once bands appeared, the blot was scanned for future reference. Blocking of the blot was

done using 5% skim milk for 30 min with constant shaking. At the end of blocking, primary antibody (prepared in 5% skim milk, anti-HA antibody was used at a titre of 1:3000) was added at the appropriate concentration and incubated overnight at 4 °C. The blot was subsequently washed with PBST (1x PBS, 0.1% Tween-20). The blot was then incubated with secondary antibody, prepared in 5% skim milk at appropriate concentration (anti-mouse antibody used at a titre of 1:4000) for 3 hours at room temperature with constant shaking. Secondary antibody was washed off with PBST, giving three washes. The blot was developed using AEC protocol. 20 mg AEC (amino-9-ethylcarbazole) was dissolved in 1 ml dimethylformamide. 833 µL 3M sodium acetate, pH 5.2 was added to 25 ml 1x PBS and the AEC solution was mixed into it. This mixture was poured on the blot and then 50 µL H₂O₂ was added. The solution was shaken gently until bands appeared on the blot. Once developed, the blot was transferred to distilled water and scanned immediately to acquire an image.

2.2.15. Hadacidin Sensitivity assay

Hadacidin sensitivity assay was performed on yAK expressing parasites (3D7^{yAK}) and vector control parasites (3D7^{EV}). Both the parasite cultures were synchronized twice using 5 % sorbitol in consecutive life cycles. 24 hours after the second synchronization, early trophozoite stage (24-30 hours post invasion) parasites were examined by Giemsa-stained smears for parasitemia. The parasitemia was adjusted to 1% and haematocrit was adjusted to 2%. Assays were set up in 6 well plates. One plate was used for 3D7^{EV} parasites and another one for 3D7^{yAK} parasites. 2 ml culture (1 % parasitemia with 2 % haematocrit) was dispensed into each well. Cell suspension was gently swirled before dispensing into each well to ensure even distribution of cells in all the wells. Wells were labelled appropriately and hadacidin was added at the appropriate concentration to wells labelled as test while equal volume of vehicle (water) was added to wells labelled as control and the cultures were mixed by shaking the plate gently. Each condition was set up in triplicate. The plate was placed in the incubator for 48 hours. At the end of 48 hours, smears were made of culture (50 µL) from each well. 1.5 ml of culture was discarded and replenished with complete medium at 2 % haematocrit (1:4 dilution). Drug and vehicle were also replenished in the respective wells and plates were transferred back in the incubator for next cycle. The assay was continued for 3-4 generations. Parasitemia was counted from each slide and graphs were generated using GraphPad Prism v5.

***Plasmodium berghei* protocols**

2.2.16. Maintenance of *Plasmodium berghei*

Plasmodium berghei ANKA strain was procured from Malaria Research and Reference Reagent Resource Center (MR4). The glycerol stock of wild type *P. berghei* parasites was injected into a healthy, 6-8 weeks old BALB/c mouse (male or female). Parasitemia was monitored by preparing Giemsa-stained smears using blood drawn through tail snip. Parasitemia was allowed to reach 30-40 % after

which either the complete blood was harvested to obtain large number of parasites or small amount of blood was passaged to a new mouse for continued maintenance of parasite line. A small amount of harvested blood was used to prepare glycerol stocks. Glycerol stocks were prepared by adding 300 μL of 30% glycerol to 200 μL of the blood, flash frozen and stored in liquid nitrogen container. Free parasites were obtained by pelleting the mouse blood collected in heparin. Pellet was resuspended in 10 ml of ice-cold 1x erythrocyte lysis buffer (1.5 M NH_4Cl , 0.1 M KHCO_3 , 0.01 M Na_2EDTA pH 7.4), incubated for 5 minutes at 4 °C and centrifuged at 500 x g for 10 minutes. The supernatant was discarded and pellet was stored in -20 °C until use for either genomic DNA isolation or western blotting.

2.2.17. Transfection of *Plasmodium berghei* parasites

Transfection of *P. berghei* parasites was performed at schizont stage. The parasitemia in an infected mouse was monitored through Giemsa stained smears and upon observation of predominantly schizont stage parasites (Janse et al. 2006), entire blood from one mouse (~ 1 ml) was harvested. The blood was collected in a 500 μL of heparin solution (200 units ml^{-1}) and mixed thoroughly. To enrich schizont stage parasites from a mixed staged culture, nycodenz density gradient centrifugation was performed. 60 % solution of nycodenz was prepared in 1x PBS and 500 μL of it was layered at the bottom of an eppendorf tube. 500 μL of heparin diluted blood was slowly layered on top of the nycodenz layer and without disturbing, the tubes were transferred to a centrifuge. Centrifugation was performed at ~ 200 x g for 15 minutes without brake. A layer of schizonts forms at the interface which was collected and washed thrice with warm incomplete RPMI. The pellet of washed parasites was then resuspended in 100 μL P5 (Lonza) transfection mix (82 μL P5 solution + 18 μL supplement 1 solution) and 10 μL plasmid DNA. Cell suspension was transferred to a cuvette and transfection was performed using Amaxa (Lonza) 4D nucleofector using pulse code FP-167 (Janse et al. 2006). Immediately after transfection, 50 μL of warm incomplete medium was added to transfection solution, mixed gently and the cell suspension was divided into two parts which were then injected in two healthy BALB/c mice. Tail snip was made 3-4 days post-transfection to examine parasite health and parasitemia and appropriate drug pressure was commenced once healthy parasites were observed. Thereafter, parasitemia was monitored regularly until drug resistant parasites emerged. The parasitemia was allowed to increase up to 30-40 % after which blood was harvested to make glycerol stocks and obtain free parasites for the purpose of genotyping.

In case of sequential genetic manipulation in *P. berghei*, slightly different approach was used since only one selection marker is available for this system (De Koning-Ward et al. 2000). *P. berghei* parasites were first transfected with vector pbCEN5-yAK that facilitated the episomal over-expression of yeast adenosine kinase to provide an alternative to the endogenous AMP synthesis pathway. The selection marker on pbCEN5 plasmid was Tgdhfr-ts (*Toxoplasma gondii* dhfr-ts bifunctional protein) that confers resistance only to pyrimethamine and not to WR99210. 7 mg pyrimethamine was dissolved in 1 ml DMSO and mixed with 100 ml drinking water (pH 3.5 - 5.0). The drug containing water was administered to mice and replenished after every 7 days. Once the transgenic parasites expressing yAK

were confirmed, they were injected into fresh BALB/c mouse and transfected with pJAZZ- Δ asl to knock-out endogenous adenylosuccinate lyase. pJAZZ vectors harbour hDHFR (Human DHFR) as a selection marker which imparts resistance WR99210. Following the transfection with pJAZZ- Δ asl, mice were administered with WR99210. WR99210 was prepared by dissolving 8 mg of drug in 1 ml absolute ethanol and to that mixture, 75 μ L of benzyl alcohol was added and volume made up to 2.5 ml using distilled water. Mice were administered the drug by subcutaneous injections (s.c.) as a single dose of 16 mg kg⁻¹ body weight for 4 consecutive days as recommended by Tania F. de Koning-Ward and co-workers (De Koning-Ward et al. 2000). Tail snips were made daily to examine parasitemia and effectiveness of drug treatment regime.

2.2.18. Genomic DNA isolation

Free parasite pellet was thawed and resuspended in 350 μ L TNE buffer (10 mM Tris pH 8.0, 5 mM EDTA pH 8.0, 100 mM NaCl). To this, 10 μ L RNase A (Stock concentration, 10 mg ml⁻¹) was added followed by addition of 50 μ L of 10 % SDS and volume was made up to 500 μ L using TNE buffer. The mixture was incubated at 37 °C for 10 minutes after which 10 μ L Pronase (10 mg ml⁻¹) was added and incubated further for 1 hour. After the incubation, 1 ml of Tris saturated phenol was added to the sample and mixed gently by inverting the tube several times. The tube was centrifuged at 10,000 x g for 10 minutes and the upper aqueous phase was transferred to a fresh eppendorf tube. The aqueous phase was treated with 1 ml of 1:1 phenol: chloroform mixture, mixed and centrifuged at 10,000 x g for 5 minutes. The upper aqueous phase was again transferred to a fresh eppendorf and mixed with 1 ml chloroform: isoamyl alcohol solution and centrifuged at 10,000 x g for 5 minutes. The supernatant was collected in a new tube and treated with 1/10th volume of 3 M sodium acetate (pH 5.2) and 1 ml absolute ethanol (of >99 % purity). The sample was mixed and centrifuged at 10,000 x g for 5 minutes and supernatant was discarded. Pellet was washed with 70 % ethanol, air dried and resuspended in water. 2 μ L of genomic DNA sample was checked on agarose gel for integrity of DNA.

Table 2.3: List of primers used in this study.

Primer No	Primer Sequences (5' to 3')
PI	GGGAATTCCATATGACCGCACCATTGGTAGTATTG
PII	CGGCTCGAGTTTAGAGTAAGATATTTTTTCGG
P1	AATGCACCTAGGATGACCGCACCATTGGTAGTATTGGGTAA
P2	AATGCACTTAAGTTATTTTTCAAATTGTGGATGTGACCAGGATCC
P3	CATGATCCGCGGCGTATTCTTAAAATGAATCACTTCCTATAAAGTCATTCT GAC
P4	CACTGACTTAAGTAGGATCACAGACTTTATGCGCATTAAAATTTCC
P5	TGCATCCATGGCCGCACAATTATCTTGGCTACGCAAGC
P6	AGTCACCTAGGGGTACAGGACAACATGGACATATGCATGG
P7	AGGACTAGTCTTGTACAAAATGAACATATTTGATC
P8	CACTGACTTAAGGGATATGTTCCAAAATCAATATCTAAC
P9	ATACCGGAATTCATCATAAAAAACTGAATTTAGTTGTAGG
P10	ATGCCATGGCTATTAGGACCTACACCAATCCAAAC
P11	GCCCCTTCCGCGGGGAGGACTAGTCATGTGAACCAACTGAAAAACATAT CG
P12	TAATTTTTTTTACAAAATGCTTAAGCCATGTGTTTTTGATAATAAAGATAC ATCAG
P13	AACATATTTATTAATCTAGAATTCGAGATATATGTAAAATTTAATGGAGC TG
P14	TGTTATTATTTTTACCGTTCCATGGGGGAATACGCAAATGATGAGC
P15	AACTCGACCCGGGATGGTACCAAATTTAATGGAGGTGCTAATGCAGG
P16	TGTTATCCTAGGTCCTCCTCCTCCGTCGAGCCATCCACACCTTC
P17	TTAGGTGACACTATAGAACTCGAGGGTACAACAAAAGAGGTATTGG
P18	ATAATGTGCTGCACCTGGCCTAGGATTTTTTTTTATATATTCCTGTGAGAA GTGC
P19	TTAGGTGACACTATAGAACTCGAGCCAGTGAAGATATTAATAATATAGCA TATGG
P20	ATAATGTGCTGCACCTGGCCTAGGATTTTTTTTTATATATTCCTGTGAGAA GTGC
P21	ATATCACCTAGGATGGATGTACATGTGAACCAACTG
P22	AATCTACTTAAGTTAATTTTTTTTTATATATTCCTGTGAGAAGTGC
P23	TATTTTCATATTAAGTATATAATATTCCTGCATCACCAACTACCTTGTTTTA GAGCTAGAAATAGCAAGTT
P24	AACTTGCTATTTCTAGCTCTAAAACAAGGTAGTTGGTGATGCAGGAATAT TATATACTTAATATGAAATA
P25	AACTTGCTATTTCTAGCTCTAAAACGAGAAAACCCCACTGTAATAT TATATACTTAATATGAAATA
P26	TATTTTCATATTAAGTATATAATATTACAGTTGGTGGGGTTTTCTCGTTTTA GAGCTAGAAATAGCAAGTT
P27	TATCGCGGATCCATGACCGCACCATTGGTAGTATTGGG
P28	CACTTCTAGAGGCATAATCTGGAACATCGTACGGATACGC
P29	TATTGTACAGCTACTAGTTACATA
P30	AAACTATGTAAC TAGTAGCTGTAC

P31	TTTTTTATAATGTAAAAATAAAGGG
P32	TATATGAATTACAAATATTGCATAAAG
P33	ACAGTTGGTGGGGTTTTCTC
P34	GAGAAAACCCACCAACTGT
P35	CCTGCATCACCAACTACCTT
QC1	TGCAGATGCAGGTTGACCATGGG
QC2	ACGCGCTAATATGTTAAGCA

Chapter 3

Results, Discussion and Future Directions

This chapter provides comprehensive account of results obtained for the objectives laid out in the study. All three objectives of the study have been provided with an introduction (a literature review) followed by results and discussion. First objective of the study was to generate transgenic *Plasmodium* lines expressing an alternate pathway for AMP synthesis to facilitate decoupling of AMP synthesis from fumarate production. Since adenosine kinase mediated purine salvage dominates in other apicomplexan parasites, we chose this enzyme to bypass HG(X)PRT mediated AMP synthesis in *Plasmodium falciparum* and *Plasmodium berghei*. Transgenic parasites expressing yeast adenosine kinase were generated, validated and used for further studies. Attempts were made to knock-out and knock-down enzymes of endogenous AMP synthesis pathway using available gene disruption techniques such as double-crossover homologous recombination, CRISPR-Cas9 and conditional protein knock-down via DHFR degradation domain-trimethoprim combination (Muralidharan et al. 2011). In *P. berghei* transgenic parasites, ASL knock-out was attempted using pJAZZ construct procured from Plasmogem. Despite considerable efforts and use of different strategies, desired gene knock-outs could not be obtained in either *P. falciparum* or *P. berghei* parasites, metabolically rewired to express an alternate AMP synthesis enzyme, suggesting that ADSS/ASL mediated AMP synthesis and perhaps fumarate production are indispensable to the parasite during asexual life-cycle. We also used a chemical genetics approach and inhibited AMP synthesis via adenylosuccinate synthetase using hadacidin. Growth phenotypes of transgenic parasites in presence and absence of hadacidin were analysed. Discussion includes succinct account of key results, future experiments, and analysis of failure to obtain desired gene knock-outs. At the end of this chapter, our attempts to standardize metabolomics with *P. falciparum* culture have been detailed.

3. Results, Discussion and Future Directions

3.1. Results

3.1.1. Generation and Validation of *P. falciparum* line expressing alternative purine salvage enzyme

Introduction

Import of purines and the purine salvage pathways in parasitic protozoa:

Parasitic protozoa are purine auxotrophs. Whether parasitism preceded the loss of purine *de novo* synthesis or loss of certain metabolic pathways led the way to parasitism is a matter of discussion (Armenta-Medina et al., 2014; Coyne et al., 2011; Jackson et al., 2016; Janouskovec and Keeling, 2016). Biosynthesis of purine ring is energetically expensive as the synthesis of one nucleotide requires approximately 50 molecules of ATP, considering the cost of synthesis of phosphoribosyl pyrophosphate and amino acids required for building purine ring structure. (Lynch and Marinov, 2015). Salvage pathways on the other hand, permit use of preformed nucleobases and nucleosides imported by parasites from the host cytosol and their conversion into nucleotides in relatively fewer steps. In Apicomplexan parasites, the majority of purine salvage is known to occur via adenosine kinase (AK) and hypoxanthine guanine phosphoribosyltransferase (HGPRT) with a minor contribution from adenine phosphoribosyltransferase (APRT) in few parasitic protozoa (Boitz and Ullman, 2006). However, in *Plasmodium spp.* parasites, the functional redundancy of purine salvage is eliminated by the lack of AK and APRT - confirmed by absence of these genes from the genome of parasites - and synthesis of adenine and guanine nucleotides is brought about solely through HGPRT (Fig. 3.1).

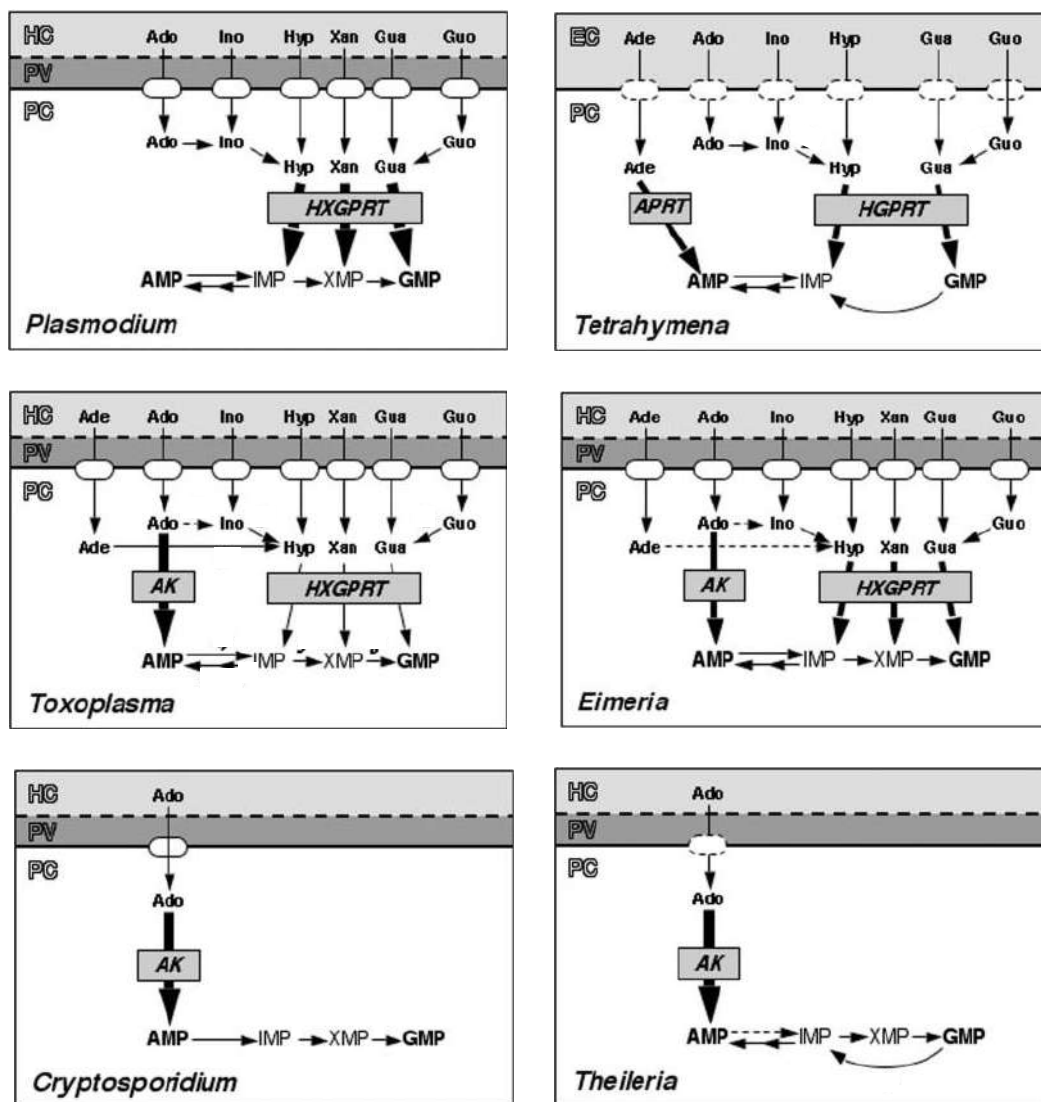


Figure 3.1: Overview of purine salvage pathways in Apicomplexan parasites. Besides *Tetrahymena* and *Plasmodium*, all other Apicomplexan organisms salvage purine via adenosine kinase. *Tetrahymena* possess APRT in addition to HG(X)PRT and can salvage adenine nucleotides via both the reactions. Image reproduced from Chaudhary, Kshitiz, John A. Darling, Leah M. Fohl, William J. Sullivan, Robert G K Donald, Elmer R. Pfefferkorn, Buddy Ullman, and David S. Roost. 2004. "Purine Salvage Pathways in the Apicomplexan Parasite *Toxoplasma Gondii*." *Journal of Biological Chemistry* 279 (30): 31221–27 (Chaudhary et al. 2004) with permission. Abbreviations: Ade, adenine; Ado, adenosine; Ino, inosine; Hyp, hypoxanthine; Xan, xanthine; Gua, guanine; Guo, guanosine.

The human host erythrocytes themselves lack the *de novo* purine synthesis pathway, importing preformed nucleobase / nucleosides from plasma (Fig. 3.2). The import is facilitated by two kinds of transporters: human equilibrative nucleoside transporter (hENT1) and human facilitative nucleobase transporter (hFNT1) of which, the former mediates import of adenosine while the latter imports hypoxanthine (Quashie, Ranford-Cartwright, and De Koning 2010). Parasite plasma membrane (PPM) harbours PfNT1 which mediates purine transport inside to the parasite, predominantly transporting hypoxanthine, adenosine and inosine while also displaying substrate specificity towards xanthosine, guanine and guanosine (Bissati et al. 2008).

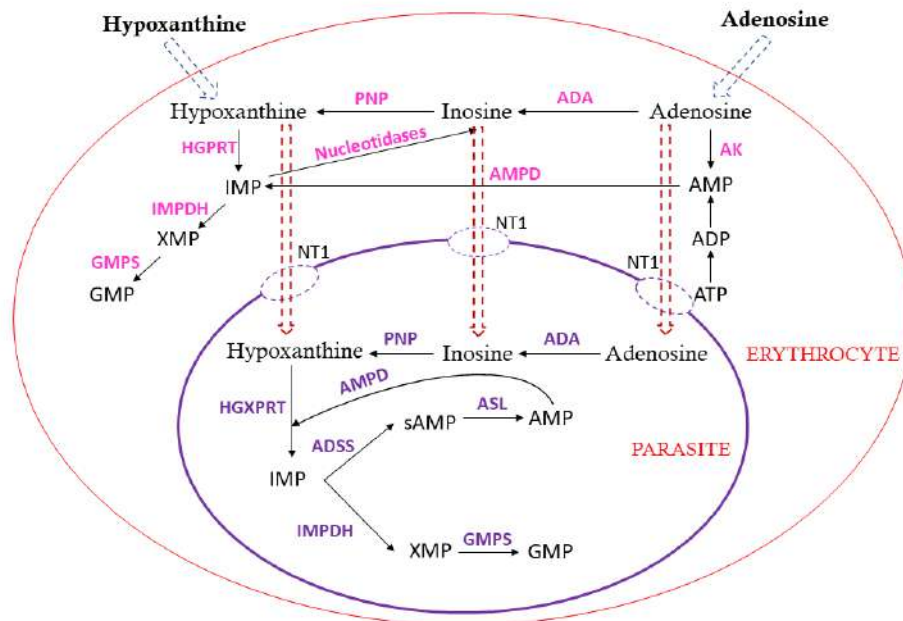


Figure 3.2: Purine nucleotide metabolism in parasite-infected erythrocyte. Schematic representation of purine nucleotide metabolism in erythrocytes and *Plasmodium* parasite compartments. Mature human erythrocytes are incapable of synthesizing purine rings de novo and therefore rely on salvage of preformed nucleobases/ nucleosides from plasma via human equilibrative nucleoside transporter (hENT1) and human facilitative nucleobase transporter (hFNT1). Parasite-infected erythrocytes uptake twice as much purine as compared to uninfected erythrocyte and adenosine uptake is higher as compared to hypoxanthine (Quashie et al. 2010). Adenylate nucleotides are synthesized via adenosine kinase whereas guanine nucleotides are synthesized via HGPRT/IMPDH/GMPS reactions. Parasites take up purine nucleobases/nucleosides from host erythrocytes via the PfNT1 transporter that demonstrates specificity for hypoxanthine, adenosine and inosine. Other nucleobases/nucleosides such as xanthosine, guanine and guanosine are also transported by PfNT1 but they contribute minimally towards AMP/GMP production and hence are not shown in the schematic. IMP is a nodal nucleotide from which both AMP and GMP can be synthesized. Abbreviations: ADSS, adenylosuccinate synthetase; ASL, adenylosuccinate lyase; AMPD, AMP deaminase; GMP, guanosine monophosphate; NK, nucleoside kinase; HG(X)PRT, hypoxanthine guanine (xanthine) phosphoribosyltransferase; IMP, inosine 5'-monophosphate; ADA, adenosine deaminase; PNP, purine nucleoside phosphorylase; XMP, xanthosine-5'-monophosphate; sAMP, succinyl AMP; IMPDH, IMP dehydrogenase; GMPS, GMP synthetase; AK, adenosine kinase. Erythrocyte enzymes are shown in pink and parasite enzymes are shown in purple. Dashed blue arrows indicate transport into the erythrocyte, dashed red arrows indicate transport into the parasite.

Purine salvage in *P. falciparum* is majorly driven by hypoxanthine since depletion of hypoxanthine upon addition of xanthine oxidase, enzyme that converts hypoxanthine to uric acid, has been shown to inhibit parasite growth *in-vitro* (Berman and Human 1991; Berman, Human, and Freese 1991). Adenosine is also transported via a separate low affinity transporter besides PfNT1 (Quashie et al. 2008) and can be readily deaminated by adenosine deaminase (ADA) to inosine; inosine is phosphorylated by purine nucleoside phosphorylase (PNP) to hypoxanthine. PfPNP additionally displays substrate specificity towards guanosine (Daddona et al. 1986), converting it to guanine which can be utilised by PfHG(X)PRT but guanosine intake and utilization contributes only a minor flux. *P. falciparum* HGPRT is referred to as HG(X)PRT as it can also catalyse phosphoribosylation of xanthine (Keough et al.

1999). The enzyme catalyses transfer of phosphoribosyl group from phosphoribosyl pyrophosphate (PRPP) to N9 of hypoxanthine, generating inosine 5' monophosphate (IMP) that serves as a nodal point from which both adenosine 5' monophosphate (AMP) and guanosine 5' monophosphate (GMP) are formed. Adenylate nucleotides are generated via adenylosuccinate synthetase/lyase (ADSS/ASL) reactions from inosine 5' monophosphate (IMP) whereas guanylate nucleotides are generated via IMP dehydrogenase/ GMP synthetase (IMPDH/GMPS) reactions (Fig. 3.3). Deamination of AMP back to IMP is catalysed by AMP deaminase (AMPD). ADSS, ASL and AMPD reactions carry out cyclic interconversion of IMP and AMP via a pathway termed purine nucleotide cycle (PNC) (Fig. 3.3)

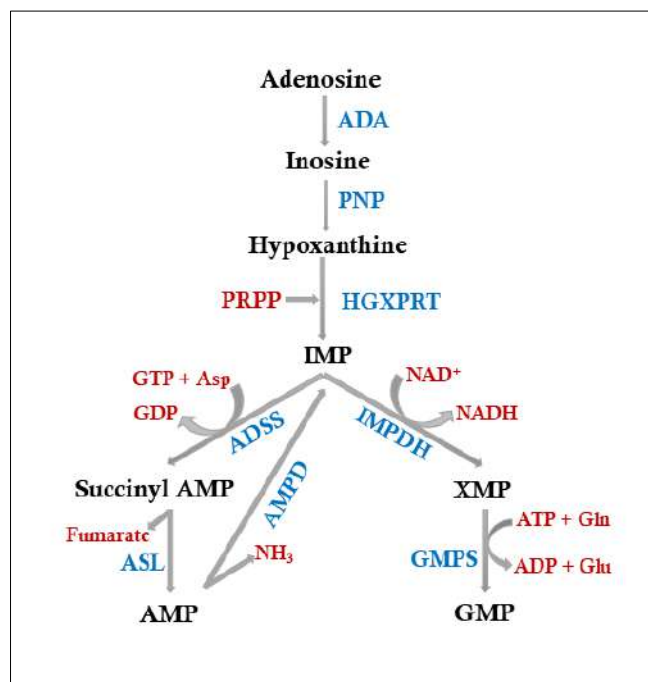


Figure 3.3: Purine nucleotide synthesis in *Plasmodium falciparum* parasite. The schematic represents details of AMP and GMP synthesis in *Plasmodium* parasites. IMP is a nodal intermediate that can be utilized either by ADSS or IMPDH priming it for AMP and GMP synthesis, respectively. During AMP synthesis, one molecule of GTP is utilized, bringing the tally of high energy molecules used by pathway of AMP synthesis to 3 (PRPP, ATP, GTP), making the pathway energy expensive. Abbreviations: Asp, aspartate; Gln, glutamine; Glu, glutamate, NAD, nicotinamide adenine dinucleotide; PRPP, phosphoribosyl pyrophosphate; AMPD, AMP deaminase. Enzymes are denoted in blue, pathway intermediates in black and co-substrates/by-products are denoted in red colour.

The retention of HG(X)PRT and absence of the AK gene in Plasmodia is intriguing as AMP generation from AK is rather energy efficient with only one molecule of ATP utilized to convert a molecule of adenosine into AMP in a one-step reaction: $\text{adenosine} + \text{ATP} \xrightarrow{\text{AK}} \text{AMP} + \text{ADP}$

On the other hand, the precursor hypoxanthine required for HG(X)PRT reaction should be imported from host erythrocyte cytosol wherein its abundance is low and erythrocytes themselves salvage hypoxanthine from plasma. Alternatively, hypoxanthine can be generated within parasite from adenosine imported from host as explained above, although adenosine concentration in plasma is also shown to be low (<1 μM) (Plagemann, Wohlhueter, and Kraupp 1985). HG(X)PRT reaction utilizes phosphoribosyl pyrophosphate (PRPP) that is formed from ribose-5-phosphate and ATP - generation

of substrate itself involves utilization of a molecule of ATP. The subsequent ADSS/ASL reactions utilize GTP and aspartate and as generation of GTP itself requires ATP, the whole pathway (HGXPRT/ADSS/ASL) becomes more energy consuming than the AK reaction. Among various Apicomplexan parasites, AK is retained in all except *Plasmodium* and *Tetrahymena* (Fig. 3.1). *Tetrahymena spp.* is the only Apicomplexan that expresses an adenine phosphoribosyltransferase (APRT), although this route of AMP synthesis is non-essential and redundant (Akematsu et al., 2018).

Conservation of HG(X)PRT in *Plasmodium spp.* could be significant as fumarate is generated as a by-product in the adenylosuccinate lyase reaction, (Fig. 3.3) that leads to formation of AMP. A functional purine nucleotide cycle (PNC) that interconverts AMP and IMP (Fig. 3.3) can further amplify the production of fumarate in the parasite. In mammalian cells, fumarate is generated via multiple routes: as a by-product during urea cycle, as a breakdown product of tyrosine metabolism and as a by-product of the purine nucleotide cycle. In *Plasmodium* parasites, which lack amino acid metabolism, fumarate is only produced via two routes and funnelled into TCA cycle: through ADSS/ASL pathway and through glutamine (glutamine → glutamate → α -ketoglutarate - that is channelled into TCA), apart from the canonical pyruvate that is fed into TCA. Carbon flux through TCA is minimal during intra-erythrocytic stages of parasite life cycle (Bulusu et al., 2011; MacRae et al. 2013; Olszewski et al. 2010), in the context of which, anaplerosis of TCA metabolites could be essential for maintaining homeostasis of cellular energy metabolism. Therefore, PNC generated fumarate could be a plausible link between nucleotide and energy metabolism within the parasites of genus *Plasmodium* (Jayaraman et al., 2012).

Objectives of the study

With this background information, we sought to understand the contribution of fumarate produced in ADSS/ASL reactions to the overall metabolism of *Plasmodium*. To do so, it was essential to either decrease or completely abolish fumarate production via ADSS/ASL reactions. Since HG(X)PRT mediated purine salvage is the singular route of AMP synthesis in *Plasmodium spp.*, a complete knock-out of either adenylosuccinate synthetase or adenylosuccinate lyase from wild type parasites would be lethal; therefore, generation of a transgenic parasite line expressing an alternate pathway of AMP synthesis (one independent of fumarate generation) was essential. As mentioned earlier, adenosine kinase mediated AMP synthesis is a common route in many Apicomplexans; hence, yeast AK (yAK) was heterologously expressed in the parasites.

A similar approach was adopted by Painter and co-workers to show that the only function of *Plasmodium* mitochondrial electron transport chain is regeneration of ubiquinone, which is required as an electron acceptor by the enzyme dihydroorotate dehydrogenase (DHODH). The authors generated transgenic *P. falciparum* parasite line expressing *Saccharomyces cerevisiae* dihydroorotate dehydrogenase that uses fumarate instead of ubiquinone as an electron acceptor and studied the susceptibility of transgenic parasites to inhibitors of mitochondrial electron transport chain such as atovaquone (Painter et al. 2007). Few other studies also demonstrate that yeast genes can be successfully cloned and

expressed in *Plasmodium* and are fully functional (Ganesan et al., 2011; De Koning-Ward et al., 2000a; Maier et al., 2006). We chose Adenosine kinase (*ADO1*) gene from *Saccharomyces cerevisiae* for transgenic episomal expression in *Plasmodium falciparum* and *Plasmodium berghei*.

Efficacy of genetic manipulation in *P. falciparum* and *P. berghei*

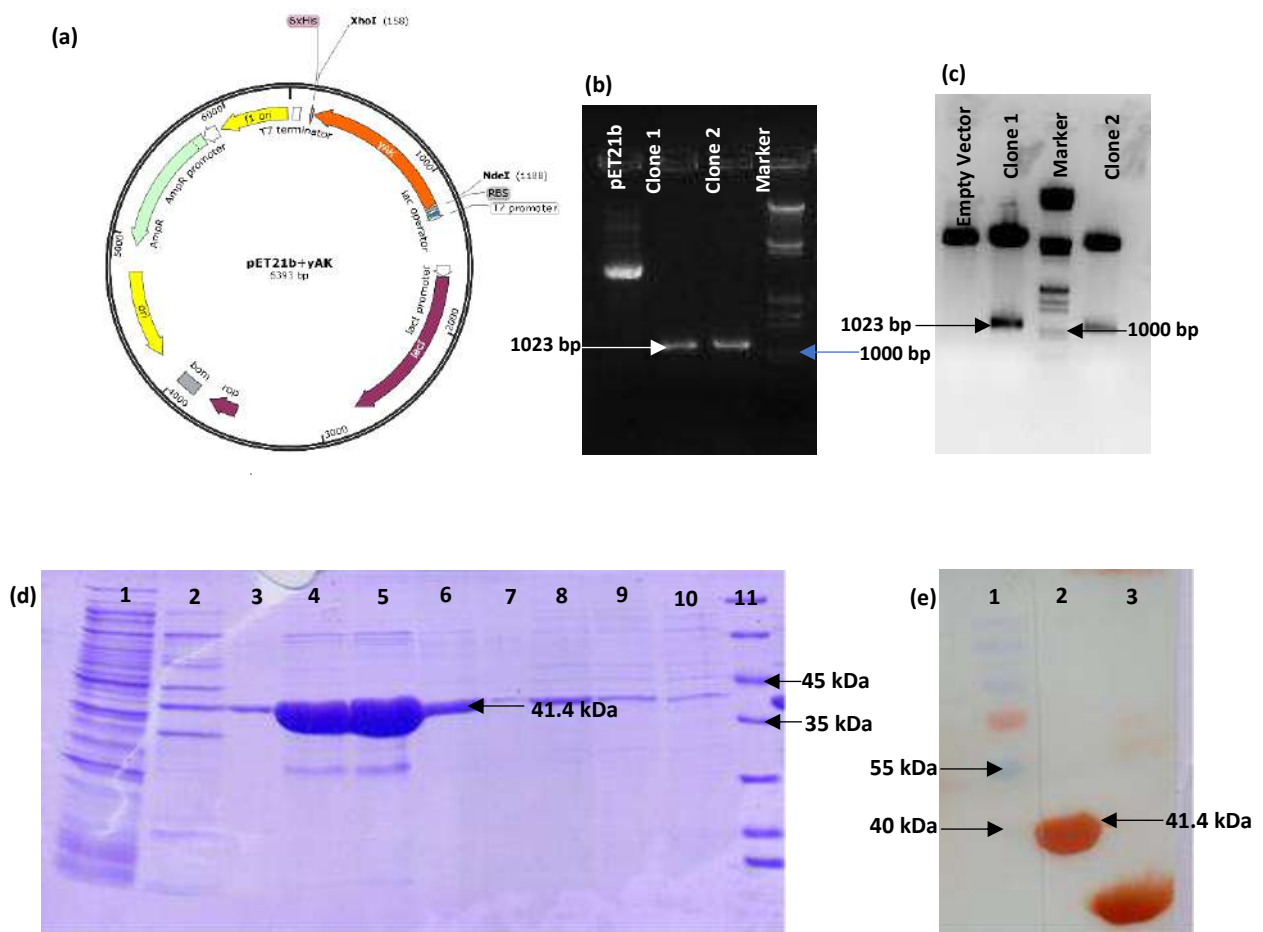
Although, the genomes of both *P. falciparum* and *P. berghei* are haploid, genetic manipulations work with better efficiency in rodent malaria parasite, *P. berghei* as compared to human malaria parasite, *P. falciparum*. This difference in efficiency of genetic manipulations between these two species could be attributed to the differential intra-erythrocytic developmental time in the respective hosts. The total duration of the asexual blood stage development is 22-24 hours in case of *P. berghei* and 48 hours in case of *P. falciparum* parasites. The transfection efficiencies of *P. falciparum* are in the range of 10^{-6} - 10^{-8} whereas advent of nucleofector technology has accorded high transfection efficiencies of 10^{-2} to 10^{-3} in *P. berghei* (Janse et al., 2006). Therefore, all genetic manipulations that were performed in *P. falciparum* to investigate the significance of fumarate to the overall metabolism of the asexual stages, were replicated in *P. berghei*. Paucity of robust positive selectable markers for *P. berghei* restricts the ability to carry out sequential genetic manipulations on the same parasite (de Koning-Ward, et. al., 2015). Only three selectable markers are available for *P. berghei*: human dihydrofolate reductase (DHFR), mutant forms of bifunctional DHFR–thymidylate synthase (*dhfr-ts*) from *Toxoplasma gondii* and *P. berghei*. The modified *P. berghei* *dhfr-ts* gene harbours Ser110→Asn mutation that makes it resistant to pyrimethamine (van Dijk et al. 1994) (unlike wild type *P. berghei* *dhfr-ts* which is pyrimethamine-sensitive) and the modified *T. gondii* *dhfr-ts* gene harbours similar mutations that render it pyrimethamine resistant (Donald and Roos 1993) (unlike wild type *T. gondii* *dhfr-ts* which is pyrimethamine-sensitive). All three of these markers confer resistance to pyrimethamine, but only human DHFR confers resistance to the drug WR99210 as well (Koning-ward et al., 2000). Therefore, for sequential genetic manipulation in *P. berghei*, the parasites must be first transfected with plasmid vectors containing Tg or Pb *dhfr-ts*, transgenic parasites selected with pyrimethamine, followed by transfection with plasmid vector containing hDHFR and selection with WR 99210 (De Koning-Ward et al. 2000). This strategy was followed in the current study for achieving transgenic expression of yeast adenosine kinase (using Tg*dhfr-ts* selection marker) and subsequently to knock out adenylosuccinate lyase (using hDHFR selection marker) in the same parasites. The results obtained for aforementioned study objectives are detailed in the following sections.

Results

3.1.1.1. Cloning, expression, purification and activity check of recombinant yAK

Prior to expression in *P. falciparum* and *P. berghei*, we verified the activity of recombinant yeast adenosine kinase *in-vitro*. *ADO1* gene of *S. cerevisiae*, coding for adenosine kinase was cloned in pET21b plasmid in-frame with C-terminal 6x His tag (Fig. 3.4 a). Plasmid constructs were verified by colony PCR, insert release (Fig. 3.4 b, c) and DNA sequencing. *E. coli* Rosetta competent cells were

transformed with a confirmed pET21b-yAK plasmid, recombinant protein was expressed and purified by Ni-NTATM affinity chromatography and confirmed by Western-blotting using anti-His antibodies (Fig. 3.4 d-e). An assay mix containing adenosine and [γ -³²P]-ATP was used to evaluate the activity of the enzyme. yAK catalyses the transfer of γ -phosphate of ATP onto adenosine, converting the later to [α -³²P]-AMP. The reaction mix was spotted onto thin layer chromatography plate that was placed in mobile phase consisting of mixture of 1-butanol, glacial acetic acid and water (50: 25: 25). Upon separation of reaction components on TLC, spot corresponding to [α -³²P]-AMP was observed (Fig. 3.4 f) confirming the activity of recombinant yAK. Free ³²P_i was also seen on TLC plates which could arise from dephosphorylation of AMP catalysed by contaminating nucleotidases in the protein preparation.



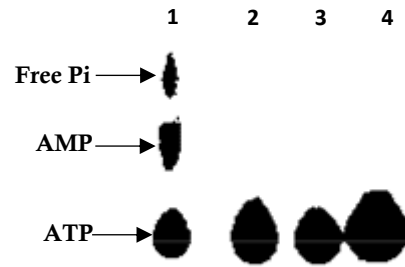


Figure 3.4: pET21b-yAK clone confirmation, recombinant protein expression and validation, in-vitro activity evaluation of recombinant yAK (a) Plasmid map of yAK cloned in pET21b generated using SnapGene Viewer. (b) Colony PCR confirming presence of yAK gene in clones. Two clones tested positive by PCR with gene specific primers. (c) Insert release from clones upon digestion with NdeI/XhoI showed fragment of correct size (1023 bp) (d) Recombinant protein purified by Ni-NTA was examined by SDS-PAGE (12 % gel). lane 1, cell lysate; lane 2, 20 mM imidazole wash; lane 3, spill-over from 4th well; lane 4, 250 mM imidazole elute 1; lane 5, 250 mM imidazole elute 2, lane 6, 250 mM imidazole elute 3; lane 7, 250 mM imidazole elute 4; Lane 8, 500 mM imidazole elute 1; lane 9, 500 mM imidazole elute 2, lane 10, 1000 mM imidazole elute 1, lane 11, protein molecular mass marker (e) Western-blotting using anti-His antibody. lane 1, pre-stained protein molecular mass marker; lane 2, purified recombinant yAK; lane 3, positive control for primary antibody. (f) Activity of purified yAK was checked by thin layer chromatography using adenosine and $[\gamma\text{-}^{32}\text{P}]\text{-ATP}$ as substrates. Reaction of recombinant yAK was monitored-by following the transfer of γ - phosphate of $[\gamma\text{-}^{32}\text{P}]\text{-ATP}$ onto adenosine, generating $[\alpha\text{-}^{32}\text{P}]\text{-AMP}$ - on TLC. Free $^{32}\text{P}_i$ seen in lane 1 could be due to contaminating nucleotidases (from *E. coli* lysate) in the protein preparation. lane 1, reaction mix containing recombinant yAK; lane 2, 3, reaction mix without yAK; lane 4, $[\gamma\text{-}^{32}\text{P}]\text{-ATP}$.

3.1.1.2. Generation and confirmation of transgenic *P. falciparum* parasites expressing yAK

Plasmid vector pFCENv2 was chosen for the episomal expression of yeast adenosine kinase in *P. falciparum* as it contains a centromeric sequence from *Plasmodium spp.* that ensures efficient segregation (>99 %) of the plasmid during each life cycle in all merozoites. This would ensure uniform and constitutive expression of the yAK protein. The expression of the transgene is driven by calmodulin (5' CAM) promoter and the cells harbouring the plasmid gain resistance against blasticidin (BSD) (Iwanaga et al. 2012). pFCENv2-yAK plasmid that would express C-terminal HA tagged yAK was generated as described in Materials and Methods. *Plasmodium falciparum* 3D7 parasites were transfected with the confirmed plasmid clone (Fig. 3.5 a) by two methods, viz., pre-loading of erythrocytes with DNA followed by parasite infection and direct transfection of ring-stage parasites, both using Bio-Rad electroporator (Skinner-Adams et al. 2003). Details of the protocols used are described in the Methods section (Chapter 2). Simultaneously, parasites were also transfected with empty vector (EV) i.e., plasmid vector pFCENv2 without yAK using both transfection methods used for pFCENv2-yAK to be used as drug resistant control during subsequent experiments. Blasticidin (at a concentration of $2.5 \mu\text{g ml}^{-1}$) was administered 48 hours post transfection and drug resistant parasites were obtained 25-40 days post transfection for both pFCENv2-yAK and pFCENv2-EV. DNA was isolated from transgenic parasites, *P. falciparum* 3D7^{yak} and *P. falciparum* 3D7^{EV}, and used as a template in PCR (performed using yAK specific primers, PI/PII, Table 2.3) to confirm presence of yAK in *P. falciparum* 3D7^{yak}. Expression of protein was confirmed by Western blotting (Fig. 3.5 c) using anti-HA antibodies.

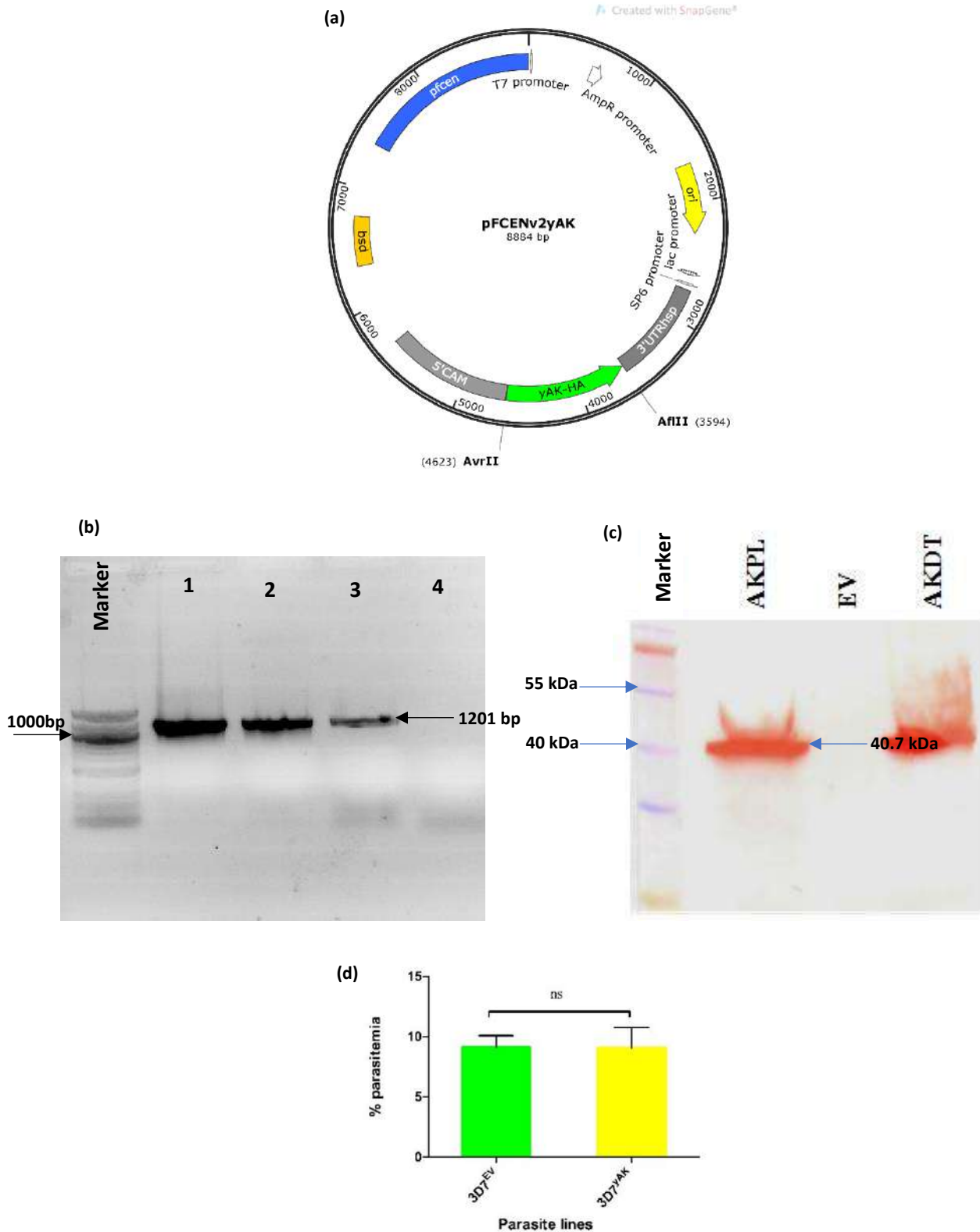


Figure 3.5: Confirmation of transgenic *P. falciparum* parasites expressing yAK. (a) Vector map of pFCENV2-yAK plasmid clone transfected in *P. falciparum*. Abbreviations: pfcen, *P. falciparum* centromeric fragment; bsd, blasticidin; 5' CAM, calmodulin promoter; 3'UTRhspl, 3' untranslated region of heat shock protein gene; ori, origin. (b) PCR performed using yAK specific primers confirmed the presence of pFCENV2-yAK in drug resistant parasites. lane 1, positive control (PCR using yeast genomic DNA as template); lane 2, PCR using DNA isolated from transgenic parasites obtained by the pre-loading transfection (AKPL) method as template; lane 3, PCR using transgenic parasites obtained by the ring stage direct transfection (AKDT) method as template; lane 4, Transgenic parasites obtained by transfection of vector control (empty vector, EV). Lane labelled as 'Marker' contains 1 Kbp DNA marker. (c) Western blotting performed using anti-HA antibody confirmed the expression of

yAK (tagged with HA tag at C terminus) in the *P. falciparum* 3D7^{yAK} transgenic parasites. lane 1, protein molecular mass marker; lane 2, transgenic parasites obtained by pre-loading transfection (AKPL) method; lane 3, transgenic parasites obtained by transfection of vector control (empty vector, EV); lane 4, transgenic parasites obtained by ring stage direct transfection (AKDT) method (d) Growth phenotypes of both parasite lines, 3D7^{EV} and 3D7^{yAK}, were found to be similar in routine culture conditions in presence of 100 μ M hypoxanthine and blasticidin (2.5 μ g ml⁻¹). Shown is the bar graphs comparing % parasitemia values of 3D7^{EV} and 3D7^{yAK} at 48 hours (starting culture condition, 1 % parasitemia, 2 % haematocrit). Experiment was performed in duplicate. p value = 0.9750 with two-tailed student's t test. Graph plotted using GraphPad Prism 5.0

Growth phenotypes of *P. falciparum* 3D7^{yAK} and 3D7^{EV} were found to be similar in routine cultures supplemented with 100 μ M hypoxanthine as purine source and blasticidin (2.5 μ g ml⁻¹) as selection marker (Fig. 3.5 d). Both parasite lines completed one life cycle in ~ 48 hours with similar fold-increase in parasitemia; indicating that expression of a heterologous yeast adenosine kinase or presence of blasticidin in the culture media did not alter growth and replication pattern of the parasites.

3.1.1.3. Generation and confirmation of transgenic *P. berghei* parasites expressing yAK

Similar to pFCENv2-yAK plasmid vector, a construct was generated for episomal expression of yAK in *P. berghei* ANKA strain of parasites using Plasmodium Artificial Chromosomes (PAC) developed by Iwanaga and co-workers. PACs contain centromere of chromosome 5 of *P. berghei*, pbcen5, that confers improved segregation efficiency to episomal plasmids. The expression of the transgene is driven by a *P. berghei* EF1 α promoter whereas selection of transgenic parasites is mediated through *Toxoplasma gondii* dhfr-ts (Tgdhfr-ts), a positive selection marker that confers resistance to pyrimethamine, expression of which is driven by *P. berghei* dhfr-ts promoter (Iwanaga et al. 2010). pbCEN5-yAK clones that contain yAK tagged with HA at the C-terminus (Fig. 3.6 a) were confirmed by insert release and DNA sequencing after which wild type *P. berghei* ANKA parasites were transfected with the confirmed clone using the protocol described earlier (Janse et al. 2006)(described in detail in the Methods, Chapter 2). Drug resistant parasites were obtained 7 days post transfection and were confirmed for presence of yAK gene via PCR (Fig. 3.6 b). Protein expression was confirmed by Western-blotting analysis using anti-HA antibodies (Fig. 3.6 c). *P. berghei* ANKA^{yAK} parasites showed growth phenotype similar to the wild type parasites suggesting that expression of heterologous yeast adenosine kinase does not affect the growth and replication pattern of the transgenic parasites.

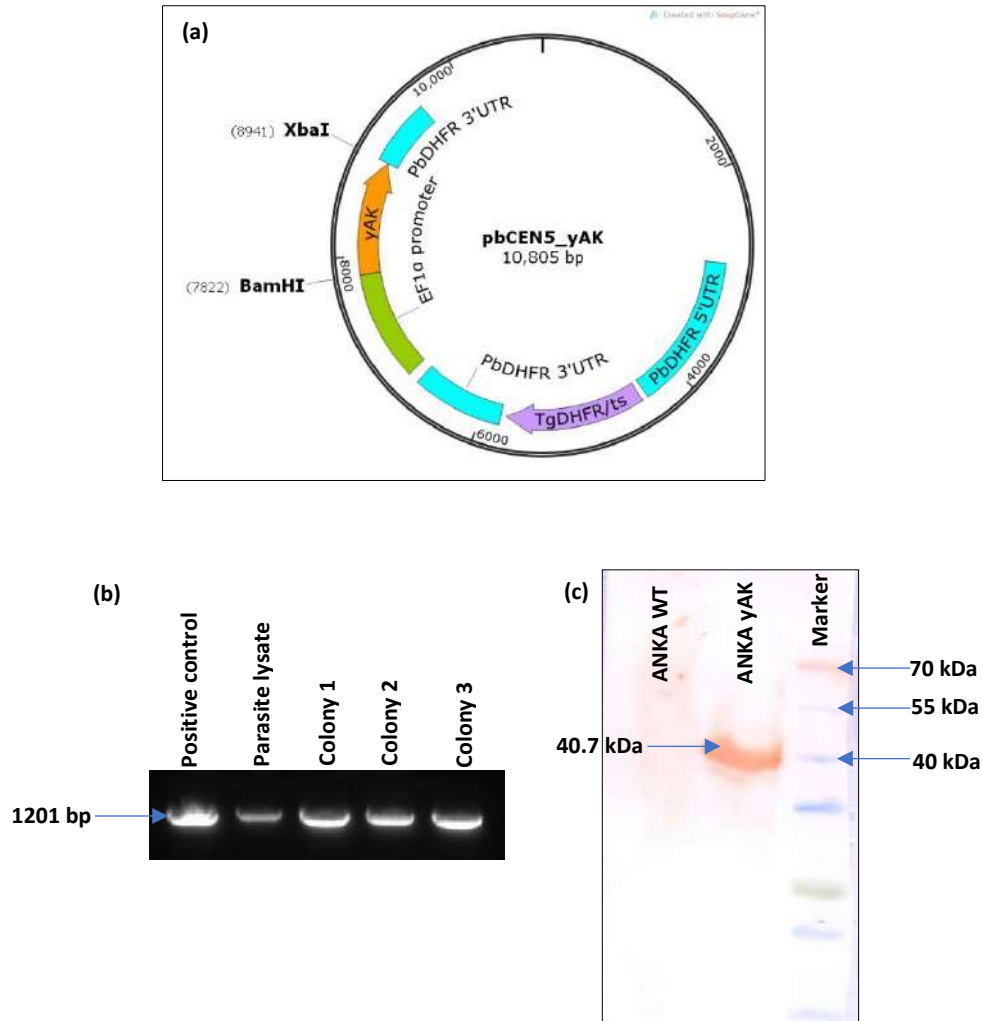


Figure 3.6: Confirmation of *P. berghei* parasites expressing yAK. (a) Vector map of pbCEN5-yAK transfected in *P. berghei* for episomal expression of yeast adenosine kinase. Abbreviations: Tgdhfr-ts, *Toxoplasma gondii* dihydrofolate reductase-thymidylate synthase bifunctional gene; PbDHFR-5'UTR, 5' untranslated region of *P. berghei* DHFR; PbDHFR-3'UTR, 3' untranslated region of *P. berghei* DHFR gene. (b) Drug resistant parasites were isolated from mouse erythrocytes and lysed by heating to release cellular contents. The parasite lysate was used as template for PCR (with yAK cloning primers, P27/P28, Table 2.3) wherein amplicon of correct size was observed. Some amount of lysate was transformed into *E. coli* DH5 α competent cells and (ampicillin resistant) colonies obtained were screened for presence of pbCEN5-yAK plasmid through PCR. All colonies obtained answered positive for presence of yAK amplicon. (c) Western blotting was performed using anti-HA antibody at 1:3000 titre and parasite lysate of ANKA^{yAK} (lane 2) showed protein band of expected size, while parasite lysate of ANKA^{WT} (lane 1) did not pick up any band on Western blot.

These two newly generated parasite lines are valuable reagents that can be used to abolish fumarate generation through ADSS/ASL pathway and study its impact on the overall parasite metabolism. One approach (to abolish fumarate production) is to knock out one of the two genes, *asl* or *adss*. Deletion of ADSS, catalysing the first step of conversion of IMP to sAMP, would eliminate substrate for the subsequent ASL reaction that generates fumarate. Attempts were made to knock out both *adss* and *asl* genes from genome of *P. falciparum* 3D7^{yAK} and to knock-out *asl* from the genome of *P. berghei* ANKA^{yAK}.

3.1.2. Attempts of gene(s) disruption in *P. falciparum* and *P. berghei*

Introduction

The ability to perform genetic manipulations in both *P. berghei* and *P. falciparum* parasites has improved significantly in last three decades, from the time when first transfections were attempted (Van Dijk et al., 1995; Wu et al., 1995). Various technologies have been developed by different groups across the world. Figure 3.7 enlists the advancement of transfection and genetic manipulation techniques developed for *P. berghei* (shown in pink boxes) and *P. falciparum* (shown in blue boxes) in chronological fashion. The complete genome sequence of *P. falciparum* was published in 2002 by Gardner and co-workers (Gardner et al. 2002) which revealed that the haploid genome is distributed across 14 chromosomes amounting to 22.8 megabases (Mb) and ranging in size from approximately 0.643 to 3.29 Mb. *Plasmodium* genome is AT rich with overall (A+T) composition of 80.6 % that rises up to 90 % in intronic and intergenic regions. Approximately 5,300 protein-encoding genes were identified (Gardner et al. 2002).

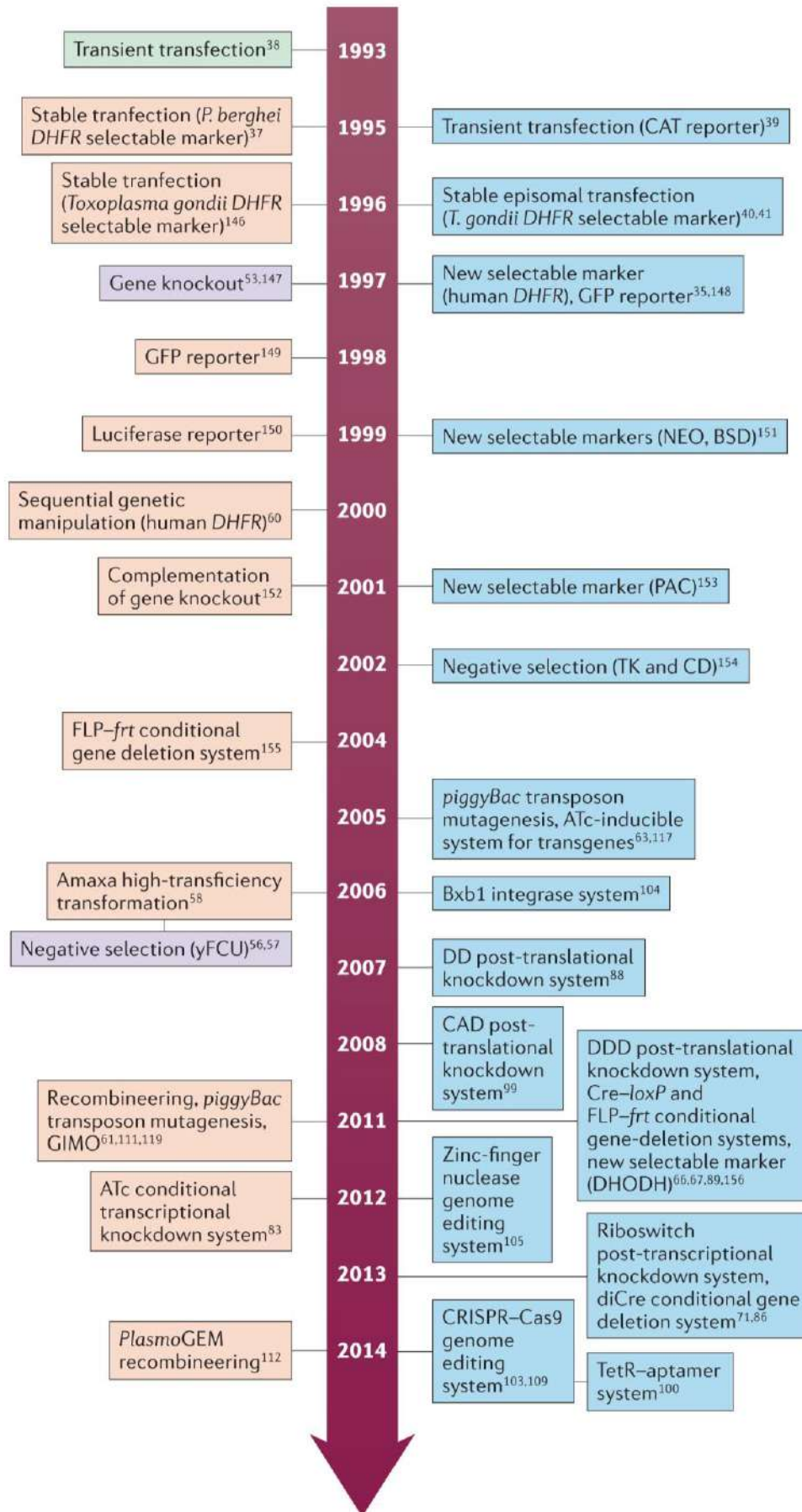


Figure 3.7: Transfection techniques developed for malaria parasites over last few decades. Technologies that are developed for *P. falciparum* are represented by blue boxes while technologies exclusive for *P. berghei* are represented in pink boxes. Purple boxes represent technologies that were developed and applied to both species. The first transient transfection was attempted in *P. gallinaceum* (shown in green box on top). Genetic manipulation techniques in Plasmodium parasites has evolved significantly in the last decade Image reproduced from Koning-Ward, Tania F. de, Paul R. Gilson, and Brendan S. Crabb. 2015. "Advances in Molecular Genetic Systems in Malaria." *Nature Reviews Microbiology* 13 (6): 373–87 with permission.

Genome editing techniques

Targeted gene disruptions are immensely helpful in delineating functions of genes and the associated proteins. In order to perform targeted gene disruption of the gene of interest (GOI) in *Plasmodium*, a homologous sequence(s) must be provided through a plasmid vector, since DNA breaks are repaired by means of homologous recombination (HR) in *Plasmodium spp.* Initially, 'single crossover' mediated integration of a selectable marker, a bifunctional protein, dihydrofolate reductase-thymidylate synthase (dhfr-ts), into the genome was developed (Crabb and Cowman, 1996; Wu et. al., 1996). That was followed by the development of plasmid constructs capable of undergoing 'double crossover' recombination. Two fragments of homology sequences that could undergo 'double crossover' homologous recombination at the genomic locus of the GOI were cloned on either side of a positive selection marker. Transgenic parasites carrying copies of these constructs into their genome (either by single or double crossover recombination) are generally selected by drug on and off cycles. But selection of transgenic parasites harbouring only the integrated copies of plasmids proves difficult due to persistence of episomal copies even after several rounds of drug (on and off) cycles. To get rid of episomes, which fail to undergo recombination and therefore genomic integration, negative selection marker was cloned in these vectors. Negative selection marker commonly used in *Plasmodium* is yFCU, a bifunctional protein with combined activities of yeast cytosine deaminase (CD) and uridyl phosphoribosyltransferase (UPRT) (Maier et al., 2006; Orr et. al., 2012). This chimeric protein is more potent (>1000 fold) than CD alone and this increased potency is due to a more efficient conversion of 5-fluoro cytosine (5-FC) into 5-fluoro uracil by CD with subsequent conversion of 5-fluoro uracil to 5-fluoro uridine monophosphate (5-fluoro-UMP) by the yUPRT (Maier et al. 2006). Addition of 5-FC to the growth media (for *P. falciparum*) or into the drinking water of mice (for *P. berghei*) kills the parasites harbouring episomal copies of the plasmids that express yFCU. Subsequent conversion of 5-fluoro-UMP into the toxic 5-fluoro-UTP and 5-fluoro-dUMP is catalysed by host cellular enzymes. 5-fluoro-UTP and 5-fluoro-dUMP are then incorporated into RNA and inhibit thymidylate synthase (Maier et al., 2006).

However, suboptimal transfections efficiencies in *P. falciparum* coupled with the extremely low probability of double crossover recombination made it a daunting task to obtain knock out of the target gene in this species. Several different transfection protocols have been developed to achieve higher transfection efficiencies. Most commonly followed transfection protocols in *P. falciparum* are transfection of ring stage parasites and transfection of uninfected erythrocytes followed by infection with schizont stage parasites (Hasenkamp et. al., 2012; Skinner-Adams et al., 2003). Recent studies demonstrated that electroporation of schizont stage *P. falciparum* parasites using Amaxa 4D

nucleofector (Lonza) improved transfection efficiencies (Ghorbal et al., 2014). Few other groups have also devised transfection protocols for different intra-erythrocytic stages of *P. falciparum* using Amaxa 4D nucleofector (Caro et al., 2012; Carrasquilla et al., 2019). In the same study, Ghorbal and co-workers also demonstrated electroporation of linearized plasmid construct in *P. falciparum* and found that desired transfectants were obtained in same time frame with both circular and linearized plasmid constructs (Ghorbal et al. 2014). But use of linearized plasmid eliminated the need to get rid of episomal plasmid copies (via negative selection), which is an important time saving advancement in itself.

Integration of plasmid construct in the genome via recombination is a chance event owing to stochastic occurrence of double-stranded breaks in the genome during DNA replication and repair. The chance of double-stranded breaks randomly occurring at the site of the gene of interest (for homologous recombination to take place with the sequence provided on the knock out construct) in the genome is low. Plasmid constructs containing homology sequences (such as pHHT1, pCC etc.) for recombination rely on this chance event and hence obtaining parasites with target gene deletion using these plasmid constructs is a time consuming process (Ganesan et al. 2011; Maier et al. 2006). To circumvent this issue, techniques were devised to intentionally introduce double stranded breaks in the genome (at the desired location) and trigger homology directed DNA repair.

i) Zinc Finger Nucleases (ZFNs)

The first one of these genome engineering techniques used in *Plasmodium* was Zinc Finger Nucleases (ZFNs) (Straimer et al. 2012). ZFNs are artificial restriction enzymes generated by fusing zinc finger DNA-binding domain to a DNA-cleavage domain (Carroll, 2011). The DNA binding domain (30 amino acids) typically contains between 3 and 6 individual zinc finger repeats and each repeat can recognize between 9-18 bp specifically. This assembly is combined with a DNA cleavage domain, which is essentially non-specific cleavage domain of type II restriction enzyme, FokI, generating a sequence specific DSB. The cleavage domain is an obligate dimer requiring two ZFs to target a non-palindromic DNA segment (Fig. 3.8) (Kim et al., 1996). Straimer and co-workers established an improved method of genome editing in *P. falciparum* using these ZFNs. The study demonstrated that parasites carrying the desired editing event could be obtained rapidly and with an efficiency that approached 100% in cases when the outcome yielded a selectable phenotype (Straimer et al. 2012).

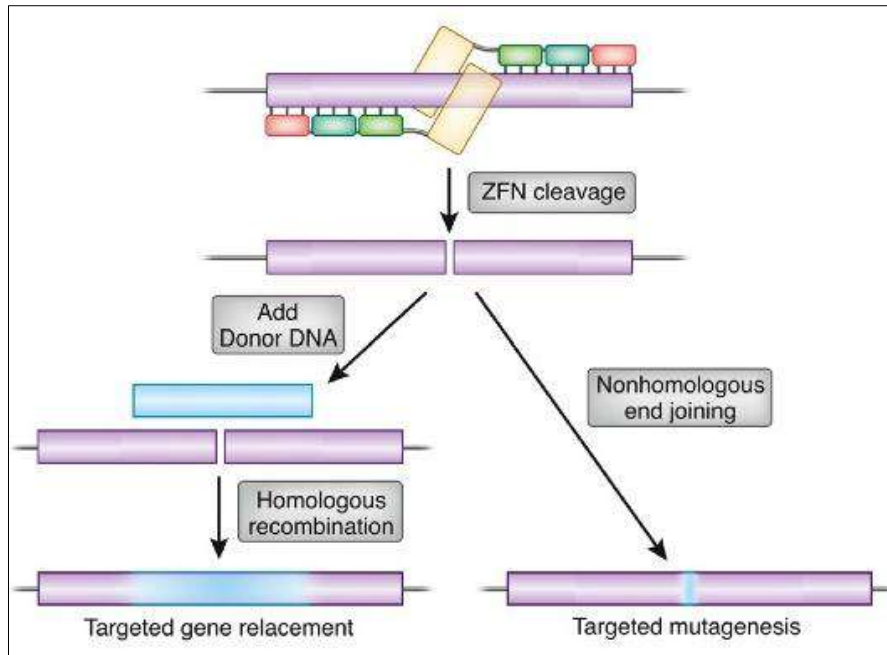


Figure 3.8: Schematic representation showing the workings of zinc finger nucleases. Pink, blue and green boxes represent zinc finger motifs that bind DNA in a sequence specific manner. These zinc fingers are associated with cleavage domain (represented as yellow box) that creates a single stranded DNA break; one on each strand by a single subunit of an obligate heterodimer. The DSB can be repaired either by non-homologous end joining pathway or homologous recombination depending upon the host organism. Image reproduced from Carroll, D. Genome engineering with zinc-finger nucleases. *Genetics Society of America*, 2011, 188(4), pp 773-782 with permission.

Although this technique is efficient, its use in the field of *Plasmodium* genetics is limited due to high cost and laborious design process.

ii) CRISPR-Cas9

Clustered Regularly Interspaced Short Palindromic Repeats (CRISPR) and CRISPR associated protein-9 (Cas9) is a bacterial and archaeal adaptive immune system that facilitates RNA-guided site specific DNA cleavage (Barrangou et al. 2007; El Beheiry et al. 2015; Bhaya, Davison, and Barrangou 2011; Cong et al. 2013; Cong and Zhang 2014). This adaptive defence system comprises of a multistep process by which small specific fragments of foreign DNA are first recognized as being non-self and then incorporated into the host genome between short DNA repeats. Subsequently, these fragments, also known as spacers, are transcribed and processed into small non-coding RNAs, which in conjunction with the host Cas proteins are used as surveillance and adaptive immune mechanism by which the incoming foreign DNA is recognized - if there is a close or absolute sequence match between the small RNA and incoming nucleic acid - and eventually destroyed or silenced (Bhaya et. al., 2011). CRISPR-Cas has a unique property that it can acquire new spacers and / or lose old spacers readily and can respond efficiently to viral predators that are also evolving at a high rate. This RNA guided nuclease system from *Streptococcus pyogenes* was harnessed to introduce double-stranded breaks in mammalian and many other eukaryotic systems by expression of its key components: *SpCas9*, RNA-guided DNA endonuclease; *tracrRNA*, tracer RNA which binds to Cas9 nuclease and *crRNA*,

CRISPR RNA that contains the 20 nucleotide sequence that guides the nuclease to the target locus (Cong et al., 2013). A chimeric hybrid of tracrRNA and mature crRNA (tracrRNA:crRNA duplex) was generated which was found to be as effective as the individual RNAs and is termed 'single guide' RNA (sgRNA) (Jiang and Doudna 2017). The target DNA site needs to be flanked by a protospacer adjacent motif (PAM) sequence, which in case of *S. pyrogenes* is 5'-NGG-3'. PAM sequence serves as binding signal for Cas9 and presence of this sequence flanking the target site is obligatory for Cas9 mediated double-stranded break generation (Fig. 3.9) (Anders et al., 2014).

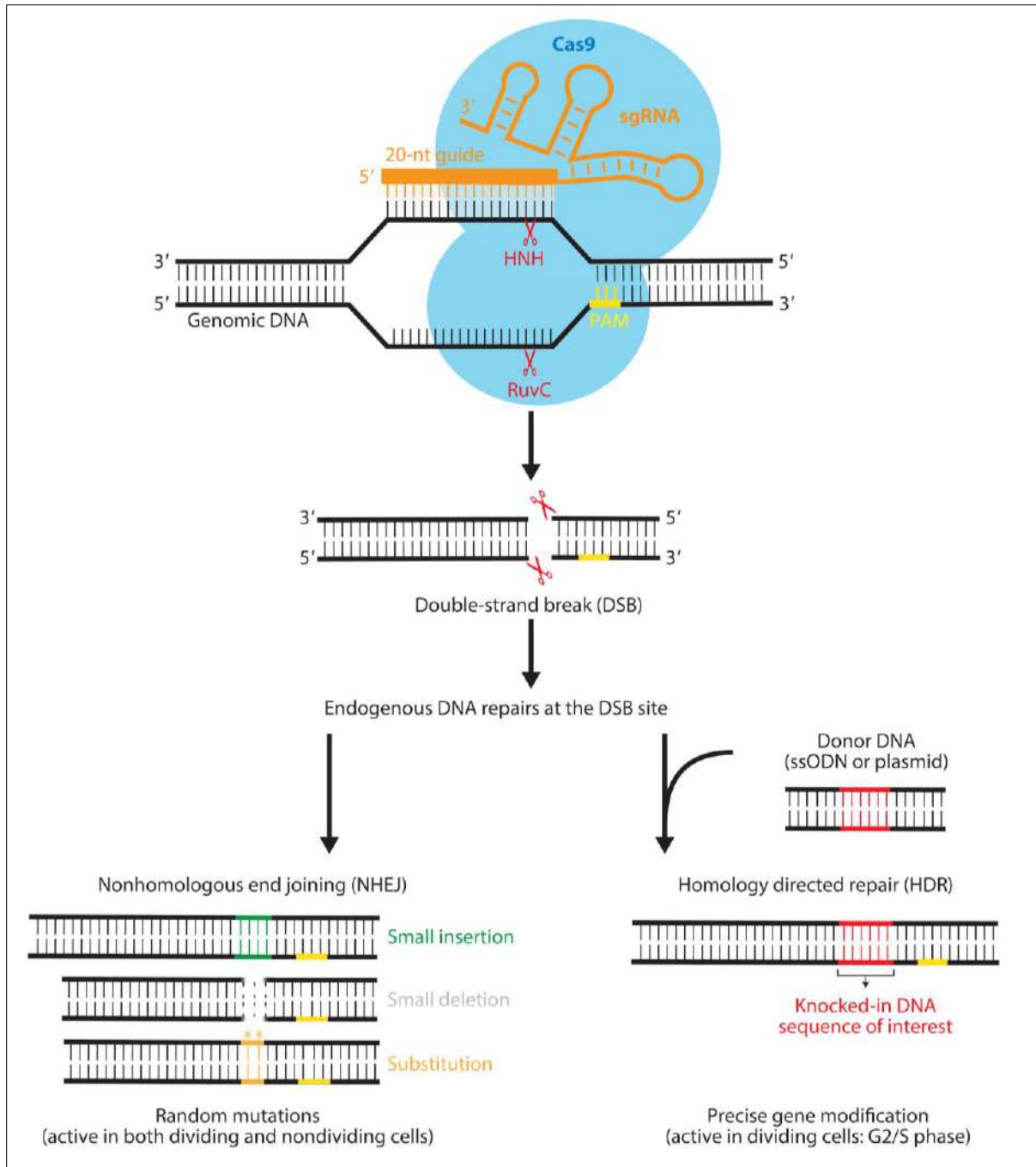


Figure 3.9: Schematic representation of mechanism of recognition and cleavage by CRISPR-Cas9. Target recognition by guide RNA leads to R-loop formation and strand scission mediated by RuvC-HNH domains (blue) and driven by complementary base pairing between the guide RNA (orange) and target DNA (black). Presence of a PAM sequence (yellow) is prerequisite for recognition of the target DNA. Depending upon the system, the DSB is repaired either via non homologous end joining or homology directed repair. Image reproduced from Jiang, Fuguo, and Jennifer A Doudna. 2017. "CRISPR – Cas9 Structures and Mechanisms," *Annu. Rev. Biophys.* 2017. 46:505–29 with permission.

This technology has been recently adapted for use in *P. falciparum* (Ghorbal et al., 2014; Mogollon et al., 2016; Kuang et al., 2017; Wagner et al., 2014; Cui Zhang et al., 2014). In the first report of CRISPR in *Plasmodium*, Ghorbal and co-workers developed a two-plasmid system: pUF1-Cas9 plasmid, contains gene coding for *SpCas9*-flanked by nuclear localization signal (NLS), 3X FLAG tag and is

maintained episomally and (Fig. 3.10 a) a pL6 plasmid (Fig. 3.10 b) harbouring sgRNA assembly and homology arms as donor DNA (for homology directed repair since NHEJ pathway is absent in *P. falciparum*). This plasmid is designed to integrate into *P. falciparum* genomic locus of interest via double crossover recombination. pUF1-Cas9 plasmid construct harbours yDHODH positive selection marker that confers resistance against DSM-1 (that inhibits PfDHODH) while pL6 plasmid harbours hDHFR positive selection marker and yFCU negative selection marker. Using these two plasmids, Ghorbal and co-workers demonstrated deletion of two different genes: eGFP gene integrated at a non-essential locus and knob-associated histidine rich protein (KAHRP) that is non-essential for parasite growth and survival (Ghorbal et al. 2014).

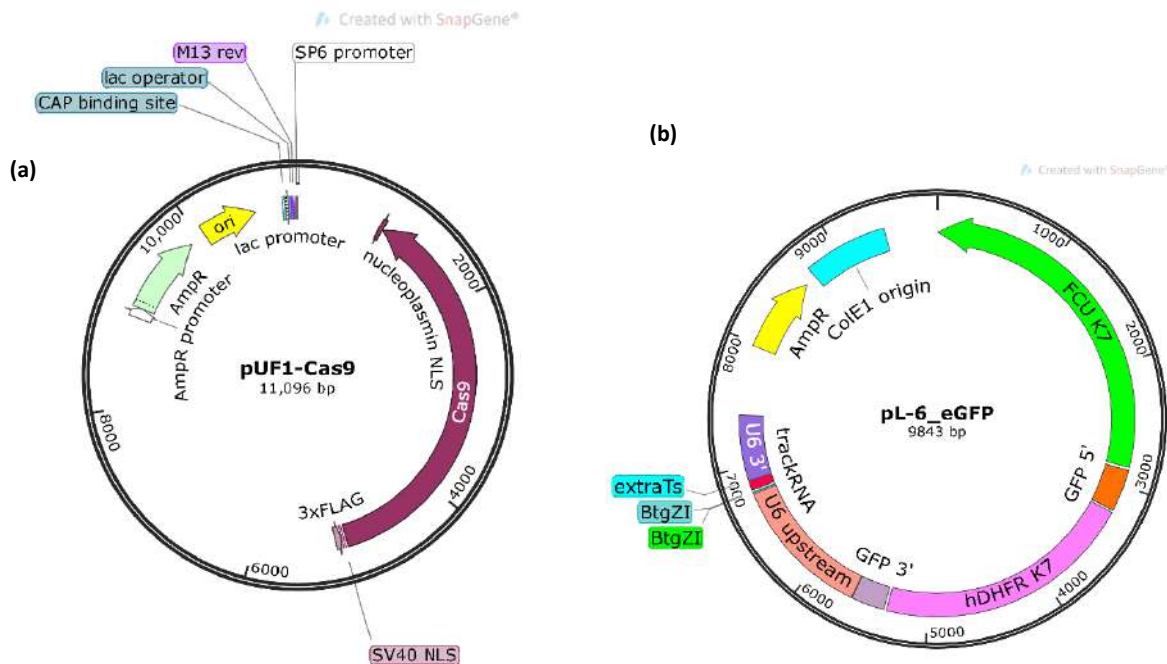


Figure 3.10: Plasmid maps of pUF1-Cas9 and pL6-eGFP. The pUF1-Cas9 plasmid contains coding sequence of SpCas9 endonuclease under 5' hsp promoter. The plasmid is maintained episomally in *P. falciparum*. The pL6 episome contains sgRNA expression cassette driven by U6 RNA polymerase III promoter. The positive selection marker cassette, hDHFR is flanked by 5' and 3' homology sequences to mediate homology directed repair of a double-stranded break. pUF1-Cas9 and pL6 constructs and associated plasmid maps were a kind gift from Dr. Jose-Juan Lopez-Rubio.

CRISPR-Cas9 mediated genome editing has proved to be a valuable resource to *Plasmodium* biology since its inception. Table 3.1 enlists some of the genes that have been modified using CRISPR-Cas9. Table adapted from Lee, Marcus C.S., Scott E. Lindner, Jose Juan Lopez-Rubio, and Manuel Llinás. 2019. "Cutting Back Malaria: CRISPR/Cas9 Genome Editing of Plasmodium." *Briefings in Functional Genomics* 18 (5): 281–89 under Creative Commons CC BY license (Lee et al. 2019).

Table 3.1: List of *Plasmodium* genes modified using CRISPR-Cas9 genome editing technique.

Genome-editing experiment	Target	Organism	Reference	
Gene knockout or replacement	<i>kahrp</i>	<i>P. falciparum</i>	(Ghorbal et al. 2014)	
	<i>kahrp, pfeba175</i>	<i>P. falciparum</i>	(Wagner et al. 2014)	
	<i>pfvap1</i>	<i>P. falciparum</i>	Nacer et al.	
	<i>pfset2</i>	<i>P. falciparum</i>	Lu et al.	
	<i>pfptef</i>	<i>P. falciparum</i>	Chan et al.	
	<i>pfshelp2</i>	<i>P. falciparum</i>	Miliu et al.	
	<i>pycdpk3, pyctrp</i>	<i>P. yoelii</i>	Zhang et al.	
	<i>pyapiap2</i> , multiple	<i>P. yoelii</i>	Zhang et al.	
	<i>pf glo1 and pf glo2</i>	<i>P. falciparum</i>	Wezena et al.	
	<i>pfcdpk2</i>	<i>P. falciparum</i>	Bansal et al.	
	<i>csp</i>	<i>P. falciparum</i>	Marin-Mogollon et al.	
	<i>pf p230p</i>	<i>P. falciparum</i>	Marin-Mogollon et al.	
	<i>pycdpk3, pyctrp</i>	<i>P. yoelii</i>	Qian et al.	
	<i>pf rh2a, pf rh2b</i>	<i>P. falciparum</i>	Campino et al.	
	<i>pfcdpk1</i>	<i>P. falciparum</i>	Bansal et al.	
	<i>pyalba4</i>	<i>P. yoelii</i>	Walker and Lindner	
	<i>pkdbpa</i> replacement with <i>pvd bp</i>	<i>P. knowlesi</i>	Mohring et al.	
	Point mutation	<i>pfkelch13, pforc1</i>	<i>P. falciparum</i>	Ghorbal et al.
		<i>pfcarl</i>	<i>P. falciparum</i>	LaMonte et al.,
<i>pfugt, pfact</i>		<i>P. falciparum</i>	Lim et al.	
<i>pfcdpk1</i>		<i>P. falciparum</i>	Bansal et al.,	
<i>pfmdr1</i>		<i>P. falciparum</i>	Ng et al.,	
<i>pfcp sf</i>		<i>P. falciparum</i>	Sonoiki et al.,	
<i>pfmdr1</i>		<i>P. falciparum</i>	Vanaerschot et al.,	
<i>pfatp4</i>		<i>P. falciparum</i>	Crawford et al.	
<i>ul13</i>		<i>P. falciparum</i>	Wong et al.,	
<i>pfact1</i>		<i>P. falciparum</i>	Das et al.,	
<i>pfap2-i, pfmsp5</i> promoter		<i>P. falciparum</i>	Santos et al.,	
<i>pf dhodh</i>		<i>P. falciparum</i>	White et al.,	
<i>pf coronin</i>		<i>P. falciparum</i>	Demas et al.,	
<i>pfatg18</i>		<i>P. falciparum</i>	Breglio et al.,	
<i>pfkelch13</i>		<i>P. falciparum</i>	Nair et al.,	
<i>pfkelch13</i>		<i>P. falciparum</i>	Payungwoung et al.,	
Intron deletion		<i>var2csa</i>	<i>P. falciparum</i>	Bryant et al.
Epitope tagging or conditional knockdown (DD, glmS or TetR-DOZI-binding aptamer)	<i>pfset7</i>	<i>P. falciparum</i>	Chen et al.,	
	<i>plasmepsinix, plasmepsinx</i>	<i>P. falciparum</i>	Nasamu et al.,	
	<i>pftric-θ</i>	<i>P. falciparum</i>	Spillman et al.	
	<i>pfclpp, pfclpr</i>	<i>P. falciparum</i>	Florentin et al.,	
	<i>pyp28</i>	<i>P. yoelii</i>	Zhang et al.	
	<i>pfck2β1, pfck2α, pfstk</i>	<i>P. falciparum</i>	Kuang et al.	

	<i>pfhsp70x</i>	<i>P. falciparum</i>	Cobb <i>et al.</i> ,
	<i>pfgdv1</i>	<i>P. falciparum</i>	Filarsky <i>et al.</i> ,
	<i>pfhsp70x</i>	<i>P. falciparum</i>	Kudyba <i>et al.</i>
	<i>pfhsp101</i>	<i>P. falciparum</i>	Ho <i>et al.</i> ,
	<i>pysep1</i>	<i>P. yoelii</i>	Qian <i>et al</i>
	<i>pfatg8</i>	<i>P. falciparum</i>	Walczak <i>et al.</i> ,
	<i>pyccp2, pydhc1</i>	<i>P. yoelii</i>	Liu <i>et al.</i>
	<i>pyalba4</i>	<i>P. yoelii</i>	Walker and Lindner
	<i>pkama1, pkron2, pkmyoA, pkcrt, pkK13</i>	<i>P. knowlesi</i>	Mohring <i>et al.</i>
Conditional KO (loxPintron)	DiCre driver lines	<i>P. falciparum</i>	Knuepfer <i>et al.</i>
	<i>pfshelph2</i>	<i>P. falciparum</i>	Miliu <i>et al.</i> ,
	<i>pfrhoph3</i>	<i>P. falciparum</i>	Sherling <i>et al.</i> ,
Reporter lines	<i>gfp-luciferase</i>	<i>P. yoelii</i>	Lu <i>et al.</i>
	<i>gfp (calmodulin, gapdh and hsp70 promoters)</i>	<i>P. falciparum</i>	Mogollon <i>et al.</i>
	<i>gfp</i>	<i>P. knowlesi</i>	Mohring <i>et al.</i>

In addition, CRISPR has been recently used to perform epigenetic editing in *P. falciparum* (Xiao *et al.*, 2019). The study demonstrated activation of reticulocyte binding protein homolog 4 (rh4) by histone hyperacetylation and repression of erythrocyte binding protein 175 (eba-175) by histone hypoacetylation mediated by dead Cas9 (dCas9). dCas9 is fused to Histone Acetyl Transferase (GCN5) to enhance the expression of the desired gene whereas its fused with Histone deacetylase Sir2a to mediate repression of the target gene (Xiao *et al.* 2019).

Complete knockout/deletion or replacement of an essential gene can prove lethal for parasite; therefore, to study the functionality of such genes, techniques which can afford flexibility of conditional modification are required.

iii) Conditional gene regulation in *Plasmodium spp.*

Conditional knockdown can be performed on the mRNA or the protein of the target gene. Transcription of the target gene can be modulated by replacing the endogenous promoter of the gene with a regulatable promoter. Tet-OFF system was devised for use in *Plasmodium spp.*, in which the promoter of gene of interest is replaced with a weak promoter that contains multiple tetracycline operator sites (TetO). Gene expression is induced when a transcriptional trans activator domain (TRAD) binds tetO sites and recruits transcriptional factors to boost promoter activity. Gene expression is repressed in presence of anhydrotetracycline (AT) which prevents binding of TRADs to the tetO sites. This technique has been successfully applied in *P. berghei* using its native apetala 2 family transcription factors as TRADs. Using this modified system, three genes in *P. berghei* were downregulated: prolifin-involved in actin cytoskeleton reconstruction, N-myristoyl transferase which helps in anchoring proteins to membranes and heat shock protein 101 (HSP101) which is a translocon component (Meissner *et al.* 2005; Pino *et al.* 2012).

Another promising technique that allows conditional gene regulation is the self-cleaving ribozymes. Ribozymes are RNA molecules that catalyse cleavage of mRNA into which they are integrated. Their enzymatic activity can also be modulated to respond to different ligand molecules. Insertion of ribozyme sequence into target gene leads to formation of chimeric mRNA with the ribozyme at its 3' end. The activity of glmS ribozyme, that is found in Gram-positive bacteria, can be regulated using glucosamine-6-phosphate and controlled gene attenuation is achieved by controlling the concentration of glucosamine-6-phosphate in the culture medium (Prommana et al. 2013).

Conditional knock down of the protein levels is achieved by promoting premature degradation of the target protein inside the cell, post translationally. Degradation could be facilitated by tagging the gene of interest with a destabilization domain such as *E. coli* DHFR degradation domain (DDD)(Svensson et al., 2006; Iwamoto et al., 2010) and the FK506-binding protein (FKBP) based destabilization domain (DD) (Chu et al., 2008; Banaszynski et al., 2006; Armstrong and Goldberg, 2007). These protein domains are structurally unstable and promote their own ubiquitinylation mediated degradation, in turn also causing endoplasmic reticulum associated degradation of the protein to which they are attached (de Koning-Ward et al., 2015). These destabilization (DD)/degradation (DDD) domains can be stabilized by Shield-1 and trimethoprim, respectively. In presence of the respective ligands, the domains and thereby the protein to which they are attached are stable; when the ligands are removed, they undergo degradation. Varying concentrations of ligands in the growth medium can achieve varying degrees of protein knock down.

Both DD and DDD have been used in *Plasmodium spp.* for obtaining protein knockdown. FKBP destabilization domain has been used to understand functions of essential genes such as cGMP-dependent protein kinase (PfPKG), cdc2-related protein kinase 4 (PfCRK4)(Ganter et al. 2017), autophagy-related protein PfATG18 (Bansal et al. 2017), parasite-specific bromodomain protein, PfBDP1 etc. However, the ligand Shield-1 is expensive and results in slower growth of *Plasmodium* parasites at the concentration used (0.5 μ M). An alternative degradation domain that can be stabilized by an inexpensive ligand, trimethoprim, was found to be effective in downregulation of protein levels in *P. falciparum*.

E. coli DHFR Degradation Domain was used first in *Plasmodium* by Muralidharan and co-workers. They generated a regulatable fluorescent affinity (RFA) tag by combining DDD with GFP and HA tags. The RFA tag was fused to 3' end of the target gene via single crossover recombination between pGDB plasmid harbouring ~ 1 kbp 3' DNA fragment of the target gene with the genomic locus (Fig.3.11).

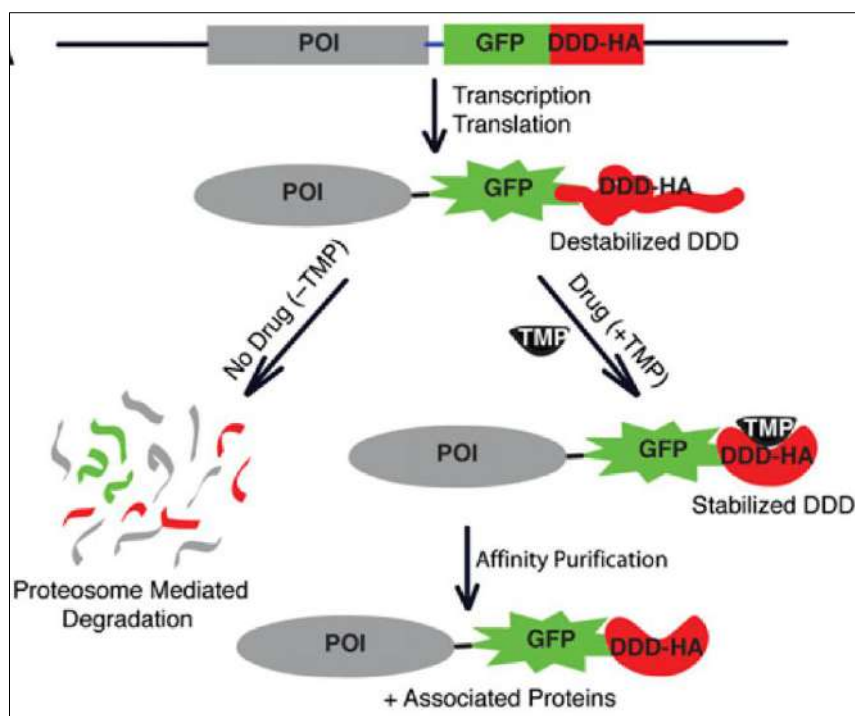


Figure 3.11: Conditional knock down of protein using DDD. The protein of interest is fused with RFA (DDD+GFP+HA) tag. Binding of TMP stabilizes the DDD and thereby the entire chimeric protein assembly. However, removal of TMP leads to ubiquitinylation and concomitant proteasome mediated degradation of the chimera. Image reproduced from Asparagine repeat function in a *Plasmodium falciparum* protein assessed via a regulatable fluorescent affinity tag Vasant Muralidharan, Anna Oksman, Mari Iwamoto, Thomas J. Wandless, Daniel E. Goldberg *Proceedings of the National Academy of Sciences* Mar 2011, 108 (11) 4411-4416; DOI: 10.1073/pnas.1018449108 under CC BY-NC-ND or CC BY license.

DDD-GFP-HA is fused to the C-terminal of the target protein resulting in a chimeric protein. This chimeric protein was stabilized in presence of trimethoprim; removal of trimethoprim results in degradation of DDD thereby degrading of target protein. Trimethoprim is toxic to *P. falciparum* parasites at the concentration required to be used for DDD stabilization (10 μ M). Therefore, parasites resistant to trimethoprim were generated by Muralidharan and co-workers by integrating hDHFR at a non-essential plasmepsin I (PMI) locus, generating knock-out parasite line (PMIKO) (Muralidharan et al., 2011).

The technique has been used to study the significance of many essential of *Plasmodium* genes: caseinolytic protease (Clp) family of proteins found in apicoplast that function as chaperons (Florentin et al. 2017); HSP101, an essential component of the PTEX export translocon (Kushwaha et al. 2018); endoplasmic reticulum chaperone PfGRP170 that is shown to be essential for asexual development (Kudyba et al. 2019) etc. Earlier in our laboratory, attempts were made to knock-down *P. falciparum* fumarate hydratase (PfFH) using this technique; however, the strategy failed to achieve drop in protein levels presumably due to mitochondrial localization of PfFH (Jayaraman et al. 2018). In this study, we attempted to generate parasite lines capable of conditional knock-down of adenylosuccinate synthetase and adenylosuccinate lyase, to evaluate effects of decreased cellular fumarate levels.

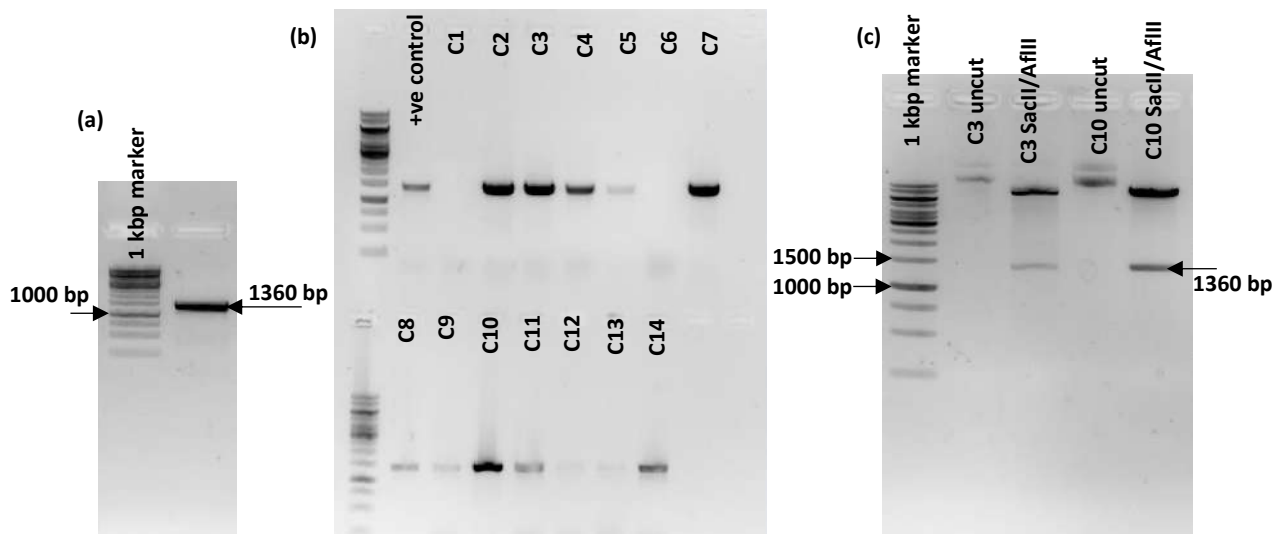
Objectives of the study

The objective of this part of the study was to use different knock out and knock down techniques to facilitate disruption of adenylosuccinate synthetase (*adss*) and adenylosuccinate lyase (*asl*) genes and study the effects of absence of fumarate (generated as a by-product during these reactions) on the overall metabolism of asexual stage parasites.

Results

3.1.2.1. Generation of plasmid constructs for disruption of *asl* gene by double homologous recombination and transfection of *P. falciparum* 3D7^{yak} parasites

For the purpose of *asl* gene disruption by double homologous recombination, pCC plasmid developed by Maier and co-workers was used (Maier et al. 2006). 5' and 3' homology arms were cloned sequentially in pCC1 parent vector. The clones of pCC1-5'*asl* were confirmed by colony PCR (Fig. 3.12 b), inset release (Fig. 3.12 c) and DNA sequencing. Confirmed clone of pCC1-5'*asl* was used to clone the 3' homology arm of *asl*. The pCC1-5'*asl*-3'*asl* (pCC1- Δ *asl*) clone was confirmed by colony PCR (Fig. 3.12 e), inset release (Fig. 3.12 f) and DNA sequencing.



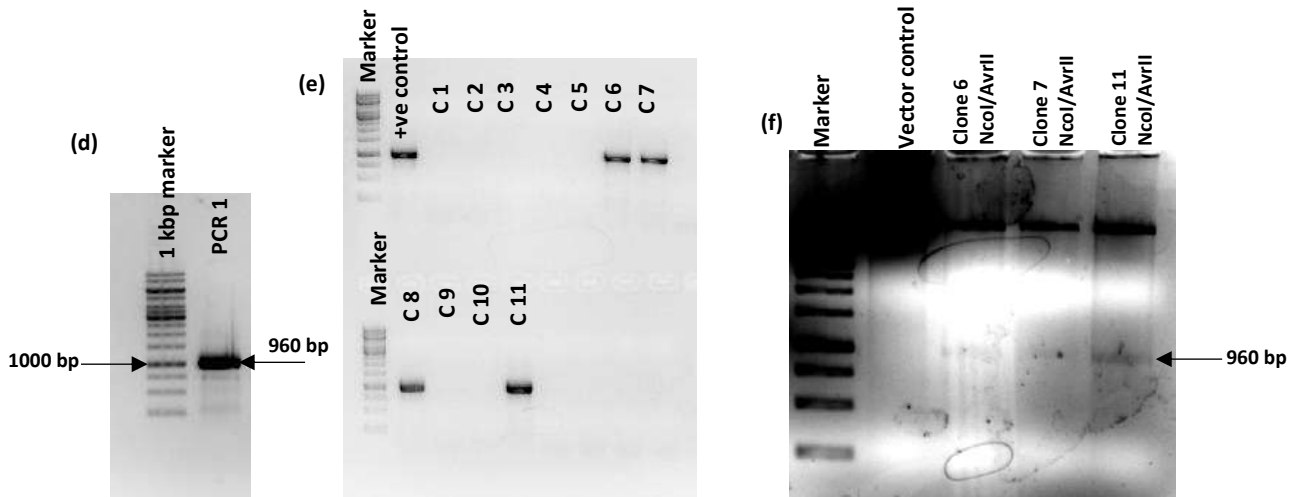


Figure 3.12: Cloning of homology arms in pCC1 vector (a) PCR amplification of 1360 bp 5' *asl* DNA segment from *P. falciparum* 3D7 genomic DNA, done using primer pair P3/P4 (Table 2.3) (b) Colony PCR of multiple colonies obtained for pCC1-5'*asl* clone, performed using primers P3/P4. Of the 10 colonies that tested positive for the pCC1-5'*asl*, 2 were chosen and further confirmed by (c) insert release, which confirmed the presence of 1.3 kbp insert in the clones and DNA sequencing. Confirmed clone of pCC1-5'*asl* was used to clone 3' homology arm of *asl*. (d) PCR amplification of 970 bp of 3'*asl* fragment from *P. falciparum* 3D7 genomic DNA, done using primers P5/P6 (Table 2.3). (e) Insert and vector ligation mix was transformed in *E. coli* DH5 α competent cells and ampicillin resistant colonies were screen by colony PCR (using primers P5/P6). Few colonies were found to be positive. Plasmids were isolated from three positive colonies and further confirmed by (f) insert release upon digestion with *Nco*I and *Avr*II. DNA fragment of correct size was seen upon insert release. One of the confirmed clones of final pCC1- Δ *asl* construct was used for transfection in *P. falciparum* 3D7^{AK}.

The final *asl* knock out construct, pCC1- Δ *asl* (Fig. 3.13) was transfected into *P. falciparum* 3D7^{AK} using several different transfection techniques on multiple occasions. Linearized DNA constructs have a greater propensity to undergo double homologous recombination inside a cell, hence pCC1- Δ *asl* linearized with *Hinc*II restriction enzyme was transfected into ring stage and schizont stage parasites in independent transfections. pCC1 plasmid contains two *Hinc*II sites within the *yFCU* region, releasing a fragment of 747 bp upon digestion. Since negative selection is not required to select against episomal copies when linear plasmid is transfected, the loss of *yFCU* can be tolerated. Linearized pCC1- Δ *asl* was purified by gel extraction prior to transfection in *P. falciparum* 3D7^{AK} parasite line.

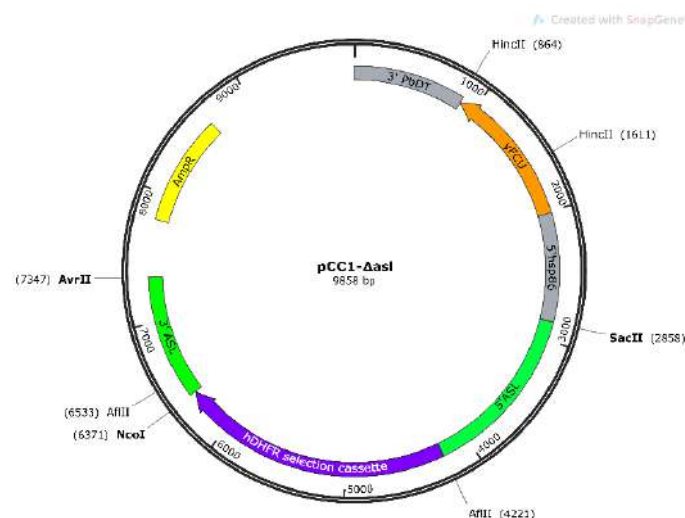
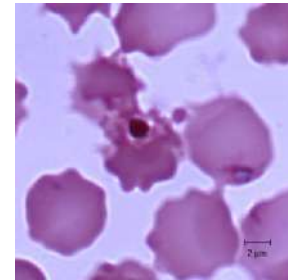
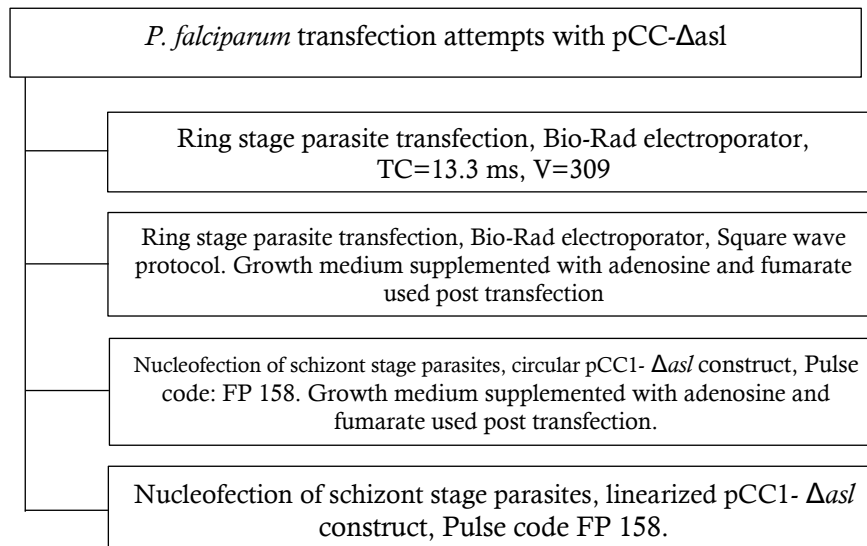


Figure 3.13: Map of final knock out construct, pCC1- Δ *asl*. Important segments are highlighted and marked appropriately. Homology arms were cloned on either side of hDHFR expression cassette. The sites of plasmid linearization, *Hinc*II, are

marked. Digestion with HincII releases a 747 bp DNA fragment from *yFCU* region disrupting the negative selection marker. Since unintegrated linear plasmid would be digested by parasite, negative selection marker becomes dispensable. Plasmid map was generated using SnapGene Viewer.

In all methods used for transfection, healthy parasites appeared few days post-transfection following which drug pressure was initiated. Administration of drug killed parasites; dead parasites were cleared from the cultures upon daily media change. All transfected cultures were maintained under drug pressure (2.5 nM WR99210) for 8-10 weeks but drug resistant parasites failed to appear in cultures. On few occasions, pyknotic parasites were seen in transfected cultures but these parasites did not survive and eventually got cleared from the cultures.

The following flowchart summarizes the attempts made to obtain *asl* KO *P. falciparum* parasites using different transfection techniques:



In few attempts, pyknotic parasites were observed few weeks after transfection but these parasites failed to survive and proliferate.

3.1.2.2. Generation of plasmid constructs for disruption of *adss* and *asl* genes using CRISPR-Cas9 genome editing technique and transfection of *P. falciparum* 3D7^{yAK} parasites

Homology arms of *adss* gene were cloned in pL6-eGFP plasmid as described in Materials and Methods. Positive clones were confirmed by colony PCR (Fig. 3.14) and DNA sequencing.

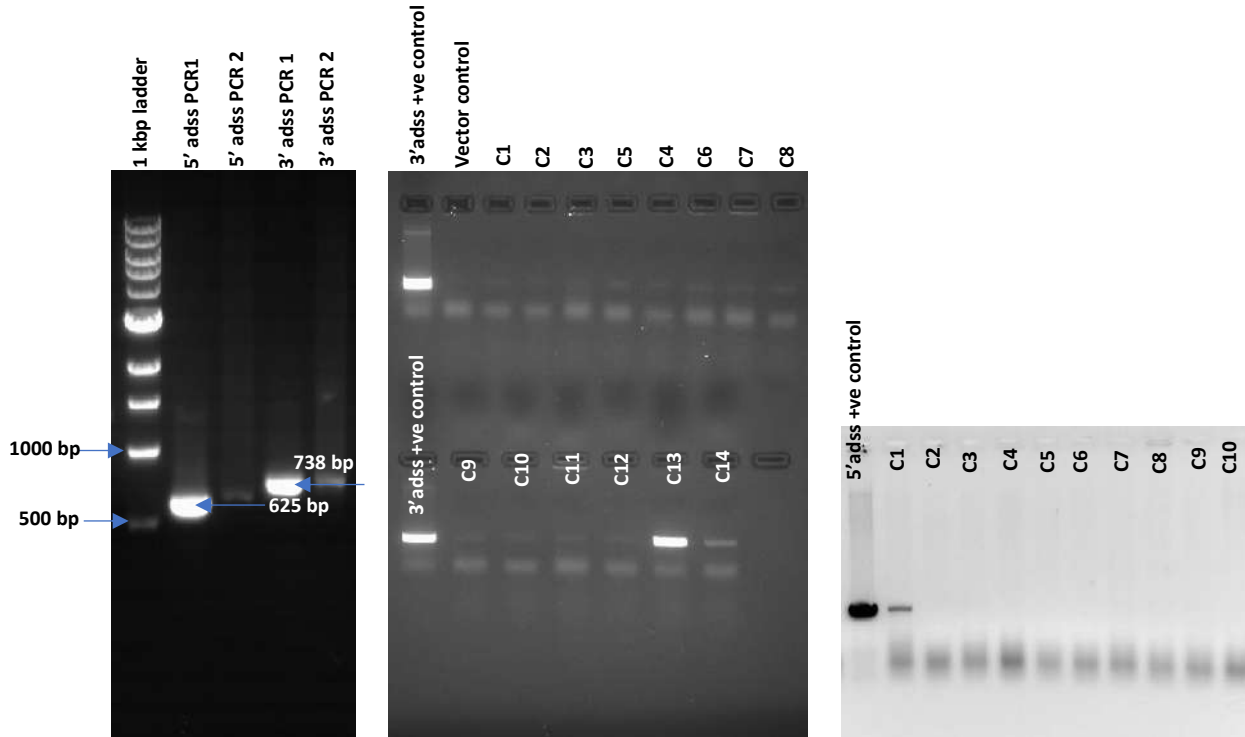


Figure 3.14: Cloning and confirmation of 5' and 3' *adss* homology arms. (a) DNA segments corresponding to 5' and 3' homology arms for knockout of *adss* gene were amplified from *P. falciparum* genomic DNA for cloning into pL6-eGFP plasmid vector. (b) 3' *adss* fragment (amplified using primers P9/P10 (Table 2.3)) was cloned in pL6-eGFP and transformed in *E. coli* DH5 α competent cells. Colonies obtained were confirmed by colony PCR using primers P9/P10. Two colonies (C13, C14) tested positive by PCR. Plasmids were isolated from these colonies and used for cloning 5' homology arm of *adss* gene. (c) 5' *adss* homology fragment (amplified using primers P7/P8 (Table 2.3)) was cloned in pL6-3' *adss* clone and transformed colonies were confirmed by colony PCR using primers P7/P8. Only one colony tested positive, which was further confirmed DNA sequencing.

Cloning of sgRNA for adss

The next step in creating a knockout vector for CRISPR involves cloning of the desired guide RNA (20 nt excluding PAM sequence) into pL6-*adss* construct. Cloning of this 20-nt DNA segment posed multiple difficulties. Several approaches were tried for the cloning which are summarized in Materials and Methods (Chapter 2). Cloning using *a*) sgRNA cloning between BtgZI restriction sites in pL6-eGFP vector and *b*) In-Fusion (Clontech) cloning kit did not yield sgRNA cloned pL6 vector. The *c*) overlap PCR method resulted in successful cloning of sgRNA in pL6-*adss* plasmid. The methodology is described in Materials and Methods. It was observed that cloning of sgRNA was relatively difficult in pL6 vector containing the homology arms for the gene of interest possibly due to the increased AT content of the plasmid owing to AT rich homology arm sequences. It was easier to clone sgRNA in empty pL6 vector followed by cloning of homology arms. pL7- Δ *adss*

clones obtained after successful cloning of sgRNA in pL6-adss plasmid were confirmed by PCR (Fig. 3.15 a) and DNA sequencing (Fig. 3.15 b)

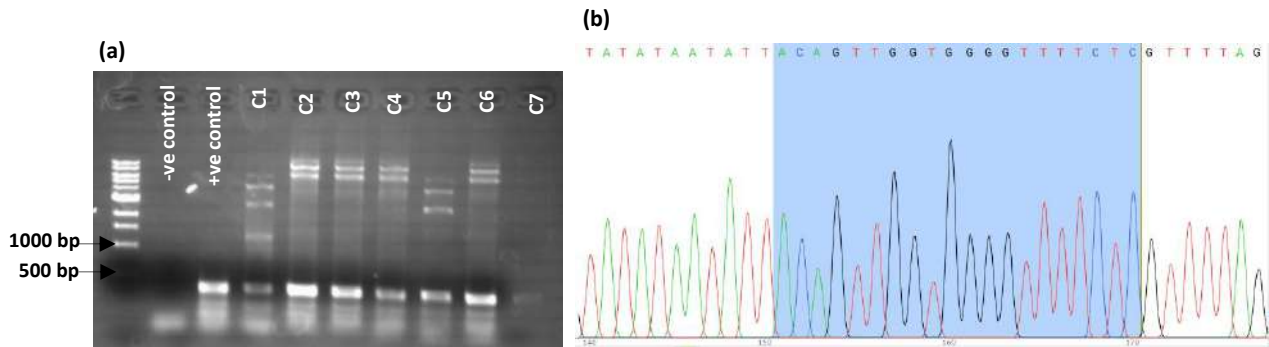


Figure 3.15: Confirmation of sgRNA cloning into pL6-adss vector. (a) Confirmation PCR using primers P25/P33 (Table 2.3) on colonies obtained upon transformation of In-Fusion reaction mix indicated presence of sgRNA fragments. pL6-adss vector without sgRNA was used as negative control. Amplicon obtained in PCR3 was used as template for positive control (50 ng concentration). (b) Few clones were then confirmed by DNA sequencing and found to be positive.

Following the generation of pL7- Δ adss construct, generation of pL7- Δ asl construct was undertaken. To begin with, sgRNA for *asl* was cloned in pL6-eGFP vector using overlap PCR method. Positive clones were confirmed by colony PCR using primers P32/P35 (Fig. 3.16 a) and DNA sequencing (Fig. 3.16 b)

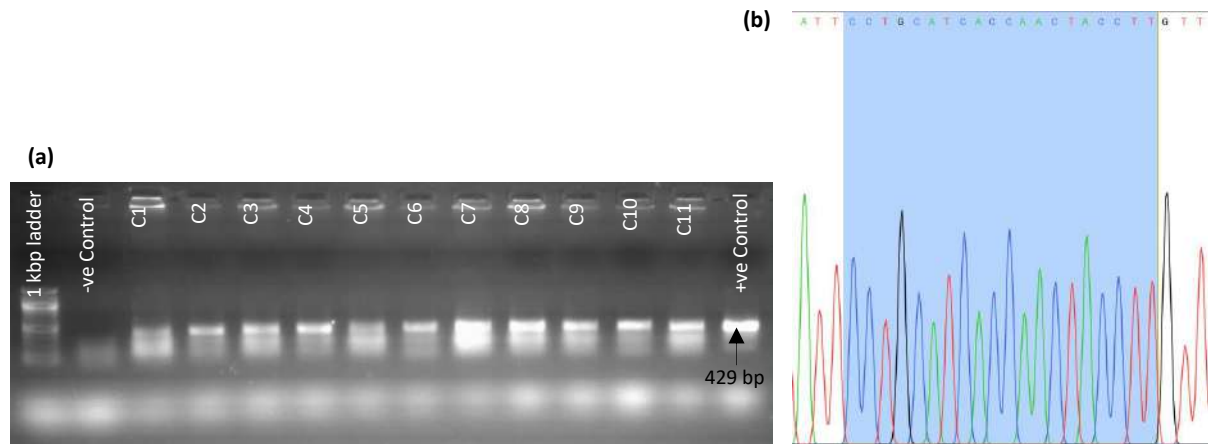


Figure 3.16: Confirmation of sgRNA cloning into pL6-eGFP vector. (a) Confirmation PCR using primers P32/P35 (Table 2.3) on colonies obtained upon transformation of In-Fusion reaction mix indicated presence of sgRNA fragments. pL6-eGFP vector without sgRNA was used as negative control. Amplicon obtained in PCR 3 was used as template for positive control (50 ng concentration). (b) Few clones were then confirmed by DNA sequencing and found to be positive.

pL6-sgRNA(*asl*) clone was then used for cloning of 5' and 3' homology arm sequences. Homology arms of *asl* gene were cloned in pL6-sgRNA(*asl*) plasmid as described in Materials and Methods. Positive clones were confirmed by colony PCR, insert release (Fig. 3.17) and DNA sequencing.

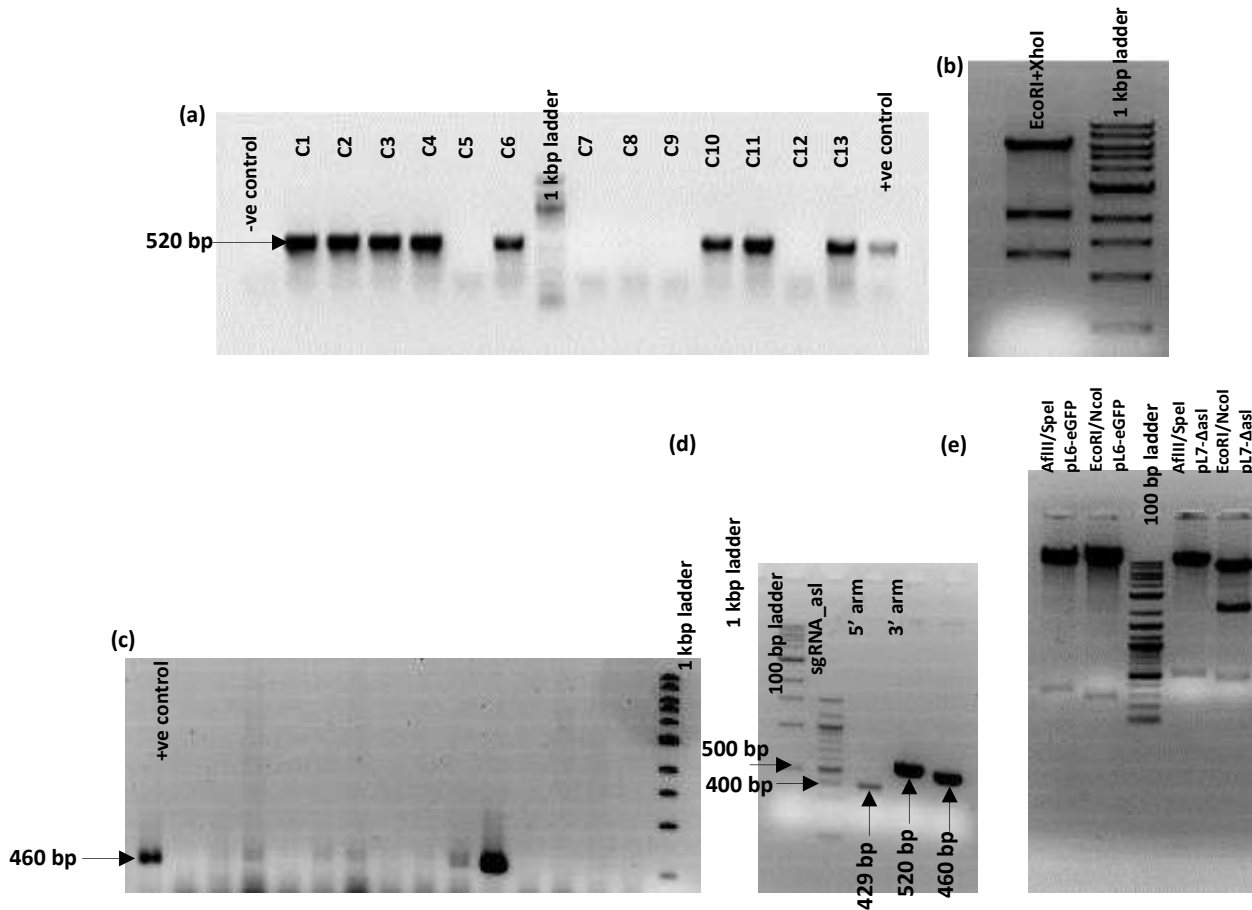
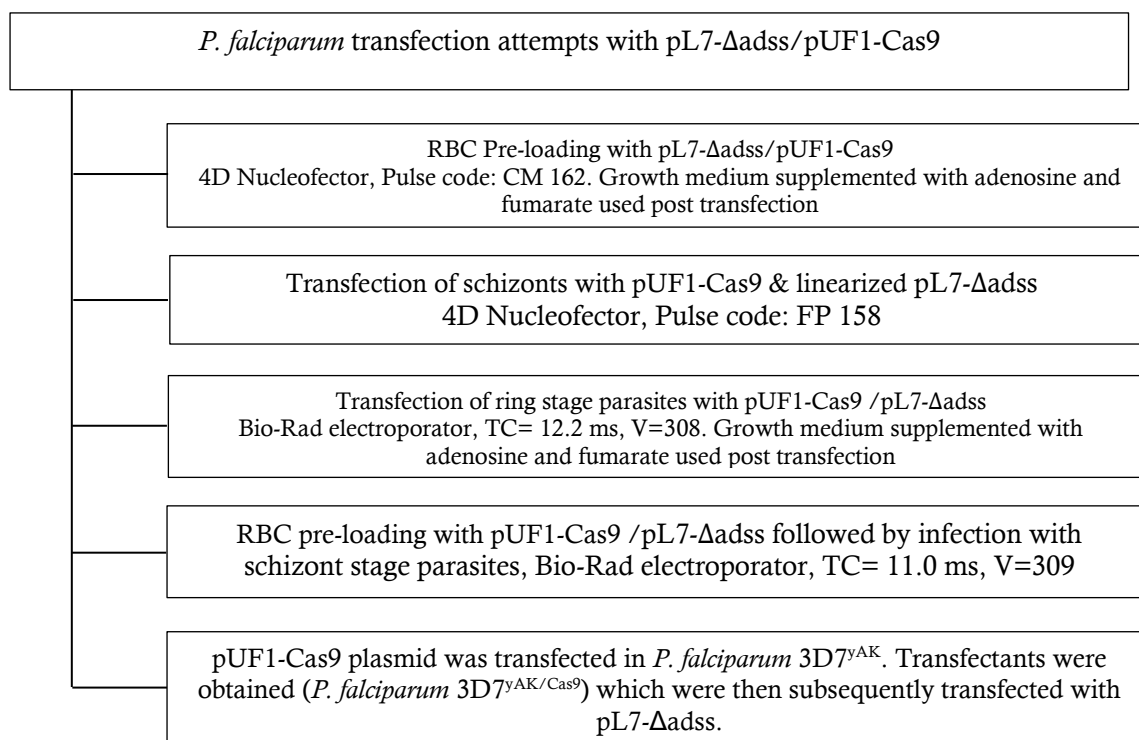


Figure 3.17: Cloning and confirmation of 3' and 5' asl homology arms. DNA segments corresponding to 5' homology arm of asl gene was amplified from *P. falciparum* 3D7 genomic DNA using primers P11/P12 (Table 2.3) and cloned in a confirmed pL6-sgRNA (asl) clone and *E. coli* DH5 α competent cells were transformed with the ligation mix. Colonies obtained were screened by (a) colony PCR using primers P11/P12 and (b) insert release (using restriction enzymes EcoRI and XhoI). The confirmed pL6-sgRNA-5'asl clone was then used to clone 3' homology arm of asl. 3' homology arm DNA segment was amplified from *P. falciparum* 3D7 genomic DNA using primers P13/P14 (Table 2.3) and cloned in a confirmed pL6-sgRNA-5'asl clone and *E. coli* DH5 α competent cells were transformed with the ligation mix. (c) Colonies obtained were screened by colony PCR using primers P13/P14. (d) Plasmid DNA from one positive colony was isolated used as template for 3 PCR reactions to confirm presence of sgRNA, 5' homology arm and 3' homology arm in final clone pL7- Δ asl. (e) pL7- Δ asl clone was also confirmed by restriction mapping using 4 different restriction enzymes before sending for DNA sequencing. Restriction mapping released DNA fragments of expected size.

The confirmed clone of pL7- Δ adss plasmid vector was then purified and transfected along with pUF1-Cas9 plasmid, in *P. falciparum* 3D7^{yAK} strain. Transfections were done multiple times using different transfection techniques, different growth conditions post-transfection and circular or linearized forms of pL7- Δ adss plasmid. Transfected cultures were maintained for 8-10 weeks but none of the transfections yielded drug resistant parasites. In one of the transfections with pUF1-Cas and pL7- Δ adss, very few parasites were observed in Giemsa-stained smears ~25 days post transfection but unfortunately, due to unknown reasons, the culture lysed and could not be retrieved. Similar transfections were attempted again but did not yield any drug-resistant parasites. Multiple events of transfection are summarized in the following schematic.



3.1.2.3. Generation of plasmid constructs for conditional knock down of ADSS and ASL and transfection of *P. falciparum* PMIKO strain

Knock out of essential genes may prove difficult in spite of providing an alternate pathway for generation of the end product(s) due to haploid nature of the *Plasmodium* genome. Hence, a system which affords conditional knock down of protein was adopted. As detailed in the earlier section, this technique developed by Muralidharan *et. al.* involves tagging the endogenous copy of the gene of interest with a regulatable (*E. coli* DDD) fluorescent (GFP) affinity (HA) tag (RFA tag) at its 3' end. The cloning method is described in Materials and Methods. Final knock-down constructs pGDB- Δ adss (Fig. 3.18 a) and pGDB- Δ asl (Fig. 3.18 b) were confirmed by colony PCR (Fig. 3.18 c) and DNA sequencing.

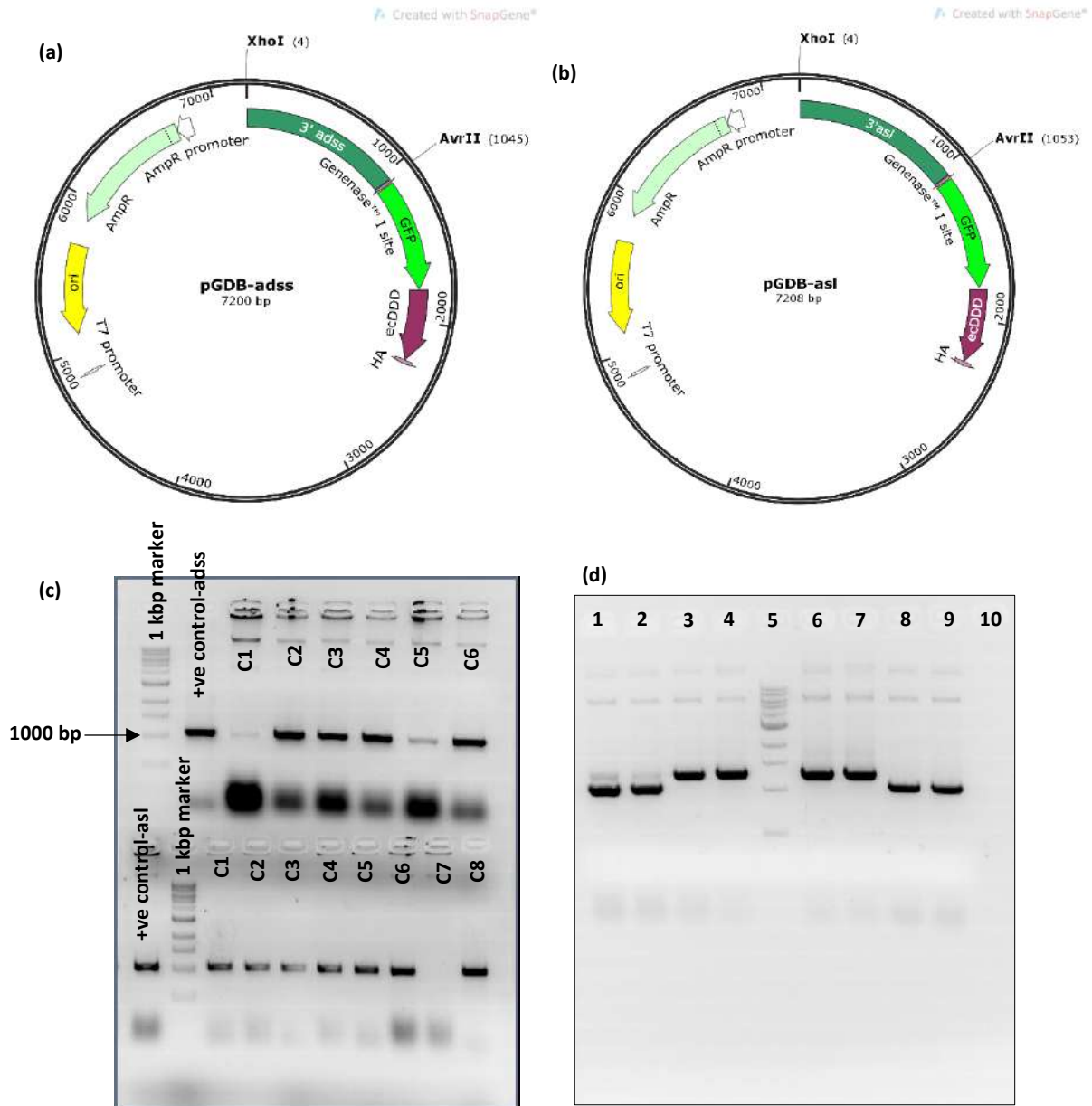
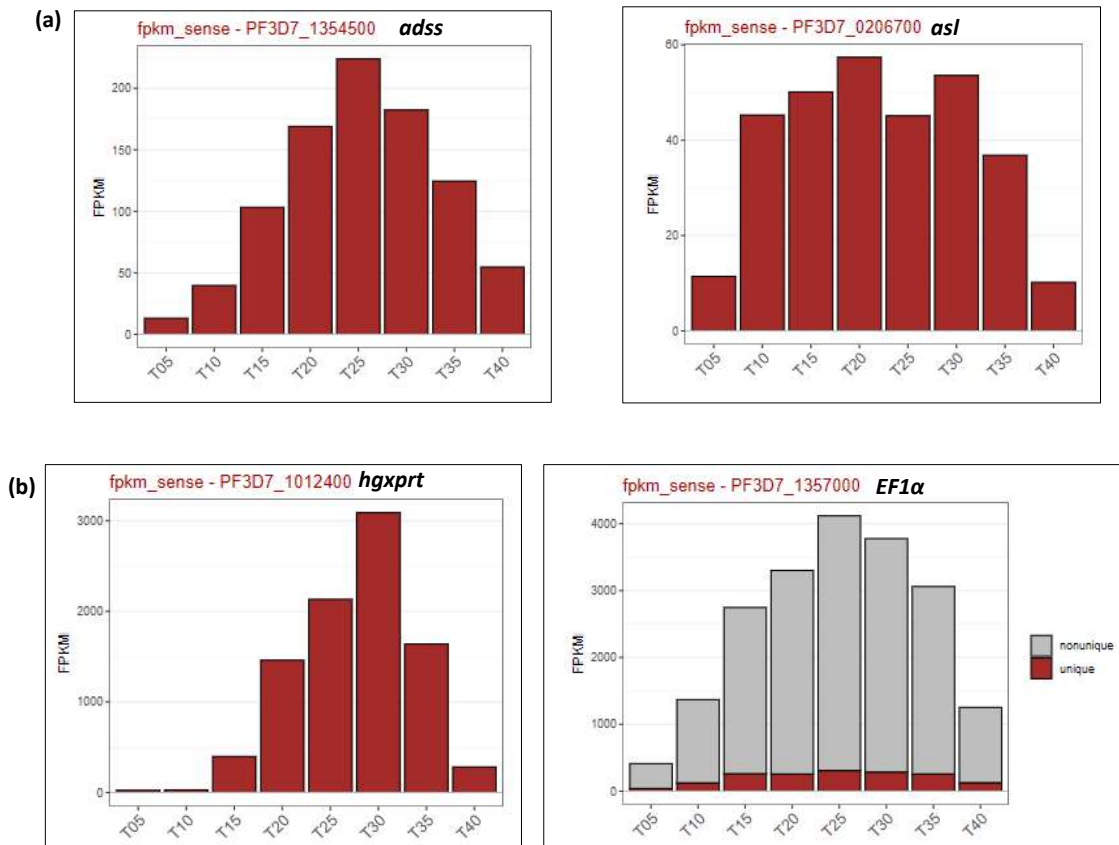


Figure 3.18: Generation and confirmation of pGDB- Δ adss and pGDB- Δ asl plasmid vectors and transfectants. (a) Schematic representation of pGDB- Δ adss construct and (b) pGDB- Δ asl construct. (c) The inserts were cloned in linearized pGDB vector using AQUA cloning technique (Beyer et al. 2015) and transformed in *E. coli* DH5 α competent cells. The colonies obtained were screened by colony PCR (Using primers P17 & P18 for *adss* and P19 & P20 for *asl* gene, Table 2.3). Few colonies were chosen and further confirmed by DNA sequencing. (d) Episomal copies of plasmids were present in both the transfectants cultures. lane 1, *adss* positive control. PCR performed with P17/P18; lane 2, *adss* test (parasite lysate) (PCR performed with P17/P18); lane 3, *adss* positive control (PCR performed with P17 and GFP reverse primer); lane 4, *adss* test (parasite lysate) (PCR performed with P17 and GFP reverse primer); lane 5, 1 kbp DNA marker; lane 6, *asl* positive control (PCR performed with P19 and GFP reverse primer); lane 7, *asl* test (parasite lysate) (PCR performed with P19 and GFP reverse primer); lane 8, *adss* positive control (PCR performed with P19/P20); lane 9, *adss* test (parasite lysate) (PCR performed with P19/P20). All primer sequences are reported in Table 2.3.

Trimethoprim is toxic to *P. falciparum* wild type parasites. Hence pGDB constructs are transfected to a strain of parasites that has hDHFR gene integrated into its genome in place of plasmepsin I, the PM1KO (Liu et al., 2005). *P. falciparum* PM1KO parasites were transfected with confirmed clones of

pGBD- Δ adss and pGDB- Δ asl by RBC pre-loading protocol. Freshly collected RBCs were transfected and immediately infected with tightly synchronized schizont stage *P. falciparum* PM1KO parasites (A kind gift from Prof. Daniel E. Goldberg, Department of Medicine, Division of Infectious Diseases, Washington University School of Medicine, USA). *P. falciparum* PM1KO parasites were cultured in continued presence of 10 μ M trimethoprim (TMP) before and after transfection. Blasticidin (BSD) pressure was commenced 24 hours post-transfection and drug resistant parasites were obtained, for both pGBD- Δ adss and pGDB- Δ asl transfectants, within 21-25 days. The events of successful genomic integration are low in *P. falciparum* and hence, drug ‘on and off’ cycles need to be performed once the parasites appear in culture. Parasites were tested for presence of episomal copies by performing PCR on drug resistant parasites (Fig. 3.18 d) and were found to be positive. Successful integration of pGBD- Δ adss or pGDB- Δ asl plasmid into the parasite genome at the correct location, would result in expression of the RFA tag driven by the endogenous promoter of the respective genes. Before commencing drug on-and-off cycles, parasites were viewed under confocal microscope to estimate the number of parasites expressing GFP. Few GFP positive parasites were observed in both pGDB-adss and pGDB-asl cultures. It should be noted that the levels of expression of both *adss* and *asl* are low during intra-erythrocytic stages, as demonstrated by RNA-seq experiments (Fig. 3.19 a) compared to some other genes such as *hgxp1t* and *EF1 α* (Fig. 3.19 b) (Bahl et al. 2003); therefore, GFP signal was also weak in both pGDB-adss (Fig. 3.19 c) and pGDB-asl parasite lines (Fig. 3.19 d).



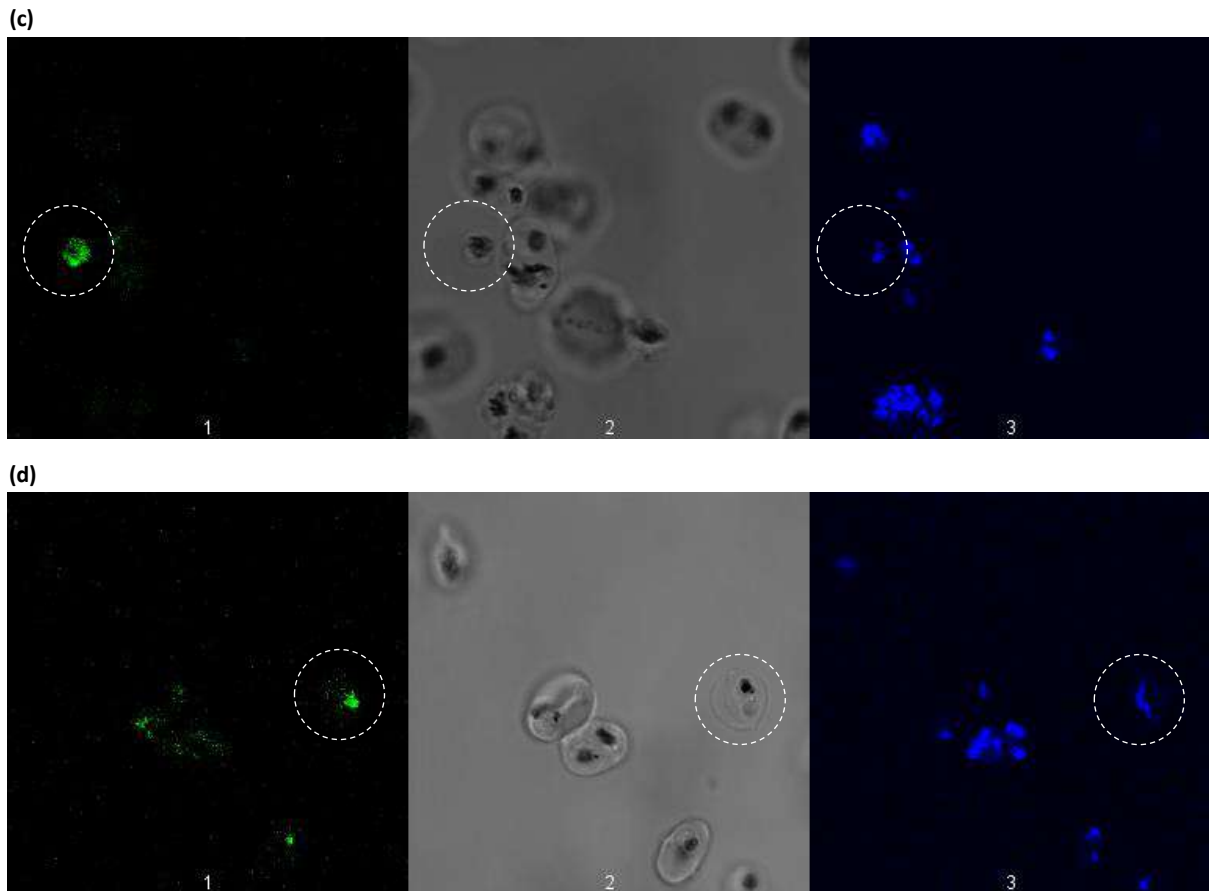


Figure 3.19: Expression levels of *adss*, *asl* and live cell imaging of transgenic parasites. Expression levels of (a) *adss* (left panel) and *asl* (right panel) are very low during intra-erythrocytic life stages as determined by RNA-seq (Bahl et al. 2003) taken from PlasmoDB (<https://plasmodb.org/plasmo/app>) (b) Expression levels of *hgxprt* and *EF1 α* are shown for comparison. X-axis represents hours in *P. falciparum* post-invasion while Y-axis represents Transcript levels of fragments per kilobase of exon model per million mapped reads (FPKM). Confocal microscopic images of (c) pGDB-*adss* parasites and (d) pGDB-*asl* parasites. Panel 1 shows fluorescence from GFP, panel 2 shows DIC of same field and panel 3 represents fluorescence from Hoechst[®] staining. GFP positive parasites have been circled with white dotted circles.

pGDB-*adss* and pGDB-*asl* parasites were observed under a confocal microscope (live cell imaging) and a very small proportion of parasites were found to be GFP positive in both cultures (Fig. 3.19 c, d). Usually, genomic integration events are facilitated by multiple drug “on-and-off” cycles (Muralidharan et al. 2011); this approach, although widely employed, is time-consuming and therefore we decided to sort GFP positive cells using fluorescent assisted cell sorting (FACS). Tightly synchronized, MACS purified pGDB-*adss* parasites were subjected to FACS (Fig. 3.20), GFP positive cells were sorted and put back in culture with fresh erythrocytes. 4% of total cell population was found to be GFP positive, indicating that the genomic integration of plasmid via single crossover recombination is rare before drug cycling. After a few generations in culture, stocks of GFP positive pGDB-*adss* parasites were made and stored in liquid nitrogen. These parasites become crucial reagents to study effect of controlled knock-down of adenylosuccinate synthetase protein by modulating the concentration of trimethoprim

in the culture. A controlled knock-down of protein levels can in turn modulate the amounts of fumarate produced in the cell, a scenario that can be useful for evaluating the contribution of fumarate generated by ADSS/ASL pathway to the overall metabolism by supplementing the parasites with ^{13}C labelled glucose, ^{13}C labelled glutamine and ^{13}C labelled aspartate with wild type parasites as control (using metabolomics).

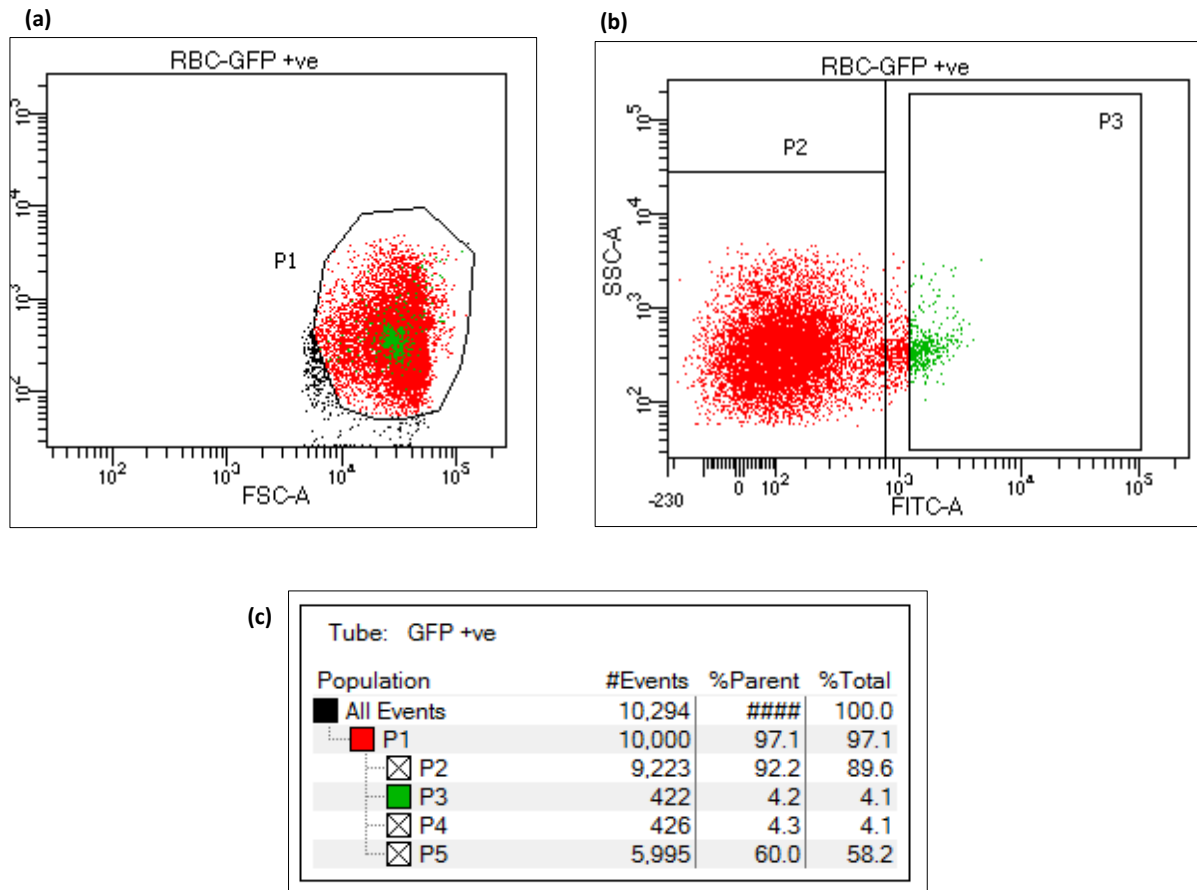


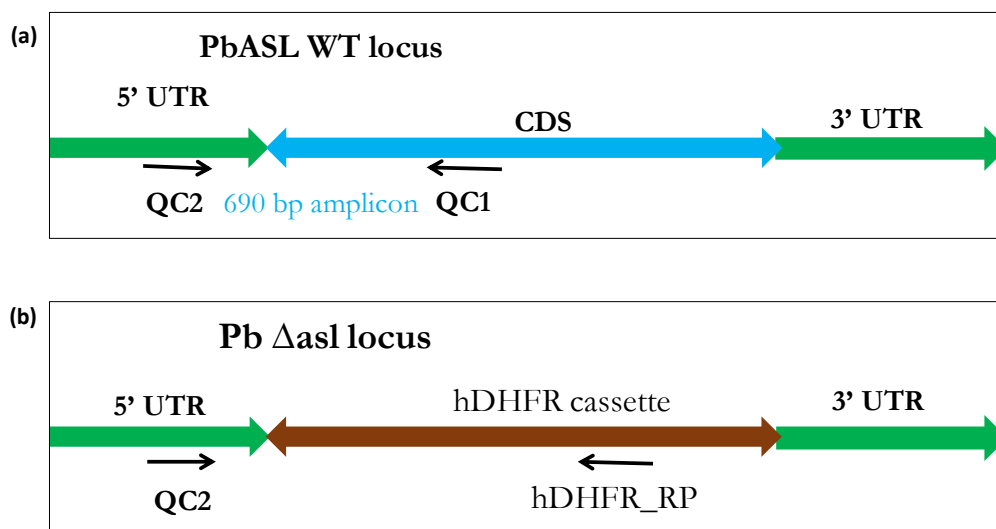
Figure 3.20: Fluorescent assisted cell sorting of GFP positive pGBD- Δ adss genome integrant. (a-b) Dot plots of GFP positive *P. falciparum*. Total number of events are represented by P1, GFP negative events are represented by P2 while GFP positive events are represented by population P3. 4 % of the total cell population was found to be GFP positive. Events in gate P3 were collected and put back in culture with fresh erythrocytes. (c) Number of events in each gate are tabulated.

3.1.2.4. Attempts to knock-out *asl* from genome of *P. berghei* ANKA^{yak} parasites

The parasite line *P. berghei* ANKA^{yak} was used to knock out *asl* gene. This line is pyrimethamine resistant due to the presence of pbCEN5-yAK that harbours Tg dhfr-ts selection marker, expression of which is driven by Pb dhfr-ts promoter (Fig. 3.6 a). Final KO construct pJAZZ- Δ asl (PbGEM-228093) that was procured from Plasmogem consortium (Schwach et al., 2015) contains hDHFR marker cassette (expression of hDHFR is driven by EF1 α promoter, a strong promoter) that provides resistance against both pyrimethamine and WR99210. The construct was confirmed by PCR (Fig. 3.21 c) and restriction mapping (Fig. 3.21 d) using 6 different restriction enzymes and was found to be correct. Once confirmed, the construct was digested with NotI and *P. berghei* ANKA^{yak} parasites were

transfected with it, following the method described in Materials and Methods. Presence of Tg dhfr-ts gene in *P. berghei* ANKA^{yak} parasites confers pyrimethamine resistance. However, these parasites are sensitive to high concentrations of WR99210. Simultaneous presence of Tg dgfr-ts (from pbCEN5-yAK plasmid) along with hDHFR (by integration of pJAZZ-asl into the genome of *P. berghei* ANKA^{yak}) increases WR99210-resistance by ~10-fold. De Koning-Ward and co-workers showed in their study that hDHFR gene that confers resistance to WR99210 can be used as a new selectable marker. They also found that hDHFR can be used in conjunction with the existing pyrimethamine resistance markers (Tg/Pb dhfr-ts) at higher concentrations (16 mg kg⁻¹) of WR. In a personal communication with Dr. Chris J Janse - Head of the Leiden Malaria Research Group, he mentioned that they use this approach to perform sequential genetic manipulations in *P. berghei*; they transfect *P. berghei* parasites first with plasmid containing Tg/Pb dhfr-ts marker, select parasites with pyrimethamine and then transfect the transgenic parasites with a second plasmid containing hDHFR marker and select using WR99210 (dosage: 16 mg kg⁻¹ body weight). He added that the best combination is first using the resistant Pb dhfr-ts gene or the Tg-dhfr-ts gene driven by the *P. berghei* dhfr-ts promoter since this promoter is somewhat weaker than the EF1 α promoter, although one can possibly use plasmids wherein expression of both markers is driven by the EF1 α promoter. Therefore, we adopted the same strategy to knock out *asl* following the episomal expression of yAK gene in *P. berghei*.

Drug pressure was initiated 48 hours post-transfection and selection of transfectants was carried out by subcutaneous (s.c.) injection of a single dose of WR9210 at a concentration of 20 mg per kg body weight on three consecutive days. Pyrimethamine pressure was maintained throughout the course of transfection (at a concentration of 2.5 mg ml⁻¹).



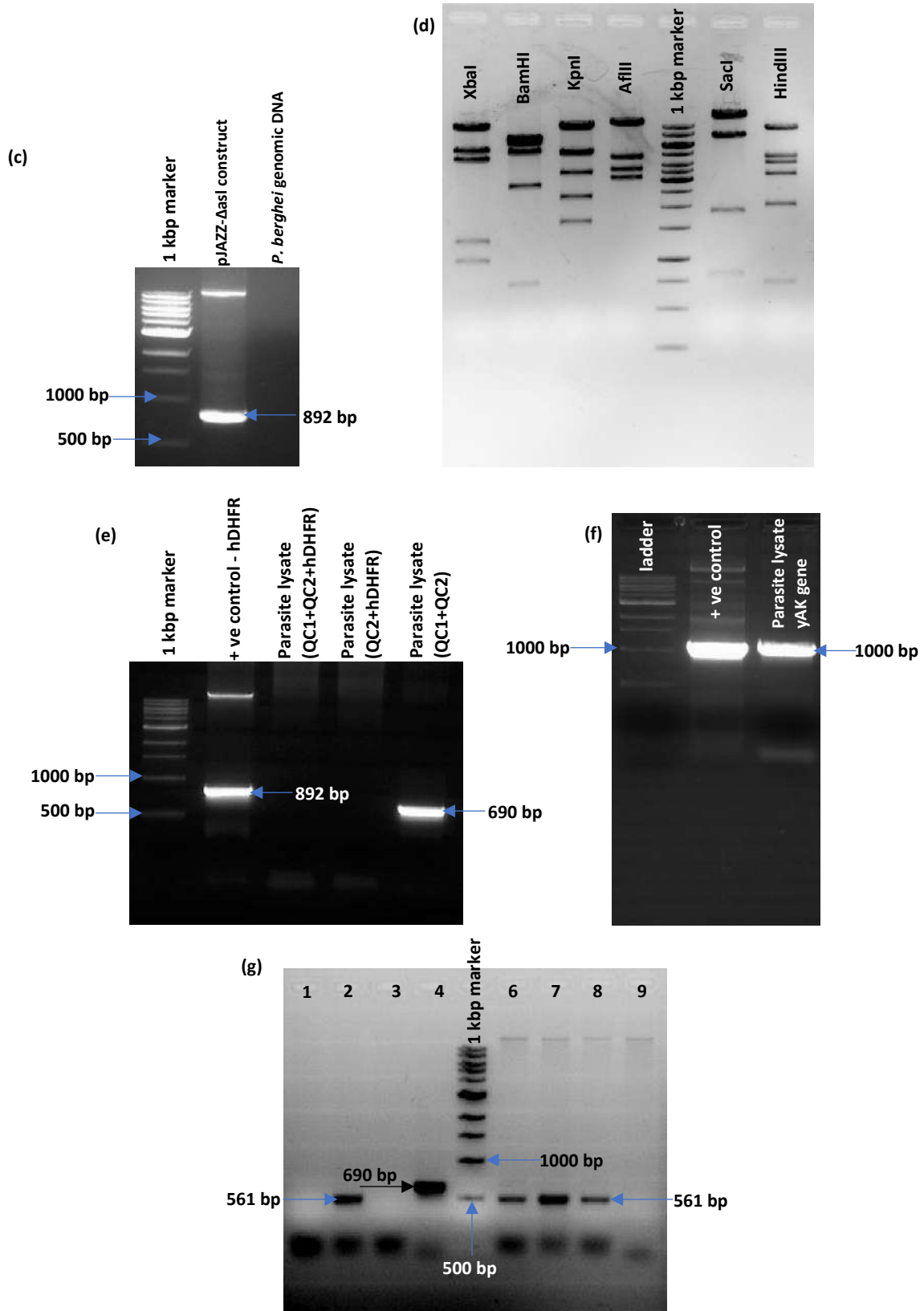


Figure 3.21: Confirmation of pJAZZ-Δasl construct and transfectants. Schematic representation showing the locations of primers used for checking *asl* gene location in (a) wild type parasites and (b) as expected in parasites with *asl* gene disruption. pJAZZ-Δasl construct procured from PlasmogEM was confirmed by (c) PCR and (d) restriction mapping (e) PCR with QC1/QC2 primers on transfectant parasite lysate confirmed the retention of *asl* gene (f) Episomal copy yAK gene was still retained in WR99210 resistant parasites (g) The parasite lysate also showed presence of hDHFR selection marker. lane 1, PCR performed

on drug resistant parasite lysate with hDHFR gene specific primers without MgCl₂/DMSO; lane 2, PCR performed on drug resistant parasite lysate with hDHFR gene specific primers with MgCl₂ in reaction mix; lane 3, PCR performed on drug resistant parasite lysate with hDHFR gene specific primers with DMSO in reaction mix; lane 4, PCR performed on drug resistant parasite lysate with QC1/QC2 primers; lane 5, 1 kbp DNA marker; lane 6, PCR performed on pJAZZ-ΔasI construct with hDHFR gene specific primers without MgCl₂/DMSO; lane 7, PCR performed on pJAZZ-ΔasI construct with hDHFR gene specific primers with MgCl₂; lane 8, PCR performed on pJAZZ-ΔasI construct with hDHFR gene specific primers with DMSO; lane 9, PCR performed on pJAZZ-ΔasI construct with QC1/QC2 primers.

Drug resistant parasites were seen 7 days post drug pressure initiation. The parasitemia was allowed to increase upto 30-40 % after which mice were bled and parasites were isolated from erythrocytes. PCR performed on the parasite lysate revealed that the *asI* gene locus was undisrupted (Fig. 3.21 e). The episomal copy of yAK was still retained in these parasites (Fig. 3.21 f). However, these parasites showed presence of hDHFR gene suggesting integration of the selection marker at a non-specific location into the parasite genome (Fig. 3.21 g).

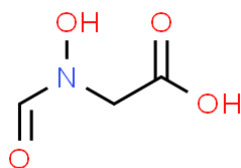
The reasons for the failure to obtain desired knock-outs in both *P. falciparum* and *P. berghei* parasites are discussed in section 3.2.

Alternatively, a chemical biology approach was used wherein a small molecule, hadacidin that specifically inhibits parasite adenylosuccinate synthetase (the enzyme that catalyses conversion of IMP to succinyl-AMP (sAMP)) was used to abolish fumarate generation in *P. falciparum* 3D7^{yAK}. Details of the chemical biology approach are discussed in the next section.

3.1.3. Hadacidin inhibition studies with transgenic parasites, *P. falciparum* 3D7^{yAK}

Introduction

Genetic manipulation techniques such as knock-out, knock-down or gene mutations have been immensely helpful in different types of cells to study the function of an enzyme or its associated substrates/products. However, these techniques have certain limitations like the lack of temporal control, lethality-leading to cell/organismal death, and in certain cell types-low transfection efficiencies, all of which make the generation of knockouts a daunting exercise. In such scenarios, tools that can perturb the activity of the enzyme - without having to alter the genome - are required to study the function of the said enzyme or its corresponding substrates/products. Selective small-molecule inhibitor(s) of the enzyme of interest serve the purpose and are useful chemical biology tools (Child, 2014). N-formyl hydroxyamino acetic acid is a small molecule that shows inhibitory activity against human adenocarcinoma (HAD) and hence is also known by the trivial name, **hadacidin** (Shigeura and Gordon 1962a, 1962b).



Hadacidin is L-aspartic acid analogue that inhibits parasite adenylosuccinate synthetase (ADSS) activity (Webster et al. 1984). Human erythrocytes lack adenylosuccinate synthetase enzyme (Bryk and Wiśniewski 2017; Lowy and Dorfman 1970) and are insensitive to hadacidin mediated inhibition; therefore, parasite growth arrest observed upon administration of hadacidin is exclusively through inhibition of PfADSS. *P. falciparum* 3D7^{yAK} parasites that can synthesize AMP independent of ADSS/ASL pathway can be used to study the impact of absence of fumarate, brought about by inhibiting PfADSS using hadacidin, on the overall parasite metabolism. With a known mechanism of action, hadacidin becomes a suitable chemical biology tool to investigate the metabolic significance of fumarate and hence was employed in the present study.

Results

3.1.3.1. Yeast adenosine kinase rescues hadacidin-induced growth defect

Transgenic parasites capable of synthesizing AMP via adenosine kinase are anticipated to be resistant to hadacidin inhibition. To test this hypothesis, we performed hadacidin inhibition studies on 3D7^{yAK} and 3D7^{EV} parasites *in vitro*. Growth of 3D7^{yAK} parasites was not inhibited in presence of high concentration of hadacidin (1 mM) whereas 3D7^{EV} parasites did not survive at the same concentration. Initially, experiment was performed for 48 hours i. e. one generation (Fig. 3.22).

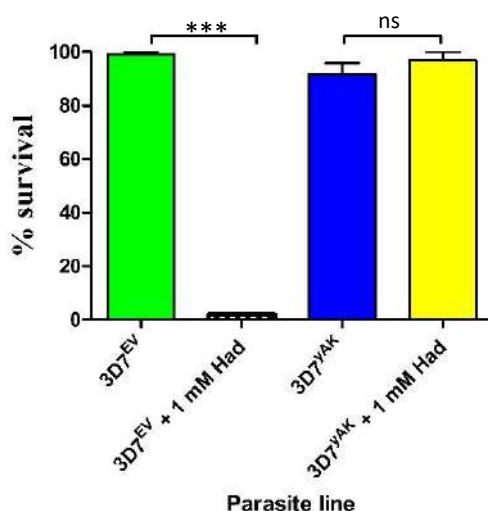


Figure 3.22: Hadacidin sensitivity. Over a period of 48 hours, i.e., one generation, parasites expressing an alternate enzyme for AMP generation (yAK) survive whereas parasites lacking yAK do not survive. Parasitemia was counted by making Giemsa-stained smears at each time point (T = 0 and T = 48 hours). Mean \pm SD values are represented and error bars indicated on top of each bar graph, n=2, ***p < 0.001. Graphs were plotted using GraphPad Prism v5.

The survival of 3D7^{yAK} parasites in presence of hadacidin attests that the yAK expressed in a heterologous manner in *P. falciparum* is functional and synthesizes AMP. However, these experiments were performed over a single generation and do not reflect upon necessity of fumarate, as the fumarate formerly present in the cells might be sufficient to support growth for one generation.

3.1.3.2. Growth pattern in prolonged presence of hadacidin highlights importance of fumarate

To examine whether the 3D7^{yAK} parasites survive without newly generated fumarate, both 3D7^{yak} and 3D7^{EV} parasite cultures were grown in presence of 500 μM (~ 3 times the IC_{50} for 3D7 wild type parasites, (Mehrotra et al. 2010)) hadacidin for longer time periods and in media supplemented with different purine sources: hypoxanthine alone (100 μM), adenosine alone (100 μM) and combination of hypoxanthine and adenosine (100 μM of each) (Fig. 3.23). Comparative analysis of growth rates in media containing only different purine sources showed that 3D7^{yAK} and 3D7^{EV} parasites grow best in the medium supplemented with both hypoxanthine and adenosine (100 μM) and growth in adenosine-supplemented medium was found to be better compared to parasite growth in hypoxanthine-supplemented medium (Fig. 3.23 a, c). Growth vigour/ replication rates of parasites in different purine sources are in the order:

Hypoxanthine + Adenosine > Adenosine > Hypoxanthine

As expected, 3D7^{EV} parasites failed to survive in presence of hadacidin, in all media conditions, (Fig. 3.23 b) with very few parasites seen in smears made at 48-hour time point. 3D7^{yAK} parasites on the other hand, survived and continued to grow, albeit with lesser vigour for 8 days i.e., 4 generations, indicating that AMP generated through yAK is partially rescuing the parasites from hadacidin inhibition (Fig. 3.23 d). The rescue of growth (from hadacidin inhibition) in presence of different purine sources does not follow the same order as the growth of control cultures (without hadacidin) (Fig. 3.23 d).

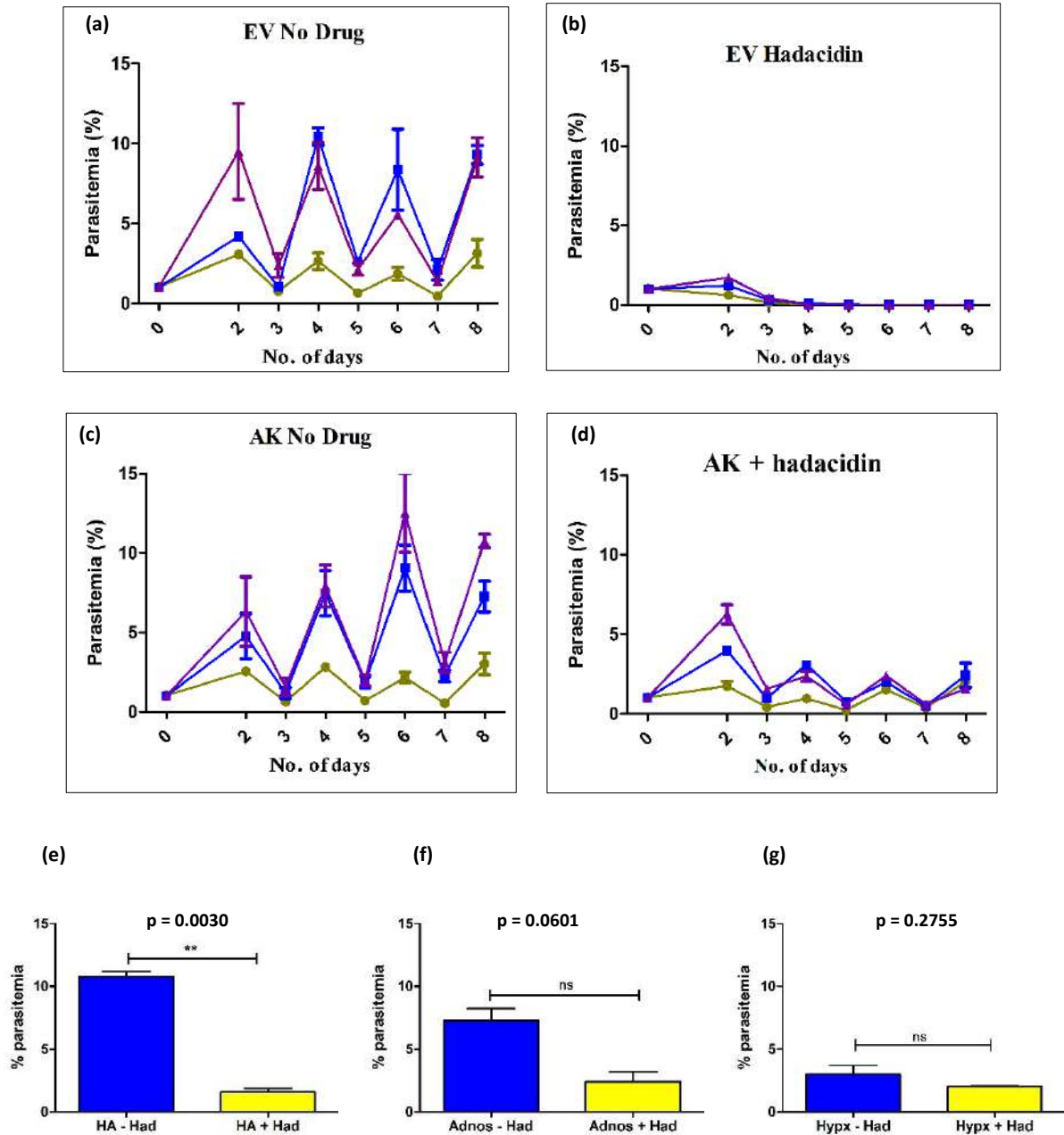


Figure 3.23: Comparative analysis of growth of parasites in presence of different purine sources. (a) Control $3D7^{EV}$ parasites without the drug show normal growth phenotype. Growth rates are the highest in growth media containing both purine sources. (b) As anticipated, $3D7^{EV}$ do not survive the unavailability of AMP and fumarate in the cellular milieu. (c) The growth rates of γ AK containing parasites is also the best in media containing both hypoxanthine and adenosine. (d) Similar trend is also followed in presence of hadacidin in the media for first 3 generation after which growth vigour seems to decline in all conditions. Unavailability of fumarate affects growth of parasites irrespective of the purine source present in the media indicating that fumarate is essential for parasite survival. The mean \pm SD for of two replicas is shown. % Parasitemia values were normalized to account for dilution (1:4) on day 3, 5 and 7. Green line indicates hypoxanthine only condition, blue line indicates adenosine only condition and purple line indicates (hypoxanthine + adenosine) condition. To support the observation that the inhibitory effect of hadacidin is more pronounced in medium supplemented with equimolar concentrations of hypoxanthine and hadacidin, statistical analysis was performed on % parasitemia data on day 8 of hadacidin treatment (e, f, g). p values are indicated for each plot which show that growth difference is more pronounced in medium supplemented with hypoxanthine + adenosine than in adenosine alone followed by hypoxanthine alone medium.

As seen from Figure 3.23, when growth rates/replication rates are higher in media supplemented with a combination of hypoxanthine/adenosine and with adenosine alone, inhibitory effect of hadacidin is

more pronounced. This observation is supported by the statistical analysis performed on data of day 8 of treatment (Fig. 3.23 e, f, g). The difference in growth rates and survival efficiency in media supplemented with different purine sources (in presence of hadacidin) can be explained as follows:

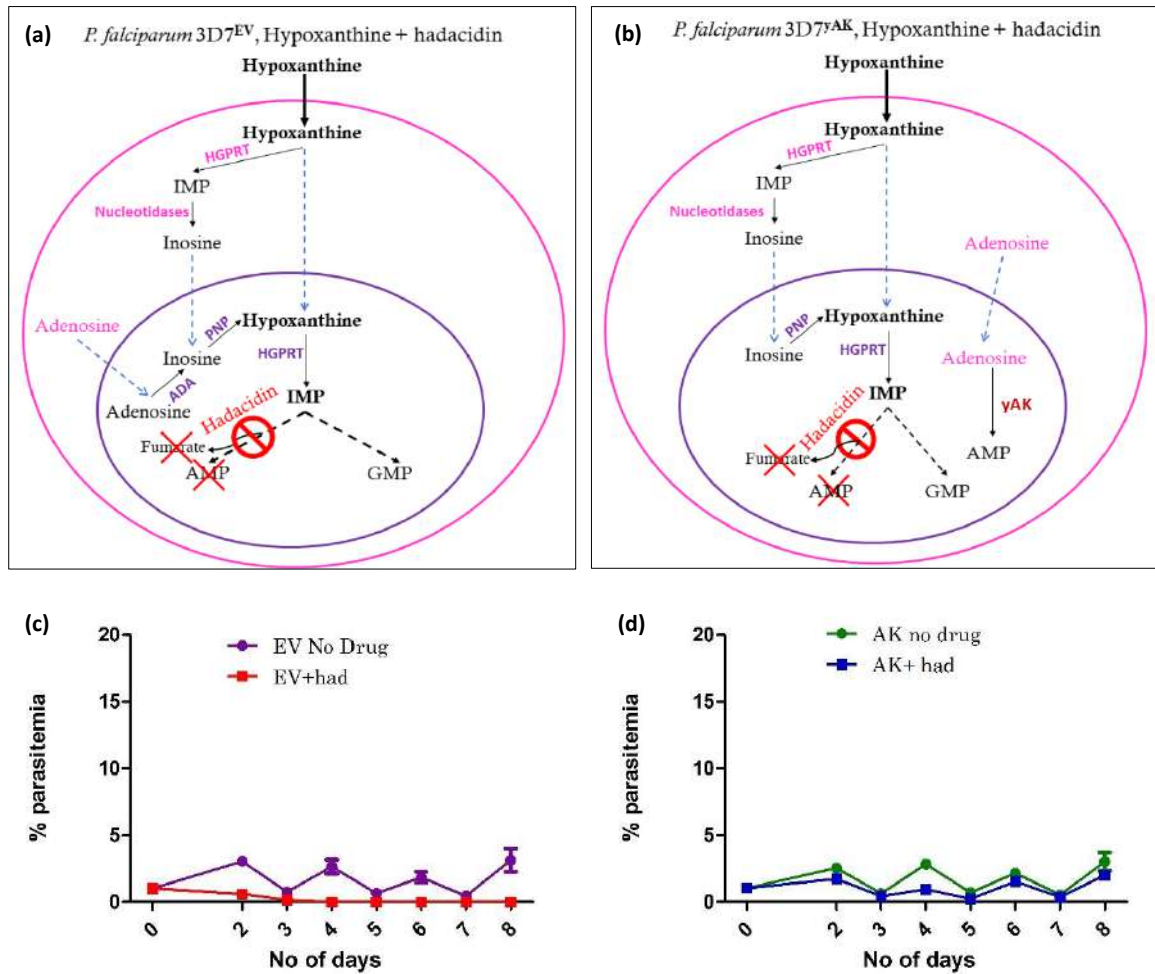


Figure 3.24: Schematic representation of AMP and fumarate production in hadacidin treated parasites grown in medium supplemented with only hypoxanthine. (a) 3D7^{EV} parasites fail to survive in presence of hadacidin as AMP synthesis through ADSS/ASL pathway is inhibited and no other pathway for AMP synthesis is available to the parasites. (b) 3D7^{yAK} parasites can synthesize GMP from hypoxanthine and AMP through episomally expressed yeast adenosine kinase using adenosine available from erythrocytes. But fumarate production is abrogated in both strains, presumably leading to slightly reduced growth seen in 3D7^{yAK} over four generations (8 days). Transport of metabolites is shown in blue dashed arrows, one step reactions are represented as black solid arrows, multistep reactions are shown in black dashed arrows, erythrocyte enzymes/metabolites are shown in pink, parasite enzymes are shown in purple. Same colour scheme is followed in the subsequent figure 3.25 and 3.26. Data presented in figure 3.23 has been re-plotted to compare (c) 3D7^{EV} and (d) 3D7^{yAK} parasites with and without hadacidin treatment. Purple solid circles represent 3D7^{EV} without hadacidin while red solid squares represent 3D7^{EV} in presence of hadacidin. Green solid circles represent 3D7^{yAK} parasites without hadacidin and blue solid circles 3D7^{yAK} parasites in presence of hadacidin. The same colour scheme is followed in the subsequent figures 3.25 and 3.26

Hypoxanthine: As shown in Fig. 3.24, in 3D7^{EV} and 3D7^{yAK} parasites, the exogenously supplemented hypoxanthine upon entering the erythrocyte can either be metabolised into IMP and inosine (by sequential action of HGPRT and nucleotidases, respectively) or transported directly across parasite plasma membrane via PfNT1 transporter. Utilization of hypoxanthine by host enzymes would diminish as maturing parasites gradually ingest erythrocyte cytosol by micropinocytosis (Rudzinska,

Trager, and Bray 1965; Slomianny, Prensier, and Charet 1985) for degradation and utilization of haemoglobin.

Addition of hadacidin to parasite cultures impairs AMP and fumarate production by inhibiting the endogenous (ADSS/ASL) pathway, leading to the death of 3D7^{EV} parasites, as expected. AMP can be synthesized in 3D7^{yAK} parasites (through episomally expressed yeast adenosine kinase) using adenosine salvaged from host erythrocyte; however, the yAK reaction does not generate fumarate, conceivably resulting in sub-optimal growth of 3D7^{yAK} parasites. In addition to the lack of fumarate generated through ADSS/ASL pathway, the low physiological concentration of adenosine in human erythrocytes (<1 μM) (Plagemann et al. 1985) and its absence in the synthetic RPMI 1640 used to grow cultures, may also contribute to moderate growth defect observed over subsequent generations in 3D7^{yAK} parasites.

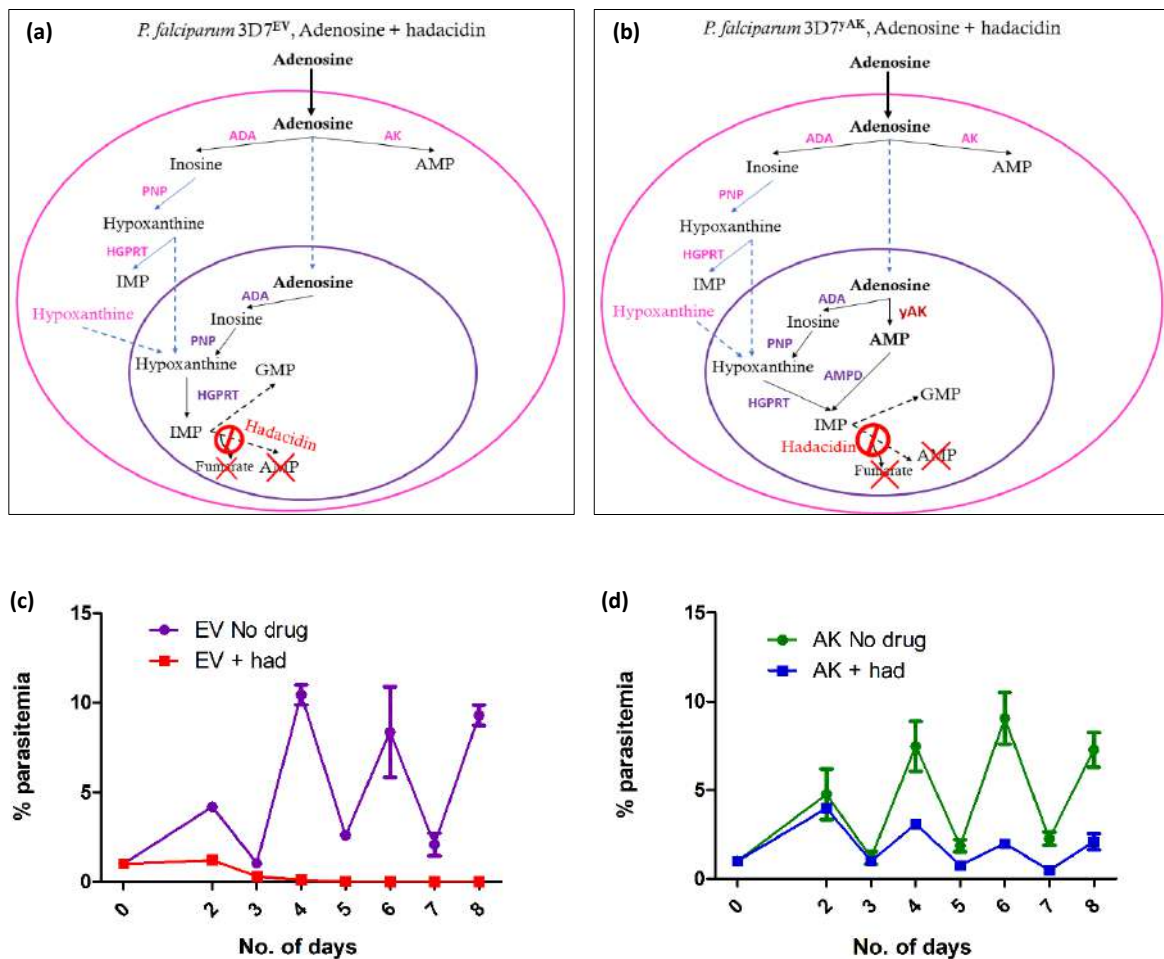


Figure 3.25: Schematic representation of AMP and fumarate production in hadacidin treated parasites grown in medium supplemented with only adenosine. Exogenously supplied adenosine would encounter three fates within erythrocyte cytosol. It can be used as substrate by erythrocytic adenosine deaminase and adenosine kinase or it can be transported directly across to the parasite via the PfNT1 transporter, present on parasite plasma membrane. Adenosine transported across parasite in (a) 3D7^{EV} parasites needs to be converted by parasite's adenosine deaminase to inosine which gets converted to hypoxanthine by purine nucleoside phosphorylase. Presence of hadacidin inhibits conversion of hypoxanthine to AMP, leading to death of these parasites. Although small amount of erythrocytic AMP is shown to be transported to parasite (Cassera et al. 2008), this amount seems to be insignificant and insufficient to support growth of 3D7^{EV} parasites. (b)

In case of 3D7^{yAK} parasites, the erythrocytic fate of adenosine is same as explained above. Within the parasite, adenosine can be partitioned between yAK and PfADA reactions leading to continuous synthesis of AMP and GMP, respectively, via these two routes. (c) 3D7^{EV} parasites in presence and absence of hadacidin and (d) 3D7^{yAK} parasites in presence and absence of hadacidin.

Adenosine: As shown in Figure 3.25, exogenously supplemented adenosine (100 μM) upon entering erythrocytes can be partitioned three ways in 3D7^{EV} and 3D7^{yAK} parasites: converted to inosine by erythrocytic adenosine deaminase (hADA), converted to AMP by erythrocytic adenosine kinase (hAK) and/or transported to parasites via PfNT1 and other low-affinity transporters. Small proportion of AMP synthesized within erythrocytes has been reported to be transported across parasite plasma membrane (Cassera et al. 2008); although our study shows that this AMP transport is insignificant as the 3D7^{EV} parasites (parasites that cannot synthesize AMP via alternate pathway) die in this media condition, in presence of hadacidin. A fraction of hADA reaction product, inosine can be transported to parasite or inosine can be converted to hypoxanthine by erythrocytic purine nucleoside phosphorylase (Sandberg et al. 1955) and transported to the parasites, although as mentioned previously, the contributions from erythrocyte metabolism decrease as parasites mature and ingest host cell cytosol.

Hadacidin sensitivity experiments under adenosine only condition show that although 3D7^{yAK} parasites can synthesize AMP, absence of collateral fumarate production leads to reduction in parasite growth and fitness (Fig. 3.23 d) when observed over multiple generations. On the other hand, 3D7^{EV} parasites, being unable to synthesize both metabolites, perish in less than 48-hours (Fig. 3.23 b).

Apart from fumarate, one may raise the possibility of perturbations in GMP levels when adenosine is provided as the sole purine precursor. However, this metabolic scenario is unlikely to exist. As adenosine can be converted to hypoxanthine owing to the functioning of *P. falciparum* adenosine deaminase (ADA), purine nucleoside phosphorylase (PNP) and HG(X)PRT reactions, GMP synthesis in both parasite lines will remain unaffected (Fig. 3.25). In 3D7^{yAK} parasites, adenosine would be partitioned between *P. falciparum* adenosine deaminase and yeast adenosine kinase, the former generating GMP and later generating AMP. The *in-vitro* enzymatic efficiency of yeast adenosine kinase is much higher ($K_{\text{cat}}/K_{\text{m}} = 34.35 \mu\text{M}^{-1} \text{s}^{-1}$) (Barrado et al. 2003) compared to *P. falciparum* adenosine deaminase ($K_{\text{cat}}/K_{\text{m}} = 0.23 \mu\text{M}^{-1} \text{s}^{-1}$) (Jaruwat et al. 2019), based on which it can be argued that yAK may drain the available adenosine, leaving only a small fraction for adenosine deaminase reaction, thereby depleting cellular GMP pools and resulting in severe growth defect seen in hadacidin-administered cultures. But it should be noted that growth of both parasite lines is remarkably good in control cultures (without hadacidin) under identical media conditions (Fig. 3.23 a, c), indicating that sufficient amount of GMP is produced with adenosine as precursor. In addition, hadacidin administration results in severe growth impairment (3.23 d) even in culture media containing both hypoxanthine and adenosine i.e. media containing precursors for synthesis of both AMP and GMP (explained in detail in the following section, figure 3.26), suggesting that GMP depletion is not a major cause of growth deficit seen in adenosine (only) media.

The two experiments together show that providing precursors for AMP and GMP fail to restore growth of hadacidin treated parasites completely and strongly suggest that severe growth defect observed in hadacidin treated parasites is in all likelihood due to the unavailability of fumarate.

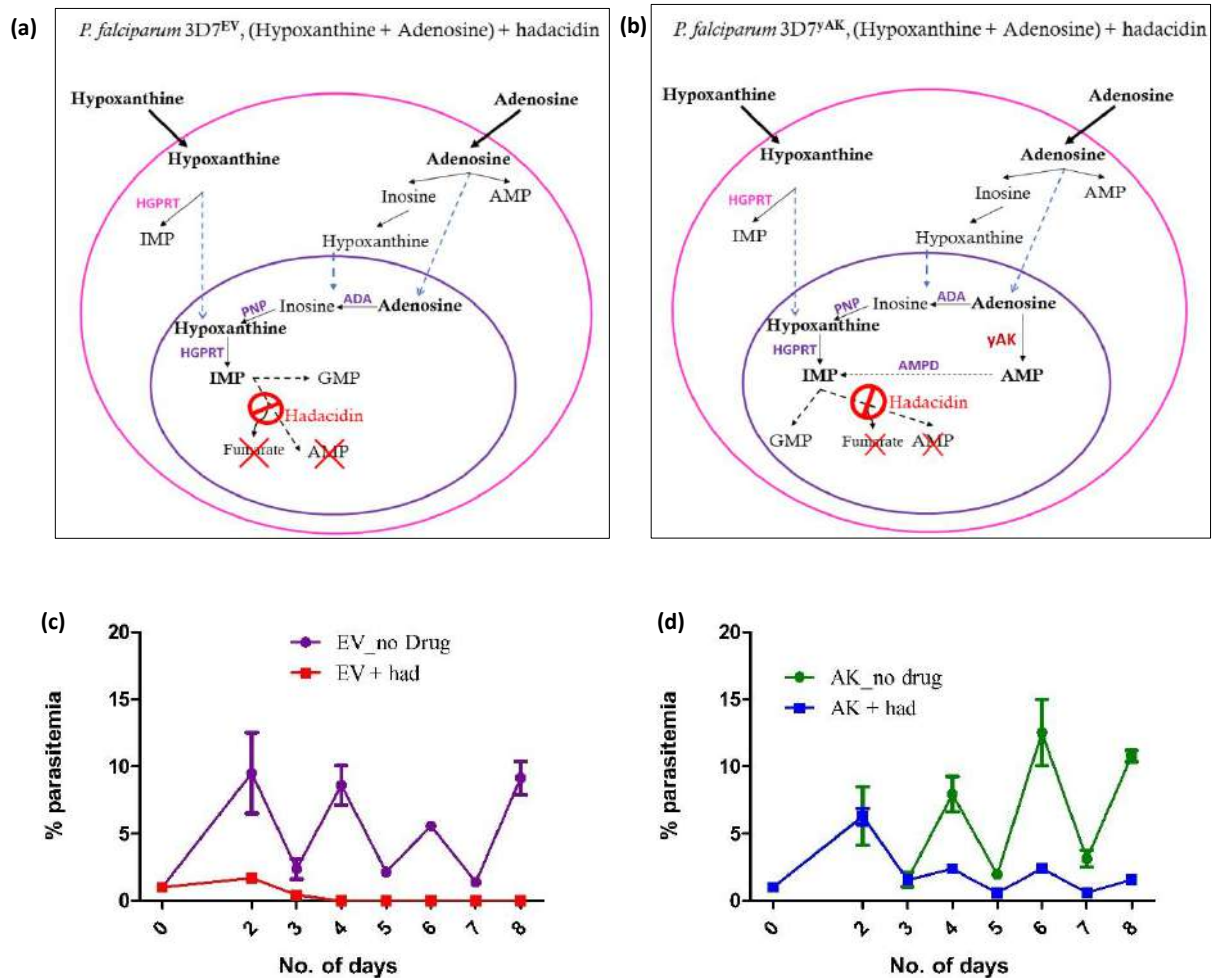


Figure 3.26: Schematic representation of AMP and fumarate production in hadacidin treated parasites grown in medium supplemented with hypoxanthine and adenosine. In both parasite lines, the fate of hypoxanthine and adenosine within the erythrocyte is identical. Both parasite lines grow best in this media condition as shown in Fig. 3.8 a, c. Presence of hadacidin abrogates AMP synthesis completely in (a) 3D7^{EV} parasites, causing death of these parasites. (b) In 3D7^{AK} parasites, although AMP synthesis through ADSS/ASL pathway is abrogated due to hadacidin, AMP can still be synthesized through γ AK and parasites survive. However, fumarate production from ADSS/ASL pathway is abolished, which possibly manifests as severe growth defect. (c) 3D7^{EV} parasites in presence and absence of hadacidin and (d) 3D7^{AK} parasites in presence and absence of hadacidin.

Adenosine + hypoxanthine: Figure 3. 23 (a, c) shows that replication rates (growth vigour) of both parasite lines are best in (control-culture) media supplemented with equimolar concentrations (100 μ M) of both hypoxanthine and adenosine, probably due to abundance of purine nucleotides generated via the salvage pathway. However, hadacidin-induced growth defect is highly pronounced in this condition presumably because the depleting fumarate concentration (over multiple generations) is insufficient to support higher growth rates seen in parasites grown in this media condition. Metabolic scenario in

cultures supplemented with both purine sources are schematically represented in Figure 3.26. In hadacidin-administered 3D7^{yAK} parasite culture, with adenosine synthesizing AMP and hypoxanthine synthesizing GMP, purine nucleotide concentrations would be abundant, driving enhanced parasite growth while simultaneously exhausting cellular fumarate stores in initial few generations (first 2 generations after hadacidin addition). As new fumarate is not produced from ASL reaction, parasite growth in subsequent generations (third and fourth generation) is severely diminished.

Supplementation of the culture medium containing hadacidin with 5 mM fumarate or 5 mM malate (in independent experiments) did not show any significant growth advantage over the medium containing hadacidin alone. This suggests that the decrease in parasitemia that we observe over prolonged culture of 3D7^{yAK} parasites in the presence of hadacidin could be attributed to: depletion of fumarate levels, non-optimal AMP levels or a combination of variations in both metabolite levels. External supplementation of fumarate/malate in the culture medium does not guarantee optimal availability of these metabolites in the mitochondrion where they can be utilized. Moreover, overexpression of an AMP synthesizing enzyme in the transgenic parasites could result in loss of cross-regulation of adenylate and guanylate pools, a situation that cannot be rescued by external supplementation of fumarate/malate.

The possibility of non-specific effects of hadacidin also needs to be considered. Hadacidin is known to be a potent competitive inhibitor of aspartate binding to adenylosuccinate synthetase (Eaazhisai et al. 2004; Jahngen and Rossomando 1984; Raman et al. 2004). The absence of significant differences in growth of 3D7^{yAK} parasites over one cycle (48 hours) indicates that off-target effects of hadacidin, if any, do not have dramatic consequences. A targeted metabolome profiling of 3d7^{yAK} parasites in presence and absence of hadacidin should provide the metabolic basis for the fitness compromise of these parasites, thereby shedding light on the metabolic significance of fumarate generated during AMP synthesis, if any.

It should be recalled that all enzymes of the TCA cycle in *P. falciparum* (except fumarate hydratase and malate: quinone oxidoreductase) can be deleted. This suggests that fumarate produced from glutamine via α -ketoglutarate or through branched-chain keto acid dehydrogenase (BCKDH) routes is not essential for intra-erythrocytic parasite survival (Fig. 1.6). The essentiality of FH therefore could be to utilize fumarate generated from purine nucleotide cycle. Earlier studies from our laboratory had demonstrated that fumarate is not a metabolic waste but is indeed metabolized by the parasites (Bulusu et al. 2011) but the metabolic essentiality of fumarate to the overall parasite metabolism remains unanswered. Studies addressing the metabolic significance of fumarate would also address the question of why do the *Plasmodium* parasites synthesis AMP through ADSS/ASL pathway rather than APRT or AK pathways. A targeted metabolomics study on 3D7^{yAK} parasites in presence or absence of hadacidin using ¹³C labelled glutamine and aspartate may provide further understanding.

All cells including parasites exhibit the potential for metabolic plasticity (Guggisberg et al. 2018; Jia et al. 2019). A reduced metabolic flux from one pathway can lead to rewiring of metabolism to increase flux through another pathway. Inhibition of fumarate generation from purine nucleotide cycle can therefore possibly be compensated by increased flux of glutamine derived fumarate in hadacidin-treated parasites. The RPMI 1640 growth medium used in parasite culturing contains 2 mM glutamine which can be sufficient to fulfil increased glutamine requirements, if any, in hadacidin-administered parasites. To test this hypothesis, hadacidin-administration experiments need to be carried out in glutamine-devoid RPMI 1640 growth medium and parasite growth phenotype examined.

3.2. Discussion

Fumarate being a *by-product of nucleotide metabolism* and an *intermediate of tricarboxylic acid cycle* is a plausible link between nucleotide and energy metabolism. The transgenic parasite lines generated in this work, *P. falciparum* 3D7^{yAK} and *P. berghei* ANKA^{yAK}, and the experiments performed so far suggest that fumarate is essential for parasite growth and survival; growth of *P. falciparum* 3D7^{yAK} parasites is compromised in presence of hadacidin and we were unable to knock-out *adss/asl* in either of the transgenic parasite lines. In addition, yAK expressing parasite lines are good reagents for exploring essentiality of other parasite genes and for performing mass spectrometry-based metabolomics.

3.2.1. Persistent essentiality of *adss* and *asl* in metabolically rewired parasites

Plasmid constructs generated to delete *adss* and *asl* genes, pCC1- Δ asl, pL7- Δ adss, pL- Δ asl were transfected in *P. falciparum* 3D7^{yAK} parasites multiple times. Growth medium was supplemented with different metabolites such as adenosine, fumarate and malate to encourage growth of KO transfected parasites. Transfected cultures were maintained for more than two months with regular media changes and RBC replenishment. However, none of the attempts yielded drug resistant parasites.

Transposon mutagenesis carried out by Zhang and co-workers using *piggybac* transposon to achieve whole genome loss-of-function mutagenesis in *P. falciparum* indicated that genes lacking insertions are essential as they cannot be disrupted by piggyBac insertion. Both *adss* (PF3D7_1354500) and *asl* (PF3D7_0206700) genes were shown to have 0 insertions within their coding sequence and therefore inferred as **non-mutable in the CDS** (Zhang et al. 2018) i.e. these genes are essential and cannot be disrupted.

4454	chr13	PF3D7_1354400	V-type proton ATPase 21 kDa proteolipid subunit, putative	Non - Mutable in CDS	0.251	-2.73	0
4455	chr13	PF3D7_1354500	adenylosuccinate synthetase	Non - Mutable in CDS	0.122	-3.107	0
4456	chr13	PF3D7_1354600	60S ribosomal protein L7-2, putative	Non - Mutable in CDS	0.119	-2.982	0
4457	chr13	PF3D7_1354700	conserved Plasmodium protein, unknown function	Non - Mutable in CDS	0.13	-2.891	0
209	chr2	PF3D7_0206600	DNA-directed RNA polymerase III subunit RPC10, putative	Non - Mutable in CDS	1	0	0
210	chr2	PF3D7_0206700	adenylosuccinate lyase	Non - Mutable in CDS	0.121	-2.994	0
211	chr2	PF3D7_0206800	merozoite surface protein 2	Non - Mutable in CDS	0.988	-2.005	0
212	chr2	PF3D7_0206900.1	merozoite surface protein 5	Non - Mutable in CDS	0.988	-2.098	0

Additionally, a genome wide knock-out study performed in *P. berghei*, using knock-out constructs available in Plasmogem, also found *asl* to be an essential gene (Bushell et al. 2017; Schwach et al. 2015). The final KO construct for *adss* gene is unavailable with Plasmogem and therefore no growth phenotype results were noted for this gene (Bushell et al. 2017).

4517	TGGT1_249520			-0.42	
4518	TGGT1_223262			-0.41	
4519	TGGT1_321390			-0.41	
4520	TGGT1_263190	PF3D7_0206700	PBANKA_0304300	-0.41	0.04 Essential
4521	TGGT1_215300			-0.41	
4522	TGGT1_200410			-0.41	
4523	TGGT1_286430			-0.41	

These gene deletion attempts were made in wild type parasites with a batch approach- several genes targeted in a single experiment. The failure of these studies to obtain knock-out prompted us to generate transgenic, metabolically rewired parasite lines, capable of synthesizing AMP independent of collateral fumarate production to increase our chances of obtaining a (*asl/adss*) gene deletion strain and thereby permit examination of role of a TCA cycle intermediate.

Our experiments to knock-out *asl* gene from the genome of *P. berghei* ANKA^{YAK} using pJAZZ- Δ *asl* plasmid construct yielded drug resistant parasites. However, upon genotyping it was found that the drug selection marker was integrated at a non-specific location into the genome and the wild type *asl* locus was intact. These results strongly suggest that this gene codes for an essential enzyme and hence cannot be deleted despite rewiring parasite metabolism to synthesize AMP via an alternate pathway; the essentiality could be attributed to: depletion of fumarate, insufficient AMP or a combination of both.

Boitz and co-workers had generated Δ *adss*, Δ *asl* *Leishmania donovani* parasite lines (Boitz et al. 2013) that were found to proliferate only in medium supplemented with adenosine or adenine. *L. donovani* expresses four purine salvage pathway enzymes: HGPRT, XPRT, APRT and AK. Δ *adss* and Δ *asl* parasite lines displayed severely compromised mouse infectivity despite AMP synthesis via APRT and AK. The growth deficit was more pronounced in Δ *asl* parasites compared to Δ *adss* parasites and the authors speculate that this could be due to build-up of adenylosuccinate (sAMP) – that serves as metabolic ‘dead-end’ sink draining IMP, thereby also decreasing GMP production - at the expense of nucleotide production in Δ *asl* parasites (Boitz et al. 2013). On the other hand, in Δ *adss* parasites, majority of IMP can be converted to GMP whereas adenylosuccinate pools can be replenished from exogenously supplied adenosine (via AK) and adenine (via APRT) (Boitz et al. 2013) resulting in relatively less severe growth deficit. Another possible reason for growth deficit observed with Δ *adss* and Δ *asl* *Leishmania* parasites could be elimination of fumarate production via ADSS/ASL pathway (and accompanying lack of fumarate metabolism); although not alluded by the authors, absence of ADSS/ASL derived fumarate could be adversely affecting parasite metabolism and thereby parasite virulence.

Our attempts to knock-out *asl* from *P. falciparum* 3D7^{yAK} and *P. berghei* ANKA^{yAk} genome could encounter a similar metabolic scenario: in parasites that could have taken up the plasmid after transfection and undergone *asl* disruption, functional ADSS could generate sAMP that could not be utilized further while simultaneously draining IMP that could be utilized for GMP synthesis, all the while not generating any fumarate. This metabolic scenario would fail to support parasite growth and proliferation, and transgenic parasites would never appear in cultures.

On the other hand, although inhibition of ADSS via hadacidin is tolerated in *P. falciparum* 3D7^{yAK} parasites, adversely-affected growth phenotypes suggest functional essentiality of this enzyme and requirement of fumarate (that will not be produced from subsequent ASL reaction) for parasite growth and survival, that is conceivably preventing us from obtaining knock-out transfectants despite providing an alternate enzyme (pathway) for AMP synthesis.

Few more alternate explanations can be provided justifying the failure to obtain KO parasites in *P. falciparum*. Technical problems during electroporation resulting in suboptimal transfection efficiency are probable. A plasmid construct has to cross 4 membranes i.e. erythrocyte plasma membrane, parasitophorous vacuolar membrane (PVM), parasite plasma membrane and the parasite nuclear membrane before it can reach the nucleus of the parasite. Failure to cross these membranes could result in loss of plasmid before reaching the parasite nucleus. Different transfection techniques were attempted during the course of the study to try and increase the probability of obtaining desired KO transfectants. In a few attempts of transfection, parasites were transfected with pFCEN plasmid as a positive control and maintained under identical culture conditions post-transfection. pFCEN plasmid was successfully transfected in all those attempts, ruling out the possibility of technical difficulties during transfection.

The sgRNAs used for CRISPR-Cas9 mediated KO were designed using EuPaGDT (Tarleton and Peng, 2015), an online tool that designs sgRNA based on parameters such as off-target analysis, on-target searching, efficiency/activity prediction, searching microhomology etc. Despite all these considerations, the chosen sgRNA could prove ineffective *in-vivo*. Possibly the sgRNA we chose during this study was not optimal and more sgRNAs need to be tried out in future for both *adss* and *asl* targets.

In order to establish that the CRISPR-Cas9 technique works in our experimental setup, a non-essential gene could be used as a target and KO plasmid construct for that gene need to be transfected in *P. falciparum* 3D7^{yAK} parasite line. The non-essential gene locus chosen in most of the studies employing CRISPR-Cas9 is the knob-associated histidine rich protein (*kahrp*) (Ghorbal et al. 2014; Wagner et al. 2014). The KO construct, pL7-Δkahrp was recently received as a kind gift from Dr. Jose-Juan Lopez-Rubio, Biology of Host-Parasite Interactions Unit, Institut Pasteur, Paris, France. This construct can be used in all subsequent transfections to establish the working of the technique in our experimental setup.

Moreover, complementation of enzyme function through restoration (episomal expression) of the disrupted gene is often used to obtain knock-outs of essential genes. To this end, ASL/ADSS gene from *Plasmodium* or highly homologous to *Plasmodium* genes can be episomally expressed via pFCEN plasmid vector and the resultant parasite lines (overexpressing ASL/ADSS) can then be subsequently transfected with the respective gene KO vectors. It is possible to implement this approach in *P. falciparum* as there are 3-4 selection markers available that support sequential genetic manipulations. If the endogenous *asl* locus would be disrupted from the genome of the transgenic parasites episomally expressing *asl*, it will indicate that the failure to obtain *asl* gene knock-out in yAK expressing parasites was due to the non-availability of fumarate; whereas *asl* overexpressing transgenic parasites can synthesize both AMP and fumarate, yAK overexpressing parasites can only synthesize AMP and the demand for fumarate in these parasites could result in inability to knock-out endogenous *asl* locus. However, as suggested previously, the AMP levels in yAK parasites could be non-optimal resulting in loss of cross-regulation of adenylate and guanylate pools. AMP levels in the yAK expressing parasites need to be determined in presence and absence of hadacidin (using metabolomics); the chemical biology approach in combination with genetic approach will help us understand the essentiality of fumarate.

In case of *P. berghei* parasites, non-specific/random integration of the antibiotic selection marker (hDHFR) into the genome under drug pressure (WR99210) is an indication of the essentiality of the gene encoding adenylosuccinate lyase, despite the presence of functional adenosine kinase. However, due to the dearth of selection markers in *P. berghei*, DHFR from different organisms, with different sensitivities to WR99210 had to be used. Although, this strategy has been demonstrated to work in the murine malaria parasites (De Koning-Ward et al. 2000), it is not widely used in the field. We used pbCEN5 plasmid with Tgdhfr-ts selection marker, to express yeast adenosine kinase in *P. berghei* ANKA due to its availability in our laboratory and ease of obtaining transfectants. Pyrimethamine resistant *P. berghei* ANKA^{yAK} parasite line was obtained, validated and subsequently transfected with pJAZZ- Δ asl that carries hDHFR selection cassette. Subcutaneous WR99210 administration resulted in death of parasites initially, followed by appearance of drug resistant parasites 10 days post drug-initiation; however, the drug-resistant parasites showed retention of the wild type *asl* locus and presence of hDHFR marker (confirmed by PCR, Fig. 3.21 g), both events indicating integration of plasmid at wrong genomic locus. Wrong integration under drug pressure suggests a conceivable selection pressure for the retention (and ensuing essentiality) of *asl*, which is generation of fumarate in addition to AMP. There could have been a population of transfected parasites wherein the pJAZZ- Δ asl construct integrated at a correct genomic locus but those parasites could have been highly fitness compromised and therefore were eliminated from the mouse system within a few generations. This indicates that even in the *in-vivo* scenario where the host (mouse) metabolism could probably compensate for inadequacies in the parasite metabolism, deletion of adenylosuccinate lyase is not possible, further stressing upon the essentiality of the enzyme function.

An alternate approach comprises recycling the selection marker (hDHFR) and it is more commonly used to overcome ambiguity of selection process encountered with the currently used strategy; it needs to be attempted in future. Briefly, yAK can be expressed via its integration into a non-essential gene locus such as p230 (Manzoni et al., 2014) (through double-crossover homologous recombination) using plasmid containing hDHFR as positive selection marker and yFCU as a negative selection marker. Pyrimethamine resistant transgenic parasites can then be subjected to 5-FC treatment that kills parasites expressing yFCU and selects for those that lost yFCU (Fig. 3.27) (Braks et al. 2006)

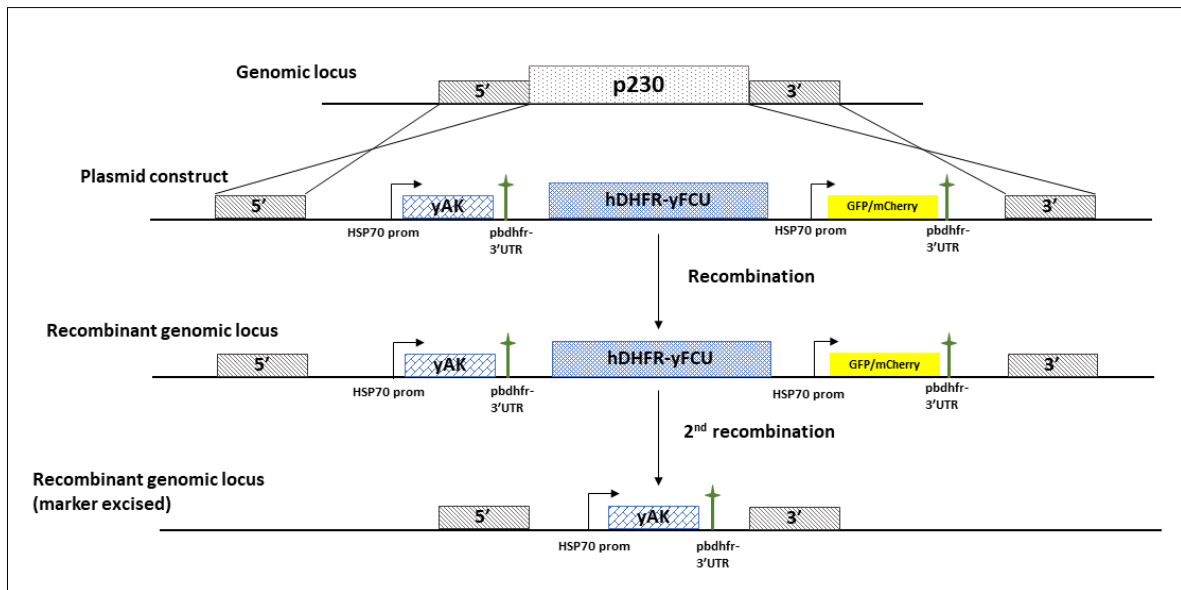


Figure 3.27: Schematic representation of workings of positive-negative selection protocol. To integrate yAK into the genome of *P. berghei*, at p230 locus, and recycle hDHFR selection marker for additional genetic manipulation, *P. berghei* wild type parasites need to be transfected with a plasmid construct harbouring yAK, hDHFR/yFCU and GFP/mCherry. Presence of two Pbdhfr-3'UTR at specific locations on the plasmid can result in excision of DNA fragment between the two sequences upon negative selection with 5-fluorouracil, resulting in loss of hDHFR-yFCU and GFP/mCherry. Parasites lacking hDHFR-yFCU and GFP/mCherry can be confirmed by genotyping and clonally selected by limiting dilution and subsequently used for deletion of *asl* (using pJAZZ- Δ asI plasmid construct).

Figure 3.27 outlines the details of positive-negative selection for integration of yAK into p230 locus of *P. berghei*. Following negative selection, parasites in which marker (hDHFR-yFCU) has been excised can be clonally selected by performing limiting dilution cloning and the parasite line used for subsequent deletion of *asl* locus.

3.2.2. Future uses of transgenic parasite lines generated

We generated parasite line expressing functional yeast adenosine kinase which synthesizes AMP from adenosine in addition to HG(X)PRT/ADSS/ASL mediated AMP production. This parasite line therefore can be used to study the essentiality of enzymes utilizing AMP such as AMP deaminase. An earlier study from our laboratory has shown that AMPD enzyme is non-essential to the complete life-cycle of *P. berghei* parasites (Nagappa et al. 2019). The authors of the study attributed non-essentiality of AMPD to the lack additional pathways for salvage of adenylate nucleotide in *Plasmodium* parasites, such as AK (found in closely related Apicomplexan parasites such as *Toxoplasma gondii*, *Theileria* etc.)

and APRT (found in *Tetrahymena*). Transgenic 3D7^{yAK} parasite line is a suitable tool to conclusively prove this inference, as AMPD activity will be imperative to utilize excess AMP (generated from two sources) that can inhibit several anabolic enzymes in the parasite (Fig. 3.28). A gene that is non-essential may become essential under an altered metabolic condition, confirming earlier hypothesis that AMPD essentiality is conditional to presence of multiple routes of AMP synthesis, thus providing a deeper understanding of the parasite metabolism.

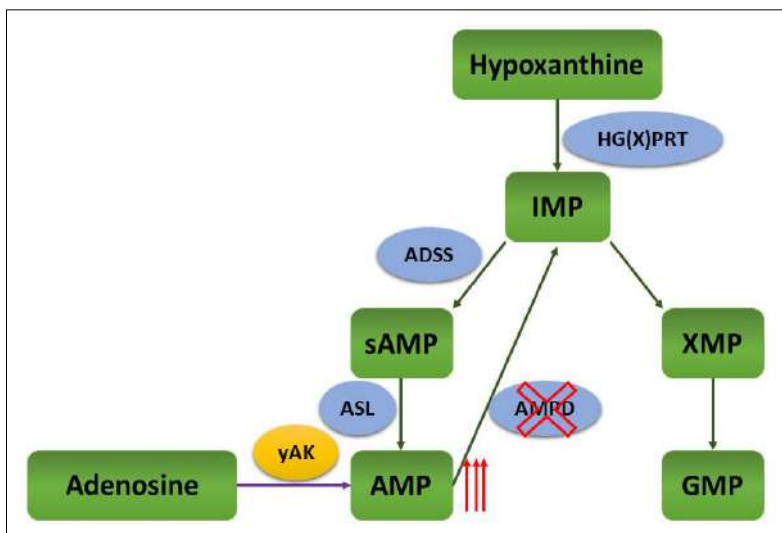


Figure 3.28: Schematic representation of potential utility of yAK expressing strain to address metabolic role of PfAMPD. yAK expressing parasites are anticipated to synthesize higher amount of AMP compared to wild type parasites, potentially inducing a need for AMP utilizing enzyme such as AMP deaminase.

Alternatively, the rewired metabolism could render an essential fumarate hydratase enzyme non-essential as explained below: As noted in the introduction section (Chapter 1), fumarate hydratase (FH) is one of the two TCA cycle enzymes essential to the parasite and attempts to knockout the enzyme were unsuccessful (Ke, H et al. 2015). The essentiality of the enzyme is attributed to its function in utilization of fumarate generated through PNC in the cytosol. The 3D7^{yAK} parasite line generated in this study survives in presence of 500 μ M (\sim 3 times the IC₅₀) hadacidin for 3-4 generations, albeit with reduced growth vigour/growth rates.

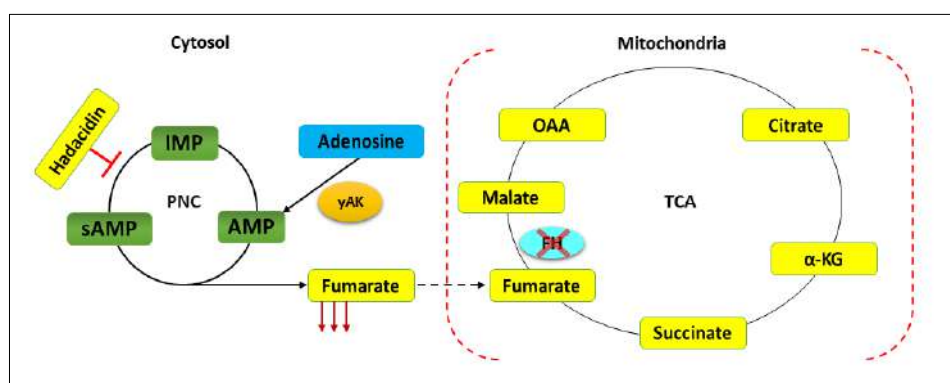


Figure 3.29: Schematic representation of potential metabolic scenario that can enable deletion of fumarate hydratase from *P. falciparum*. yAK expressing parasites could survive in presence of hadacidin as seen in this study. Sub-optimal

concentrations of hadacidin, just enough to partially inhibit ADSS reaction without severely compromising parasite growth for prolonged periods, could be used in γ AK culture to reduce cellular fumarate concentration. FH activity is postulated to be essential to recycle fumarate for regeneration of aspartate that can be fuelled back to PNC; however, FH activity could also be essential to prevent fumarate toxicity i.e. succination of cellular proteins by fumarate or reverse reaction of adenylosuccinate synthetase draining AMP. Reduction in cellular fumarate amounts in presence of hadacidin could alleviate the fumarate toxicity, thereby enabling deletion of fumarate hydratase gene.

If lower concentrations of hadacidin ($\leq IC_{50}$) are found to sustain growth of these parasites for longer time duration, this culture can be used to achieve *fh* gene deletion. The rationale behind the proposed experiment (Fig. 3.29) is that lower concentrations of hadacidin would result in partial inhibition of ADSS activity, lowering the fumarate production rather than completely abolishing it, which can sustain parasite growth as well as not result in excess fumarate accumulation (fumarate toxicity). Medium can be supplemented with malate and/or aspartate and adenosine post transfection to assist growth of the *fh* knock-out (FHKO) parasites: malate to ensure continued functionality of MQO, aspartate to fuel PNC and adenosine to feed into γ AK reaction. We speculate that these media conditions could perhaps lead to deletion of *fh* gene and establish its role in parasite metabolism. Adenosine kinase expressing parasite line therefore could be a useful resource to understand significance of enzymes in specified metabolic contexts and offer additional support to earlier observations made in different studies from our laboratory (Jayaraman et al. 2018; Nagappa et al. 2019).

In conclusion, having established a parasite line that expresses an alternate pathway for AMP generation in order to un-couple AMP synthesis from fumarate generation and demonstrated the resistance of this strain to ADSS inhibitor hadacidin, the next step in this regard is to perform metabolomics on the wild type and transgenic parasites and examine the participation and contribution of fumarate in different cellular pathways.

3.3. Future Directions

Fumarate accumulation is shown to be a hallmark of Hereditary leiomyomatosis and renal cell cancer (HLRCC) in mammalian cells; excess fumarate can react with cysteine residues in proteins leading to a PTM termed succination (Merkley et al., 2014). As the TCA cycle is found to be dispensable during the intraerythrocytic stages of *Plasmodium* parasites (Ke, H et al. 2015), the question arises of ‘what could be the significance of the TCA intermediate, fumarate, that is generated in copious amounts during AMP synthesis?’ A previous study from our laboratory had demonstrated that fumarate is not a metabolic waste, rather free parasites metabolise exogenously supplied fumarate into malate, aspartate, pyruvate, and lactate (Bulusu et. al., 2011). The sole enzyme that can act on fumarate in *Plasmodium spp.* is fumarate hydratase, (enzyme that is present in mitochondria and converts fumarate into malate) and is essential for survival and growth of asexual stage parasites as shown by another study from our laboratory (Jayaraman et al., 2018) and by Ke and co-workers (Ke et al., 2015). Essentiality of FH is attributed to its role in utilization of fumarate to prevent fumarate accumulation

in the cytosol and enable regeneration of aspartate for continued functioning of ADSS/ASL and other metabolic processes. **However, a detailed understanding of the involvement of fumarate in different cellular pathways, if any, is lacking and this study was an attempt to i) generate parasite lines that could enable us to examine the pathways affected by absence of fumarate and ii) further study the metabolism in those transgenic lines using *in vitro* assays and metabolomics (using LC-MS).**

Transgenic parasite lines episomally expressing yeast adenosine kinase, that can convert adenosine into AMP, were generated and validated in both *P. falciparum* and *P. berghei*. These lines were then used to carry out deletion of either adenylosuccinate lyase or adenylosuccinate synthetase. Deletion of either of the genes would abolish generation of fumarate. Neither of the genes could be deleted from either *P. falciparum* or *P. berghei* despite extensive efforts. Simultaneously, a chemical biology approach was attempted which involved use of the specific PfADSS inhibitor, hadacidin, (Shigeura and Gordon, 1962a, 1962b), which inhibits growth of intraerythrocytic *Plasmodium* parasites. *P. falciparum* 3D7^{yAK} parasites survived in presence of 500 μ M hadacidin for 3-4 generations (\sim 3 times IC₅₀) whereas *P. falciparum* 3D7^{EV} could not survive for more than 48 hours. Growth of *P. falciparum* 3D7^{yAK} line in presence of hadacidin and different purine sources was monitored via *in vitro* assays.

In future, relative intracellular concentrations of AMP and fumarate in these parasites need to be estimated using metabolite assay kits and/or mass spectrometry.

Comparison of metabolite levels in *P. falciparum* 3D7^{yak} parasites supplemented with and without hadacidin would reflect the changes associated with lack of fumarate from parasite metabolism. Targeted metabolomics and metabolite profiling using U-¹³C glucose and/or glutamine would help in tracing the metabolic pathways which are affected by lack of fumarate. **To this end, initial experiments to standardize metabolite extraction from *P. falciparum* parasites were performed.** The detailed protocol for intracellular metabolites extraction from *P. falciparum*, that we optimised is described below.

Metabolite extraction

Metabolite extraction procedure described by Llinás Lab was followed (Allman et al. 2016). The protocol is divided in four parts starting from preparation of parasites, enrichment of late stage parasites, plate setup and treatment and metabolite extraction.

a) Preparation of parasites

Parasites were synchronized tightly by performing 5% sorbitol synchronization in cycle one. At the end of first cycle, to achieve a shorter window of synchronization, late stage trophozoites were enriched by Percoll treatment and put back in culture with fresh erythrocytes at 2% haematocrit. At the beginning of the second cycle, parasites were synchronized again by 5% sorbitol synchronization. To test an inhibitor on wild type and/or transgenic parasites, 250 mL culture of each strain type (2% haematocrit with 10% parasitemia) is required in order to obtain

untreated and compound (inhibitor) treated samples in triplicates. To obtain good quality data, 1×10^8 parasites /condition are recommended for each replicate. With our experimental setup-culture, synchronization and enrichment techniques-a total of 5.0×10^7 to 1.0×10^8 parasites were obtained during each experiment.

b) Enrichment of late stage parasites for treatment

Magnetic assisted cell sorting (MACS) is a preferred enrichment method when performing metabolomics experiments as it is less harsh on cells and achieves close to 90% enrichment. Enrichment was performed using MACS protocol explained earlier, with a slight modification. Column washes are performed using complete RPMI in place of incomplete medium. Parasites were eluted in 5 mL complete medium and collected in 15 ml Falcon tubes. 50 μ L cell suspension was removed to perform cell count and make Giemsa-stained smears while remaining free-parasite's suspension was transferred to a T25 flask and put back in the incubator.

c) Plate setup

To each well of a 6-well plate, 4 ml pre-warmed complete medium was added. After counting the cell number, cell density was adjusted to 1×10^7 / 1ml – 1×10^8 / 1 ml as per the yield during MACS. 1 ml cell suspension was then added to the wells. Appropriate concentration of the drug or vehicle was added to the respective wells and the plate was placed in the incubator for 3 hours. At the end of incubation time, plates were removed from the incubator. 4 ml media was aspirated from each well and the remaining medium was mixed by pipetting to resuspend the cells settled at the bottom of the well.

d) Metabolite extraction

Eppendorfs were pre-chilled by placing them on ice. The cell suspension from each well was transferred to those appropriately labelled, pre-chilled eppendorfs and transferred on ice immediately. The tubes were centrifuged at 10,000 rpm for 30 sec at 4 °C. The supernatant RPMI was aspirated quickly and pellets were gently resuspended in ice cold 1x PBS (prepared in LC-MS grade water) and centrifuged at 10,000 rpm for 30 sec at 4 °C. Supernatant was aspirated from one tube and cell metabolism was quenched by adding 1 ml of ice-cold 90 % methanol and quickly resuspended by vortexing. The tube was placed on ice and remaining tubes were processed in the same manner. Once extraction/quenching of all samples was complete, all the tubes were vortexed for additional 10 sec to ensure complete dissociation of pellets and cell lysis. The samples were then centrifuged at 13,000 rpm for 10 minutes at 4 °C. While the samples were spinning more eppendorfs were chilled on ice to transfer the extracts. After the centrifugation, supernatants were transferred to respectively labelled, chilled tubes. Care was taken to avoid transfer of any cell debris. The samples were either immediately dried under nitrogen gas flow or stored in -80 °C for some time (not more than 1 month). Once dry, samples were stored at -80 °C until LC-MS analysis.

Cellular metabolites were extracted successfully using this method and run on the mass spectrometer in preliminary experiments. This established the extraction method that can be later followed by junior students in laboratory while performing metabolomics experiments. Efforts are underway to standardize metabolite separation and detection on LC-MS.

Metabolite Derivatization

To increase the sensitivity of detection, efficiency of ionization and chromatographic behaviour of TCA cycle intermediates, some amino acids and certain glycolytic intermediates, these metabolites are often derivatized. Tan and co-workers reported *O*-benzylhydroxylamine (*O*-BHA) (Tan et al. 2014) as a robust derivatization reagent and based on inputs from Walvekar and co-workers (Walvekar et al. 2018) we standardized the derivatization protocol in our laboratory.

Derivatization Protocol

Vacuum dried metabolite extracts / metabolite standards (1 μ M) were dissolved in 20-100 μ L mass-spectrometry grade water. To that, 50 μ L of 1 M EDC (1-ethyl-3-(dimethylaminopropyl) carbodiimide) (prepared in pyridine buffer, pH 5.0) was added and mixed gently. To this mix, 100 μ L of 0.5 M *O*-BHA (prepared in pyridine buffer) was added and the mixture was placed on shaker for 1 hour. At the end of one-hour incubation, 300 μ L of ethyl acetate was added to each tube and placed on shaker for 10 min. Upper layer was transferred to a fresh tube and the remaining solution was extracted with 300 μ L ethyl acetate, twice. Ethyl acetate extracts were pooled in one tube, dried under vacuum and stored in -80 °C until analysis by LC-MS.

Derivatization of metabolite standards (commercially available pure compounds) has been optimized in the laboratory and will be used in conjunction with reverse-phase chromatography to achieve maximum possible detection sensitivity.

Parallel use of two approaches: metabolite derivatization and hydrophilic interaction liquid chromatography (HILIC) (described in detail in below) would be followed for reliable quantification of intracellular metabolite levels.

Cellular metabolites span a wide range of molecules from organic acids, nucleotides/nucleosides/nucleobases, carbohydrates to sugar phosphates which are mostly polar molecules. Separation of these polar molecules in a single chromatographic method is challenging. Last few decades have seen an enormous amount of development in chromatographic techniques in order to develop methods that can separate wide variety of molecules in a single run. These efforts have led to the development of one such method, the **hydrophilic interaction liquid interaction chromatography (HILIC)** for separation of highly polar and hydrophilic compounds. Detection and quantitation of small polar molecules was traditionally done using C18 columns with an ion-pairing

agent in reverse phase liquid chromatography (RP-LC). However, ion-pairing agents stick to the components of LC, the columns and also to the ion source of the mass spectrometer. They can suppress the signals in proteomics analysis carried out in positive ion mode, demanding a dedicated MS only for metabolomics, and also tend to diminish the lifespan of the LC columns. To overcome these problems associated with the use of ion-pairing agents in RP-LC, HILIC has been extensively utilized for metabolomic analysis.

HILIC is similar to normal-phase liquid chromatography (NP-LC) with added features of reverse phase and ion-exchange chromatography (IC) as depicted in the Figure 3.30.

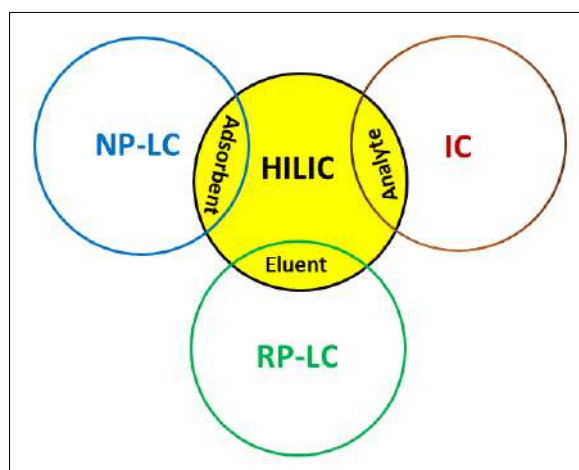
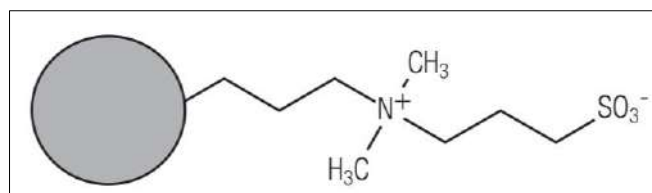


Figure 3.30: Schematic representation of features of HILIC. HILIC contains stationary phases similar to those used in normal phase liquid chromatography (NP-LC), the analyte binding principle is similar to ion exchange (IC) chromatography while mobile phase used are similar to reverse phase liquid chromatography (RP-LC)

In HILIC, the stationary phases consist of hydrophilic, polar materials which causes them to absorb water (and form a thin layer of water on the surface) from the mobile phase which consists of organic solvent (preferably acetonitrile) in aqueous buffer (such as ammonium acetate, ammonium carbonate etc.). Bare silica or silica gels have traditionally been used as stationary phase in HILIC. Polymer-based stationary phases have also been used (Buszewski and Noga, 2012). Depending upon the requirement of the sample, chemically bonded silica/polymer stationary phases are used; commonly used ones are the amide bonded silica or zwitterionic silica / polymer stationary phases of which the latter are often employed, a typical example of which is the sulfobetaine (sulfoalkylbetaine) phase. The sulfobetaine group consists of a negatively charged (acidic) sulfonic acid and a positively charged (basic) quaternary ammonium group, facilitating analyte interaction with the stationary phase predominantly via ion-exchange.



Sulfobetaine

The mobile phases used for HILIC chromatography consist of an aqueous mobile phase A and a water-soluble organic solvent as mobile phase B. Additives such as volatile buffer salts (ammonium acetate, ammonium formate, ammonium carbonate etc.) are added in either one or both mobile phases to regulate pH and ionic strength (Buszewski and Noga 2012). The interaction chemistry of HILIC is more complex than ion-exchange and normal phase chromatography and combines: partitioning between the stationary and the mobile phase, hydrogen bonding between the stationary phase and the polar functional group of the analyte as well as weak electrostatic interactions with ionizable functional groups on the analyte under strong organic conditions (Alpert 1990; Buszewski and Noga 2012) as represented in the Figure 3.31

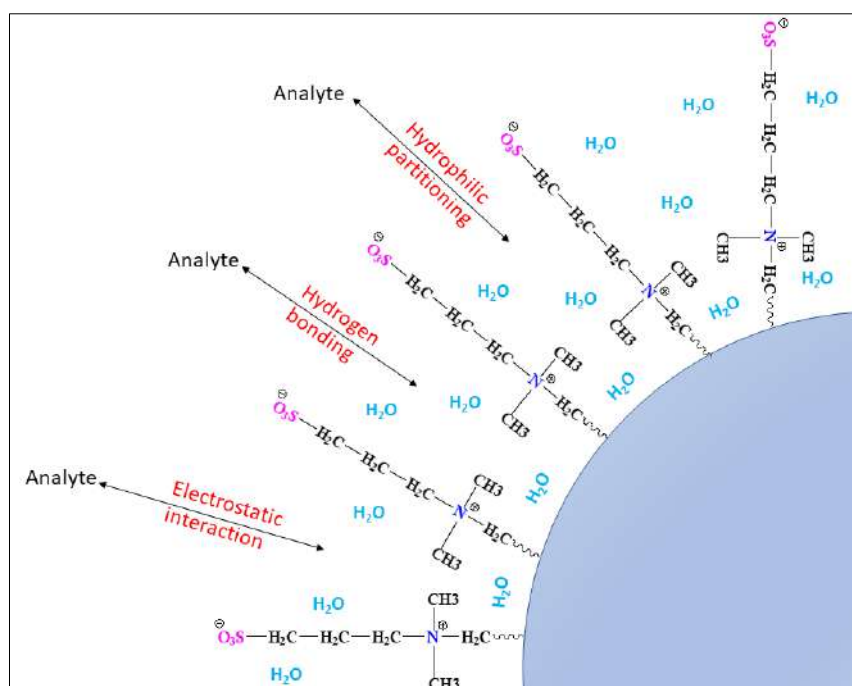


Figure 3.31: Schematic representation of retention mechanisms on HILIC. The interaction chemistry in HILIC is a combination of hydrophilic partitioning between stationary and mobile phase, hydrogen bonding between the stationary phase and the polar functional group of the analyte as well as weak electrostatic interactions with ionizable functional groups on the analyte under strong organic conditions (Alpert 1990).

In past few years HILIC has been successfully used in metabolomics application (Bajad et al. 2006; Creek et al. 2011; Liu et al. 2019; Teleki and Takors 2019; Westrop et al. 2015; Zborníková et al. 2019). Various studies have also demonstrated use of zwitterionic HILIC (ZIC-HILIC) column for

metabolomic studies of *P. falciparum* (Birrell et al. 2020; Creek et al. 2016; Vincent and Barrett 2015). HILIC also circumvents the need for metabolite derivatization which could be a source of error between replicates. Due to its obvious advantages over RP-LC as outlined above, we decided to use HILIC for our metabolomics studies.

Parallely, we will be using metabolite derivatization in conjunction with RP-HPLC (without the use of ion-pairing agents) to maximize sensitivity of detection.

MS parameters for detection of metabolite standards are being optimized. Results of standardization are summarized below.

The mass spectrometry parameters for detection of each individual metabolite standard were optimized by direct-infusion of small concentration (1 μ M, unless mentioned otherwise) of the metabolite (dissolved in 1:1 methanol: water solution) into the H-ESI source of Q-Exactive HF mass-spectrometer (Thermo Scientific, USA). All metabolites were detected in negative ion mode. Table 3.2 enlists metabolite standards and their observed masses detected on Q-Exactive HF upon direct-infusion. Mass spectrum of AMP is shown in Fig. 3.32. Spectra obtained for other metabolites are documented in Annexure I.

Table 3.2: Metabolite standards, their monoisotopic masses and observed masses. Unless otherwise mentioned, concentration of metabolite used was 1 μ M.

Metabolite	Monoisotopic mass	Observed mass (Negative ion mode)
AMP	347.063085	346.05626
GMP	363.057983	362.05087
IMP (10 μ M)	348.0470	347.04024
XMP (10 μ M)	364.042023	363.03500
ATP	506.9957	505.98846
Fumarate	116.010956	115.07565
Succinate	118.026611	117.01846
Citrate	192.027003	191.10733
Glucose-6-phosphate	260.0297	259.02206
O-BHA-fumarate	327.126654	326.12234

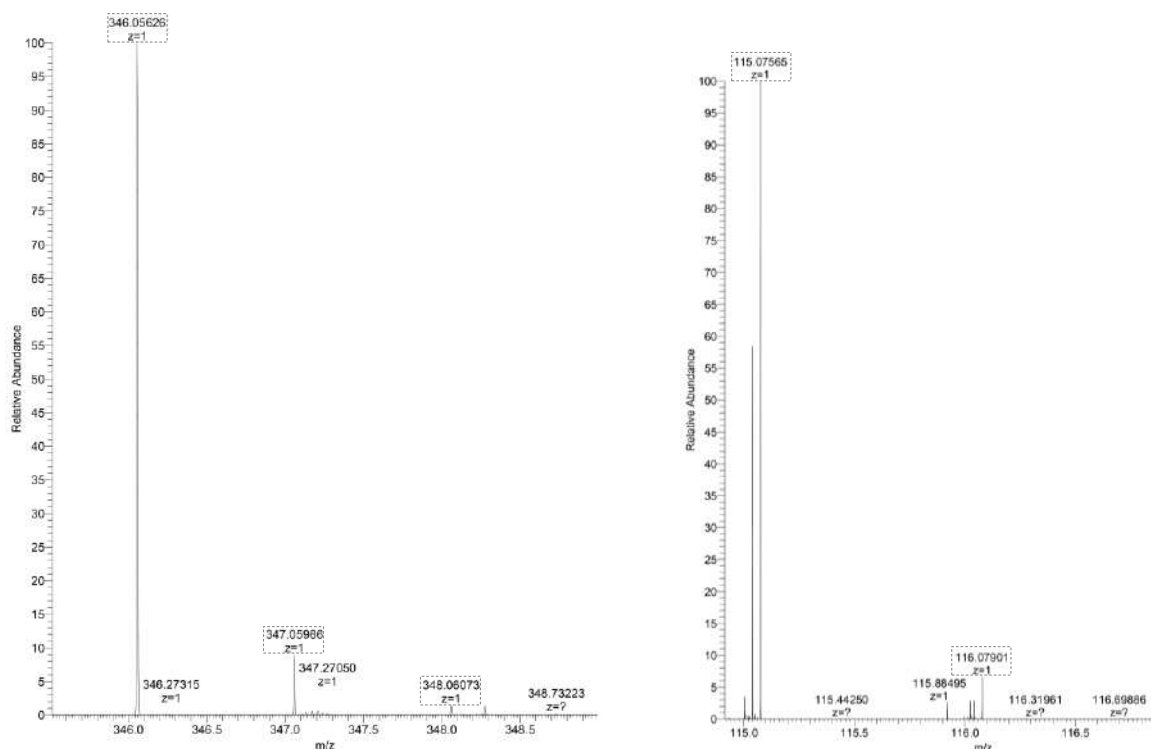


Figure 3.32: Mass spectra of AMP and fumarate. (a) 1 μ M AMP was injected into the mass spectrometer H-ESI source using a Hamilton syringe. Ion corresponding to AMP was detected by selective ion monitoring using a window of 5.0 m/z on either side of the expected m/z of 346.0630. Ions representing isotopic distribution can also be seen (347.05986 and 348.06073). (b) Fumarate spectrum was acquired in a similar manner. Isotopic distribution of fumarate can also be seen (m/z 116.07901)

This study, although encountered with significant challenges and involved standardization of new techniques; I believe, impelled our endeavours of delineating the metabolic significance of fumarate generated by ADSS/ASL reactions to the intraerythrocytic stages of Plasmodium parasite. Junior students in the laboratory are pursuing this work further.

Understanding the structural basis for the hyperthermostability of an archaeal glutaminase induced by post-translational succinimide formation

Chapter 4

Introduction

This chapter provides literature review on known mechanisms of thermostability, enzymatic and non-enzymatic deamidation processes, a brief account of other non-enzymatic post-translational modifications, functional implications of iso-aspartate formations in proteins, an account on few examples of stable succinimidylyl residues found in other proteins (examples taken from RCSB-PDB) and the influence of stable succinimides (in peptides) on structure of peptide backbones. The section also contains brief introduction to the molecular dynamic simulation tools used, replica exchange with solute scaling (REST2) and Well-tempered metadynamics (WT-MTD). A major problem encountered during simulations of biological macro-molecules is the insufficient sampling of conformational space. As MjGATase is an inherently stable protein, tools that could sample enough conformational space to reflect small changes were required; REST2 and WT-MTD mitigate this problem by sampling large conformational space.

4. Introduction

4.1. Mechanisms of protein thermostability

Surviving at temperatures ranging from 80-120 °C entails hyperthermophiles to evolve proteins and enzymes that have special structural and functional features to facilitate their optimal activity at high temperatures. Hyperthermophilic proteins are thereby desired candidates for those interested in studying molecular mechanisms of protein thermostability. Despite their extreme thermal stabilities, thermophilic proteins have high structural and sequence similarities to their mesophilic homologues. Protein stability is a function of not just primary amino acid sequence but also the tertiary structure of protein and through the course of evolution, there have been alterations in amino acid sequences and/or at post-translational level in thermophilic proteins that helped them attain better thermal stability than their mesophilic homologues. Some features that lead to improved stability of proteins from hyperthermophiles are discussed below:

4.1.1. Primary sequence of proteins and associated intrinsic properties

The amino acid sequence of proteins contributes to but is not solely responsible for higher thermostability in hyperthermophilic proteins. Although overall sequence conservation between proteins from mesophiles and hyperthermophiles is significant, mutations/substitutions at critical positions endow thermostability to the latter. Some reports show higher incorporation of arginine residue in hyperthermophiles. This could be attributed to lower reactivity of Arg due to high pKa and resonance stabilization. Arg can participate in multiple noncovalent interactions owing to its positively charged side chain (Vieille and Zeikus 2006). Another trend is decreased content of Asn, Asp and Gln due to their tendency to undergo deamidation or dehydration (Asp) at high temperatures (Pace et al., 2013). These examples are rare and no objective rules regarding variations in sequence composition seem to be followed in nature.

4.1.2. Shortening or deletion of loops

Loops are an important part of a protein structure that are not just disordered regions but play rather significant roles in protein function, stability and folding (Balasco et al., 2013). Structural differences observed in members of same protein family or similar proteins from organisms inhabiting different habitats are predominantly present on protein surfaces. Such changes often correspond to exposed loop regions connecting elements of secondary structure in the protein. Shortening of loops and increased occurrence of proline residues in the loops are known to contribute to thermostability by decreasing the floppiness in the concerned region (Pavlicek et al., 2008; Watanabe et al., 1991).

4.1.3. Hydrophobic and aromatic interactions

Hydrophobic interactions are the major forces involved in protein folding and stability. Increased content of hydrophobic residues is responsible for thermostability in adenylate kinase of *Methanocaldococcus jannaschii* (Vieille and Zeikus, 2001); Oligomerization of protein subunits via

hydrophobic interactions is involved in thermostability of 3-isopropylmalate dehydrogenase of *Thermus thermophilus* (Kirino et al., 1994).

An interaction is defined as aromatic-aromatic interaction or an aromatic pair when the distance between the phenyl ring centres is less than 7 Å (Vieille and Zeikus, 2001). Some hyperthermophilic proteins are known to have more aromatic residues as compared to their mesophilic homologues, e.g. α -amylase of *Pyrococcus furiosus* and *Bacillus licheniformis*. Similarly, a serine protease Thermitase from *Thermoactinomyces vulgaris* has more aromatic residues as compared to its mesophilic homologue from *Bacillus amyloliquefaciens*.

4.1.4. Increased occurrence of proline residues

The effect of a proline residue on a protein structure is entropic in nature. Proline decreases the entropy of a protein's unfolded state - owing to its limited conformational freedom - thereby stabilizing the folded structure (Krane 2008; Suzuki et al., 1987). Hence, introduction of proline residues in a loop makes the loop less susceptible to unfolding (Watanabe et al., 1991, 1994).

4.1.5. Increased number of hydrogen bonds, ion pairs and salt bridges

Hydrogen bonds mediate organization of distinct folds within a protein and render selectivity to protein-ligand interaction which is the basis for molecular recognition. Although individual hydrogen bonds (H bonds) contribute an average of 1.3 kcal mol⁻¹ to the stabilization (Hubbard and Haider, 2010), increase in entropy gained as the solvent is displaced from the groups is significant. Hence, increased number of H bonds aid in stabilization of folded state from an entropic viewpoint. Salt bridge is a combination of H bond and ionic bonding and is a major contributor to stability of the entropically unfavourable, folded conformation of proteins (Kumar, et.al., 2000). Although noncovalent interactions are known to be relatively weak, they can cumulatively make an important contribution to the overall stability of a conformer.

4.1.6. Post-translational modifications (PTMs)

PTMs increase the milieu of protein functions by adding functional groups on the side chains of amino acids or in certain cases by altering the protein backbone. PTMs are long known contributing factors to thermostability of proteins. Some of the well-known thermostability-endowing PTMs are discussed below.

4.1.6.1. Disulphide bond formation

Disulphide bridges are believed to stabilize a protein by decreasing the entropy of the unfolded state much like a proline residue. Their contribution to the stability of intracellular proteins comes as a surprise, since cytosolic environment is reducing which is favourable for the thiol form of cysteines. Nonetheless, disulphide bridges were shown to stabilize 5'-methylthioadenosine phosphorylase from *Sulfolobus solfataricus* (Cacciapuoti et al., 1994) and *Aquifex pyrophilus* serine protease. Inter-subunit disulphide bridges leading to oligomerization of protein are shown to be responsible for thermostability

of pyrrolidone carboxyl peptidase (PCP) of the hyperthermophile, *Pyrococcus furiosus* (Mukaiyama et al., 2004)

4.1.6.2. Methylation

Post-translational protein methylation is widely observed in proteins from prokaryotes and eukaryotes. Recent reports state that lysine methylation plays a role in thermostability of β -glycosidase from *S. Solfatarius* (Febbraio et al., 2004). Other examples of improved thermal stability mediated by lysine methylation are that of a MCM helicase from *Sulfolobus islandicus* (Niu et al., 2015) and RNA polymerase from *S. solfataricus* (Botting et al., 2010). In another report by Zhang and co-workers, methylation was the most prevalent PTM type, accounting for 40 % of the PTMs employed by bacteria for environmental adaptation in a deep-sea hydrothermal vent (Zhang et al., 2016).

4.1.6.3. Glycosylation

Although the precise mechanistic details of effect of glycosylation on protein thermostability is poorly understood, it appears to be rather entropic in nature (Shental-Bechor and Levy, 2008). The stabilization effect was shown to depend on the position of the glycans; thus, the same degree of glycosylation may be resulting in differential thermal effect depending on the location of the sugars (Fonseca-Maldonado et al., 2013). N-linked glycosylation is characterized by enzymatic addition of glucose, mannose and n-acetylglucosamine onto an asparaginyl residue. The oligosaccharide chain is specifically added onto an asparaginyl residue in the peptide sequence Asn-X-Ser or Asn-X-Thr (X being any amino acids except Pro). O-linked glycosylation on the other hand, begins with enzymatic addition of N-acetyl-galactosamine followed by other carbohydrates onto serine or threonine residues. Both kinds of glycosylation modifications play a role in protein folding, interaction, stability, and mobility, as well as in signal transduction (Roth et al., 2012)

4.1.7. Counter selection of thermolabile amino acids

Statistically significant changes in sequence composition between mesophilic and thermophilic proteins have been reported. The amino acids Asn, Gln, Met, and Cys are thermolabile i.e., they are not stable at high temperatures and tend to undergo deamidation (Asn and Gln) or oxidation (Met and Cys) (Kumar et. al., 2000). These amino acids are less common in thermophilic proteins and the thermolabile residues that do occur are usually buried.

4.1.8. Oligomerization

Oligomerization is a critical contributing factor of protein thermostability in many hyperthermophilic organisms. Proteins such as protein L-isoaspartyl-O-methyltransferase (PIMT) is reported in all organisms but PIMT from *Sulfolobus tokodaii* was found to be unique in that it is a hexamer (Tanakai et al., 2004). Phosphoribosylanthranilate isomerase (TrpF) is monomeric in most mesophiles and was found to be homo-tetrameric in *Thermotoga maritima* (Tanaka et al., 2000). Apart from these, there are several other examples where hyperthermophilic proteins are shown have higher oligomeric state than their mesophilic homologues (Vieille and Zeikus, 2001). Oligomers provide additional interface

interactions like disulphide and salt bridges, hydrophobic interactions that can contribute to the thermostability of the protein. (Höcker et al., 2001; Dams and Jaenicke, 1999; Hess et al., 1995).

4.1.9. Release of conformational strain

Left-handed helices are rare in proteins but when they do occur, they contribute to protein stability in cases where they themselves are stabilized by intra-molecular interactions. Left-handed helices are less stable as compared to right-handed helices as they lead to close contacts between atoms of the residues involved. This leads to a strain in the protein. In hyperthermophiles, the residues in left-handed helices are found to be replaced by Gly as it relieves the strain. Examples include increased thermal stabilization of DNA binding protein HU from *Bacillus stearothermophilus* and *E. coli* RNAaseHI. The release of conformational strain results in improved thermodynamic stabilities of these proteins (Kawamura et al., 1996; Kimuras et.al., 1992). This factor has not been extensively studied in hyperthermophilic proteins.

A single mechanism is never responsible for bestowing thermostability over a thermophilic protein. Hyperthermophilic enzymes deploy combinations of the above-mentioned mechanisms to achieve extreme thermal stability. In some instances, a point mutation or a post-translational modification could be responsible for thermostability which may not obey any tangible rules. Formation of a stable succinimide appears to be one such mechanism deployed by *Methanocaldococcus jannaschii* glutamine amidotransferase (MjGATase). This mechanism generates a small network of interactions, the 'conformational lock' that is the driving force for hyperthermostability, the details of this study are presented in this section of the thesis.

4.2. Deamidation

Protein deamidation is a post-translational modification (PTM) that is known to occur in ageing proteins *in vivo* or prolonged stored proteins *in vitro* and is the process of removal of amide group (-NH₂) from the side chain of asparaginyl or glutaminyl residues leading to release of ammonia (NH₃). L-Asparaginyl deamidation in proteins results in formation of either L- aspartyl, D-aspartyl, L-iso-aspartyl or D-iso-aspartyl residues while L-glutaminyl deamidation can generate either glutamyl or pyrroglutamyl residues (5-oxoproline). Two types of deamidation reactions take place in a living cell.

a) Enzymatic deamidation

Enzymatic deamidation of a glutamine residue in protein can be brought about by two classes of enzymes namely, Ca⁺² dependent transglutaminase (TG) and peptidoglutaminases. Transglutaminase enzyme can deamidate, transamidate or esterify specific Gln residues in proteins (Lorand and Graham, 2003) while peptidoglutaminase deamidates a glutaminyl residue into a glutamate residue (Kikuchi et al., 1971). Of the TGs that can deamidate glutaminyl residues in proteins, the ones acting on gliadin, a class of proline and glutamine rich proteins found in wheat and other cereals, is of specific importance as they deamidate Gln to Glu and the glutamate containing gliadins are the epitopes that activate T cells in coeliac disease (Shan et al., 2002). *E. coli* cytotoxic factor is functionally closely associated with

TGs and brings about selective deamidation of specific Gln residues of Rho family GTPases, RhoA, thereby resulting in activation of Rho and Ras and subsequent destruction of host cells during infection (Flatau et al., 1997; Sugai et al., 1999). Deamidation inhibits the GTPase activity of Rho and Ras resulting in unregulated actin stress-fibre formation. Peptidoglutaminases can be further classified into two classes, peptidoglutaminase I and peptidoglutaminase II. Peptidoglutaminase-I is specific for derivatives substituted at amino group while peptidoglutaminase II is responsible for deamidation of amide group of glutaminyl residue in a protein/peptide. Both the enzymes were found to be inactive towards free L-glutamine. Asparaginyl residues were not substrates of these enzymes (Kikuchi et al., 1971).

Enzymes that can deamidate an internal asparaginyl residue in a protein are not known, perhaps because spontaneous non-enzymatic deamidation of asparagine resulting in formation of either (L/D)-aspartate or (L/D)-iso aspartate serves as a “molecular clock” for the protein as discussed below. Nonetheless, enzymes deamidating the N-terminal asparaginyl residue in proteins are known and are a part of N-end rule pathway of *in vivo* protein degradation. The enzyme is termed Protein N-terminal asparagine amidohydrolase in humans and other multi cellular organisms (NTAN1) and deamidates asparaginyl residue to an aspartyl residue that renders the protein susceptible to arginylation (i.e. cross-linking with arginine) or poly ubiquitination and subsequent degradation as per the N-end rule pathway (Cantor et.al., 2011). NTAN1 is specific for N-terminal Asn residues and does not act upon internal or free asparagine or C-terminal or internal glutaminyl residues.

b) Non-enzymatic deamidation

The spontaneous, non-enzymatic deamidation of asparagine residue proceeding via L/D-succinimidyl intermediate is a widely studied non-enzymatic post-translational modification occurring primarily in ageing proteins *in vivo* or prolonged stored proteins *in vitro*. Deamidation of asparaginyl residue proceeds at a higher rate (two orders of magnitude higher) compared to glutaminyl deamidation, with the later involving formation of glutarimide intermediate and its subsequent hydrolysis to glutamate. The ubiquitous presence of the repair enzyme protein L-isoaspartyl (D-aspartyl) methyltransferase (PIMT) in organisms from all three kingdoms of life is a strong indication that deamidation of asparagine is physiologically more relevant and is found to be more widespread thereby generating the need for a rectifying enzyme. Deamidation of asparaginyl residues occurring in biosimilars (such as therapeutic peptides and antibodies) upon their prolonged storage is a prevalent problem in pharmaceutical industry. It leads to effects such as altered epitope recognition and binding affinity of antibodies, loss of structure and thereby efficacy of therapeutic peptides. Due to the heavy losses that have to be incurred by pharmaceutical industries on account of inactivation of biologics, determination of probable deamidation sites in peptides/ antibodies is of at-most importance. Isomerization of aspartyl residue to iso-aspartate is also a frequently occurring PTM in ageing proteins exemplified by isoaspartylation of several aspartate residues in α -crystallin (Lyon et al., 2019) and Asp23 in β -amyloid fibrils (Warmack et al., 2019). Deamidation / isoaspartylation is also shown to regulate functions of

several proteins as exemplified by p53. The influence of spontaneous deamidation / isoaspartylation on protein function is discussed in section 4.5.

4.2.1. Reaction mechanisms of non-enzymatic deamidation

Spontaneous deamidation of asparaginyl residues proceeds via nucleophilic attack by a deprotonated backbone nitrogen atom of succeeding residue (n+1) on the conformationally correctly aligned side chain of asparagine (n). This leads to cyclization of the side chain γ carbon of asparagine with the backbone nitrogen and concomitant release of ϵ amide group of Asn side chain as ammonia (NH_3) (Fig. 4.1). This five membered succinimide ring is metastable with the C-N bond on either side of imide nitrogen being highly prone to hydrolysis. Cleavage of $\text{C}_\gamma\text{-N}$ bond leads to formation of Asp whereas hydrolysis of C-N bond leads to formation of iso-Asp (Fig. 4.2). The hydrogen bonded to C_α is labile and therefore succinimide ring can undergo racemization giving rise to D-Asp/D-isoAsp. The susceptibility of a given asparaginyl residue to spontaneous deamidation in a protein is mainly governed by the primary sequence of the protein. The side chain of the n+1 residue (the succeeding residue) is the most important factor. Analyses of several hundred protein sequences have shown that asparaginyl residue which is followed by a glycyl residue has the highest propensity to undergo deamidation. Glycyl residue with its smallest side chain does not pose any steric hindrance to the alignment of asparagine side chain suitable for deamidation reaction to take place. Protein structures in which asparagine deamidation or aspartate isomerization intermediate (Succinimide) and/or products have been observed, the modification is present predominantly in the loop region. Loops being flexible structures, provide conformational environment conducive for the process of deamidation.

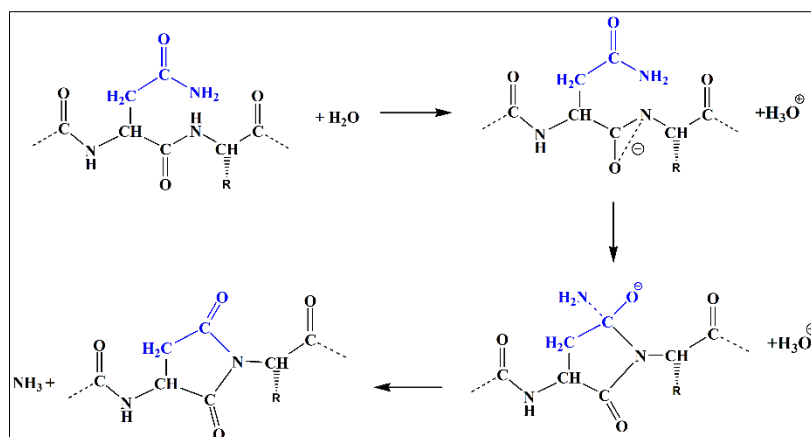


Figure 4.1: Mechanism of deamidation of asparagine via imide formation. Deamidation of an asparaginyl residue begins with deprotonation of nitrogen of the successive amino acid residue that is followed by cyclization and formation of a five membered succinimide ring. Schematic was generated using ChemDraw Ultra.

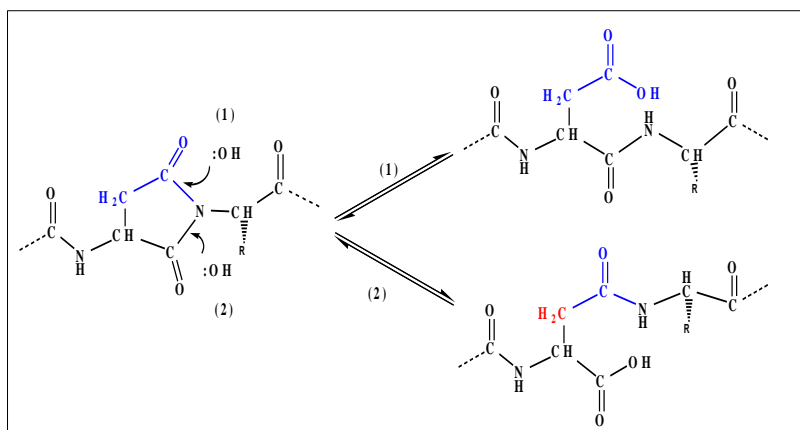


Figure 4.2: Hydrolysis products of succinimide. The hydrolysis product of succinimide depends on which of the C-N bond is attacked. Breakage of C_γ-N bond generates Asp (1) while that of C_α-N leads to formation of iso-Asp (2). Schematic was generated using ChemDraw Ultra.

Another possible mechanism of asparagine deamidation is termed ‘**cleavage mechanism**’. Here the imide intermediate is formed when the amide nitrogen (N_ε) of Asn deprotonates and reacts with the backbone carboxylic carbon of the same asparaginyl residue, leading to cleavage of protein backbone (Fig. 4.3). This mechanism of deamidation plausibly occurs in peptides where an asparaginyl residue is succeeded by a proline residue which lacks the hydrogen attached to backbone nitrogen, suitable for a base catalysed deamidation.

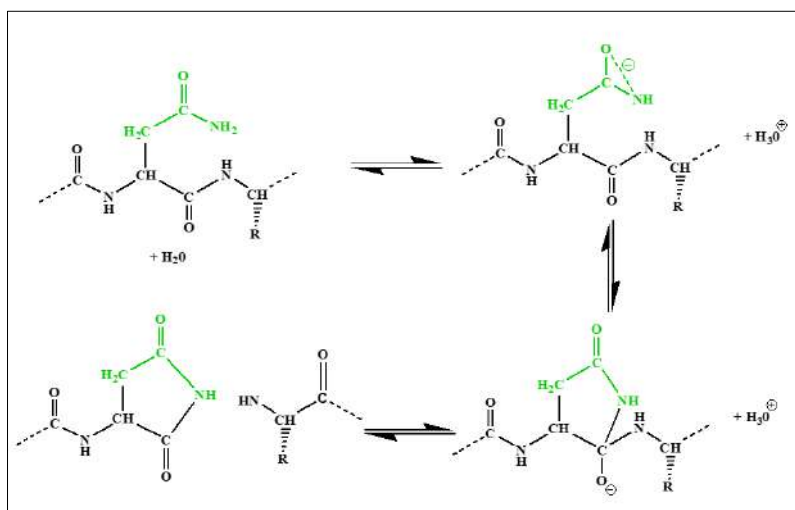


Figure 4.3: Cleavage mechanism of deamidation. This mechanism of deamidation also proceeds via succinimide formation but instead of nitrogen of succeeding residue, amide nitrogen of Asn itself is part of SNN ring.

At lower pH (<5), **acid catalysis** prevails as a mechanism of asparagine deamidation. The rate of this reaction increases as the pH drops below 2. As the [H⁺] increases with drop in pH, the oxygen attached to C_γ of asparagine is protonated and the electrons on the carbon are delocalized to create a partial positive charge over the carbon atom. In presence of H₂O, the OH⁻ ions attack C_γ while amide nitrogen

leaves as NH_4^+ ion, leading to formation of aspartate. Alternatively, a succinimide intermediate is formed with concomitant release of NH_4^+ as shown in Fig. 4.4.

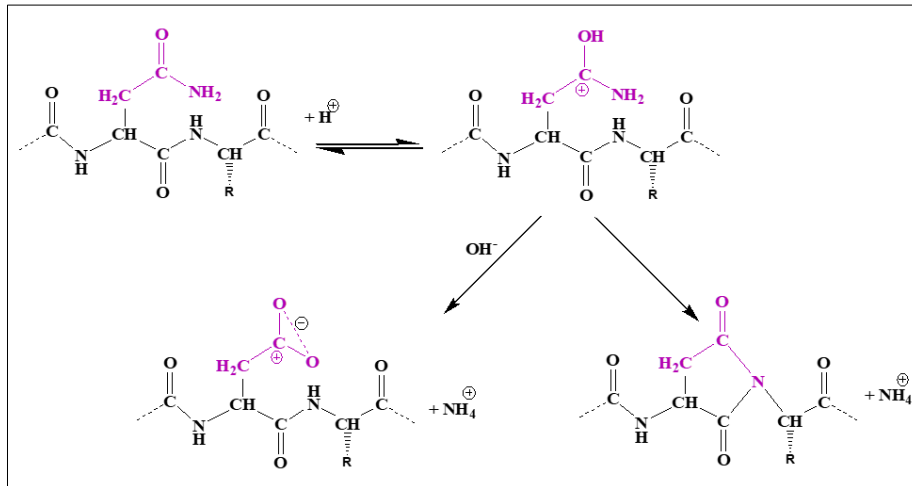


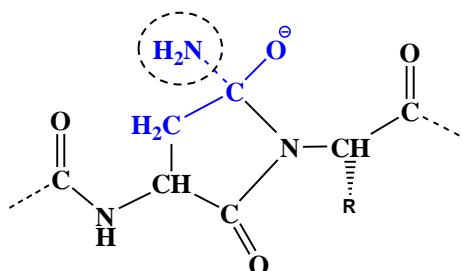
Figure 4.4: Acid hydrolysis mechanism of deamidation

Glutamine can also follow similar mechanisms of deamidation albeit at a much slower rate (Kossiakoff et. al., 1988; Geiger and Clarke, 1987)

4.2.2. Factors affecting deamidation in peptides and proteins

- Structural determinants:* The influence of protein's primary sequence on deamidation has been analysed and the commonly accepted premise is that an Asn residue followed by a glycine residue has the maximum probability of undergoing deamidation. This largely holds true for peptides but in proteins the tertiary structure could pose additional complexity and Asn-Gly pairs in proteins could be deliberately placed to act as biological clocks controlling the ageing of the protein.
- The acidity of the nitrogen of succeeding residue:* The acidity of the backbone nitrogen atom that takes part in formation of five membered succinimide ring is influenced by the environment around it; inductive effect and electrostatic effect determined by the peptide/protein sequence and structure playing a major role (Robinson and Robinson, 2004). This nitrogen needs to be deprotonated and should not be involved in hydrogen bonding.
- Steric hindrance:* Formation of a succinimide intermediate is contingent on the availability of conformational space to accommodate a five membered ring within the protein/peptide. Therefore, in proteins much like the previous factor, the three-dimensional structure governs the steric hindrance posed to cyclization. This factor has been exploited to predict the propensity of deamidation of a given Asn/Gln in a protein for which three-dimensional structure is available (Robinson, 2002)

- d) *The probability of the leaving group* (NH_2) of the tetrahedral intermediate (existing momentarily just before succinimide ring formation) is influenced by inductive and electrostatic effects to certain extent in addition to effect of buffer ions and pH of the solution (Robinson and Robinson, 2004).



4.3. An account of other non-enzymatic post-translational modifications

Post-translational modifications increase the repertoire of protein functionality to a significant extent. PTMs govern variety of attributes such as thermal stability, localization, protein turnover, protein-protein interactions etc in many proteins. PTMs are a proof that subtle changes brought about in certain proteins can have a huge impact on the overall cellular functioning. However, PTMs occurring in ageing proteins or accumulated over time in certain proteins can also contribute to disease phenotypes. Over the years, extensive research has been carried out on PTMs mediated by cellular enzymes with almost 400 of them listed in UniProt. However, research regarding spontaneous non-enzymatic PTMs is in nascent state. These spontaneous non-enzymatic chemical reactions (PTMs) occur primarily due to oxidative or metabolic stress and do not always follow an apparent pattern. They can be classified into two groups namely, reversible and irreversible. Reversible modifications can be repaired by non-enzymatic dissociation or by enzyme mediated reactions and therefore do not have dire physiological consequences. Irreversible non-enzymatic PTMs on the other hand, are indicators of redox and/or metabolic imbalance rather than regulatory events like the enzyme-mediated PTMs. They can be kept in check to a limited extent by controlling redox status of the cell and ensuring metabolic homeostasis. Some of those PTMs have been discussed in detail.

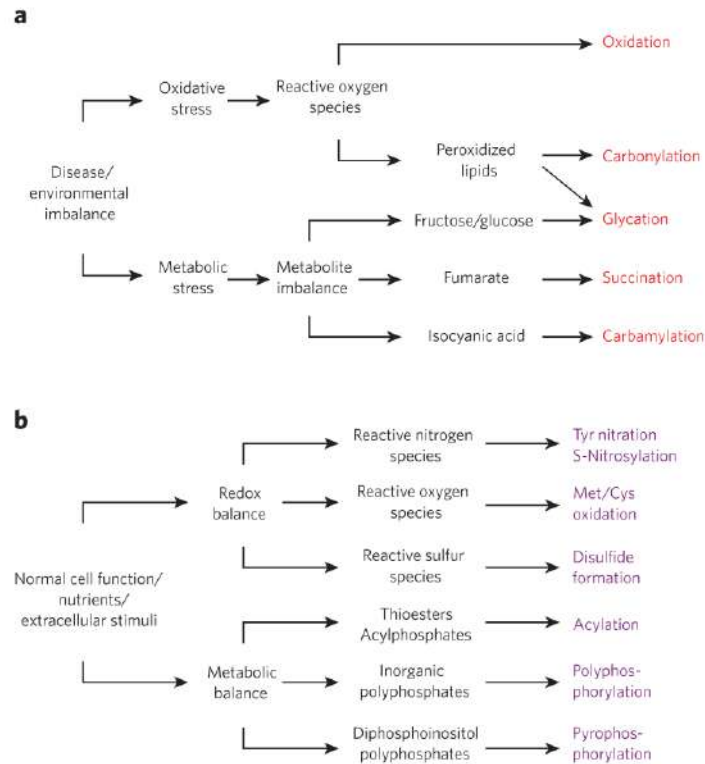
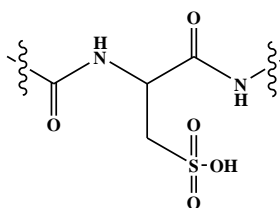


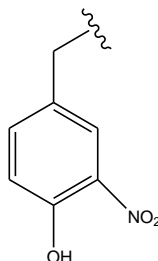
Figure 4.5: A brief summary of non-enzymatic PTMs. (a) Irreversible non-enzymatic PTMs. Cells subjected to an extreme environmental imbalance or ones that exhibit disease state experience oxidative stress due to accumulation of reactive oxygen species which can, in turn, carry out irreversible oxidation of proteins thereby rendering them non-functional. Similarly, metabolic imbalance resulting in accumulation of sugars, fumarate or other metabolites leads to irreversible modifications of proteins making them non-functional. (b) Reversible non-enzymatic PTMs. Even during normal cell functioning, metabolic or redox imbalance can set in which leads to reversible modifications of certain proteins. Figure adapted from Harmel, Robert and Dorothea Fiedler. 2018. "Features and Regulation of Non-Enzymatic Post-Translational Modifications." *Nature Chemical Biology* 14(3):244–52 with permission.

4.3.1. Oxidation

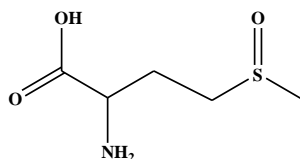
- a) Cysteine Oxidation: Reactive molecules such as reactive oxygen species (ROS), reactive nitrogen species (RNS) and reactive sulphide species (RSS) are involved in the process of protein oxidation. Representative examples include cysteine oxidation, tyrosine nitration and methionine sulfoxidation. Reversible oxidation of cysteinyl residues in proteins is a common PTM observed in proteins *in vivo* and *in vitro* and it often leads to formation of disulphide bond between two cysteinyl residues thereby increasing protein stability. The local environment around a cysteine determines its propensity to undergo oxidation. The modification can be reversed by an anti-oxidant such as glutathione (GSH) (Harmel and Fiedler, 2018).



- b) Tyrosine nitration was previously thought of as irreversible but recent studies suggest that it might be reversible although, specific de-nitrases have not been isolated and characterized yet (Abdelmegeed and Song, 2014). This modification serves roles in both physiological (such as alteration of protein activity, influence on protein phosphorylation, sensitivity to proteolytic degradation) and pathological conditions i.e. implication in diseases (Abello et al., 2009; J. R. Lee et al., 2009).



- c) Methionine sulfoxidation: Methionine can be oxidized by addition of oxygen to its sulfur atom to form methionine sulfoxide. The modification is reversible *in vivo*. The interconversion of methionine and methionine sulfoxide (MetO) is a regulatory process responsible for controlling actin assembly in mammalian cells, scavenging ROS from macrophages leading to survival of *Mycobacterium tuberculosis* (Abulimiti et al., 2003) and brings about conformational changes in certain proteins (Gustavsson et al., 1999).

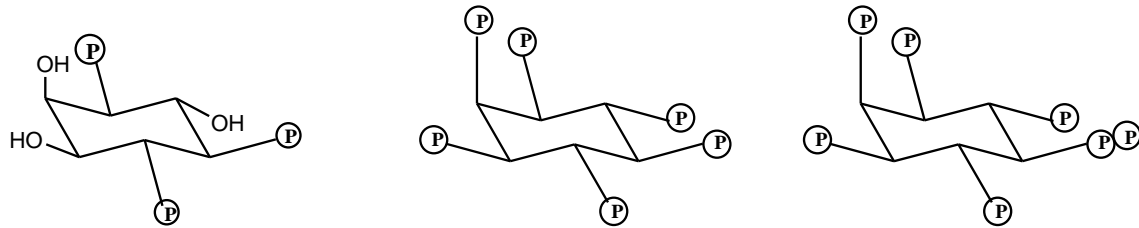


4.3.2. Lysine Acylation

It is an evolutionarily conserved modification which acts as a regulatory switch during many cellular processes. Acetyl-CoA is the principal acylation molecule that is generated via β -oxidation of fatty acids, conversion of pyruvate via pyruvate dehydrogenase complex and also as a by-product of amino acid degradation pathway. The significance of histone (lysine) acetylation and deacetylation is known since long (Baeza et al., 2016; Nakayasu et al., 2017). Enzyme independent lysine acetylation events have also been reported (Wagner and Payne, 2013; Baeza et al., 2015; Andrew M. James et al., 2017). In addition to the reactivity of lysine residue, the concentration of acetyl-CoA (and of succinyl CoA responsible for succinylation) and the intrinsic properties of these intermediates govern the non-enzymatic acetylation and succinylation. Other intermediates that can acylate lysine residue are glutaryl-CoA and butaryl-CoA and 3-hydroxy-3-methyl-glutaryl-CoA. Some high energy intermediates have also been shown to act as acyl group donors; these include, thioesters and acyl phosphates such as 1,3-bisphosphoglycerate. Lysine acylation can be removed enzymatically by a plethora of specific sirtuins, a highly conserved family of NAD⁺ dependent deacetylases (Kupis et al., 2016).

4.3.3. Polyphosphorylation

Enzyme-independent polyphosphorylation of proteins is perhaps a nascent area of research. Polyphosphorylation depends on inorganic polyphosphates as phosphate donors. There is a singular study showing that polyphosphorylation of topoisomerase I and nuclear signal recognition I (NSRI) inhibits the interaction between those two proteins which results in reduced release of supercoiled DNA (Azevedo et al., 2015). The highly phosphorylated, diffusible inositol polyphosphates (InsPs) and inositol pyrophosphates (PP-InsPs) serve as cellular messengers.



They can transmit signals by binding directly to target protein and altering their localization, activity and protein-protein interaction. Alternatively, these molecules can transfer a phosphoryl group onto a previously phosphorylated serine residue through a non-enzymatic reaction, requiring only ATP as a cofactor (Wu et al., 2016). Interaction between dynactin multi-subunit protein complex with dynein protein is augmented by pyrophosphorylation of the later (Saiardi et. al., 2016). These recent studies underline regulatory role of polyphosphorylation and pyrophosphorylation modifications.

4.3.4. Succination

Fumarate has been shown to act as oncometabolite by altering protein functionality post-translationally via cysteine- S- succination. Increased levels of fumarate as a result of mutations in the enzyme fumarate hydratase (FH) is a hallmark of hereditary leiomyomatosis and renal carcinoma (HLRCC) (Menko et al., 2014; Y. Yang et al., 2012). Recent studies by Kulkarni and co-workers have found new targets of succination in cancer cells (Kulkarni et al., 2019).

4.3.5. S-cyanylation

The addition of hydrogen cyanide onto cysteine residues of proteins is a non-enzymatic PTM shown to be regulating primary metabolic pathways such as glycolysis, Calvin cycle and S-adenosyl-methionine cycle in *Arabidopsis thaliana* (García et al., 2019).

4.3.6. Glycation

Glycation is marked by condensation of glucose, fructose or methylglyoxal with reactive amino acid side chains such as the primary amines of lysine or guanidino group in arginine through Millard reaction resulting in formation of stable adducts (Šoškić et al., 2008; Zheng et al., 2019). Glycation of proteins due to continuous and increased exposure to glucose is a hallmark of diabetes (Rhee and Kim, 2018; Šoškić et al., 2008; Ulrich and Cerami, 2001). Recent study by Zheng and co-workers reported intense histone glycation in breast cancer tumours (Zheng et al., 2019). Initial glycation products can undergo further chemical reactions and rearrangements to form advanced glycation end-products

(AGEs). AGEs contribute to progression of diabetes, ageing, atherosclerosis, Alzheimer's disease and kidney disease (Šoškić et al., 2008).

4.4. Functional implications of iso-aspartate formation

Deamidation of asparaginyl or dehydration of aspartyl, giving rise to iso-aspartyl (iso-Asp or iso-D) residue as one of the end products has always been viewed in the light of destabilization of protein structure and eventual loss of function (Robinson, 2002; Robinson and Robinson, 2004, 2001; Brennan and Clarke, 1993). Iso-Asp formation leads to addition of a $-CH_2-$ group to the polypeptide backbone which may not be tolerated well in a protein. However, there are instances where Asp to iso-Asp conversion is perhaps important for the functionality of a protein or acts as a regulatory switch mediating certain cellular functions under physiological and pathological conditions. Some of those examples are reviewed below.

- Integrin-ligand interactions are central to cell-cell and cell-extracellular matrix (ECM) adhesions. Integrin $\alpha\beta_3$ interacts with fibronectin protein present in ECM. The specific sequence motif recognized by $\alpha\beta_3$ on fibronectin is RGD (Arg-Gly-Asp). Some variants of fibronectins contain a repeating sequence motif NGR (Asn-Gly-Arg). It was observed that deamidation of Asn to form iso-Asp in the motif (iso-DGR) leads to activation of latent RGD-dependent integrins such as $\alpha\beta_3$ (Corti and Curnis, 2011; Curnis et al., 2010, 2006). Studies have implicated a role of integrin $\alpha\beta_3$ in angiogenesis during tumour formation. Therefore, iso-DGR fibronectin, interacting with $\alpha\beta_3$ could possibly play a role in angiogenesis (Di Matteo et al., 2006).
- Residues N29 and N30 in p53 are deamidated to iso-Asp in native protein. Carboxy methylation of these iso-Asp residues by PIMT enzyme suppresses the activity of p53. PIMT methylated p53 has been shown to exhibit higher affinity for HDM2, a ubiquitin E3 ligase. Deamidation in this protein does not seem to be an aging defect but rather a beneficial PTM, preventing binding with HDM2 and thereby, protecting it from degradation. PIMT is therefore thought to act as a regulatory signal maintaining steady-state levels of p53 (Lee et al., 2012).
- Amyloid β fibrils are known to undergo numerous post-translational modifications one of which is isoaspartylation at Asp7, Asp14 and Asp23. Whereas iso-Asp residues at positions 7 and 14 are not pathologically relevant, iso-Asp23 is shown to accelerate the aggregation rate of A β fibrils (Warmack et al., 2019). Iso-Asp at position 23 was also shown to enhance the stability of A β fibrils. A similar observation was also made in case of A β fibrils harbouring a hereditary Asp23Asn mutation, known as the Iowa mutation. Asn containing fibrils also aggregated faster and were more stable. The authors of this study attribute this to the possible deamidation of Asn, a process that can form iso-Asp (Warmack et al., 2019).

4.5. Stable succinimides in proteins and their functions

There are very few structures of proteins available which harbour stable succinimide in them. PDB database contains 57 entries of proteins with a succinimide residue. In a subset of those proteins a functional role has been assigned or predicted for this modified non-natural residue. Succinimide is abbreviated as SUI [(3-amino-2,5-dioxo-1-pyrrolidinyl) acetic acid] or SNN (L-3-aminosuccinimide).

Table 4.1 contains the list of PDB entries with succinimide annotated as a modified residue or a ligand.

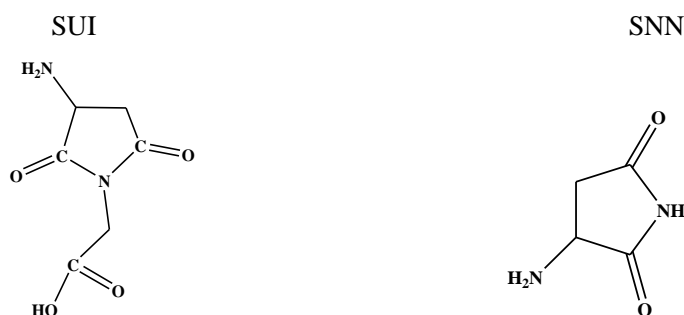


Table 4.1: Proteins containing stable succinimide residue

PDB ID	Protein description	Publication
1GKT	Endothiapepsin structures	(Coates et al., 2001)
1GVT, 1GVU, 1GVV, 1GVW, 1GVX	Endothiapepsin structures	(Coates et al., 2002)
1OEW, 1OEX	Endothiapepsin structures	(Erskine et al., 2003)
2JJI, 2JJJ	Endothiapepsin in complex with a gem-diol inhibitor.	(Coates et al., 2008)
2OWC, 2OWW, 2OWX 2VS2	<i>Thermus thermophilus</i> amyloamylase Neutron diffraction structure of Endothiapepsin in complex with a gem- diol inhibitor.	(Barends et al., 2007)
3URI, 3URJ, 3URL 1WL8	Endothiapepsin-DB5 complex. Pyrococcus horikoshii glutamine amidotransferase	(Bailey et al., 2012)
1AT5	Hen egg white lysosome	(Noguchi et. al., 1998)
5LU8, 5LU9, 5LUA, 5LUB, 5NIJ, 5OBT, 4D3X, 4D3Y, 4D3Z, 4N6N, 4N6O	Legumain	(Dall et. al. 2015; Zauner et al., 2018; Zauner et. al., 2018)
3IFJ, 3IGD, 2IMZ, 3NZM, 3CO3	Inteins	(Callahan et. al. 2011b; Liu et. al. 2014; Van Roey et. al. 2007)
4CUO	Plant peroxidase	(Palm et al. 2014)
6DHI, 6AZT	Endopeptidases	(Haywood et. al., 2018; James et. al., 2018)
6AKQ, 6AL0, 6AL1, 6ICC, 6ICF 4DX3, 4DXK	Putative zinc metalloproteases Enolase	(Tamura et al., 2019)
6A56	Lectin AJLec from Sea Anemone	(Unno et al., 2018)
5JIW	<i>Thermus aquaticus</i> amyloamylase	(Roth et al., 2017)
3I4W, 3K82	Post synaptic density 95 protein	(Cámara-Artigas et al., 2010)

3ESM	Uncharacterized protein from <i>Nocardia farcinia</i>	
2OMK	Thiamin pyrophosphokinase from <i>Bacteroides</i>	
1JBE	ApoCheY from <i>E. coli</i>	(Simonovic and Volz, 2001)

Among the above-mentioned structures, a functional role for succinimide residue has been assigned for only following few examples. Amylomaltases are specialized glycoside hydrolases that are characterized by hydrolysis of β -1,4 linked complex glycans. The structures of amylomaltases from *Thermus aquaticus* (5JIW) and *T. thermophilus* (2OWC, 2OWW, 2OWX) have been solved by X-ray crystallography with and without the substrate glycans. The residues D370 and G371 are conserved in all amylomaltases and in proteins from both the organisms, the D370 residue was found to exist in the form of succinimide (Barends et al., 2007; Sträter et al., 2017). It was initially thought to be an artefact of high temperature protein purification process but was later shown to be involved in binding to the substrate glycan (Glc + 5 ring). The authors discern that presence of unmodified aspartate side chain would have introduced a steric clash with the substrate glycan. Mutation of D370 to serine resulted in increase in K_m for glycan ascertaining the need for succinimide to enzyme functionality (Sträter et al., 2017). In case of both these amylomaltases, there is a negatively charged residue in the vicinity that forms a negatively charged shield over the succinimide ring plane like *Methanocaldococcus jannaschii* GATase D110 which protects succinimide from hydrolysis (discussed in detail in chapter five).

Although there is no structure available, methionyl human growth hormone (Met-hGH) containing an intact succinimide was isolated and characterized by Teschima G. *et. al* back in 1990 (Teshimas et al., 1991). The protein had been incubated at 45 °C for 4 months. Methionyl hGH was shown to undergo deamidation at Asn149 and isomerization at Asp130. Asp130 in Met-hGH is located in a flexible region of the protein and hence is prone to isomerization. MS/MS analysis of the protein identified peptide fragment with mass difference of 17 units (Da) which verified the presence of intact succinimide.

Similarly, porcine somatotropin (PST) protein containing stable succinimide was isolated when incubated under acidic conditions. RP-HPLC and peptide mapping experiments showed the presence of a peptide with intact succinimide (Violand et al., 1992).

Legumain is an asparaginyl endopeptidase (AEP) found mainly in endolysosomes and contributes to antigen processing and TLR maturation and is also implicated in tumour progression. In addition to the protease activity, human AEP was found to also possess peptide ligase activity independent of ATP. Formation of a bond is an endergonic process and requires energy from a high energy molecule such as ATP. Plant legumins were previously known to possess both ligase and cyclase activities, the mechanisms of which are still unknown. Upon solving the crystal structure of human legumain, Elfriede Dall and co-workers observed that residue Asp147 is present in the modified form succinimide (Suc147). The authors proposed that Suc147 acts as a high-energy coupling agent required for amide bond formation. Presence of succinimide surpasses the need for ATP. Single site mutants, D147S and

D147G, although showed reduced proteolytic activity, totally lacked the ligase activity (Dall et al., 2015) verifying the role of Suc147 in granting ligase activity to human legumain.

Another class of proteins that are known to harbour succinimide residue in their native structure are inteins. Inteins are mobile amino acid sequences capable of excising themselves from a protein (splicing). The process is analogous to mRNA splicing that removes intronic regions. Inteins are ubiquitously present in proteins of organisms from all domains of life. The splicing signal is perceived as a regulatory mechanism for generating functional proteins depending on environmental stimuli. Most known inteins are characterized by presence of C-terminal succinimide residue, formed as a result of their splicing from the pro-protein (Callahan et al., 2011; Liu et al., 2014; Van Roey et al., 2007).

CheY is a well characterized member of response regulator superfamily. The structure of *E. coli* CheY protein was solved at 1.1 Å resolution and was found to contain a stable succinimide. The succinimide was speculated to be stabilized by its interaction with a sulfate ion (Simonovic and Volz, 2001, 2002). The protein crystal was diffracted after 8 years of storage at 4 °C. Analysis of all the above-mentioned protein structures revealed the presence of succinimide in loop regions, a scenario similar to that in MjGATase (Fig. 4.6)

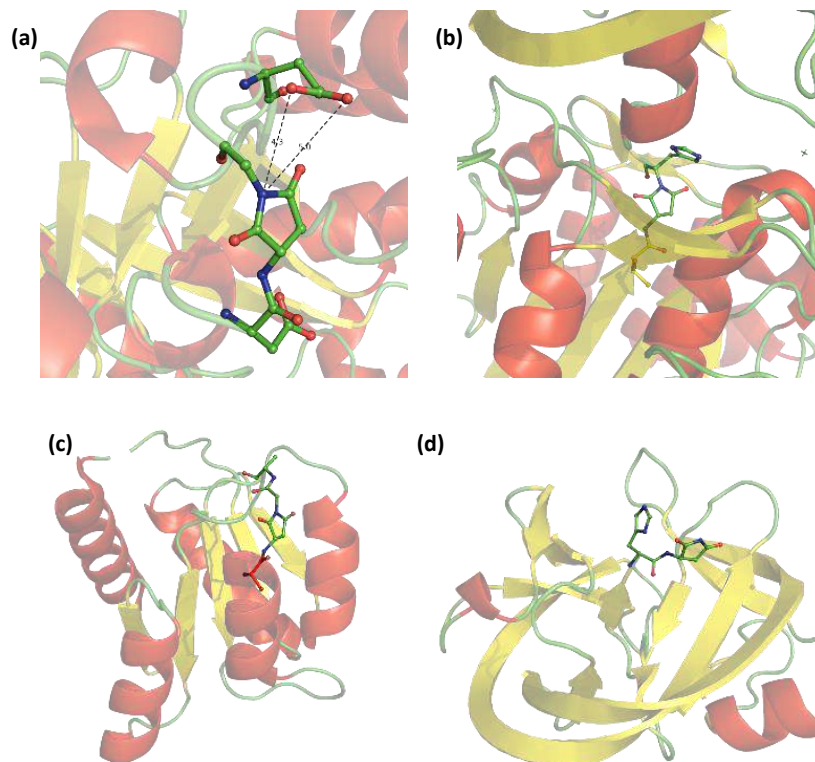


Figure 4.6: Stable succinimide residues in proteins. (a) The succinimide residue in *T. thermophilus* and *T. aquaticus* amyloamylase enzymes shows a presence of a negatively charged residue in the vicinity. (b) Succinimide in human legumain is possibly protected from hydrolysis by a histidine residue present over the succinimide ring plane. (c) Stable succinimide residue in *E. coli* CheY protein and (d) Inteins.

4.6. The influence of a stable succinimide on peptide backbone

Capasso and colleagues have performed extensive studies on the conformations adopted by succinimide or aminosuccinyl (Asu) containing peptides (Capasso and Di Cerbo, 2000; Capasso et al., 1995; Catak et al., 2006; demasi et al., 2009). They provide empirical evidence indicating that peptides of different lengths and sequences possessing Asu residue adopt type II' β -turn conformation. Turns are non-canonical structural conformations found in proteins that are characterized by a hydrogen bond between main chain carbonyl oxygen (i) and N(H) of residues ($i+x$, $x=1, 2, 3\dots$). Depending upon the number of atoms involved in formation of turns, turns are categorized as α , β , γ , δ and π turn (Kuo Chen Chou et al., 2000). β -turns are formed when a hydrogen bond is formed between C=O of i^{th} residue and N(H) of $(i+3)^{\text{rd}}$ residue of a polypeptide. β -turns were originally identified in proteins by Venkatachalam (Venkatachalam, 1968) and were further classified depending upon the Φ , Ψ values of the residues involved, as type I, II, and III and I', II' and III' (when signs of Φ and Ψ reversed). Capasso and colleagues found that succinimide containing peptides always adopted type II' β -turn conformation (Capasso et al., 1995)

In addition to a β -turn (4 \rightarrow 1), the succinimide harbouring segment in MjGATase also assumes an α -turn (5 \rightarrow 1) conformation, both leading to reversal of polypeptide chain in that region. An α -turn is characterized by hydrogen bond between carbonyl oxygen of residue i and N(H) of residue $i+4$. α -turns are relatively lesser studied conformational elements in proteins. They were first identified and studied by C. Ramakrishnan (Natraj et al., 1995) and found to be a widespread occurrence in proteins. Following the same criteria as β -turn, α -turns are categorized further in several different types (Kou Chen Chou et al., 1997). In proteins, turns generally occur on solvent exposed surfaces and might thereby be playing a role in antigen determination and variation. Moreover, turns aid in tight packing of globular proteins (Kou Chen Chou et al., 1997).

4.7. Glutamine amidotransferase (GATase)

Glutamine amidotransferases (GATase) as the name suggests are enzymes that 'transfer nitrogen from glutamine' to other molecules and are hence entailed in biosynthesis of nitrogen containing molecules. Glutamine contains one atom of nitrogen as an amide and another atom of nitrogen as an amine. The fundamental reaction carried out by GATases is as follows.



The NH_3 released by GATases is then used by a synthetase/ synthase domain or subunit that aminates the acceptor substrate. Glutamine amide nitrogen is utilized in the synthesis of the vitamins, NAD and NADP, purine and pyrimidine nucleotides. The amide group of glutamines is also used to produce carbamoyl phosphate for the synthesis of pyrimidines. Therefore, glutamine amidotransferases are a class of essential enzymes required for survival and proliferation of organisms from all three domains

of life. GATase domain can occur as a standalone enzyme subunit coded by a single gene. In this case, the synth(ase)etase subunit is encoded by a separate gene. Examples of two subunit type amidotransferases include, anthranilate synthase, amidodeoxychorismate and bacterial CPS. Some other amidotransferases are encoded by a single gene translating into multi-domain type enzyme, exemplified by asparagine synthetase, glutamine: PRPP amidotransferase, glucosamine-6- phosphate synthase among others. In most of the known cases, activation of the GATase enzyme is conditional to the binding of ligands to the acceptor domain/subunit. The conformational changes occurring in the acceptor subunit upon ligand binding, appear to be crucial to GATase activation. The ammonia generated in the active GATase is then tunnelled to the acceptor domain/subunit for further reaction (Ballut et al., 2015; Douangamath et al., 2002; Huang et al., 2001; Mouilleron and Golinelli-Pimpaneau, 2007).

Two types of glutamine amidotransferases have been identified in nature.

- **Class-I (also known as trpG-type or triad):** The name trpG is derived from TrpG subunit of anthranilate synthase, encoded by the Trp operon genes. In these glutamine amidotransferases, a triad of conserved Cys-His-Glu forms the active site, wherein the catalytic cysteine is essential for the amidotransferase activity. MjGATase belongs to this class of amidotransferases.
- **Class-II (also known as purF-type or Ntn):** These enzymes have a conserved Cys at the N-terminus. purF is the gene that encodes Glutamine: PRPP amidotransferase.

4.7.1. Structural features of Glutamine amidotransferases

RCSB PDB harbours 166 entries of GATase domain structures. Five structures of glutamine hydrolysing domains were selected randomly and superimposed using PyMol on MjGATase structure that we solved. We observed that although there is not much sequence similarity among them (Fig. 4.7 a), the folds in protein tertiary structure remained similar (Fig. 4.7 b). The Pfam database enlists hundreds of unique domain organisations or architectures among which GATase family (PF00117) domain is found. Class I GATases are characterized by the presence of 7 β sheets of mixed polarity surrounded by α helices and loops (Smith, 1995). The Cys-His-Glu catalytic triad of all class I GATases is situated towards the C terminal end of the β sheet cluster. The catalytic cysteine residue along with backbone nitrogen atoms of neighbouring tyrosine and glycine residues forms an oxyanion hole that stabilizes the negative charge on the transition state intermediate during hydrolytic reaction (Chittur et al., 2001; Korolev et al., 2002).

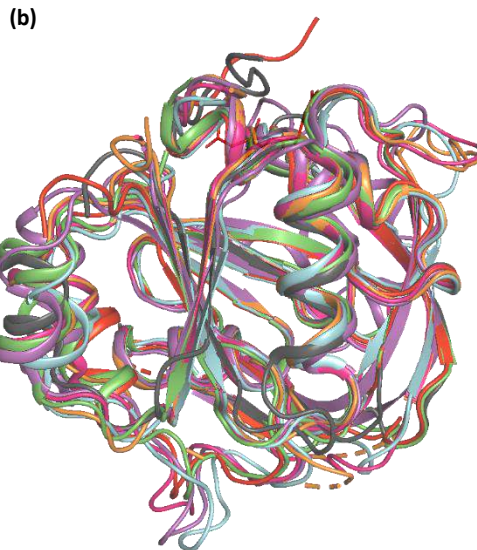
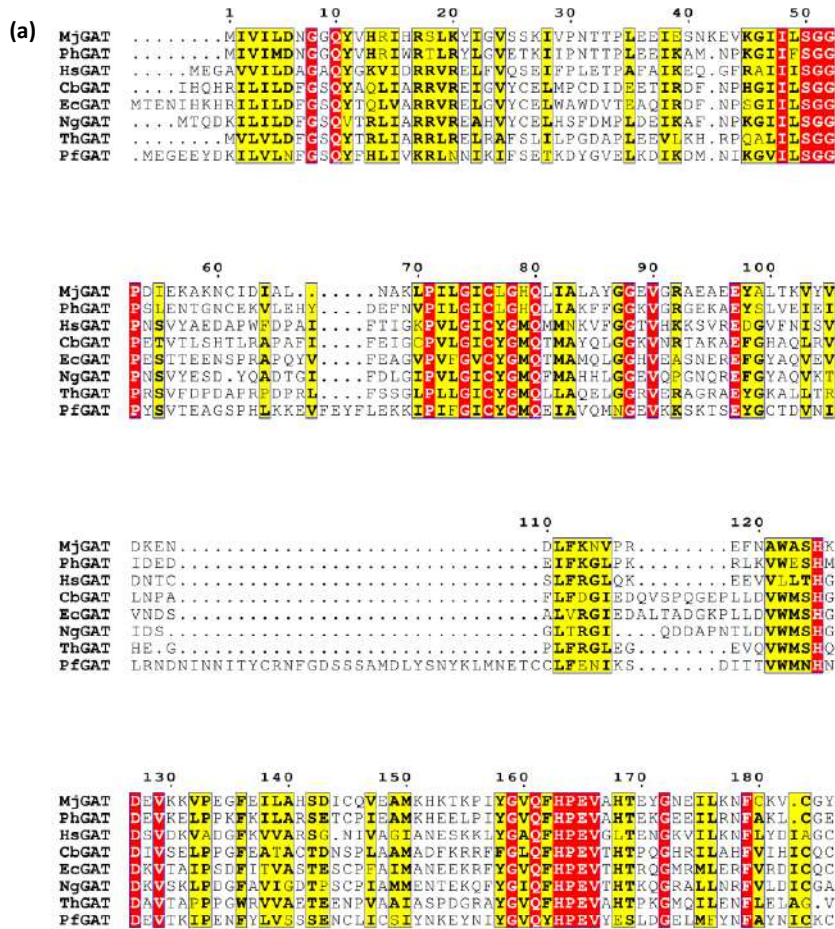


Figure 4.7: Multiple sequence alignment of GATase sequences from eight different organisms. (a) Although there is low sequence similarity between the proteins, their (b) structures show the same folds. Abbreviations: MjGAT: *M. jannaschii* GATase (red), PhGAT: *Pyrococcus horikoshii* GATase (green), HsGAT: *Homo sapiens* GATase (grey), EcGAT: *E. coli* GATase (blue), NgGAT: *Neisseria gonorrhoeae* GATase (pink), ThGAT: *Thermus thermophilus* GATase (cyan), PfGAT: *Plasmodium falciparum* GATase (purple). Colours of each GATase structures are mentioned in brackets.

Methanocaldococcus jannaschii is the first ever Archean whose genome was sequenced in 1996 (Bult et al., 2016) This opened new avenues for understanding the reasons for how an organism can survive and proliferate at extreme temperature (≥ 85 °C) and pressure conditions (~ 200 atm) where no life could be envisioned. Survival and proliferation are phenomena that are governed by functionality of proteins, so organisms that can thrive at such extreme conditions would have proteins that are folded rigidly and employ mechanisms to stabilize and maintain those folds and thus protein stability. Majority of information that we possess today regarding protein stability has come from studies on thermophilic proteins (Vieille and Zeikus, 2006). Thermophilic proteins crystallize better than their mesophilic counterparts and are hence desirable candidates for structural studies. Owing to this paradigm, a lot of proteins from *M. jannaschii* have been structurally studied. In our laboratory, we study biochemistry of enzymes from purine salvage pathway of *Plasmodium falciparum*. As it is a mesophilic protozoan parasite whose proteins are at times difficult to express in heterologous fashion and obtain in soluble fractions, proteins from *M. jannaschii* were studied and findings were extrapolated wherever applicable. Mesophilic, thermophilic or psychrophilic proteins often possess similar folds although they differ significantly in their thermal stabilities (Liao et al. 2018). Hence, we chose thermophilic homologues of those *Plasmodium falciparum* proteins from *Methanocaldococcus jannaschii*. Earlier studies in our laboratory had focused on solving the structures of adenylosuccinate synthetase, fumarate hydratase and ATP pyrophosphorylase from *M. jannaschii*.

4.8. Molecular Dynamic Simulation

Molecular dynamic simulations (MDS) have proven immensely useful in capturing the internal motions in protein molecules that are difficult to be experimentally captured sometimes. By coupling structure and dynamics data, MDS allows investigation of the conformational energy landscapes accessed by proteins. MDS has been historically used to delineate functional dynamics of proteins (Sultan et al., 2018; Yang et al., 2012), mechanisms of protein folding/unfolding pathways (Freddolino et al., 2010; Liwo et. al. 2005) and protein stability mechanisms (Baker et al., 2017; Dong et al., 2018). Protein function is a result of dynamic interactions of atoms within the protein molecule. By the use of a force field i.e., potential energy landscapes, simulations unravel protein dynamics as a function of time, temperature or any other desired parameter. The spatial and temporal resolution granted by MD simulations permits us to view proteins in action, a feature that static protein structure can-not provide. In solution, proteins can access various conformational states given their inherent dynamic nature but these conformational states are not represented in crystal structures. In such scenario, MD simulation try to access those states and provide atomistic details about different conformational states in response to different simulated environmental conditions (such as temperature, pH, time). Therefore, MD simulations can be used to interpret experimentally obtained results as well as predict the outcome of an experiment.

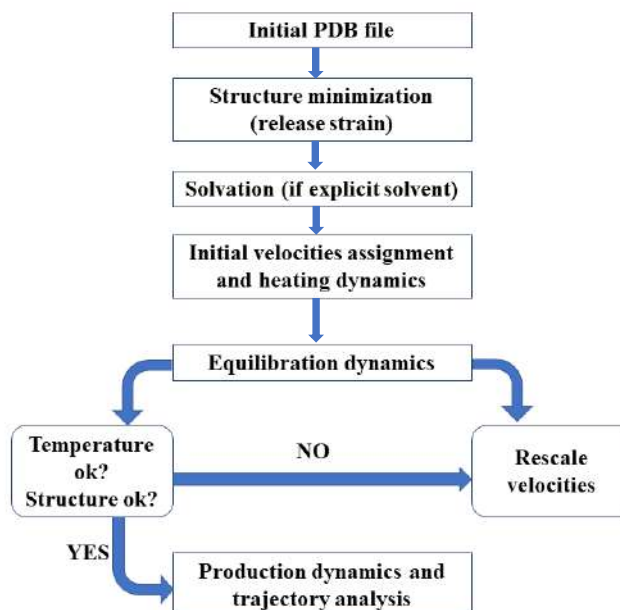


Figure 4.8: Flowchart of steps involved in molecular dynamic simulation of proteins. Figure adapted from Patodia, Sachin. 2014. "Molecular Dynamics Simulation of Proteins: A Brief Overview." *Journal of Physical Chemistry & Biophysics* 4(6): 4–7 in accordance with the Open Access license.

In recent times, molecular dynamic simulations have been used to understand the influence of post-translational modifications on protein stability. Glycosylation as mentioned earlier, is a PTM known to impart thermostability to some proteins; MD simulations have been used to predict glycosylation sites and/or glycosylation patterns involved in granting higher stability to the protein (Shental-Bechor and Levy 2008).

A major limitation encountered during simulations of biological molecules is the insufficient sampling of conformational space given their large size. Limited sampling of conformational space limits meaningful characterization of dynamics and function of the system. Often times, the changes within protein structure are evident only when most of the probable conformational space is explored. But that would mean carrying out computationally laborious and time-consuming simulations. To mitigate this problem, methods such as replica-exchange molecular dynamics (REMD) and metadynamics have been developed among others. These two methods were used in our study to sample all of the possible conformational space for the inherently stable hyper-thermophilic protein MjGATase. *(The simulations were carried out by Dr. Sudip Das, from Prof. Balasubramanian Sundaram's laboratory, Chemistry and Physics of Materials Unit, JNCASR as a collaborative project)*

Large systems such as proteins hardly relax as the energy barrier to cross from one conformational state to another is too high and hence the system poses a threat of falling within multiple local energy minima at room temperature simulations.

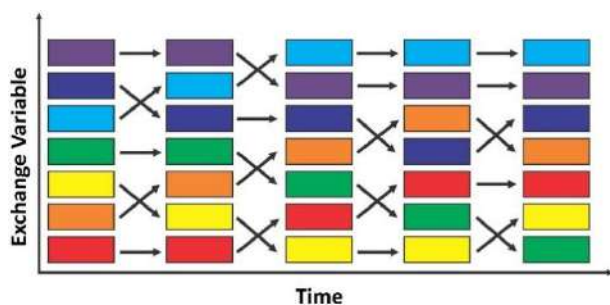


Figure 4.9: Representation of replica exchange method (REM). Image adapted from Rafael C. Bernardi, Marcelo C.R.Melo, Klaus Schulten, Enhanced sampling techniques in molecular dynamics simulations of biological systems, *Biochimica et Biophysica Acta (BBA) - General Subjects*, 1850, 2015, 872-877 with permission.

To overcome this difficulty, the system can be heated by increasing its potential energy thereby forcing the system to cross the energy barrier and access different conformations. The state of the system (protein) or the replica, at a given temperature is defined by the positions of all atoms at that temperature and these replicas can be exchanged freely between different temperatures in the replica exchange method (REM). However, for a large system of several

hundred amino acids, the number of replicas to

be handled can be enormous presenting a need to use high end computers. In the improved method of **replica exchange with solute scaling (REST2)**, the problem of scaling is mitigated thereby making it an attractive choice for simulation of biomolecules. Instead of tempering the whole system, REST2 method specifically scales the potential energy surface of the region of interest (solute) resulting in significant decrease in the number of replicas; thus, making it computationally effective thereby enabling the study of the system without an a priori knowledge of the major conformational changes (Fig. 4.9). Hence, the temperature value in REST2 is an effective temperature value rather than an actual temperature. REST2 enables larger replica exchange probability i.e. better sampling of replicas between different temperatures and therefore efficient MD sampling of conformational space between higher and lower temperatures.

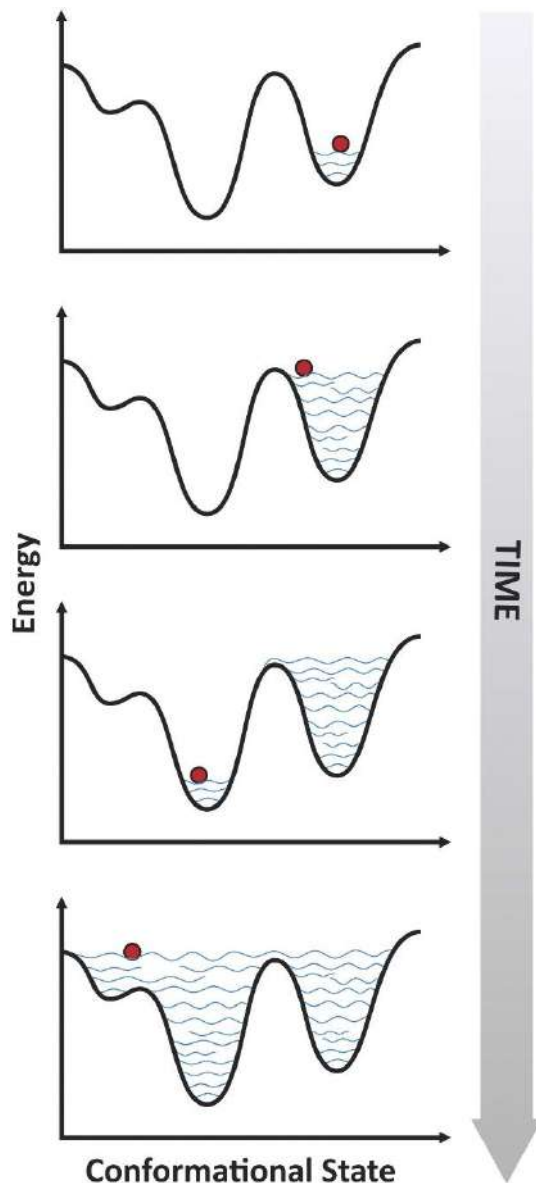


Figure 4.10: Diagrammatic illustration of concept of metadynamics. The method involves filling of free energy wells using “computational sand” as described by Darve and Phorille, preventing the system from revisiting the same energy well. Image adapted from Rafael C. Bernardi, Marcelo C.R.Melo, Klaus Schulten, Enhanced sampling techniques in molecular dynamics simulations of biological systems, *Biochimica et Biophysica Acta (BBA) - General Subjects*, 1850, 2015, 872-877 with permission.

Another powerful algorithm that is used for reconstruction of the free energy landscapes to visit rarely occurring events in a biomolecule is **metadynamics**. This method uses a set of collective variables (CV) (such as radius of gyration of a stretch of residues, interatomic distances, angles, torsions etc.) to describe the system. The free energy surface is a function of these collective variables. The metadynamics algorithm inserts a memory in sampling thereby, discouraging the system from revisiting a previously sampled conformational state. This enhances the scope for exploration of available free energy landscape. Darve and Phorille (Darve and Pohorille, 2001) described this method as “*filling the free energy wells with computational sand.*” Once the sand fills one free energy well, the system can -not visit it again and moves in search of another plausible well thereby searching through the entire free energy landscape (Fig. 4.10). This facet which allows crossing of energy barriers is much desirable for studying protein folding (Bussi et al., 2006), molecular docking (Gervasio et al., 2005) and conformational changes (Spiwok et al., 2007) in inherently stable proteins.

Objectives of the study

This chapter describes the study of solving the crystal structure of Glutamine amidotransferase (GATase) subunit of Guanosine 5' monophosphate synthetase (GMPS) from *M. jannaschii*. The structure was then used for molecular dynamic simulations to further understand the factors contributing to the unusually high thermal stability of MjGATase gained via a succinimide modification.

Chapter 5

Materials and Methods, Results, Discussion and Future Directions

This chapter contains Materials and Methods, Results, Discussion and Future directions of this section of the thesis. Methods used to purify, crystallize and solve structure of MjGATase (wild type and mutants) have been reported in detail. Structure of MjGATase solved by X-ray crystallography has been thoroughly analysed with specific focus on the succinimidyl residue: its interactions with neighbouring residues, long-range contacts and tertiary contacts connecting the stable succinimidyl residue with the active site residues. Structure of WT MjGATase covalently bound to the non-hydrolysable glutamine analogue, acivicin (5CS) was also solved. In addition, structure of D110G mutant, in which succinimide forms but readily undergoes hydrolysis, was also solved and analysed. Further, the stabilizing interactions of succinimidyl residue have been discussed. We postulate that post-translational succinimide formation might be more widespread among hyperthermophilic organisms than we currently presume. At the end, I have briefly reported the results obtained by advanced simulation tools used in the study (*All simulations were performed by Dr. Sudip Das, Ph.D. from Prof. Balasubramanian Sundaram's laboratory, Chemistry and Physics of Materials Unit, JNCASR*). Finally, the future prospects for this section of the thesis have been discussed.

5.1. Materials and Methods

All chemicals used were of highest purity and were procured from Sigma-Aldrich. Akta Basic HPLC and Q-sepharose resin were from GE Healthcare Life Sciences, UK. Mass spectra were recorded at Molecular Biophysics Unit, India Institute of Science, Bangalore, India using high resolution ESI-Q-TOF (Maxis Impact, Bruker Daltonics, Germany) coupled to Agilent HPLC system and at Central Instrumentation facility (CIF), Molecular Biology and Genetics Unit, JNCASR using Q Exactive HF (Thermo Scientific, USA) coupled to a Dionex UltiMate 3000 UHPLC/ EASY-nLC 1200 (nano LC system, Thermo Scientific). X-ray diffraction data for wild type (WT) and mutant MjGATase crystals were collected on Rigaku RU200 X-ray diffractometer equipped with a rotating anode type light source with an osmic mirror that gives a monochromatic light source of wavelength 1.54179 Å. An image plate of type MAR scanner, 345 nm was used for detection.

5.1.1. Protein purification

Gene for GATase subunit from *M. jannaschii* genomic DNA was cloned into pET3str using NdeI and BamHI restriction sites, and subcloned into cassette I of pST39 expression vector using XbaI and BamHI restriction sites. Plasmids carrying gene for GATase subunit were transformed into Rosetta (DE3) pLysS *E. coli* overexpression strain. The cells containing the plasmid construct were grown at 37 °C in terrific broth containing 100 µg ml⁻¹ ampicillin and 34 µg ml⁻¹ chloramphenicol to an OD₆₀₀ value of 0.6. and thereafter the cells were induced with IPTG to a final concentration of 0.3 mM and grown for additional period of 3 hours. At the end of 3 hours, cell pellet was collected by centrifugation at 3400 g for 10 minutes at 4 °C, and re-suspended in 30 ml of lysis buffer (20 mM Tris-HCl pH 7.4, 10 % glycerol, 0.1 mM EDTA, 1 mM PMSF, 2 mM DTT, pH 8.0) and lysed by sonication. The cell lysate was centrifuged at 24,000 g for 30 minutes at 4 °C to remove cell debris. The supernatant was heated at 70 °C for 30 minutes to denature and precipitate *E. coli* proteins. The denatured endogenous bacterial proteins were removed by centrifugation at 24,000 g for 30 minutes at 4 °C. In order to precipitate nucleic acids, supernatant was treated with 0.01 % of polyethyleneimine and centrifuged at 24,000 g for 30 minutes. The resulting supernatant was loaded onto a Q-sepharose anion-exchange column equilibrated with buffer A (20 mM Tris-HCl pH 8.0, 10 % glycerol, 0.1 mM EDTA, 1 mM PMSF, 2 mM DTT, pH 8.0) at a flow rate of 3.0 ml min⁻¹. The column was washed with 50 ml of buffer A. The protein was eluted with a linear gradient of buffer B (Buffer A containing 1 M NaCl). Elution was monitored by measuring absorbance at 280 nm. Fractions containing protein were collected, and concentrated using centrifugal concentrators (Centricon, Millipore, USA, 10.0 kDa MWCO). Protein concentration was estimated by the method of Bradford using BSA (1 mg ml⁻¹) as a standard.

5.1.2. Crystallization and data collection

Crystallization of both MjGATase_WT and mutant proteins (MjGATase_D110G, MjGATase_N109S) was set up under 1:1 mixture of silicon and paraffin oil using the micro-batch method (Chayen et. al., 1992). Initially, all conditions available with Hampton Research crystal screen were used. Protein crystals were not obtained under any of the conditions. The solubility of MjGATase

at room temperature is very high and hence lowering of the temperature was required to lower the solubility leading to crystallization. Crystals of MjGATase_WT suitable for X-ray diffraction (Fig. 5.1 a) were obtained at 4 °C in 100 mM sodium acetate, pH 5.6 and 35 % PEG 6000. Crystals of MjGATase_D110G enzyme (Fig. 5.1 b) were obtained at 4 °C in 100 mM sodium acetate, pH 5.6 and 10 % PEG 6000. Several attempts were made to crystallize MjGATase_N109S mutant enzyme under the same conditions as well as various conditions of the Hampton Screens but all of the crystals that were obtained, failed to provide good quality diffraction data. Repeatedly, the crystals obtained were multi lattice type (Fig 5.1 c) and resulted in twinned diffraction pattern (Fig. 5.2 c) which could not be used to solve structure of this mutant enzyme.

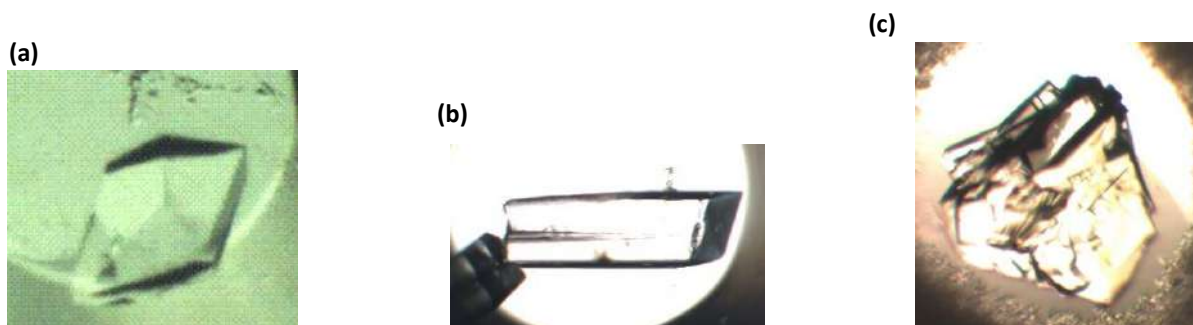


Figure 5.1: Images of crystals of (a) MjGATase_WT, (b) MjGATase_D110G and (c) MjGATase_N109S. MjGATase_N109S crystals were multi-lattice type and did not yield good diffraction pattern.

Both MjGATase_WT and MjGATase_D110G enzyme crystals were soaked in reservoir solution supplemented with 25 % ethylene glycol as cryo-protectant for 10 minutes prior to diffraction. The crystal of MjGATase_WT diffracted to a resolution of 1.665 Å and a total of 232 frames were collected. The same crystal was then carefully unmounted from the diffractometer and soaked in a solution of acivicin for 8 hours and diffracted again under the same conditions. It also diffracted to a resolution of 1.665 Å (Fig. 5.2 a). The crystal of MjGATase_D110G diffracted to a resolution of 2.214 Å and 137 frames were collected (Fig. 5.2 b). Details of the data collection and refinement are provided in Table 5.1.

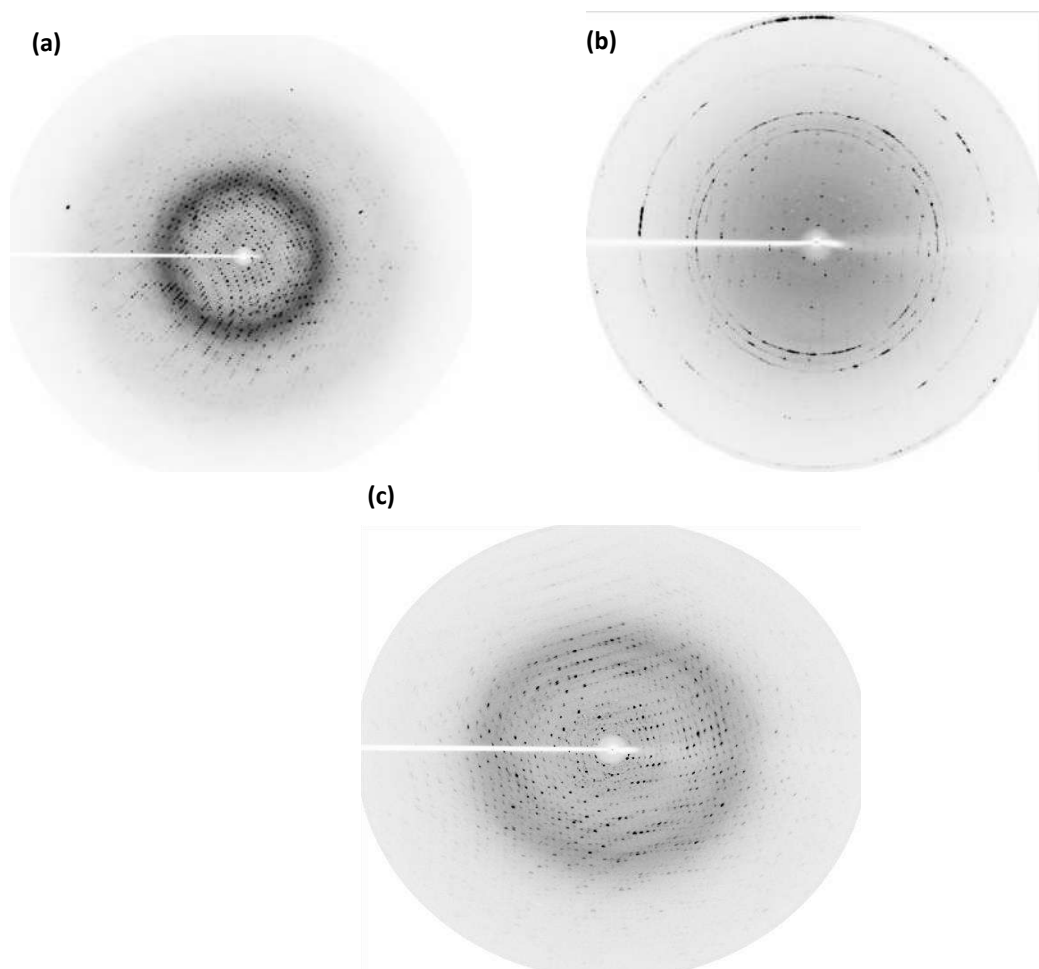


Figure 5.2: Representative images of diffraction patterns of (a) MjGATase_WT, (b) MjGATase_D110G and (c) MjGATase_N109S

5.1.3. Structure solution and refinement

Diffraction images were processed using iMOSFLM (Battye et al., 2011). The space group of the crystal of apo and acivicin bound MjGATase was P32 while that of MjGATase_D110G was P212121. Structure solutions were obtained using molecular replacement method (MR) and Phaser module of CCP4 (McCoy et al., 2007; Winn et al., 2011). For phasing the reflections from MjGATase_WT crystal, structure of GATase from *Pyrococcus horikoshii* (PDB ID: 1WL8) was used as template as it shares 59 % identity with MjGATase sequence. The MjGATase_WT structure was used as a template for molecular replacement to solve the structure of MjGATase_D110G. For refinement of the structures, Refmac module of CCP4 (Murshudov et al., 2011; Murshudov et. al., 1997; Winn et al., 2011) and AutoBuild module of Phenix (Adams et al., 2010; Terwilliger et al., 2007) were used. Refmac placed an asparagine residue at position 109 where a clear density for a cyclic structure could be seen. Based on our earlier results it was known that N109 was deaminated to a succinimidyl residue (SNN) in native MjGATase (Kumar et al., 2016). Hence, N109 was replaced by SNN using the coordinates of SNN available in the SMILES library. After fitting SNN, several rounds of refinement were carried out using Refmac and SNN fitted correctly within the electron density. In case of the

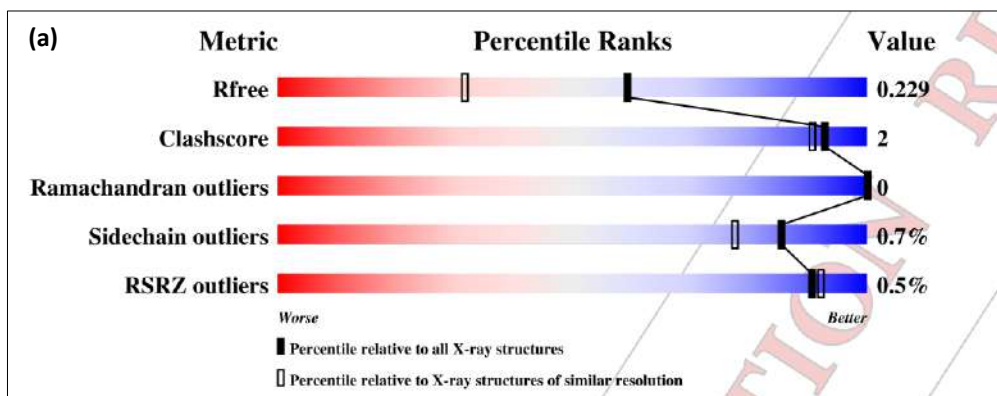
liganded structure, co-ordinates for acivicin (5CS) were also procured from SMILES and included in the structure co-ordinates file and multiple rounds of refinement were then carried out. After refinement of structures, validation reports were generated for each structure using wwPDB validation service. The graphic indicating the percentile scores (ranging between 0-100) for global validation metrics of the entry are shown in Figure 5.3.

Table 5.1: Summary of data-collection and refinement statistics

Property	MjGATase	MjGATase with acivicin	MjGATase D110G
PDB ID	7D40	7D95	7D96
Data collection statistics			
Resolution Range	56.53 - 1.67	56.59 - 1.67	50.99 - 2.29
Wavelength (Å)	1.54179	1.54179	1.54179
Space group	P 32	P 32	P 21 21 21
Unit cell parameters			
a, b, c	65.28Å 65.28Å 97.14Å	65.35Å 65.35Å 97.37Å	36.18Å 66.65Å 79.18Å
α, β, γ	90.00 ⁰ 90.00 ⁰ 120.00 ⁰	90.00 ⁰ 90.00 ⁰ 120.00 ⁰	90.00 ⁰ 90.00 ⁰ 90.00 ⁰
% completeness	99.7 (83.6)	99.7 (89.5)	91.2 (97.8)
Avg. Mosaicity	0.60	0.80	0.50
Total reflections	11997 (42843)	11242 (41922)	1248 (5936)
Unique reflections	1730 (6644)	1737 (7137)	299 (1258)
Multiplicity	6.9 (6.4)	6.5 (5.9)	4.3 (4.7)
N ⁰ mol. / asym. Unit	2	2	1
I/(σ)I	20.7 (6.0)	19.9 (4.1)	10.2 (4.1)
CC _{1/2}	0.973 (0.766)	0.981 (0.858)	0.970 (0.881)
R _{meas}	0.134 (0.303)	0.094 (0.371)	0.143 (0.396)
R _{merge} (%)	12.4 (27.8)	8.6 (33.8)	12.6 (35.5)
Wilson B factor (Å ²)	18.5	21.4	19.1
Data Refinement statistics			
R _{work} /R _{free}	0.1610/0.2144	0.1993/0.2350	0.2797/0.2884
No. of atoms			

Protein	3482	3206	1495
Ligand	0	1	0
No. of non-H atoms			
Protein	2895	2940	1421
Ligand	0	0	0
Water	524	266	54
rms deviation			
Bond Angle ($^{\circ}$)	2.2051	2.0224	1.6129
Bond Length (\AA)	0.0240	0.0124	0.0128
Avg. B, all atoms	23.0	25.0	18.0
<u>Residues in Ramachandran plot</u>			
<u>Favoured</u>	358 (98%)	360 (99%)	176 (97 %)
<u>Allowed</u>	7 (2%)	4 (1%)	5 (3 %)
<u>Outliers</u>	1 (0%)	0	0

Values for the highest resolution shell are given in parentheses.



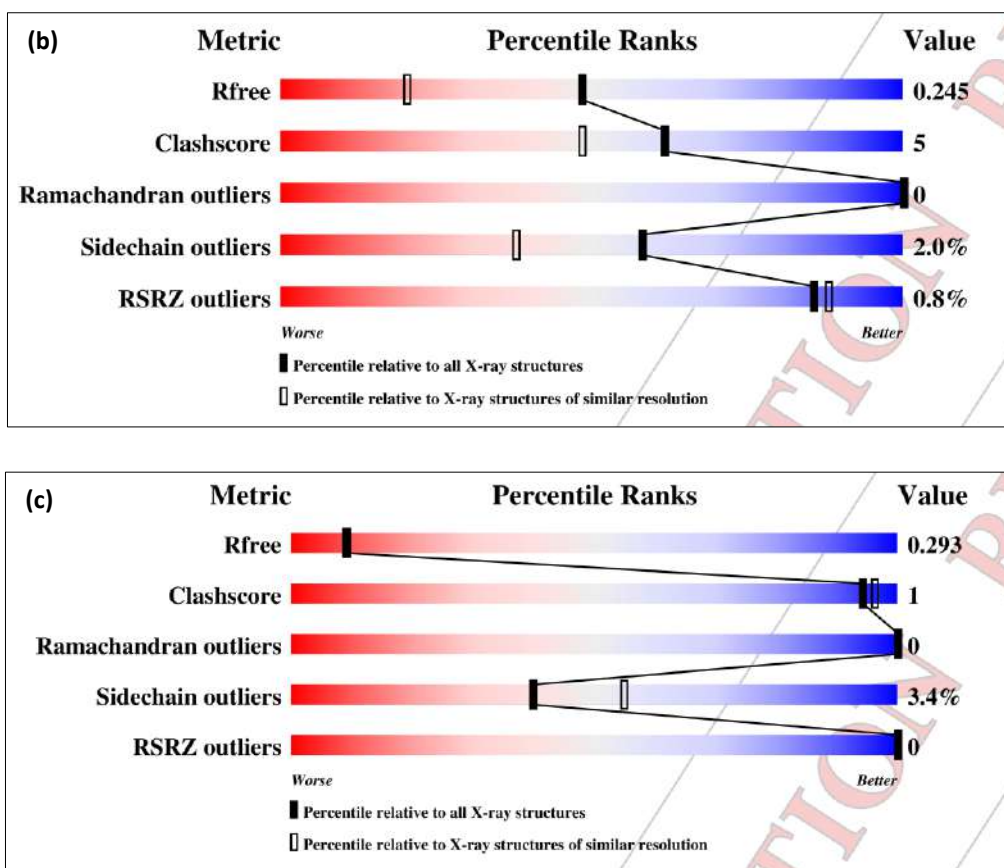


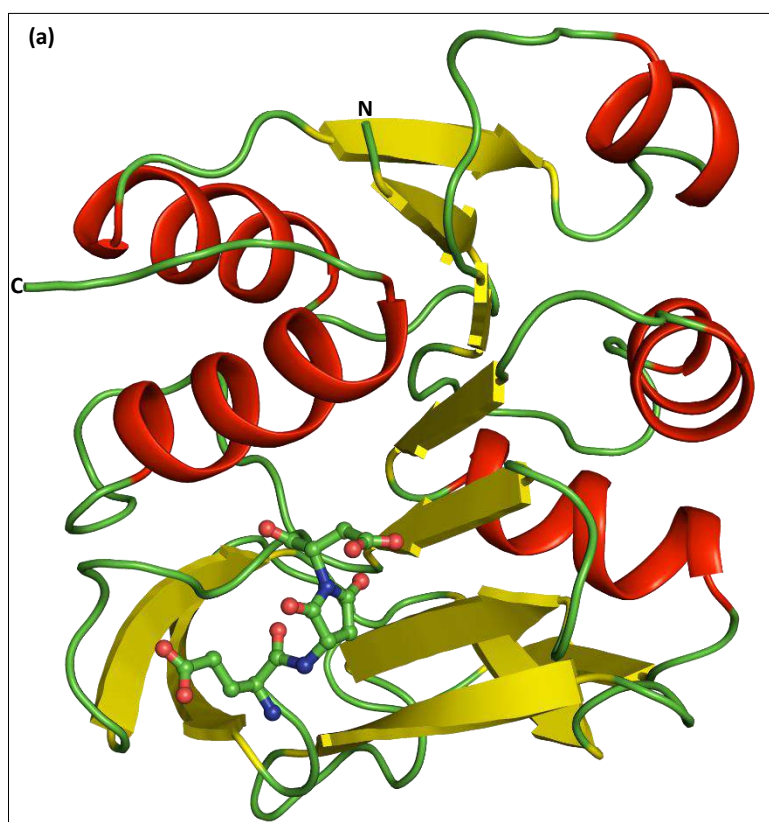
Figure 5.3: Validation reports generated via wwPDB validation service. (a) Validation report of apo structure of MjGATase_WT, (b) acivicin bound MjGATase_WT and (c) MjGATase_D110G

5.2. Results and Discussion

5.2.1. Crystal structure of MjGATase

The structure of MjGATase was previously obtained using solution NMR (PDB ID: 2LXN) (Ali et al., 2013). At that time, the deamidation of Asn109 as a post-translational modification was unknown. The discovery that Asn 109 residue in MjGATase undergoes deamidation as a post-translational modification was made later in the course of the same study (Kumar et al., 2016). The presence of a succinimidyl residue (SNN) at position 109 was confirmed by extensive mass spectrometric analysis of the intact protein as well as peptides from tryptic digestion. However, a structure depicting the presence and placement of succinimidyl residue in the protein, that could explain how it imparts thermostability was absent and that is the focus of this study. X-Ray crystallographic structure could not only ascertain the existence of succinimidyl residue at position 109 but also enabled the visualization and understanding of the structural features involved in stabilization of this otherwise meta-stable intermediate in the protein.

The overall structure of MjGATase is shown in Figure 5.4 a. The glutamine hydrolysing domain/subunit of Class I Glutamine amidotransferases from organisms across all three kingdoms of life share common structural features. The central region comprises of 7 mixed β -sheets (Fig. 5.4 b) which are surrounded by α helices and loops (Smith et.al., 1995). The active site triad (Cys-His-Glu, Cys76, His163, Glu165 in MjGATase) is at the C terminal end of β -sheets. All these features are conserved in MjGATase enzyme.



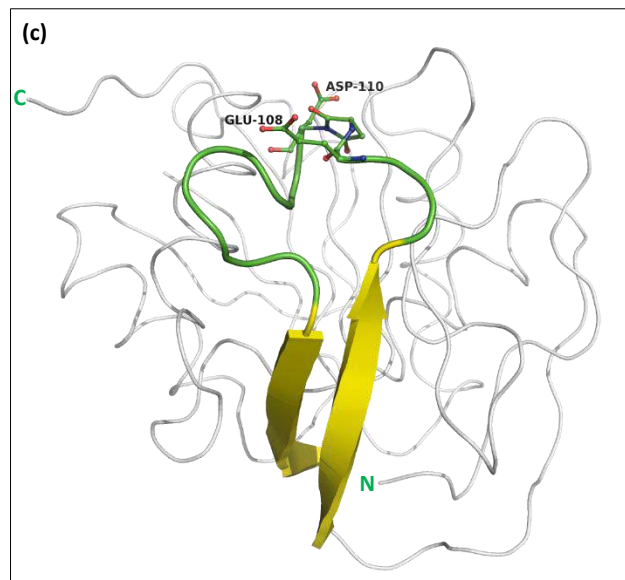
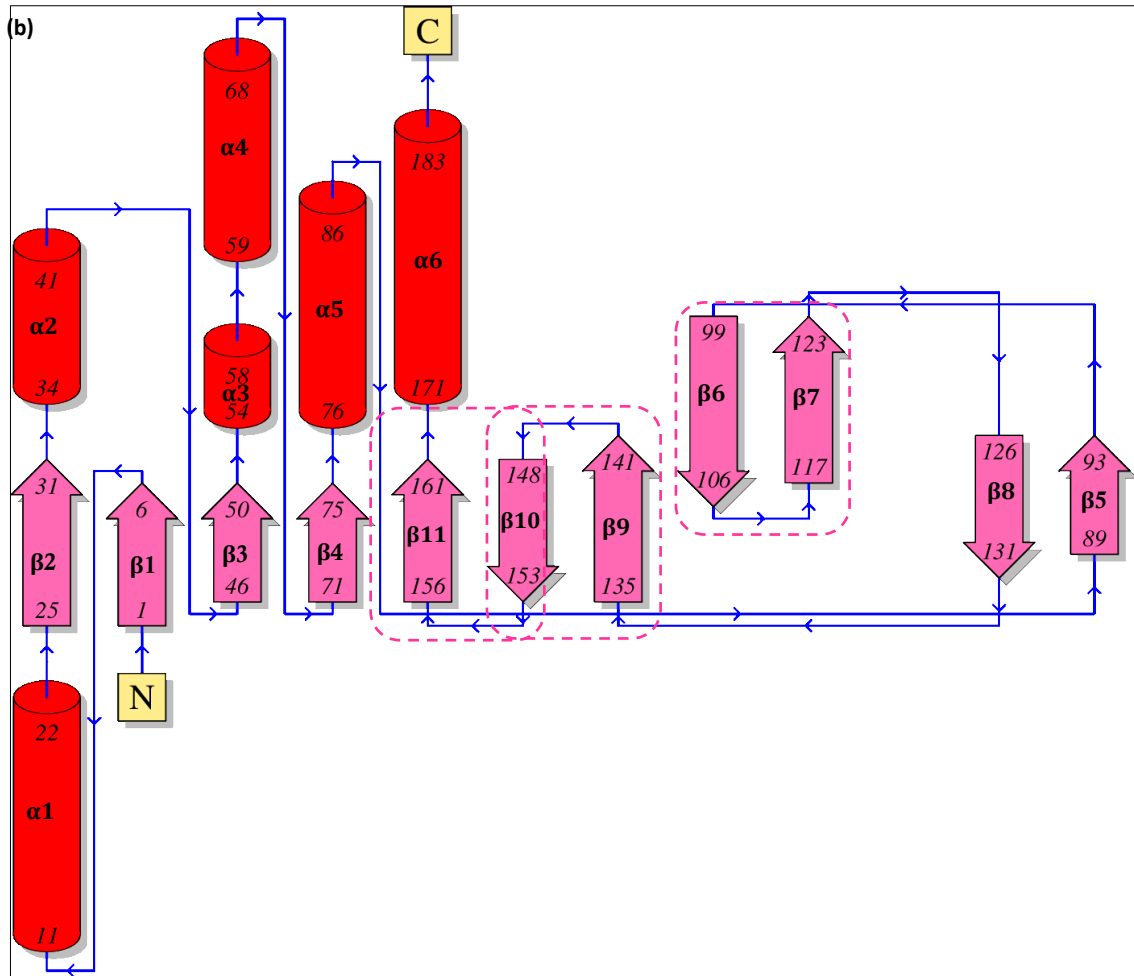


Figure 5.4: Structural features of MjGATase containing a succinimidyl residue. (a) Ribbon diagram of the overall structure of MjGATase solved at 1.67 Å resolution. The tripeptide region 108-110 harbouring succinimidyl residue (SNN109) is represented as ball and stick. (b) Topology diagram of MjGATase. Central region of the protein comprises of 7 mixed β -sheets which are surrounded by α -helices, a structural feature conserved in all GATase central region in class I glutamine amidotransferase family proteins. There are three β -hairpins present in the MjGATase structure which are highlighted in pink dotted boxes. (c) Ribbon diagram representing β -hairpin formed by $\beta 6$ - $\beta 7$ which are connected by a 12-residue long loop, the tip of which contains the tripeptide (108-110) harbouring succinimidyl residue represented as ball and stick model.

MjGATase protein contains three β -hairpin structural motifs that consist of (β 6- β 7), (β 9- β 10) and (β 10- β 11). The β 6- β 7 hairpin consisting of residues 99-123 harbours the succinimidyl residue in the loop region (Fig. 5.4 c). A clear density could be observed for succinimidyl residue at a resolution of 1.67 Å (Fig. 5.5 a-d)

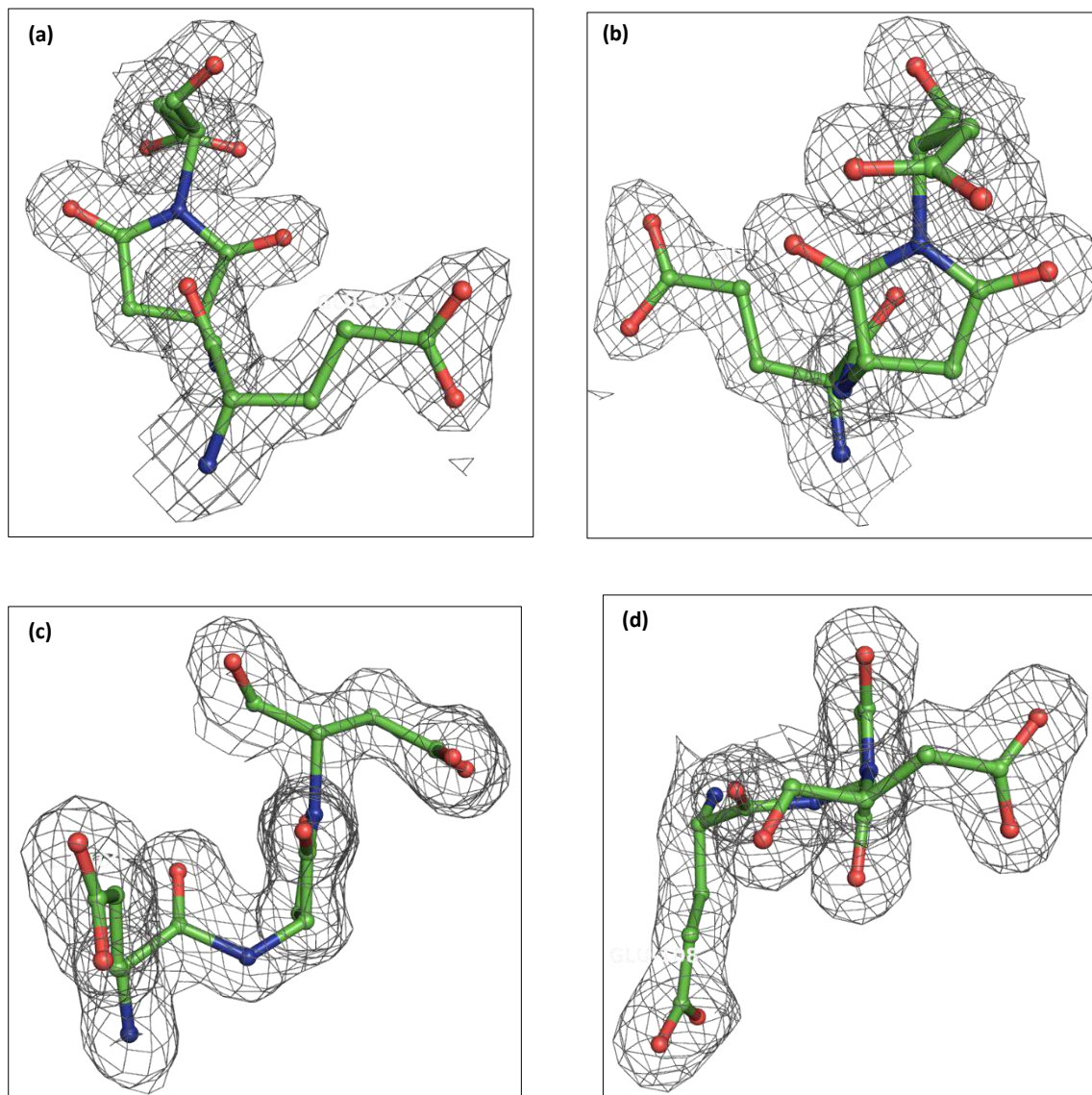


Figure 5.5: Clear electron density for the tripeptide region harbouring succinimidyl residue could be seen at 1.67 Å resolution. (a-d) Four different representations of the electron density are shown to emphasize the presence of the electron density in the region. All electron density maps ($2F_o - F_c$) are contoured at 1σ .

Although deamidation is a frequently occurring PTM in ageing proteins and in proteins stored for longer duration (Gracy et. al., 1998)(Daniel et. al., 1996), the succinimide intermediate formed during the course of the modification is seldom stable and hence often not been captured in X-Ray crystallographic structures. However, even in the instances where electron density for a succinimidyl residue is observed, it is not modelled correctly simply owing to the fact that its existence is

unanticipated. This can be exemplified by two structures of *Pyrococcus horikoshii* GATase, one containing SNN residue (PDB ID: 1WL8) (Fig. 5.6 a) while the other deposited structure did not report a SNN residue although electron density for it was evident (Fig. 5.6 b). Another similar example found in the literature is that of structures of amylomaltase from *Thermus thermophilus* and *Thermus aquaticus*. The acarbose bound amylomaltase structure was deposited by Przytylski *et al.* which showed electron density corresponding to a succinimidyl residue but authors modelled an Ala in the place (Fig. 5.6 d) ((Przytylski *et al.*, 2000). Later, a study by Barends *et al.* showed a succinimidyl residue at position 370 in *Thermus thermophilus* amylomaltase and also pointed out the corresponding succinimidyl residue in case of the *T. aquaticus* amylomaltase (Fig. 5.6 c) (Barends *et al.*, 2007).

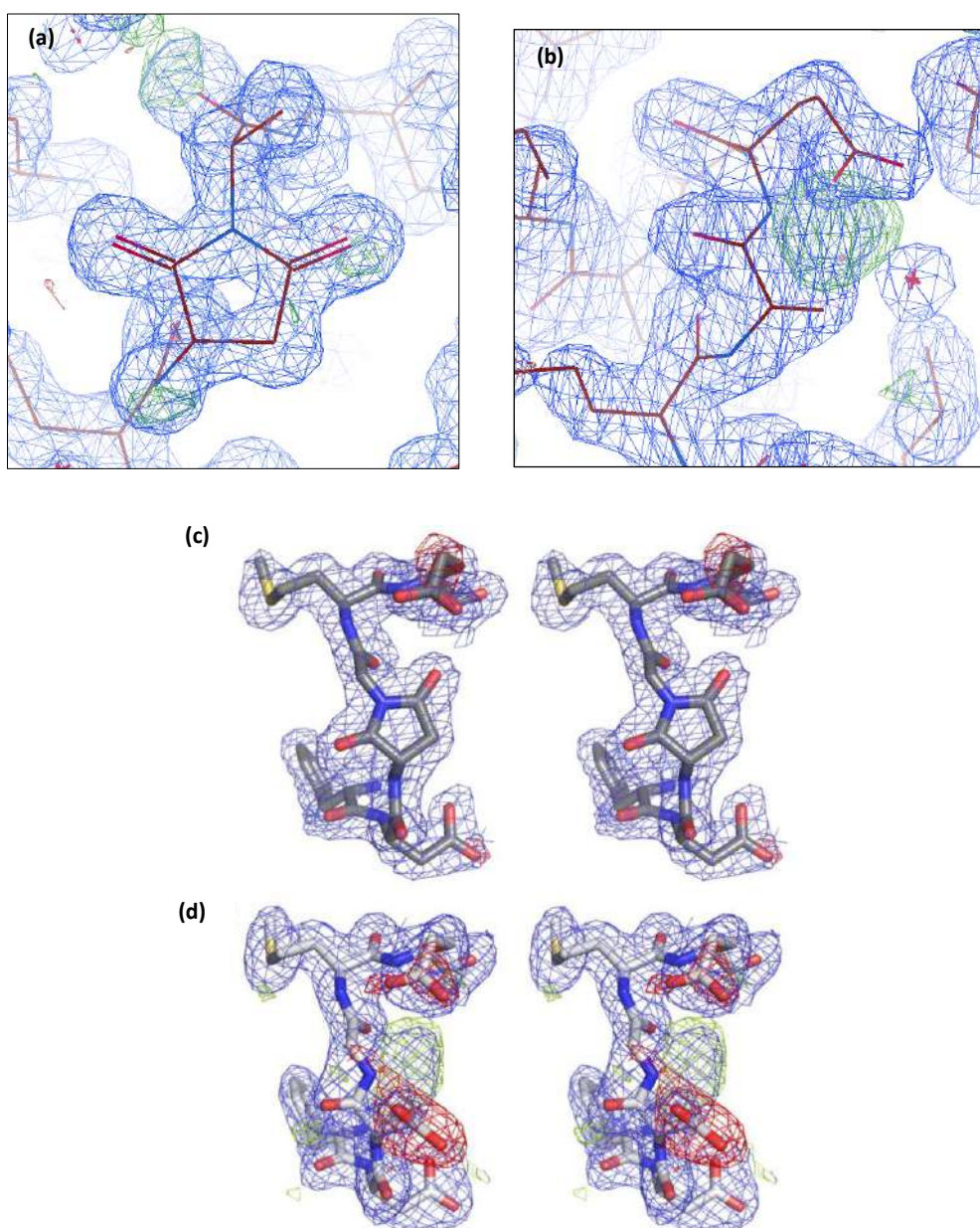
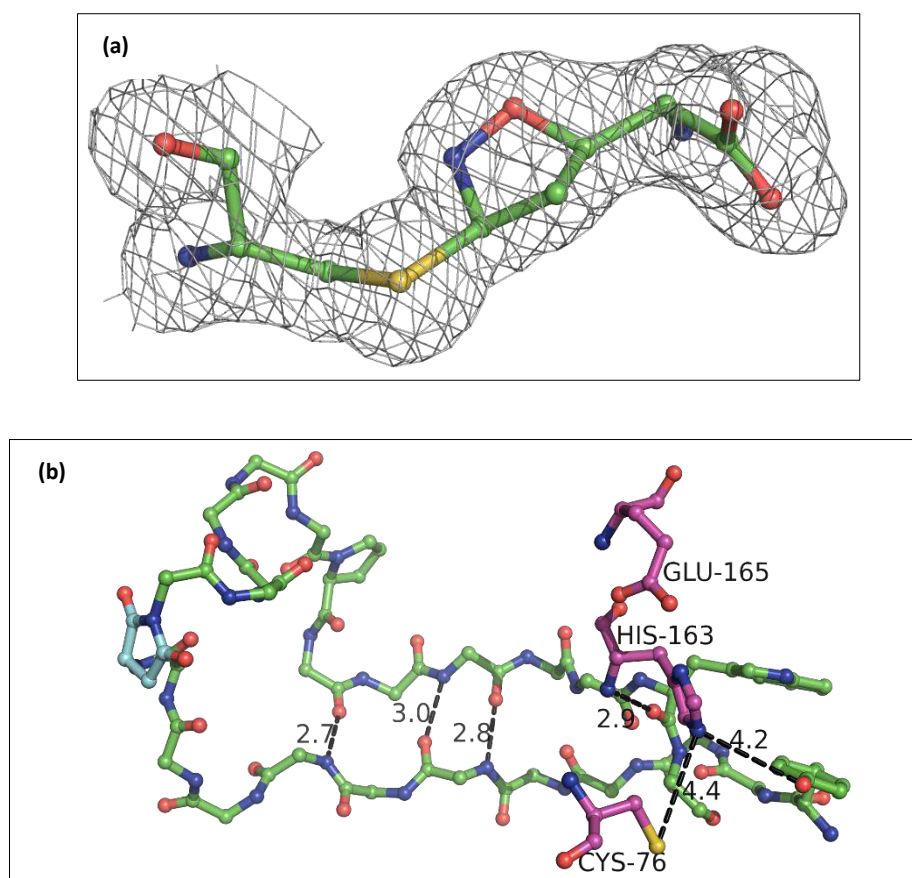


Figure 5.6: Missed electron density of succinimidyl residues in proteins. (a) Electron density map of residues 111-113 of *P. horikoshii* GATase with a succinimidyl residue modelled at position 112. (b) In the structure of the same protein solved previously the green blob of electron density is seen that could accommodate a succinimidyl residue but instead an Ala

residue was modelled. Figures were generated using Crystallographic Object-Oriented Toolkit (Coot). (c) Electron density map of the region of amyloamylase, residues 369-371, from *T. aquaticus* with a succinimidyl residue at position 370. The neighboring residue is a negative charged residue with a orientation similar to Asp110 of MjGATase. (d) Electron density map of similar region from *T. thermophilus* amyloamylase. A green blob of electron density is seen wherein a succinimidyl residue could be modelled. Panel (c) and (d) reproduced from Barends TR, Bultema JB, Kaper T, van der Maarel MJ, Dijkhuizen L, Dijkstra BW. Three-way stabilization of the covalent intermediate in amyloamylase, an alpha-amylase-like transglycosylase. *J Biol Chem*. 2007 Jun 8;282(23):17242-9 under Creative Common Licences.

Structure of ligand bound MjGATase was also solved to examine if any major conformational changes would be observed upon ligand binding and would they be cascaded to the SNN containing region of the protein. The crystal of apo protein, post diffraction was unmounted and soaked in a solution of acivicin for 8 hours and diffracted again. Acivicin is a glutamine analogue that binds GMP synthetase irreversibly by forming a covalent bond with the catalytic cysteine (Chittur et al., 2001) (Cys76 in case of MjGATase). A clear density for acivicin could be seen at a resolution of 1.67 Å (Fig. 5.7 a). The coordinates of acivicin (5CS) were obtained from SMILES library and after ligand addition, the structure was subjected to multiple rounds of refinement. Binding of acivicin to the catalytic cysteine did not bring about any major conformational change in MjGATase as seen in Fig. 5.7 b-c. Active site residues of MjGATase are located close to the end of the β hairpin harbouring the succinimidyl residue (Fig. 5.7 b-c).



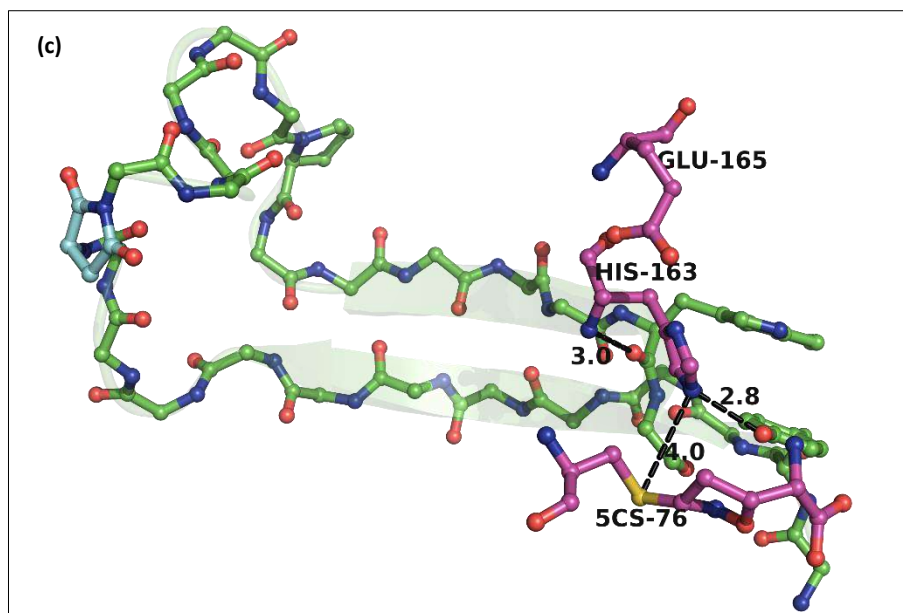


Figure 5.7: Structural analysis of acivicin bound MjGATase. (a) Electron density for Cys 76 covalently modified by acivicin (5-CS) contoured to 1σ . (b) A segment of MjGATase apo and (c) ligand bound structure. No significant conformational changes were observed in the vicinity of the active site. Shown in the images (b-c) is a ball and stick representation of β -hairpin harbouring succinimidyl residue and its association with the active site residues. Active site residues are coloured in magenta, succinimidyl residue is coloured in cyan and β -hairpin residues are coloured in green, all represented as ball and stick model. Numbers above dotted lines are distances in Å.

Among all the GATase structures available in PDB database, only a few entries correspond to a ligand bound GATase. These are listed in Table 5.2.

Table 5.2: List of PDB entries with ligand bound GATase subunits

PDB ID	Name of protein	Ligand
1OX5	<i>Saccharomyces cerevisiae</i> Imidazole Glycerophosphate Synthase	Acivicin (5CS)
2W7T	<i>Trypanosoma brucei</i> CTP Synthetase	Acivicin (5CS)
4WIN	<i>Plasmodium falciparum</i> C89A GMP synthetase	Glutamine (GLN)

Superimposition of the structure of acivicin bound MjGATase and *T. brucei* CTP Synthetase showed that in both cases the ligand was bound in similar orientation within the active site cavity (Fig. 5.8 a). Superimposition of the structures *P. falciparum* C89A GMP synthetase mutant and MjGATase shows that the two ligands, glutamine and acivicin, respectively, occupy different regions of the pocket (Fig. 5.8 b). However, the C_{δ} carbon of ligand glutamine is at a 3 Å distance from sulphur atom of Cys76 of MjGATase. This indicates that the amide is positioned close to the catalytic Cys for hydrolysis while the remaining atoms of the two ligands occupy different spaces. Interestingly, all the catalytically important residues superpose well (5.8 b). The residues surrounding the ligand (within 4 Å distance cut-off) are fairly conserved in both *M. jannaschii* and *P. falciparum* (listed in table 5.3).

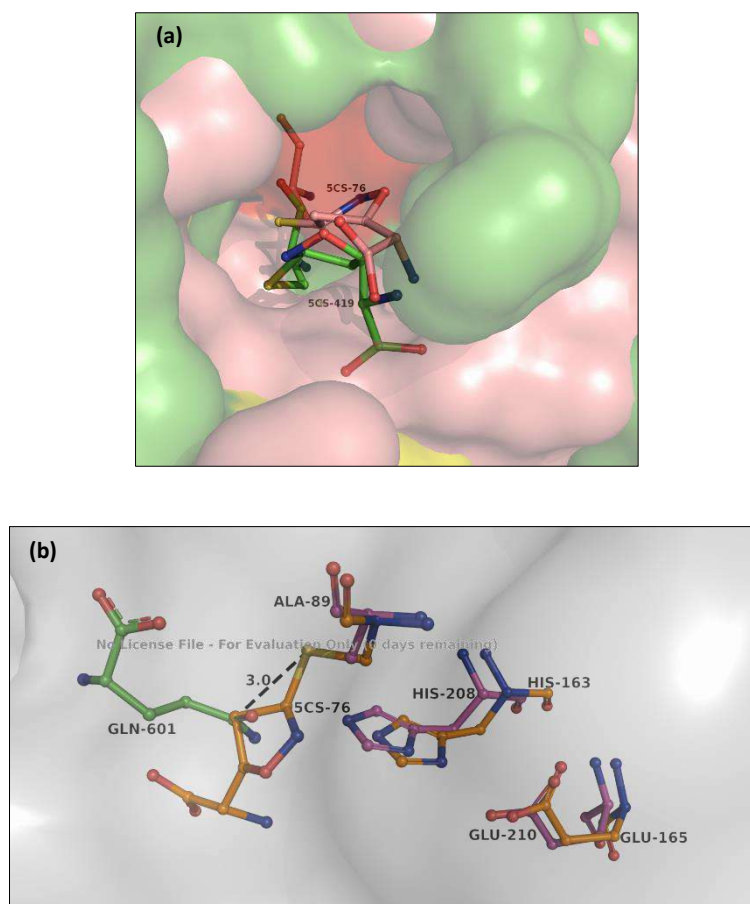


Figure 5.8: Comparison of ligand bound structures of GATases. (a) Superimposition of MjGATase (Mauve coloured surface) on TbGATase (Green surface) shows similar orientation of acivicin ligands. Acivicin is covalently bonded to catalytic cysteine in both the cases. MjGATase acivicin is represented as mauve coloured ball and stick model while TbGATase is represented as green ball and stick model. (b) Superposition of acivicin (5CS) bound MjGATase on glutamine (GLN 601) bound PfGATase (C89A mutant). The catalytic residues of MjGATase, His163, Glu165 and acivicin bound Cys76 are represented as ball and stick model and coloured in orange. PfGATase catalytic residues, His208, Glu210 and Ala89 (Mutant C89A) are also represented as ball and stick model and coloured in pink. The ligand glutamine is coloured in green. Numbers above dotted lines are distances in Å.

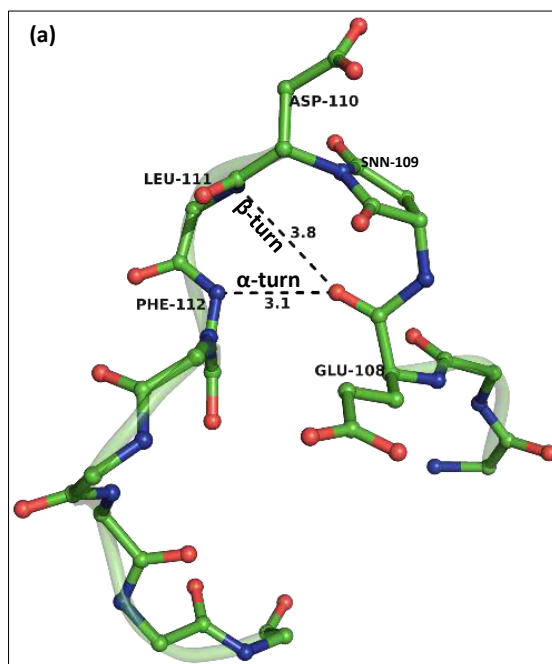
Table 5.3: Contacts made by acivicin in MjGATase and glutamine in PfGATase (C89A)

Acivicin interacting residues in MjGATase	Glutamine interacting residues in PfGATase
Q10	Y60
G52	G58
G51	G57
L77	Y90
Q80	Q93
C76	A89 (C89)
G78	D172
Y98	H170
Q161	N169
H163	H208
H79	

*Conserved residues from MjGATase and PfGATase are highlighted in bold.

5.2.2. Structural Implication of a stable succinimidyl residue in MjGATase

As mentioned in section 4.6, peptides containing succinimidyl / aminosuccinyl residues adopt type II' β -turn conformation (Capasso et. al., 1995). In case of MjGATase the loop segment harbouring succinimidyl residue is 12 amino acid long and shows presence a type II' β -turn formed by residues E108 (*i*) and L111 (*i*+3) (Fig. 5.9 a). The values of main chain torsion angle for Glu108 are $\Phi = -56.3^\circ$ and $\Psi = -38.7^\circ$ which fall within allowed region of Ramachandran plot and the SNN109-Asp110 moiety assumes a type II' β -turn conformation with SNN109 and Asp110 at second and third positions, respectively, of the turn. With a bond distance of 3.8 Å, the hydrogen bond formed between CO of Glu108 and NH of L111 is a weak hydrogen bond. The length of the hydrogen bond is influenced by the by the value of $\Psi_{2(\text{SNN109})}$ which in this case is restrained close to -120° ($\Psi = -128.8$) due to cyclic succinimidyl residue. This conformational preference also suggests that type II' β -turn might be playing a role in deamidation process in proteins (Capasso et al. 2004).



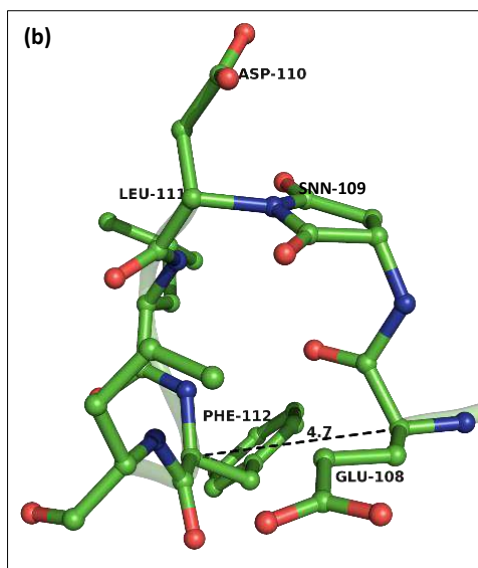


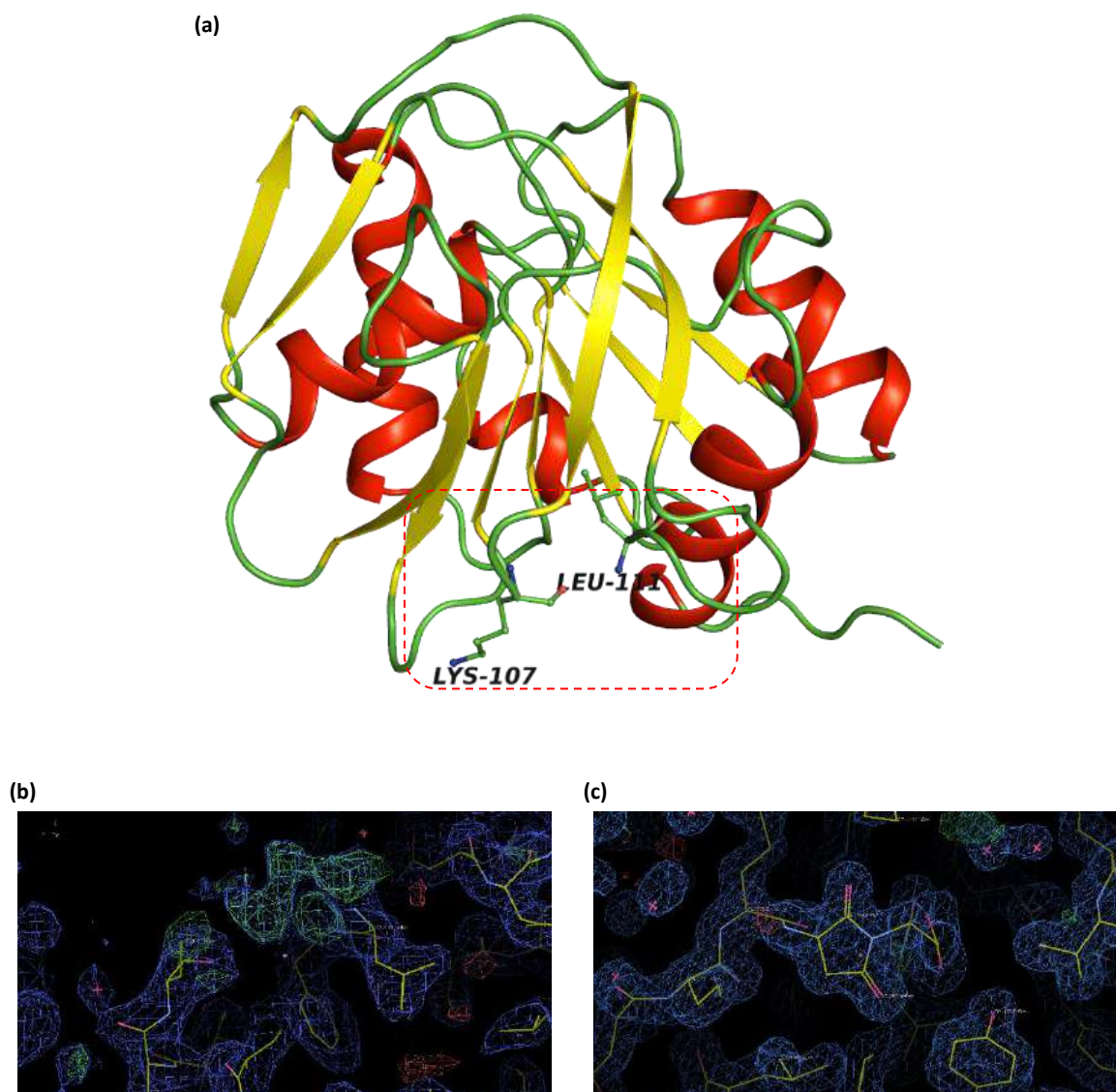
Figure 5.9: The tight-turn conformations assumed by residues in the SNN harbouring loop in MjGATase. (a) The backbone carbonyl oxygen of E108 can hydrogen bond with backbone nitrogen of L111 (β -turn) and backbone nitrogen of F112 (α -turn). (b) The distance between C_{α} of E108 and C_{α} of F112 is shown. Bond Numbers above dotted lines are distances in Å.

Besides the type II' β -turn hydrogen bond, a hydrogen bond is also observed between CO of Glu108 (*i*) and NH of Phe112 (*i*+4) constituting an α -turn secondary structural element (Fig. 5.9 a). This bonding is also involved in reversal of polypeptide direction analogous to the β -turn. As compared to β -turns and γ -turns, α -turns are less studied. Analysis of large number of protein structures by *C. Ramakrishnan* and colleagues shows that α -turns can have different characteristic main chain conformational angles and amino acid preferences (Chou, 1997; Natraj et al., 1995). The distance between C_{α} of Glu108 and C_{α} of Phe112 is 4.7 Å which is within the observed range of end-to-end C_{α} distances in case of these turns (4.7-6.7 Å) (Fig. 5.9 b). This hydrogen bond network seems to stabilize the local polypeptide segment, in turn, contributing to overall protein folding and stability. The loop region (containing succinimidyl residue) assuming these tight turn conformations might not strictly follow the dihedral angle criteria satisfied by most polypeptide segments assuming these structures since the dihedral angles of SNN residue are unusual and restrained ($\Phi = 42.6^{\circ}$ and $\Psi = -128.8^{\circ}$) which can influence the dihedral angles of preceding and succeeding residues. Apart from the hydrogen bonds leading to formation of tight turns, several other interactions seem to be involved in the stabilization of SNN and therefore the protein. These are discussed in section 5.2.4.

5.2.3. Structure of MjGATase_D110G mutant

The importance of the succeeding residue for stabilization of succinimide in MjGATase was examined previously through thermal and chemical denaturation and activity measurements on a mutant in which Asp110 was mutated to Gly by site-directed mutagenesis (Kumar et al., 2016). The mutant D110G was found to be stable and active up to 85 °C; increase in temperature beyond 85 °C resulted

in precipitation of the enzyme and concomitant loss of activity. The crystals of MjGATase_D110G were obtained under conditions described in Materials and Methods (Section 5.1). The crystal has two molecules of protein in the asymmetric unit. The overall structure is shown in Figure 5.10 a. The electron density for residues 108-110 was fragmented (Fig. 5.10 b) thereby thwarting attempts to place any residue in this region. The absence of electron density is an evidence for enhanced flexibility in the absence of the succinimide constraint that could be a result of the local disorder caused by disruption of contacts made by D110 in WT. On the other hand, two different populations of proteins i.e. one with SNN and another with its hydrolysed product Asp/isoAsp could be coexisting in the crystal. We further analysed a different crystal from the same condition by mass spectrometry and it revealed that the major protein population in that crystal was of the protein wherein the succinimidyl residue was intact (Fig. 5.10 d).



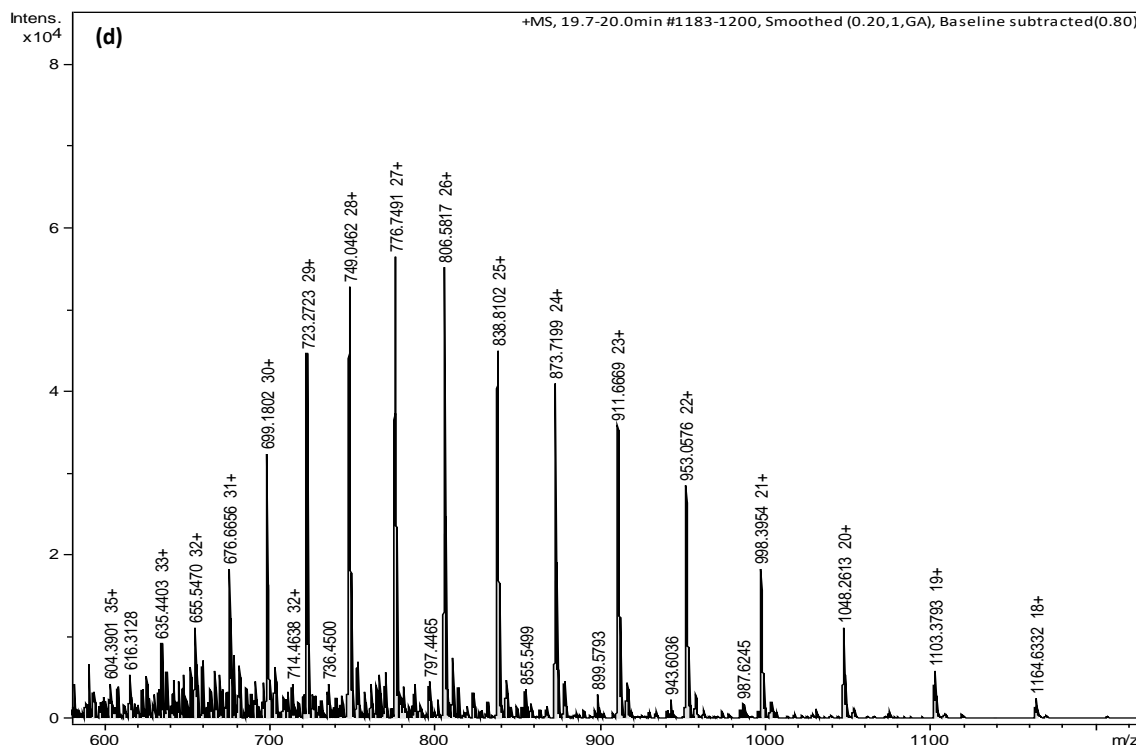


Figure 5.10: Structural analysis of MjGATase_D110G mutant. (a) Overall structure of D110G mutant of MjGATase is represented as a ribbon diagram. The position of missing residue 108-110 is highlighted in red dotted box. (b) Fragmented electron density in the region 108-110 of MjGATase_D110G is evident in the figure. Electron densities for residues K107 and L111 are complete (residues represented as ball and stick inside corresponding electron densities). (c) Electron density of the wild type protein structure showing clear density in the corresponding 108-110 region. Electron densities for both structures are represented as 1σ contour. (d) ESI-MS spectrum of MjGATase_D110G crystal (Deconvoluted using mass spectrometry software from Bruker). Majorly observed mass is 20,945 Da that corresponds to a protein with a succinimide residue.

Superimposition of MjGATase_WT structure onto MjGATase_D110G structure does not indicate drastic shifts in the positions of any residues with the associated root mean square deviation of 0.339 Å (Fig. 5.11 a). Very small shifts are observed in K107, Y158 and L111. The active site residues and the residues connecting E(SNN)D region to active site such as Val160 and Gln161 superimpose well with the WT. This suggests that a SNN harbouring loop region provides 'extra' stability to an already thermostable enzyme. The floppiness instigated in this region by a point mutation of Asp to Gly causes only a local disorder and not a global one. The electron density for the rest of the protein backbone was of good quality. However, the localized flexibility is translocated into the mutant protein upon heating, leading to loss of stability if heated beyond 85 °C. This also re-affirms the role of the succeeding residue in stabilization of the succinimide ring as shown previously (Kumar et al., 2016).

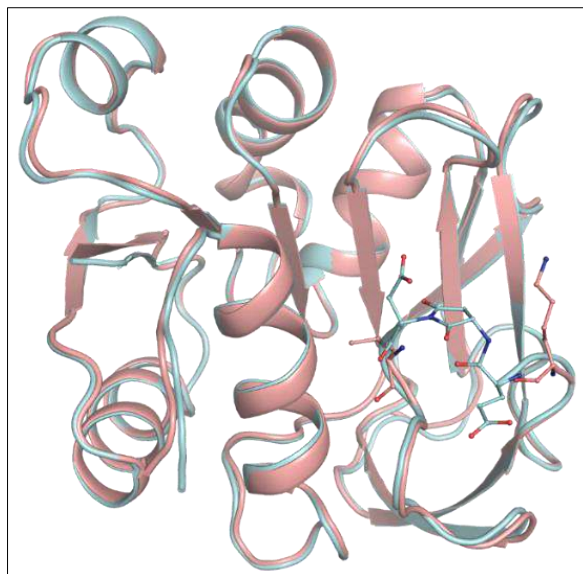


Figure 5.11: Superimposition of MjGATase_D110G mutant structure over MjGATase_WT structure. Overall structure superimposition yields a rms deviation of 0.339 Å. WT enzyme is represented in cyan while mutant structure is represented in mauve colour.

5.2.4. Interactions stabilizing succinimidyl residue in MjGATase

The stability of succinimidyl intermediate seems to be governed by more than one factor. The negatively charged succeeding residue plays a key role in shielding the SNN ring from approach of water thereby preventing hydrolysis of the intermediate. The preceding residue seems to shield the other side from water approach, again by formation of a set of hydrogen bonds and $n \rightarrow \pi^*$ interactions. The interactions of succinimidyl residue - which is present on a solvent exposed loop region - with the residues from the core of the protein lead to stabilization of different segments of the protein. Each of these factors are discussed below in detail.

5.2.4.1. The succeeding residue, Asp 110

As reported previously, studies on MjGATase_D110G have shown that the succeeding residue influences the stability of SNN in a pH dependent manner. In this mutant, succinimide is formed but is rapidly hydrolysed to Asp/ β -Asp above pH 5.0 (Kumar et al., 2016). Asp 110 is oriented over the SNN ring plane in manner that forms a negatively charged cloud over SNN, (Fig. 5.5) which impedes the approach of water molecule towards SNN, preventing its hydrolysis. The orientation that the Asp side chain adopts is held in place by interactions with Tyr158, Val182, Lys151 and SNN109 itself (Fig. 5.12 a). The $O_{\delta 2}$ of Asp110 forms a close contact with OH of Tyr158 (2.7 Å). C_{β} atom of Asp110 makes a van der Waals interaction with C_{γ} of Val182 (4.2 Å) while the oxygen atoms of the carboxylate side chain of Asp110 form hydrogen bonds with its backbone amide group, which is a part of SNN as a result of cyclization.

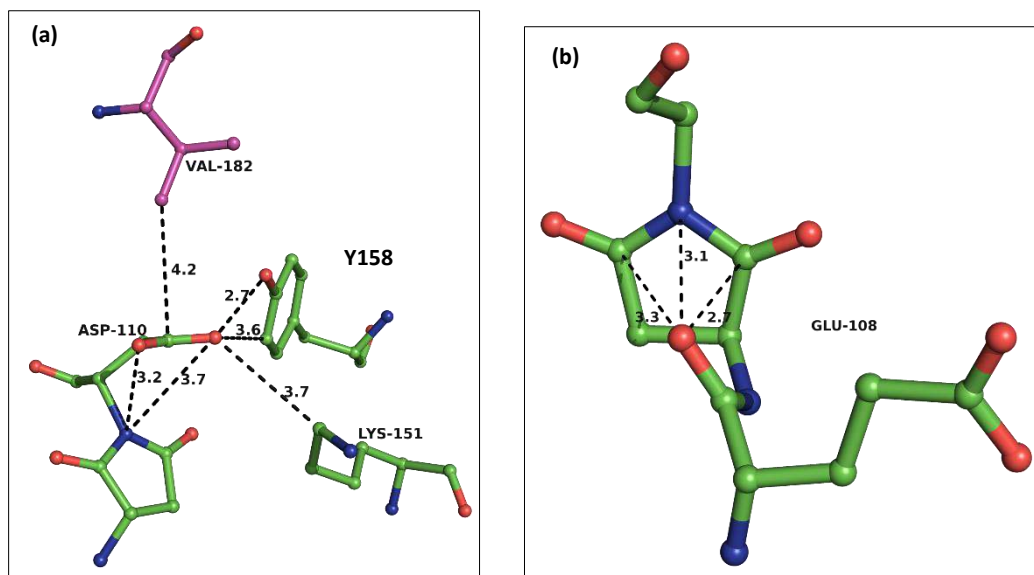


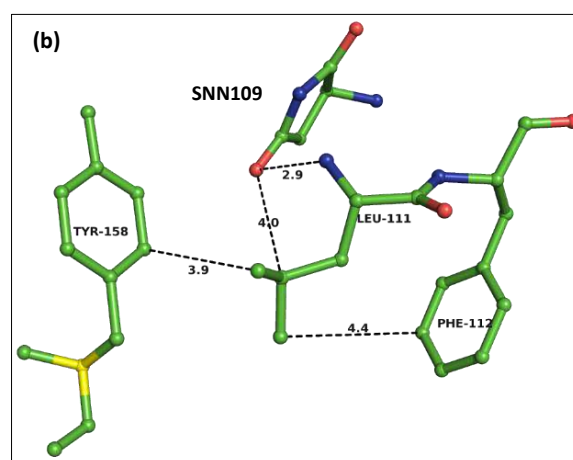
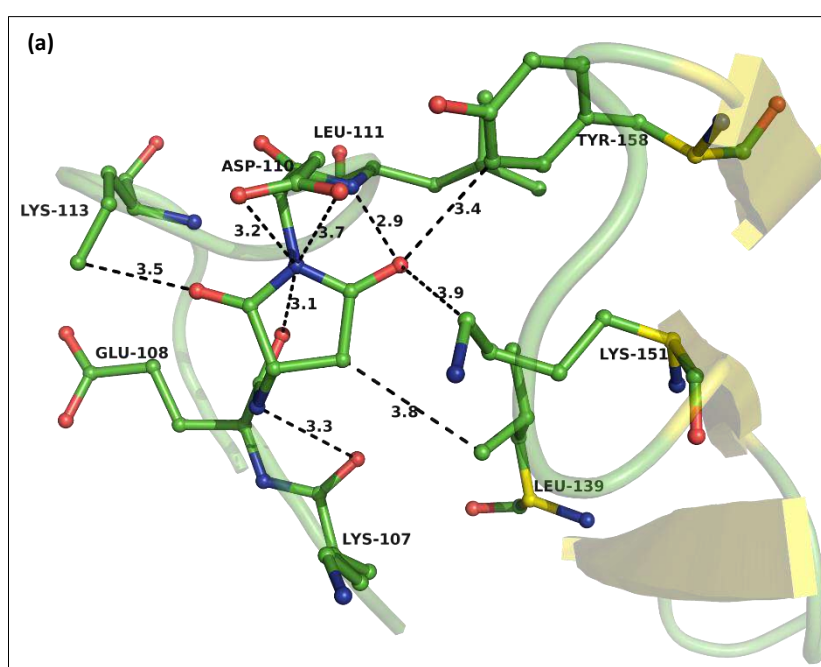
Figure 5.12: Interactions stabilizing succinimidyl residue in MjGATase. (a) Asp 110 which forms a negatively charged cloud over the SNN ring plane is held in place by its interactions with Y158, K151, V182 and SNN109 itself. (b) Glu 108 CO forms a hydrogen bond with NH of SNN109 and $n \rightarrow \pi^*$ interactions with C and C_γ atoms of succinimidyl residue. These contacts protect the succinimidyl residue from approach of water from its rear-end. All the distances between atoms are represented as black dashed lines. Numbers alongside the lines are distances in Å. Amino acid residues are represented in ball and stick models. Numbers above dotted lines are distances in Å.

5.2.4.2. Orientation of the preceding residue, Glu 108

The backbone carbonyl oxygen of Glu108 is within bonding distance of the nitrogen of SNN109. This oxygen can also participate in $n \rightarrow \pi^*$ interaction with the two carbonyl carbons of SNN109 (Fig. 5.12 b). In an $n \rightarrow \pi^*$ interaction, a nucleophile (oxygen from one carbonyl group) donates a lone pair (n) electron density into empty π^* orbital of nearby carbonyl group (carbon of another carbonyl group). The resulting mixing of these orbitals releases energy which is the basis for this interaction. The energy associated with an $n \rightarrow \pi^*$ interaction involving amide bonds has been estimated to be 0.27 kcal/mol (Newberry et al., 2013), however, the abundance of amide bonds in a protein molecule hints at prodigious contributions of these interactions to protein stabilization. Recently, these interactions have also been implicated in substrate assisted catalysis in aspartic proteases, wherein the substrate adopts a conformation leading to formation of an $n \rightarrow \pi^*$ interaction with the enzyme main chain and this aids in catalysis (Windsor et. al., 2019). Extensive studies on $n \rightarrow \pi^*$ interactions have been pursued by Ronald T. Raines' group who believe that the contributions of these interactions in protein chemistry have not fully been understood (Bartlett et al., 2013; Newberry et al., 2013, 2014; Newberry and Raines, 2017; Windsor et. al., 2019). The preceding Glu residue is conserved in a group of archaeal GATases as seen from the sequence alignment of 100 GATase sequences all belonging to either Thermococci or Methanococci (Fig. 5.15 a). Among the tripeptide E(N/D)(D/E), E is conserved in 94% sequences (Fig. 5.15 b). This suggests that this residue might have a role to play in the process of deamidation/dehydration of Asn/Asp, respectively. MjGATase mutant where Glu is mutated to Ala would throw light on whether this residue is possibly involved either in the process of cyclization of Asn or stabilization of cyclized intermediate succinimide.

5.2.4.3. Interactions of succinimidyl residue with residues from protein core

As mentioned earlier, succinimidyl residue is present on a solvent exposed loop of MjGATase and makes H bonds and van der Waals contacts with 3 residues from core β -sheets; Leu139 (β 9), Lys151 (β 10) and Tyr158 (β 11) (Fig. 5.13 a). The residues close to SNN (within 4 Å distance) are Lys107, Glu108, Leu111, Lys113 and the above-mentioned residues from the core of the protein. These interactions are possibly involved in stabilization of the core through SNN i.e., surface loop driven core stabilization. Leu111 which is the part of SNN containing loop is positioned in such a way that it holds Tyr158 and Phe112 via van der Waals interaction (Fig. 5.13 b). Tyr158 in turn is connected to SNN109 and Phe112 is connected to Glu108. Hence, L111 which is sandwiched between Tyr158 and Phe112 seems to be holding the whole assembly in place. These residues are conserved among GATases from many archaeal organisms (Fig. 5.13 c)



	107	108	109	110	111	113	139	151	158
(c) Methanocaldococcus_jannaschii	K	E	N	D	L	K	I	K	Y
Pyrococcus_horikoshii	D	E	D	E	I	K	I	K	Y
Methanobacterium	E	E	N	D	I	K	I	K	Y
Thermococcus_celericrescens	E	E	N	G	I	R	I	K	Y
Methanotorris_igneus	E	E	N	D	L	K	I	K	Y
Palaeococcus_ferrophilus	D	E	N	E	V	K	I	K	Y
Archaeoglobus_veneficus	E	E	D	E	I	E	I	R	Y
Ferroglobus_placidus	D	K	D	E	L	E	L	R	F
Methanothermobacter_wolfeii	D	E	D	D	I	R	I	K	Y
Methanocaldococcus_villosus	D	E	D	D	I	K	I	K	Y

Figure 5.13: Contacts of SNN: (a) Residues Lys107, Lys113, Tyr158, Glu108, Asp110, Leu111, Leu139 and Lys151 are positioned within 4 Å from SNN109. Of these, Tyr158, Leu139 and Lys151 are a part of core β -sheets of the protein. These residues are shown as ball and stick model while the protein backbone is shown as transparent ribbon diagram. (b) L111 is sandwiched between F112 and Y158 making it a key SNN interacting residue. Dashed lines represent the distances between atoms in Å units. (c) Sequence conservation of SNN interacting residues in archaeal GATases. Numbers above dotted lines are distances in Å.

5.2.4.4. Connection of the succinimidyl residue with the active site

The activity of an enzyme is a function of its structure. Only an enzyme in its correctly folded state is capable of catalytic activity. Conditions such as high temperature, higher salt concentration or presence of a chaotrope result in partial or complete unfolding of protein and precipitation/aggregation, thereby resulting in the loss of catalytic activity. MjGATase enzyme, in the absence of SNN is soluble, retains its tertiary structure and is active up to 85 °C but increase in temperature from 85 to 100 °C causes the protein to precipitate out of solution owing to which its activity can-not be measured and is inactive (Kumar et al., 2016). Intact enzyme activity at 100 °C indicates that, the succinimidyl residue which we have shown to be responsible for structural stability, could possibly be involved in stabilization of the active site. Succinimidyl residue interacts with active site via tertiary interactions as seen from crystal structure (Fig. 5.14). L111 is the key residue mediating this interaction as it makes van der Waals contact with V160 which in turn is connected to Cys76 (acivicin modified Cys76 {5CS-76} in ligand bound MjGATase) thorough a strong hydrogen bond (2.8 Å).

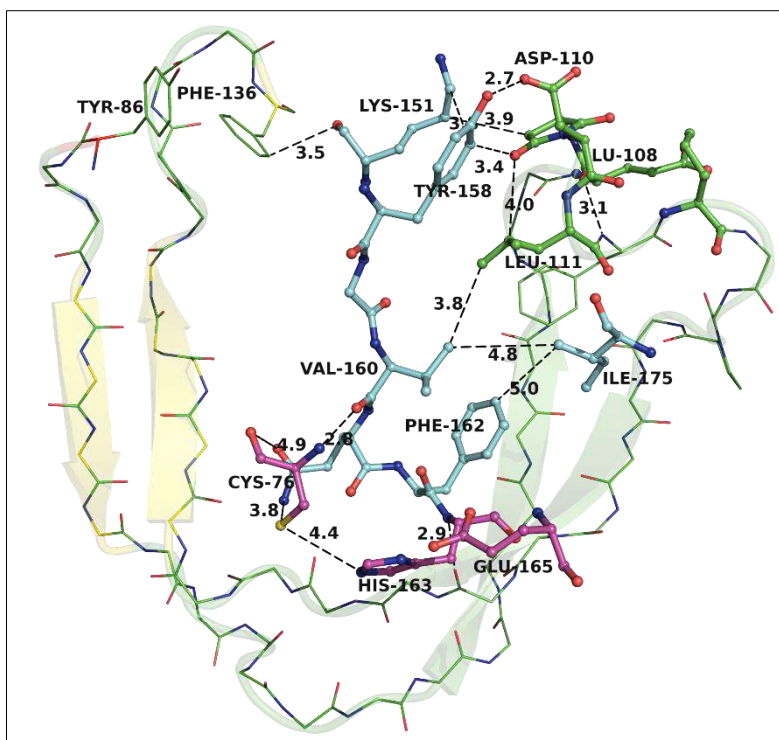


Figure 5.14: Contacts made by succinimidyl residue with the active site residues. Although succinimidyl residue does not directly contact active site residues, the tertiary interactions with the active site are evident. The contacts relay from succinimidyl residue via Leu 111 and Val 160 to the catalytic Cys 76. Moreover, Phe112 connects with Phe162 which further connects with Cys 76. An extended β -hairpin starting from residue Tyr 86 to Phe 136 is shown in the figure. The ends of β -hairpin are in connection with succinimidyl residue via Tyr 158 and Lys 151. Residues mediating its contacts with the active site are represented as ball and stick model and coloured in cyan. Active site residues are represented by magenta coloured ball and stick model. Residues in the extended β -hairpin harbouring SNN109 are coloured in green and are represented as lines. Distances between atoms are shown as dashed black lines with the respective values mentioned next to the dashed lines. Numbers above dotted lines are distances in Å.

5.2.5. Stable succinimide formation as an adaptive mechanism of protein thermostability in hyperthermophiles

Besides *M. jannaschii* and *P. horikoshii* GATases, there are very few examples where a stable succinimide is observed in proteins. RCSB PDB harbours 54 {37 SNN (1-3-aminosuccinimide) and 17 SUI(3-amino-2,5-dioxo-1-pyrrolidinyl) acetic acid)} entries of proteins/peptides with succinimidyl residue mapped in their structure. Out of total 54 structures, one structure belongs to thermostable protein from a mesophile (PDB ID: 4CUO) and the remaining five belong to proteins from hyperthermophiles (PDB ID: 2OWC, 2OWW, 2OWX, 5JIW, 1WL8). In all of these six protein structures, the succinimidyl residue is followed by a negatively charged residue similar to that in MjGATase. The succinimidyl residue in amyloamylase from *T. thermophilus* has been implicated in substrate binding, while a structure stabilizing role has been proposed for the homologue from *T. aquaticus*. For the remaining 4 thermostable proteins with a stable succinimidyl residue, no role is yet assigned for the residue. In the remaining 45 entries, apart from involvement in self-splicing in inteins, the role of the succinimidyl residue is yet to be understood. As mentioned earlier, the homologue from *P. horikoshii* in its crystal structure also shows the presence of a succinimidyl residue that is formed by dehydration of D112, with

the residue E113 shielding it. PSI-BLAST output obtained using MjGATase sequence as query showed that the tripeptide sequence E(N/D)(D/E) is almost completely conserved (Fig. 5.15 a). PSI-BLAST allows the user to build a PSSM (position-specific scoring matrix) using the results of the first BlastP run (Altschul et al., 1997). The search was limited to database of non-redundant protein sequences of archaea. Uncultured/environmental sample sequences were excluded for ease of analysis. Number of hits parameter was set to 250. BLOSUM62 substitution matrix was chosen by default by NCBI. After 3 rounds of iteration with top 100 hits, the sequences were aligned and curated to remove redundant entries and we were left with 84 sequences which were used for further analysis. The 84 non-redundant protein sequences belonged to organisms of domain Archaea, phylum Euryarchaeota. The class of organisms was either Thermococci or Methanococci and the sequence of the tripeptide is either END, EDD or ENE (Fig. 5.15 a). Using WebLogo 3.0, a web-based application designed for the generation of sequence logos, the SNN harbouring loop was analysed (Fig. 5.15 b). It was observed that the preceding residue Glu is conserved in 94 % of the sequences indicating that this residue is either essential for formation or stability of the succinimidyl residue. In case of MjGATase, the preceding residue is engaged in multiple bond formation with the succinimidyl residue thereby shielding it from the rear end from approach of water molecules. Asn and Asp are both capable of forming succinimidyl intermediate during deamidation and dehydration respectively, and hence conservation of these amino acids across archaeal GATase protein sequences suggests that stabilization of succinimidyl residue formed as an intermediate of an otherwise detrimental process might be an evolutionarily selected mechanism. As the stabilization of the succinimidyl intermediate is also mediated by the succeeding negatively charged residue, conservation of a negatively charged residue (D/E) at this position is anticipated. **Our findings suggest a novel mechanism of thermostability and it might be more widespread than currently perceived.**

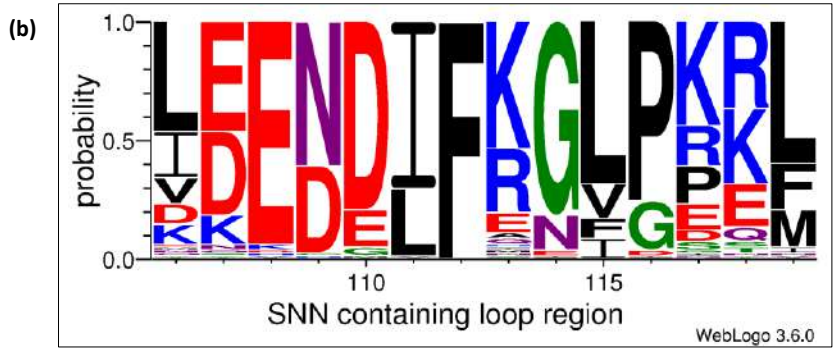
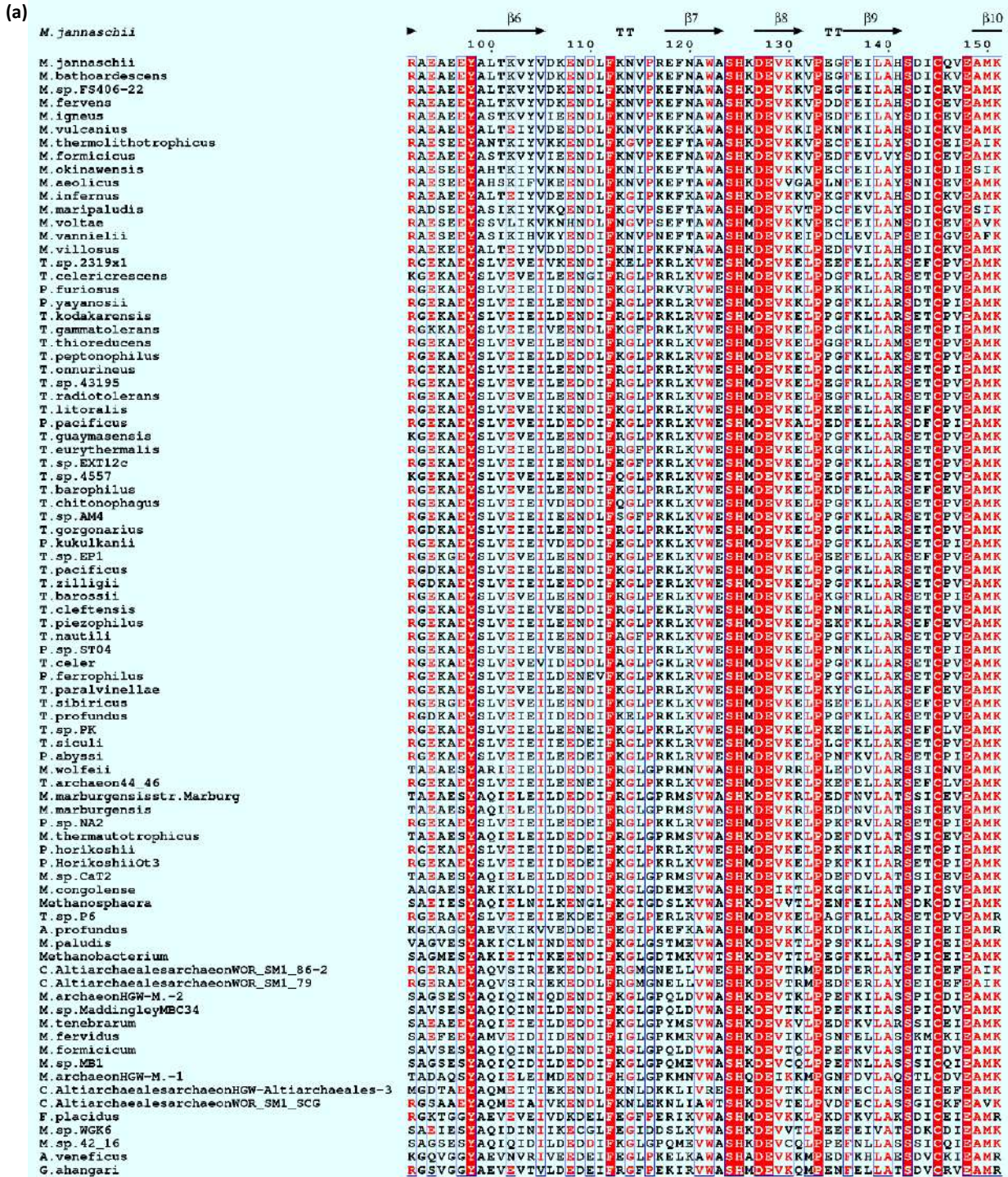


Figure 5.15: Sequence alignment of Archaeal GATases. (a) Protein BLAST (NCBI-BLAST) performed using MjGATase protein sequence as query yielded 100 hits, all belonging to GATase subunit of GMP synthetase belonging to organisms from the domain Archaea. Data curation provided 84 hits. (b) The preceding Glu is the most conserved residue among the tripeptide END with 94% conservation. Image was generated using WebLogo 3.

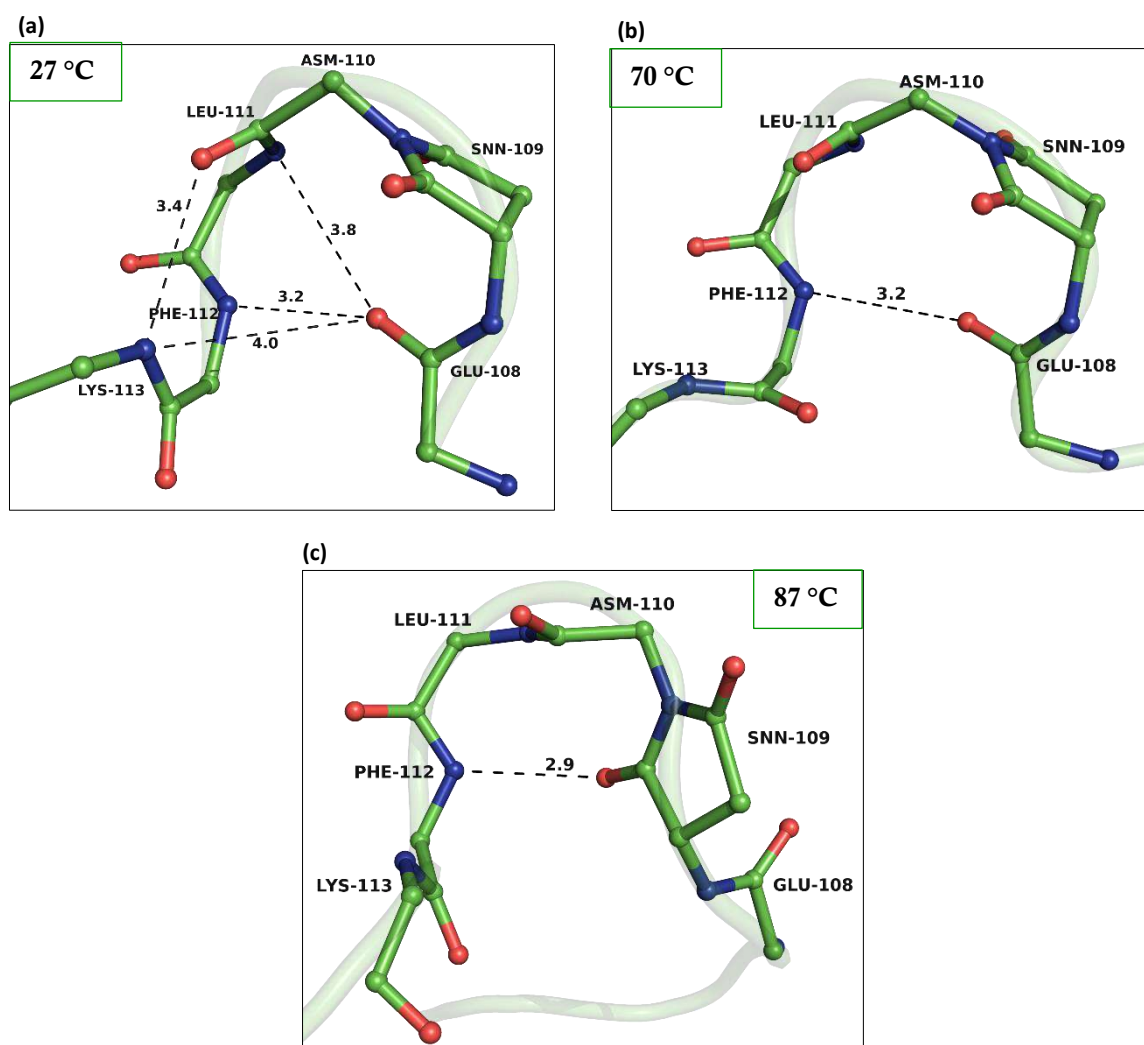
5.2.6. Molecular Dynamic Simulation

Crystal structure depicts the molecular arrangements within proteins only at a fixed spatial and temporal resolution. However, in solution, proteins are in constant motion i.e. dynamic state. The intramolecular interactions and thereby the protein function depend on this dynamic state which varies with changes in the surrounding environmental factors such as temperature of the solution, ionic strength of the solvent etc. For instance, crystal structure of a hyperthermophilic protein obtained at below 0 °C may not truly reflect its structure at 80 °C - the optimum growth temperature of hyperthermophiles. To understand how thermostable proteins withstand such high temperatures, what kind of intramolecular interactions aid in preventing the proteins from unfolding, the temperature of the system needs to be increased and dynamics of the protein needs to be visualized at elevated temperatures. However, doing this experimentally can be difficult; an attractive alternative is the use of computer simulations. Molecular dynamic simulations (MDS) predict how every atom in a protein or any other molecular system will move over time in response to different environmental cues (Hollingsworth and Dror, 2018).

In case of MjGATase mutant N109S that lacks a succinimidyl residue, the enzyme becomes inactive at a much lower temperature compared to WT (Kumar et al., 2016). We were interested in trying to understand how the structural dynamics between the two proteins changes as a function of temperature for which, we resorted to molecular dynamic simulations. *All simulations were performed by Dr. Sudip Das, from Prof. Balasubramanian Sundaram's laboratory, Chemistry and Physics of Materials Unit, JNCASR.* Often times, simulations with complex macro molecules such as proteins are faced with a challenge of inadequate sampling during regular MDS. To circumvent this problem, improved methods such as replica exchange with solute scaling (REST2) and Well-tempered metadynamics (WT-MTD) were used. The results of the simulations are briefly discussed below.

Since good quality diffraction data could not be collected from MjGATase_N109S crystals, the structure of this mutant was generated by replacing SNN109 with S109 (using PyMol) and the resulting structure was energy minimized. This was used as a starting structure for MDS. As seen from the crystal structure, due to the presence of a succinimidyl residue in the loop region, a network of hydrogen bonds is formed resulting in an α -turn and a β -turn secondary structural elements. Within MD simulation time scales, MjGATase_WT and MjGATase_SNN109S did not show any difference in stability due to inadequate sampling of conformations. Therefore, to enhance conformational sampling, replica exchange with solute (enzyme) scaling (REST2) (Wang et. al., 2011) simulation was performed. Few replicas from REST2 simulations were chosen (belonging to effective temperatures of 27, 70 and 87 °C) and were subjected to regular MD simulation for 300 ns at temperatures, 27 °C, 70 °C and 87 °C,

respectively. In case of WT protein, the network of hydrogen bonds existing in the crystal structure weakened as a function of temperature (Fig. 5.16 a-c). In case of MjGATase_N109S, to begin with, replacement of SNN109 with S109 seems to have broken a few interactions existing in the WT protein. As the effective temperature increased, these fewer interactions weakened (5.16 d-e) and were eventually completely lost (5.16 f). This could explain the lower stability of the N109S mutant at higher temperature. The tight turn induced in the loop region by the cyclic succinimidyl residue leads to formation of a network of hydrogen bonds, that weakens but is not completely abolished at higher temperatures. Further, the cyclic succinimidyl residue constraints loop flexibility, even at the highest temperature examined through MDS. When this conformational constraint of cyclic residue is removed, the loop region can no longer adopt the tight turn conformations, subsequently abolishing the hydrogen bond network.



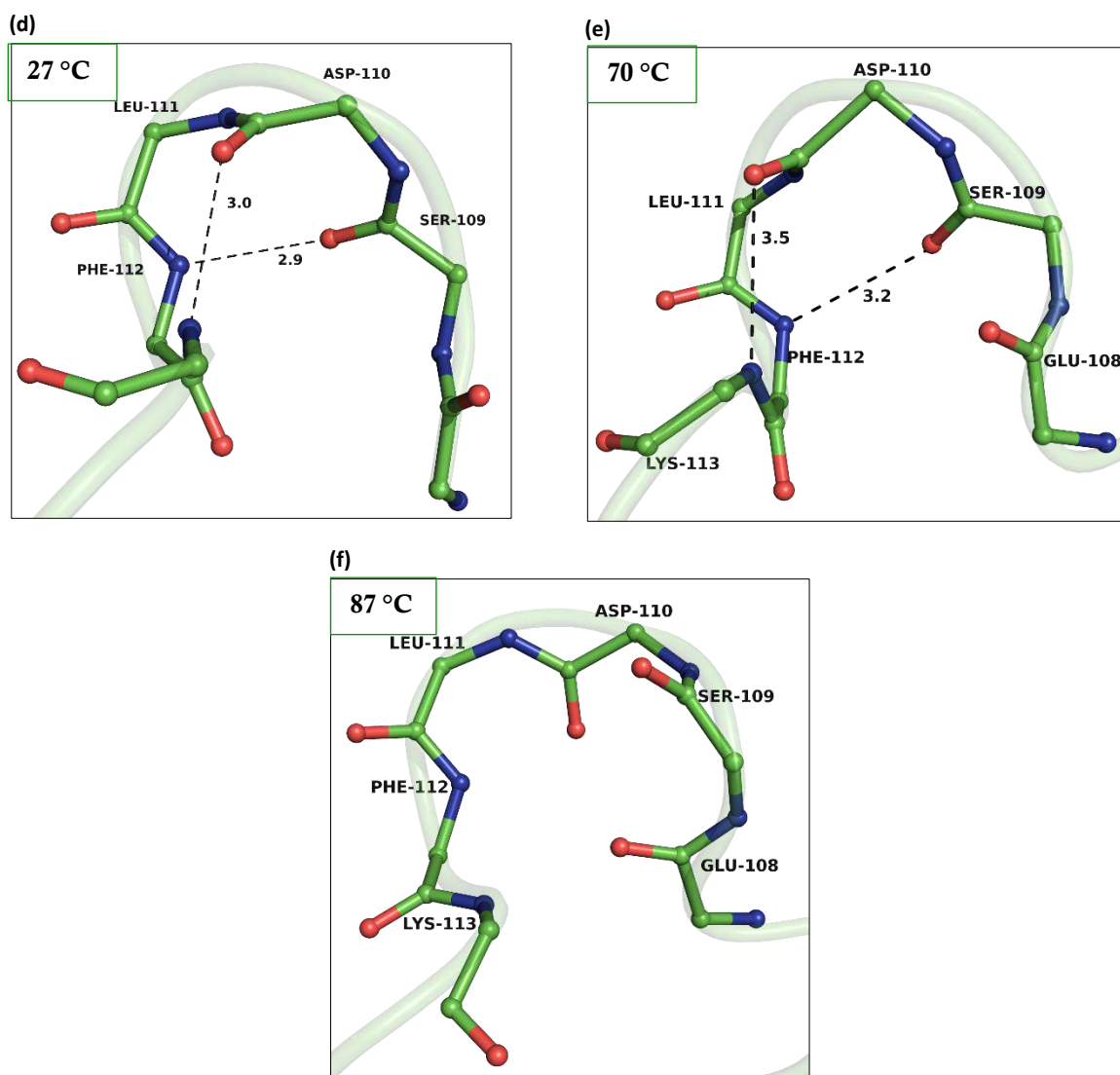


Figure 5.16: Contributions of hydrogen bond networks in maintaining structural stability at elevated temperatures. Network of hydrogen bonds existing in MjGATase_WT at (a) 27 °C, (b) 70 °C and (c) 87 °C. In MjGATase_N109S at (d) 27 °C, only two hydrogen bonds exist which are weakened at (e) 70 °C and no hydrogen bonds were found to exist in simulation at (f) 87 °C. All hydrogen bonds are represented as black dashed lined with the corresponding bond lengths noted on top/bottom of the line. For each temperature simulation, the most frequently represented structure was chosen and the corresponding co-ordinate file was used to generate figures in PyMol. Only the peptide backbone atoms are shown as ball and stick model for the sake of clarity and coloured according to atom type (carbon, green; oxygen, red; nitrogen, blue; colour scheme maintained all throughout). Numbers above dotted lines are distances in Å.

The key results from REST2 simulation were further validated by well-tempered metadynamics, a popular biased enhanced sampling technique (Barducci et al., 2008). WT-MTD was performed at 27 °C. By applying biasing force (in this case, radius of gyration (Rg) of residues 108-115), the sampling was boosted and it was observed that in the absence of the succinimide constraint in the MjGATase_N109S mutant, the loop exists in a locally, unfolded conformation, at higher free energy (at a higher free energy minimum corresponding to Rg value of ~ 7 Å) (Fig. 5.17). On the other hand, there is little or no effect on the local conformation of the corresponding segment in the WT enzyme (Fig. 5.17)

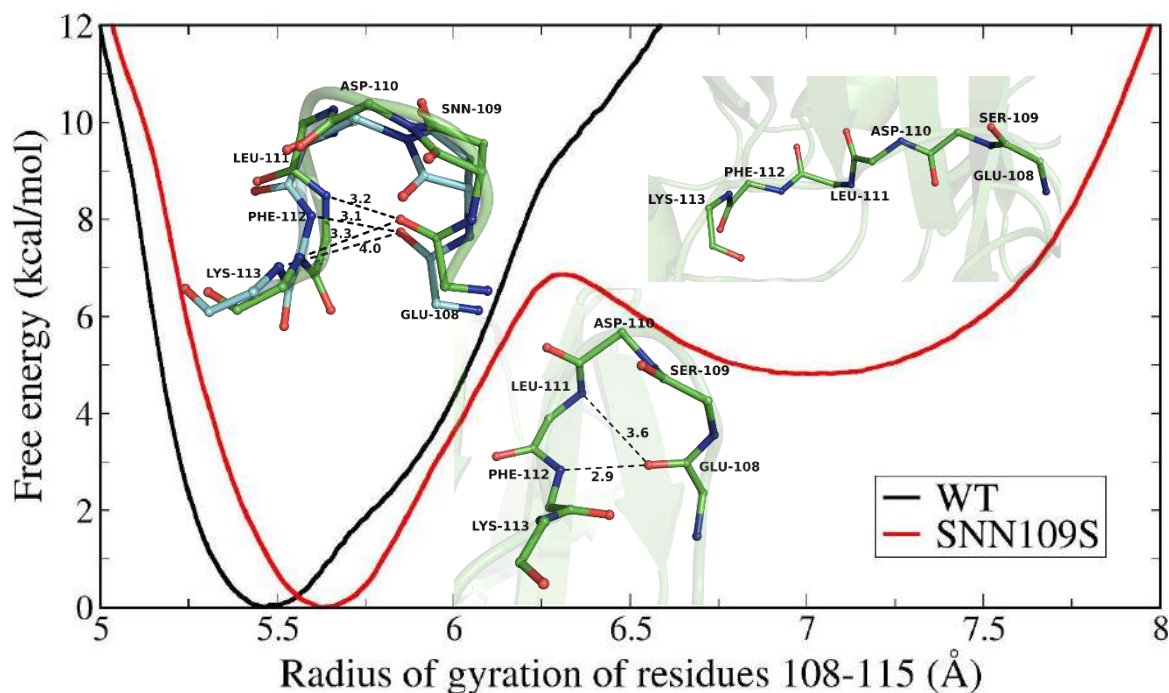


Figure 5.17: Results of WT-MTD: Black solid line represents free energy profile of MjGATase_WT and red solid line represents the same for MjGATase_N109S. Structural conformations of each minima are shown as ball and stick model over the corresponding minimum. Figure Courtesy, Sudip Das.

The free energy profiles in Figure 5.17 establish two distinct minima in the MjGATase_N109S (SNN109S) mutant corresponding to the folded and extended conformations of the loop as against a single minimum in case of the WT enzyme. This further affirms that succinimidyl residue, through imposition of a conformational restraint, decreases the floppiness of the loop in which it is situated. This phenomenon has a long-range effect on the overall structure and stabilizes the protein. Abrogation of this constraint opens up the loop as a function of temperature, an effect that's cascaded into the rest of the protein leading to the destabilization of the protein structure as the temperature increases.

5.3. Future Directions

Mechanisms of attaining thermostability are umpteen and not all are fully understood yet. However, the interest of scientific community in understanding newer mechanism is ever increasing. This interest stems from the need to transform industrially important mesophilic enzymes into more robust thermally stable enzymes that can be used in bioreactors at higher temperatures.

In the present study we attempted to understand a previously unknown mechanism of thermostability found in glutamine amidotransferase from a hyperthermophilic archaeon, *Methanocaldococcus jannaschii*. The serendipitous finding of succinimide formation in MjGATase and its role in imparting enhanced thermal stability to the protein was the focus of an earlier study from our laboratory. Those studies, through extensive mass spectrometric and site directed mutagenesis analyses had proved that stable succinimide, formed by spontaneous, non-enzymatic deamidation of Asn109, is responsible for imparting enhanced thermal stability to MjGATase. In the present study, we solved the crystal structure of MjGATase wild type enzyme and mutant D110G and delineated structural features that mediate

the stability of the succinimide modification and in turn, the stability of the entire protein. The structural observations were further substantiated by molecular dynamic simulation studies. Our study has unravelled a new mechanism of thermostability and added to the known pool of mechanisms of thermostability known so far. It also raises more questions regarding the evolutionary pressure for selection of this PTM as a thermostabilization mechanism, its widespread occurrence, techniques for easy detection of intact (stable) succinimides in proteins and factors that facilitate deamidation at Asn109 in MjGATase. Studies need to be undertaken in future to attempt to answer these questions and an outline for the same has been provided in this section.

5.3.1. Evolutionary selection of a succinimidyl residue

In the course of this study, various other known mechanisms of thermostability were reviewed. One such mechanism is the increased occurrence of proline residues in thermophilic enzymes compared to their mesophilic counterparts. Stability of a protein structure is determined by the net difference in free energy of the folded and the unfolded forms (Matthews et. al., 1987) and free energy is a combination of entropy and enthalpy ($\Delta G = \Delta H - T\Delta S$). Different amino acids contribute differently to the configurational entropy of unfolding. It depends majorly upon the number of conformations available to the residue in the unfolded state. Prolyl residue in a polypeptide chain restricts the flexibility of the segment due to its restricted Φ values (Matthews et. al., 1987), thereby contributing minimally to the free energy of unfolding. The conformational constraint imposed by SNN is similar (to proline) in that the cyclization of the side chain in the succinimidyl residue constrains the Ψ value to -120° . This raised a question, could a proline residue substitute for a SNN residue and confer similar thermal stability to MjGATase? Or to rephrase the question, in the course of evolution why was a SNN residue chosen (at position 109) rather than a commonly occurring Pro residue? Additional studies were undertaken in the laboratory to answer this question results of which are summarized below. A mutant (MjGATase_N109P) of MjGATase was created by site-directed mutagenesis that harboured a prolyl residue at position 109 in place of succinimide. **Preliminary experiments which involved subjecting protein to boiling temperatures showed that N109P precipitates out of solution at about 80 °C and hence is thermally more unstable than wild type enzyme as well as the N109S mutant.** Further, thermal denaturation examined by circular dichroism showed that N109P melts at 78 °C, a temperature that is 10 °C lower than even that of N109S mutant of MjGATase. It should be noted that the WT protein, under the experimental conditions does not unfold even at 100 °C. In order to understand the reasons behind decreased thermal stability of this mutant, it was imperative to solve its structure. Therefore, N109P protein was crystallized and structure was solved at 1.9 Å, in P1 space group, using the MjGATase_WT structure as a template for molecular replacement. The structure solution and refinement statistics are noted in table 5.4.

Table 5.4: Structure solution and data refinement statistics

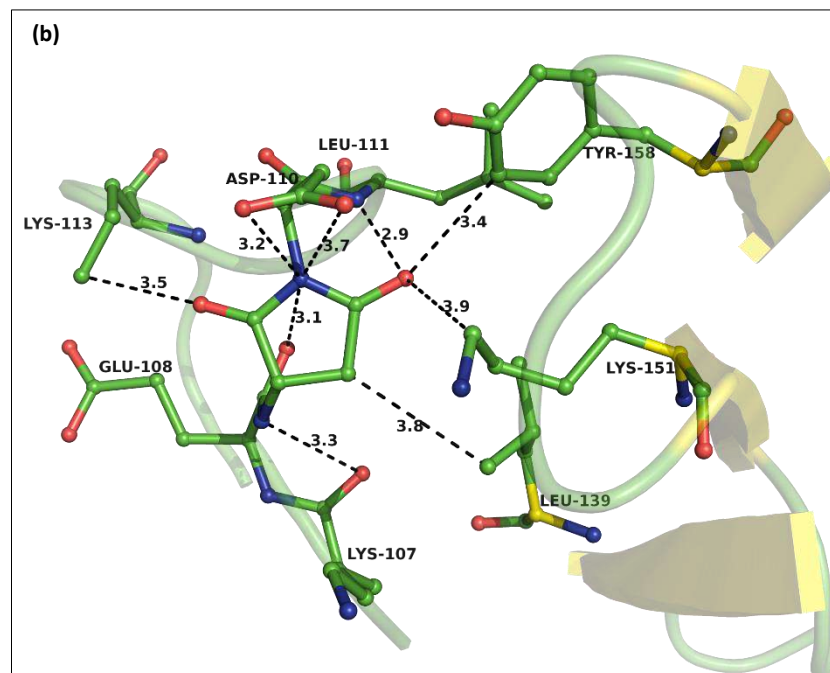
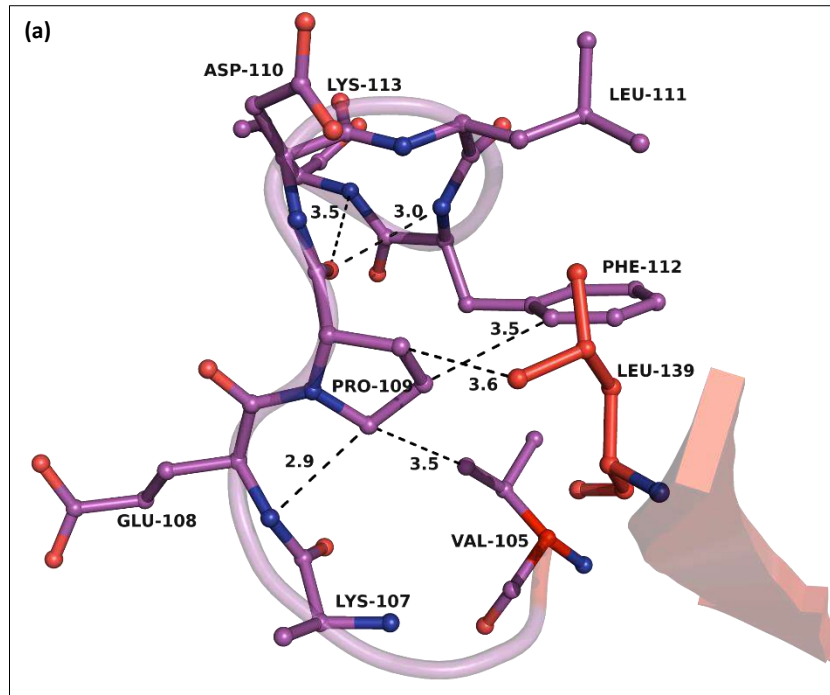
Property	MjGATase_N109P
PDB ID	7D97
Data collection statistics	
Resolution range	35.49 – 1.89
Wavelength	1.54179
Space group	P 1
a, b, c	35.50Å 68.05Å 75.35Å
α , β , γ	90.95 ⁰ , 90.47 ⁰ , 91.45 ⁰
% completeness	96.8 (73.3)
Avg. Mosaicity	0.80
Total reflections	3362 (11939)
Unique reflections	1628 (5717)
Multiplicity	2.1 (2.1)
(I/ σ (I))	5.3 (3.4)
CC _{1/2}	0.988 (0.702)
R _{meas}	0.089 (0.321)
R _{merge} (%)	6.5 (23.5)
Wilson B factor (Å ²)	12.4
N ⁰ mol. / asym. Unit	4
Data refinement statistics	
R _{work} /R _{free}	0.2041/0.2640
<u>No. of atoms</u>	
Protein	6253
Ligand	0
<u>No. of non-H atoms</u>	
Protein	5668
Ligand	0
Water	585

<u>rms deviation</u>	
Bond Angle (°)	1.6245
Bond Length (Å)	0.0082
Avg. B, all atoms (Å ²)	14.0

<u>Residues in Ramachandran plot</u>	
Favoured	705 (96%)
Allowed	27 (4%)
Outliers	6 (1%)

Values for the highest resolution shell are given in parentheses.

Analysis of N109P protein structure revealed that some of the interactions that were important in maintaining the stability of SNN109 in the WT structure (Fig. 5.18 b), are lost in the mutant (Fig. 5.18 a). In N109S mutant as well, the critical interactions are lost (Fig. 5.18 c) (Since structure of N109S could not be solved, contact analysis was performed on the structure obtained by molecular dynamic simulations). Interactions with K151 and Y158, residues from the core region of the protein, are lost; these interactions (along with L139) connect the solvent exposed loop containing SNN to the core of the protein, possibly leading to decreased floppiness of the loop in the wild type protein.



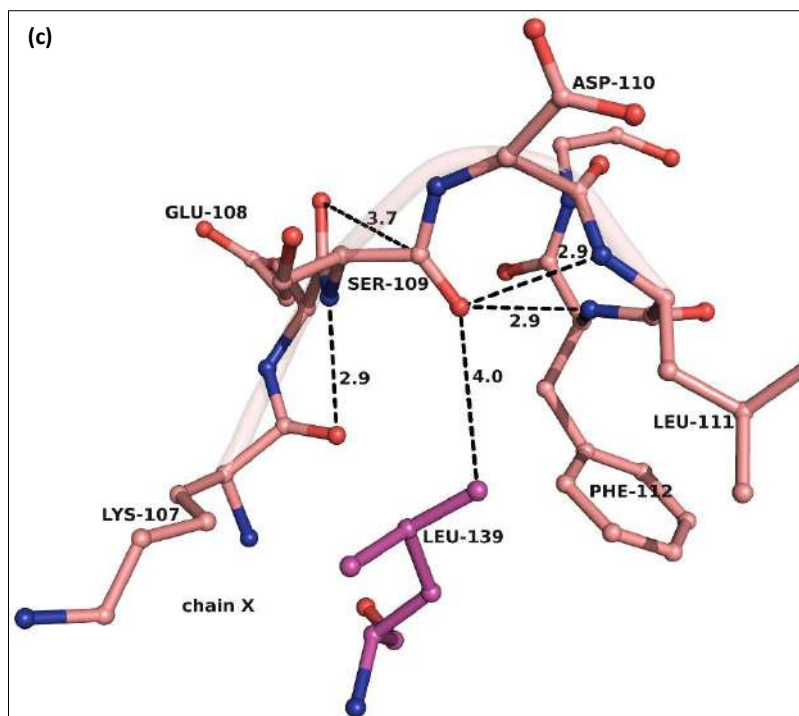
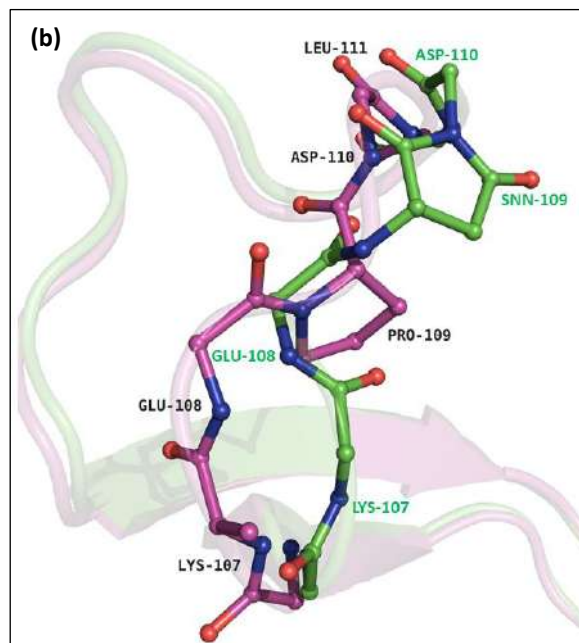
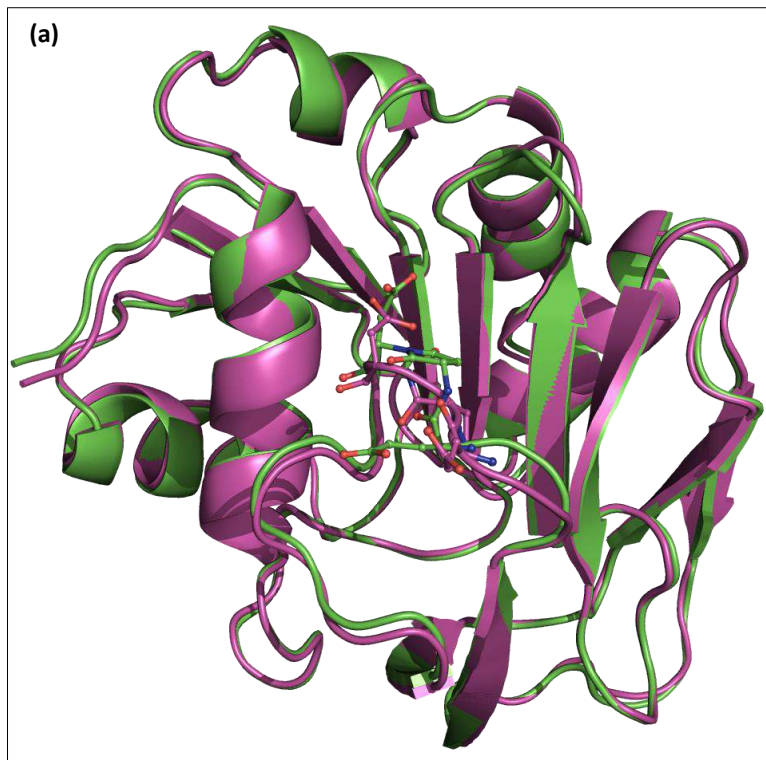


Figure 5.18: Comparison of interactions of Pro109, SNN109 and S109 at 4 Å distance cut-off. (a) Crystal structure of MjGATase_N109P protein revealed that residues Val105, Lys107, Glu108, Asp110, Phe112, Lys113 and Leu139 are positioned within 4 Å distance from Pro109. Contacts with Lys151 and Tyr158 are lost in this mutant. (b) As seen from the crystal structure and described in section 6.4.3., SNN interacts with residues from the loop harbouring it as well as residues from the core of the protein as seen from the crystal structure. (c) The structure of MjGATase_N109S could not be solved from the collected diffraction data. Therefore, contact analysis for this mutant was performed on the structure obtained from in silico modelling (in PyMol) and energy minimization. In N109S mutant as well, contacts with residues from the core of the protein are absent, whereas other contacts are conserved. Numbers above dotted lines are distances in Å.

Overlay of the structure of MjGATase_N109P on the WT structure (Fig. 5.19 a) showed RMSD of 0.390 with a slight deviation in the loop region as shown in Figure 5.19 b. A major difference can be spotted in the way the side chains are positioned in the mutant (Fig. 5.19 c). Figure 5.19 d illustrates that in the loop region, backbone of the mutant traces a different path compared to the peptide backbone of the WT. The orientation of Glu108 in the WT promotes formation of H bonds between the its CO NH of Leu111 and Phe112, which constitute the α -turn and β -turn, respectively. Due to the different orientation of Glu108 in the mutant N109P of MjGATase, these H bonds are lost, thereby prohibiting the formation of the same tight turns, which we speculate are involved in decreasing the floppiness of the loop (Fig. 5.19 e). In case of N109S mutant as well, the backbone CO of Glu108 has adopted a different orientation, thereby abolishing α - and β -turns (Fig. 5.19 f). However, the polypeptide chain in MjGATase_N109P bends in a manner that H-bonds are formed between Pro109 CO---Phe112 NH (3.0 Å, β -turn) and Asp110 CO---Lys113 NH (3.1 Å, β -turn) depicting two β turns, respectively (Fig. 5.19 g).



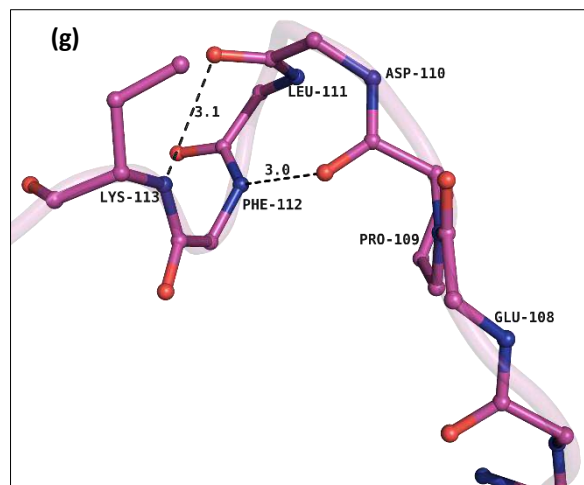
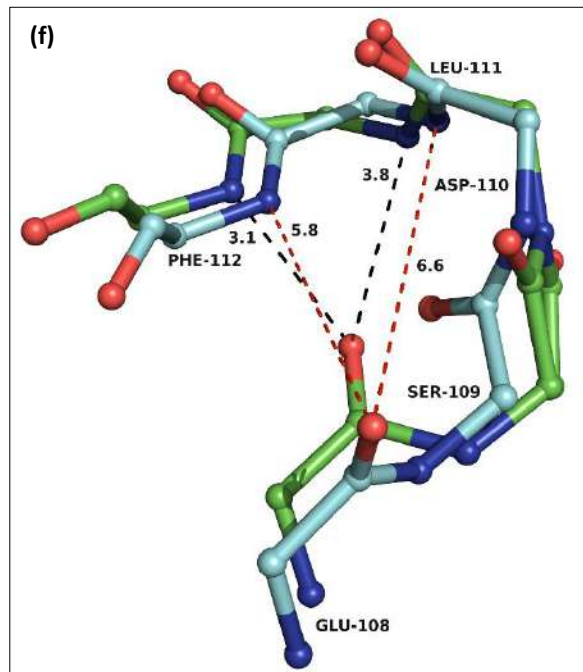
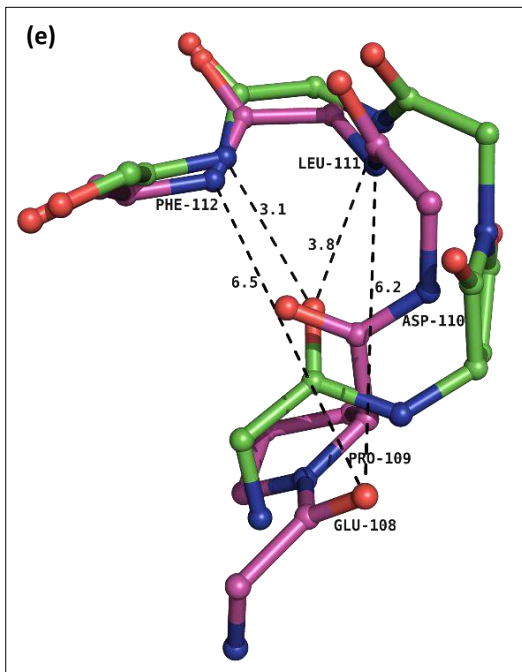
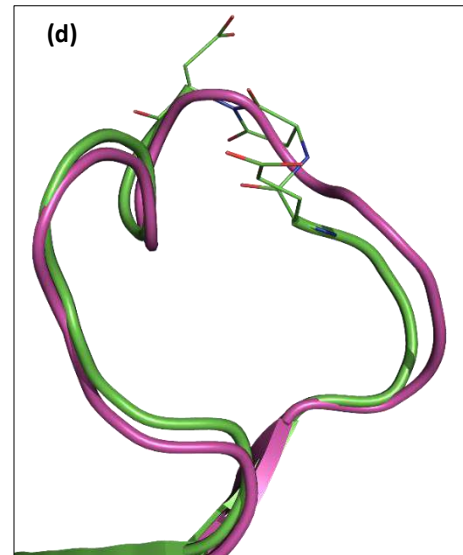
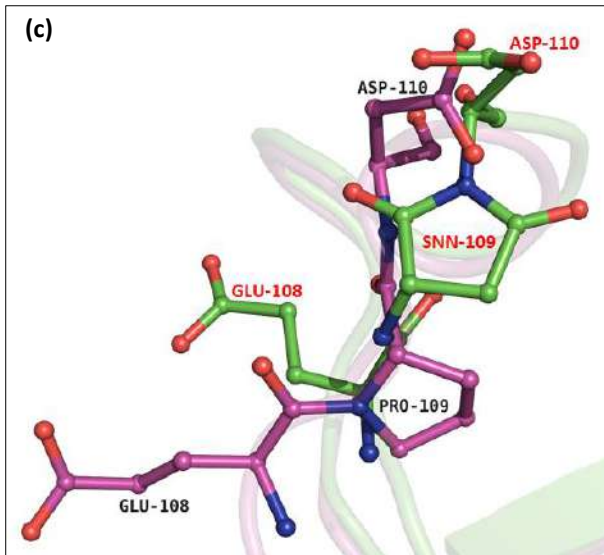


Figure 5.19: Comparison of the structures of WT and N109P mutant of MjGATase. (a) Superimposition of the structures of WT and N109P mutant of MjGATase. (b) A close-up of the loop region containing SNN revealed different paths traced by the backbone of residues K107-L111. For clarity, only the main chain of the residues (except SNN109 and Pro109) is represented as ball and stick model. WT residues are labelled in green colour while N109P mutant residues are labelled in black colour. (c) An even more conspicuous difference is seen in the positioning of side chains of the amino acids in the E(SNN)(P)D tripeptide. The side chains of Glu108 and Asp110 are oriented in completely different manner. The backbone CO of Glu108 which is involved in the formation of α and β -turn is flipped and is in a position where it can no-longer form the hydrogen bonds required for these turns. WT residues are labelled in red colour and N109P residues are labelled in black colour. (d) The tight-turn structural motifs formed due to the presence of a succinimide moiety are lost and the loop appears to be more extended than that in the WT. (e-f) The backbone CO of Glu108 that forms H bonds responsible for tight-turns is moved away thereby, abolishing formation of the tight-turn structural motifs in both N109P and N109S mutant proteins. Shown in the figure are the distances between CO of Glu108 and its H-bonded partners in the wild type and the mutants. MjGATase_WT is represented in green, MjGATase_N109P in magenta and MjGATase_N109S in cyan colour in all panels. In case of both mutants, the α and β turn forming H bonds are lost, which were formed by Glu108 CO---Phe112 NH and Glu108 CO---Leu111 NH, respectively, in the WT protein. (g) However, a new set of H bonds are formed between Pro109 CO---Phe112 NH and D110 CO---K113 NH, leading to formation of two β -turns. Numbers above dotted lines are distances in Å.

These structural differences, although subtle, seem to have a long-range impact on the overall structural stability of the mutant. The results also suggest that the effect of substitutions on protein stability are difficult to predict and rather than the global difference in entropies of folded and unfolded state, it is the local packing efficiencies in the folded proteins that determine thermostability (Vieille et. al., 1996) (Fig. 5.20). The trend of Φ , Ψ values in the polypeptide region 105-113 is shown in Figure 5.20 a. The same values are also plotted on a Ramachandran map for easy comparison (Fig. 5.20 b). The differences in the dihedral angle values suggest that conformational constraints imposed by two different residues having cyclized side chains is different and these differences are more evident in the structures (Fig. 5.20 c-e). Our experimental observation that thermal stability of (MjGATase) WT > N109S > N109P is corroborated by the structural differences observed between these three proteins (Fig. 5.20 c-e).

(a)	Residue	Φ	Ψ
MjGATase_WT	V105	-84.6	118.2
	D106	-90.6	-30.0
	K107	-144.8	112.2
	E108	-56.3	-38.7
	SNN109	42.6	-128.8
	D110	-100.2	-47.5
	L111	-60.4	-27.4
	F112	-118.2	19.6
	K113	-53.6	133.6
MjGATase_N109P	V105	-74.4	130.1
	D106	-75.9	-59.5
	K107	-123.5	-111.3
	E108	-134.4	50.4
	P109	-71.3	146.6
	D110	-61.5	-31.4
	L111	-65.0	-23.2
	F112	-110.5	24.8
	K113	-62.6	128.8

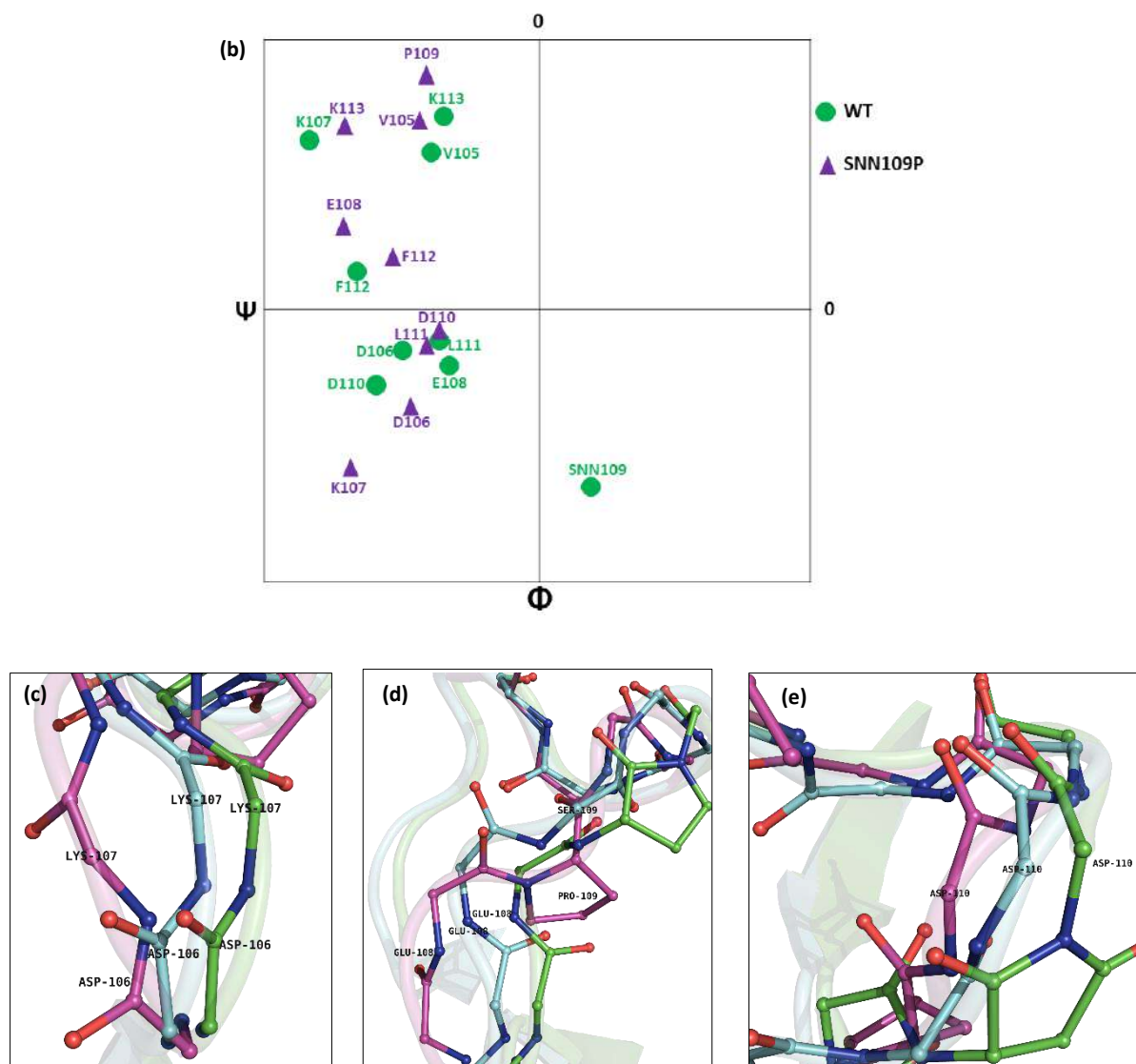


Figure 5.20: Differences in constraints imposed by SNN and Pro residues and comparison of MjGATase WT and mutant structures. Although both SNN and Pro are residues with cyclized side chains, the constraints imposed on preceding and succeeding residues due to their presence is different. (a) Table lists the Φ and Ψ values of residues in the loop region of MjGATase_WT and MjGATase_N109P. (b) The values are plotted on a Ramachandran map. Green circles denote MjGATase_WT residues while purple triangles depict MjGATase_N109P residues. A clear deviation is seen for residues 106-110. (c-e) A zoomed in view of the same region in the structures shows that N109S structure (modelled) is more similar to WT than N109P protein structure. WT is represented in green colour, N109S in cyan and N109P structure in magenta. It can be seen that the structure of N109S lies in between the structure of WT and N109P corroborating our experimental observations on the thermostability of these three proteins. Thermostabilities of the three proteins can be ranked ordered as WT > N109S > N109P.

The thermodynamic effect of proline substitutions on stability have been shown to display an enthalpic component in addition to an entropic one; however, in case of MjGATase, the succinimidyl residue seems to offer superior enthalpic gain (though largely through Van der Waal's interactions) in addition to entropic gain (due to conformational constraint). Prolyl residue at position 109 has lost interactions with Y158 and K151, which are key residues from the core of the protein. This indicates that although proline can decrease the conformational entropy of unfolding (Matthews et al., 1987), this entropic

contribution is masked by decreased enthalpic contributions as a consequence of loss of van der Waals and electrostatic interactions and therefore, a succinimidyl residue containing protein would have been selected in the course of evolution.

Molecular dynamic simulations need to be performed on the solved structure, which will further assist in investigating the decreased stability of MjGATase_N109P mutant.

5.3.2. Detection of stable succinimidyl residue in proteins

Stable succinimidyl residues in proteins go undetected mainly because their occurrence in intact proteins is not anticipated; however, they could be more widespread than currently perceived. Our observation with GATase sequences from ~100 other thermophilic Archaea showed that the E(N/D)(D/E) tripeptide sequence is conserved. Moreover, a stable SNN is present in *Pyrococcus horikoshii* GATase crystal structure. These observations led us to hypothesize that stable succinimides could be more prevalent and might be involved in granting structural stability to proteins. A bona fide way of detection of succinimidyl residue in proteins is through observation of crystal structure depicting electron density of SNN; however, it is not always possible to obtain crystal structures of proteins and hence other full-proof methods for detecting SNN need to be explored. High resolution mass spectrometry (of intact proteins) holds promise as a suitable method to detect succinimidyl residue in relatively smaller proteins, wherein a mass loss of 17 Da (-17.026549 Da, in case of deamidation reaction) can be observed with confidence.

Alternatively, peptide mapping can be used to trace succinimidyl residue in proteins; although, neutral or high pH conditions used during the conventional protein digestion could lead to hydrolysis of succinimide. This challenge can be overcome by either minimizing the exposure of protein to neutral or high pH conditions or carrying out the digestion under mildly acidic condition. A method for protein digestion under mildly acidic condition was developed by Huang and co-workers which was based on the use of acid labile surfactant RapiGest (RG), for digestion of proteins at pH 6.0, followed by degradation of the surfactant before LC-MS/MS analysis of the resultant peptide fragments (Huang et al., 2009).

Another method developed recently by Mingyan Cao and co-workers describes amalgamation of two approaches: low-pH digestion and hydrophobic interaction chromatographic (HIC) separation (of intact proteins) (Cao et al. 2019). In this strategy (performed on BisA, a bispecific monoclonal antibody), peptide mapping was performed at low-pH (5.4 - 5.8) and this was followed by LC-MS/MS of the resultant peptides which revealed three species: an unmodified BisA, BisA with a deamidation hydrolysis product (Asp/iso-Asp) and a species containing intact succinimide. Although this approach granted successful detection of intact succinimide, the complexity of sample preparation may forbid its use in routine protein analysis. The group also simultaneously described a chromatographic separation of intact proteins – the hydrophobic interaction chromatography that separates molecules based on hydrophobicity. Protein molecules contain hydrophobic and hydrophilic patches and upon

introduction of a high-salt buffer (mobile phase A; 50mM sodium phosphate and 1M sodium sulfate, pH 6.5), the hydrophobic patches (that are usually buried inside) are exposed. The hydrophobic regions adsorb to the stationary phase (MAbPac HIC-10 column, Thermo Scientific) in presence of high salt mobile phase A. Separation is achieved by decreasing salt gradient (mobile phase B; 50mM sodium phosphate, pH 6.5) under which protein molecules elute in order of increasing hydrophobicity (Cao et al. 2019). Hydrophobicity of unmodified protein, in this case BisA, would be different from the completely deamidated and succinimide containing protein and hence separation of the three species is achieved. This chromatographic separation method does not involve complex sample preparation steps and is therefore more suitable for easier and faster detection of succinimides in intact proteins.

5.3.3. Can this PTM be engineered to enhance stability and reduce floppiness?

Over the last few decades, a great many mechanisms of thermostability have been discovered and studied in detail; however, only a few of them have displayed the potential to be engineered into other proteins. Four general strategies have been identified for engineering thermal stabilization in proteins (Vieille et al. 1996);

- i) More efficient protein core packing
- ii) α -helix stabilization
- iii) surface loop driven core stabilization
- iv) prevention of chemical degradation

Enhanced thermal stabilization of MjGATase was achieved naturally through a PTM that introduced conformational constraint in a loop region which in turn, stabilized the entire protein and also prevented deamidation mediated degradation of the protein (a combination of strategies iii and iv from the above-mentioned list). **A better understanding of this newer mechanism of thermostability now raises the question, if this PTM can be engineered in mesophilic proteins to confer thermal and structural stability.**

The role of surface exposed loops in protein stabilization has been the focus of many studies for a long time and it has been shown that manipulation of the loops and turn structures is a common strategy imparting thermostability. In this context, we postulate that attempts can be made to introduce E(N/D)(D/E) tripeptide sequence in the (long) loops of mesophilic proteins to enhance thermal stability. However, the tripeptide sequence alone may not be sufficient to grant structural stability as analysis of MjGATase structure shows that succinimidyl residue is stabilized owing to its interactions with residues in the surrounding microenvironment. Therefore, the positioning of the tripeptide sequence at correct location in the protein structure would be a crucial consideration. To search structural features conducive for incorporation of a stable succinimidyl residue in the protein of interest, one can use computational tools that search for desired structural motifs/features in proteins. Examples of such tools include 3D-PP, a tool for discovering conserved three-dimensional protein patterns (Valdés-Jiménez et al. 2019) and LFM-Pro (local feature mining in proteins) (Sacan et al. 2007) etc.

These tools sample structural features rather than sequence and consider characteristics such as hydrophobicity, solvent accessibility to capture physico-chemical properties of the site of interest (Sacan et al. 2007). It is worthwhile noting that such an exercise will be non-trivial and will require both extensive computational and experimental approaches.

Our experimental results strongly highlight the role of the succeeding residue in stabilization of the succinimide ring structure. And based on the data obtained from sequence alignment, it can be conjectured that the preceding residue, Glu, that is highly conserved in all GATases may have a role either in formation or stabilization of the succinimide. Asparagine is a thermolabile residue which undergoes irreversible deamidation upon increase in temperature. Protein unfolding proceeds at a much higher rate following chemical degradation. Prediction of the sites that have a higher tendency to deamidate can be used to engineer the residues preceding (n-1) and succeeding (n+1) the labile Asn to Glu (n-1) and Glu/Asp (n+1) respectively, and assess if the resulting mutations can lead to formation of a stable succinimidyl residue that can impart enhanced structural stability. Introduction of a conformationally constrained succinimidyl residue in loop regions of mesophilic proteins would be similar to the incorporation of prolyl residues in loop regions to enhance thermostability, in that, the cyclization of the side chain would decrease the conformational entropy between the folded and the unfolded state but the overall effect would be determined by the enthalpic contributions and the three-dimensional structure of the protein around the site of mutation. To corroborate our finding, structures of more thermophilic GATases containing E(N/D)(D/E) sequence but having lower overall sequence identity to MjGATase/PhGATase need be solved in future. If succinimidyl residue is observed in such GATases, it would reaffirm our finding of post-translational formation of succinimidyl residue as a mechanism granting thermal stability to hyperthermophilic GATases. We also found that not only in the GATase subunit of thermophilic archaeal GMPS is the END sequence conserved, the GATase subunit of anthranilate synthase (a triad glutamine amidotransferase like GMPS) from *Phaeodactylum tricorutum* (mesophilic diatom, algae) contains the END tripeptide sequence in a conserved location. Residues that interact with succinimidyl residue in MjGATase are also found to be conserved in GATase of *Phaeodactylum tricorutum*; however, the overall sequence identity (with MjGATase) is only 36%. A structure of this GATase needs to be solved in order to see if a succinimidyl residue would be observed. Many more such examples could be found upon search for sequence conservation using MjGATase as a query sequence.

Assessment of spontaneous, non-enzymatic deamidation/isoaspartylation of therapeutic antibodies is an important facet of therapeutic antibody development since this PTM leads to mass change, charge heterogeneity and structural alteration. Loops of antibodies, that harbour the complementarity determining regions (CDR), are majorly susceptible to deamidation as shown by studies with 37 monoclonal antibodies (Sydow et al., 2014) and 131 clinical stage antibodies (Lu et al., 2019) among many others. Major finding from these and other studies highlight the impact of the succeeding residue on propensity of deamidation of an asparaginy residue. In this context, mutation of the n+1 Gly

residue to another amino acid residue (Asp/Glu based on our observation with MjGATase and PhGATase), such as an aspartyl or glutamyl residue could possibly stabilize the succinimidyl intermediate without affecting the deamidation propensity.

A recent study by Huawei Qiu and co-workers on anti-CD52 antibody (MAB1) demonstrated that in the CDR of the antibody where deamidation is prevalent, mutation of Asn to remove the deamidation site leads to dramatic decrease in antigen binding affinity (Qiu et al. 2019). However, mutation of the succeeding Gly residue to Arg (G34R), Lys (G34K) and Gln (G34Q) largely retained the antigen binding affinity even after deamidation. The wild type antibody, under the same conditions, lost the antigen binding affinity to a significant extent (K_D change from 4.3 nM to 1230 nM) (Qiu et al. 2019). Analysis of the deposited structure of MAB1 (PDB ID 6OBD) showed a conformation of Asn33 conducive for deamidation i.e. Asn33 side chain is oriented in close proximity of the backbone amide nitrogen of the succeeding residue (“near attack conformation”)(Sadiq and Coveney 2015; Ugur et al. 2015) (Fig. 5.21).

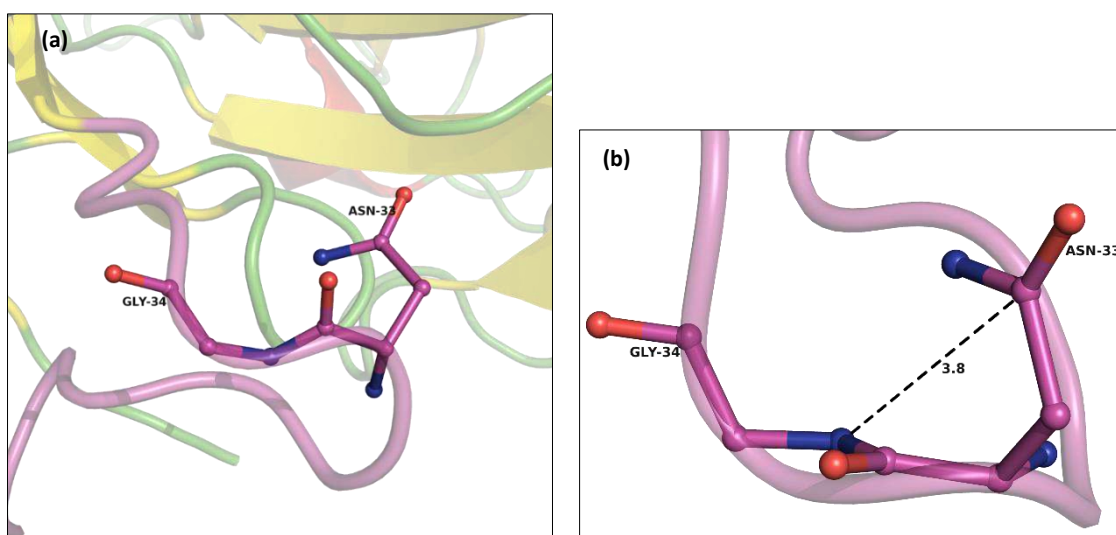


Figure 5.21: Conformation of Asn undergoing deamidation in anti-CD52 binding antibody (MAB1). Asn33 of MAB1 is shown to undergo deamidation thereby resulting in decreased antigen binding affinity. (a) The Asn is situated in a surface exposed loop of the light chain and is succeeded by a Gly residue. (b) Zoom-in of the same region from MAB1 showing the near attack conformation assumed by Asn33 side chain that is conducive for deamidation reaction. Mutation of Gly34 to either Lys, Arg or Gln resulted in stabilization of the antibody via decrease in deamidation. Numbers above dotted lines are distances in Å

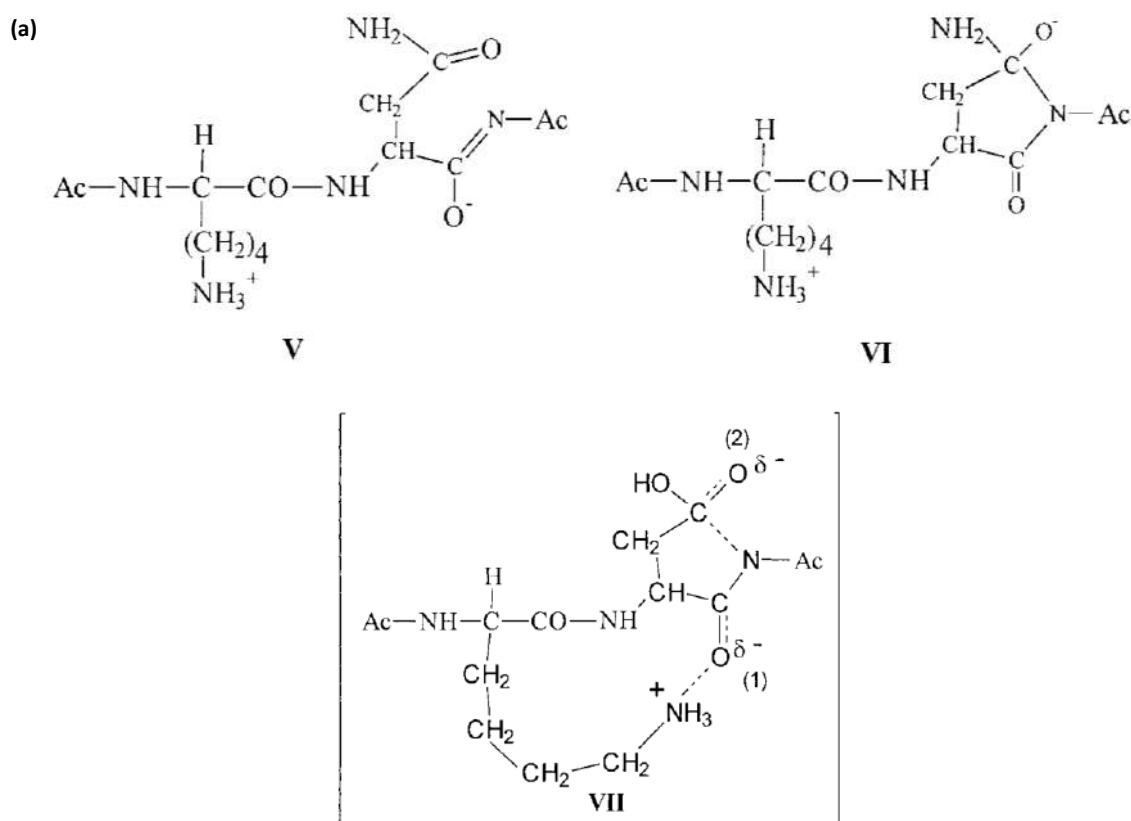
5.3.4. Factors governing succinimide formation in MjGATase

Study presented in this thesis deals with understanding the structural factors responsible for succinimide induced hyperthermostability of MjGATase. It is seen that maintenance of stable succinimidyl residue is a function of the primary amino acid sequence and the three-dimensional structure surrounding the site of PTM.

Information about the factors that determine the propensity of Asn109 to deamidate is missing and further studies need to be undertaken to examine the same. Studies performed on denatured proteins

and synthetic peptides have shown that the rate of succinimide formation is greatly influenced by the carboxy terminal (n+1) amino acid residue (Li et al. 2005; Robinson 2002; Robinson and Robinson 2004b, 2004a). It is well established that presence of a small residue such as glycine that lacks β -carbon enhances the tendency of Asn to undergo deamidation (or tendency of Asp to undergo isomerization). However, in case of MjGATase and PhGATase, succinimide forming Asn and Asp (respectively) are succeeded by negatively charged residues (Asp and Glu, respectively). Similarly, in case of amylomaltase from *T. thermophilus* and *T. aquaticus*, (stable) SNN is succeeded by a negatively charged residue, as noted in section 4.5. These observations are contrary to the information known thus far and hence demand further investigation.

Capasso and co-workers have shown that a lysine residue in the immediate vicinity of an asparagine residue can increase deamidation rate (Capasso et. al., 2000). Authors suggested that presence of a positively charged lysine residue, close in space (to an Asn), may act through electronic effect as shown in Figure 5.22 a. Electronic effect does not require lysine to be situated sequentially close to the site of deamidation, but close in space.



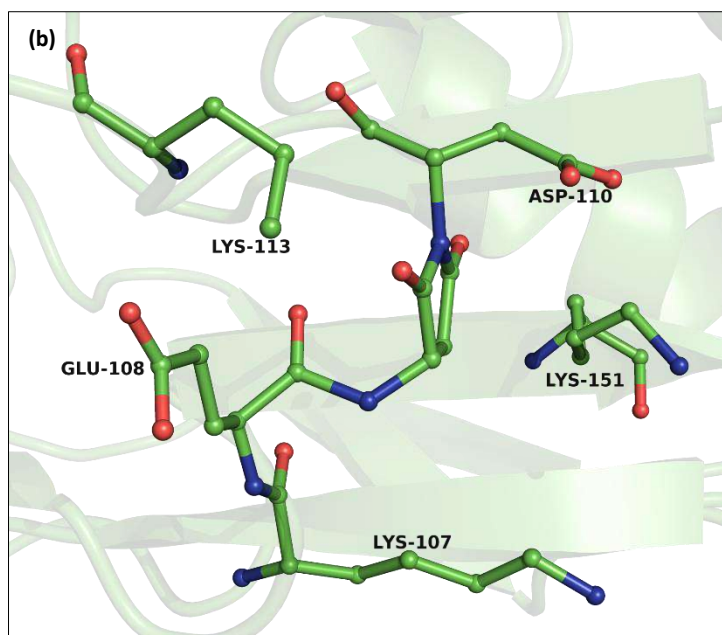


Figure 5.22: Effect of lysine on deamidation. (a) Presence of a lysine side chain close to an asparagine might facilitate deamidation of Asn by exerting electronic effect via interaction with the negative charge on the carbonyl oxygen. Figure reproduced from Capasso, S., Balboni, G., & Di Cerbo, P. (2000). *Effect of lysine residues on the deamidation reaction of asparagine side chains*, *Biopolymers: Original Research on Biomolecules*, 53(2), 213-219. (b) In MjGATase, K113 is located close to the deamidation site and can possibly enable deamidation reaction.

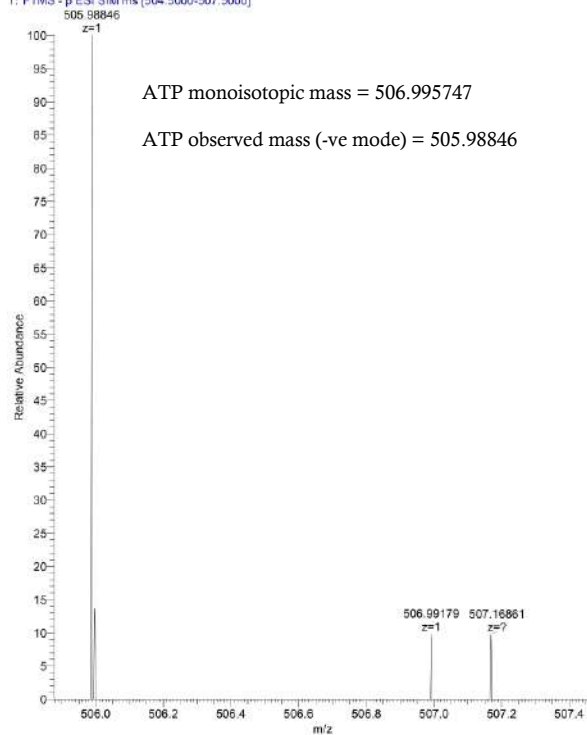
In MjGATase, there are three lysine residues in the vicinity (within 4 Å distance) of deamidation site (K107, K113, K151). Of these three lysine residues, K113 appears to be oriented in a position so as to interact with the side chain of Asn109 (although electron density for all atoms of the side chain of Lys113 was not mapped in the crystal structure, the orientation of C γ of Lys113 indicates that the amide nitrogen of the side chain could be situated close to CO of Asn109 (Fig. 5.22 b)). K113 residue might be involved in increasing the acidity of backbone nitrogen (Radkiewicz et al. 2001) (through its interaction with the carboxyl oxygen of Asn109 side chain) of Asp110, thereby enabling deamidation reaction. This hypothesis needs further experimental evidence; site-directed mutagenesis of K113 to alanine might shed light on whether this residue plays a role in formation of succinimide.

Besides, the backbone acidity of NH of the succeeding residue, another factor that is shown to assist deamidation in peptides is the special orientation of the side chain of deamidating Asn. The carbonyl carbon of the side chain of Asn needs to be present in close proximity of the backbone NH of the succeeding residue, a conformation termed as ‘near attack conformation’ (Sadiq and Coveney 2015) (and not pointing away from it). In order to fulfil the near attack conformation criteria, the Ψ angle of Asn109 needs to be -120° , which is indeed the case in MjGATase ($\Psi_{\text{Asn109}} = -128.8^\circ$). Another criterion is the distance between NH of the succeeding residue (n+1) and carbonyl carbon of the side chain of

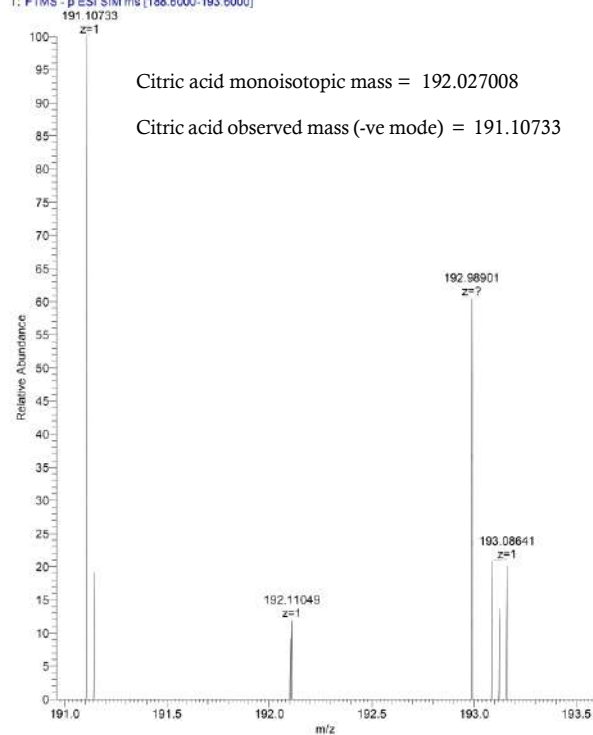
the deamidating residue (n). This distance needs to be within 3.5 Å for a successful nucleophilic attack to take place. Since no protein with unmodified Asn109 is obtained during the purification process, it is difficult to experimentally observe if this criteria is fulfilled in case of MjGATase; however, molecular dynamic simulations with a simulated structure of MjGATase in which SNN109 is replaced with Asn109 (and energy minimized) could be used to evaluate the same.

Annexure I

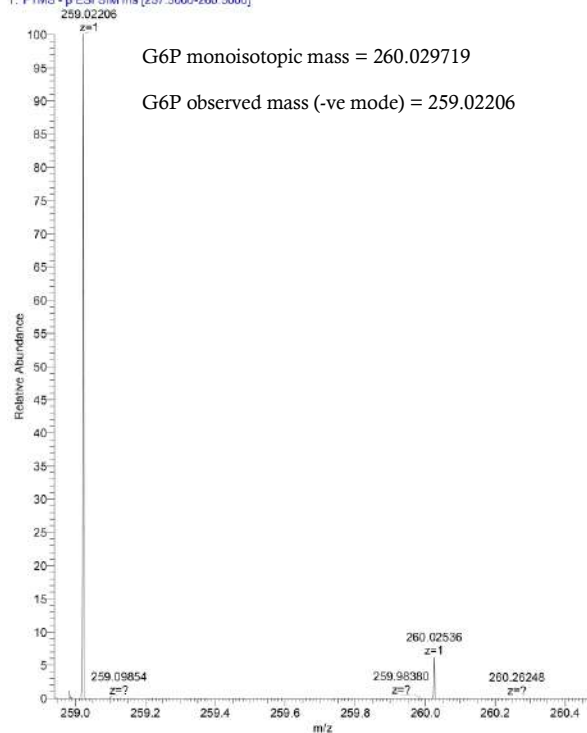
ATP_1um_DI_Negative_240k #1 RT: 0.01 AV: 1 NL: 3.28E3
T: FTMS -p ESI SIM ms [504.5000-507.5000]



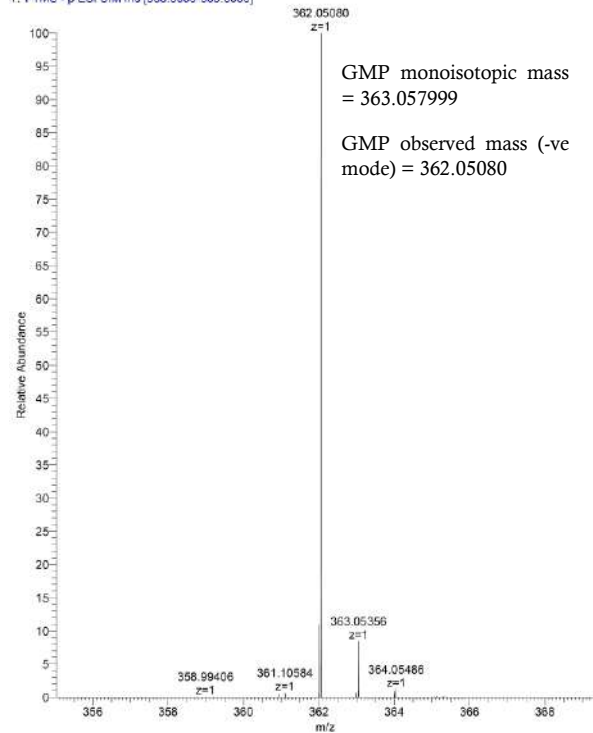
CitricAcid_1um_DI_Ne 50k_03 #1 RT: 0.01 AV: 1 NL: 5.51E3
T: FTMS -p ESI SIM ms [188.6000-193.6000]



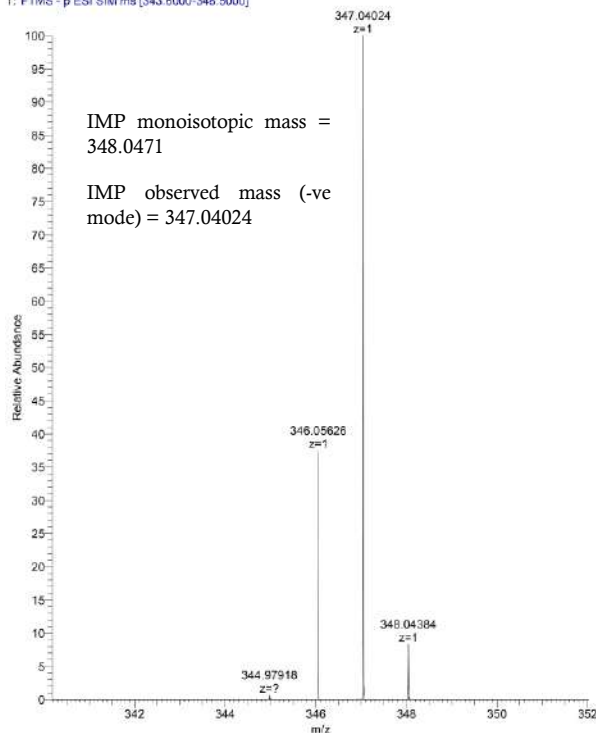
Glucose Phosphate_1um_DI_Negative_120k #1 RT: 0.00 AV: 1 NL: 4.74E6
T: FTMS -p ESI SIM ms [257.5000-260.5000]



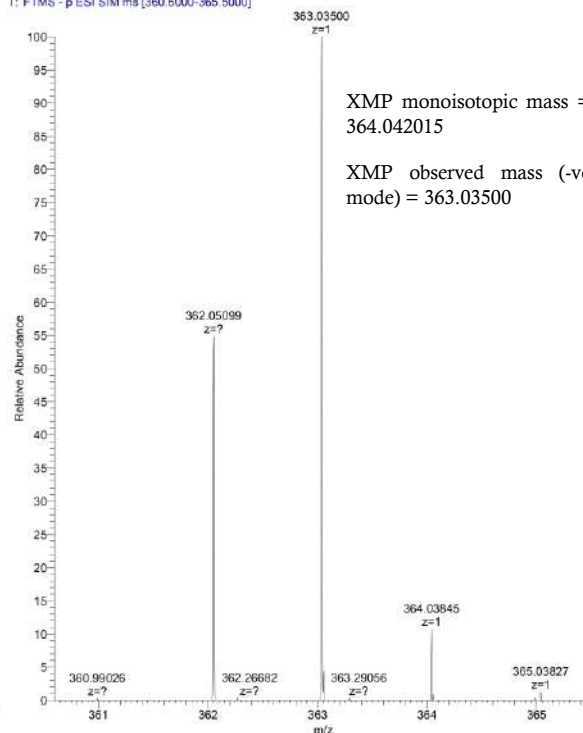
GMP_1um_DI_Negative_120k #28-97 RT: 0.12-0.42 AV: 70 NL: 5.74E6
T: FTMS -p ESI SIM ms [358.6000-363.6000]



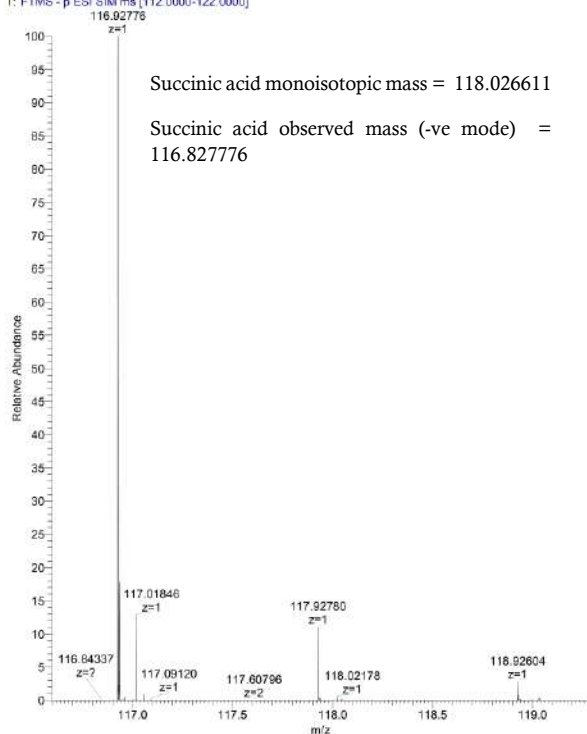
10µM_IMP_Ne_01 #371-384 RT: 0.93-0.97 AV: 14 NL: 1.22E6
T: FTMS - p ESI SIM ms [343.6000-348.5000]



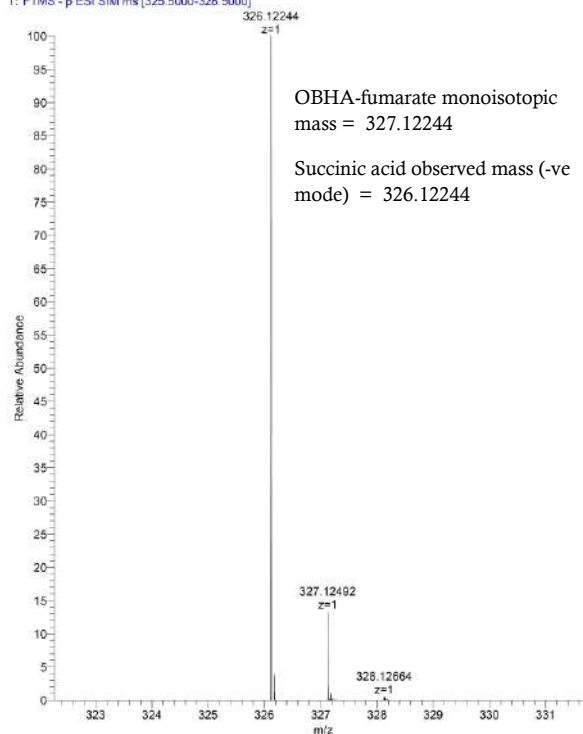
10µM_XMP_Ne_01 #1 RT: 0.00 AV: 1 NL: 3.52E5
T: FTMS - p ESI SIM ms [360.6000-365.5000]



1µM_Succinate_01 #79-90 RT: 0.53-0.61 AV: 12 NL: 1.59E6
T: FTMS - p ESI SIM ms [112.0000-122.0000]



OHBA_Fumaric_acid_1um_DI_Negative_120k #12-45 RT: 0.26-0.99 AV: 34 NL: 3.81E6
T: FTMS - p ESI SIM ms [325.5000-328.5000]



Mass spectra of metabolite standards: 1 µM of each of the metabolite standards were injected into the mass spectrometer H-ESI source using a Hamilton syringe. Ion corresponding to each metabolite was detected by selective ion monitoring using a window of 5.0 m/z on either side of the expected m/z of the respective metabolite. Isotopic distribution could be observed for all metabolite standards.

Annexure II

MjGATase_WT

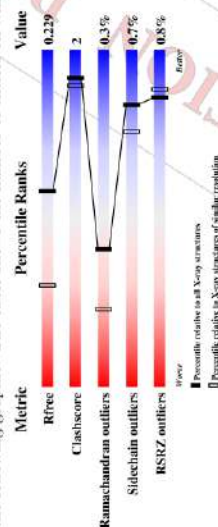
1 Overall quality at a glance

The following experimental techniques were used to determine the structure:

X-RAY DIFFRACTION

The reported resolution of this entry is 1.67 Å.

Percentile scores (ranging between 0-100) for global validation metrics of the entry are shown in the following graphic. The table shows the number of entries on which the scores are based.



Metric	Whole archive (#Entries)	Similar resolution (#Entries, resolution range(Å))
R _{free}	130704	6780 (1.70-1.66)
Clashscore	141614	7510 (1.70-1.66)
Ramachandran outliers	138981	7173 (1.70-1.66)
Sidechain outliers	138945	7172 (1.70-1.66)
RSRZ outliers	127900	6661 (1.70-1.66)

The table below summarises the geometric issues observed across the polymeric chains and their fit to the electron density. The red, orange, yellow and green segments on the lower bar indicate the fraction of residues that contain outliers for >=3, 2, 1 and 0 types of geometric quality criteria respectively. A grey segment represents the fraction of residues that are not modelled. The numeric value for each fraction is indicated below the corresponding segment, with a dot representing fractions <=5%. The upper red bar (where present) indicates the fraction of residues that have poor fit to the electron density. The numeric value is given above the bar.

Mol	Chain	Length	Quality of chain
1	A	188	94% 6%
1	B	188	94% 5%

The following table lists non-polymeric compounds, carbohydrate monomers and non-standard residues in protein, DNA, RNA chains that are outliers for geometric or electron-density-fit criteria:



Preliminary Full wwPDB X-ray Structure Validation Report

Sep 13, 2020 – 03:21 AM EDT

This is a Preliminary Full wwPDB X-ray Structure Validation Report.

This report is produced by the standalone wwPDB validation server.

The structure in question has not been deposited to the wwPDB.

This report should not be submitted to journals.

We welcome your comments at validation@mail.wwpdb.org

A user guide is available at

<https://www.wwpdb.org/validation/2017/XrayValidationReportHelp>

with specific help available everywhere you see the  symbol.

The following versions of software and data (see references ) were used in the production of this report:

MolProbity	: 4.02b-407
Mogul	: 1.8.5 (274361), CSD as541be (2020)
Xtrange (Phenix)	: 1.13
EDS	: 2.14.2
Percentile statistics	: 20191225.v01 (using entries in the PDB archive December 25th 2019)
Refmac	: 5.8.0158
CCP4	: 7.0.044 (Gargrove)
Ideal geometry (proteins)	: Eng & Huber (2001)
Ideal geometry (DNA, RNA)	: Parkinson et al. (1996)
Validation Pipeline (wwPDB-VP)	: 2.14.2

2 Entry composition [i](#)

There are 2 unique types of molecules in this entry. The entry contains 3419 atoms, of which 0 are hydrogens and 0 are deuteriums.

In the tables below, the ZeroOcc column contains the number of atoms modelled with zero occupancy, the AltConf column contains the number of residues with at least one atom in alternate conformation and the Trace column contains the number of residues modelled with at most 2 atoms.

- Molecule 1 is a protein.

Mol	Chain	Residues	Atoms			ZeroOcc	AltConf	Trace		
			Total	C	N				O	S
1	A	188	1453	933	243	270	7	0	0	0
1	B	188	1442	928	241	266	7	0	0	0

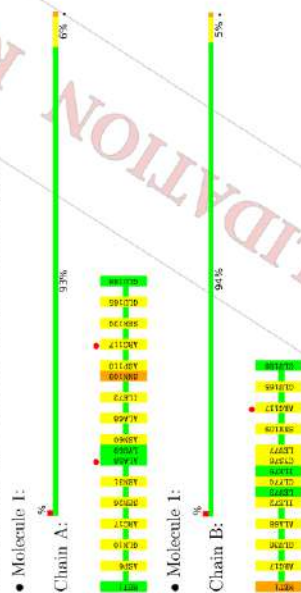
- Molecule 2 is water.

Mol	Chain	Residues	Atoms		ZeroOcc	AltConf
			Total	O		
2	S	524	524	524	0	0

Mol	Type	Chain	Res	Chirality	Geometry	Clashes	Electron density
1	SNN	A	109	-	-	X	-

3 Residue-property plots

These plots are drawn for all protein, RNA, DNA and oligosaccharide chains in the entry. The first graphic for a chain summarises the proportions of the various outlier classes displayed in the second graphic. The second graphic shows the sequence view annotated by issues in geometry and electron density. Residues are color-coded according to the number of geometric quality criteria for which they contain at least one outlier: green = 0, yellow = 1, orange = 2 and red = 3 or more. A red dot above a residue indicates a poor fit to the electron density ($RSRZ > 2$). Stretches of 2 or more consecutive residues without any outlier are shown as a green connector. Residues present in the sample, but not in the model, are shown in grey.



4 Data and refinement statistics

Property	Value	Source
Space group	P 32	Depositor
Cell constants	65.28Å 97.14Å 90.00° 90.00° 120.00°	Depositor
a, b, c, α, β, γ	56.53 – 1.67 36.84 1.67	Depositor
Resolution (Å)	99.4 (56.53-1.67)	EDS
% Data completeness (in resolution range)	99.4 (36.84-1.67)	EDS
R_{merge}	(Not available)	Depositor
R_{split}	(Not available)	Depositor
$\langle I/\sigma(I) \rangle$	4.27 (at 1.08Å)	Xtriage
Refinement program	REFMAC 5.8.0158	Depositor
R, R_{free}	0.167 0.218	DCC
R_{free} test set	0.181 0.220	wwPDB-VP
Wilson B-factor (Å ²)	2667 reflections (5.04%)	Xtriage
Anisotropy	18.5	Xtriage
Bulk solvent k_{vol} (e/Å ³), B_{vol} (Å ²)	0.015	EDS
L-test for twinning ^a	0.34, 43.8	Xtriage
Estimated twinning fraction	$\langle L \rangle = 0.49$; $\langle L^2 \rangle = 0.33$ 0.022 for -h,-k,l 0.466 for h,-k,-l 0.023 for -k,-h,-l	Xtriage
F_o/F_c correlation	0.96	EDS
Total number of atoms	3419	wwPDB-VP
Average B, all atoms (Å ²)	23.0	wwPDB-VP

Xtriage's analysis on translational NCS is as follows: The largest off-origin peak in the Patterson function is 3.98% of the height of the origin peak. No significant pseudotranslation is detected.

^a Intensities estimated from amplitudes.

^b Theoretical values of $\langle |L| \rangle > \langle L^2 \rangle$ for acentric reflections are 0.5, 0.333 respectively for untwinned datasets, and 0.375, 0.2 for perfectly twinned datasets.



5 Model quality [1](#)

5.1 Standard geometry [1](#)

Bond lengths and bond angles in the following residue types are not validated in this section: SNN

The Z score for a bond length (or angle) is the number of standard deviations the observed value is removed from the expected value. A bond length (or angle) with $|Z| > 5$ is considered an outlier worth inspection. RMSZ is the root-mean-square of all Z scores of the bond lengths (or angles).

Mol	Chain	Bond lengths		Bond angles	
		RMSZ	# Z > 5	RMSZ	# Z > 5
1	A	1.17	3/1473 (0.2%)	1.08	3/1991 (0.2%)
1	B	1.16	3/1464 (0.2%)	1.08	4/1981 (0.2%)
All	All	1.16	6/2937 (0.2%)	1.08	7/3972 (0.2%)

All (6) bond length outliers are listed below:

Mol	Chain	Res	Type	Atoms	Z	Observed(Å)	Ideal(Å)
1	B	165	GLU	CD-OE1	5.88	1.32	1.25
1	A	165	GLU	CD-OE1	5.64	1.31	1.25
1	B	36	GLU	CD-OE1	5.33	1.31	1.25
1	A	124	SER	CB-OG	5.28	1.49	1.42
1	A	26	SER	CB-OG	5.23	1.49	1.42
1	B	74	GLY	N-CA	5.14	1.53	1.46

All (7) bond angle outliers are listed below:

Mol	Chain	Res	Type	Atoms	Z	Observed(°)	Ideal(°)
1	A	17	ARG	NE-CZ-NH2	-9.81	115.40	120.30
1	B	17	ARG	NE-CZ-NH2	-9.56	115.52	120.30
1	B	1	MET	CG-SD-CE	-7.17	88.72	100.20
1	B	17	ARG	NE-CZ-NH1	7.17	123.80	120.30
1	A	17	ARG	NE-CZ-NH1	7.03	123.81	120.30
1	A	6	ASP	CB-CG-OD1	6.01	123.71	118.30
1	B	17	ARG	CG-CD-NE	-5.56	100.13	111.80

There are no chirality outliers.

There are no planarity outliers.

5.2 Too-close contacts [1](#)

In the following table, the Non-H and H(model) columns list the number of non-hydrogen atoms and hydrogen atoms in the chain respectively. The H(added) column lists the number of hydrogen atoms added and optimized by MolProbity. The Clashes column lists the number of clashes within the asymmetric unit, whereas Symm-Clashes lists symmetry related clashes.

Mol	Chain	Non-H	H(model)	H(added)	Clashes	Symm-Clashes
1	A	1453	0	1427	7	17
1	B	1442	0	1412	2	17
2	S	521	0	0	1	0
All	All	3419	0	2839	9	17

The all-atom clashscore is defined as the number of clashes found per 1000 atoms (including hydrogen atoms). The all-atom clashscore for this structure is 2.

All (9) close contacts within the same asymmetric unit are listed below, sorted by their clash magnitude.

Atom-1	Atom-2	Interatomic distance (Å)	Interatomic overlap (Å)	Clash overlap (Å)
1:A:109:SNN:N1	1:A:110:ASP:CA	1.71	1.53	1.53
1:A:10:GLN:OE1	1:A:10:GLN:NE2	1.75	1.19	1.19
1:A:109:SNN:C2	1:A:110:ASP:CA	2.62	0.76	0.76
1:A:109:SNN:N1	1:A:110:ASP:CB	2.52	0.72	0.72
1:A:109:SNN:C5	1:A:110:ASP:CA	2.72	0.58	0.58
1:A:117:ARG:NH1	2:S:630:HOHO	2.36	0.58	0.58
1:B:68:ALA:HB3	1:B:72:ILE:HD11	1.98	0.46	0.46
1:A:68:ALA:HB3	1:A:72:ILE:HD11	1.99	0.44	0.44
1:B:76:CVS:O	1:B:77:LEU:C	2.59	0.41	0.41

All (17) symmetry-related close contacts are listed below. The label for Atom-2 includes the symmetry operator and encoded unit-cell translations to be applied.

Atom-1	Atom-2	Interatomic distance (Å)	Clash overlap (Å)
1:A:117:ARG:CZ	1:B:117:ARG:NE1_655	0.42	1.78
1:A:117:ARG:NH2	1:B:117:ARG:CD1_655	0.71	1.49
1:A:117:ARG:NE1	1:B:117:ARG:CZ1_655	1.03	1.17
1:A:117:ARG:NH2	1:B:117:ARG:NE1_655	1.15	1.05
1:A:117:ARG:CD	1:B:117:ARG:CZ1_655	1.19	1.01
1:A:117:ARG:NE	1:B:117:ARG:NH11_655	1.23	0.97
1:A:117:ARG:CD	1:B:117:ARG:NH11_655	1.27	0.93
1:A:117:ARG:CD	1:B:117:ARG:NH21_655	1.42	0.78
1:A:117:ARG:NE	1:B:117:ARG:NE1_655	1.44	0.76

Continued on next page...

Continued from previous page...

Atom-1	Atom-2	Interatomic distance (Å)	Clash overlap (Å)
1:A:117:ARG:CZ	1:B:117:ARG:CZ[1_655]	1.49	0.71
1:A:117:ARG:NH1	1:B:117:ARG:NE[1_655]	1.55	0.65
1:A:117:ARG:CZ	1:B:117:ARG:CD[1_655]	1.57	0.63
1:A:117:ARG:NH2	1:B:117:ARG:CG[1_655]	1.74	0.46
1:A:117:ARG:NH2	1:B:117:ARG:CZ[1_655]	1.84	0.36
1:A:117:ARG:CG	1:B:117:ARG:NH2[1_655]	1.94	0.26
1:A:117:ARG:NH2	1:B:117:ARG:NH2[1_655]	2.11	0.09
1:A:117:ARG:NH1	1:B:117:ARG:CD[1_655]	2.11	0.09

5.3 Torsion angles [ⓘ](#)

5.3.1 Protein backbone [ⓘ](#)

In the following table, the Percentiles column shows the percent Ramachandran outliers of the chain as a percentile score with respect to all X-ray entries followed by that with respect to entries of similar resolution.

The Analysed column shows the number of residues for which the backbone conformation was analysed, and the total number of residues.

Mol	Chain	Analysed	Favoured	Allowed	Outliers	Percentiles
1	A	183/188 (97%)	179 (98%)	3 (2%)	1 (0%)	29 12
1	B	183/188 (97%)	179 (98%)	4 (2%)	0	100 100
All	All	366/376 (97%)	358 (98%)	7 (2%)	1 (0%)	41 23

All (1) Ramachandran outliers are listed below:

Mol	Chain	Res	Type
1	A	60	ASN

5.3.2 Protein sidechains [ⓘ](#)

In the following table, the Percentiles column shows the percent sidechain outliers of the chain as a percentile score with respect to all X-ray entries followed by that with respect to entries of similar resolution.

The Analysed column shows the number of residues for which the sidechain conformation was analysed, and the total number of residues.

Mol	Chain	Analysed	Rotameric	Outliers	Percentiles
1	A	150/159 (94%)	149 (99%)	1 (1%)	84 76
1	B	147/159 (92%)	146 (99%)	1 (1%)	84 76
All	All	297/318 (93%)	295 (99%)	2 (1%)	84 76

All (2) residues with a non-rotameric sidechain are listed below:

Mol	Chain	Res	Type
1	A	31	ASN
1	B	1	MET

Some sidechains can be flipped to improve hydrogen bonding and reduce clashes. All (1) such sidechains are listed below:

Mol	Chain	Res	Type
1	A	31	ASN

5.3.3 RNA [ⓘ](#)

There are no RNA molecules in this entry.

5.4 Non-standard residues in protein, DNA, RNA chains [ⓘ](#)

2 non-standard protein/DNA/RNA residues are modelled in this entry.

In the following table, the Counts column lists the number of bonds (or angles) for which Mogul statistics could be retrieved, the number of bonds (or angles) that are observed in the model and the number of bonds (or angles) that are defined in the Chemical Component Dictionary. The Link column lists molecule types, if any, to which the group is linked. The Z score for a bond length (or angle) is the number of standard deviations the observed value is removed from the expected value. A bond length (or angle) with $|Z| > 2$ is considered an outlier worth inspection. RMSZ is the root-mean-square of all Z scores of the bond lengths (or angles).

Mol	Type	Chain	Res	Link	Bond lengths		Bond angles			
					Counts	RMSZ	# Z > 2	Counts	RMSZ	# Z > 2
1	SNN	A	109	1	7.8,8	1.57	1 (14%)	7,11,11	0.93	0
1	SNN	B	109	1	7.8,8	1.77	1 (14%)	7,11,11	0.87	0

In the following table, the Chirals column lists the number of chiral outliers, the number of chiral centers analysed, the number of these observed in the model and the number defined in the Chemical Component Dictionary. Similar counts are reported in the Torsion and Rings columns. * means no outliers of that kind were identified.



Mol	Type	Chain	Res	Link	Chirals	Torsions	Rings
1	SNN	A	109	1	-	-	0/1/1/1
1	SNN	B	109	1	-	-	0/1/1/1

All (2) bond length outliers are listed below:

Mol	Chain	Res	Type	Atoms	Z	Observed(Å)	Ideal(Å)
1	B	109	SNN	C5-N1	-4.44	1.30	1.37
1	A	109	SNN	C5-N1	-3.78	1.31	1.37

There are no bond angle outliers.

There are no chirality outliers.

There are no torsion outliers.

There are no ring outliers.

1 monomer is involved in 4 short contacts:

Mol	Chain	Res	Type	Clashes	Symm-Clashes
1	A	109	SNN	4	0

5.5 Carbohydrates [i](#)

There are no monosaccharides in this entry.

5.6 Ligand geometry [i](#)

There are no ligands in this entry.

5.7 Other polymers [i](#)

There are no such residues in this entry.

5.8 Polymer linkage issues [i](#)

There are no chain breaks in this entry.

6 Fit of model and data [i](#)

6.1 Protein, DNA and RNA chains [i](#)

In the following table, the column labelled '#RSRZ > 2' contains the number (and percentage) of RSRZ outliers, followed by percent RSRZ outliers for the chain as percentile scores relative to all X-ray entries and entries of similar resolution. The OWAB column contains the minimum, median, 95th percentile and maximum values of the occupancy-weighted average B-factor per residue. The column labelled 'Q < 0.9' lists the number of (and percentage) of residues with an average occupancy less than 0.9.

Mol	Chain	Analysed	<RSRZ>	#RSRZ>2	OWAB(Å ²)	Q<0.9
1	A	187/188 (99%)	-0.66	2 (1%)	80	13, 20, 32, 44
1	B	187/188 (99%)	-0.65	1 (0%)	91	13, 20, 32, 39
All	All	374/376 (99%)	-0.65	3 (0%)	86	13, 20, 32, 44

All (3) RSRZ outliers are listed below:

Mol	Chain	Res	Type	RSRZ
1	A	58	ALA	2.6
1	B	117	ARG	2.3
1	A	117	ARG	2.0

6.2 Non-standard residues in protein, DNA, RNA chains [i](#)

In the following table, the Atoms column lists the number of modelled atoms in the group and the number defined in the chemical component dictionary. The B-factors column lists the minimum, median, 95th percentile and maximum values of B factors of atoms in the group. The column labelled 'Q < 0.9' lists the number of atoms with occupancy less than 0.9.

Mol	Type	Chain	Res	Atoms	RSCC	RSR	B-factors(Å ²)	Q<0.9
1	SNN	B	109	8/?	0.96	0.06	19,19,20,21	0
1	SNN	A	109	8/?	0.97	0.05	18,20,21,21	0

6.3 Carbohydrates [i](#)

There are no monosaccharides in this entry.

6.4 Ligands [i](#)


There are no ligands in this entry.

6.5 Other polymers ⓘ

There are no such residues in this entry.

PRELIMINARY VALIDATION REPORT

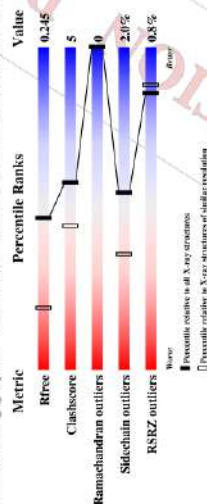
MjGATase_WT bound to acivicin

1 Overall quality at a glance 

The following experimental techniques were used to determine the structure:
X-RAY DIFFRACTION

The reported resolution of this entry is 1.67 Å.

Percentile scores (ranging between 0-100) for global validation metrics of the entry are shown in the following graphic. The table shows the number of entries on which the scores are based.



Metric	Whole archive (# Entries)	Similar resolution (# Entries, resolution range(Å))
R _{free}	130704	6780 (1.70-1.66)
Clashscore	141614	7310 (1.70-1.66)
Ramachandran outliers	138981	7173 (1.70-1.66)
Sidechain outliers	138945	7172 (1.70-1.66)
RSRZ outliers	127900	6661 (1.70-1.66)

The table below summarises the geometric issues observed across the polymeric chains and their fit to the electron density. The red, orange, yellow and green segments on the lower bar indicate the fraction of residues that contain outliers for >=3, 2, 1 and 0 types of geometric quality criteria respectively. A grey segment represents the fraction of residues that are not modelled. The numeric value for each fraction is indicated below the corresponding segment, with a dot representing fractions <=5%. The upper red bar (where present) indicates the fraction of residues that have poor fit to the electron density. The numeric value is given above the bar.

Mol	Chain	Length	Quality of chain
1	A	188	
1	B	188	

The following table lists non-polymeric compounds, carbohydrate monomers and non-standard residues in protein, DNA, RNA chains that are outliers for geometric or electron-density-fit criteria.

EB:



Preliminary Full wwPDB X-ray Structure Validation Report

Sep 14, 2020 – 02:07 AM EDT

This is a Preliminary Full wwPDB X-ray Structure Validation Report.

This report is produced by the standalone wwPDB validation server.

The structure in question has not been deposited to the wwPDB. This report should not be submitted to journals.

We welcome your comments at validation@mail.wwpdb.org

A user guide is available at

<https://www.wwpdb.org/validation/2017/XrayValidationReportHelp> with specific help available everywhere you see the  symbol.

The following versions of software and data (see references ) were used in the production of this report:

MolProbity : 4.02b-467
 Mogul : 1.8.5 (273601), CSD as511bc (2020)
 Xtriage (Phenix) : 1.13
 EDS : 2.14.2
 Percentile statistics : 20191225.v01 (using entries in the PDB archive December 25th 2019)
 Refmac : 5.8.0158
 CCP4 : 7.0.044 (Gargrave)
 Ideal geometry (proteins) : Esch & Huber (2001)
 Ideal geometry (DNA, RNA) : Parkinson et al. (1996)
 Validation Pipeline (wwPDB-VI) : 2.14.2

Mol	Type	Chain	Res	Chirality	Geometry	Clashes	Electron density
1	SNN	A	109	-	-	X	-

2 Entry composition [①](#)

There are 2 unique types of molecules in this entry. The entry contains 3206 atoms, of which 0 are hydrogens and 0 are deuteriums.

In the tables below, the ZeroOcc column contains the number of atoms modelled with zero occupancy, the AltConf column contains the number of residues with at least one atom in alternate conformation and the Trace column contains the number of residues modelled with at most 2 atoms.

- Molecule 1 is a protein.

Mol	Chain	Residues	Atoms			ZeroOcc	AltConf	Trace	
			Total	C	N				O
1	A	188	1468	939	247	275	7	0	0
1	B	188	1472	941	247	277	7	0	0

- Molecule 2 is water.

Mol	Chain	Residues	Atoms			ZeroOcc	AltConf
			Total	O			
2	W	266	266	266	0	0	

3 Residue-property plots

These plots are drawn for all proteins, RNA, DNA and oligosaccharide chains in the entry. The first graphic for a chain summarises the proportions of the various outlier classes displayed in the second graphic. The second graphic shows the sequence view annotated by issues in geometry and electron density. Residues are color-coded according to the number of geometric quality criteria for which they contain at least one outlier: green = 0, yellow = 1, orange = 2 and red = 3 or more. A red dot above a residue indicates a poor fit to the electron density (RSRZ > 2). Stretches of 2 or more consecutive residues without any outlier are shown as a green connector. Residues present in the sample, but not in the model, are shown in grey.

- Molecule 1:



5 Model quality ⁽¹⁾

5.1 Standard geometry ⁽¹⁾

Bond lengths and bond angles in the following residue types are not validated in this section: SNN, 5CS

The Z score for a bond length (or angle) is the number of standard deviations the observed value is removed from the expected value. A bond length (or angle) with $|Z| > 5$ is considered an outlier worth inspection. RMSZ is the root-mean-square of all Z scores of the bond lengths (or angles).

Mol	Chain	Bond lengths		Bond angles	
		RMSZ	# Z > 5	RMSZ	# Z > 5
1	A	1.13	2/1473 (0.1%)	1.07	5/1990 (0.3%)
1	B	1.14	3/1477 (0.2%)	1.03	6/1905 (0.3%)
All	All	1.14	5/2950 (0.2%)	1.05	11/3895 (0.3%)

Chiral center outliers are detected by calculating the chiral volume of a chiral center and verifying if the center is modelled as a planar moiety or with the opposite hand. A planarity outlier is detected by checking planarity of atoms in a peptide group, atoms in a mainchain group or atoms of a sidechain that are expected to be planar.

Mol	Chain	#Chirality outliers	#Planarity outliers
1	B	0	1

All (5) bond length outliers are listed below:

Mol	Chain	Res	Type	Atoms	Z	Observed(Å)	Ideal(Å)
1	B	36	GLU	CD-OE1	8.92	1.35	1.25
1	A	36	GLU	CD-OE2	-7.48	1.17	1.25
1	B	36	GLU	CD-OE2	6.49	1.32	1.25
1	A	25	SER	CB-OG	-5.70	1.34	1.42
1	B	158	TYR	CE1-CZ	5.38	1.45	1.38

All (11) bond angle outliers are listed below:

Mol	Chain	Res	Type	Atoms	Z	Observed(°)	Ideal(°)
1	A	17	ARG	NE-CZ-NH2	-8.21	116.19	120.30
1	A	17	ARG	NE-CZ-NH1	7.33	123.96	120.30
1	B	17	ARG	NE-CZ-NH2	-6.19	117.21	120.30
1	A	110	ASP	CB-CG-OD2	6.13	123.81	118.30
1	A	92	ARG	NE-CZ-NH1	5.87	123.23	120.30
1	B	14	ARG	NE-CZ-NH2	-5.84	117.38	120.30

Continued on next page...



Continued from previous page...

Mol	Chain	Res	Type	Atoms	Z	Observed(°)	Ideal(°)
1	B	110	ASP	CB-CG-OD2	5.80	123.52	118.30
1	A	6	ASP	CB-CG-OD2	-5.61	113.25	118.30
1	B	6	ASP	CB-CG-OD2	-5.56	113.30	118.30
1	B	17	ARG	NE-CZ-NH1	5.50	123.05	120.30
1	B	143	ASP	CB-CG-OD1	5.00	122.80	118.30

There are no chirality outliers.

All (1) planarity outliers are listed below:

Mol	Chain	Res	Type	Group
1	B	76	5CS	Mainchain

5.2 Too-close contacts ⁽¹⁾

In the following table, the Non-H and H(model) columns list the number of non-hydrogen atoms and hydrogen atoms in the chain respectively. The H(added) column lists the number of hydrogen atoms added and optimized by MolProbity. The Clashes column lists the number of clashes within the asymmetric unit, whereas Symm-Clashes lists symmetry related clashes.

Mol	Chain	Non-H	H(model)	H(added)	Clashes	Symm-Clashes
1	A	1468	0	1046	14	2
1	B	1472	0	1451	14	1
2	W	266	0	0	7	1
All	All	3206	0	2897	28	2

The all-atom clashscore is defined as the number of clashes found per 1000 atoms (including hydrogen atoms). The all-atom clashscore for this structure is 5.

All (28) close contacts within the same asymmetric unit are listed below, sorted by their clash magnitude.

Atom-1	Atom-2	Interatomic distance (Å)	Clash overlap (Å)
1:A:109:SNN:N1	1:A:110:ASP:CA	1.69	1.53
1:A:69:LYS:HD3	2:W:250:HOH:O	1.61	1.00
1:B:187:PHE:O	1:B:188:GLU:HB2	1.57	0.98
1:B:117:ARG:HG2	2:W:58:HOH:O	1.76	0.83
1:A:69:LYS:HD2	2:W:91:HOH:O	1.82	0.78
1:A:109:SNN:C2	1:A:110:ASP:CA	2.03	0.76
1:B:187:PHE:O	1:B:188:GLU:CB	2.33	0.72
1:A:109:SNN:C5	1:A:110:ASP:CA	2.68	0.66

Continued on next page...



Continued from previous page...

Atom-1	Atom-2	Interatomic distance (Å)	Clash overlap (Å)
1:A:109:SNV:N1	1:A:110:ASP:Cβ3	2.58	0.61
1:B:188:GLU:OE2	1:B:188:GLU:HA	2.00	0.61
1:B:109:SNV:H42	2:W:38:HOH:O	2.02	0.60
1:B:68:ALA:HB3	1:B:72:ILE:HD11	1.88	0.54
1:B:108:GLU:O	1:B:109:SNV:C2	2.56	0.54
1:A:98:TYR:CE1	1:A:124:SER:HB3	2.43	0.53
1:A:92:ARG:HG2	2:W:517:HOH:O	2.12	0.49
1:A:92:GLY:O	1:A:76:5CS:HF	2.13	0.49
1:B:117:ARG:CD	2:W:58:HOH:O	2.61	0.48
1:A:72:ILE:HG12	1:A:157:ILE:HG12	1.97	0.46
1:B:92:GLY:H	1:B:76:5CS:HF	1.81	0.46
1:A:72:ILE:HD11	1:A:157:ILE:HG23	1.98	0.46
1:B:117:ARG:CG	2:W:58:HOH:O	2.48	0.44
1:A:184:GLY:O	1:A:186:LYS:HE2	2.19	0.42
1:A:98:TYR:CZ	1:A:124:SER:HB3	2.56	0.41
1:B:5:LEU:HD21	1:B:64:ILE:CD1	2.49	0.41
1:B:76:5CS:HD	1:B:77:LEU:H	1.85	0.41
1:B:76:5CS:HD	1:B:77:LEU:N	2.36	0.40
1:A:109:SNV:N1	1:A:110:ASP:C	2.61	0.40
1:B:132:VAL:CG1	1:B:136:PHE:HB2	2.51	0.40

All (2) symmetry-related close contacts are listed below. The label for Atom-2 includes the symmetry operator and encoded unit-cell translations to be applied.

Atom-1	Atom-2	Interatomic distance (Å)	Clash overlap (Å)
1:A:92:ARG:NH2	2:W:238:HOH:O[2_644]	2.08	0.12
1:A:117:ARG:CG	1:B:117:ARG:NH1[1_665]	2.18	0.02

5.3 Torsion angles (1)

5.3.1 Protein backbone (1)

In the following table, the Percentiles column shows the percent Ramachandran outliers of the chain as a percentile score with respect to all X-ray entries followed by that with respect to entries of similar resolution.

The Analysed column shows the number of residues for which the backbone conformation was analysed, and the total number of residues.



Mol	Chain	Analysed	Favoured	Allowed	Outliers	Percentiles
1	A	182/188 (97%)	180 (99%)	2 (1%)	0	100 100
1	B	182/188 (97%)	180 (99%)	2 (1%)	0	100 100
All	All	364/376 (97%)	360 (99%)	4 (1%)	0	100 100

There are no Ramachandran outliers to report.

5.3.2 Protein sidechains (1)

In the following table, the Percentiles column shows the percent sidechain outliers of the chain as a percentile score with respect to all X-ray entries followed by that with respect to entries of similar resolution.

The Analysed column shows the number of residues for which the sidechain conformation was analysed, and the total number of residues.

Mol	Chain	Analysed	Rotameric	Outliers	Percentiles
1	A	152/158 (96%)	150 (99%)	2 (1%)	69 54
1	B	153/158 (97%)	149 (97%)	4 (3%)	46 25
All	All	305/316 (96%)	299 (98%)	6 (2%)	55 36

All (6) residues with a non-rotameric sidechain are listed below:

Mol	Chain	Res	Type
1	A	31	ASN
1	A	45	LYS
1	B	31	ASN
1	B	102	LYS
1	B	117	ARG
1	B	188	GLU

Some sidechains can be flipped to improve hydrogen bonding and reduce clashes. All (2) such sidechains are listed below:

Mol	Chain	Res	Type
1	A	31	ASN
1	B	31	ASN

5.3.3 RNA (1)

There are no RNA molecules in this entry.



5.4 Non-standard residues in protein, DNA, RNA chains [\(i\)](#)

4 non-standard protein/DNA/RNA residues are modelled in this entry.

In the following table, the Counts column lists the number of bonds (or angles) for which Mogul statistics could be retrieved, the number of bonds (or angles) that are observed in the model and the number of bonds (or angles) that are defined in the Chemical Component Dictionary. The Link column lists molecule types, if any, to which the group is linked. The Z score for a bond length (or angle) is the number of standard deviations the observed value is removed from the expected value. A bond length (or angle) with $|Z| > 2$ is considered an outlier worth inspection. RMSZ is the root-mean-square of all Z scores of the bond lengths (or angles).

Mol	Type	Chain	Res	Link	Bond lengths			Bond angles		
					Counts	RMSZ	# Z > 2	Counts	RMSZ	# Z > 2
1	5CS	A	76	1	8.1617	1.95	3 (37%)	7.21.23	6.72	3 (42%)
1	SNN	A	109	1	7.8.8	1.35	1 (14%)	7.11.11	1.69	1 (14%)
1	SNN	B	109	1	7.8.8	3.95	3 (42%)	7.11.11	2.88	4 (57%)
1	5CS	B	76	1	8.16.17	2.09	3 (37%)	7.21.23	6.17	3 (42%)

In the following table, the Chirals column lists the number of chiral outliers, the number of chiral centers analysed, the number of these observed in the model and the number defined in the Chemical Component Dictionary. Similar counts are reported in the Torsion and Rings columns. '-' means no outliers of that kind were identified.

Mol	Type	Chain	Res	Link	Chirals	Torsions	Rings
1	5CS	A	76	1	-	4/7 (24/26)	0/1/1/1
1	SNN	A	109	1	-	-	0/1/1/1
1	SNN	B	109	1	-	-	0/1/1/1
1	5CS	B	76	1	-	5/7 (24/26)	0/1/1/1

All (10) bond length outliers are listed below:

Mol	Chain	Res	Type	Atoms	Z	Observed(A)	Ideal(A)
1	B	109	SNN	C4-C3	-7.63	1.45	1.53
1	B	109	SNN	C5-N1	-6.14	1.28	1.37
1	B	76	5CS	OF-CF	-4.01	1.38	1.44
1	A	76	5CS	OF-CF	-3.47	1.39	1.44
1	A	109	SNN	C5-N1	-3.16	1.32	1.37
1	A	76	5CS	CE-CF	2.86	1.59	1.52
1	B	76	5CS	CE-CF	2.80	1.59	1.52
1	B	109	SNN	O5-C5	2.77	1.28	1.23
1	B	76	5CS	CE-CD	-2.67	1.50	1.53
1	A	76	5CS	O-C	2.08	1.28	1.19

All (11) bond angle outliers are listed below:

Mol	Chain	Res	Type	Atoms	Z	Observed(°)	Ideal(°)
1	A	76	5CS	CE-CF-C1	12.09	136.19	115.08
1	A	76	5CS	OF-CF-C1	-11.35	87.42	109.23
1	B	76	5CS	OF-CF-C1	-10.97	88.17	109.23
1	B	76	5CS	CE-CF-C1	10.93	134.16	115.08
1	A	76	5CS	CD-CE-CF	-5.82	98.97	107.78
1	B	76	5CS	CD-CE-CF	-4.84	100.45	107.78
1	B	109	SNN	O5-C5-C4	4.49	132.32	126.39
1	B	109	SNN	O2-C2-C3	-3.81	123.43	126.18
1	B	109	SNN	C3-C2-N1	3.23	109.79	107.30
1	B	109	SNN	O3-C5-N1	-3.19	120.71	125.00
1	A	109	SNN	C3-C2-N1	3.13	109.72	107.30

There are no chirality outliers.

All (9) torsion outliers are listed below:

Mol	Chain	Res	Type	Atoms
1	A	76	5CS	CE-CD-SG-CB
1	A	76	5CS	CE-CF-Cl-N1
1	A	76	5CS	OF-CF-Cl-C1
1	A	76	5CS	CE-CF-Cl-C1
1	B	76	5CS	CE-CD-SG-CB
1	B	76	5CS	CE-OF-Cl-N1
1	B	76	5CS	OF-CF-Cl-C1
1	B	76	5CS	CE-OF-Cl-C1
1	B	76	5CS	CA-CB-SG-CD

There are no ring outliers.

4 monomers are involved in Π short contacts:

Mol	Chain	Res	Type	Clashes	Symm-Clashes
1	A	76	5CS	1	0
1	A	109	SNN	5	0
1	B	109	SNN	2	0
1	B	76	5CS	3	0

5.5 Carbohydrates [\(i\)](#)

There are no monosaccharides in this entry.

5.6 Ligand geometry [i](#)

There are no ligands in this entry.

5.7 Other polymers [i](#)

There are no such residues in this entry.

5.8 Polymer linkage issues [i](#)

There are no chain breaks in this entry.

6 Fit of model and data [i](#)**6.1 Protein, DNA and RNA chains** [i](#)

In the following table, the column labelled '#RSRZ> 2' contains the number (and percentage) of RSRZ outliers, followed by percent RSRZ outliers for the chain as percentile scores relative to all X-ray entries and entries of similar resolution. The OWAB column contains the minimum, median, 95th percentile and maximum values of the occupancy-weighted average B-factor per residue. The column labelled 'Q<0.9' lists the number of (and percentage) of residues with an average occupancy less than 0.9.

Mol	Chain	Analysed	<RSRZ>	#RSRZ>2	OWAB(Å ²)	Q<0.9
1	A	186/188 (98%)	-0.53	1 (0%)	91, 92	15, 23, 36, 57
1	B	186/188 (98%)	-0.52	2 (1%)	80, 83	14, 23, 36, 55
All	All	372/376 (98%)	-0.53	3 (0%)	86, 88	14, 23, 36, 57

All (3) RSRZ outliers are listed below:

Mol	Chain	Res	Type	RSRZ
1	A	58	ALA	3.1
1	B	188	GLU	2.3
1	B	58	ALA	2.2

6.2 Non-standard residues in protein, DNA, RNA chains [i](#)

In the following table, the Atoms column lists the number of modelled atoms in the group and the number defined in the chemical component dictionary. The B-factors column lists the minimum, median, 95th percentile and maximum values of B factors of atoms in the group. The column labelled 'Q<0.9' lists the number of atoms with occupancy less than 0.9.

Mol	Type	Chain	Res	Atoms	RSCC	RSR	B-factors(Å ²)	Q<0.9
1	5CS	A	76	16/?	0.89	0.14	15,27,36,38	0
1	SNN	B	109	8/?	0.89	0.08	23,24,30,31	0
1	5CS	B	76	16/?	0.91	0.14	14,26,37,42	0
1	SNN	A	109	8/?	0.92	0.09	21,22,23,24	0

6.3 Carbohydrates [i](#)

There are no monosaccharides in this entry.

6.4 Ligands ⓘ

There are no ligands in this entry.

6.5 Other polymers ⓘ

There are no such residues in this entry.

PRELIMINARY VALIDATION REPORT

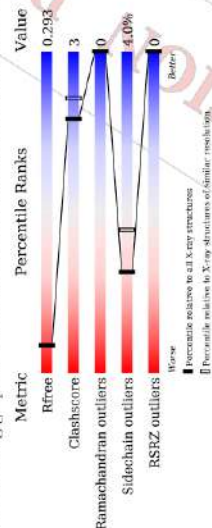
MjGATase_D110G

1 Overall quality at a glance 

The following experimental techniques were used to determine the structure:
X-RAY DIFFRACTION

The reported resolution of this entry is 2.29 Å.

Percentile scores (ranging between 0-100) for global validation metrics of the entry are shown in the following graphic. The table shows the number of entries on which the scores are based.



Metric	Whole archive (#Entries)	Similar resolution (#Entries, resolution range(Å))
R_{free}	137704	5042 (2.30-2.30)
Clashscore	141614	5643 (2.30-2.30)
Ramachandran outliers	138981	5575 (2.30-2.30)
Sidechain outliers	138945	5575 (2.30-2.30)
RSRZ outliers	127900	4938 (2.30-2.30)

The table below summarises the geometric issues observed across the polymeric chains and their fit to the electron density. The red, orange, yellow and green segments on the lower bar indicate the fraction of residues that contain outliers for >=3, 2, 1 and 0 types of geometric quality criteria respectively. A grey segment represents the fraction of residues that are not modelled. The numeric value for each fraction is indicated below the corresponding segment, with a dot representing fractions <=5%. The upper red bar (where present) indicates the fraction of residues that have poor fit to the electron density. The numeric value is given above the bar.

Mol	Chain	Length	Quality of chain
1	A	188	95%



Preliminary Full wwPDB X-ray Structure Validation Report

Sep 21, 2020 – 08:01 PM JST

Deposition ID : D_1300018696

This is a Preliminary Full wwPDB X-ray Structure Validation Report.

This report is produced by the wwPDB Deposition System during initial deposition but before annotation of the structure.

We welcome your comments at validation@mail.wwpdb.org

A user guide is available at

<https://www.wwpdb.org/validation/2017/XrayValidationReportHelp> with specific help available everywhere you see the  symbol.

The following versions of software and data (see references ) were used in the production of this report:

MolProbity	4.02b-107
Xtango (Phenix)	1.13
EDS	2.14.6
Percentile statistics	2019.125.v01 (using entries in the PDB archive December 25th 2019)
Refmac	5.8.0158
CCP4	7.0.044 (Gargrove)
Ideal geometry (proteins)	Engl & Huber (2001)
Ideal geometry (DNA, RNA)	Packinson et al. (1996)
Validation Pipeline (wwPDB-VP)	2.14.6



2 Entry composition

There are 2 unique types of molecules in this entry. The entry contains 1475 atoms, of which 0 are hydrogens and 0 are deuteriums.

In the tables below, the ZeroOcc column contains the number of atoms modelled with zero occupancy, the AltConf column contains the number of residues with at least one atom in alternate conformation and the Trace column contains the number of residues modelled with at most 2 atoms.

- Molecule 1 is a protein.

Mol	Chain	Residues	Atoms				ZeroOcc	AltConf	Trace
			Total	C	N	O	S		
1	A	185	1421	916	237	261	7	0	0

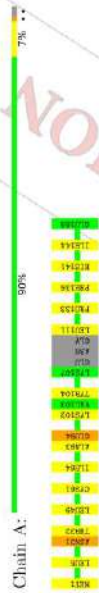
- Molecule 2 is water.

Mol	Chain	Residues	Atoms		ZeroOcc	AltConf
			Total	O		
2	W	54	54	54	0	0

3 Residue-property plots

These plots are drawn for all protein, RNA, DNA and oligosaccharide chains in the entry. The first graphic for a chain summarises the proportions of the various outlier classes displayed in the second graphic. The second graphic shows the sequence view annotated by issues in geometry and electron density. Residues are color-coded according to the number of geometric quality criteria for which they contain at least one outlier: green = 0, yellow = 1, orange = 2 and red = 3 or more. A red dot above a residue indicates a poor fit to the electron density (RSRZ > 2). Stretches of 2 or more consecutive residues without any outlier are shown as a green connector. Residues present in the sample, but not in the model, are shown in grey.

- Molecule 1:



5 Model quality [1](#)

5.1 Standard geometry [1](#)

The Z score for a bond length (or angle) is the number of standard deviations the observed value is removed from the expected value. A bond length (or angle) with $|Z| > 5$ is considered an outlier worth inspection. RMSZ is the root-mean-square of all Z scores of the bond lengths (or angles).

Mol	Chain	Bond lengths		Bond angles	
		RMSZ	# Z > 5	RMSZ	# Z > 5
1	A	0.75	0/1451	0.87	0/1962

Chiral center outliers are detected by calculating the chiral volume of a chiral center and verifying if the center is modelled as a planar moiety or with the opposite hand. A planarity outlier is detected by checking planarity of atoms in a peptide group, atoms in a mainchain group or atoms of a sidechain that are expected to be planar.

Mol	Chain	#Chirality outliers	#Planarity outliers
1	A	0	1

There are no bond length outliers.

There are no bond angle outliers.

There are no chirality outliers.

All (1) planarity outliers are listed below:

Mol	Chain	Res	Type	Group
1	A	53	ALA	Peptide

5.2 Too-close contacts [1](#)

In the following table, the Non-H and H(model) columns list the number of non-hydrogen atoms and hydrogen atoms in the chain respectively. The H(added) column lists the number of hydrogen atoms added and optimized by MolProbity. The Clashes column lists the number of clashes within the asymmetric unit, whereas Symm-Clashes lists symmetry related clashes.

Mol	Chain	Non-H	H(model)	H(added)	Clashes	Symm-Clashes
1	A	1421	0	1409	8	0
2	W	54	0	0	1	0
All	All	1475	0	1409	8	0

The all-atom clashscore is defined as the number of clashes found per 1000 atoms (including

4 Data and refinement statistics [1](#)

Property	Value	Source
Space group	P 21 21 21	Depositor
Cell constants a, b, c, α , β , γ	36.18Å 66.65Å 79.18Å 90.00° 90.00° 90.00°	Depositor
Resolution (Å)	50.99 – 2.29	Depositor
	50.99 – 2.29	EDS
% Data completeness (in resolution range)	88.6 (50.99-2.29)	Depositor
	88.6 (50.99-2.29)	EDS
$R_{average}$	(Not available)	Depositor
R_{sym}	(Not available)	Depositor
$< I/\sigma(I) >$	4.02 (at 2.29Å)	Xtriage
Refinement program	REFMAC 5.8.0238	Depositor
R, R_{free}	0.210 , 0.287	Depositor
	0.215 , 0.293	DCC
R_{free} test set	41.7 reflections (6.18%)	wwPDB-VP
Wilson B-factor (Å ²)	49.1	Xtriage
Anisotropy	-0.102	Xtriage
Bulk solvent k_{sol} (/Å ³), B_{sol} (Å ²)	0.33 , 24.3	EDS
L-test for twinning ²	$< L > \leq 0.48$, $< L^2 > = 0.31$	Xtriage
Estimated twinning fraction	No twinning to report.	Xtriage
F_o/F_c correlation	0.91	EDS
Total number of atoms	1475	wwPDB-VP
Average B, all atoms (Å ²)	18.0	wwPDB-VP

Xtriage's analysis on translational NCS is as follows: *The largest off-origin peak in the Patterson function is 8.25% of the height of the origin peak. No significant pseudotranslation is detected.*

¹ Intensities estimated from amplitudes.
² Theoretical values of $< |L| >$, $< L^2 >$ for acentric reflections are 0.5, 0.333 respectively for untwinned datasets, and 0.375, 0.2 for perfectly twinned datasets.

hydrogen atoms). The all-atom clashscore for this structure is 3.

All (8) close contacts within the same asymmetric unit are listed below, sorted by their clash magnitude.

Atom-1	Atom-2	Interatomic distance (Å)	Clash overlap (Å)
1:A:5:LEU:HD21	1:A:64:ILE:CD1	2.38	0.53
1:A:133:PRO:HG2	1:A:136:PHE:CD1	2.51	0.46
1:A:104:TYR:HB2	1:A:141:HIS:CE1	2.51	0.45
1:A:31:ASN:C	1:A:31:ASN:HD22	2.19	0.45
1:A:31:ASN:HD22	1:A:32:THR:N	2.16	0.43
1:A:49:LEU:HD13	1:A:61:CYS:HB3	2.02	0.41
1:A:5:LEU:CD2	1:A:6:ILE:CD1	2.98	0.41
1:A:94:GLU:HB2	2:W:7:HOH:O	2.21	0.41

There are no symmetry-related clashes.

5.3 Torsion angles [1](#)

5.3.1 Protein backbone [1](#)

In the following table, the Percentiles column shows the percent Ramachandran outliers of the chain as a percentile score with respect to all X-ray entries followed by that with respect to entries of similar resolution.

The Analysed column shows the number of residues for which the backbone conformation was analysed, and the total number of residues.

Mol Chain	Analysed	Favoured	Allowed	Outliers	Percentiles
1 A	181/188 (96%)	176 (97%)	5 (3%)	0	100 100

There are no Ramachandran outliers to report.

5.3.2 Protein sidechains [1](#)

In the following table, the Percentiles column shows the percent sidechain outliers of the chain as a percentile score with respect to all X-ray entries followed by that with respect to entries of similar resolution.

The Analysed column shows the number of residues for which the sidechain conformation was analysed, and the total number of residues.

Mol Chain	Analysed	Rotameric	Outliers	Percentiles
1 A	149/159 (94%)	143 (96%)	6 (4%)	31 44

All (6) residues with a non-rotameric sidechain are listed below:

Mol Chain	Res	Type
1 A	1	MET
1 A	31	ASN
1 A	94	GLU
1 A	102	LYS
1 A	111	LEU
1 A	144	ILE

Some sidechains can be flipped to improve hydrogen bonding and reduce clashes. All (1) such sidechains are listed below:

Mol Chain	Res	Type
1 A	31	ASN

5.3.3 RNA [1](#)

There are no RNA molecules in this entry.

5.4 Non-standard residues in protein, DNA, RNA chains [1](#)

There are no non-standard protein/DNA/RNA residues in this entry.

5.5 Carbohydrates [1](#)

There are no monosaccharides in this entry.

5.6 Ligand geometry [1](#)

There are no ligands in this entry.

5.7 Other polymers [1](#)

There are no such residues in this entry.

5.8 Polymer linkage issues [i](#)

There are no chain breaks in this entry.



6 Fit of model and data [i](#)

6.1 Protein, DNA and RNA chains [i](#)

In the following table, the column labelled '#RSRZ> 2' contains the number (and percentage) of RSRZ outliers, followed by percent RSRZ outliers for the chain as percentile scores relative to all X-ray entries and entries of similar resolution. The OWAB column contains the minimum, median, 95th percentile and maximum values of the occupancy-weighted average B-factor per residue. The column labelled 'Q< 0.9' lists the number of (and percentage) of residues with an average occupancy less than 0.9.

Mol Chain	Analyzed	<RSRZ>	#RSRZ>2	OWAB(A ²)	Q<0.9
1 A	185/188 (98%)	-0.49	0 100 100	10, 17, 29, 47	0

There are no RSRZ outliers to report.

6.2 Non-standard residues in protein, DNA, RNA chains [i](#)

There are no non-standard protein/DNA/RNA residues in this entry.

6.3 Carbohydrates [i](#)

There are no monosaccharides in this entry.

6.4 Ligands [i](#)

There are no ligands in this entry.

6.5 Other polymers [i](#)

There are no such residues in this entry.



MjGATase_N109P

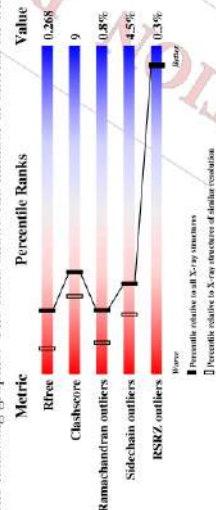
1 Overall quality at a glance 

The following experimental techniques were used to determine the structure:

X-RAY DIFFRACTION

The reported resolution of this entry is 1.80 Å.

Percentile scores (ranging between 0-100) for global validation metrics of the entry are shown in the following graphic. The table shows the number of entries on which the scores are based.



Metric	Whole archive (# Entries)	Similar resolution (# Entries, resolution range(Å))
R_{free}	130704	6207 (1.90-1.90)
Clashscore	141614	6847 (1.90-1.90)
Ramachandran outliers	138981	6760 (1.90-1.90)
Sidechain outliers	138945	6760 (1.90-1.90)
RSRZ outliers	127900	6082 (1.90-1.90)

The table below summarises the geometric issues observed across the polymeric chains and their fit to the electron density. The red, orange, yellow and green segments on the lower bar indicate the fraction of residues that contain outliers for >=3, 2, 1 and 0 types of geometric quality criteria respectively. A grey segment represents the fraction of residues that are not modelled. The numeric value for each fraction is indicated below the corresponding segment, with a dot representing fractions <=5%. The upper red bar (where present) indicates the fraction of residues that have poor fit to the electron density. The numeric value is given above the bar.

Mol	Chain	Length	Quality of chain
1	A	188	78% 20% **
1	B	188	79% 18% *
1	C	188	85% 13% **
1	D	188	76% 21% *



Preliminary Full wwPDB X-ray Structure Validation Report


Sep 13, 2020 – 02:49 AM EDT

This is a Preliminary Full wwPDB X-ray Structure Validation Report.

This report is produced by the standalone wwPDB validation server.
The structure in question has not been deposited to the wwPDB.
This report should not be submitted to journals.

We welcome your comments at validation@mail.wwpdb.org

A user guide is available at

<https://www.wwpdb.org/validation/2017/XrayValidationReportHelp>
with specific help available everywhere you see the  symbol.

The following versions of software and data (see references ) were used in the production of this report:

MolProbity : 4.02b-467
 Xtrunge (Phenix) : 1.13
 EDS : 2.14.2
 Percentile statistics : 20191225.v01 (using entries in the PDB archive December 25th 2019)
 Refmac : 5.8.0158
 CCP4 : 7.0.041 (Gargrave)
 Ideal geometry (proteins) : Engh & Huber (2001)
 Ideal geometry (DNA, RNA) : Parkinson et al. (1996)
 Validation Pipeline (wwPDB-VF) : 2.14.2

2 Entry composition

There are 2 unique types of molecules in this entry. The entry contains 6253 atoms, of which 0 are hydrogens and 0 are deuteriums.

In the tables below, the ZeroOcc column contains the number of atoms modelled with zero occupancy, the AltConf column contains the number of residues with at least one atom in alternate conformation and the Trace column contains the number of residues modelled with at most 2 atoms.

- Molecule 1 is a protein.

Mol	Chain	Residues	Atoms			ZeroOcc	AltConf	Trace			
			C	N	O				S		
1	A	185	Total	1423	919	236	261	7	0	0	0
1	B	188	Total	1414	908	235	264	7	0	0	0
1	C	187	Total	1399	898	232	262	7	0	0	0
1	D	188	Total	1432	921	235	269	7	0	0	0

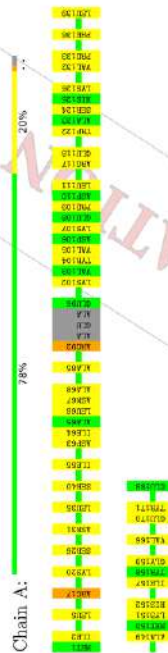
- Molecule 2 is water.

Mol	Chain	Residues	Atoms			ZeroOcc	AltConf
			O	H	D		
2	W	585	Total	585	0	0	0

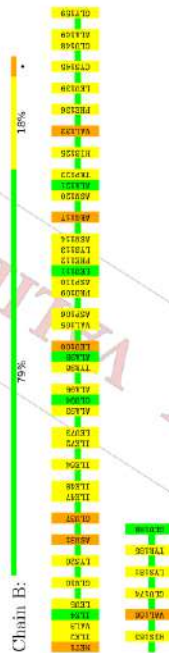
3 Residue-property plots

These plots are drawn for all protein, RNA, DNA and oligosaccharide chains in the entry. The first graphic for a chain summarises the proportions of the various outlier classes displayed in the second graphic. The second graphic shows the sequence view annotated by issues in geometry and electron density. Residues are color-coded according to the number of geometric quality criteria for which they contain at least one outlier: green = 0, yellow = 1, orange = 2 and red = 3 or more. A red dot above a residue indicates a poor fit to the electron density (RSRZ > 2). Stretches of 2 or more consecutive residues without any outlier are shown as a green connector. Residues present in the sample, but not in the model, are shown in grey.

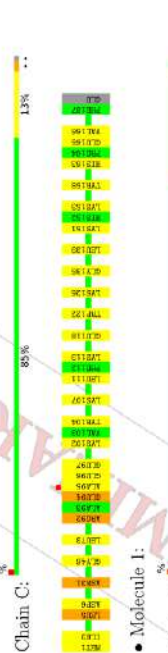
- Molecule 1:



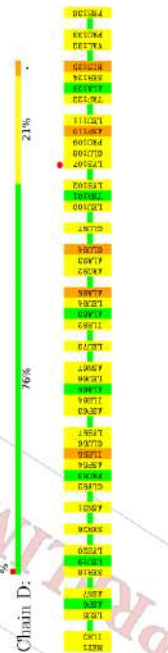
- Molecule 1:



- Molecule 1:



- Molecule 1:



4 Data and refinement statistics 

Property	Value	Source
Space group	P 1	Depositor
Cell constants a, b, c, α , β , γ	35.50Å 68.05Å 75.35Å 90.95° 90.47° 91.45°	Depositor
Resolution (Å)	35.49 1.89 35.49 1.89	Depositor EDS
% Data completeness (in resolution range)	85.3 (35.49-1.89) 93.7 (35.49-1.89)	Depositor EDS
R_{merge}	(Not available)	Depositor
R_{sym}	(Not available)	Depositor
$\langle I/\sigma(I) \rangle$	1.28 (at 1.89Å)	Xtriage
Refinement program	REFMAC5.8.0238	Depositor
R, R_{free}	0.204 0.264 0.210 0.268	Depositor DCC
R_{free} test set	2597 reflections (4.90%)	wwPDB-VP
Wilson B-factor (Å ²)	12.4	Xtriage
Anisotropy	0.058	Xtriage
Bulk solvent k_{sol} (e/Å ³), B_{sol} (Å ²)	0.34, 40.6	EDS
L^2 -test for twinning ^a	$\langle L \rangle = 0.52$, $\langle L^2 \rangle = 0.37$	Xtriage
Estimated twinning fraction	0.035 for h-k,-l 0.047 for -h,k,-l 0.055 for -h,-k,l	Xtriage
Reported twinning fraction	0.773 for H, K, L 0.089 for -h,-k,l 0.059 for h,-k,-l 0.080 for -H, K, -L	Depositor
Outliers	0 of 53050 reflections	Xtriage
F_o/F_e correlation	0.91	EDS
Total number of atoms	6253	wwPDB-VP
Average B, all atoms (Å ²)	14.0	wwPDB-VP

Xtriage's analysis on translational NCS is as follows: *The largest off-origin peak in the Patterson function is 6.00% of the height of the origin peak. No significant pseudotranslation is detected.*

^a Intensities estimated from amplitudes.

^b Theoretical values of $\langle |L| \rangle > \langle L^2 \rangle$ for acentric reflections are 0.5, 0.333 respectively for untwinned datasets, and 0.375, 0.2 for perfectly twinned datasets.

PRELIMINARY VALIDATION REPORT



The all-atom clashscore is defined as the number of clashes found per 1000 atoms (including hydrogen atoms). The all-atom clashscore for this structure is 9.

All (101) close contacts within the same asymmetric unit are listed below, sorted by their clash magnitude.

Atom-1	Atom-2	Interatomic distance (Å)	Clash overlap (Å)
I-B:10:GLN:CB	I-B:10:GLN:OE1	2.25	0.84
I-D:107:LYS:O	I-D:109:PRO:CD	2.30	0.80
I-D:109:PRO:O	I-D:110:ASP:HB2	1.86	0.76
I-D:107:LYS:O	I-D:109:PRO:N	2.22	0.71
I-D:98:ALA:HB3	I-D:125:HIS:O	1.92	0.69
I-B:10:GLN:OE1	I-B:10:GLN:NE2	2.26	0.69
I-D:107:LYS:O	I-D:109:PRO:HD3	1.93	0.68
I-C:163:HIS:ND1	I-C:165:GLU:OE2	2.26	0.68
I-C:116:LYS:CB	2-W:26:HOH:O	2.43	0.67
I-B:100:LEU:HD22	I-B:120:ASN:HB3	1.77	0.67
I-B:31:ASN:C	I-B:31:ASN:HD22	1.98	0.67
I-B:98:TYR:HB3	I-B:122:TRP:CZ2	2.30	0.66
I-A:122:TRP:CD1	I-A:166:VAL:HG21	2.33	0.64
I-D:55:ILE:HD11	I-D:84:LEU:HD12	1.81	0.63
I-C:56:LEU:HD23	I-C:31:ASN:HA	1.82	0.62
I-B:5:LEU:HD21	I-B:6:ILE:CD1	2.30	0.61
I-B:110:ASP:O	I-B:113:LYS:CG	2.49	0.60
I-C:151:LYS:HD2	I-C:158:TYR:CE2	2.36	0.59
I-B:1:MET:HE3	I-B:2:ILE:N	2.17	0.59
I-C:1:MET:HE3	I-C:2:ILE:O	2.02	0.59
I-A:132:VAL:HG12	I-A:136:PHE:HB2	1.85	0.59
I-A:20:LYS:NZ	I-D:94:GLU:OE1	2.35	0.59
I-B:163:HIS:HB3	I-B:166:VAL:HG13	1.84	0.58
I-A:40:SER:OG	2-W:90:HOH:O	2.09	0.58
I-B:1:MET:HE1	I-B:3:VAL:HG23	1.86	0.57
I-D:1:MET:HE3	I-D:2:ILE:C	2.26	0.56
I-B:93:ALA:HB3	I-B:125:HIS:O	2.05	0.56
I-A:122:TRP:CG	I-A:166:VAL:HG21	2.42	0.55
I-B:5:LEU:HD21	I-B:6:ILE:HD13	1.89	0.55
I-B:109:PRO:HB3	I-B:139:LEU:HD22	1.89	0.53
I-D:133:PRO:HB2	I-D:136:PHE:CD1	2.44	0.53
I-D:55:ILE:HD11	I-D:8:LEU:CD1	2.38	0.53
I-B:122:TRP:CD1	I-B:166:VAL:HG21	2.45	0.52
I-C:92:ARG:HD2	I-C:126:LYS:O	2.09	0.52
I-B:95:ALA:HB3	I-B:125:HIS:HE2	1.90	0.52
I-A:105:VAL:HG11	I-A:117:ARG:HH11	1.74	0.52
I-D:63:ASP:OD1	I-D:67:ASN:ND2	2.34	0.51

Continued on next page...



5 Model quality (1)

5.1 Standard geometry (1)

The Z score for a bond length (or angle) is the number of standard deviations the observed value is removed from the expected value. A bond length (or angle) with $|Z| > 5$ is considered an outlier worth inspection. RMSZ is the root-mean-square of all Z scores of the bond lengths (or angles).

Mol	Chain	Bond lengths		Bond angles	
		RMSZ	# Z > 5	RMSZ	# Z > 5
1	A	0.76	0/1454	0.89	1/1969 (0.1%)
1	B	0.78	0/1443	0.91	0/1961
1	C	0.75	0/1430	0.84	0/1946
1	D	0.75	0/1463	0.87	1/1985 (0.1%)
All	All	0.76	0/5790	0.88	2/7861 (0.0%)

There are no bond length outliers.

All (2) bond angle outliers are listed below:

Mol	Chain	Res	Type	Atoms	Z	Observed(°)	Ideal(°)
1	A	17	ARG	NE-CZ-NH1	5.20	122.90	120.30
1	D	125	HIS	CB-CA-C	5.05	120.49	110.40

There are no chirality outliers.

There are no planarity outliers.

5.2 Too-close contacts (1)

In the following table, the Non-H and H(model) columns list the number of non-hydrogen atoms and hydrogen atoms in the chain respectively. The H(added) column lists the number of hydrogen atoms added and optimized by MolProbity. The Clashes column lists the number of clashes within the asymmetric unit, whereas Symm-Clashes lists symmetry related clashes.

Mol	Chain	Non-H	H(model)	H(added)	Clashes	Symm-Clashes
1	A	1423	0	1399	24	0
1	B	1414	0	1362	30	0
1	C	1399	0	1341	20	0
1	D	1432	0	1396	30	0
2	W	585	0	0	2	0
All	All	6253	0	5498	101	0



Continued from previous page...

Atom-1	Atom-2	Interatomic distance (Å)	Clash overlap (Å)
1:A:139:LEU:HD11	1:A:151:LYS:HB2	2.01	0.42
1:B:11:ASN:HB2	1:B:174:GLU:HG2	2.01	0.42
1:A:3:LEU:HD21	1:A:64:ILE:HD13	2.01	0.42
1:B:181:LYS:HA	1:B:185:TYR:O	2.20	0.42
1:A:151:LYS:HA	1:A:157:ILE:O	2.20	0.42
1:D:54:ASP:OD2	1:D:57:LYS:HG2	2.20	0.42
1:D:122:TRP:CD1	1:D:166:VAL:HG21	2.35	0.42
1:C:2:ILE:HA	1:C:46:GLY:O	2.21	0.41
1:D:132:VAL:HG21	1:D:138:ILE:HG12	2.02	0.41
1:D:18:SER:OG	1:D:165:GLU:O	2.35	0.41
1:B:145:CYS:HB3	1:B:148:GLU:OE2	2.21	0.41
1:B:47:ILE:O	1:B:72:ILE:HA	2.20	0.41
1:D:97:GLU:O	1:D:121:SER:HA	2.21	0.41
1:D:1:MET:CE	1:D:2:ILE:C	2.88	0.41
1:A:151:LYS:HG2	1:A:152:HIS:O	2.21	0.41
1:A:107:LYS:C	1:A:109:PRO:HD3	2.40	0.41
1:B:109:PRO:HG2	1:B:112:PHE:HB2	2.01	0.41
1:B:132:VAL:HG13	1:B:136:PHE:HB2	2.03	0.40
1:C:122:TRP:CD1	1:C:168:VAL:HG21	2.56	0.40
1:A:170:GLU:HB3	1:A:171:TYR:CD2	2.56	0.40
1:A:63:ASP:OD1	1:A:67:ASN:ND2	2.54	0.40
1:C:122:TRP:HB3	1:C:166:VAL:HG21	2.04	0.40
1:D:73:LEU:HA	1:D:158:TYR:O	2.22	0.40

There are no symmetry-related clashes.

5.3 Torsion angles

5.3.1 Protein backbone

In the following table, the Percentiles column shows the percent Ramachandran outliers of the chain as a percentile score with respect to all X-ray entries followed by that with respect to entries of similar resolution.

The Analysed column shows the number of residues for which the backbone conformation was analysed, and the total number of residues.

Mol	Chain	Analysed	Favoured	Allowed	Outliers	Percentiles
1	A	181/188 (96%)	175 (97%)	6 (3%)	0	100
1	B	186/188 (99%)	179 (96%)	7 (4%)	0	100

Continued on next page...



Continued from previous page...

Atom-1	Atom-2	Interatomic distance (Å)	Clash overlap (Å)
1:A:149:ALA:HA	1:A:159:GLY:O	2.10	0.51
1:D:5:LEU:HD21	1:D:64:ILE:CD1	2.41	0.51
1:B:105:VAL:HG11	1:B:117:ARG:HH21	1.76	0.50
1:C:163:HIS:O	1:C:166:VAL:HG22	2.12	0.50
1:D:130:LEU:HD21	1:D:151:LYS:HG2	1.92	0.50
1:A:5:LEU:HD21	1:A:64:ILE:CD1	2.43	0.49
1:D:109:PRO:O	1:D:110:ASP:CB	2.59	0.49
1:C:102:LYS:HE3	1:C:118:GLU:OE1	2.13	0.48
1:A:92:ARG:CD	1:A:126:LYS:O	2.61	0.48
1:D:1:MET:HE3	1:D:2:ILE:O	2.13	0.48
1:B:1:MET:C	1:B:1:MET:HE3	2.33	0.48
1:A:92:ARG:HD2	1:A:126:LYS:O	2.14	0.48
1:D:56:GLU:OE2	1:D:56:GLU:HA	2.14	0.48
1:D:7:ASN:O	1:D:92:GLY:HA3	2.14	0.48
1:D:163:HIS:O	1:D:166:VAL:HG22	2.15	0.47
1:A:122:TRP:CB	1:A:166:VAL:HG21	2.45	0.47
1:B:105:VAL:HG11	1:B:117:ARG:HH2	2.30	0.46
1:B:31:ASN:ND2	1:B:31:ASN:C	2.68	0.46
1:B:149:ALA:HA	1:B:159:GLY:O	2.16	0.46
1:A:66:LEU:HD21	1:A:85:ALA:O	2.16	0.46
1:C:73:LEU:HA	1:C:158:TYR:O	2.16	0.46
1:D:109:PRO:HB3	1:D:139:LEU:HD22	1.97	0.46
1:B:48:ILE:HA	1:B:73:LEU:O	2.16	0.45
1:A:104:TYR:CD1	1:A:118:GLU:HG2	2.52	0.45
1:A:139:LEU:HD11	1:A:151:LYS:CB	2.47	0.45
1:D:82:ILE:O	1:D:85:ALA:HB3	2.17	0.45
1:B:20:LYS:NZ	1:C:94:GLU:HA	2.32	0.44
1:D:2:ILE:O	1:D:26:SER:HB2	2.18	0.44
1:D:66:LEU:HD23	1:D:66:LEU:HA	1.85	0.44
1:A:2:ILE:O	1:A:26:SER:HA	2.17	0.44
1:B:117:ARG:HD3	1:B:117:ARG:HA	1.48	0.43
1:C:102:LYS:HD3	1:C:104:TYR:OH	2.18	0.43
1:C:6:ASP:O	1:C:31:ASN:HB3	2.18	0.43
1:C:1:MET:CE	1:C:2:ILE:C	2.87	0.43
1:A:33:PRO:HB2	1:A:136:PHE:CD1	2.53	0.43
1:A:35:LEU:HD11	1:A:68:ALA:HA	2.00	0.43
1:B:37:GLU:HG2	1:D:100:LEU:HG	2.01	0.43
1:C:1:MET:HE3	1:C:2:ILE:C	2.39	0.43
1:C:139:LEU:HD11	1:C:151:LYS:HB2	2.01	0.43
1:C:135:GLY:O	1:C:153:LYS:HB2	2.19	0.43
1:C:95:ALA:HD1	1:C:97:GLU:HG2	2.00	0.42

Continued on next page...



Continued from previous page...

Mol Chain	Analysed	Favoured	Allowed	Outliers	Percentiles
1 C	185/188 (98%)	176 (95%)	6 (3%)	3 (2%)	9 2
1 D	186/188 (99%)	175 (94%)	8 (4%)	3 (2%)	9 2
All	738/752 (98%)	705 (96%)	27 (4%)	6 (1%)	19 9

All (6) Ramachandran outliers are listed below:

Mol Chain	Res	Type
1 D	108	GLU
1 D	110	ASP
1 C	94	GLU
1 C	107	LYS
1 D	85	ALA
1 C	96	GLU

5.3.2 Protein sidechains (1)

In the following table, the Percentiles column shows the percent sidechain outliers of the chain as a percentile score with respect to all X-ray entries followed by that with respect to entries of similar resolution.

The Analysed column shows the number of residues for which the sidechain conformation was analysed, and the total number of residues.

Mol Chain	Analysed	Rotameric	Outliers	Percentiles
1 A	147/160 (92%)	140 (95%)	7 (5%)	25 16
1 B	143/160 (89%)	135 (94%)	8 (6%)	21 11
1 C	142/160 (89%)	138 (97%)	4 (3%)	43 36
1 D	148/160 (92%)	141 (95%)	7 (5%)	26 16
All	580/640 (91%)	554 (96%)	26 (4%)	27 18

All (26) residues with a non-rotameric sidechain are listed below:

Mol Chain	Res	Type
1 A	17	ARG
1 A	31	ASN
1 A	55	ILE
1 A	92	ARG
1 A	102	LYS
1 A	111	LEU

Continued on next page...



Continued from previous page...

Mol Chain	Res	Type
1 A	124	SER
1 B	1	MET
1 B	31	ASN
1 B	37	GLU
1 B	100	LEU
1 B	106	ASP
1 B	117	ARG
1 B	132	VAL
1 B	166	VAL
1 C	5	LEU
1 C	31	ASN
1 C	92	ARG
1 C	111	LEU
1 D	20	LYS
1 D	31	ASN
1 D	55	ILE
1 D	92	ARG
1 D	94	GLU
1 D	102	LYS
1 D	111	LEU

Some sidechains can be flipped to improve hydrogen bonding and reduce clashes. All (9) such sidechains are listed below:

Mol Chain	Res	Type
1 A	7	ASN
1 A	16	HIS
1 A	31	ASN
1 B	31	ASN
1 C	16	HIS
1 C	31	ASN
1 C	114	ASN
1 D	31	ASN
1 D	168	HIS

5.3.3 RNA (1)

There are no RNA molecules in this entry.



5.4 Non-standard residues in protein, DNA, RNA chains [1](#)

There are no non-standard protein/DNA/RNA residues in this entry.

5.5 Carbohydrates [1](#)

There are no monosaccharides in this entry.

5.6 Ligand geometry [1](#)

There are no ligands in this entry.

5.7 Other polymers [1](#)

There are no such residues in this entry.

5.8 Polymer linkage issues [1](#)

There are no chain breaks in this entry.

6 Fit of model and data [1](#)

6.1 Protein, DNA and RNA chains [1](#)

In the following table, the column labelled '#RSRZ> 2' contains the number (and percentage) of RSRZ outliers, followed by percent RSRZ outliers for the chain as percentile scores relative to all X-ray entries and entries of similar resolution. The OWAB column contains the minimum, median, 95th percentile and maximum values of the occupancy-weighted average B-factor per residue. The column labelled 'Q< 0.9' lists the number of (and percentage) of residues with an average occupancy less than 0.9.

Mol Chain	Analysed	<RSRZ>	#RSRZ>2	OWAB(Å)	Q<0.9
1 A	187/188 (98%)	-0.06	0 100 100	7, 11, 19, 26	0
1 B	188/188 (100%)	-0.06	0 100 100	6, 11, 20, 26	0
1 C	187/188 (99%)	0.12	1 (0%) 91 92	7, 15, 24, 44	0
1 D	188/188 (100%)	0.02	1 (0%) 91 92	7, 14, 22, 35	0
All	748/752 (99%)	0.00	2 (0%) 91 91	6, 13, 22, 44	0

All (2) RSRZ outliers are listed below:

Mol Chain	Res	Type	RSRZ
1 C	95	ALA	5.0
1 D	107	LYS	2.2

6.2 Non-standard residues in protein, DNA, RNA chains [1](#)

There are no non-standard protein/DNA/RNA residues in this entry.

6.3 Carbohydrates [1](#)

There are no monosaccharides in this entry.

6.4 Ligands [1](#)

There are no ligands in this entry.

6.5 Other polymers [1](#)

There are no such residues in this entry.

Rights and Permissions

6/8/2020

RightsLink Printable License

ELSEVIER LICENSE TERMS AND CONDITIONS

Jun 08, 2020

This Agreement between Ms. Apama Dongre ("You") and Elsevier ("Elsevier") consists of your license details and the terms and conditions provided by Elsevier and Copyright Clearance Center.

License Number	4844131284088
License date	Jun 08, 2020
Licensed Content Publisher	Elsevier
Licensed Content Publication	Trends in Parasitology
Licensed Content Title	The Plasmodium sporozoite journey: a rite of passage
Licensed Content Author	Stefan H.I. Kappe,Karine Kaiser,Kai Matuschewski
Licensed Content Date	Mar 1, 2003
Licensed Content Volume	19
Licensed Content Issue	3
Licensed Content Pages	9
Start Page	135
End Page	143
Type of Use	reuse in a thesis/dissertation
Portion	figures/tables/illustrations

<https://s100.copyright.com/AppDispatchServlet>

1/7

4/16/2020

RightsLink Printable License

ELSEVIER LICENSE
TERMS AND CONDITIONS

Apr 16, 2020

This Agreement between Ms. Apama Dongre ("You") and Elsevier ("Elsevier") consists of your license details and the terms and conditions provided by Elsevier and Copyright Clearance Center.

License Number	4810710431252
License date	Apr 16, 2020
Licensed Content Publisher	Elsevier
Licensed Content Publication	Trends in Parasitology
Licensed Content Title	The Plasmodium sporozoite journey: a rite of passage
Licensed Content Author	Stefan H.I. Kappe,Karine Kaiser,Kai Matuschewski
Licensed Content Date	Mar 1, 2003
Licensed Content Volume	19
Licensed Content Issue	3
Licensed Content Pages	9
Start Page	135
End Page	143
Type of Use	reuse in a thesis/dissertation
Portion	figures/tables/illustrations

<https://s100.copyright.com/AppDispatchServlet>

1/7

6/9/2020

RightsLink Printable License

SPRINGER NATURE LICENSE
TERMS AND CONDITIONS

Jun 09, 2020

This Agreement between Ms. Apama Dongre ("You") and Springer Nature ("Springer Nature") consists of your license details and the terms and conditions provided by Springer Nature and Copyright Clearance Center.

License Number	4844630513323
License date	Jun 09, 2020
Licensed Content Publisher	Springer Nature
Licensed Content Publication	Springer eBook
Licensed Content Title	The Plasmodium Tricarboxylic Acid Cycle and Mitochondrial Metabolism
Licensed Content Author	Simon A. Cobbold, Malcolm J. McConville
Licensed Content Date	Jan 1, 2014
Type of Use	Thesis/Dissertation
Requestor type	academic/university or research institute
Format	print and electronic
Portion	figures/tables/illustrations
Number of figures/tables/illustrations	1
Will you be translating?	no

<https://s100.copyright.com/AppDispatchServlet>

1/5

4/21/2020

RightsLink Printable License

SPRINGER NATURE LICENSE
TERMS AND CONDITIONS

Apr 21, 2020

This Agreement between Ms. Apama Dongre ("You") and Springer Nature ("Springer Nature") consists of your license details and the terms and conditions provided by Springer Nature and Copyright Clearance Center.

License Number	4813511069279
License date	Apr 21, 2020
Licensed Content Publisher	Springer Nature
Licensed Content Publication	Springer eBook
Licensed Content Title	Purine and Pyrimidine Pathways
Licensed Content Author	Hilda A. Namanja-Magliano, Rodrigo G. Ducati, Vern L. Schramm
Licensed Content Date	Jan 1, 2013
Type of Use	Thesis/Dissertation
Requestor type	academic/university or research institute
Format	print and electronic
Portion	figures/tables/illustrations
Number of figures/tables/illustrations	1
Will you be translating?	no

<https://s100.copyright.com/AppDispatchServlet>

1/5

3/30/2020

RightsLink Printable License

SPRINGER NATURE LICENSE
TERMS AND CONDITIONS

Mar 30, 2020

This Agreement between Ms. Apama Dongre ("You") and Springer Nature ("Springer Nature") consists of your license details and the terms and conditions provided by Springer Nature and Copyright Clearance Center.

License Number	4798800585883
License date	Mar 30, 2020
Licensed Content Publisher	Springer Nature
Licensed Content Publication	Nature Reviews Microbiology
Licensed Content Title	Advances in molecular genetic systems in malaria
Licensed Content Author	Tania F. de Koning-Ward et al
Licensed Content Date	May 15, 2015
Type of Use	Thesis/Dissertation
Requestor type	academic/university or research institute
Format	print and electronic
Portion	figures/tables/illustrations
Number of figures/tables/illustrations	2
High-res required	no

<https://s100.copyright.com/AppDispatchServlet>

1/5

7/6/2020

RightsLink Printable License

ELSEVIER LICENSE
TERMS AND CONDITIONS

Jul 06, 2020

This Agreement between Ms. Apama Dongre ("You") and Elsevier ("Elsevier") consists of your license details and the terms and conditions provided by Elsevier and Copyright Clearance Center.

License Number	4863000657412
License date	Jul 06, 2020
Licensed Content Publisher	Elsevier
Licensed Content Publication	Trends in Parasitology
Licensed Content Title	Molecules targeting the purine salvage pathway in Apicomplexan parasites
Licensed Content Author	Arnaud Ghérardi,Marie-Elisabeth Sarciron
Licensed Content Date	Aug 1, 2007
Licensed Content Volume	23
Licensed Content Issue	8
Licensed Content Pages	6
Start Page	384
End Page	389
Type of Use	reuse in a thesis/dissertation

<https://s100.copyright.com/AppDispatchServlet>

1/7

7/6/2020

RightsLink Printable License

SPRINGER NATURE LICENSE
TERMS AND CONDITIONS

Jul 06, 2020

This Agreement between Ms. Apama Dongre ("You") and Springer Nature ("Springer Nature") consists of your license details and the terms and conditions provided by Springer Nature and Copyright Clearance Center.

License Number	4863010532073
License date	Jul 06, 2020
Licensed Content Publisher	Springer Nature
Licensed Content Publication	Nature Reviews Genetics
Licensed Content Title	Genome editing with engineered zinc finger nucleases
Licensed Content Author	Fyodor D. Urnov et al
Licensed Content Date	Dec 31, 1969
Type of Use	Thesis/Dissertation
Requestor type	academic/university or research institute
Format	print and electronic
Portion	figures/tables/illustrations
Number of figures/tables/illustrations	1
Will you be translating?	no

<https://s100.copyright.com/AppDispatchServlet>

1/5

6/15/2020

Zimbra

Zimbra

aparna@jncasr.ac.in

Fw: Need permission for reprint

From : CurrentScience Association <edcursci@ias.ac.in> Fri, Jun 12, 2020 02:23 PM
Subject : Fw: Need permission for reprint
To : aparna@jncasr.ac.in

Dear Ms Dongre,

Thank you for your mail seeking permission to reproduce a figure from the following article:

Figure 1 from the article 'Crosstalk between purine nucleotide metabolism and mitochondrial pathways in Plasmodium falciparum. Vijay Jayaraman, Vinay Bulusu and Hemalatha Balam. CURRENT SCIENCE, 10 March 2012, Vol. 102(5), pp. 757–766'.

We hereby grant you permission, free of cost (as it is for academic purpose and not for any commercial use), to reproduce the above mentioned figure in your PhD thesis to be submitted to Jawaharlal Nehru Centre for Advanced Scientific Research (JNCASR), Bengaluru.

Kindly acknowledge the source properly. We urge you to keep the authors informed.

Thanking you,

With regards,
 G. Madhavan
 Executive Secretary
 Current Science Association

From: aparna@jncasr.ac.in <aparna@jncasr.ac.in>
Sent: 12 June 2020 12:12
To: CurrentScience <csc@ias.ac.in>
Subject: Need permission for reprint

Dear Sir/Madam,

I am Aparna Dongre, a PhD student in Jawaharlal Nehru Centre for Advanced Scientific Research, Bangalore. I would reproduce figure 1 from article cited below

"Jayaraman, V., Bulusu, V., & Balam, H. (2012). Crosstalk between purine nucleotide metabolism and mitochondrial pathways in Plasmodium falciparum. Current Science, 102(5), 757" in my doctoral dissertation. Kindly grant me permission to do so.

Thank you.

Regards

--

Aparna Vilas Dongre
 c/o, Prof. Hemalatha Balam,
 Molecular Parasitology and Protein Engineering Lab,
 Molecular Biology and Genetics Unit,

6/15/2020

RightsLink Printable License

AMERICAN DIABETES ASSOCIATION ORDER DETAILS

Jun 15, 2020

Order Number	501576613
Order date	Jun 15, 2020
Licensed Content Publisher	American Diabetes Association
Licensed Content Publication	Diabetes
Licensed Content Title	Inactivation of Glyceraldehyde-3-Phosphate Dehydrogenase by Fumarate in Diabetes
Licensed Content Author	Matthew Blatnik,Norma Frizzell,Suzanne R. Thorpe,John W. Baynes
Licensed Content Date	Jan 1, 2008
Licensed Content Volume	57
Licensed Content Issue	1
Type of Use	Thesis/Dissertation
Requestor type	Academic institution
Format	Print, Electronic
Portion	chart/graph/table/figure
Number of charts/graphs/tables/figures	1

Rights for Main product

<https://s100.copyright.com/AppDispatchServlet>

1/2

6/11/2020

Zimbra

Zimbra

aparna@jncasr.ac.in

Re: Permission to reproduce material

From : Martine Zilversmit <zilversmit@nyu.edu> Thu, Jun 11, 2020 08:05 AM
Subject : Re: Permission to reproduce material
To : aparna@jncasr.ac.in
Cc : Susan Perkins <perkins@amnh.org>

Hi, Aparna.

I'm not sure if Susan already replied, but free to use the table. The article is a bit out of date on the diversity of the genus as many more species have been named and discovered, but the table is correct.

Best of luck,

Martine

On Mon, Jun 8, 2020 at 5:39 AM <aparna@jncasr.ac.in> wrote:

Dear Martine and Susan,

I am Aparna Dongre, a Ph.D. student in Jawaharal Nehru Center for Advanced Scientific Research, Bangalore, India. Recently, I came across your writing on **Tree of Life Plasmodium. Malaria Parasites**. It was informative article. I would like to reproduce the table titled "**Hosts and Geographic Distribution of Some Parasites**" from that article in my thesis. I would be obliged if you could grant me permission to use the material. Thank you.

Regards

--

Aparna Vilas Dongre
c/o, Prof. Hemalatha Balam,
Molecular Parasitology and Protein Engineering Lab,
Molecular Biology and Genetics Unit,
Jawaharal Nehru Centre for Advanced Scientific Research,
Jakkur, Bangalore-560064,
Karnataka, India.
Contact- (080) 2208 2813/2858

2/29/2020

RightsLink Printable License

SPRINGER NATURE LICENSE
TERMS AND CONDITIONS

Feb 29, 2020

This Agreement between Ms. Aparna Dongre ("You") and Springer Nature ("Springer Nature") consists of your license details and the terms and conditions provided by Springer Nature and Copyright Clearance Center.

License Number	4778091016839
License date	Feb 29, 2020
Licensed Content Publisher	Springer Nature
Licensed Content Publication	Nature Chemical Biology
Licensed Content Title	Features and regulation of non-enzymatic post-translational modifications
Licensed Content Author	Robert Harmel et al
Licensed Content Date	Feb 14, 2018
Type of Use	Thesis/Dissertation
Requestor type	academic/university or research institute
Format	print and electronic
Portion	figures/tables/illustrations
Number of figures/tables/illustrations	1
High-res required	no

<https://s100.copyright.com/AppDispatchServlet>

1/5

ELSEVIER LICENSE
TERMS AND CONDITIONS

Dec 01, 2020

This Agreement between Ms. Aparna Dongre ("You") and Elsevier ("Elsevier") consists of your license details and the terms and conditions provided by Elsevier and Copyright Clearance Center.

License Number	4851911464196
License date	Jun 18, 2020
Licensed Content Publisher	Elsevier
Licensed Content Publication	Biochimica et Biophysica Acta (BBA) - General Subjects
Licensed Content Title	Enhanced sampling techniques in molecular dynamics simulations of biological systems
Licensed Content Author	Rafael C. Bernardi, Marcelo C.R. Melo, Klaus Schulten
Licensed Content Date	May 1, 2015
Licensed Content Volume	1850
Licensed Content Issue	5
Licensed Content Pages	6
Start Page	872
End Page	877
Type of Use	reuse in a thesis/dissertation
Portion	figures/tables/illustrations
Number of figures/tables/illustrations	2
Format	both print and electronic
Are you the author of this Elsevier article?	No
Will you be translating?	No
Title	Study of the Structural Basis for the hyperthermostability of an Archaeal Glutaminase Induced By Post-Translational Succinimide Formation
Institution name	Jawahar Lal Nehru Centre for Advanced Scientific Research (JNCASR)
Expected presentation date	Jun 2020
Portions	Figure 2, Figure 3
Requestor Location	Ms. Aparna Dongre Student's residence, JNCASR Jakkur, Bangalore

<https://s100.copyright.com/MyAccount/web/jsp/viewprintablelicensefrommyorders.jsp?ref=517cf31f-d3e7-411b-848e-d37a4865f5db&email=>

1/5

References

- Abdelmegeed, Mohamed A. and Byoung Joon Song. 2014. "Functional Roles of Protein Nitration in Acute and Chronic Liver Diseases." *Oxidative Medicine and Cellular Longevity* 2014.
- Abello, Nicolas, Huib A. M. Kerstjens, Dirkje S. Postma, and Rainer Bischoff. 2009. "Protein Tyrosine Nitration: Selectivity, Physicochemical and Biological Consequences, Denitration, and Proteomics Methods for the Identification of Tyrosine-Nitrated Proteins." *Journal of Proteome Research* 8(7):3222–38.
- Abulimiti, Abuduaini, Xiaolei Qiu, Jing Chen, Yang Liu, and Zengyi Chang. 2003. "Reversible Methionine Sulfoxidation of Mycobacterium Tuberculosis Small Heat Shock Protein Hsp16.3 and Its Possible Role in Scavenging Oxidants." *Biochemical and Biophysical Research Communications* 305(1):87–93.
- Adams, Paul D., Pavel V. Afonine, Gábor Bunkóczi, Vincent B. Chen, Ian W. Davis, Nathaniel Echols, Jeffrey J. Headd, Li Wei Hung, Gary J. Kapral, Ralf W. Grosse-Kunstleve, Airlie J. McCoy, Nigel W. Moriarty, Robert Oeffner, Randy J. Read, David C. Richardson, Jane S. Richardson, Thomas C. Terwilliger, and Peter H. Zwart. 2010. "PHENIX: A Comprehensive Python-Based System for Macromolecular Structure Solution." *Acta Crystallographica Section D: Biological Crystallography* 66(2):213–21.
- Akematsu, Takahiko, Andrew Findlay, Yasuhiro Fukuda, Ronald E. Pearlman, Josef Loidl, Eduardo Orias, and Eileen P. Hamilton. 2018. "Resistance to 6-Methylpurine Is Conferred by Defective Adenine Phosphoribosyltransferase in Tetrahymena." *Genes* 9(4).
- Alderson, Nathan L., Yuping Wang, Matthew Blatnik, Norma Frizzell, Michael D. Walla, Timothy J. Lyons, Nadja Alt, James A. Carson, Ryoji Nagai, Suzanne R. Thorpe, and John W. Baynes. 2006. "S-(2-Succinyl)Cysteine: A Novel Chemical Modification of Tissue Proteins by a Krebs Cycle Intermediate." *Archives of Biochemistry and Biophysics* 450(1):1–8.
- Alexander, David L., Jeffrey Mital, Gary E. Ward, Peter Bradley, and John C. Boothroyd. 2005. "Identification of the Moving Junction Complex of Toxoplasma Gondii: A Collaboration between Distinct Secretory Organelles." *PLoS Pathogens* 1(2):0137–49.
- Ali, Rustam, Sanjeev Kumar, Hemalatha Balaram, and Siddhartha P. Sarma. 2013. "Solution Nuclear Magnetic Resonance Structure of the GATase Subunit and Structural Basis of the Interaction between GATase and ATPase Subunits in a Two-Subunit-Type GMPS from Methanocaldococcus Jannaschii." *Biochemistry* 52(25):4308–23.
- Ali, Syed Nasir and Keith Alec Fletcher. 1985. "Carbohydrate Metabolism of Malarial Parasites-I. Metabolism of Lactate in Plasmodium Knowlesi Infected Monkey Erythrocytes." *Comparative Biochemistry and Physiology -- Part B: Biochemistry And* 80(4):725–29.
- Allman, Erik L., Heather J. Painter, Jasmeet Samra, Manuela Carrasquilla, and Manuel Llinás. 2016. "Metabolomic Profiling of the Malaria Box Reveals Antimalarial Target Pathways." *Antimicrobial Agents and Chemotherapy* 60(11):6635–43.
- Alpert, Andrew J. 1990. "Hydrophilic-Interaction Chromatography for the Separation of Peptides, Nucleic Acids and Other Polar Compounds." *Journal of Chromatography A* 499(C):177–96.
- Altschul, Stephen F., Thomas L. Madden, Alejandro A. Schäffer, Jinghui Zhang, Zheng Zhang, Webb Miller, and David J. Lipman. 1997. "Gapped BLAST and PSI-BLAST: A New Generation of Protein Database Search Programs." *Nucleic Acids Research* 25(17):3389–3402.
- Anders, Carolin, Ole Niewoehner, Alessia Duerst, and Martin Jinek. 2014. "Europe PMC Funders Group Structural Basis of PAM-Dependent Target DNA Recognition by the Cas9 Endonuclease." *Nature* 513(7519):569–73.
- Annette M. Gero, Graham V. Brown and William J. O'Sullivan. 1984. "Pyrimidine de Novo Synthesis during the Life Cycle of the Intraerythrocytic Stage of Plasmodium Falciparum." *The Journal of Parasitology* 70(4):536–41.

- Aragón, Juan and John Lowenstein. 1980. "The Purine-Nucleotide Cycle and Recovery from Exercise." *European Journal of Biochemistry* 377:371–77.
- Arinze, Ifeanyi J. 2005. "Facilitating Understanding of the Purine Nucleotide Cycle and the One-Carbon Pool: Part II: Metabolism of the One-Carbon Pool." *Biochemistry and Molecular Biology Education* 33(4):255–59.
- Armenta-Medina, Dagoberto, Lorenzo Segovia, and Ernesto Perez-Rueda. 2014. "Comparative Genomics of Nucleotide Metabolism: A Tour to the Past of the Three Cellular Domains of Life." *BMC Genomics* 15(1):800.
- Armstrong, Christopher M. and Daniel E. Goldberg. 2007. "An FKBP Destabilization Domain Modulates Protein Levels in *Plasmodium Falciparum*." *Nature Methods* 4(12):1007–9.
- Arrow, Kenneth J., Claire Panosian, and Hellen Gelband. 2004. *Saving Lives, Buying Time: Economics of Malaria Drugs in an Age of Resistance*.
- Athmer, Lance, Jason Kindrachuk, Fawzy Georges, and Scott Napper. 2002. "The Influence of Protein Structure on the Products Emerging from Succinimide Hydrolysis." *Journal of Biological Chemistry* 277(34):30502–7.
- Azevedo, Cristina, Thomas Livermore, and Adolfo Saiardi. 2015. "Protein Polyphosphorylation of Lysine Residues by Inorganic Polyphosphate." *Molecular Cell* 58(1):71–82.
- Baer, Kerstin, Christian Klotz, Stefan H. I. Kappe, Thomas Schnieder, and Ute Frevert. 2007. "Release of Hepatic *Plasmodium Yoelii* Merozoites into the Pulmonary Microvasculature." *PLoS Pathogens* 3(11):e171.
- Baeza, Josue, Michael J. Smallegan, and John M. Denu. 2015. "Site-Specific Reactivity of Nonenzymatic Lysine Acetylation." *ACS Chemical Biology* 10(1):122–28.
- Baeza, Josue, Michael J. Smallegan, and John M. Denu. 2016. "Special Issue: Mitochondria & Metabolism Mechanisms and Dynamics of Protein Acetylation in Mitochondria." *Trends in Biochemical Sciences* 41(3):231–44.
- Bahl, Amit, Brian Brunk, Jonathan Crabtree, Martin J. Fraunholz, Bindu Gajria, Gregory R. Grant, Hagai Ginsburg, Dinesh Gupta, Jessica C. Kissinger, Philip Labo, Li Li, Matthew D. Mailman, Arthur J. Milgram, David S. Pearson, David S. Roos, Jonathan Schug, Christian J. Stoeckert, and Patricia Whetzel. 2003. "PlasmoDB: The *Plasmodium* Genome Resource. A Database Integrating Experimental and Computational Data." *Nucleic Acids Research* 31(1):212–15.
- Bailey, D., E. P. Carpenter, A. Coker, S. Coker, J. Read, A. T. Jones, P. Erskine, C. F. Aguilar, M. Badasso, L. Toldo, F. Rippmann, J. Sanz-Aparicio, A. Albert, T. L. Blundell, N. B. Roberts, S. P. Wood, and J. B. Cooper. 2012. "An Analysis of Subdomain Orientation, Conformational Change and Disorder in Relation to Crystal Packing of Aspartic Proteinases." *Acta Crystallographica Section D: Biological Crystallography* 68(5):541–52.
- Bajad, Sunil U., Wenyun Lu, Elizabeth H. Kimball, Jie Yuan, Celeste Peterson, and Joshua D. Rabinowitz. 2006. "Separation and Quantitation of Water Soluble Cellular Metabolites by Hydrophilic Interaction Chromatography-Tandem Mass Spectrometry." *Journal of Chromatography A* 1125(1):76–88.
- Baker, Emily G., Christopher Williams, Kieran L. Hudson, Gail J. Bartlett, Jack W. Heal, Kathryn L. Porte, Goff, Richard B. Sessions, Matthew P. Crump, and Derek N. Woolfson. 2017. "Engineering Protein Stability with Atomic Precision in a Monomeric Miniprotein." *Nature Chemical Biology* 13(7):764–70.
- Balasco, Nicole, Luciana Esposito, Alfonso De Simone, and Luigi Vitagliano. 2013. "Role of Loops Connecting Secondary Structure Elements in the Stabilization of Proteins Isolated from Thermophilic Organisms." *Protein Science* 22:1016–23.
- Banaszynski, Laura A., Ling chun Chen, Lystranne A. Maynard-Smith, A. G. Lis. Ooi, and Thomas J. Wandless. 2006. "A Rapid, Reversible, and Tunable Method to Regulate Protein Function in Living Cells Using Synthetic Small Molecules." *Cell* 126(5):995–1004.

- Bansal, Priyanka, Anuj Tripathi, Vandana Thakur, Asif Mohammed, and Pushkar Sharma. 2017. "Autophagy-Related Protein ATG18 Regulates Apicoplast Biogenesis in Apicomplexan Parasites." *MBio* 8(5).
- Barducci, Alessandro, Giovanni Bussi, and Michele Parrinello. 2008. "Well-Tempered Metadynamics: A Smoothly Converging and Tunable Free-Energy Method." *Physical Review Letters* 100(2):1–4.
- Barends, Thomas R. M. M., Jelle B. Bultema, Thijs Kaper, Marc J. E. C. E. C. van der Maarel, Lubbert Dijkhuizen, Bauke W. Dijkstra, Thomas R. M. M. Barends, Jelle B. Bultema, Marc J. E. C. E. C. van der Maarel, Bauke W. Dijkstra, and Lubbert Dijkhuizen. 2007. "Three-Way Stabilization of the Covalent Intermediate in Amylomaltase, an α -Amylase-like Transglycosylase." *Journal of Biological Chemistry* 282(23):17242–49.
- Barrado, Patricia, María José Rodríguez, Antonio Jiménez, and María Fernández Lobato. 2003. "Expression in Escherichia Coli of a Recombinant Adenosine Kinase from Saccharomyces Cerevisiae: Purification, Kinetics and Substrate Analyses." *Yeast* 20(13):1145–50.
- Barrangou, Rodolphe, Christophe Fremaux, H  l  ne Deveau, Melissa Richards, Patrick Boyaval, Sylvain Moineau, Dennis A. Romero, and Philippe Horvath. 2007. "CRISPR Provides Acquired Resistance against Viruses in Prokaryotes." *Science* 315(5819):1709–12.
- Bartlett, Gail J., Robert W. Newberry, Brett Vanveller, Ronald T. Raines, and Derek N. Woolfson. 2013. "Interplay of Hydrogen Bonds and $n \rightarrow \pi^*$ Interactions in Proteins." *Journal of the American Chemical Society* 135(49):18682–88.
- Battye, T. Geoff G., Luke Kontogiannis, Owen Johnson, Harold R. Powell, and Andrew G. W. Leslie. 2011. "IMOSFLM: A New Graphical Interface for Diffraction-Image Processing with MOSFLM." *Acta Crystallographica Section D: Biological Crystallography* 67(4):271–81.
- El Beheiry, Mohamed, Jean-Baptiste Masson, Zhe Liu, Liangqi Xie, Benjamin Guglielmi, Maxime Dahan, Wulan Deng, Lana Bosanac, Robert Tjian, Elisa T. Zhang, Spencer C. Knight, Lea B. Witkowsky, and Jennifer A. Doudna. 2015. "Dynamics of CRISPR-Cas9 Genome Interrogation in Living Cells." *Science* 350(6262):823–26.
- Berman, P. A. and L. Human. 1991. "Hypoxanthine Depletion Induced by Xanthine Oxidase Inhibits Malaria Parasite Growth in Vitro." *Advances in Experimental Medicine and Biology* 309(Part A):165–68.
- Berman, P. A., L. Human, and J. A. Freese. 1991. "Xanthine Oxidase Inhibits Growth of Plasmodium Falciparum in Human Erythrocytes in Vitro." *Journal of Clinical Investigation* 88(6):1848–55.
- Beyer, Hannes M., Patrick Gonschorek, Sophia L. Samodelov, Matthias Meier, Wilfried Weber, and Matias D. Zurbriggen. 2015. "AQUA Cloning: A Versatile and Simple Enzyme-Free Cloning Approach." *PloS One* 10(9):e0137652.
- Bhaya, Devaki, Michelle Davison, and Rodolphe Barrangou. 2011. "CRISPR-Cas Systems in Bacteria and Archaea: Versatile Small RNAs for Adaptive Defense and Regulation." *Annual Review of Genetics* 45(1):273–97.
- Billker, O., M. K. Shaw, G. Margos, and R. E. Sinden. 1997. "The Roles of Temperature, PH and Mosquito Factors as Triggers of Male and Female Gametogenesis of Plasmodium Berghei in Vitro." *Parasitology* 115(1):1–7.
- Birrell, Geoffrey W., Matthew P. Challis, Amanda de Paoli, Dovile Anderson, Shane M. Devine, Gavin D. Heffernan, David P. Jacobus, Michael D. Edstein, Ghizal Siddiqui, and Darren J. Creek. 2020. "Multi-Omic Characterization of the Mode of Action of a Potent New Antimalarial Compound, JPC-3210, against Plasmodium Falciparum." *Molecular and Cellular Proteomics* 19(2):308–25.
- Bissati, Kamal El, Megan J. Downie, Seong Kyoung Kim, Michael Horowitz, Nicola Carter, Buddy Ullman, and Choukri Ben Mamoun. 2008. "Genetic Evidence for the Essential Role of PfNT1 in the Transport and Utilization of Xanthine, Guanine, Guanosine and Adenine by Plasmodium Falciparum." *Molecular and Biochemical Parasitology* 161(2):130–39.
- Blatnik, Matthew, Suzanne R. Thorpe, and John W. Baynes. 2008. "Succination of Proteins by Fumarate: Mechanism of Inactivation of Glyceraldehyde-3-Phosphate Dehydrogenase in Diabetes." Pp. 272–75

- in *Annals of the New York Academy of Sciences*. Vol. 1126. Blackwell Publishing Inc.
- De Bock, Katrien, Maria Georgiadou, Sandra Schoors, Anna Kuchnio, Brian W. Wong, Anna Rita Cantelmo, Annelies Quaegebeur, Bart Ghesquière, Sandra Cauwenberghs, Guy Eelen, Li Kun Phng, Inge Betz, Bieke Tembuysen, Katleen Brepoels, Jonathan Welti, Ilse Geudens, Inmaculada Segura, Bert Cruys, Francesco Bifari, Ilaria Decimo, Raquel Blanco, Sabine Wyns, Jeroen Vangindertael, Susana Rocha, Russel T. Collins, Sebastian Munck, Dirk Daelemans, Hiromi Imamura, Roland Devlieger, Mark Rider, Paul P. Van Veldhoven, Frans Schuit, Ramon Bartrons, Johan Hofkens, Peter Fraisl, Sucheta Telang, Ralph J. Deberardinis, Luc Schoonjans, Stefan Vinckier, Jason Chesney, Holger Gerhardt, Mieke Dewerchin, and Peter Carmeliet. 2013. "Role of PFKFB3-Driven Glycolysis in Vessel Sprouting." *Cell* 154(3):651–63.
- Bogusky, R. T., L. M. Lowenstein, and J. M. Lowenstein. 1976. "The Purine Nucleotide Cycle. A Pathway for Ammonia Production in the Rat Kidney." *Journal of Clinical Investigation* 58(2):326–35.
- Boitz, Jan M., Rona Strasser, Phillip A. Yates, Armando Jardim, and Buddy Ullman. 2013. "Adenylosuccinate Synthetase and Adenylosuccinate Lyase Deficiencies Trigger Growth and Infectivity Deficits in *Leishmania Donovanii*." *Journal of Biological Chemistry* 288(13):8977–90.
- Boitz, Jan M. and Buddy Ullman. 2006. "Leishmania Donovanii Singly Deficient in HGPRT, APRT or XPRT Are Viable in Vitro and within Mammalian Macrophages." *Molecular and Biochemical Parasitology* 148(1):24–30.
- Botting, Catherine H., Paul Talbot, Sonia Paytubi, and Malcolm F. White. 2010. "Extensive Lysine Methylation in Hyperthermophilic Crenarchaea: Potential Implications for Protein Stability and Recombinant Enzymes." *Archaea* 2010:1–6.
- Braks, Joanna A. M. M., Blandine Franke-Fayard, Hans Kroeze, Chris J. Janse, and Andrew P. Waters. 2006. "Development and Application of a Positive - Negative Selectable Marker System for Use in Reverse Genetics in *Plasmodium*." *Nucleic Acids Research* 34(5).
- Brennan, Todd V and Steven Clarke. 1993. "Spontaneous Degradation of Polypeptides at Aspartyl and Asparaginy Residues : Effects of the Solvent Dielectric." *Protein Science* 2:331–38.
- Bryk, Agata H. and Jacek R. Wiśniewski. 2017. "Quantitative Analysis of Human Red Blood Cell Proteome." *Journal of Proteome Research* 16(8):2752–61.
- Buckwitz, Detlef, Gisela Jacobasch, and Christa Gerth. 1990. "Phosphofructokinase from *Plasmodium Berghei*: A Kinetic Model of Allosteric Regulation." *Molecular and Biochemical Parasitology* 40(2):225–32.
- Bulusu, Vinay, Vijay Jayaraman, and Hemalatha Balaram. 2011. "Metabolic Fate of Fumarate, a Side Product of the Purine Salvage Pathway in the Intraerythrocytic Stages of *Plasmodium Falciparum*." *Journal of Biological Chemistry* 286(11):9236–45.
- Bulusu, Vinay, Bharath Srinivasan, Monnanda Ponnappa Bopanna, and Hemalatha Balaram. 2009. "Elucidation of the Substrate Specificity, Kinetic and Catalytic Mechanism of Adenylosuccinate Lyase from *Plasmodium Falciparum*." *Biochimica et Biophysica Acta - Proteins and Proteomics* 1794(4):642–54.
- Bushell, Ellen, Ana Rita Gomes, Theo Sanderson, Kai Wengelnik, Julian C. Rayner, Oliver Billker, Ellen Bushell, Ana Rita Gomes, Theo Sanderson, Burcu Anar, Gareth Girling, Colin Herd, Tom Metcalf, Katarzyna Modrzynska, Frank Schwach, Rowena E. Martin, Michael W. Mather, Geoffrey I. Mcfadden, Leopold Parts, Gavin G. Rutledge, Akhil B. Vaidya, Kai Wengelnik, Julian C. Rayner, and Oliver Billker. 2017. "Functional Profiling of a *Plasmodium* Genome Reveals an Abundance of Essential Genes Article Functional Profiling of a *Plasmodium* Genome Reveals an Abundance of Essential Genes." *Cell* 170(2):260-272.e8.
- Bussi, Giovanni, Francesco Luigi Gervasio, Alessandro Laio, and Michele Parrinello. 2006. "Free-Energy Landscape for β Hairpin Folding from Combined Parallel Tempering and Metadynamics." *Journal of the American Chemical Society* 128(41):13435–41.
- Buszewski, Bogusław and Sylwia Noga. 2012. "Hydrophilic Interaction Liquid Chromatography (HILIC)- a Powerful Separation Technique." *Analytical and Bioanalytical Chemistry* 402(1):231–47.

- Cacciapuoti, Giovanna, Marina Porcelli, Costanzo Bertoldo, Mario De Rosa, and Vincenzo Zappia. 1994. "Purification and Characterization of Extremely Thermophilic and Thermostable 5'-Methylthioadenosine Phosphorylase from the Archaeon *Sulfolobus Solfataricus*: Purine Nucleoside Phosphorylase Activity and Evidence for Intersubunit Disulfide Bonds." *Journal of Biological Chemistry* 269(40):24762–69.
- Callahan, Brian P., Natalya I. Topilina, Matthew J. Stanger, Patrick Van Roey, and Marlene Belfort. 2011. "Structure of Catalytically Competent Intein Caught in a Redox Trap with Functional and Evolutionary Implications." *Nature Structural and Molecular Biology* 18(5):630–33.
- Cámara-Artigas, Ana, Javier Murciano-Calles, Jose A. Gavira, Eva S. Cobos, and Jose C. Martínez. 2010. "Novel Conformational Aspects of the Third PDZ Domain of the Neuronal Post-Synaptic Density-95 Protein Revealed from Two 1.4Å X-Ray Structures." *Journal of Structural Biology* 170(3):565–69.
- Cantor, Jason R., Everett M. Stone, and George Georgiou. 2011. "Expression and Biochemical Characterization of the Human Enzyme N-Terminal Asparagine Amidohydrolase." *Biochemistry* 50(14):3025–33.
- Cao, Mingyan, Sri Hari Raju Mulagapati, Bhargavi Vemulapalli, Jihong Wang, Sergei V. Saveliev, Marjeta Urh, Alan Hunter, and Dengfeng Liu. 2019. "Characterization and Quantification of Succinimide Using Peptide Mapping under Low-PH Conditions and Hydrophobic Interaction Chromatography." *Analytical Biochemistry* 566(October 2018):151–59.
- Capasso, S., L. Mazzarella, F. Sica, and A. Zagari. 2004. "Solid-State Conformations of Aminosuccinyl Peptides: Crystal Structure of tert-Butyloxycarbonyl-L-Leucyl-L-Aminosuccinyl-L-Phenylalaninamide." *Biopolymers* 28(1):139–47.
- Capasso, Sante, Gianfranco Balboni, and Paola Di Cerbo. 2000. "Effect of Lysine Residues on the Deamidation Reaction of Asparagine Side Chains." *Biopolymers* 53(2):213–19.
- Capasso, Sante and Paola Di Cerbo. 2000. "Formation of an RNase A Derivative Containing an Aminosuccinyl Residue in Place of Asparagine 67." *Biopolymers* 56(1):14–19.
- Capasso, Sante, Lelio Mazzarella, and Adriana Zagari. 1995. "Folding of Aminosuccinyl Peptides: Thermodynamic Data from Temperature Dependent Circular Dichroism Measurements." *Chirality* 7(8):605–9.
- Caro, Florence, Mathew G. Miller, and Joseph L. DeRisi. 2012. "Plate-Based Transfection and Culturing Technique for Genetic Manipulation of *Plasmodium Falciparum*." *Malaria Journal* 11:1–10.
- Carrasquilla, Manuela, Theo Sanderson, Ruddy Montandon, Julian Rayner, and Marcus Lee. 2019. "Quantitation of Vector Uptake Reveals Non-Poissonian Transfection Dynamics in *Plasmodium Falciparum*." *BioRxiv*.
- Carroll, Dana. 2011. "Genome Engineering with Zinc-Finger Nucleases." *Genetics* 188(4):773–82.
- Cassera, María B., María B., Keith Z. Hazleton, Paul M. Riegelhaupt, Emilio F. Merino, Minkui Luo, Myles H. Akabas, and Vern L. Schramm. 2008. "Erythrocytic Adenosine Monophosphate as an Alternative Purine Source in *Plasmodium Falciparum*." *Journal of Biological Chemistry* 283(47):32889–99.
- Cassera, María Belén, Yong Zhang, Keith Z. Hazleton, and Vern L. Schramm. 2011. "Purine and Pyrimidine Pathways as Targets in *Plasmodium Falciparum*." *Bone* 11(16):2103–15.
- Catak, Saron, Gérald Monard, Viktorya Aviyente, and Manuel F. Ruiz-López. 2006. "Reaction Mechanism of Deamidation of Asparaginyl Residues in Peptides: Effect of Solvent Molecules." *Journal of Physical Chemistry A* 110(27):8354–65.
- Chan, Maurice and Tiow Suan Sim. 2004. "Functional Analysis, Overexpression, and Kinetic Characterization of Pyruvate Kinase from *Plasmodium Falciparum*." *Biochemical and Biophysical Research Communications* 326(1):188–96.
- Chan, Maurice, Doreen S. H. Tan, and T. S. Sim. 2007. "*Plasmodium Falciparum* Pyruvate Kinase as a Novel Target for Antimalarial Drug-Screening." *Travel Medicine and Infectious Disease* 5(2 SPEC. ISS.):125–31.

- Chayen, Naomi E., Patrick D. Shaw Stewart, and David M. Blow. 1992. "Microbatch Crystallization under Oil a New Technique Allowing Many Small-Volume Crystallization Trials." 122:176–80.
- Child, Matthew Andrew. 2014. "Chemical Biology Approaches for the Study of Apicomplexan Parasites." 192(0):1–9.
- Chittur, Sridar V., Thomas J. Klem, Cynthia M. Shafer, and V. Jo Davisson. 2001. "Mechanism for Acivicin Inactivation of Triad Glutamine Amidotransferases [†]." *Biochemistry* 40(4):876–87.
- Chou, Kou Chen. 1997. "Prediction and Classification of α -Turn Types." *Biopolymers - Nucleic Acid Sciences Section* 42(7):837–53.
- Chou, Kuo Chen. 2000. "Prediction of Tight Turns and Their Types in Proteins." *Analytical Biochemistry* 286(1):1–16.
- Chu, Bernard W., Laura A. Banaszynski, Ling chun Chen, and Thomas J. Wandless. 2008. "Recent Progress with FKBP-Derived Destabilizing Domains." *Bioorganic and Medicinal Chemistry Letters* 18(22):5941–44.
- Coates, L., P. T. Erskine, M. P. Crump, S. P. Wood, and J. B. Cooper. 2002. "Five Atomic Resolution Structures of Endothiapepsin Inhibitor Complexes: Implications for the Aspartic Proteinase Mechanism." *Journal of Molecular Biology* 318(5):1405–15.
- Coates, L., P. T. Erskine, S. P. Wood, D. A. A. Myles, and J. B. Cooper. 2001. "A Neutron Laue Diffraction Study of Endothiapepsin: Implications for the Aspartic Proteinase Mechanism [†]." *Journal of Molecular Biology* 318(5):1405–15.
- Coates, Leighton, Han Fang Tuan, Stephen Tomanicek, Andrey Kovalevsky, Marat Mustyakimov, Peter Erskine, and Jon Cooper. 2008. "The Catalytic Mechanism of an Aspartic Proteinase Explored with Neutron and X-Ray Diffraction." *Journal of the American Chemical Society* 130(23):7235–37.
- Cobbold, Simon A. and Malcolm J. Mcconville. 2014. "The Plasmodium Tricarboxylic Acid Cycle and Mitochondrial Metabolism Overview of Carbon Metabolism of Plasmodium Spp . Asexual Stages." 1–18.
- Cobbold, Simon A., Ashley M. Vaughan, Ian A. Lewis, Heather J. Painter, Nelly Camargo, David H. Perlman, Matthew Fishbaugher, Julie Healer, Alan F. Cowman, Stefan H. I. Kappe, and Manuel Llinás. 2013. "Kinetic Flux Profiling Elucidates Two Independent Acetyl-Coa Biosynthetic Pathways in Plasmodium Falciparum." *Journal of Biological Chemistry* 288(51):36338–50.
- Cong, Le, F. Ann Ran, David Cox, Shuailiang Lin, Robert Barretto, Patrick D. Hsu, Xuebing Wu, Wenyan Jiang, and Luciano a Marraffini. 2013. "Multiplex Genome Engineering Using CRISPR/Cas Systems." *Science* 339(6121):819–23.
- Cong, Le and Feng Zhang. 2014. "Genome Engineering Using Crispr-Cas9 System." *Chromosomal Mutagenesis: Second Edition* 8(11):197–217.
- Corti, A. and F. Curnis. 2011. "Isoaspartate-Dependent Molecular Switches for Integrin-Ligand Recognition." *Journal of Cell Science* 124(4):515–22.
- Cowman, Alan F. and Brendan S. Crabb. 2006. "Invasion of Red Blood Cells by Malaria Parasites." *Cell* 124(4):755–66.
- Cox, Francis Eg. 2010. "History of the Discovery of the Malaria Parasites and Their Vectors." *Parasites & Vectors* 3(1):5.
- Coyne, Robert S., Linda Hannick, Dhanasekaran Shanmugam, Jessica B. Hostetler, Daniel Bami, Vinita S. Joardar, Justin Johnson, Diana Radune, Irtisha Singh, Jonathan H. Badger, Ujjwal Kumar, Milton Saier, Yufeng Wang, Hong Cai, Jianying Gu, Michael W. Mather, Akhil B. Vaidya, David E. Wilkes, Vidyalakshmi Rajagopalan, David J. Asai, Chad G. Pearson, Robert C. Findly, Harry W. Dickerson, Martin Wu, Cindy Martens, Yves Van de Peer, David S. Roos, Donna M. Cassidy-Hanley, and Theodore G. Clark. 2011. "Comparative Genomics of the Pathogenic Ciliate *Ichthyophthirius multifiliis*, Its Free-Living Relatives and a Host Species Provide Insights into Adoption of a Parasitic Lifestyle and Prospects for Disease Control." *Genome Biology* 12(10):R100.
- Crabb, Brendan S. and Alan F. Cowman. 1996. "Characterization of Promoters and Stable Transfection

- by Homologous and Nonhomologous Recombination in *Plasmodium Falciparum*." *Proceedings of the National Academy of Sciences of the United States of America* 93(14):7289–94.
- Creek, Darren J., Hwa H. Chua, Simon A. Cobbold, Brunda Nijagal, James I. MacRae, Benjamin K. Dickerman, Paul R. Gilson, Stuart A. Ralph, and Malcolm J. McConville. 2016. "Metabolomics-Based Screening of the Malaria Box Reveals Both Novel and Established Mechanisms of Action." *Antimicrobial Agents and Chemotherapy* 60(11):6650–63.
- Creek, Darren J., Andris Jankevics, Rainer Breitling, David G. Watson, Michael P. Barrett, and Karl E. V Burgess. 2011. "Toward Global Metabolomics Analysis with Hydrophilic Interaction Liquid Chromatography: Mass Spectrometry: Improved Metabolite Identification by Retention Time Prediction." *Analytical Chemistry* (83):8703–10.
- Cui Zhang, a Bo Xiao, a Yuanyuan Jiang, a Yihua Zhao, a Zhenkui Li, a Han Gao, a Yuan Ling, a Jun Wei, a Shaoneng Li, a Mingke Lu, A., a Jing Yuan a Xin-zhuan Su, b Huiting Cui, Cui Zhang, Bo Xiao, and Yuanyuan Jiang. 2014. "Efficient Editing of Malaria Parasite Genome Using the CRISPR / Cas9." *Microbiology* 5(4):1–9.
- Curnis, Flavio, Angela Cattaneo, Renato Longhi, Angelina Sacchi, Anna Maria Gasparri, Fabio Pastorino, Paola Di Matteo, Catia Traversari, Angela Bachi, Mirco Ponzoni, Gian Paolo Rizzardì, and Angelo Corti. 2010. "Critical Role of Flanking Residues in NGR-to-IsoDGR Transition and CD13/Integrin Receptor Switching." *Journal of Biological Chemistry* 285(12):9114–23.
- Curnis, Flavio, Renato Longhi, Luca Crippa, Angela Cattaneo, Eleonora Dondossola, Angela Bachi, and Angelo Corti. 2006. "Spontaneous Formation of L-Isoaspartate and Gain of Function in Fibronectin." *Journal of Biological Chemistry* 281(47):36466–76.
- Daddona, P. E., W. P. Wiesmann, W. Milhouse, J. W. Chern, L. B. Townsend, M. S. Hershfield, and H. K. Webster. 1986. "Expression of Human Malaria Parasite Purine Nucleoside Phosphorylase in Host Enzyme-Deficient Erythrocyte Culture. Enzyme Characterization and Identification of Novel Inhibitors." *Journal of Biological Chemistry* 261(25):11667–73.
- Dall, Elfriede, Julia C. Fegg, Peter Briza, and Hans Brandstetter. 2015. "Structure and Mechanism of an Aspartimide-Dependent Peptide Ligase in Human Legumain." *Angewandte Chemie - International Edition* 54(10):2917–21.
- Dams, Thomas and Rainer Jaenicke. 1999. "Stability and Folding of Dihydrofolate Reductase from the Hyperthermophilic Bacterium *Thermotoga Maritima*." *Biochemistry* 38(28):9169–78.
- Daniel, R. M., M. Dines, and H. H. Petach. 1996. "The Denaturation and Degradation of Stable Enzymes at High Temperatures." *The Biochemical Journal* 317 (Pt 1):1–11.
- Darve, Eric and Andrew Pohorille. 2001. "Calculating Free Energies Using Average Force." *The Journal of Chemical Physics* 115:926.
- Das, Aparup, Anupkumar R. Anvikar, Lauren J. Cator, Ramesh C. Dhiman, Alex Eapen, Neelima Mishra, Bhupinder N. Nagpal, Nutan Nanda, Kamaraju Raghavendra, Andrew F. Read, Surya K. Sharma, Om P. Singh, Vineeta Singh, Photini Sinnis, Harish C. Srivastava, Steven A. Sullivan, Patrick L. Sutton, Matthew B. Thomas, Jane M. Carlton, and Neena Valecha. 2012. "Malaria in India: The Center for the Study of Complex Malaria in India." *Acta Tropica* 121(3):267–73.
- DEMASI, D., S. CAPASSO, F. SICA, and A. ZAGARI. 2009. "Conformationally Restrained Peptides: Crystal Structure of Tert-Butyloxycarbonyl-L-Alanyl-D-Alanyl-D-Aminosuccinyl-Glycyl-L-Alanine Methyl Ester." *International Journal of Peptide and Protein Research* 47(4):227–30.
- Van Dijk, M. R., A. P. Waters, and C. J. Janse. 1995. "Stable Transfection of Malaria Parasite Blood Stages." *Science* 268(5215):1358–62.
- van Dijk, Melissa R., Glenn A. McConkey, Rinke Vinkenoog, Andrew P. Waters, and Chris J. Janse. 1994. "Mechanisms of Pyrimethamine Resistance in Two Different Strains of *Plasmodium Berghei*." *Molecular and Biochemical Parasitology* 68(1):167–71.
- Donald, R. G. K. and D. S. Roos. 1993. "Stable Molecular Transformation of *Toxoplasma Gondii*: A Selectable Dihydrofolate Reductase-Thymidylate Synthase Marker Based on Drug-Resistance

- Mutations in Malaria.” *Proceedings of the National Academy of Sciences of the United States of America* 90(24):11703–7.
- Dong, Yun-wei, Ming-ling Liao, Xian-liang Meng, and George N. Somero. 2018. “Structural Flexibility and Protein Adaptation to Temperature: Molecular Dynamics Analysis of Malate Dehydrogenases of Marine Molluscs.” *Proceedings of the National Academy of Sciences* 115(6):201718910.
- Van Dooren, Giel G., Luciana M. Stimmler, and Geoffrey I. McFadden. 2006. “Metabolic Maps and Functions of the Plasmodium Mitochondrion.” *FEMS Microbiology Reviews* 30(4):596–630.
- Douangamath, Alice, Martina Walker, Silke Beismann-Driemeyer, M. Cristina Vega-Fernandez, Reinhard Sterner, and Matthias Wilmanns. 2002. “Structural Evidence for Ammonia Tunneling across the (β)₈ Barrel of the Imidazole Glycerol Phosphate Synthase Bienenzyme Complex.” *Structure* 10(2):185–93.
- Dunn, Cameron R., Mark J. Banfield, John J. Barker, Christopher W. Higham, Kathleen M. Moreton, Dilek Turgut-Balik, R. Leo Brady, and J. John Holbrook. 1996. “The Structure of Lactate Dehydrogenase from Plasmodium Falciparum Reveals a New Target for Anti-Malarial Design.” *Nature Structural Biology* 3(11):912–15.
- Eaazhisai, K., R. Jayalakshmi, P. Gayathri, R. P. Anand, K. Sumathy, H. Balam, and M. R. N. Murthy. 2004. “Crystal Structure of Fully Liganded Adenylosuccinate Synthetase from Plasmodium Falciparum.” *Journal of Molecular Biology* 335(5):1251–64.
- Erskine, Peter T., Leighton Coates, Sanjay Mall, Raj S. Gill, Steve P. Wood, Dean A. A. Myles, and Jon. B. Cooper. 2003. “Atomic Resolution Analysis of the Catalytic Site of an Aspartic Proteinase and an Unexpected Mode of Binding by Short Peptides.” *Protein Science* 12(8):1741–49.
- Febbraio, Ferdinando, Annapaola Andolfo, Fabio Tanfani, Raffaella Briante, Fabrizio Gentile, Silvestro Formisano, Carlo Vaccaro, Andrea Scirè, Enrico Bertoli, Piero Pucci, and Roberto Nucci. 2004. “Thermal Stability and Aggregation of Sulfolobus Solfataricus β -Glycosidase Are Dependent upon the N- ϵ -Methylation of Specific Lysyl Residues .” *Journal of Biological Chemistry* 279(11):10185–94.
- Flatau, Gilles, Emmanuel Lemichez, Michel Gauthier, Pierre Chardin, Sonia Paris, Carla Fiorentini, and Patrice Boquet. 1997. “Toxin-Induced Activation of the G Protein P21 Rho by Deamidation of Glutamine.” *Nature* 387(6634):729–33.
- Fleck, S. L., M. Pudney, and R. E. Sinden. 1996. “The Effect of Atovaquone (566680) on the Maturation Plasmodium Falciparum Gametocytes in Vitro and Viability Of.” *Parasitology Research* 309–12.
- Florentin, Anat, David W. Cobb, Jillian D. Fishburn, Michael J. Cipriano, Paul S. Kim, Manuel A. Fierro, Boris Striepen, and Vasant Muralidharan. 2017. “PfClpC Is an Essential Clp Chaperone Required for Plastid Integrity and Clp Protease Stability in Plasmodium Falciparum.” *Cell Reports* 21(7):1746–56.
- Folmes, Clifford D. L., Timothy J. Nelson, Almudena Martinez-Fernandez, D. Kent Arrell, Jelena Zlatkovic Lindor, Petras P. Dzeja, Yasuhiro Ikeda, Carmen Perez-Terzic, and Andre Terzic. 2011. “Somatic Oxidative Bioenergetics Transitions into Pluripotency-Dependent Glycolysis to Facilitate Nuclear Reprogramming.” *Cell Metabolism* 14(2):264–71.
- Fonseca-Maldonado, Raquel, Davi Serradella Vieira, Juliana Sanchez Alpointi, Eric Bonneil, Pierre Thibault, and Richard John Ward. 2013. “Engineering the Pattern of Protein Glycosylation Modulates the Thermostability of a GH11 Xylanase.” *Journal of Biological Chemistry* 288(35):25522–34.
- Fraser, T. S., S. H. Kappe, D. L. Narum, K. M. VanBuskirk, and J. H. Adams. 2001. “Erythrocyte-Binding Activity of Plasmodium Yoelii Apical Membrane Antigen-1 Expressed on the Surface of Transfected COS-7 Cells.” *Molecular and Biochemical Parasitology* 117(1):49–59.
- Freddolino, Peter L., Christopher B. Harrison, Yanxin Liu, and Klaus Schulten. 2010. “Challenges in Protein-Folding Simulations.” *Nature Physics* 6(10):751–58.
- Frezza, Christian. 2017. “Mitochondrial Metabolites: Undercover Signalling Molecules.” *Interface Focus* 7(2):20160100.

- Fry, Mitchell and Mary Pudney. 1992. "Site of Action of the Antimalarial Hydroxynaphthoquinone, 2-[Trans-4-(4'-Chlorophenyl) Cyclohexyl]-3-Hydroxy-1,4-Naphthoquinone (566C80)." *Biochemical Pharmacology* 43(7):1545–53.
- Ganesan, Suresh M., Joanne M. Morrissey, Hangjun Ke, Heather J. Painter, Kamal Laroiya, Margaret A. Phillips, Pradipsinh K. Rathod, Michael W. Mather, and Akhil B. Vaidya. 2011. "Yeast Dihydroorotate Dehydrogenase as a New Selectable Marker for Plasmodium Falciparum Transfection." *Molecular and Biochemical Parasitology* 177(1):29–34.
- Ganter, Markus, Jonathan M. Goldberg, Jeffrey D. Dvorin, Joao A. Paulo, Jonas G. King, Abhai K. Tripathi, Aditya S. Paul, Jing Yang, Isabelle Coppens, Rays H. Y. Jiang, Brendan Elsworth, David A. Baker, Rhoel R. Dinglasan, Steven P. Gygi, and Manoj T. Duraisingh. 2017. "Plasmodium Falciparum CRK4 Directs Continuous Rounds of DNA Replication during Schizogony." *Nature Microbiology* 2:17017.
- García, Irene, Lucía Arenas-Alfonseca, Inmaculada Moreno, Cecilia Gotor, and Luis C. Romero. 2019. "HCN Regulates Cellular Processes through Posttranslational Modification of Proteins by S-Cyanylation." *Plant Physiology* 179(1):107–23.
- Garcia, Javier E., Alvaro Puentes, and Manuel E. Patarroyo. 2006. "Developmental Biology of Sporozoite-Host Interactions in Plasmodium Falciparum Malaria: Implications for Vaccine Design." *Clinical Microbiology Reviews* 19(4):686–707.
- Gardner, Malcolm J., Neil Hall, Eula Fung, Owen White, Matthew Berriman, Richard W. Hyman, Jane M. Carlton, Arnab Pain, Karen E. Nelson, Sharen Bowman, Ian T. Paulsen, Keith James, Jonathan A. Eisen, Kim Rutherford, Steven L. Salzberg, Alister Craig, Sue Kyes, Man Suen Chan, Vishvanath Nene, Shamira J. Shallom, Bernard Suh, Jeremy Peterson, Sam Angiuoli, Mihaela Peretea, Jonathan Allen, Jeremy Selengut, Daniel Haft, Michael W. Mather, Akhil B. Vaidya, David M. A. Martin, Alan H. Fairlamb, Martin J. Fraunholz, David S. Roos, Stuart A. Ralph, Geoffrey I. McFadden, Leda M. Cummings, G. Mani Subramanian, Chris Mungall, J. Craig Venter, Daniel J. Carucci, Stephen L. Hoffman, Ronald W. Davis, Claire M. Fraser, and Bart Barrell. 2002. "Genome Sequence of the Human Malaria Parasite Plasmodium Falciparum." *Nature* 419(6906):498–511.
- Geiger, T. and S. Clarke. 1987. "Deamidation, Isomerization, and Racemization at Asparaginyl and Aspartyl Residues in Peptides. Succinimide-Linked Reactions That Contribute to Protein Degradation." *Journal of Biological Chemistry* 262(2):785–94.
- Geneva: World Health Organization. 2019. *World Malaria Report 2019*.
- Gervasio, Francesco Luigi, Alessandro Laio, and Michele Parrinello. 2005. "Flexible Docking in Solution Using Metadynamics." *Journal of the American Chemical Society* 127(8):2600–2607.
- Ghorbal, Mehdi, Molly Gorman, Cameron Ross Macpherson, Rafael Miyazawa Martins, Artur Scherf, Jose-Juan Juan Lopez-Rubio, Rafael Miyazawa Martins, Jose-Juan Juan Lopez-Rubio, Mehdi Ghorbal, Molly Gorman, Cameron Ross Macpherson, Rafael Miyazawa Martins, Artur Scherf, Jose-Juan Juan Lopez-Rubio, Rafael Miyazawa Martins, Jose-Juan Juan Lopez-Rubio, and Mehdi Ghorbal. 2014. "Genome Editing in the Human Malaria Parasite Plasmodium Falciparum Using the CRISPR-Cas9 System." *Nature Biotechnology* 32(8):819–21.
- Gracy, Robert W., John M. Talent, and Anita I. Zvaigzne. 1998. "Molecular Wear and Tear Leads to Terminal Marking and the Unstable Isoforms of Aging." *The Journal of Experimental Zoology* 282(12):18–27.
- Guggisberg, Ann M., Philip M. Frasse, Andrew J. Jezewski, Natasha M. Kafai, Aakash Y. Gandhi, Samuel J. Erlinger, and Audrey R. Odom John. 2018. "Suppression of Drug Resistance Reveals a Genetic Mechanism of Metabolic Plasticity in Malaria Parasites." *MBio* 9(6).
- Gustavsson, N., U. Härndahl, A. Emanuelsson, P. Roepstorff, and C. Sundby. 1999. "Methionine Sulfoxidation of the Chloroplast Small Heat Shock Protein and Conformational Changes in the Oligomer." *Protein Sci* 8(11):2506–12.
- Harmel, Robert and Dorothea Fiedler. 2018. "Features and Regulation of Non-Enzymatic Post-Translational Modifications." *Nature Chemical Biology* 14(3):244–52.

- Hartuti, Endah Dwi, Daniel Ken Inaoka, Keisuke Komatsuya, Yukiko Miyazaki, Russell J. Miller, Wang Xinying, Mohamad Sadikin, Erwahyuni Endang Prabandari, Danang Waluyo, Marie Kuroda, Eri Amalia, Yuichi Matsuo, Nuki B. Nugroho, Hiroyuki Saimoto, Amila Pramisanidi, Yoh Ichi Watanabe, Mihoko Mori, Kazuro Shiomi, Emmanuel Oluwadare Balogun, Tomoo Shiba, Shigeharu Harada, Tomoyoshi Nozaki, and Kiyoshi Kita. 2018. "Biochemical Studies of Membrane Bound Plasmodium Falciparum Mitochondrial L-Malate:Quinone Oxidoreductase, a Potential Drug Target." *Biochimica et Biophysica Acta - Bioenergetics* 1859(3):191–200.
- Hasenkamp, Sandra, Karen T. Russell, and Paul Horrocks. 2012. "Comparison of the Absolute and Relative Efficiencies of Electroporation-Based Transfection Protocols for Plasmodium Falciparum." *Malaria Journal* 11(1):210.
- Haywood, Joel, Jason W. Schmidberger, Amy M. James, Samuel G. Nonis, Kirill V. Sukhoverkov, Mikael Elias, Charles S. Bond, and Joshua S. Mylne. 2018. "Structural Basis of Ribosomal Peptide Macrocyclization in Plants." *ELife* 7:1–22.
- Hedstrom, Lizbeth. 2009. "IMP Dehydrogenase: Structure, Mechanism, and Inhibition." *Chemical Reviews* 109(7):2903–28.
- Hess, Daniel, Kerstin Krüger, Achim Knappik, Peter Palm, and Reinhard Hensel. 1995. "Dimeric 3-Phosphoglycerate Kinases from Hyperthermophilic Archaea: Cloning, Sequencing and Expression of the 3-Phosphoglycerate Kinase Gene of Pyrococcus Woesei in Escherichia Coli and Characterization of the Protein. Structural and Functional Comparison ." *European Journal of Biochemistry* 233(1):227–37.
- Höcker, Birte, Catharina Jürgens, Matthias Wilmanns, and Reinhard Sterner. 2001. "Stability, Catalytic Versatility and Evolution of the (β α)8-Barrel Fold." *Current Opinion in Biotechnology* 12(4):376–81.
- Hollingsworth, Scott A. and Ron O. Dror. 2018. "Molecular Dynamics Simulation for All." *Neuron* 99(6):1129–43.
- Huang, Holly Z., Andrew Nichols, and Dingjiang Liu. 2009. "Direct Identification and Quantification of Aspartyl Succinimide in an IgG2 MAb by RapiGest Assisted Digestion." *Analytical Chemistry* 81(4):1686–92.
- Huang, Xinyi, Hazel M. Holden, and Frank M. Raushel. 2001. "Channeling of Substrates and Intermediates in Enzyme-Catalyzed Reactions." *Annual Review of Biochemistry* 70(1):149–80.
- Hubbard, Roderick E. and Muhammad Kamran Haider. 2010. "Hydrogen Bonds in Proteins: Role and Strength." *Encyclopedia of Life Sciences* 1:1–6.
- Iwamoto, Mari, Tomas Björklund, Cecilia Lundberg, Deniz Kirik, and Thomas J. Wandless. 2010. "A General Chemical Method to Regulate Protein Stability in the Mammalian Central Nervous System." *Chemistry and Biology* 17(9):981–88.
- Iwanaga, Shiroh, Tomomi Kato, Izumi Kaneko, and Masao Yuda. 2012. "Centromere Plasmid: A New Genetic Tool for the Study of Plasmodium Falciparum." *PLoS ONE* 7(3).
- Iwanaga, Shiroh, Shahid M. Khan, Izumi Kaneko, Zoe Christodoulou, Chris Newbold, Masao Yuda, Chris J. Janse, and Andrew P. Waters. 2010. "Functional Identification of the Plasmodium Centromere and Generation of a Plasmodium Artificial Chromosome." *Cell Host and Microbe* 7(3):245–55.
- Jackson, Andrew P., Thomas D. Otto, Martin Aslett, Stuart D. Armstrong, Frederic Bringaud, Alexander Schlacht, Catherine Hartley, Mandy Sanders, Jonathan M. Wastling, Joel B. Dacks, Alvaro Acosta-Serrano, Mark C. Field, Michael L. Ginger, and Matthew Berriman. 2016. "Kinetoplastid Phylogenomics Reveals the Evolutionary Innovations Associated with the Origins of Parasitism." *Current Biology* 26(2):161–72.
- Jahngen, Edwin G. E. and Edward F. Rossomando. 1984. "Adenylosuccinate Synthetase from Dictyostelium Discoideum: Effects of Hadacidin Analogs and Binding of [14C]Hadacidin." *Archives of Biochemistry and Biophysics* 229(1):145–54.
- James, Amy M., Joel Haywood, Julie Leroux, Katarzyna Ignasiak, G. Elliott, Jason W. Schmidberger,

- Mark F. Fisher, Samuel G. Nonis, Charles S. Bond, and Joshua S. Mylne. 2018. "The Macrocyclizing Protease Butelase 1 Remains Auto-Catalytic and Reveals the Structural Basis for Ligase Activity."
- James, Andrew M., Kurt Hoogewijs, Angela Logan, Andrew R. Hall, Shujing Ding, Ian M. Fearnley, and Michael P. Murphy. 2017. "Non-Enzymatic N-Acetylation of Lysine Residues by AcetylCoA Often Occurs via a Proximal S-Acetylated Thiol Intermediate Sensitive to Glyoxalase II." *Cell Reports* 18(9):2105–12.
- Janouskovec, Jan and Patrick J. Keeling. 2016. "Evolution: Causality and the Origin of Parasitism." *Current Biology* 26(4):R174–77.
- Janse, Chris J., Blandine Franke-Fayard, Gunnar R. Mair, Jai Ramesar, Corinna Thiel, Sabine Engelmann, Kai Matuschewski, Geert Jan Van Gemert, Robert W. Sauerwein, and Andrew P. Waters. 2006. "High Efficiency Transfection of Plasmodium Berghei Facilitates Novel Selection Procedures." *Molecular and Biochemical Parasitology* 145(1):60–70.
- Jaruwat, Aritsara, Pinpunya Riangrunroj, Sakunrat Ubonprasert, Udom Sae-ueng, Buabarn Kuaprasert, Yongyuth Yuthavong, Ubolsree Leartsakulpanich, and Penchit Chitnumsub. 2019. "Crystal Structure of Plasmodium Falciparum Adenosine Deaminase Reveals a Novel Binding Pocket for Inosine." *Archives of Biochemistry and Biophysics* 667:6–13.
- Jayaraman, Vijay, Vinay Bulusu, and Hemalatha Balam. 2012. "Crosstalk between Purine Nucleotide Metabolism and Mitochondrial Pathways in Plasmodium Falciparum." *Current Science* 102(5):757–66.
- Jayaraman, Vijay, Arpitha Suryavanshi, Pavithra Kalale, Jyothirmai Kunala, and Hemalatha Balam. 2018. "Biochemical Characterization and Essentiality of Plasmodium Fumarate Hydratase." *Journal of Biological Chemistry* 293(16):5878–94.
- Jia, Dongya, Mingyang Lu, Kwang Hwa Jung, Jun Hyoung Park, Linglin Yu, José N. Onuchic, Benny Abraham Kaiparettu, and Herbert Levine. 2019. "Elucidating Cancer Metabolic Plasticity by Coupling Gene Regulation with Metabolic Pathways." *Proceedings of the National Academy of Sciences of the United States of America* 116(9):3909–18.
- Jiang, Fuguo and Jennifer A. Doudna. 2017. "CRISPR – Cas9 Structures and Mechanisms." 505–31.
- Kappe, Stefan H. I., Karine Kaiser, and Kai Matuschewski. 2003. "The Plasmodium Sporozoite Journey: A Rite of Passage." *Trends in Parasitology* 19(3):135–43.
- Kato, Kentaro, D. C. Ghislain. Mayer, Sanjay Singh, Marion Reid, and Louis H. Miller. 2005. "Domain III of Plasmodium Falciparum Apical Membrane Antigen 1 Binds to the Erythrocyte Membrane Protein Kx." *Proceedings of the National Academy of Sciences of the United States of America* 102(15):5552–57.
- Kawamura, Shunsuke, Yoshimitsu Kakuta, Isao Tanaka, Kunio Hikichi, Satoru Kuhara, Nobuyuki Yamasaki, and Makoto Kimura. 1996. "Glycine-15 in the Bend between Two α -Helices Can Explain the Thermostability of DNA Binding Protein HU from Bacillus Stearothermophilus." *Biochemistry* 35(4):1195–1200.
- Ke, Hangjun, Suresh M. Ganesan, Swati Dass, Joanne M. Morrissey, Sovitj Pou, Aaron Nilsen, Michael K. Riscoe, Michael W. Mather, and Akhil B. Vaidya. 2019. "Mitochondrial Type II NADH Dehydrogenase of Plasmodium Falciparum (PfNDH2) Is Dispensable in the Asexual Blood Stages." *PLoS ONE* 14(4).
- Ke, Hangjun, Ian A Lewis, Manuel Lliná, and Akhil B. Vaidya Correspondence. 2015. "Genetic Investigation of Tricarboxylic Acid Metabolism during the Plasmodium Falciparum Life Cycle." *CellReports* 11:164–74.
- Ke, Hangjun, Ian A. Lewis, Joanne M. Morrissey, Kyle J. McLean, Suresh M. Ganesan, Heather J. Painter, Michael W. Mather, Marcelo Jacobs-Lorena, Manuel Lliná, and Akhil B. Vaidya. 2015. "Genetic Investigation of Tricarboxylic Acid Metabolism during the Plasmodium Falciparum Life Cycle." *Cell Reports* 11(1):164–74.

- Keough, Dianne T., Ai Lin Ng, Donald J. Winzor, Bryan T. Emmerson, and John De Jersey. 1999. "Purification and Characterization of Plasmodium Falciparum Hypoxanthine-Guanine-Xanthine Phosphoribosyltransferase and Comparison with the Human Enzyme." *Molecular and Biochemical Parasitology* 98(1):29–41.
- Kikuchi, Mamoru, Hiroshi Hayashida, Eiichi Nakano, and Kenji Sakaguchi. 1971. "Peptidoglutaminase. Enzymes for Selective Deamidation of γ -Amide of Peptide-Bound Glutamine." *Biochemistry* 10(7):1222–29.
- Kim, Jun Seob, Da Hyeong Cho, Paul Heo, Suk Chae Jung, Myungseo Park, Eun Joong Oh, Jaeyun Sung, Pan Jun Kim, Suk Chan Lee, Dae Hee Lee, Sarah Lee, Choong Hwan Lee, Dongwoo Shin, Yong Su Jin, and Dae Hyuk Kweon. 2016. "Fumarate-Mediated Persistence of Escherichia Coli against Antibiotics." *Antimicrobial Agents and Chemotherapy* 60(4):2232–40.
- Kim, Yang Gyun, Jooyeun Cha, and Srinivasan Chandrasegaran. 1996. "Hybrid Restriction Enzymes: Zinc Finger Fusions to Fok I Cleavage Domain." *Proceedings of the National Academy of Sciences of the United States of America* 93(3):1156–60.
- Kimuras, Shigenobu, Shigenori Kanaya, and Haruki Nakamura. 1992. "Thermostabilization of Escherichia Coli Ribonuclease HI by Replacing Left-Handed Helical Lys96 with Gly or Asn*." *Biochemistry* 22014–17.
- KIRINO, Hiromi, Makoto AOKI, Miho AOSHIMA, Yumiko HAYASHI, Masayuki OHBA, Akihiko YAMAGISHI, Takayoshi WAKAGI, and Tairo OSHIMA. 1994. "Hydrophobic Interaction at the Subunit Interface Contributes to the Thermostability of 3-isopropylmalate Dehydrogenase from an Extreme Thermophile, Thermus Thermophilus." *European Journal of Biochemistry* 220(1):275–81.
- Kondoh, Hiroshi, Matilde E. Leonart, Yasuhiro Nakashima, Masayuki Yokode, Makoto Tanaka, David Bernard, Jesus Gil, and David Beach. 2007. "A High Glycolytic Flux Supports the Proliferative Potential of Murine Embryonic Stem Cells." *Antioxidants and Redox Signaling* 9(3):293–99.
- De Koning-Ward, Tania F., David A. Fidock, Vandana Thathy, Robert Menard, Rosalina M. L. L. Van Spaendonk, Andrew P. Waters, and Chris J. Janse. 2000. "The Selectable Marker Human Dihydrofolate Reductase Enables Sequential Genetic Manipulation of the Plasmodium Berghei Genome." *Molecular and Biochemical Parasitology* 106(2):199–212.
- Koning-ward, Tania F. De, David a Fidock, Vandana Thathy, Robert Menard, Rosalina M. L. Van Spaendonk, Andrew P. Waters, and Chris J. Janse. 2000. "The Selectable Marker Human Dihydrofolate Reductase." *Molecular and Biochemical Parasitology* 106:199–212.
- de Koning-Ward, Tania F., Paul R. Gilson, and Brendan S. Crabb. 2015. "Advances in Molecular Genetic Systems in Malaria." *Nature Reviews Microbiology* 13(6):373–87.
- Korolev, S., T. Skarina, E. Evdokimova, S. Beasley, A. Edwards, A. Joachimiak, and A. Savchenko. 2002. "Crystal Structure of Glutamine Amidotransferase from Thermotoga Maritima." *Proteins: Structure, Function and Genetics* 49(3):420–22.
- Kossiakoff, A. A. 1988. "Principal Determinant." 1321(April):1985–88.
- Krane, Stephen M. 2008. "The Importance of Proline Residues in the Structure, Stability and Susceptibility to Proteolytic Degradation of Collagens." 703–10.
- Krishna, S., C. J. Woodrow, R. J. S. Burchmore, K. J. Saliba, and K. Kirk. 2000. "Hexose Transport in Asexual Stages of Plasmodium Falciparum and Kinetoplastidae." *Parasitology Today* 16(12):516–21.
- Krungkrai, Jerapan, Anthony Cerami, and Graeme B. Henderson. 1990. "Pyrimidine Biosynthesis in Parasitic Protozoa: Purification of a Monofunctional Dihydroorotase from Plasmodium Berghei and Crithidia Fasciculata." *Biochemistry* 29(26):6270–75.
- Kuang, Dexuan, Jichen Qiao, Zhou Li, Weiwei Wang, Hui Xia, Lubin Jiang, Jiejie Dai, Qiang Fang, and Xueyu Dai. 2017. "Tagging to Endogenous Genes of Plasmodium Falciparum Using CRISPR/Cas9." *Parasites and Vectors* 10(1):4–11.
- Kudyba, Heather M., David W. Cobb, Manuel A. Fierro, Anat Florentin, Dragan Ljolje, Balwan Singh, Naomi W. Lucchi, and Vasant Muralidharan. 2019. "The Endoplasmic Reticulum Chaperone

- PfGRP170 Is Essential for Asexual Development and Is Linked to Stress Response in Malaria Parasites." *Cellular Microbiology* 21(9).
- Kulkarni, Rhushikesh A., Daniel W. Bak, Darmood Wei, Sarah E. Bergholtz, Chloe A. Briney, Jonathan H. Shrimp, Aktan Alpsoy, Abigail L. Thorpe, Arissa E. Bavari, Daniel R. Crooks, Michaela Levy, Laurence Florens, Michael P. Washburn, Norma Frizzell, Emily C. Dykhuizen, Eranthie Weerapana, W. Marston Linehan, and Jordan L. Meier. 2019. "A Chemoproteomic Portrait of the Oncometabolite Fumarate." *Nature Chemical Biology* 15(4):391–400.
- Kumar, Sandeep, Chung-Jung Tsai, and Ruth Nussinov. 2000. "Factors Enhancing Protein Thermostability." *Protein Engineering, Design and Selection* 13(3):179–91.
- Kumar, Sanjeev, Sunita Prakash, Kallol Gupta, Aparna Dongre, Padmanabhan Balaram, and Hemalatha Balaram. 2016. "Unexpected Functional Implication of a Stable Succinimide in the Structural Stability of Methanocaldococcus Jannaschii Glutaminase." *Nature Communications* 7:12798.
- Kupis, Wioleta, Jan Palyga, Ewa Tomal, and Ewa Niewiadomska. 2016. "The Role of Sirtuins in Cellular Homeostasis." *Journal of Physiology and Biochemistry* 72(3):371–80.
- Kushwaha, Ambuj K., Liana Apolis, Daisuke Ito, and Sanjay A. Desai. 2018. "Increased Ca⁺⁺ Uptake by Erythrocytes Infected with Malaria Parasites: Evidence for Exported Proteins and Novel Inhibitors." *Cellular Microbiology* 20(9):e12853.
- Lamarque, Mauld, Sébastien Besteiro, Julien Papoin, Magali Roques, Brigitte Vulliez-Le Normand, Juliette Morlon-Guyot, Jean François Dubremetz, Sylvain Fauquenoy, Stanislas Tomavo, Bart W. Faber, Clemens H. Kocken, Alan W. Thomas, Martin J. Boulanger, Graham A. Bentley, and Maryse Lebrun. 2011. "The RON2-AMA1 Interaction Is a Critical Step in Moving Junction-Dependent Invasion by Apicomplexan Parasites." *PLoS Pathogens* 7(2):e1001276.
- Lambros, Chris and Jerome P. Vanderberg. 1979. "Synchronization of Plasmodium Falciparum Erythrocytic Stages in Culture." *Journal of Parasitology* 65(3):418–20.
- Lee, Jae Cheol, Sung Ung Kang, Yeji Jeon, Jong Woo Park, Jueng Soo You, Shin Won Ha, Narkhyun Bae, Gert Lubec, So Hee Kwon, Ju Seog Lee, Eun Jung Cho, and Jeung Whan Han. 2012. "Protein L-Isoaspartyl Methyltransferase Regulates P53 Activity." *Nature Communications* 3(May):910–27.
- Lee, Jung Rok, Jae Kyung Kim, Soo Jae Lee, and Kwang Pyo Kim. 2009. "Role of Protein Tyrosine Nitration in Neurodegenerative Diseases and Atherosclerosis." *Archives of Pharmacal Research* 32(8):1109–18.
- Lee, Marcus C. S. and David A. Fidock. 2014. "CRISPR-Mediated Genome Editing of Plasmodium Falciparum Malaria Parasites." *Genome Medicine* 6(8):1–4.
- Lee, Marcus C. S., Scott E. Lindner, Jose Juan Lopez-Rubio, and Manuel Llinás. 2019. "Cutting Back Malaria: CRISPR/Cas9 Genome Editing of Plasmodium." *Briefings in Functional Genomics* 18(5):281–89.
- Li, Bei, Eric M. Gorman, Kimberly D. Moore, Todd Williams, Richard L. Schowen, Elizabeth M. Topp, and Ronald T. Borchardt. 2005. "Effects of Acidic N + 1 Residues on Asparagine Deamidation Rates in Solution and in the Solid State." *Journal of Pharmaceutical Sciences* 94(3):666–75.
- Liu, Jun, Ilya Y. Gluzman, Mark E. Drew, and Daniel E. Goldberg. 2005. "The Role of Plasmodium Falciparum Food Vacuole Plasmepsins." *Journal of Biological Chemistry* 280(2):1432–37.
- Liu, Qing, Jingwei Cai, Robert G. Nichols, Yuan Tian, Jintao Zhang, Philip B. Smith, Yan Wang, Chao Yan, and Andrew D. Patterson. 2019. "A Quantitative HILIC-MS/MS Assay of the Metabolic Response of Huh-7 Cells Exposed to 2,3,7,8-Tetrachlorodibenzo-p-Dioxin." *Metabolites* 9(118).
- Liu, Z., S. Frutos, M. J. Bick, M. Vila-Perello, G. T. Debelouchina, S. A. Darst, and T. W. Muir. 2014. "Structure of the Branched Intermediate in Protein Splicing." *Proceedings of the National Academy of Sciences* 111(23):8422–27.
- Liwo, A., M. Khalili, and H. A. Scheraga. 2005. "Ab Initio Simulations of Protein-Folding Pathways by Molecular Dynamics with the United-Residue Model of Polypeptide Chains." *Proceedings of the National Academy of Sciences* 102(7):2362–67.

- Lorand, Laszlo and Robert M. Graham. 2003. "Transglutaminases: Crosslinking Enzymes with Pleiotropic Functions." *Nature Reviews Molecular Cell Biology* 4(2):140–56.
- Lowy, B. and B. Z. Dorfman. 1970. "Adenylosuccinase Activity in Human and Rabbit Erythrocyte Lysates." *Journal of Biological Chemistry* 245(12):3043–46.
- Lu, Xiaojun, R. Paul Nobrega, Heather Lynaugh, Tushar Jain, Kyle Barlow, Todd Boland, Arvind Sivasubramanian, Maximiliano Vásquez, and Yingda Xu. 2019. "Deamidation and Isomerization Liability Analysis of 131 Clinical-Stage Antibodies." *MAbs* 11(1):45–57.
- Lynch, Michael and Georgi K. Marinov. 2015. "The Bioenergetic Costs of a Gene." *Proceedings of the National Academy of Sciences of the United States of America* 112(51):15690–95.
- Lyon, Yana A., Miranda P. Collier, Dylan L. Riggs, Matteo T. Degiacomi, Justin L. P. Benesch, and Ryan R. Julian. 2019. "Structural and Functional Consequences of Age-Related Isomerization in α -Crystallins." *Journal of Biological Chemistry* jbc.RA118.007052.
- MacRae, James I., Matthew Wa Dixon, Megan K. Dearnley, Hwa H. Chua, Jennifer M. Chambers, Shannon Kenny, Iveta Bottova, Leann Tilley, Malcolm J. Mcconville, Matthew Wa Dixon, Megan K. Dearnley, Hwa H. Chua, Jennifer M. Chambers, Shannon Kenny, Iveta Bottova, Leann Tilley, and Malcolm J. Mcconville. 2013. "Mitochondrial Metabolism of Sexual and Asexual Blood Stages of the Malaria Parasite Plasmodium Falciparum." *BMC Biology* 11(1):67.
- Maier, Alexander G., Joanna A. M. Braks, Andrew P. Waters, and Alan F. Cowman. 2006. "Negative Selection Using Yeast Cytosine Deaminase/Uracil Phosphoribosyl Transferase in Plasmodium Falciparum for Targeted Gene Deletion by Double Crossover Recombination." *Molecular and Biochemical Parasitology* 150(1):118–21.
- Manzoni, Giulia, Sylvie Briquet, Veronica Risco-Castillo, Charlotte Gaultier, Selma Topçu, Maria Larisa Ivănescu, Jean François Franetich, Bénédicte Hoareau-Coudert, Dominique Mazier, and Olivier Silvie. 2014. "A Rapid and Robust Selection Procedure for Generating Drug-Selectable Marker-Free Recombinant Malaria Parasites." *Scientific Reports* 4:1–10.
- Di Matteo, Paola, Flavio Curnis, Renato Longhi, Giorgio Colombo, Angelina Sacchi, Luca Crippa, Maria Pia Protti, Mirco Ponzoni, Salvatore Toma, and Angelo Corti. 2006. "Immunogenic and Structural Properties of the Asn-Gly-Arg (NGR) Tumor Neovasculature-Homing Motif." *Molecular Immunology* 43(10):1509–18.
- Matthews, B. W., H. Nicholson, and W. J. Becktel. 1987. "Enhanced Protein Thermostability from Site-Directed Mutations That Decrease the Entropy of Unfolding.Pdf." *Proceedings of the National Academy of Sciences of the United States of America* 84(19):6663–67.
- McCoy, Airlie J., Ralf W. Grosse-Kunstleve, Paul D. Adams, Martyn D. Winn, Laurent C. Storoni, and Randy J. Read. 2007. "Phaser Crystallographic Software." *Journal of Applied Crystallography* 40(4):658–74.
- Mehrotra, Sonali, Monnanda P. Bopanna, Vinay Bulusu, and Hemalatha Balaram. 2010. "Adenine Metabolism in Plasmodium Falciparum." *Experimental Parasitology* 125(2):147–51.
- Meissner, Markus, Efrosinia Krejany, Paul R. Gilson, Tania F. de Koning-Ward, Dominique Soldati, and Brendan S. Crabb. 2005. "Tetracycline Analogue-Regulated Transgene Expression in Plasmodium Falciparum Blood Stages Using Toxoplasma Gondii Transactivators." *Proceedings of the National Academy of Sciences of the United States of America* 102(8):2980–85.
- Ménard, Robert, Ali A. Sultan, Claudio Cortes, Rita Altszuler, Melissa R. Van Dijk, Chris J. Janse, Andrew P. Waters, Ruth S. Nussenzweig, and Victor Nussenzweig. 1997. *Circumsporozoite Protein Is Required for Development of Malaria Sporozoites in Mosquitoes*. Vol. 385.
- Menko, Fred H., Eamonn R. Maher, Laura S. Schmidt, Lindsay A. Middleton, Kristiina Aittomäki, Ian Tomlinson, Stéphane Richard, and W. Marston Linehan. 2014. "Hereditary Leiomyomatosis and Renal Cell Cancer (HLRCC): Renal Cancer Risk, Surveillance and Treatment." *Familial Cancer* 13(4):637–44.
- Merkley, Eric D., Thomas O. Metz, Richard D. Smith, John W. Baynes, and Norma Frizzell. 2014. "The

- Succinated Proteome.” *Mass Spectrometry Reviews* 33(2):98–109.
- Mikolajczak, Sebastian A., Ashley M. Vaughan, Niwat Kangwanrangsang, Wanlapa Roobsoong, Matthew Fishbaugher, Narathatai Yimamnuaychok, Nastaran Rezakhani, Viswanathan Lakshmanan, Naresh Singh, Alexis Kaushansky, Nelly Camargo, Michael Baldwin, Scott E. Lindner, John H. Adams, Jetsumon Sattabongkot, and Stefan H. I. Kappe. 2015. “Plasmodium Vivax Liver Stage Development and Hypnozoite Persistence in Human Liver-Chimeric Mice.” *Cell Host and Microbe* 17(4):526–35.
- Mitchell, G. H., A. W. Thomas, G. Margos, A. R. Dlugewski, and L. H. Bannister. 2004. “Apical Membrane Antigen 1, a Major Malaria Vaccine Candidate, Mediates the Close Attachment of Invasive Merozoites to Host Red Blood Cells.” *Infection and Immunity* 72(1):154–58.
- Mogollon, Catherin Marin, Fiona J. A. Van Pul, Takashi Imai, Jai Ramesar, Seâverine Chevalley-Maurel, Guido M. De Roo, Sabrina A. J. Veld, Hans Kroeze, Blandine M. D. Franke-Fayard, Chris J. Janse, and Shahid M. Khan. 2016. “Rapid Generation of Marker-Free P. Falciparum Fluorescent Reporter Lines Using Modified CRISPR/Cas9 Constructs and Selection Protocol.” *PLoS ONE* 11(12).
- Mony, Binny M., Monika Mehta, Gotam K. Jarori, and Shobhona Sharma. 2009. “Plant-like Phosphofruktokinase from Plasmodium Falciparum Belongs to a Novel Class of ATP-Dependent Enzymes.” *International Journal for Parasitology* 39(13):1441–53.
- Moon, Robert W., Joanna Hall, Fania Rangkuti, YungShwen Shwen Ho, Neil Almond, Graham H. Mitchell, Arnab Pain, Anthony A. Holder, and Michael J. Blackman. 2013. “Adaptation of the Genetically Tractable Malaria Pathogen Plasmodium Knowlesi to Continuous Culture in Human Erythrocytes.” *Proceedings of the National Academy of Sciences of the United States of America* 110(2):531–36.
- Moss, By Karen M. and John D. McGivan. 1975. “Characteristics of Aspartate Deamination by the Purine Nucleotide Cycle in the Cytosol Fraction of Rat Liver.” 25:275–83.
- Mouilleron, Stéphane and Béatrice Golinelli-Pimpaneau. 2007. “Conformational Changes in Ammonia-Channeling Glutamine Amidotransferases.” *Current Opinion in Structural Biology* 17(6):653–64.
- Mukaiyama, Atsushi, Kazufumi Takano, Mitsuru Haruki, Masaaki Morikawa, and Shigenori Kanaya. 2004. “Kinetically Robust Monomeric Protein from a Hyperthermophile.” *Biochemistry* 43(43):13859–66.
- Muralidharan, Vasant, Anna Oksman, Mari Iwamoto, Thomas J. Wandless, and Daniel E. Goldberg. 2011. “Asparagine Repeat Function in a Plasmodium Falciparum Protein Assessed via a Regulatable Fluorescent Affinity Tag.” *Proceedings of the National Academy of Sciences of the United States of America* 108(11):4411–16.
- Murphy, A. D. 1998a. “Metabolic Changes of the Malaria Parasite during the Transition from the Human to the Mosquito Host.”
- Murphy, A. D. 1998b. “Metabolic Changes of the Malaria Parasite During the Transition From the Human To the Mosquito Host.”
- Murshudov, Garib N., Pavol Skubák, Andrey A. Lebedev, Navraj S. Pannu, Roberto A. Steiner, Robert A. Nicholls, Martyn D. Winn, Fei Long, and Alexei A. Vagin. 2011. “REFMAC5 for the Refinement of Macromolecular Crystal Structures.” *Acta Crystallographica Section D: Biological Crystallography* 67(4):355–67.
- Murshudov, Garib N., Alexei A. Vagin, and Eleanor J. Dodson. 1997. “Refinement of Macromolecular Structures by the Maximum-Likelihood Method.” *Acta Crystallographica Section D: Biological Crystallography* 53(3):240–55.
- Nagappa, Lakshmeesha Kempaiah, Dipti Singh, Sandeep Dey, Kota Arun Kumar, and Hemalatha Balaram. 2019. “Biochemical and Physiological Investigations on Adenosine 5' Monophosphate Deaminase from Plasmodium Spp.” *Molecular Microbiology* 112(2):699–717.
- Nakayasu, Ernesto S., Meagan C. Burnet, Hanna E. Walukiewicz, Christopher S. Wilkins, Anil K. Shukla, Shelby Brooks, Matthew J. Plutz, Brady D. Lee, Birgit Schilling, Alan J. Wolfe, Susanne

- Müller, John R. Kirby, Christopher V Rao, John R. Cort, and Samuel H. Payne. 2017. "Ancient Regulatory Role of Lysine Acetylation in Central Metabolism." *MBio* 8(6).
- Natarajan, Kedar Nath. 1968. "Metabolism of P. Berghei-Pi Incorporation into High Energy Phosphates." *Experimental Parasitology* 22:27–32.
- Natraj, D. V, N. Srinivasan, R. Sowdhamini, and C. Ramakrishnan. 1995. "Alpha-Turns In Protein Structures." *Current Science* 69(5):434–47.
- Newberry, Robert W., Gail J. Bartlett, Brett VanVeller, Derek N. Woolfson, and Ronald T. Raines. 2014. "Signatures of N→ π^* Interactions in Proteins." *Protein Science* 23(3):284–88.
- Newberry, Robert W. and Ronald T. Raines. 2017. "The N→ π^* Interaction." *Accounts of Chemical Research* 50(8):1838–46.
- Newberry, Robert W., Brett Vanveller, Ilia A. Guzei, and Ronald T. Raines. 2013. "N → π^* Interactions of Amides and Thioamides: Implications for Protein Stability." *Journal of the American Chemical Society* 135(21):7843–46.
- Newsholme, P., R. Curi, S. Gordon, and E. A. Newsholme. 1986. "Metabolism of Glucose, Glutamine, Long-Chain Fatty Acids and Ketone Bodies by Murine Macrophages." *Biochemical Journal* 239(1):121–25.
- Niikura, Mamoru, Keisuke Komatsuya, Shin Ichi Inoue, Risa Matsuda, Hiroko Asahi, Daniel Ken Inaoka, Kiyoshi Kita, and Fumie Kobayashi. 2017. "Suppression of Experimental Cerebral Malaria by Disruption of Malate:Quinone Oxidoreductase." *Malaria Journal* 16(1):247.
- Niu, Yanling, Yisui Xia, Qinhong Cao, Xiaojiang S. Chen, Yang Fu, Huiqiang Lou, and Jiamin Cui. 2015. "The Helicase Activity of Hyperthermophilic Archaeal MCM Is Enhanced at High Temperatures by Lysine Methylation." *Frontiers in Microbiology* 6(November):1–12.
- Noguchi, Shuji, Kazuki Miyawaki, and Yoshinori Satow. 1998. "Succinimide and Isoaspartate Residues in the Crystal Structures of Hen Egg-White Lysozyme Complexed with Tri- N -Acetylchitotriose."
- O' Sullivan, W. J. and K. Ketley. 1980. "Biosynthesis of Uridine Monophosphate in Plasmodium Berghei." *Annals of Tropical Medicine and Parasitology* 74(2):109–14.
- Oelshlegel, Fred J., Barry J. Sander, and George J. Brewer. 1975. "Pyruvate Kinase in Malaria Host-Parasite Interaction." *Nature* 255(5506):345–47.
- Olafsson, Pétur and Ulrich Certa. 1994. "Expression and Cellular Localisation of Hexokinase during the Bloodstage Development of Plasmodium Falciparum." *Molecular and Biochemical Parasitology* 63(1):171–74.
- Olafsson, Pétur, Hugues Matile, and Ulrich Certa. 1992. "Molecular Analysis of Plasmodium Falciparum Hexokinase." *Molecular and Biochemical Parasitology* 56(1):89–101.
- Olaszewski, Kellen L., Michael W. Mather, Joanne M. Morrissey, Benjamin A. Garcia, Akhil B. Vaidya, Joshua D. Rabinowitz, and Manuel Llinás. 2010. "Branched Tricarboxylic Acid Metabolism in Plasmodium Falciparum." *Nature* 466(7307):774–78.
- Oppenheim, Rebecca D., Darren J. Creek, James I. Macrae, Katarzyna K. Modrzynska, Paco Pino, Julien Limenitakis, Valerie Polonais, Frank Seeber, Michael P. Barrett, Oliver Billker, Malcolm J. McConville, and Dominique Soldati-Favre. 2014. "BCKDH: The Missing Link in Apicomplexan Mitochondrial Metabolism Is Required for Full Virulence of Toxoplasma Gondii and Plasmodium Berghei." *PLoS Pathogens* 10(7).
- Orr, Rachael Y., Nisha Philip, and Andrew P. Waters. 2012. "Improved Negative Selection Protocol for Plasmodium Berghei in the Rodent Malarial Model." *Malaria Journal* 11(1):103.
- Pace, Amanda L., Rita L. Wong, Yonghua Taylor Zhang, Yung-Hsiang Kao, and Y. John Wang. 2013. "Asparagine Deamidation Dependence on Buffer Type, PH, and Temperature." *Journal of Pharmaceutical Sciences* 102(6):1712–23.
- Painter, Heather J., Joanne M. Morrissey, Michael W. Mather, and Akhil B. Vaidya. 2007. "Specific Role

- of Mitochondrial Electron Transport in Blood-Stage Plasmodium Falciparum." *Nature* 446(7131):88–91.
- Palm, Gottfried J., Anurag Sharma, Moni Kumari, Santosh Panjekar, Dirk Albrecht, Medicherla V. Jagannadham, and Winfried Hinrichs. 2014. "Post-Translational Modification and Extended Glycosylation Pattern of a Plant Latex Peroxidase of Native Source Characterized by X-Ray Crystallography." *The FEBS Journal* 281(18):4319–33.
- Palmer, Clovis S., Matias Ostrowski, Brad Balderson, Nicole Christian, and Suzanne M. Crowe. 2015. "Glucose Metabolism Regulates T Cell Activation, Differentiation, and Functions." *Frontiers in Immunology* 6(JAN).
- Pavlicek, Jiri, Steven L. Coon, Surajit Ganguly, Joan L. Weller, Sergio A. Hassan, Dan L. Sackett, and David C. Klein. 2008. "Evidence That Proline Focuses Movement of the Floppy Loop of Arylalkylamine N-Acetyltransferase (EC 2.3.1.87)." *Journal of Biological Chemistry* 283(21):14552–58.
- Pino, Paco, Sarah Sebastian, Eunbin Arin Kim, Erin Bush, Mathieu Brochet, Katrin Volkmann, Elyse Kozlowski, Manuel Llinás, Oliver Billker, and Dominique Soldati-Favre. 2012. "A Tetracycline-Repressible Transactivator System to Study Essential Genes in Malaria Parasites." *Cell Host and Microbe* 12(6):824–34.
- Piroli, Gerardo G., Allison M. Manuel, Michael D. Walla, Matthew J. Jepson, Jonathan W. C. Brock, Mathur P. Rajesh, Ross M. Tanis, William E. Cotham, and Norma Frizzell. 2014. "Identification of Protein Succination as a Novel Modification of Tubulin." *Biochemical Journal* 462(2):231–45.
- Plagemann, Peter G. W., Robert M. Wohlhueter, and Martin Kraupp. 1985. "Adenosine Uptake, Transport, and Metabolism in Human Erythrocytes." *Journal of Cellular Physiology* 125(2):330–36.
- Prommana, Parichat, Chairat Uthaipibull, Chayaphat Wongsombat, Sumalee Kamchonwongpaisan, Yongyuth Yuthavong, Ellen Knuepfer, Anthony A. Holder, and Philip J. Shaw. 2013. "Inducible Knockdown of Plasmodium Gene Expression Using the GlmS Ribozyme" edited by A. G. Craig. *PLoS ONE* 8(8):e73783.
- Przylas, I., Y. Terada, K. Fujii, T. Takaha, W. Saenger, and N. Sträter. 2000. "X-Ray Structure of Acarbose Bound to Amylomaltase from *Thermus Aquaticus*. Implications for the Synthesis of Large Cyclic Glucans." *European Journal of Biochemistry* 267(23):6903–13.
- Qiu, Huawei, Ronnie Wei, Julie Jaworski, Ekaterina Boudanova, Heather Hughes, Scott VanPatten, Anders Lund, Jaime Day, Yanfeng Zhou, Tracey McSherry, Clark Q. Pan, and Rebecca Sendak. 2019. "Engineering an Anti-CD52 Antibody for Enhanced Deamidation Stability." *MAbs* 11(7):1266–75.
- Quashie, Neils B., Dominique Dorin-Semblat, Patrick G. Bray, Giancarlo A. Biagini, Christian Doerig, Lisa C. Ranford-Cartwright, and Harry P. De Koning. 2008. "A Comprehensive Model of Purine Uptake by the Malaria Parasite *Plasmodium Falciparum*: Identification of Four Purine Transport Activities in Intraerythrocytic Parasites." *Biochemical Journal* 411(2):287–95.
- Quashie, Neils B., Lisa C. Ranford-Cartwright, and Harry P. De Koning. 2010. "Uptake of Purines in *Plasmodium Falciparum*-Infected Human Erythrocytes Is Mostly Mediated by the Human Equilibrative Nucleoside Transporter and the Human Facilitative Nucleobase Transporter." *Malaria Journal* 9(1):36.
- Radkiewicz, J. L., H. Zipse, S. Clarke, and K. N. Houk. 2001. "Neighboring Side Chain Effects on Asparaginyl and Aspartyl Degradation: An Ab Initio Study of the Relationship between Peptide Conformation and Backbone NH Acidity." *Journal of the American Chemical Society* 123(15):3499–3506.
- Raman, Jayalakshmi, Sonali Mehrotra, Ranjith P. Anand, and Hemalatha Balaram. 2004. "Unique Kinetic Mechanism of *Plasmodium Falciparum* Adenylosuccinate Synthetase." *Molecular and Biochemical Parasitology* 138(1):1–8.
- Rathod, Pradipsinh K. and Karl H. Rieckmann. 1982. "Enzymes of Purine and Pyrimidine Metabolism from the Human Malaria Parasite, *Plasmodium Falciparum* Malaria Evolution in South Asia View Project 2018 GORDON CONFERENCE DRUG RESISTANCE View Project SEE PROFILE."

Article in Molecular and Biochemical Parasitology.

- Rhee, Sang Youl and Young Seol Kim. 2018. "The Role of Advanced Glycation End Products in Diabetic Vascular Complications." *Diabetes and Metabolism Journal* 42(3):188–95.
- RIVADENEIRA, ENID M., MOISES WASSERMAN, and CARLOS T. ESPINAL. 1983. "Separation and Concentration of Schizonts of Plasmodium Falciparum by Percoll Gradients." *The Journal of Protozoology* 30(2):367–70.
- Robinson, N. E. 2002. "Protein Deamidation." *Proceedings of the National Academy of Sciences* 99(8):5283–88.
- Robinson, N. E. and A. B. Robinson. 2001. "Molecular Clocks." *Proceedings of the National Academy of Sciences of the United States of America* 98(3):944–49.
- Robinson, N. E. and A. B. Robinson. 2004a. "Molecular Clocks: Deamidation of Asparaginyl and Glutaminyl Residues in Peptides and Proteins." *Althouse Press, Cave Junction, OR* 1–11.
- Robinson, N. E. and A. B. Robinson. 2004b. "Prediction of Primary Structure Deamidation Rates of Asparaginyl and Glutaminyl Peptides through Steric and Catalytic Effects." *Journal of Peptide Research* 63(5):437–48.
- Van Roey, Patrick, Brian Pereira, Zhong Li, Kaori Hiraga, Marlene Belfort, and Victoria Derbyshire. 2007. "Crystallographic and Mutational Studies of Mycobacterium Tuberculosis RecA Mini-Inteins Suggest a Pivotal Role for a Highly Conserved Aspartate Residue." *Journal of Molecular Biology* 367(1):162–73.
- Roth, E. 1990. "Plasmodium Falciparum Carbohydrate Metabolism: A Connection between Host Cell and Parasite." *Blood Cells* 16(2–3):453–60.
- Roth, Ziv, Galit Yehezkel, and Isam Khalaila. 2012. "Identification and Quantification of Protein Glycosylation." *International Journal of Carbohydrate Chemistry* 2012.
- RUDZINSKA, MARIA A., WILLIAM TRAGER, and R. S. BRAY. 1965. "Pinocytotic Uptake and the Digestion of Hemoglobin in Malaria Parasites* †." *The Journal of Protozoology* 12(4):563–76.
- Sabina, R. L., J. L. Swain, B. M. Patten, T. Ashizawa, W. E. O'Brien, and E. W. Holmes. 1980. "Disruption of the Purine Nucleotide Cycle. A Potential Explanation for Muscle Dysfunction in Myoadenylate Deaminase Deficiency." *Journal of Clinical Investigation* 66(6):1419–23.
- Sacan, Ahmet, Ozgur Ozturk, Hakan Ferhatosmanoglu, and Yusu Wang. 2007. "LFM-Pro: A Tool for Detecting Significant Local Structural Sites in Proteins." *Bioinformatics* 23(6):709–16.
- Sadiq, S. Kashif and Peter V. Coveney. 2015. "Computing the Role of near Attack Conformations in an Enzyme-Catalyzed Nucleophilic Bimolecular Reaction." *Journal of Chemical Theory and Computation* 11(1):316–24.
- Saiardi, Adolfo. 2016. "Protein Pyrophosphorylation: Moving Forward." *Biochemical Journal* 473(21):3765–68.
- Salcedo-Sora, J. Enrique, Eva Caamano-Gutierrez, Stephen A. Ward, and Giancarlo A. Biagini. 2014. "The Proliferating Cell Hypothesis: A Metabolic Framework for Plasmodium Growth and Development." *Trends in Parasitology* 30(4):170–75.
- SANDBERG, A. A., G. R. LEE, G. E. CARTWRIGHT, and M. M. WINTROBE. 1955. "Purine Nucleoside Phosphorylase Activity of Blood. I. Erythrocytes." *The Journal of Clinical Investigation* 34(12):1823–29.
- Schwach, Frank, Ellen Bushell, Ana Rita Gomes, Burcu Anar, Gareth Girling, Colin Herd, Julian C. Rayner, and Oliver Billker. 2015. "PlasmoGEM, a Database Supporting a Community Resource for Large-Scale Experimental Genetics in Malaria Parasites." *Nucleic Acids Research* 43(D1):D1176–82.
- Shan, Lu, Øyvind Molberg, Isabelle Parrot, Felix Hausch, Ferda Filiz, Gary M. Gray, Ludvig M. Sollid, and Chaitan Khosla. 2002. "Structural Basis for Gluten Intolerance in Celiac Sprue." *Science* 297(5590):2275–79.

- Shental-Bechor, D. and Y. Levy. 2008. "Effect of Glycosylation on Protein Folding: A Close Look at Thermodynamic Stabilization." *Proceedings of the National Academy of Sciences* 105(24):8256–61.
- Sherman, IW. 1979. "Biochemistry of Plasmodium (Malaria Parasites)." *Microbiol Rev* 43(4):453–95.
- Shigeura, Harold T. and Charles N. Gordon. 1962a. *Hadacidin, a New Inhibitor of Purine Biosynthesis*. Vol. 237.
- Shigeura, Harold T. and Charles N. Gordon. 1962b. *The Mechanism of Action of Hadacidine*. Vol. 237.
- Shivakumaraswamy, Santosh, Lakshmi Prasoon Thota, Richard Haser, Hemalatha Balaram, Nushin Aghajari, Lionel Ballut, Sébastien Violot, Santosh Shivakumaraswamy, Lakshmi Prasoon Thota, Manu Sathya, Jyothirmai Kunala, Bauke W. Dijkstra, Raphaël Terreux, Richard Haser, Hemalatha Balaram, and Nushin Aghajari. 2015. "Active Site Coupling in Plasmodium Falciparum GMP Synthetase Is Triggered by Domain Rotation." *Nature Communications* 6(May).
- Shoemark, Deborah K., Matthew J. Cliff, Richard B. Sessions, and Anthony R. Clarke. 2007. "Enzymatic Properties of the Lactate Dehydrogenase Enzyme from Plasmodium Falciparum." *FEBS Journal* 274(11):2738–48.
- Simonovic, Miljan and Karl Volz. 2001. "A Distinct Meta-Active Conformation in the 1.1-Å Resolution Structure of Wild-Type ApoCheY." *Journal of Biological Chemistry* 276(31):28637–40.
- Simonovic, Miljan and Karl Volz. 2002. "Atomic Resolution Structure of a Succinimide Intermediate in E. Coli CheY." *Journal of Molecular Biology* 322(4):663–67.
- Skinner-Adams, Tina S., Paula M. Lawrie, Paula L. Hawthorne, Donald L. Gardiner, and Katharine R. Trenholme. 2003. "Comparison of Plasmodium Falciparum Transfection Methods." *Malaria Journal* 2:1–4.
- Slomianny, C., G. Prensier, and P. Charet. 1985. "Ingestion of Erythrocytic Stroma by Plasmodium Chabaudi Trophozoites: Ultrastructural Study by Serial Sectioning and 3-Dimensional Reconstruction." *Parasitology* 90(3):579–87.
- Slowiaczek, Peter and M. H. N. Tattersall. 1982. "The Determination of Purine Levels in Human and Mouse Plasma." *Analytical Biochemistry* 125(1):6–12.
- Smith, J. L. 1995. "Structures of Glutamine Amidotransferases from the Purine Biosynthetic Pathway." *Biochemical Society Transactions* 23(4):894–98.
- Šoškić, Vukić, Karlfried Groebe, and André Schratzenholz. 2008. "Nonenzymatic Posttranslational Protein Modifications in Ageing." *Experimental Gerontology* 43(4):247–57.
- Spadafora, Carmenza, Lucia Gerena, and Karen M. Kopydlowski. 2011. "Comparison of the in Vitro Invasive Capabilities of Plasmodium Falciparum Schizonts Isolated by Percoll Gradient or Using Magnetic Based Separation." *Malaria Journal* 10:2–5.
- Spiwok, Vojtěch, Petra Lipovová, and Blanka Králová. 2007. "Metadynamics in Essential Coordinates: Free Energy Simulation of Conformational Changes." *The Journal of Physical Chemistry B* 111(12):3073–76.
- Srivastava, Anubhav, Darren J. Creek, Krystal J. Evans, David De Souza, Louis Schofield, Sylke Müller, Michael P. Barrett, Malcolm J. McConville, and Andrew P. Waters. 2015. "Host Reticulocytes Provide Metabolic Reservoirs That Can Be Exploited by Malaria Parasites." *PLoS Pathogens* 11(6):1–22.
- Srivastava, Indresh K., Hagai Rottenberg, and Akhil B. Vaidya. 1997. "Atovaquone, a Broad Spectrum Antiparasitic Drug, Collapses Mitochondrial Membrane Potential in a Malarial Parasite." *Journal of Biological Chemistry* 272(7):3961–66.
- Storm, Janet, Sonal Sethia, Gavin J. Blackburn, Achuthanunni Chokkathukalam, David G. Watson, Rainer Breitling, Graham H. Coombs, Sylke Müller, and Sylke Müller. 2014. "Phosphoenolpyruvate Carboxylase Identified as a Key Enzyme in Erythrocytic Plasmodium Falciparum Carbon Metabolism." *PLoS Pathogens* 10(1).

- Straimer, Judith, Marcus C. S. Lee, Andrew H. Lee, Bryan Zeitler, April E. Williams, Jocelynn R. Pearl, Lei Zhang, Edward J. Rebar, Philip D. Gregory, Manuel Llinás, Fyodor D. Urnov, and David A. Fidock. 2012. "Site-Specific Genome Editing in Plasmodium Falciparum Using Engineered Zinc-Finger Nucleases." *Nature Methods* 9(10):993–98.
- Sträter, Norbert, Timm Maier, Wolfgang Zimmermann, Wolfram Saenger, Nicola Bexten, Christian Roth, and Nicole Weizenmann. 2017. "Amylose Recognition and Ring-Size Determination of Amylomaltase." *Science Advances* 3(1):e1601386.
- Sugai, Motoyuki, Kiyotaka Hatazaki, Akira Mogami, Hiroyuki Ohta, Sylvie Y. Pérès, Frédéric Héroult, Yasuhiko Horiguchi, Minako Masuda, Yoko Ueno, Hitoshi Komatsuzawa, Hidekazu Suginaka, and Eric Oswald. 1999. "Cytotoxic Necrotizing Factor Type 2 Produced by Pathogenic Escherichia Coli Deamidates a Gln Residue in the Conserved G-3 Domain of the Rho Family and Preferentially Inhibits the GTPase Activity of RhoA and Rac1." *Infection and Immunity* 67(12):6550–57.
- Sullivan, Lucas B., Dan Y. Gui, Aaron M. Hosios, Lauren N. Bush, Elizaveta Freinkman, and Matthew G. Vander Heiden. 2015. "Supporting Aspartate Biosynthesis Is an Essential Function of Respiration in Proliferating Cells." *Cell* 162(3):552–63.
- Sultan, Mohammad M., Gert Kiss, and Vijay S. Pande. 2018. "Towards Simple Kinetic Models of Functional Dynamics for a Kinase Subfamily." *Nature Chemistry* 10(9):903–9.
- Suzuki, Yuzuru, Kazumi Oishi, Hajime Nakano, and Takashi Nagayama. 1987. "A Strong Correlation between the Increase in Number of Proline Residues and the Rise in Thermostability of Five Bacillus Oligo-1,6-Glucosidases." *Applied Microbiology and Biotechnology* 26(6):546–51.
- Svensson, Anna-Karin E., Jill A. Zitzewitz, C. Rober. Matthews, and Virginia F. Smith. 2006. "The Relationship between Chain Connectivity and Domain Stability in the Equilibrium and Kinetic Folding Mechanisms of Dihydrofolate Reductase from E. Coli." *Protein Engineering, Design and Selection* 19(4):175–85.
- Sydow, Jasmin F., Florian Lipsmeier, Vincent Larraillet, Maximiliane Hilger, Bjoern Mautz, Michael Mølhøj, Jan Kuentzer, Stefan Klostermann, Juergen Schoch, Hans R. Voelger, Joerg T. Regula, Patrick Cramer, Apollon Papadimitriou, and Hubert Kettenberger. 2014. "Structure-Based Prediction of Asparagine and Aspartate Degradation Sites in Antibody Variable Regions" edited by S. Dübel. *PLoS ONE* 9(6):e100736.
- Talman, Arthur M., Olivier Domarle, F. Ellis McKenzie, Frédéric Arieu, and Vincent Robert. 2004. "Gametocytogenesis: The Puberty of Plasmodium Falciparum." *Malaria Journal* 3(1):24.
- Tamura, Risako, Rika Oi, Satoko Akashi, Mika K. Kaneko, Yukinari Kato, and Terukazu Nogi. 2019. "Application of the NZ-1 Fab as a Crystallization Chaperone for PA Tag-Inserted Target Proteins." *Protein Science* 28(4):823–36.
- Tan, Bo, Zhaohai Lu, Sucai Dong, Genshi Zhao, and Ming Shang Kuo. 2014. "Derivatization of the Tricarboxylic Acid Intermediates with O-Benzylhydroxylamine for Liquid Chromatography-Tandem Mass Spectrometry Detection." *Analytical Biochemistry* 465:134–47.
- Tanabe, K. 1990. "Glucose Transport in Malaria Infected Erythrocytes." *Parasitology Today* 6(7):225–29.
- Tanaka, Michael Hennig, Reinhard Sterner, and Kasper Kirschner. 2000. "Structure and Function of Mutationally Generated Monomers of Dimeric Phosphoribosylanthranilate Isomerase from Thermotoga Maritima." *Structure* 8(3):265–76.
- Tanakai, Yoshikazu, Kouhei Tsumoto, Yoshiaki Yasutake, Mitsuo Umetsu, Min Yao, Harumi Fukada, Isao Tanaka, and Izumi Kumagai. 2004. "How Oligomerization Contributes to the Thermostability of an Archaeon Protein: Protein L-Isoaspartyl-O-Methyltransferase from Sulfolobus Tokodaii." *Journal of Biological Chemistry* 279(31):32957–67.
- Tarleton, Rick and Duo Peng. 2015. "EuPaGDT: A Web Tool Tailored to Design CRISPR Guide RNAs for Eukaryotic Pathogens." *Microbial Genomics* 1(4):1–7.
- Teleki, Attila and Ralf Takors. 2019. "Quantitative Profiling of Endogenous Metabolites Using Hydrophilic Interaction Liquid Chromatography–Tandem Mass Spectrometry (HILIC-MS/MS)." *Journal of Chromatography B* 1617:1–12.

- Methods in Molecular Biology* 1859:185–207.
- Terwilliger, Thomas C., Ralf W. Grosse-Kunstleve, Pavel V. Afonine, Nigel W. Moriarty, Peter H. Zwart, Li Wei Hung, Randy J. Read, and Paul D. Adams. 2007. “Iterative Model Building, Structure Refinement and Density Modification with the PHENIX AutoBuild Wizard.” *Acta Crystallographica Section D: Biological Crystallography* 64(1):61–69.
- Teshimas, Glen, John T. Stultsg, Victor Ling, and Eleanor Canova-davis. 1991. “Isolation and Characterization of a Succinimide Variant of Methionyl Human Growth Hormone.” 13544–47.
- Tornheimsb, Keith, Henrianna Pangllii, and E. Costello. 1986. “The Purine Nucleotide Cycle and Ammoniogenesis in Rat Kidney Tubules.” (12).
- Trager, W. and J. B. Jensen. 1977. “Cultivation of Erythrocytic Stages.” *Bulletin of the World Health Organization* 55(2–3):363–65.
- Ugur, Ilke, Antoine Marion, Viktorya Aviyente, and Gerald Monard. 2015. “Why Does Asn71 Deamidate Faster than Asn15 in the Enzyme Triosephosphate Isomerase? Answers from Microsecond Molecular Dynamics Simulation and QM/MM Free Energy Calculations.” *Biochemistry* 54(6):1429–39.
- Ulrich, P. and A. Cerami. 2001. “Protein Glycation, Diabetes, and Aging.” *Recent Progress in Hormone Research* 56:1–21.
- Unno, Hideaki, Azusa Nakamura, Shingo Mori, Shuichiro Goda, Kenichi Yamaguchi, Keiko Hiemori, Hiroaki Tateno, and Tomomitsu Hatakeyama. 2018. “Identification, Characterization, and X-Ray Crystallographic Analysis of a Novel Type of Lectin AJLec from the Sea Anemone *Anthopleura Japonica*.” *Scientific Reports* 8(1).
- Valdés-Jiménez, Alejandro, Josep L. Larriba-Pey, Gabriel Núñez-Vivanco, and Miguel Reyes-Parada. 2019. “3D-PP: A Tool for Discovering Conserved Three-Dimensional Protein Patterns.” *International Journal of Molecular Sciences* 20(13).
- Vaughan, Ashley M. and Stefan H. I. Kappe. 2017. “Malaria Parasite Liver Infection and Exoerythrocytic Biology.” *Cold Spring Harbor Laboratory Press* 1–22.
- Veletzky, Luzia, Khalid Rehman, Tilman Lingscheid, Wolfgang Poepl, Felix Loetsch, Heinz Burgmann, and Michael Ramharter. 2014. “In Vitro Activity of Immunosuppressive Drugs against *Plasmodium Falciparum*.” *Malaria Journal* 13(1).
- Venkatachalam, C. M. 1968. “Stereochemical Criteria for Polypeptides and Proteins. V. Conformation of a System of Three Linked Peptide Units.” *Biopolymers* 6(10):1425–36.
- Vieille, Claire, Doug S. Burdette, and J. Gregory Zeikus. 1996. “Thermozymes.” *Biotechnology Annual Review* 2(C):1–83.
- Vieille, Claire and Gregory J. Zeikus. 2006. “Hyperthermophilic Enzymes: Sources, Uses, and Molecular Mechanisms for Thermostability.” *Microbiology and Molecular Biology Reviews* 65(1):324.
- Vincent, Isabel M. and Michael P. Barrett. 2015. “Metabolomic-Based Strategies for Anti-Parasite Drug Discovery.” *Journal of Biomolecular Screening* 20(1):44–55.
- Violand, B. N., M. R. Schlittler, E. W. Kolodziej, P. C. Toren, M. A. Cabonce, N. R. Siegel, K. L. Duffin, J. F. Zobel, C. E. Smith, and J. S. Tou. 1992. “Isolation and Characterization of Porcine Somatotropin Containing a Succinimide Residue in Place of Aspartate 129.” *Protein Science* 1(12):1634–41.
- Wagner, Gregory R. and R. Mark Payne. 2013. “Widespread and Enzyme-Independent N ϵ -Acetylation and N ϵ -Succinylation of Proteins in the Chemical Conditions of the Mitochondrial Matrix.” *Journal of Biological Chemistry* 288(40):29036–45.
- Wagner, Jeffrey C., Randall J. Platt, Stephen J. Goldfless, Feng Zhang, and Jacquie C. Niles. 2014. “Efficient CRISPR-Cas9-Mediated Genome Editing in *Plasmodium Falciparum*.” *Nature Methods* 11(9):915–18.

- Walvekar, Adhish, Zeenat Rashida, Hemanth Maddali, and Sunil Laxman. 2018. "A Versatile LC-MS/MS Approach for Comprehensive, Quantitative Analysis of Central Metabolic Pathways." *Wellcome Open Research* 3(0):122.
- Wang, Lingle, Richard A. Friesner, and B. J. Berne. 2011. "Replica Exchange with Solute Scaling: A More Efficient Version of Replica Exchange with Solute Tempering (REST2)." *Journal of Physical Chemistry B* 115(30):9431–38.
- Warburg, Otto. 1956. "On the Origin of Cancer Cells." *Science* 123(3191):309–14.
- Warmack, Rebecca A., David R. Boyer, Chih-Te Zee, Logan S. Richards, Michael R. Sawaya, Duilio Cascio, Tamir Gonen, David S. Eisenberg, and Steven G. Clarke. 2019. "Structure of Amyloid- β (20-34) with Alzheimer's-Associated Isomerization at Asp23 Reveals a Distinct Protofilament Interface." *Nature Communications* 10(1):3357.
- Watanabe, Kunihiko, Kyoko Chishiro, Kazuhisa Kitamura, and Yuzuru Suzuki. 1991. "Proline Residues Responsible for Thermostability Occur with High Frequency in the Loop Regions of an Extremely Thermostable Oligo-1,6-Glucosidase from *Bacillus Thermoglucosidasius* KP1006." *Journal of Biological Chemistry* 266(36):24287–94.
- Watanabe, Kunihiko, Tomoko Masuda, Hiroyuki Ohashi, Hisaaki Mihara, and Yuzuru Suzuki. 1994. "Multiple Proline Substitutions Cumulatively Thermostabilize *Bacillus Cereus* ATCC7064 Oligo-1,6-Glucosidase." *European Journal of Biochemistry* 283:277–83.
- Webster, H. Kyle, June M. Whaun, Marvin D. Walker, and Teresa L. Bean. 1984. "Synthesis of Adenosine Nucleotides from Hypoxanthine by Human Malaria Parasites (*Plasmodium Falciparum*) in Continuous Erythrocyte Culture: Inhibition by Hadacidin but Not Alanosine." *Biochemical Pharmacology* 33(9):1555–57.
- Westrop, Gareth D., Roderick A. M. Williams, Lijie Wang, Tong Zhang, David G. Watson, Ana Marta Silva, and Graham H. Coombs. 2015. "Metabolomic Analyses of *Leishmania* Reveal Multiple Species Differences and Large Differences in Amino Acid Metabolism." *PLoS ONE* 10(9).
- Windsor, Ian W., Brian Gold, and Ronald T. Raines. 2019. "An N \rightarrow π^* Interaction in the Bound Substrate of Aspartic Proteases Replicates the Oxyanion Hole." *ACS Catalysis* 9(2):1464–71.
- van der Windt, Gerritje J. W. and Erika L. Pearce. 2012. "Metabolic Switching and Fuel Choice during T-Cell Differentiation and Memory Development." *Immunological Reviews* 249(1):27–42.
- Winn, Martyn D., Charles C. Ballard, Kevin D. Cowtan, Eleanor J. Dodson, Paul Emsley, Phil R. Evans, Ronan M. Keegan, Eugene B. Krissinel, Andrew G. W. Leslie, Airlie McCoy, Stuart J. McNicholas, Garib N. Murshudov, Navraj S. Pannu, Elizabeth A. Potterton, Harold R. Powell, Randy J. Read, Alexei Vagin, and Keith S. Wilson. 2011. "Overview of the CCP4 Suite and Current Developments." *Acta Crystallographica Section D: Biological Crystallography* 67(4):235–42.
- Woodrow, C. J., R. J. Burchmore, and S. Krishna. 2000. "Hexose Permeation Pathways in *Plasmodium Falciparum*-Infected Erythrocytes." *Proceedings of the National Academy of Sciences of the United States of America* 97(18):9931–36.
- Wright, Gavin J. and Julian C. Rayner. 2014. "*Plasmodium Falciparum* Erythrocyte Invasion: Combining Function with Immune Evasion." *PLoS Pathogens* 10(3):1–7.
- Wu, Mingxuan, Lucy S. Chong, David H. Perlman, Adam C. Resnick, and Dorothea Fiedler. 2016. "Inositol Polyphosphates Intersect with Signaling and Metabolic Networks via Two Distinct Mechanisms."
- Wu, Yimin, Laura A. Kirkman, and Thomas E. Wellems. 1996. "Transformation of *Plasmodium Falciparum* Malaria Parasites by Homologous Integration of Plasmids That Confer Resistance to Pyrimethamine." *Proceedings of the National Academy of Sciences of the United States of America* 93(3):1130–34.
- Wu, Yimin, C. David Sifri, Hsien Hsien Lei, Xin Zhuan Su, and Thomas E. Wellems. 1995. "Transfection of *Plasmodium Falciparum* within Human Red Blood Cells." *Proceedings of the National Academy of Sciences of the United States of America* 92(4):973–77.

- Xiao, Bo, Shigang Yin, Yang Hu, Maoxin Sun, Jieqiong Wei, Zhenghui Huang, Yuhao Wen, Xueyu Dai, Huiling Chen, Jianbing Mu, Liwang Cui, and Lubin Jiang. 2019. "Epigenetic Editing by CRISPR/DCas9 in *Plasmodium Falciparum*." *Proceedings of the National Academy of Sciences of the United States of America* 116(1):255–60.
- Yang, Lee-Wei, Silvina Matysiak, Shang-Te Danny Hsu, Gabriela Mustata Wilson, and Yasumasa Joti. 2012. "Functional Dynamics of Proteins." *Computational and Mathematical Methods in Medicine* 2012:1–3.
- Yang, Ming, Tomoyoshi Soga, Patrick J. Pollard, and Julie Adam. 2012. "The Emerging Role of Fumarate as an Oncometabolite." *Frontiers in Oncology* 2 JUL(July):1–7.
- Yang, Youfeng, Vladimir Valera, Carol Sourbier, Cathy D. Vocke, Minghui Wei, Lisa Pike, Ying Huang, Maria A. Merino, Gennady Bratslavsky, Min Wu, Christopher J. Ricketts, and W. Marston Linehan. 2012. "A Novel Fumarate Hydratase-Deficient HLRCC Kidney Cancer Cell Line, UOK268: A Model of the Warburg Effect in Cancer." *Cancer Genetics* 205(7–8):377–90.
- Yogev, Ohad, Adi Naamati, and Ophry Pines. 2011. "Fumarate: A Paradigm of Dual Targeting and Dual Localized Functions." *FEBS Journal* 278(22):4230–42.
- Zauner, Florian B., Elfriede Dall, Christof Regl, Luigi Grassi, Christian G. Huber, Chiara Cabrele, and Hans Brandstetter. 2018. "Crystal Structure of Plant Legumain Reveals a Unique Two-Chain State with PH-Dependent Activity Regulation." *Plant Cell* 30(3):686–99.
- Zauner, Florian B., Brigitta Elsässer, Elfriede Dall, Chiara Cabrele, and Hans Brandstetter. 2018. "Structural Analyses of Arabidopsis Thaliana Legumain Reveal Differential Recognition and Processing of Proteolysis and Ligation Substrates." *Journal of Biological Chemistry* 293(23):8934–46.
- Zborníková, Eva, Zdeněk Knejzlík, Vasili Haurlyliuk, Libor Krásný, and Dominik Rejman. 2019. "Analysis of Nucleotide Pools in Bacteria Using HPLC-MS in HILIC Mode." *Talanta* 205(July):120161.
- Zhang, Min, Chengqi Wang, Thomas D. Otto, Jenna Oberstaller, Xiangyun Liao, Swamy R. Adapa, Kenneth Udenze, Iraad F. Bronner, Deborah Casandra, Matthew Mayho, Jacqueline Brown, Suzanne Li, Justin Swanson, Julian C. Rayner, Rays H. Y. Jiang, and John H. Adams. 2018. "Uncovering the Essential Genes of the Human Malaria Parasite *Plasmodium Falciparum* by Saturation Mutagenesis." *Science* 360(6388).
- Zhang, Weipeng, Jin Sun, Huiluo Cao, Renmao Tian, Lin Cai, Wei Ding, and Pei Yuan Qian. 2016. "Post-Translational Modifications Are Enriched within Protein Functional Groups Important to Bacterial Adaptation within a Deep-Sea Hydrothermal Vent Environment." *Microbiome* 4:1–10.
- Zheng, Liang, Simone Cardaci, Livnat Jerby, Elaine D. Mackenzie, Marco Sciacovelli, T. Isaac Johnson, Edoardo Gaude, Ayala King, Joshua D. G. Leach, Ruangelie Edrada-Ebel, Ann Hedley, Nicholas A. Morrice, Gabriela Kalna, Karen Blyth, Eytan Ruppín, Christian Frezza, and Eyal Gottlieb. 2015. "Fumarate Induces Redox-Dependent Senescence by Modifying Glutathione Metabolism." *Nature Communications* 6.
- Zheng, Qingfei, Nathaniel D. Omans, Rachel Leicher, Adewola Osunsade, Albert S. Agustinus, Efrat Finkin-Groner, Hannah D'Ambrosio, Bo Liu, Sarat Chandarlapaty, Shixin Liu, and Yael David. 2019. "Reversible Histone Glycation Is Associated with Disease-Related Changes in Chromatin Architecture." *Nature Communications* 10(1).